Jour. Research U.S. Geol. Survey
Vol. 5, No. 1, Jan.–Feb. 1977, p. 49–52

PROCEDURE FOR ESTIMATING THE TEMPERATURE OF A HOT-WATER COMPONENT IN A MIXED WATER BY USING A PLOT OF DISSOLVED SILICA VERSUS ENTHALPY

By A. H. TRUESDELL and R. O. FOURNIER, Menlo Park, Calif.

Abstract.—A graphical method using a plot of dissolved silica versus enthalpy allows quick determination of the temperature of the hot-water component of a nonboiling thermal spring. The method is applicable to warm spring waters that either have not lost heat before mixing or have lost heat by separation of steam before mixing.

Fournier and Truesdell (1974) published graphical and analytical procedures for estimating the temperature and proportion of a hot-water component mixed with a cold water. These procedures, valid for warm springs of large flow rate, were based on heat and silica balances. This paper presents simplified graphical procedures for obtaining those results. The method makes use of the dissolved silica-versus temperature graph of Fournier and Rowe (1966, fig. 5), replotted in figure 1 as dissolved silica versus enthalpy of liquid water in equilibrium with steam. To simplify the procedure, we have chosen to plot enthalpy in International Table calories (cal_{IT}) per gram (above 0°C) rather than joules per gram because the enthalpy of liquid water is numerically approximately the same as the temperature.

In using figure 1, one may assume either that no steam or heat had been lost from the hot-water component before mixing or that steam had separated from the hot-water component at an intermediate temperature before mixing. In either event, it is necessary to assume that no loss of heat occurs after mixing, that the initial silica content of the deep hot water is controlled by the solubility of quartz, and that no further solution or deposition of silica occurs before or after mixing. These assumptions are discussed in greater detail in Fournier and Truesdell (1974).

PROCEDURE

Assuming no loss of steam or heat before mixing; then do the following:

1. Determine or estimate the temperature and silica content of nonthermal ground water in the region and plot as a point in figure 1, the silica-versus-enthalpy graph. Plot temperature in degrees Celsius as calories. This is shown as point A in figure 2.
2. Plot the temperature and silica content of the warm spring water as another point on the graph, point B in figure 2 (again plotting temperature as calories).
3. Draw a straight line through the two points and extend that line to intersect the quartz solubility curve, point C in figure 2. Point C is the enthalpy and silica content of the deep hot-water component.
4. Obtain the temperature of the hot-water component from its enthalpy by using steam tables (Keenan and others, 1969) or figure 3.
5. Determine the fraction of hot water in the warm spring by dividing the distance AB by AC.

It is possible that point B may plot at too high a silica value for the extension of line AB to intersect the quartz solubility curve. This may be due to the assumption of too low a value for the silica content of the nonthermal water, and this value may be increased if it seems reasonable. Alternately, the hot-water component may have lost heat, but not silica, before mixing. If heat was lost by separation of steam, it is possible to evaluate the situation.

Assuming steam loss from an adiabatically cooled liquid before mixing with cold water; then do the following:

1. Plot the temperature and silica contents of the warm and cold waters as in the above procedure (fig. 4, points A and D).
2. Draw a straight line between those points (A and D) and extend that line to the liquid-water enthalpy equivalent of the temperature at which

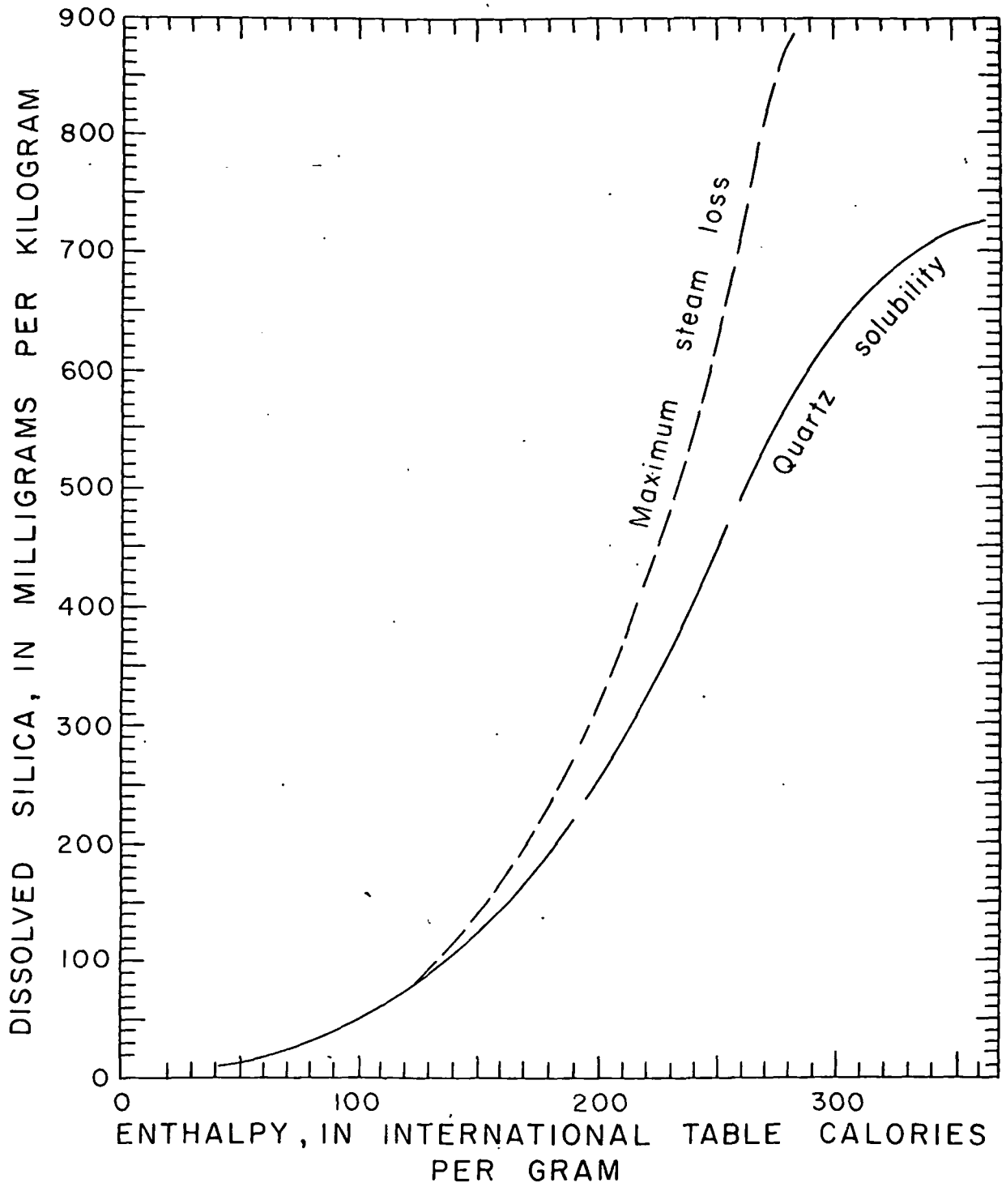

FIGURE 1.—Dissolved silica–enthalpy graph for determining temperature of a hot-water component mixed with cold water yielding warm spring water.

steam is assumed to have escaped before mixing (point E for 100°C in fig. 4).

3. Move horizontally across the diagram parallel to the abscissa until the maximum steam-loss curve is intersected (point F in fig. 4). Point F gives the enthalpy of the hot-water component before the onset of boiling, and point G gives the original silica content before loss of steam occurred.

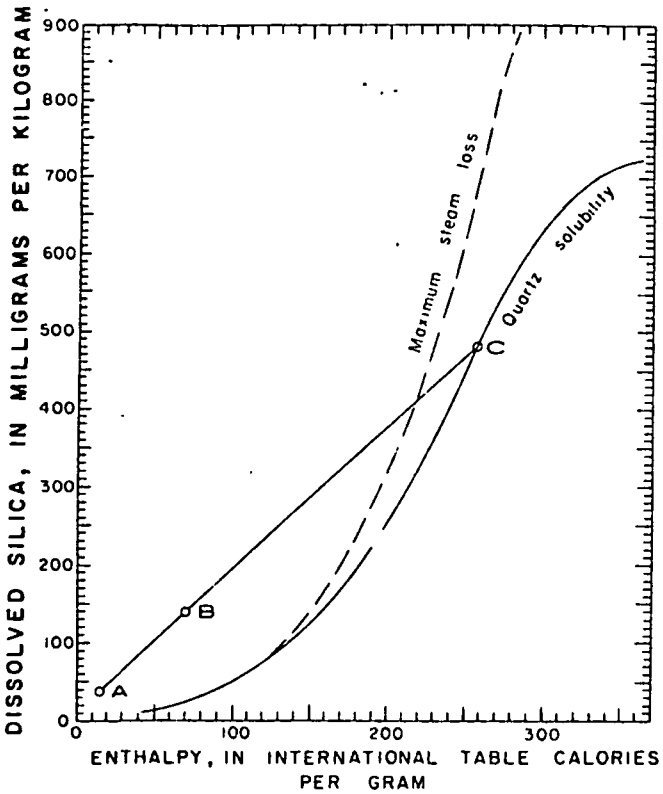

FIGURE 2.—Dissolved silica–enthalpy graph to be used when assumption is made that no steam or heat has been lost before mixing. See text for explanation.

4. Determine the fraction of hot water (after steam loss) in the warm spring by dividing the distance AD by AE. The weight fraction of original hot water lost as steam before mixing, x, is given by the formula

$$x = 1 - \frac{\text{silica value at point G}}{\text{silica value at point F}}.$$

If steam is lost at temperatures above 100°C, point F will lie on an intermediate steam loss (ISL) curve between the 100°C maximum steam loss (MSL) curve and the quartz solubility (QS) curve. The relative distance of the ISL curve from the QS and MSL curves is in the proportion $(H_{QS}-H_{ISL})/(H_{ISL}-H_{100})$ where H_{QS} is the enthalpy of liquid water at the quartz solubility curve at a given value of silica, H_{ISL} is the enthalpy of liquid water at the actual temperature of steam loss, and H_{100} is the enthalpy of liquid water at 100°C.

If steam separates at less than 1 atmospheric pressure, the enthalpy of the residual liquid water will be

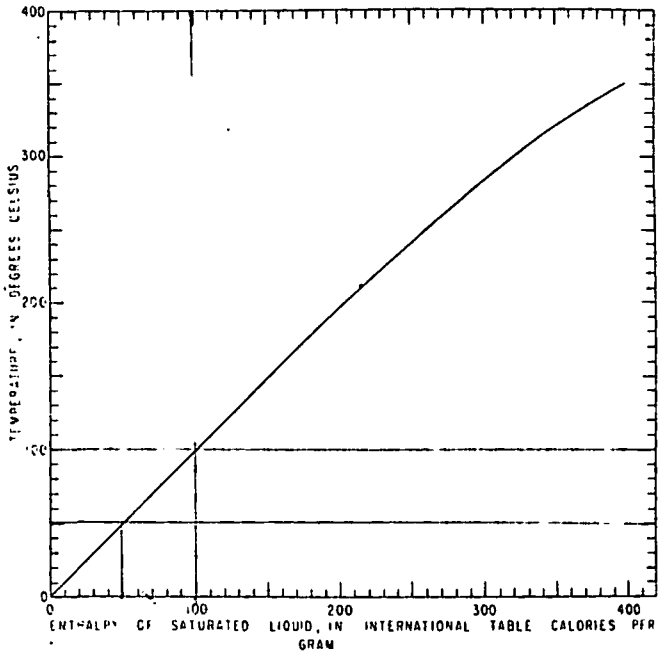

FIGURE 3.—Temperature-enthalpy relations for liquid water in equilibrium with steam.

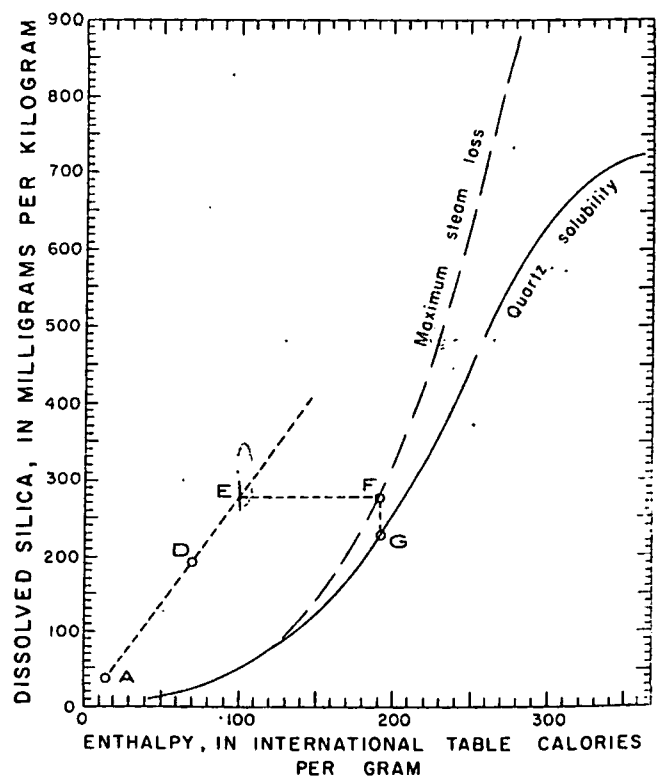

FIGURE 4.—Dissolved silica–enthalpy graph to be used when assumption is made that steam separated at 100°C from the hot-water component before mixing. See text for explanation.

less than 100 cal_{IT}/g. Point F will then be positioned on a different maximum steam-loss curve located slightly to the left of the maximum steam-loss line shown in figure 4. However, the change in position of the maximum steam loss curve as a function of the atmospheric pressure (altitude) is generally trivial.

DISCUSSION

The maximum enthalpy of the hot-water component that can be reliably determined is set by the point at which an extended line, such as AB (fig. 2), would be tangent to the quartz solubility curve. For most reasonable silica contents of nonthermal water, this will be at about 300 cal_{IT}/g (~285°C). Higher initial enthalpies of the hot-water component would cause an extended line to intersect the quartz solubility curve at two points, and the lower enthalpy point probably would be erroneously selected as the solution to the mixing problem. Although this presents a problem in interpretation, another problem inherent in dealing with very high enthalpy waters (above 275 to 300 cal_{IT}/g) is probably more serious. Quartz precipitates relatively quickly from such waters, and, therefore, temperatures derived from any relation assuming no silica precipitation are likely to be in error.

This method does allow easy evaluation of the effects of variations in assumed silica content and temperature of nonthermal water. The method also allows results obtained assuming no steam loss to be compared quickly with results obtained assuming steam loss at various intermediate temperatures. Similar graphical methods can be used to accommodate other silica phases such as chalcedony and cristobalite.

REFERENCES CITED

Fournier, R. O., and Rowe, J. J., 1966, Estimation of underground temperatures from the silica content of water from hot springs and wet-steam wells: Am. Jour. Sci., v. 264, p. 685–687.

Fournier, R. O., and Truesdell, A. H., 1974, Geochemical indicators of subsurface temperature—Part 2, Estimation of temperature of fraction of hot water mixed with cold water: U.S. Geol. Survey Jour. Research, v. 2, no. 3, p. 263–270.

Keenan, J. H., Keyes, F. G., and Moore, J. G., 1969, Steam tables, Thermodynamic properties of water, including vapour, liquid, and solid phases: New York, John Wiley & Sons, 162 p.

MINERALOGICAL MAGAZINE, SEPTEMBER 1981, VOL. 44, PP. 325-31

Partition geochemistry of sediments from DSDP 424 in the Galapagos Hydrothermal Mounds Field

S. P. VARNAVAS* AND D. S. CRONAN

Applied Geochemistry Research Group, Department of Geology, Imperial College, London

[Paper read 8 November 1979]

ABSTRACT. Sediments from DSDP 424, a core taken in a hydrothermal mound in the Galapagos Mounds Field, comprise biogenic oozes, siliceous ash-rich layers and two varieties of hydrothermal precipitates, an Fe-rich clay (nontronite), and Mn oxides. Compositionally, these sediments differ considerably from one another and vary in proportion down the core to basement. Geochemical partition studies on the sediments have indicated a variable fractionation of the elements that they contain between clays, carbonate, and Mn oxides with the hydrothermal phases being strongly depleted in trace elements. The hydrothermal sediments are thought to have been formed as a result of the fractional precipitation of Fe silicates and Mn oxides from ascending hydrothermal solutions which are depleted in trace elements due to subsurface precipitation of sulphides, and have had insufficient time to scavenge trace metals from sea water due to their rapid precipitation

THE Galapagos Spreading Center (fig. 1) forms part of the global mid-ocean ridge system. It is spreading at a half rate of 35 mm/yr (Klitgord and Mudie, 1974) and heat flow and bottom-water temperature measurements show an increase of these parameters in this area relative to that surrounding (Sclater *et al.*, 1974; Detrick *et al.*, 1974) indicating that it is hydrothermally active.

Hydrothermal mounds are located within an area of high heat flow, between 18 and 25 km from the spreading axis. Their height varies from less than a metre to over 20 m, the small mounds having gentle slopes while the larger ones have steeper slopes. Within the mounds, black Mn-oxide crusts have been observed overlying orange Fe oxides, which in turn overlie green nontronite (Corliss *et al.*, 1978). The chemistry of these deposits showed that Fe and Mn were strongly fractionated. Fe was found almost exclusively in the nontronite or Fe oxides while Mn formed a separate phase consisting of todorokite and birnessite (Corliss *et al.*, 1978).

In the present study, some hydrothermal deposits drilled at DSDP 424 in a sea-floor mound field 22 km south of the Galapagos Spreading Center have been investigated as follows: (1) The bulk chemical composition of the deposits has been determined, and the profiles of the vertical distribution of their metals studied. (2) The phases present in the sediments have been separated chemically and the proportional distribution of metals in each determined. (3) An attempt has been made to deduce the process of formation of the deposits.

Lithology—stratigraphy

The general lithology of the sediments drilled at DSDP 424 has been summarized by Hekinian *et al.* (1978). The following material was recovered: hydrothermal deposits, foraminifer-nanofossil ooze, siliceous-nanofossil ooze, and siliceous-ash-rich layers. The hydrothermal deposits can be divided into two classes: (*a*) green smectite of nontronitic composition, and (*b*) Mn oxides.

The top of the core down to 13.8 m consists of hydrothermal sediment, made up essentially of green nontronitic mud intermixed with Mn oxide. At 13.8–14.2 m, a thin layer of foraminifer-nanofossil ooze occurs, in which Mn oxides are present. Hydrothermal sediments similar to those found in the upper part of the sediment sequence occur in the core at 14.2–15.1 m and 15.5–16.2 m, with foraminifer-nanofossil ooze between them. Between 16.2 and 19.0 m there is a layer of carbonate sediments which is followed by another horizon of green nontronitic mud (19.0–19.5 m). From 19.5 m down to the bottom of the sediment column the core is composed of foraminiferal-nanofossil ooze.

* Present address: Department of Geology, University of Patras, Patras, Greece.

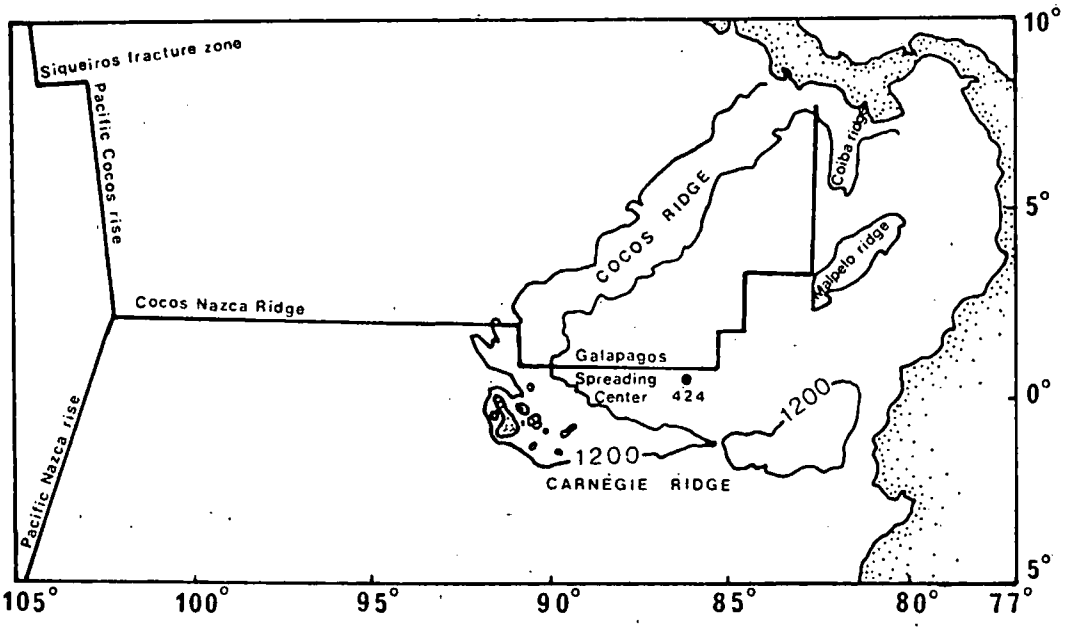

FIG. 1. Location of the Galapagos Spreading Centre.

From the presence of radiolaria, which are abundant and well preserved in a large part of the core, the age of the basal sediments has been determined to be not greater than 1.2 Ma.

Chemistry of the deposits

Bulk chemical composition. Chemical analyses of nineteen samples from various depths of DSDP 424 were carried out by Atomic Absorption Spectrophotometry for Mn, Fe, Ni, Co, Pb, Zn, Ca, Mg, and Al. The results are given on a carbonate-free basis in Table I. The attack used was a total $HF-HClO_4$ dissolution leaving no residue. The accuracy of the determinations was checked by analysis of international standards, and the precision of the determinations were better than $\pm 10\%$. The Atomic Absorption instrument used was a Perkin Elmer 403, and the readings it gave were corrected for Ca interference in high-carbonate samples. Silica was determined separately.

The chemical composition of the deposits shows that certain sediment horizons occur which are markedly ferruginous, whereas in other layers the concentration of Fe is lower and in some cases is similar to that in normal pelagic clays. Fe is depleted in the Mn crusts at the top of the sediment sequence while its concentration in the underlying green hydrothermal sediments ranges between 21 and 22.5%. Mn is depleted in these latter sediments. From 19.5 m down to the basement, where carbonate sediments occur, the concentration of Fe tends to decrease and at the basement it reaches values which are comparable with those of normal pelagic sediments. It is observed that at the top of each of the ferruginous horizons a thin Mn-rich layer occurs, whereas at greater depths the whole of each ferruginous horizon is exceedingly depleted in Mn.

The trace-element data for the highly ferruginous and manganiferous horizons show that these sediments are extremely depleted in trace metals such as Ni, Co, Zn, and Cu, when compared with the average composition of Pacific surface pelagic clays and especially Mn nodules and mid-ocean ridge metalliferous sediments at large (Cronan, 1969, 1976*a*). In the upper Fe-rich clays (0–13.8 m) the concentrations of these metals do not show any significant variation with increasing depth. In contrast, there is a tendency for their concentration to increase with depth in the carbonate sediments (fig. 2). The maximum concentrations of Ni, Co, and Zn occur at 17.4 m (346, 60, 418 ppm, respectively), while Cu shows its highest concentration at 30.6 m (324 ppm). In both cases these depths fall within the foraminifer–nanofossil ooze layers. The vertical variations of Ni, Co, Cu, and Zn are, in large part, positively correlated with each other.

In contrast to the other trace metals, Pb does not show any depletion in the Fe-rich sediments,

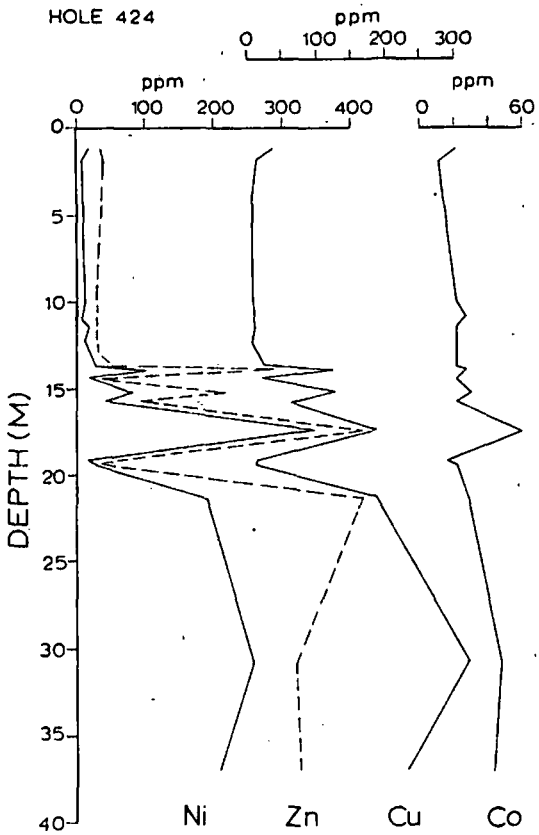

FIG. 2. Variations of Ni, Zn, Cu, and Co with depth in DSDP 424.

its concentrations being similar to the average concentration of Pb in normal pelagic clays. Furthermore, the vertical variations of Pb show a different pattern from that produced by the vertical distributions of Ni, Co, Cu, and Zn. A decrease in the concentration of Pb with increasing depth within the upper ferruginous horizon occurs which continues into the carbonate sediments below. The two peaks in the concentration of Pb which have been found at depths of 1.20 and 19.10 m are associated with the Mn-rich layers occurring at the tops of the ferruginous horizons.

The Fe- and Mn-rich sediments are characterized by a very low Al content, while in the other sediments the concentration of Al varies with that of $CaCO_3$. The concentration of SiO_2 ranges between 39.03 and 47.32% on a CFB. There is a tendency for its concentration to decrease with increasing depth in DSDP 424. A positive linear correlation (fig. 3) between SiO_2 and Fe concentrations was found.

The average chemical composition of the Galapagos green hydrothermal clay material shows similarities with those of clay-rich sediments described from the Gulf of Aden (Cann *et al.*, 1977), and from transform fault A in the FAMOUS area (Hoffert *et al.*, 1978).

Partition analysis. The use of partition analysis has become an important tool in the elucidation of the distribution of elements between various coexisting phases of marine sediments which are too fine-grained for it to be possible to physically separate their individual constituents (Goldberg and Arrhenius, 1958; Chester and Hughes, 1967; Cronan, 1976*a*). In the present investigation, partition analysis has been carried out on ten samples in order to investigate the distribution of Ca, Mn, Fe, Ni, Co, Pb, Zn, Cu, and Al between their constituent phases. The method used was a modification of that of Chester and Hughes (1967), described in detail by Cronan (1976*a*). The samples were leached first with acetic acid to remove carbonate phases and adsorbed ions, secondly with hydroxylamine HCl to remove reducible Mn and ferromanganese oxides, thirdly with HCl to remove iron oxides and attack silicates, and finally with HF, $HClO_4$ to take up the residue resistent to the previous attacks. The partition data are summarized in Table II, where the sediments have been divided into Fe-rich clays, carbonates, and Mn-rich sediments. The relatively pure manganese oxide crust from the top of the core was not subjected to partition analysis because insufficient material was available.

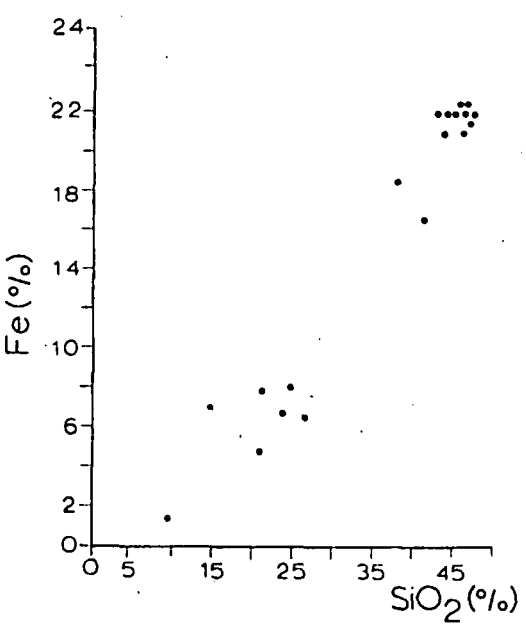

FIG. 3. Fe against SiO_2 in samples analysed.

Table I: Chemical composition of sediments from the Galapagos spreading center (Leg 54, Hole 424), expressed on a carbonate-free basis.

	Sample Number	Depth m	Ca %	$CaCO_3$ %	Mn %	Fe %	Ni ppm	Co ppm	Pb ppm	Zn ppm	Cu ppm	Mg %	Al %	SiO_2 %	Fe/Mn
1	6	Top	1.02	0.01	33.00	7.2	81	16	48	126	39	1.65	0.15	13.84	0.22
2	15	1.20	0.33	0.01	3.80	22.0	17	22	150	35	14	2.20	0.09	42.72	5.79
3	39	1.94	0.17	0.01	0.35	22.5	7	12	80	39	8	2.30	0.06	45.99	64.2
4	48	9.87	0.18	0.01	0.078	22.0	12	22	95	28	9	2.50	0.03	45.22	282
5	51	10.97	0.19	0.01	0.077	22.0	7	27	80	29	11	2.65	0.05	47.32	285
6	38	11.38	0.15	0.01	0.054	22.0	17	22	50	30	12	2.70	0.07	46.56	407
7	2	12.21	0.17	0.01	0.063	22.5	12	22	50	27	9	2.47	0.05	46.32	357
8	25	12.91	0.17	0.01	0.067	22.0	17	22	50	33	12	2.40	0.07	45.06	328
9	28	13.72	0.21	0.01	0.090	21.0	27	22	50	54	24	2.70	0.43	47.00	233
10	19	13.91	17.25	40.98	0.314	13.1	101	27	35	289	125	2.77	2.19	36.19	41.82
11	18	14.40	0.22	0.01	0.105	22.0	17	22	50	38	20	2.50	0.17	44.67	209
12	1	15.22	15.50	36.53	0.300	12.6	82	30	46	218	129	3.17	2.14	39.28	42.0
13	32	15.75	4.02	7.34	0.108	17.8	40	22	45	94	63	2.89	1.16	44.57	164
14	47	17.41	18.50	44.16	0.457	12.0	346	60	41	418	189	3.72	4.30	42.65	26.2
15	12	19.10	0.52	0.01	10.75	18.4	16	17	294	57	13	2.15	0.05	38.08	1.72
16	54	19.36	0.29	0.01	0.080	21.0	27	22	49	35	14	2.75	0.21	43.95	262
17	35	21.30	20.75	49.89	0.409	9.4	190	29	37	418	189	7.65	4.19	41.35	23.1
18	7	30.69	11.50	26.35	1.603	8.9	261	49	71	323	324	3.10	3.74	35.66	5.59
19	14	36.90	30.75	75.32	2.068	5.1	210	44	75	329	233	3.34	5.27	39.03	2.50
Average of nine ferruginous samples			0.19	0.01	0.107	21.9	16	22	62	35	13	2.55	0.13	45.79	

Table II Summary of partition analyses. The results are expressed as percentages of bulk composition.

		Ca	Mn	Fe	Ni	Co	Pb	Zn	Cu	Al
Fe-rich clays	A	51.62	31.06	1.19	5.88	8.33	1.01	3.57	8.88	13.54
	B	32.58	29.72	2.39	51.64	7.58	65.30	8.81	39.39	6.38
	C	0.98	33.52	95.08	34.64	15.15	4.46	43.78	15.27	48.48
	D	14.83	5.69	0.21	7.84	68.93	28.74	43.85	36.44	31.61
	E	0.75	0.61	21.07	20.00	21.00	69.00	67.00	21.00	0.27
Carbonate sediments	A	95.65	41.93	1.42	13.61	12.50	16.82	5.44	18.33	2.81
	B	1.00	5.00	2.11	22.75	15.00	4.76	6.31	21.12	2.65
	C	0.00	49.23	80.97	62.30	72.50	59.37	68.0	33.71	57.88
	D	3.35	3.85	14.78	1.35	0.00	19.05	20.17	26.86	36.67
	E	17.87	0.22	7.22	126.00	25.00	22.00	202.00	89.00	1.84
Mn-rich sediments	A	65.39	2.23	0.76	0.00	0.00	0.00	1.76	7.69	20.00
	B	19.23	89.49	2.76	81.25	11.76	94.90	3.77	46.15	0.00
	C	1.92	4.93	93.01	0.00	11.76	0.00	21.05	0.00	40.00
	D	13.46	3.35	3.47	18.75	76.48	5.10	68.42	46.15	40.00
	E	0.52	10.75	18.45	16.00	17.00	294.00	57.00	13.00	0.05

A: Acetic acid leach (HAc).

B: Acid-reducing agent leach (i.e. hydroxylamine hydrochloride).

C: HCl leach.

D: HCl-insoluble residue.

E: Bulk composition (Ca, Mn, Fe and Al in wt. %, remainder in ppm).

When co
indicate tha
the partitio
the carbona
(Table II).

In the Fe-
associated w
minerals. Fe
a non-auth
low over a
located in th
fraction. Co
insoluble re
between the
insoluble res
distributions
Co, Pb, Zn,
the Fe-rich c
of some basa
Since there
these sedimen
ated with th
reflect its ra
surface of th
HCl-soluble
admixed cl

Except fo
(Mn, Fe, Ni
carbonate
HCl-soluble
of normal
elements are
clay fractio
nificant co
the acetic-
removal of
cium carbon
material.

The Mn-
different fr
carbonate se
observed for
ates. This
of Fe-rich cl
In the Mn-
associated w
tion, while C
HCl-insolub
distributed e
the HCl-ins
is equally d
and the HCl
acetic acid-
of Mn asso
soluble fract
proportion
ments.

When considered over all, the partition data indicate that there are considerable differences in the partition of elements between the Fe-rich clays, the carbonate sediments, and the Mn-rich sediments (Table II).

In the Fe-rich clays most of the Fe and Al are associated with the HCl-soluble fraction in the clay minerals, Fe in the nontronite and Al probably in a non-authigenic aluminosilicate, but Al is very low over all. The majority of the Ni and Pb are located in the minor hydroxylamine HCl-soluble fraction. Cobalt is more concentrated in the HCl-insoluble residue, while Zn is equally distributed between the HCl-soluble fraction and the HCl-insoluble residue. Other elements show more even distributions. The presence of significant amounts of Co, Pb, Zn, and Al in the HCl-insoluble residue of the Fe-rich clays would suggest the incorporation of some basaltic detrital material in these sediments. Since there is little or no carbonate material in these sediments, the high proportion of Mn associated with the acetic acid-soluble fraction may reflect its removal from adsorption sites on the surface of the Fe-rich clays, and hydroxylamine-HCl-soluble Mn may be present in physically admixed oxides.

Except for Ca, the majority of the elements (Mn, Fe, Ni, Co, Pb, Zn, Cu, and Al) in the carbonate sediments are associated with the HCl-soluble fraction. This may reflect the processes of normal pelagic sedimentation, where these elements are incorporated into the non-authigenic clay fraction of the sediments. However, the significant concentrations of Mn, Pb, and Cu in the acetic-acid-soluble fraction points to the removal of these elements from biogenic calcium carbonate or from coatings on carbonate material.

The Mn-rich sediments show partition patterns different from those of Fe-rich clays and the carbonate sediments, but are more similar to those observed for the Fe-rich clays than for the carbonates. This is most likely to be due to the presence of Fe-rich clay material admixed in these sediments. In the Mn-rich sediments, Mn, Ni, and Pb are associated with the acid-reducible Mn oxide fraction, while Co and Zn are predominately in the HCl-insoluble detrital residue. Copper is equally distributed between the acid-reducible fraction and the HCl-insoluble residue. The minor aluminum is equally distributed between the HCl-soluble and the HCl-insoluble fractions, with some in the acetic acid-soluble fraction. The high percentage of Mn associated with the hydroxylamine HCl-soluble fraction indicates the presence of a large proportion of reducible Mn oxides in the sediments.

Discussion

The observations described in this paper support discussion of a number of problems. What are the reasons for the strikingly different compositions of the different hydrothermal constituents of the sediments, and why are they all so low in trace elements? Are the deposits primary precipitates, or are they diagenetic in origin? Do the data indicate episodic or continuous accumulation of hydrothermal precipitates in the Galapagos Mounds Area? Where do they fit into the global mid-ocean ridge hydrothermal fractionation sequence (Cronan, 1976*b*, 1980), parts of which are being found in more and more locations on the sea floor.

The fact that the Mn-crusts present at the top of the sediments contain very little Fe, while the underlying Fe-rich clays are depleted in Mn, indicates that a fractionation between Fe and Mn occurs in the sediments. The experimental conditions for the direct precipitation of nontronite from solutions containing Fe and Si require a reducing environment (Harder, 1976). Therefore during the precipitation of the nontronite, Mn remains in solution and precipitates later above the Fe silicates as Mn oxide when the redox potential rises, although some may escape altogether by dispersion through sea water.

That the Fe/Mn ratios vary vertically down the core, indicates that hydrothermal solutions have been discharged periodically in the mounds area rather than during one continuous process. The layers with high Fe/Mn ratios represent sediments deposited during the early phases of discharge of hydrothermal solutions whereas those having lower Fe/Mn ratios are sediments which have been formed from the residual solutions of the hydrothermal activity under more oxidizing conditions. This is consistent with observations on the Santorini hydrothermal deposits made by Smith and Cronan (1975), where the sediments from close to the fumarolic outlets are characterized by high Fe/Mn ratios in contrast to those away from the fumarolic outlets where the Fe/Mn ratios are low. Fluctuations in the Fe/Mn ratios are also reported from sediments near Stromboli (Bonatti *et al.*, 1972), which suggest a similar process of sedimentation. Likewise, there is a marked fractionation of Mn from Fe in the Red Sea hydrothermal deposits, where a pattern including Mn- and Fe-rich geochemical zones was found around the Atlantis II Deep (Bignell *et al.*, 1976). Thus, there is evidence to conclude that the geochemical conditions which occurred during the precipitation of the Galapagos deposits were similar to those occurring in the Red Sea and the Santorini hydrothermal areas. The main difference is that in the Galapagos deposits

the results of this process are exhibited vertically, whereas in the Santorini and the Red Sea sediments they are exhibited horizontally.

It is notable that the concentrations of Ni, Co, Zn, and Cu are extremely low in the Galapagos hydrothermal sediments, particularly in the ferruginous horizons. Two possible explanations are envisaged for the depletion of these metals. (1) The hydrothermal solutions which are responsible for their formation are depleted in these metals. (2) The rapid precipitation of the major hydrothermal phases does not allow significant scavenging of the metals from sea water. Cronan (1976*b*) suggested that circulating sea water within the fractures and fissures of the upper part of the oceanic crust could mix with hydrothermal solutions and cause precipitation of metal sulphides and possibly other phases below the sea floor. This would lead to a depletion of sulphide-forming elements, such as most of the trace elements determined in this work, in the hydrothermal solutions at discharge.

Although sub-sea-floor precipitation processes can explain why the Galapagos hydrothermal sediments are not enriched in trace metals, they are not able to explain why the concentrations of trace metals in these sediments are lower than the average concentrations which occur in normal pelagic sediments. It is known that 'scavenging' of metals from sea water by suspended material and transfer of them to the sea floor is an important process in the incorporation of trace metals into deep-sea sediments (Goldberg, 1954), and is a function of a number of factors. The factor which is probably most important in explaining the extremely low concentrations of trace metals in the Galapagos hydrothermal sediments is their rate of deposition. In view of the young age of the deposits, their rate of deposition must have been very rapid and the time of their residence in the sea water was so short that scavenging of metals would have been very limited.

Therefore, it is concluded that a combination of two factors determines the low trace-element content of the hydrothermal sediments; the rapid deposition of the hydrothermal precipitates together with the depletion of the hydrothermal solutions in trace metals as a result of sub-sea-floor precipitation processes.

An attempt has been made in the present study to investigate the form in which Si is present in the Galapagos sediments, and to determine the possible form in which it was precipitated from the hydrothermal solutions. The selective chemical analyses indicate that Fe is associated chiefly with the HCl-soluble fraction, which, along with the fact that there is a positive linear correlation (fig. 3) between Fe and the total SiO_2 leads to the conclusion that the majority of Fe and Si in the sediments examined occur in the form of nontronite. This could have been formed either by direct precipitation from the hydrothermal solutions or from their reaction with silica-bearing sediments, or diagenetically from the reaction between Fe-hydroxides and SiO_2 after their precipitation from the hydrothermal solutions as two separate phases.

To examine the possibility of diagenetic formation of an Fe-rich clay mineral, after the precipitation of Fe and Si from the hydrothermal solutions, the following reaction should be considered.

$$\text{Fe-hydroxides} + SiO_2 \xrightarrow{\text{diagenesis}} \text{Fe-rich clay mineral}$$

If this reaction takes place in the Galapagos sediments, then the proportion of Fe present in the sediments associated with the Fe-rich clays should increase with time. This can be tested by examining variations down the core in the distribution of Fe between the fraction soluble in HCl and the other fractions, because the Fe which is present in the form of Fe silicate in the clay minerals will be dissolved in HCl. There is no tendency for the proportion of the Fe associated with the HCl-soluble fraction to increase with increasing depth in the core and thus it is considered that no transformation of one Fe phase to another occurs in the present sediments. It is, therefore, reasonable to conclude that the Fe-rich nontronitic clays found in the Galapagos sediments either precipitate directly from the hydrothermal solutions, or form by reaction of the hydrothermal solution with, and replacement of, the indigenous sediments of the area which are SiO_2-bearing biogenic oozes.

In comparison with other hydrothermal deposits on the sea floor, those from the Galapagos Mounds Area described here can be classified as sharply fractionated deposits. In the global mid-ocean ridge hydrothermal fractionation sequence (Cronan, 1980) they would form after the precipitation of sulphides, which, as mentioned, probably occur within the oceanic crust below them, and before the precipitation of widely dispersed Fe-Mn oxides, which probably occur on the sea floor away from the immediate vicinity of the Mounds area. Their sharply fractionated nature is probably due to rapid cooling, mixing, and changes in Eh and other properties of the hydrothermal solutions on discharge.

Conclusions

Hydrothermal sediments from DSDP 424 can be divided into an Fe-rich smectite (nontronite) phase and a Mn oxide phase. Both hydrothermal phases are low in trace elements, thought to be due to (i) the subsurface precipitation of the elements

concerned in sulphides and (ii) the rapid precipitation of the hydrothermal phases precluding the scavenging of trace metals from sea water.

Down-core variations in the proportion of the different hydrothermal phases present, reflected in part by variation in the Fe/Mn ratio, demonstrate that selective fractionation of Mn phases from Fe phases has taken place at discrete times in the past and that the hydrothermal precipitation has not been a continuous process.

The partition of elements between the different phases is as follows: Fe is principally present in the HCl-soluble Fe-rich clay fraction of all the sediments; Ca is largely present in biogenic debris, and Al as non-authigenic aluminosilicate detritus. The remaining elements are variably partitioned between these phases and Mn additionally occurs in an authigenic Mn-oxide phase in the Mn-rich sediments.

In the global mid-ocean ridge hydrothermal fractionation sequence of Cronan (1980), the deposits are thought to lie between early formed sulphides and later formed widely dispersed ferromanganese oxides.

Acknowledgements. We thank the Deep Sea Drilling Project under the auspices of the NSF for the samples used in this work. Financial support for the study was provided by the NERC. S. Varnavas thanks the Greek State Scholarship foundation for a Ph.D. studentship under the supervision of D.S.C. This paper is a contribution to IGCP 111.

REFERENCES

Bignell, R. D., Cronan, D. S., and Tooms, J. S. (1976). *Trans. Instn. Min. Metall.* (B), **85**, B274–8.

Bonatti, E., Honnorez, J., Joensuu, O., and Rydell, H. S. (1972). *In* Stanley, D. J. (ed.), *Symposium on the Sedimentation in the Mediterranean Sea:* VIII International Sediment. Congress, Heidelberg, 701–10.

Cann, J. R., Winter, C. K., and Pritchard, R. G. (1977). *Mineral. Mag.* **41**, 193–9.

Chester, R. and Hughes, M. J. (1967). *Chem. Geol.* **2**, 249–62.

Corliss, J. B., Lyle, M., Dymond, J., and Crane, K. (1978). *Earth Planet. Sci. Lett.* **40**, 12–24.

—— Edmond, J. M., Gordon, L. I., von Herzen, R. P., Ballard, R. D., Green, K., Williams, D., Bainbridge, A., Crane, K., and van Andel, T. H. (1979). *Science*, **203**, 1073–83.

Cronan, D. S. (1969). *Geochim. Cosmochim. Acta*, **33**, 1562–5.

—— (1976*a*). *Bull. Geol. Soc. Am.* **87**, 928–34.

—— (1976*b*). *Nature*, **262**, 567–9.

—— (1980). *Underwater Minerals*. Academic Press, London, 362 pp.

Detrick, R. S., Williams, D. L., Mudie, J. D., and Sclater, J. G. (1974). *Geophys. JR Astr. Soc.* **38**, 627–36.

Goldberg, E. D. (1954). *J. Geol.* **62**, 249–65.

—— and Arrhenius, G. (1958). *Geochim. Cosmochim. Acta*, **13**, 153–212.

Harder, H. (1976). *Chem. Geol.* **18**, 169–80.

Hekinian, R., Rosendahl, B. R., Cronan, D. S., Dmitriev, V., Fodor, R. V., Goll, R. M., Hoffert, M., Humphries, S. E., Mattey, D. P., Natland, J., Petersen, N., Roggenthen, W., Schrader, E. L., Srivastava, R. K., and Warren, M. (1978). *Oceanol. Acta*, **1**, 473–82.

Hoffert, M., Perseil, A., Hekinian, R., Choukroune, P., Needham, H. D., Francheteau, J., and Le Pichon, X. (1978). Ibid, **1**, 73–86.

Klitgord, K. D. and Mudie, J. D. (1974). *Geophys. J. R. Astr. Soc.* **38**, 563–8.

Sclater, J. G., von Herzen, R. P., Williams, D. L., Anderson, R. N., and Klitgord, K. (1974). Ibid. **38**, 609–26.

Smith, P. A. and Cronan, D. S. (1975). *3rd Oceanology International, Brighton, England*, 111–14.

[*Manuscript received 8 September 1980; revised 11 December 1980*]

Marine Geology, 17(1974): 151—164

POSTDEPOSITIONAL INJECTIONS OF URANIUM-RICH SOLUTIONS INTO EAST PACIFIC RISE SEDIMENTS

H. RYDELL, T. KRAEMER, K. BOSTRÖM and O. JOENSUU

Rosenstiel School of Marine and Atmospheric Science, University of Miami, Miami, Fla. (U.S.A.)

(Accepted for publication May 21, 1974)

ABSTRACT

Rydell, H., Kraemer, T., Boström, K. and Joensuu, O., 1974. Postdepositional injections of uranium-rich solutions into East Pacific Rise sediments. *Mar. Geol.*, 17: 151—164.

An 8.5 m long apparently undisturbed core from a hilltop on the crest of the East Pacific Rise has uranium and thorium isotope distributions that are very unusual. The core is very poor in ^{232}Th, and very rich in U, particularly at the 500-cm level, where a value of about 150 ppm is reached. At the same depth the $^{230}Th_{xs}$ reaches very large negative values. These facts could be accounted for if one assumes that solutions rich in U and poor in Th had been postdepositionally injected into the sediments about 90,000—110,000 years ago. The top of the sediment received much of its U from seawater, judging from the $^{234}U/^{238}U$ ratio. Possibly carbonate rich solutions were the carriers of the injected uranium.

INTRODUCTION

Sediments on active oceanic ridges are geochemically very different from other pelagic sediments; detailed investigations of them could throw light over petrogenetic processes that are associated with the formation of new oceanic crust (Boström, 1973). For this reason we have acquired several 8—9 m long sediment cores from the crest of the East Pacific Rise, some of the sediments occurring on small hills. These sediments have been discussed by Boström et al. (1974), in which the geochemistry, mineralogy, sedimentation rates, and physiographic setting of one of these cores (GS 7202-35) have been described in greater detail. The data in Table I show that the core is geochemically fairly homogeneous, the extreme values differing less than a factor of two from the averages except for U (see also Fig.1). Also significant to our discussion is the presence of uncontorted layering, the absence of mixed faunas, and the abundance of unbroken shells, which all suggest that no slumping or disturbance took place in the sediment. Studies of other cores from this part of the ridge (Boström and Peterson, 1969; Boström et al., 1974) show that the core GS7202-35 is very representative of

TABLE I

Chemical concentrations and accumulation rates for core GS-7202-35P*

Units	Constituent	Concentration range			Concentration average	Rates of accumulation (mg/cm² 1000 yr)
In % on a total basis	$CaCO_3$	52	—	75	67	563
	$SrCO_3$	0.22	—	0.29	0.24	2.0
	NaCl	4.4	—	6.2	5.2	44
	KCl	0.28	—	0.70	0.46	3.9
	"$MgCO_3$"	1.1	—	1.7	1.3	11
In % on a carbonate- and salt-free basis	SiO_2	12.3	—	15.5	14.3	34
	SiO_2 biol.	10.4	—	13.4	12.4	28
	Al	0.21	—	0.49	0.32	0.72
	Ti	0.020	—	0.044	0.033	0.074
	Fe	25.1	—	33.0	28.3	63.4
	Mn	8.88	—	14.1	10.7	24
	P_2O_5	2.49	—	5.82	4.18	9.4
In ppm on a carbonate- and salt-free basis	B (total)	520	—	1400	820	0.18
	B (clay fract.)	500	—	1370	770	0.17
	Ba	2900	—	6400	4200	0.94
	Cu	1200	—	2000	1500	0.33
	Co	76	—	140	97	0.022
	Ni	530	—	820	675	0.15
	Zn	570	—	770	640	0.14
	Pb	160	—	440	300	0.065
	As	320	—	870	490	0.11
	V	800	—	1200	950	0.21
	Sc[1]	2(?)	—	4.5	≈ 3.2	0.0008
In ppm on a carbonate- and salt-free basis	Y	95	—	200	130	0.029
	La[1]	110	—	180	140	0.031
	Hg	0.15	—	0.40	0.25	0.000056
	Zr	110	—	180	150	0.032
	U	12.6	—	181	44.8	0.010

[1] Very approximative results, obtained from acetic acid treated fraction.
[2] Three suspiciously low values disregarded.

* Results of chemical analyses of 15 samples from core GS7202-35P (Univ. of Miami). $CaCO_3$, $SrCO_3$, NaCl, KCl, and "$MgCO_3$" represent what is dissolved in 0.2-molar acetic acid at 50°C. Some Mg may derive from the solid and liquid abiogen fractions (such as pore waters and clays), but the proportions are difficult to establish; hence all Mg is reported as "$MgCO_3$". To some extent this remark also pertains to KCl. The accumulation rates are based on an age for the core of 600,000 years and an in-situ uncompressed density of dry matter of 0.59/cm³ which is the average of 11 measured densities, maximum spread being ± 10% of this value. This density is somewhat lower than the commonly assumed average of 0.70—0.75 g/cm³, but this circumstance does not change the overall patterns described in the literature (Boström, 1970; Boström et al., 1973; Bender et al., 1971).

Note the anomalously low Al and Ti values, indicating that neither continental nor oceanic crust is supplying much debris to this location.

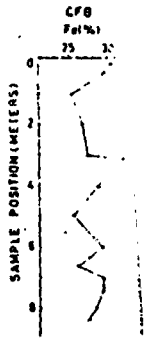

Fig.1. Eleme
corrected v
basis. (Data
$A^{230}Th/A^{23}$
general distri
show maxim
least part of

the type of
and Mn and

It is kno
1972; Bons
is anomalou
of basaltic
with this hy
Bonatti, 19
GS 7202-35
Since carbo
(Boström, 1
Lengai in th

METHODS

Our isoto
using a solid
and Th by
depositon.
(Ku, 1966).
were done b

DISCUSSION

The analy
and in Figs.
et al. (197-
Comparis

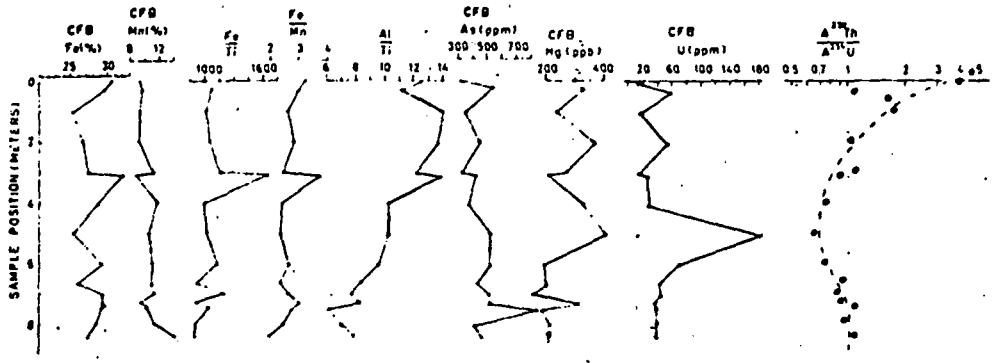

Fig.1. Elemental and isotope data for core GS 7202-35 (14°47.9'S, 113°30.1'W, corrected waterdepth 3044 m). CFB represents analyses on a carbonate- and salt-free basis. (Data after Boström et al., 1974; and this work, Table II). The dashed line through $A^{230}Th/A^{234}U$ points has no defined physical meaning, but is only intended to show the general distribution of these activity ratios. Note that the elements As, Hg, and U all show maxima at about 35 cm, 200 cm and 500 cm, suggesting an identical source for at least part of these elements.

the type of sediments that occur in this area of the Pacific, being rich in Fe and Mn and poor in Al and Ti.

It is known from other studies (Veeh and Boström, 1971; Scott et al., 1972; Bonatti et al., 1972; Rydell and Bonatti, 1973) that the ratio $^{234}U/^{238}U$ is anomalous in many volcanic deposits. These ratios may be due to leaching of basaltic crust by percolating hot seawater, but there are several weaknesses with this hydrothermal leaching hypothesis (Corliss, 1971; Rydell and Bonatti, 1973; Boström, 1973; Fisher, 1973). We have chosen to study core GS 7202-35 in detail to further illuminate the problems mentioned above. Since carbonate emanations are possible sources of active ridge sediments (Boström, 1973), we have included a study of carbonate lavas from Oldoinyo Lengai in this work for comparison.

METHODS

Our isotopic analyses were done (H.R.) by alpha-particle spectrometry, using a solid-state detector and multichannel analyzer after separation of U and Th by coprecipitation, solvent extraction, ion exchange, and electrodeposition. ^{232}U and ^{234}Th tracers were used to correct for analytical losses (Ku, 1966). The element analyses of the sediments and the carbonate lava were done by previously discussed methods (Boström et al., 1972, 1973).

DISCUSSION OF RADIOMETRIC DATA

The analytical results for core GS 7202-35 are given in Tables II and III and in Figs.1 and 2, some of them having already been discussed in Boström et al. (1974).

Comparison of our data with data for other cores from the East Pacific

02-35P*

Rates of accumulation (mg/cm² 1000 yr)
563
2.0
44
3.9
11
34
28
0.72
0.074
63.4
24
9.4
0.18
0.17
0.94
0.33
0.022
0.15
0.14
0.065
0.11
0.21
0.0008
0.029
0.031
0.000056
0.032
0.010

ıction.

P (Univ. of Miami).
in 0.2-molar acetic
fractions (such as
hence all Mg is
Cl. The accumula-
ı-situ uncompressed
ed densities,
lower than the
ce does not change
öm et al., 1973;

continental nor

TABLE II

Distribution of U and Th and their isotopes in core GS 7202-35*

Sample depth (cm)	$CaCO_3$ (%)	^{234}U (ppm)	$^{234}U/^{238}U$	^{234}U (DPH)	^{230}Th (DPH)	$^{230}Th/^{234}U$	$^{230}Th_{xs}$ (DPH)
Gravity core							
0–5	70	14.69 ± 0.23	1.12 ± 0.02	721 ± 11	3276 ± 17	4.54 ± 0.07	2555 ± 20
Pistoncore							
5–9	72	10.24 ± 0.17	1.06 ± 0.02	481 ± 8	1922 ± 15	4.00 ± 0.07	1441 ± 17
32–37	69	46.02 ± 0.45	1.09 ± 0.02	2211 ± 21	2350 ± 21	1.06 ± 0.02	139 ± 30
63–66	68	17.37 ± 0.24	1.08 ± 0.02	823 ± 11	1317 ± 11	1.60 ± 0.03	494 ± 16
100–105	67	13.83 ± 0.12	1.08 ± 0.01	654 ± 5	1132 ± 8	1.73 ± 0.02	478 ± 10
200–205	75	41.57 ± 0.40	1.05 ± 0.02	1915 ± 18	1988 ± 17	1.04 ± 0.01	73 ± 25
300–305	73	10.83 ± 0.15	1.05 ± 0.02	502 ± 7	543 ± 8	1.08 ± 0.02	41 ± 11
313–318	64	20.67 ± 0.15	1.05 ± 0.01	953 ± 7	769 ± 14	0.81 ± 0.02	−184 ± 15
400–405	69	23.92 ± 0.17	1.03 ± 0.01	1084 ± 8	815 ± 9	0.75 ± 0.01	−269 ± 12
500–505	72	148.15 ± 0.61	1.00 ± 0.01	6489 ± 27	4287 ± 55	0.66 ± 0.01	−2202 ± 61
600–605	68	55.05 ± 0.38	1.02 ± 0.01	2471 ± 17	1844 ± 27	0.75 ± 0.01	−627 ± 27
665–671	67	39.49 ± 0.34	1.01 ± 0.01	1752 ± 15	1614 ± 18	0.92 ± 0.01	−138 ± 23
700–705	52	37.17 ± 0.27	1.00 ± 0.01	1634 ± 12	1407 ± 16	0.86 ± 0.01	−227 ± 19
730–735	72	30.36 ± 0.27	1.02 ± 0.01	1362 ± 12	1254 ± 20	0.92 ± 0.02	−108 ± 23
743–748	59	31.09 ± 0.29	1.02 ± 0.01	1393 ± 13	1564 ± 19	1.12 ± 0.02	171 ± 23
800–805	66	30.28 ± 0.26	1.02 ± 0.01	1356 ± 12	1298 ± 10	0.96 ± 0.01	−58 ± 15
844–848	65	29.95 ± 0.27	1.04 ± 0.01	1372 ± 12	1510 ± 10	1.10 ± 0.01	139 ± 16

* All ratios expressed as activity ratios. All isotopic data on a carbonate-free basis; all errors equal 1 sigma and are calculated by the relation $\sqrt{N}/N$ where N is the number of counts.

Th^{232} < 1 ppm at all sample depths; $^{230}Th_{xs} = {}^{230}Th - {}^{234}U$.

TABLE III

Chemical compositions of some deep-sea sediments and carbonatites*

	1	2	3	4
Si	6.7 —11.7	22 —27	4.81	< 0.05
Ti	0.03— 0.15	0.34— 0.75	0.44	—
Al	0.3 — 3.9	7.7 —10.5	1.74	< 0.05
Fe	9.9 —28	4.1 — 5.6	5.22	0.42
Mn	3.1 —11	0.30— 0.58	0.53	0.37
P	0.5 — 1.8	0.06— 0.07	0.91	—
Ba	0.4 — 2.7	0.04— 0.10	0.36	1.2
Al'	0.8 —23	60 —66	23.2	0.6
Fe'	59 —72	31 —37	69.7	53
Mn'	18 —27	2 — 5	7.1	—
P'	3.1 — 4.6	~ 0.4	12.2	—
Ba'	1.1 —16	0.07—0.7	4.8	150

* Compositional variations in deep-sea sediments (columns 1 and 2) and carbonatites (columns 3 and 4). All concentrations of sediments given in % of the carbonate- and salt-free fraction. The expressions Al', Fe', etc., represent Al/Σ, Fe/Σ etc., where Σ = (Al + Fe + Mn), using concentrations expressed in %.

1 = ranges in concentrations of sediments from the East Pacific Rise at 5—15°S and 100—115°W; based on 12 cores, some up to 8.5 m long (data after Boström, 1973).

2 = ranges in concentrations in surface sediments from the Northwest Pacific (north of 10°N, west of 165°W), based on 12 sediment cores; many of which were analyzed in detail. Similar values are found in almost all of the open North Pacific north of 7°N (data after Bostrom, 1973).

3 = average composition of carbonatites based on 96—164 analyses and adjusted to 100%. Many carbonatites are considerably poorer in Si and Al and richer in Fe, Mn, Ba and P (Heinrich, 1966).

4 = composition of carbonate lava from Oldoinyo Lengai, Tanganyika. These values agree well with those reported by Dawson (1966) and Poole (1963).

Rise (e.g., Bender et al., 1971) suggests that our core has had an interesting history with respect to U and perhaps other elements as well. A number of points stand out in particular:

(1) Although the entire core has a very high U content, the 500-cm layer contains an exceptionally high U value of approximately 150 ppm on a carbonate free basis. To our knowledge this is the highest U value found for any deep-sea sediment, including other sediments on the East Pacific Rise and the Red Sea geothermal deposits, which are all thought to result from hydrothermal activity and which have high U contents compared to other pelagic sediments.

(2) The ^{232}Th content of our core is essentially insignificant, being less than 1 ppm at all depths sampled. Low ^{232}Th contents have been found in East Pacific Rise sediments and in the Red Sea geothermal deposits, but not as low as the values we find for this core.

(3) The top 350 cm of the core has $^{230}Th_{xs}$ values which define a sedimentation rate that disagrees with other estimates of the sedimentation

* All ratios expressed as activity ratios. All isotopic data on a carbonate-free basis; all errors equal 1 sigma and are calculated by the relation $\sqrt{N}/N$ where N is the number of counts.
Th^{232} < 1 ppm at all sample depths; $^{230}Th_{xs} = {}^{230}Th - {}^{234}U$.

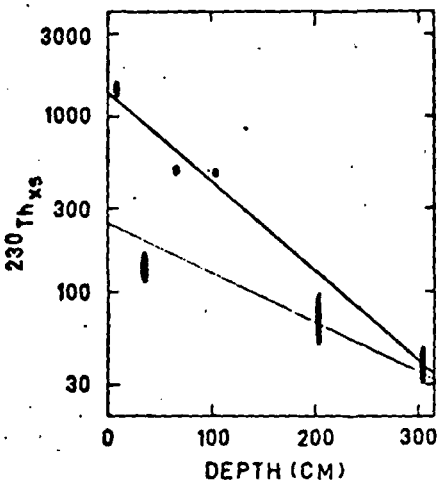

Fig.2. Plot of $^{230}Th_{xs}$ versus depth in the core GS 7202-35. As in Table II, from which the data is obtained, $^{230}Th_{xs}$ is defined as the difference in activity between ^{230}Th and ^{234}U.

Coarse upper line corresponds to best fit by some "good" points (that is, those which are characterized by small errors and by relatively low U concentrations, and hence are less likely to be disturbed by postdepositional injections). The expression for this regression line is:

$$\log {}^{230}Th_{xs} = 3.13 - 0.00503D$$

where D is the core depth in cm.

The thin, lower, line has a slope that gives an age of 350,000 years B.P. for the 500 cm depth; the expression for this line is:

$$\log {}^{230}Th_{xs} = 2.22 - 0.00194D$$

Although these data points in general are "poor" by above-mentioned criteria, they do, nevertheless, harmonize better with other age indicators, see text.

rate, both by paleontologic and paleomagnetic methods (Boström et al., 1974).

These observations and other known data on this core and its geological setting are difficult to reconcile with each other. We will first discuss to what extent postdepositional injections of U-rich solutions can reconcile these isotope patterns with other known facts, and then discuss how well "ordinary" sedimentation and slumping processes can explain the origin of these sediments and their U—Th isotope relations.

The post depositional injection hypothesis

We will here discuss the U—Th data in detail in order to learn to what extent a postdepositional injection can explain U—Th distribution in this sediment. The U content fluctuates considerably throughout the length of the core, indicating that, to a varying degree, all depths of the core may have been affected by an injection of a U-rich fluid. Particularly high U values are found at 32—37 cm, 200—205 cm, 500—505 cm, and 600—605 cm. All

these points have U concentrations exceeding 40 ppm, the highest U value being at the 500—505-cm layer (150 ppm), which also has a striking deficiency of ^{230}Th with respect to ^{234}U. This 500-cm level has been dated micropaleontologically giving an age of about 350,000 years from the extinction of *Pseudoemiliania lacunosa* (Boström et al., 1974). If the U-rich injection were concommitant with the deposition of this layer, the $^{230}Th/^{234}U$ ratio should be within a few percent of equilibrium. However, the actual value is more than 30% out of equilibrium, indicating a much later time of injection.

The time of addition of the U can be roughly estimated, using the 500-cm sample. Excluding this value, the average U content for the core is 28 ppm (CFB) which converts to 1244 DPH. If the age at 500 cm is taken to be 350,000 years, then ^{230}Th would be a few percent from equilibrium with ^{234}U. If, after this, U was introduced without Th, as seems to be the case, then ^{230}Th would have to start toward establishing a new equilibrium. The time for this start can be estimated by the relationship:

$$T = -\frac{t_{1/2}{}^{230}\mathrm{Th}}{0.693} \ln\left(1 - \frac{A^{230}\mathrm{Th}}{A^{234}\mathrm{U}}\right)$$

which, upon substitution of the "corrected values" becomes:

$$\frac{\mathrm{DPH}\ {}^{230}\mathrm{Th}_{500\,cm} - \mathrm{DPH}\ {}^{234}\mathrm{U}_{ave}}{\mathrm{DPH}\ {}^{234}\mathrm{U}_{500\,cm} - \mathrm{DPH}\ {}^{236}\mathrm{U}_{ave}} = 0.580$$

and gives an age of 94,000 years B.P. for the addition of U. The exact average in U content for an unaffected state is difficult to estimate, but probably does not vary much; using the extreme variations in reasonable averages in U content we obtain intrusion ages of between 90,000 and 110,000 years B.P. by the above mentioned method.

Additional anomalies are found deeper in the core at 743—748 cm and 844—848 cm. Here the $^{230}Th/^{234}U$ activity ratio should, according to the paleontological data, be at equilibrium; yet there is a 10% excess of ^{230}Th, suggesting that these samples have lost U while others have acquired it. As is shown by the data in Table II, the variations are statistically significant.

We, therefore, conclude that these observations can only be reconciled if it is assumed that injection of a U-rich, Th-poor solution occurred in the sediments after their deposition. This gentle injection may have represented a final phase in the hydrothermal process which produced the ridge sediments at this location.

The "ordinary" sedimentation hypothesis

A few points near the top of the core (0—312 cm) are low in U relative to the rest of the core and are not far from the values for East Pacific Rise sediments found by other workers (Ku, 1966; Bender et al., 1971; Kraemer, 1971), which show apparently good radiometric decay curves. In this interval (0—312 cm, see Fig.2), where we have positive $^{230}Th_{xs}$ values, a line can be drawn which is in reasonable agreement with a sedimentation rate of about

0.74 cm/10^3 years. It is also of interest to note that the samples in this range also contain higher $^{234}U/^{238}U$ activity ratios than the rest of the core, even approaching the seawater ratio at the top of the core. These facts could be interpreted as support for the hypothesis that these values are largely undisturbed and represent a valid sedimentation rate, the U being derived from seawater and undergoing normal radioactive decay. However, extrapolation of the line in Fig.2 gives an age of 630,000 years for the 500-cm layer and an age of more than 1.0 m.y. for the 850-cm layer at the bottom of the core. These dates conflict with the paleontological date at 500 cm of about 350,000 years, based on the *Pseudoemiliania lacunosa* extinction (S. Gartner, in Boström et al., 1974). (According to S. Gartner, personal communication, it is not likely that this age can be "stretched" further back in time than about 390,000 years ago.) Furthermore, the crustal age at this site should only be about 800,000 years according to magnetic anomaly-patterns (Herron, 1972). The situation is further complicated by the fact that the sediment cover at station GS 7202-35 probably is much thicker than 10 m, as is suggested both by the exceptionally good quality of the depth recordings and the total lack of "bottoming out" traces on the coring device.

These observations could possibly be explained if we assume that the radiometrically determined sedimentation rate for the top 300 cm of the core is largely correct, but that a decrease in the sedimentation rate occurred somewhere between 500 and 300 cm, which would explain the apparent disagreement between the extrapolated radiometric age and the paleontological and paleomagnetic age indicators.

Speculating as to why there should be a change of sedimentation rate between 500 and 300 cm, one would envision that sedimentation initially was proceeding at a prodigeous rate because of debouching hydrothermal solutions, out of which deposited copious amounts of precipitates rich in iron and manganese.

After a considerable thickness of this material was built up over the hill as well as around the orifice, a slump, perhaps caused by an earthquake, clogged the vent, thus drastically limiting the volume of solution which could egress directly into the seawater. This, in turn, built up a pressure within the vent which may have been partly relieved by migration of the solutions through the previously deposited sediments, enriching them in U, and partly may have forced the solutions to ascend through other preexisting vents and openings in the basalts into the overlying sediment blanket. These processes also caused considerable decrease in the sedimentation rate at the site in question by restricting the amount of material that could freely enter the seawater and subsequently deposit. These processes therefore explain why an injection (or several) was forced to take place. We are unable however, to explain the U—Th isotope pattern in this core by exclusively resorting to "normal" exogenic processes such as sedimentation or slumping; none of them could, in our opinion, cause the build-ups of several zones with $^{230}Th_{xs}$ at depth in the core e.g. at 743—748 and 844—848 cm.

The solutions that deposited U in this sediment (and probably also As and Hg to some extent, see Fig.1) are most likely produced by volcanic processes, but the mechanism by which these emanations originate is unknown. Seawater may descend into heated lava substratums in the sea floor and resurface elsewhere. (Elder, 1965; Boström, 1967; Corliss, 1971; Lister, 1972; Rydell and Bonatti, 1973) bringing with it material from leaching processes. However, leaching of basalt probably does not produce solutions that are sufficiently enriched in Fe, Mn, etc., to explain the Fe/Al, Mn/Al, etc., ratios observed in the sediments, since hot-water leaching of basalt does not descriminate efficiently against Al. This observation is borne out by a large number of studies in hot-spring areas in basaltic terrains (Barth, 1950; Naboko, 1963). This subject has been discussed extensively in Boström, 1973, pp.191—204).

Other possible metalliferous solutions would be chloride brines, as found in the Red Sea; however, no mid-oceanic evaporite sequences are known that would produce brines, nor are there any imprints, like Cl-amphiboles, from brines in mid-oceanic rocks (Boström, 1973). Furthermore, the U-isotope ratios and concentrations in the sediment are very different from corresponding values in coatings on submarine volcanoes (Veeh and Boström, 1971; Rydell and Bonatti, 1973). We, therefore, can only conclude that leaching of basaltic crust by seawater or brines is an unlikely source for U in the postdepositional processes described in this paper. The much higher rate of accumulation for unconsolidated sediments as compared to that of concretionary iron oxides also suggests different modes of origin (Boström et al., 1973).

Much geological and physico-chemical evidence suggests that a solution rich in carbon dioxide could bring up Fe, Mn, Ba, P, Al, Ti, etc., in the proportions observed in East Pacific Rise sediments (Boström, 1973). If this conclusion is correct, one should also expect U—Th relations to reflect such a source. In Tables III and IV it is shown that the element distribution in a carbonatitic lava is indeed very similar to what is observed in East Pacific Rise sediments. We, therefore, suspect that the ascending mineralizing solutions could have been rich in carbon dioxide, although most certainly not extreme enough in composition to warrant the term carbonatitic. This interpretation is supported by (1) the extensive carbon dioxide emission during most volcanic processes that can be expected at plate edges (Green, 1972), and (2) the fact that carbon dioxide can act as a carrier of Fe, Mn, etc., provided the CO_2 activity is sufficiently large (Puchelt, 1973; Boström, 1973). CO_2 is, furthermore, an excellent carrier of U in aqueous phases (see Fig.3).

Another explanation for this postdepositional injection of U-rich solutions may be that although the early phase of the sediment build-up was due to carbonate emanations, later phases of volcanic activity were characterized primarily by hot dilute solutions which were not necessarily very rich in Fe and Mn. However, U tends to be strongly enriched over Th in such

TABLE IV

U—Th distributions in sediments and in carbonate lava*

	1	2	3
$^{234}U/^{238}U$	1.04 (ave)	0.98	1.15
^{238}U (ppm)	35.3 (ave)	6.79	3
^{232}Th (ppm)	< 1	0.86	10

* Comparison of U and Th isotope data for core GS 7202-35 (1), for carbonate lava from Oldoinyo Lengai (2) and for Pacific pelagic sediment far from the East Pacific Rise (3). All concentrations are reported on a carbonate-free basis.

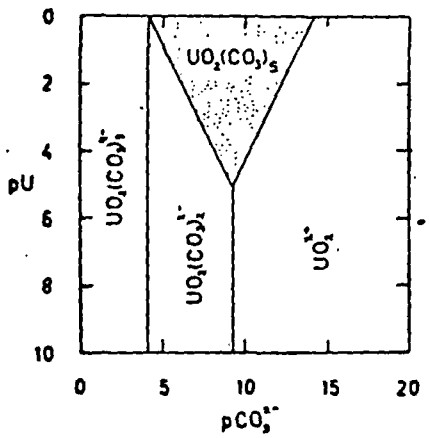

Fig.3. Stability conditions in the system CO_2—H_2O—U at 25°C and 1 atm. pressure. The operator p represents (as in the symbol pH) the negative decadic logarithm for the activities of U and CO_3^{2-}. Note that $UO_2(CO_3)$ is stable only in a very limited pU—pCO_3^{2-} interval; under other conditions U is soluble as a UO_2^{2+} complex. Sergeyeva et al. (1972) have shown that such UO_2^{2+} complexes are very soluble even at 150°C, indicating that carbonate-coupling of UO_2^{2+} may be a common mechanism to form U-rich solutions in Nature.

solutions, as is indicated by the U/Th ratios in hydrothermal deposits (Rodgers and Adams, 1969). This second explanation conforms better with traditional viewpoints on the origin of hydrothermal deposits, but introduces the complication that early and late mineralizing solutions on active ridges may be quite different. Possibly these variations are due to preferential loss of CO_2 during early stages of the volcanic process. Such processes have recently been discussed by Tugarinov and Naumov, 1972, but their applicability on the active ridge processes still must be further studied.

Physico-chemical data for U and Th and their compounds suggest that solutions over a wide range of CO_2 content can easily transport U (see Fig.3) even under highly variable temperature conditions, much more easily than Th, which is extremely insoluble except at very low pH values (Hyde, 1960; Pourbaix et al., 1963; Sergeyeva et al., 1972). Data for Th and U compounds (Sillèn and Martell, 1964; Naumov et al., 1971) furthermore show that in

addition to CO_2 (or CO_3^{2-} and HCO_3^-) also hydroxyl complexes and sulfate complexes of UO_2^{2+} are capable of transporting U in solution, whereas analogous complexes for Th are either unknown or have such unfavorable free energies of formation that they cannot easily be synthesized and studied. This very fact, however, suggests that they are incapable of forming Th-rich solutions.

The lack of crystallinity in the sediment indicates that the introducing solutions could not have been very hot; prolonged heating even at 150—200°C would probably have converted the amorphous ferric hydroxides to hematite (Boström et al., 1972), which has not been observed in this core.

The ascending solutions are seemingly not very reducing. Thus, even at depth in the sediment, the ratio Fe/Mn (Fig.1) shows very small variations, whereas reduction would have caused a large-scale redistribution of Mn upwards. This nonreducing condition could be due to mixing of reducing ascending solutions by descending oxygenated seawater, forming solutions of intermediary oxidation potentials. However, the strong redoxbuffering capacity alone of manganese and iron oxides in the sediment would quickly nullify the effect of even very reducing solutions as long as their overall reducing capacity is small, as often is the case when a dilute solution interacts with readily reacting solids (Boström, 1965).

Extent of postdepositional injections on the East Pacific Rise

It is remarkable that the foram tests are corroded to the extent they are in this core, since the coring site is located well above the carbonate compensation depth (Revelle, 1944; Bramlette, 1961; Berger, 1973). In the East Pacific such corroded foram tests have been noticed in two general areas:

(1) In sediments from the very crestal areas of the East Pacific Rise, such as in the cores Amphitrite 27 (10°33'S, 110°52'W) and Amphitrite 11 (7°28'S, 113°32'W), both at the Scripps Institution of Oceanography in La Jolla, and in core GS 7202-35 (this work).

(2) In sediments from the Bauer Deep, where extensive dissolution of $CaCO_3$ can be widely observed even at bottom depths of only about 3500—4000 m (Revelle, 1944; Bramlette, 1961; Boström and Peterson, 1969; Boström, 1973; Sayles and Bischoff, 1973). In other East Pacific Rise sediments, even those found only a few hundred kilometers from the spreading centre, corrosion of foram tests seems to be absent.

Such anomalous corrosion could be another indication of postdepositional injections of solutions into the sediments; corrosion studies of calcareous fossils may, therefore, be a fast method to map the extent of the area that possibly is affected by postdepositional injections; radiometric methods are obviously not very well suited for this task in view of the workload involved.

Other indications of postdepositional injections and rearrangements of matter in the sediments have been reported by Arrhenius (1952); thus indurations and remobilizations of the constituents Mn, P_2O_5 and SiO_2 in

the Swedish Deep-Sea Expedition core 41 (at 3°20'S, 97°53'W) were interpreted by him as evidence for rising hydrothermal solutions.

CONCLUSIONS

(1) An 8.5 m long core from the crest of the East Pacific Rise shows complex U—Th isotope distributions. The original sediment formed from rapidly egressing hydrothermal solutions.

(2) After the formation of an extensive sediment cover postdepositional injections of ascending U-rich, Th-poor solutions took place in the sediments. The main part of the sediment at 500 cm was deposited at about 350,000 years B.P., whereas an injection at that level occurred about 90,000—110,000 years ago. Probably the injection episode was forced by slumps that clogged the main orifice for the hydrothermal solutions, which therefore were forced to seek other escape paths.

(3) The ascending solutions show similarities with carbonate emanations, that is, they are rich in U and poor in Th; they furthermore show similarities in their isotopic ratios. This suggestion is further enhanced by the distribution patterns of Fe, Mn, Si, Al, Ti, P, Ba, and REE in both carbonate emantions and in active ridge sediments. Leaching of basalt is probably an insufficient source for the high concentrations of U present in the core.

(4) Such postdepositional injection processes may have been occurring on a larger scale than earlier realized.

ACKNOWLEDGEMENT

This research was supported by the National Science Foundation, grant NSF-GX-40428.

Contribution from the Rosenstiel School of Marine and Atmospheric Science, University of Miami, Miami, Florida, U.S.A.

REFERENCES

Arrhenius, G., 1952. Sediments from the East Pacific. Reports of the Swedish Deep-Sea Expedition 1947—1948, V. Göteborgs Kungl. Vetenskap-Vitterhetssamhälle, Gothenburg, 227 pp.

Barth, T. F. W., 1950. Volcanic geology, hot springs and geysers of Iceland. Carnegie Inst. Wash. Publ., No. 587.

Bender, M., Broecker, M., Gornitz, V., Middle, U., Kay, R., Sun, S. S. and Biscay, P., 1971. Geochemistry of three cores form the East Pacific Rise. Earth Planet. Sci. Lett., 12: 425—433.

Berger, W., 1973. Plate stratigraphy, oceanic fertility and the paleobathymetry of Deep Sea carbonate. Abstract of paper given at European Geophys. Soc. Meet., Zurich, 1973. Sedimentology (in press).

Bernat, M. and Goldberg, E. D., 1969. Thorium isotopes in the marine environment. Earth Planet. Sci. Lett., 5: 308—312.

Bonatti, E., Fisher, D. E., Joensuu, O. and Rydell, H. S., 1971. Postdepositional mobility of some transition elements, phosphorus, uranium and thorium in deep-sea sediments. Geochim. Cosmochim. Acta, 35: 189—201.

Bonatti, E., Fisher, D. E., Joensuu, O., Rydell, H. and Beyth, M., 1972. Iron—manganese—barium deposit from the Northern Afar rift (Ethiopia). Econ. Geol., 67: 717—730.
Boström, K., 1965. Some aspects of the analysis of mineral forming conditions. Arkiv Min. Geol., 3: 545—572.
Boström, K., 1967. The problem of excess manganese in pelagic sediments. In: P. H. Abelson (Editor), Researches in Geochemistry, 2. John Wiley and Sons, New York, N. Y., pp. 421—452.
Boström, K., 1970. Submarine volcanism as a source for iron. Earth Planet. Sci. Lett., 9: 348—354.
Boström, K., 1973. The origin and fate of ferromanganoan active ridge sediments. Acta Univ. Stockholmiensis, 27: 149—243.
Boström, K. and Peterson, M. N. A., 1969. Origin of aluminium-poor ferro-manganoan sediments in areas of high heat-flow on the East Pacific Rise. Mar. Geol., 7: 427—447.
Boström, K., Joensuu, O., Valdes, S. and Riera, M., 1972. Geochemical history of South Atlantic Ocean sediments since late Cretaceous. Mar. Geol., 12: 85—121.
Boström, K., Kraemer, T. and Gartner, S., 1973. Provenance and accumulation rates of opaline silica, Al, Ti, Fe, Mn, Cu, Ni, and Co in Pacific pelagic sediments. Chem. Geol., 11: 123—148.
Boström, K., Joensuu, O., Kraemer, T., Rydell, H., Valdes, S., Gartner, S. and Taylor, G., 1974. New finds of exhalative deposits on the East Pacific Rise. Geol. Fören. Stockh. Förhandl. (in press).
Bramlette, M. N., 1961. Pelagic sediments. In: M. Sears (Editor), Oceanography. Am. Assoc. Adv. Sci., Washington, D. C., pp. 345—366.
Corliss, J. B., 1971. The origin of metal-bearing submarine hydrothermal solutions. J. Geophys. Res., 76: 8128—8138.
Dawson, J. B., 1966. Oldoinyo Lengai-an active volcano with sodium carbonatite lava flows. In: O. F. Tuttle and J. Gittins (Editors), Carbonatites. Interscience Publishers, New York, N.Y., pp. 155—168.
Elder, J. W., 1965. Physical processes in geothermal areas. In: H. K. Lee (Editor), Terrestrial heat flow. American Geophysical Union Monograph Series No.8. Washington, D.C., pp. 211—239.
Fisher, D. E., 1973. The effect of oceanic weathering on U concentrations in deep-sea basalts (manuscript in preparation).
Green, H. W., 1972. A CO_2-charged asthenosphere. Nature Phys. Sci., 238: 2—5.
Heinrich, E. Wm., 1966. The Geology of Carbonatites. Rand McNally and Co., Chicago, Ill.
Herron, E. M., 1972. Sea-floor spreading and Cenozoic history of the East Central Pacific. Geol. Soc. Am. Bull., 83: 1671—1692.
Hyde, E., 1960. Radiochemistry of Thorium. National Academy of Sciences, National Research Council, Nuclear Science Series.
Kraemer, T. F., 1971. Rates of Accumulation of Iron, Manganese, and Certain Trace Elements on the East Pacific Rise. M.S. Thesis, Florida State Univ., Tallahassee, Fla., 94 pp.
Ku, T-L., 1966. Uranium Series Disequilibrium in Deep-Sea Sediments. Ph.D. Thesis, Columbia University, N.Y., 157 pp.
Lister, C. R. B., 1972. On the thermal balance of a mid-oceanic ridge. Geophys. J. R. Astron. Soc., 26: 515—535.
Naboko, S. I., 1953. Gidrotermalnyi metamorfizm porod u vulkanitjeskikh oblastjakh. Izd Adad. Nauk, Moscow.
Naumov, G. B., Ryzhenko, B. N. and Khodakovskiy, I. L., 1971. Spravochnik termodinamiches kich velichin. Atomizdet, Moscow.
Poole, J. H. J., 1963. Radioactivity of sodium carbonate lava from Oldoinyo Lengai, Tanganyika. Nature, 198: 1291.
Pourbaix, M., Zoubov, N. and Muylder, T. V., 1963. Atlas d'Equilibres electrochimiques. Gauthier-Villars, Cie, Paris.

Puchelt, N., 1973. Recent iron sediment formation at the Kameni islands, Santorini (Greece). In: G. C. Amstutz and A. J. Bernal (Editors), Ores in Sediments. Springer Verlag, Berlin, pp. 227—245.
Revelle, R. R., 1944. Marine bottom samples collected in the Pacific by the Carnegie on its seventh cruise. Carnegie Inst. Wash. Publ., No. 556.
Rodgers, J. J. and Adams, J. A. S., 1969. Thorium. In: K. H. Wedepohl (Editor), Handbook of Geochemistry, II-1. Springer Verlag, Berlin, chapter 90.
Rydell, H. S. and Bonatti, E., 1973. Uranium in submarine metalliferous deposits. Geochim. Cosmochim. Acta, 37: 2557—2565.
Sayles, F. L. and Bischoff, J. L., 1973. Ferromanganoan sediments in the Equatorial East Pacific. Earth Planet. Sci. Lett., 19: 330—336.
Scott, M. R., Osmond, J. K. and Cochran, J. K., 1972. Sedimentation rates and sediment history in the South Indian Basin. In: D. E. Hayes (Editor), Antarctic Oceanology, II. The Australian—New Zealand sector — Antarctic Res. Ser., No. 19.
Sergeyeva, E. I., Nikitin, A. A., Khodakovskiy, I. L. and Naumov, G. B., 1972. Experimental investigation of equilibria in the system (UO_3—CO_2—H_2) in the temperature interval 25—200° C. Geochem. Int., 9 (6): 900—910. (Transl. from Geochimia, No. 11, 1972.)
Sillèn, L. G. and Martell, A. E., 1964. Stability Constants of Metal-Ion complexes. The Chemical Society, London.
Tugarinov, A. I. and Naumov, V. B., 1972. Physicochemical parameters of hydrothermal mineral formation. Geochem. Int., 9 (2): 161—167.
Veeh, H. H. and Bostrom, K., 1971. Anomalous $^{234}U/^{238}U$ on the East Pacific Rise. Earth Plan. Sci. Lett., 10: 372—374.

...veries at Great Bear Lake, Northwest ...ritories: Canada Dept. Mines, Mines ...ach, Invest. Min. Res. and Min. Ind., no. ... p. 55–92

... J. H., and Williams, G. A., 1954, Strati...phic relations of the Triassic Shinarump ...lomerate and a prominent sandstone unit ...the Chinle formation in southeastern Utah ...stract): Geol. Soc. America Bull., v. 65, p. ...

... L. R., Stern, T. W., and Milkey, R. G., 1953, ...reliminary determination of the age of some ...anium ores of the Colorado Plateau by the ...Uranium method: U. S. Geol. Survey ...c. 271, 19 p.

... L. R., Stern, T. W., and Milkey, R. G., ...54, Nuclear geology: N. Y., John Wiley & ...ons, Inc., 264 p.

... L. R., Stern, T. W., and Sherwood, A. M., ...956, Coffinite, a uranous silicate with hydroxyl ...substitution: a new mineral: Am. Mineralogist, ...41, p. 675–688

...chi, T., and Nambu, M., 1956, On the ...genesis of chalcopyrite lattice in bornite: ...Tohaku Univ., Japan, Sci. Rep. Research ...Inst., A, v. 8, p. 31–44

...pson, M. E., Ingram, B., and Gross, E. B., ...1956, Abernathyite, a new uranium mineral of ...the metatorbernite group: Am. Mineralogist, ...v. 41, p. 82–103

...pson, M. E., Roach, C., and Braddock, W., ...1956, New occurrences of native selenium: ...Am. Mineralogist, v. 41, p. 156–157

...telot, H. A., 1952, Reconnaissance for uranif...erous rocks in northeastern Wind River basin, ...Wyoming: U. S. Geol. Survey TEM-445, 14 p.

...s, A. F., Jr., Chew, R. T., 3d, and Lovering, ...T. G., 1955, Mineralogy of the uranium deposit ...at the Happy Jack mine, White Canyon dis...trict, San Juan County, Utah: U. S. Geol. Survey TEI-514, 48 p.

Vickers, R. C., 1953, An occurrence of autunite, Lawrence County, South Dakota: U. S. Geol. Survey Circ. 286, 5 p.

Vine, J. D., and Prichard, G. E., 1956, Geology and uranium occurrences in the Miller Hill area, Carbon County, Wyoming: U. S. Geol. Survey TEI-227, 77 p.

Warren, C. H., 1903, Native arsenic from Arizona: Am. Jour. Sci., 4th ser., v. 16, p. 337–339

Waters, A. C., and Granger, H. C., 1953, Volcanic debris in uraniferous sandstones and its possible bearing on the origin and precipitation of uranium: U. S. Geol. Survey Circ. 224, 26 p.

Weeks, A. D., Coleman, R. G., and Thompson, M. E., 1956, Summary of the mineralogy of the Colorado Plateau uranium ores: U. S. Geol. Survey TEI-583, 50 p.

Whitmore, D. R. E., Berry, L. G., and Hawley, J. E., 1946, Chrome micas: Am. Mineralogist, v. 31, p. 1–21

Willard, M. E., and Proctor, P. D., 1946, White Horse alunite deposit, Marysvale, Utah: Econ. Geology, v. 41, p. 619–643

Williams, H., 1936, Pliocene volcanoes of the Navajo-Hopi country: Geol. Soc. America Bull., v. 47, p. 111–172

Wright, R. J., 1955, Ore controls in sandstone uranium deposits of the Colorado Plateau: Econ. Geology, v. 50, p. 135–155

Wyant, D. G., 1952, Lost Creek (Wamsutter) schroeckingerite deposit, Sweetwater County, Wyoming: U. S. Geol. Survey TEM-10B, 9 p.

Yoder, H. S., Jr., and Eugster, H. P., 1955, Synthetic and natural muscovites: Geochimica and Cosmichimica Acta, v. 8, nos. 5/6, p. 225–280

Department of Geology, Columbia University, New York, N. Y.

Manuscript Received by the Secretary of the Society, May 2, 1958

PROGRESS REPORT ON THE CHEMICAL ENVIRONMENT OF PITCHBLENDE

by
Leo J. Miller and Paul F. Kerr

ABSTRACT

Several reactions which are described involve the reduction of uranyl ions in acidic solutions to pitchblende. A similarity exists between the texture of synthetic and natural pitchblende. The synthetic pitchblende consists of fibers which apparently radiate from a common center. There is an indication that the crystallite size of the synthetic pitchblende becomes larger at higher temperatures. Oxidized synthetic pitchblende has a smaller lattice constant than the unoxidized material.

INTRODUCTION

The purpose of this report is to review research on the synthesis of pitchblende in the Mineralogical Laboratory of Columbia University from October 1, 1953 to April 1, 1954. The work to date covers the initial stages of a much broader investigation, the objectives of which are threefold: (1) to investigate the solutions in which uranium ions capable of precipitating pitchblende may exist, (2) to define the chemical environment in which pitchblende will precipitate, and (3) to study the correlation between the crystallinity and mode of aggregation of synthetic and natural pitchblende. This paper deals with initial experiments concerning the chemical environment in which pitchblende will precipitate from acid solution.

A REVIEW OF THE LITERATURE

Between 1824 and 1927 ten chemists had successfully produced pitchblende (UO_2) in the laboratory. From 1927 until the Second World War little experimentation was completed on the chemistry of uranium oxides. During and after the war a tremendous quantity of literature was published concerning UO_2. Little of this work has a direct bearing on the synthesis of pitchblende from solution, but

deals with the dry fusion of salts of uranium to produce UO_2, UO_3 and U_3O_8.

Arfvedson (1824) obtained UO_2 by reduction of KUO_2Cl_3 with dry hydrogen. Ebelman (1824) claimed to have precipitated pure cubic crystals of UO_2 from $NaUO_4$. Peligot (1824) ignited uranyl salts to obtain U_3O_8. Wöhler (1942) treated a solution of $(NH_4)_2\ UO_4$ with HCl and an excess of NH_3Cl and after evaporation, fusing and leaching obtained UO_2. Kessler (1857) dissolved UO_2 with HNO_3 and reprecipitated it with H_2S at a temperature of 30° C. Zimmermann (1880) precipitated uranium from solution by using either $(NH)_2S$ or NH_4OH at 100° C. Hillebrand (1893) confirmed Wöhler's experiment of 1842. Oechsner de Connich (1908) produced UO_2 from $UO_3 \cdot H_2O$ by reduction with hydrogen at a low red heat. Biltz and Muller (1927) prepared UO_3 from $UO_4 \cdot xH_2O$. Katz and Rabinowitch (1951) summarized the precipitation of UO_2 by stating: "Uranyl salts can give UO_2 either by straight thermal decomposition, e.g.,

$$UO_2Br_2 \xrightarrow{\text{heat}} UO_2 + Br_2$$

or by reduction, e.g.,

$$UO_2Cl_2 + H_2 \longrightarrow UO_2 + 2HCl."$$

Gruner (1952) demonstrated that pitchblende would precipitate from acid uranyl solutions from 50° C to 215° C by using either H_2S or organic reagents. Lang (1953) published an annotated bibliography on the solid-state reactions of the uranium oxides.

EXPERIMENTAL PROCEDURE

Uranyl sulfate solutions saturated with a reductant are sealed below a reducing atmosphere within thick walled pyrex tubes and heated to a desired temperature within galvanized iron bombs. The pressure of these experiments is the vapor pressure of the liquid and the pressure of the gas. A high pressure reaction vessel has been tested and is now being assembled for future syntheses of pitchblende. In this equipment variables of temperature, pressure and concentration can be carefully controlled.

Hydrogen ion concentration measurements are determined by a Leeds and Northrup pH meter. Additional electrodes for the measurement of oxidation-reduction potentials are being calibrated for future use on experiments.

Quantitative analysis of solutions for uranium is a difficult and time consuming operation. Fortunately a Cary spectrophotometer is available which can be used for rapid quantitative uranium analysis. The initial calibration curves of UO_2^{++}, U^{+4} and $UO_2Fe(CN)_6^{--}$ have followed Beer's law and indicate an accuracy of 1% (Tschernichow and Guldina, 1934; Scott and Dixon, 1945).

The precipitate from pitchblende experiments is analyzed by a Phillips X-ray diffractometer. Data obtained with this instrument may be used to calculate the lattice constant, crystallite size and particle orientation. The particle size and form of the precipitate may be further examined under an electron microscope.

CHEMISTRY OF THE REACTIONS

The experiments to date have been performed in acid solutions in which the very stable uranyl ion, UO_2^{++} has been the chief constituent. It has the properties of a doubly charged, large metallic ion. The trioxides of the actinide group of elements, of which uranium is a member, have a tendency to form complicated polyacids. However, due to the formation of the uranyl ion in acid solutions, and the slight solubility of the diuranates in general, this tendency is partially repressed. The uranyl ion, UO_2^{++}, forms a significant couple in acid solution with the U^{+4} ion according to the equation (Latimer, 1952)

$$(1)\quad UO_2^{++} + 4H^+ + 2e^- = U^{+4} + 2H_2O, \quad E^o = 0.334$$

Given sufficient time the U^{+4} ion precipitates as pitchblende, UO_2, so the essential reaction is

$$(2)\quad UO_2^{++} + 2e = UO_2 \text{ (pitchblende)}, \quad E^o = 0.334$$

Confirming Gruner's work of 1952, pitchblende has been precipitated from uranyl sulfate solutions by the use of hydrogen sulfide gas at temperatures between 50°C and 233°C with estimated pressures from 0.1 to 29 atmospheres (Exp. 1 through 15). It has been found that a catalyst is not necessary and the reaction is essentially (see Exp. 1, 2, 3):

$$(3)\quad H_2S + UO_2^{++} + 4H^+ = S + UO_2 + 2H_2O, \quad E^o = 0.193$$

An experiment was designed to see if the oxidation of the sulfide ion to sulfur was the only source of electrons in the reaction (Exp. 8). It is thought that the sulfide ion could be oxidized to the sulfate ion

thus giving up 8 electrons. The experiment designed to test this hypothesis failed. Another experiment is now being attempted.

Pitchblende was also precipitated from uranyl sulfate solutions containing sodium sulfide (Exp. 11). This reaction is similar to equation (3) since Na_2S hydrolyses in water to form H_2S.

Sulfur dioxide readily reduces the uranyl ion according to the general equation (Exp. 15):

$$(4)\quad UO_2^{++} + SO_2 + 2H_2O = UO_2 + H_2SO_4 + 2H^+$$

Unlike equation (3) E^o has not been measured. Sulfur is not precipitated in this reaction since sulfur goes from a +4 to a +6 polar charge.

Ferrous sulfate failed to reduce the uranyl ion (Exp. 2). Theoretically the ferrous ion should precipitate pitchblende due to the relatively high potential difference of the reaction in comparison with the H^+, H_2 electrode. The equation is:

$$(5)\quad UO_2^{++} + 2Fe^{++} + 4H^+ = U^{+4} + 2Fe^{+3} + 2H_2O, \quad E^o = 0.436$$

This reaction will be investigated in future experiments.

THE PITCHBLENDE PRECIPITATE

In certain experiments pitchblende formed at the interface between the liquid and the gas as sheets of hemispherical globules (Plate 5). The sheets had a downward bend due to the curvature of the meniscus. Globules were attached to the underside of the sheet with the convex surface facing down. This botryoidal texture is similar to the texture of the pitchblende at the Eldorado mine, Great Bear Lake, Canada (Kidd and Haycock, 1935). The globules range in size from 50 microns in diameter precipitated at 190° C (Exp. 3) to 9 microns precipitated at 135° C. They are internally banded with two shades of gray. The authors have observed this same banding in pitchblende specimens from deposits of the Front Range and Great Bear Lake. Further investigation may shed some light on the different types of pitchblende Kidd and Haycock report from the latter uranium district.

The globules of pitchblende when viewed beneath the electron microscope have a fibrous structure (Sciacca, Part II of this Report). The size of the fibers varies with the amount of crushing in the sample preparation. Also, they may vary in size due to a difference in temper-

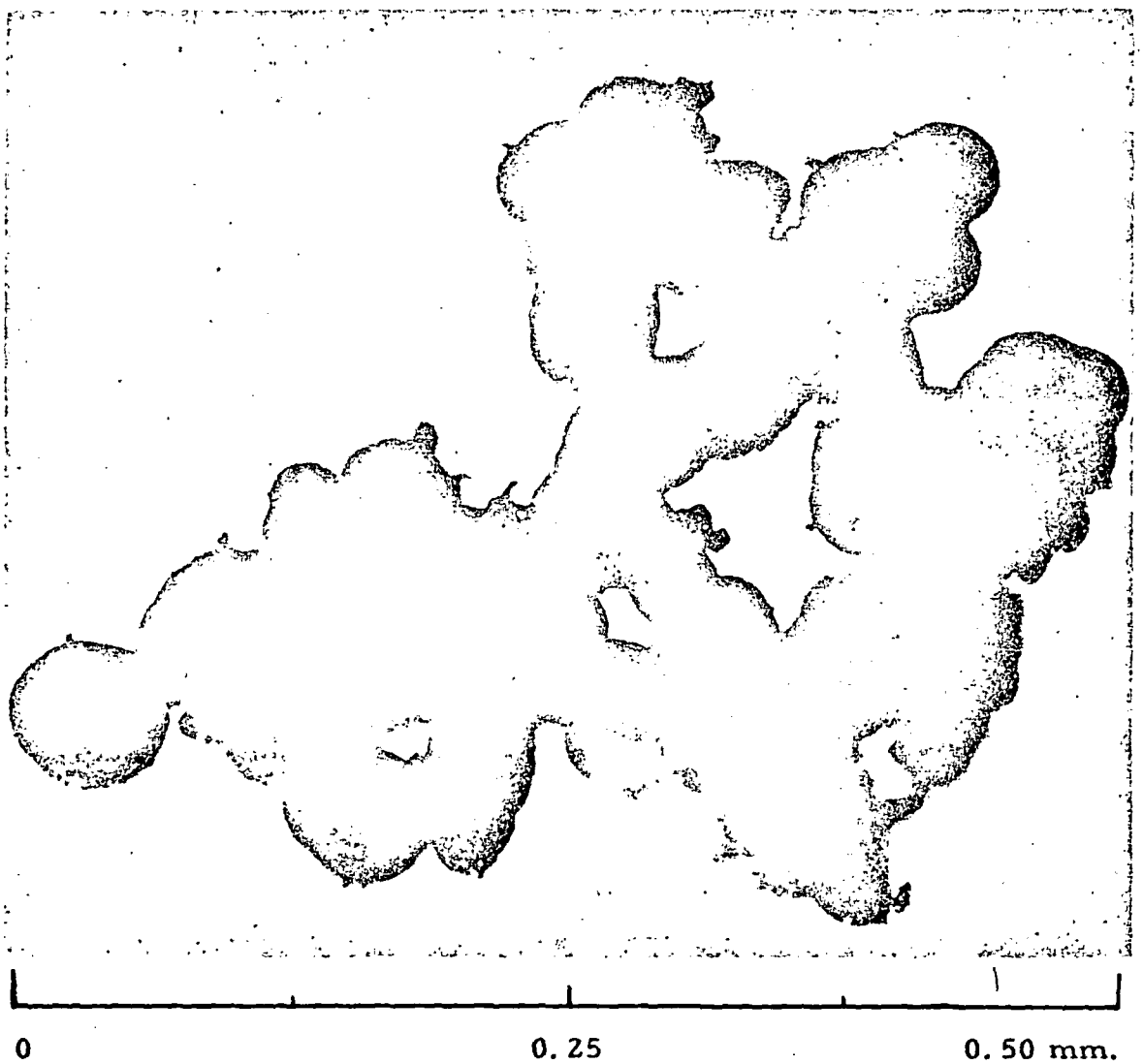

Photomicrograph of synthetic, botryoidal pitchblende precipitated at 190° C.

Plate 5

ature of precipitation but this remains to be proven. One of the larger fibers measured is over 4 microns long and 1/2 a micron wide. A suitable hypothesis for particle orientation would be that the fibers are arranged in a radial pattern in respect to the center of the hemispherical globule. The radius of many of the smaller hemispheres is 4 microns which is in agreement with the above measured fiber lengths.

The X-ray data are discussed more fully in Part II of this Annual Report by William Croft. At this point it will suffice to describe a few general correlations between structure, size and environment of precipitation.

The lattice constant, 5.467 Å ± 0.002 Å, of the synthetic pitchblende is remarkably large. This is probably due to the purity of the material and temperature of precipitation (Exp. 1). The above pitchblende was precipitated at 215° C while at lower temperatures the lattice constant is near 5.461 Å ± 8 Å (Exp. 1, 5).

One of the most significant changes is the variation in crystallite size with temperature. The size ranges from 100 Å at 135° C to 500 Å at 215° C (Exp. 1, 5). As more experimental data are accumulated a correlation between crystallite size and temperature of precipitation may be realized.

Synthetic pitchblende formed at 233°C under oxidizing conditions has a smaller lattice constant but the same crystallite size as pitchblende formed at 215°C under reducing conditions (Exp. 1, 8). Assuming that the small temperature difference is unimportant, oxidation is probably the reason for the small lattice constant of oxidized natural pitchblende (Cohen, Part II of this Report).

INTERPRETATION OF RESULTS

It has been demonstrated by Gruner (1953) and confirmed in this report that pitchblende is readily precipitated by hydrogen sulfide. Many field geologists have indicated the association of organic matter with pitchblende (Gruner et al, 1953; Miller, 1953). It is evident that one possible mechanism for the concentration of pitchblende in nature is the contact of acid solutions of uranyl ions with decaying or decayed organic matter. The temperature of the solutions is important only in the sense of speeding up the reaction and shifting the equilibrium of equation (3) to the right.

Bain (1953) felt that many Colorado Plateau pitchblende deposits were formed by processes of secondary enrichment. Near the outcrop pitchblende has a high $\frac{UO_3}{UO_2}$ ratio and in this condition is more susceptible to leaching by acid ground waters (Phair and Levine, 1953). If these waters migrate into an environment of hydrogen sulfide such as might be present in petroliferous regions (Gruner, 1952) pitchblende will precipitate and given sufficient time may form a rich "secondary" ore deposit.

The experiments have demonstrated that sulfur dioxide will precipitate pitchblende. That sulfur dioxide is a common gas in volcanic and hot spring areas has been demonstrated by several geologists (Graton, 1945). It is possible, therefore, that uranyl solutions mixing with SO_2 can be one mechanism for the emplacement of hydrothermal vein pitchblende such as is present in the Marysvale district (Kerr et al, 1953).

REFERENCES

Arfvedson, J. A. (1824) Contribution toward a closer knowledge of uranium, Annalen der Physik et de Chemie (Poggendorf), 1, p. 245.

Bain, G. W. (1953) Experimental simulation of Plateau type uranium deposits, A. E. C. report RMO-44, p. 45.

Biltz, W. and Muller, H. (1927) On uranium oxide XLI of systematic affinity principles, Z. anorg-allgem-chem., 163, p. 257.

Ebelman, J. J. (1842) Research on several compounds of uranium, Annalen de Chemie, 43, p. 286.

Graton, L. C. (1945) Conjecture regarding volcanic heat, Am. Jour. Sci., 243A, p. 190.

Gruner, J. W. (1952) New data of syntheses of uranium minerals, A. E. C. Annual Report, June 1952, RMO-983, Part I.

———— ; Gardiner, L. and Smith, D. K., Jr. (1953) A. E. C. Annual Report, RME-3044.

Hillebrand, W. F. (1893) The preparation and specific gravity of crystallized uranium dioxide, U. S. G. S. Bull. 113, p. 37.

Katz, J. J. and Rabinowitch, E. (1951) The Chemistry of Uranium, McGraw Hill Book Co., Inc., New York, 609 pp.

Kerr, P. F.; Hamilton, P. K.; Brophy, Gerald P.; Simpson, W. L.; Cohen, William; Dahl, Harry; and Green, Jack (1953) A. E. C. Annual Report RME-3046.

Kessler, L. (1857) Procedure for the preparation and analysis of uranium oxide, Jour. of Pharm. Chim., 31, p. 182.

Kidd, D. F. and Haycock, M. H. (1935) Mineragraphy of the ores of Great Bear Lake, Geol. Soc. Am., Bull. 46, pp. 901-903.

Lang, S. M. (1953) An annotated bibliography of selected references on the solid-state reactions of the uranium oxides, Nat. Bur. Stds. circular 535, pp. 1-95.

Latimer, W. M. (1952) Oxidation Potentials, Prentice Hall, Inc., New York, pp. 300-304, 2nd Ed.

Miller, L. J. (1953) Uranium ore controls of the Happy Jack mine, White Canyon, San Juan Co., Utah, being published as A. E. C. RMO.

Oechsner de Connich, F. W. (1908) Uranium compounds, Bull. de la Classe des Sciences, Acad. Royale de Belgique, 992.

Peligot, E. (1842) Research on uranium, Annalen de Chemie, 43, p. 255.

Phair, G. and Levine, H. (1953) Notes on the differential leaching of uranium, radium and lead from pitchblende in H_2SO_4 solutions, Jour. Econ. Geol., 48, no. 5, pp. 358-369.

Scott, T. R. and Dixon, P. (1945) A colorimetric method for the determination of uranium in leach liquors, Analyst, 70, p. 462.

Tschernichow, J. and Guldina, E. (1934) Colorimetric determination of uranium in uranium ores, Zeit. für Anal. Chem., 96, p. 257.

von Wöhler, F. (1842) Preparation of uranium, Annalen de Chemie, 41, p. 345.

Zimmerman, J. L. C. (1880) On the decomposition and transformation product of uranyl sulfide, Annalen de Chemie, 204, p. 204.

APPENDIX C

Laboratory Experiments in the Synthesis of Pitchblende

X-ray data are absent in several of the following tables because insufficient pitchblende precipitated during the experiment for complete analysis. Experiments 4, 7, 9, 10, 13 and 14 are not included since they either do not add any new concepts to the report or they are still in progress.

EXPERIMENT #1

Conducted 12/8/53

Purpose

The experiment was designed to make synthetic pitchblende following Gruner (1952). The purpose was also to investigate the product produced and interpret the conditions of formation in terms of natural occurrence.

Procedure

A concentration of 0.273 M $UO_2SO_4 \cdot 3H_2O$ and 0.043 M $FeSO_4 \cdot 7H_2O$ in 0.0372 N H_2SO_4 saturated with H_2S was heated in a sealed purex tube within an iron bomb at 215°C for 48 hours and allowed to cool.

Results

Pitchblende separated out into a dual precipitate; a fine brown powder below and a black crust above. Powder photographs of the brown and the black pitchblende are identical. On standing free from the liquor the brown turned black. The solution above the precipitate was not analyzed quantitatively. Qualitative analysis with potassium ferrocyanide gave a positive test for iron and a negative test for uranium was obtained using the salt of phosphorus bead. Spectrometric data gave a lattice constant near 5.467 ± .001 Å.

Analytical Data 12/30/53

Reagents	Amounts	Concentrations
$UO_2SO_4 \cdot 3H_2O$, C.P.	1.1480 gms. in 10 ml. of solution	0.273 M
$FeSO_4 \cdot 7H_2O$, Analytical	0.120 gms. in 10 ml. of solution	0.043 M
H_2S	Unknown	Saturated
H_2SO_4, C.P.	5 ml.	0.0372 N

Starting pH	Ending pH	Temp. of exp.	Pressure of exp.	Time of exp.	Precipitate	Remaining solution
1.73	acid	215°C	Estimated 21 atmospheres	48 hrs.	Pitchblende (UO_2)	(Fe, U, SO_4^{--})

EXPERIMENT #1

Spectrometer Data

hkl(α)	2 θ	I	d	lattice	Crystallite size Å
111	28.26	10.1	3.1552	5.465	532
200	32.74	5.1	2.7329	5.466	898
220	46.98	5.4	1.9327	5.466	608
311	55.73	4.7	1.6483	5.467	632
222	58.45	0.9	1.5778	5.465	798
400	68.61	0.9	1.3668	5.467	1290
331	75.79	1.6	1.2543	5.467	725
420	78.13	1.3	1.2224	5.467	454
422	87.30	1.2	1.1159	5.467	442
333 511	94.11	1.4	1.0523	5.468	545
440	105.68	0.5	.96649	5.467	483
531	112.90	1.4	.92422	5.468	406
600 442	115.40	0.8	.91125	5.468	438
620	126.00	0.9	.86447	5.468	566
533	134.98	0.7	.83377	5.467	438
622	138.28	0.7	.82428	5.467	498

Supplementary Data on File

X-ray patterns (Rm. 417 Scher.)
(1) 2 patterns of Experiment #1 UO_2

X-ray diffractometer curves (Rm. 417 Scher.)
(1) 1 curve of Experiment #1 UO_2

Electron Micrographs (Rm. 417 Scher.)
(1) 5 pictures of Experiment #1 UO_2

EXPERIMENT #2

Conducted 12/30/53

Purpose

The experiment was designed to discover if H_2S was required for the precipitation of UO_2 from a uranyl sulfate-ferrous sulfate solution.

Procedure

A concentration of 0.273 M $UO_2SO_4 \cdot 3H_2O$ and .043 M $FeSO_4 \cdot 7H_2O$ in 0.0372 N H_2SO_4 without H_2S was heated in a sealed pyrex tube within an iron bomb at 215°C for 48 hours and allowed to cool.

Results

The solution remained yellow with a flaky red precipitate at the bottom and on the walls of the tube. The red material is believed to be hematite but was not precipitated in sufficient quantity for X-ray examination. The experiment indicated that Fe^{++} in itself will not precipitate UO_2 from a uranyl sulfate solution. The experiment will be repeated at a later date to determine the nature of the red precipitate.

Analytical Data

Reagents	Amounts	Concentrations
$UO_2SO_4 \cdot 3H_2O$, C.P.	1.1480 gms. in 10 ml. of solution	0.273 M
$FeSO_4 \cdot 7H_2O$, Analytical	0.120 gms. in 10 ml. of solution	0.043 M
H_2SO_4, C.P.	5 ml.	0.0372 N

Starting pH	Ending pH	Temp. of exp.	Pressure of exp.	Time of exp.	Precipitate	Remaining solution
1.73	acid	215°C	Estimated 21 atmospheres	48 hrs.	Probably Fe_2O_3	UO_2^{++}, SO_4 Fe

EXPERIMENT #3

Conducted 1/4/54

Purpose

The experiment was designed to discover if a uranyl sulfate solution saturated with H_2S would precipitate UO_2 in the absence of Fe^{++}.

Procedure

A concentration of 0.249 M $UO_2SO_4 \cdot 3H_2O$ in 5 ml. of 0.0372 N H_2SO_4 saturated with H_2S was heated in a sealed pyrex tube within an iron bomb at 190°C for 115 hours and allowed to cool.

Results

Solids separated out into a dual precipitate; a fine brown powder below and a black crust above. Although the tube has not been open at the time of this writing it seems likely that the material is UO_2. The precipitate has the identical form of the UO_2 in Experiment #1. It appears from this experiment that Fe^{++} is not needed for the precipitation of pitchblende.

Analytical Data

Reagents	Amounts	Concentrations
$UO_2SO_4 \cdot 3H_2O$, C.P.	1.0470 gms. in 10 ml. of solution	0.249 M
H_2S	Unknown	Saturated
H_2SO_4, C.P.	5 ml.	0.0372 N

Starting pH	Ending pH	Temp. of exp.	Pressure of experiment	Time of exp.	Precipitate	Remaining solution
1.73	acid	190°C	Estimated 12 atmos.	115 hrs.	Probably UO_2	Clear

1/6/54

An examination of the synthetic pitchblende under the petrographic microscope revealed that the precipitate consists of hard black crusts made up of hemispherical globules. The hemispheres are on the order of 0.05 mm. in diameter. The internal structure appears to be banded and suggests a similarity to the botryoidal pitchblende occurrences at Great Bear Lake and in the Front Range. Attempts to polish the material for study under the reflecting microscope were unsuccessful. It is hoped that with better cementing material this technique may be used. A photomicrograph of the crust accompanies this memorandum.

EXPERIMENT #5

Conducted 1/10/54

Purpose

The experiment was designed to test the difference, if any, between pitchblende formed at 135° C and that formed at 215° C.

Procedure

A concentration of 0.249 M $UO_2SO_4 \cdot 3H_2O$ in 0.0372 N H_2SO_4 saturated with H_2S was heated for 39 hours at 135° C in a sealed pyrex tube and allowed to cool.

Results

A black precipitate of pitchblende formed on the bottom of the tube. The solution was a yellowish green indicating that the reaction had not gone to completion at the lower temperature. The X-ray diffractometer curve has not been completely measured at the time of this writing. A marked line broadening is present which indicates, since the material is pure, a smaller crystallite size. Several experiments will be run to confirm and possibly extend this observation over a wider temperature range.

Analytical Data

Reagents	Amounts	Concentrations
$UO_2SO_4 \cdot 3H_2O$, C.P.	1.0470 gms. in 10 ml. of solution	0.249 M
H_2S	Unknown	Saturated
H_2SO_4, C.P.	2 ml.	0.0372 N

Starting pH	Ending pH	Temp. of exp.	Pressure of experiment	Time of exp.	Precipitate	Remaining solution
1.73	acid	135°C	Estimated 3 atmos.	39 hrs.	Pitchblende (UO_2)	Yellow-green

Supplement to

Experiment #5

The crystallite size of the pitchblende crystallized in this experiment is on the order of 100 Angstrom units as compared to 500 Angstrom units for Experiment #1. The lattice constant is also smaller by about .007 Angstrom units. The data on crystallite size computed for various lines follows:

Spectrometer Data

hkl	2 θ	I	d	lattice	crystallite size
111	28.25	10.	3.1574	5.469	109
200	32.80	4.52	2.7281	5.456	140
220	47.00	5.14	1.9317	5.463	113
311	55.80	4.90	1.6461	5.460	121
222	58.42	0.95	1.5783	5.467	168
400	68.75	--	1.3644	5.458	--
331	76.00	1.81	1.2511	5.454	82
420	78.30	1.67	1.2200	5.456	117
422	87.52	1.79	1.1137	5.456	102
333 511	94.45	1.81	1.0494	5.453	97
440	106.00	1.61	.96445	5.456	143
531	113.27	--	.92230	5.456	--
600 442	115.6	--	.91025	--	--
620	126.5	1.06	.86294	--	101
533	135.7	--	.83192	--	--
622	139.0	--	.82232	--	--

EXPERIMENT #6

Conducted 1/30/54

Purpose

The experiment was designed to precipitate pitchblende at 50°C in sufficient quantity to calculate the crystallite size.

Procedure

A concentration of 0.2088M $UO_2SO_4 \cdot 3H_2O$ in 0.0372 N H_2SO_4 saturated with H_2S was heated in a sealed pyrex tube at 50°C for 5 days.

Results

A small amount of black material, probably pitchblende, was mixed with a small amount of a chalky brown precipitate. Neither precipitate was in sufficient quantity for a positive identification. The solution was a greenish yellow. The pH had increased 0.30 units. This experiment is at present being repeated as Experiment #9 for a longer time.

Analytical Data

Reagents	Amounts	Concentrations
$UO_2SO_4 \cdot 3H_2O$, C.P.	8.7748 gms. in 100 ml. of solution	0.2088
H_2S	Unknown	Saturated
H_2SO_4, C.P.	5 ml.	0.0372 N

Starting pH	Ending pH	Temp. of exp.	Pressure of experiment	Time of exp.	Precipitate	Remaining solution
1.73	2.03	50°C	Estimated 0.1 atmos.	5 days	Probably UO_2 and sulfur	Yellow-green

EXPERIMENT #8

Purpose

Conducted 1/29/54

The experiment was designed to determine if the HS^- and S^{--} ions were the only source of electrons in the solution for the reduction of UO_2^{++}. Theoretically the 6.10×10^{-4} moles of H_2S added should precipitate 6.10×10^{-4} moles of UO_2 according to the equation:

$$H_2S + UO_2^{++} \longrightarrow 2H^+ + S + UO_2$$

Procedure

A concentration of 0.2088 M $UO_2SO_4 \cdot 3H_2O$ in 0.0372 N H_2SO_4 saturated with H_2S was heated in a sealed pyrex tube within a micro reaction vessel at 233° C for 17-1/2 hours and allowed to cool.

Results

The bomb broke during the experiment. This breakage allowed the H_2S to escape and consequently the UO_2 precipitated in an oxidizing environment. The authenticity of the above equation will be investigated in future experiments.

The significant result, however, is that X-ray measurements show that the pitchblende which precipitated in the oxidizing atmosphere has a smaller lattice constant than pitchblende produced in a completely reducing environment by previous experiments. The oxidized pitchblende has a lattice constant close to 5.434 Å while the reduced pitchblende has a lattice constant near 5.467 Å.

Analytical Data

Reagents	Amounts	Concentrations
$UO_2SO_4 \cdot 3H_2O$, C.P.	8.7748 gms. in 100 ml. of solution	0.2088 M
H_2S	6.10×10^{-4} moles	Saturated
H_2SO_4, C.P.	5 ml.	0.0372 N

Starting pH	Ending pH	Temp. of exp.	Pressure of experiment	Time of exp.	Precipitate	Remaining solution
1.73	2.03	233° C	Estimated 29 atmos.	17-1/2 hrs.	UO_2 and sulfur	Clear positive test for U

EXPERIMENT #8

Spectrometer Data

$a = 5.434 \pm .007$

hkl	2θ	d	Lattice	Crystallite size Å
111	28.43	3.1378	5.435	516
200	32.97	2.7136	6.427	595
220	47.30	1.9201	5.430	410
311	56.09	1.6385	5.435	382
222	58.86	1.5676	5.430	
400	69.18	1.3568	5.427	
331	76.32	1.2466	5.434	
420	78.68	1.2151	5.434	
422	87.97	1.1092	5.434	
333 511	94.88	1.0457	5.433	
440	106.5	0.9619	5.441	
531	113.9	0.91946	5.439	
600 442	116.5	0.90628	5.438	
620	127.3	0.85993	5.439	
533	136.7	0.82900	5.436	
622	140.2	0.81916	5.433	

EXPERIMENT #11

Conducted 2/12/54

Purpose

The experiment was conducted to determine if Na_2S was capable of precipitating pitchblende from solution. Sodium sulfide will react with water to give one mole of hydrogen sulfide which in turn should reduce the uranyl ion to pitchblende:

$$Na_2S + 2H_2O \rightleftharpoons H_2S + 2NaOH$$

Procedure

To a solution of 0.2088 M $UO_2SO_4 \cdot 3H_2O$ was added 0.06744 M $NA_2S. 9H_2O$. This solution was heated at 205°C for three days within a sealed pyrex tube.

Results

A large amount of leaf-like pitchblende formed on the bottom of the tube. Not enough precipitate was available for a complete analysis by the X-ray spectrometer but there was an adequate supply for identification. The change in hydrogen ion concentration will be measured at a later date.

Analytical Data

Reagents	Amounts	Concentrations
$UO_2SO_4 \cdot 3A_2O$, C.P.	8.7748 gms. in 100 ml. of solution	0.2088 M
$Na_2S \cdot 9H_2O$, C.P.	0.1620 gms. in 10 ml. of solution	0.0674 M
H_2SO_4, C.P.	5 ml.	0.0372 N

Temperature of exper.	Pressure of exper.	Time of exper.	Precipitate	Solution
205° C	Estimated 14 atmos.	3 days	UO_2	Yellow U^{+6}

EXPERIMENT #15

Conducted 3/12/54

Purpose

The experiment was designed to precipitate pitchblende by reduction with SO_2. Theoretically SO_2 should be oxidized in an aqueous solution thereby releasing 2 electrons for the reduction of the UO_2^{++} ion.

$$SO_2 + 2H_2O \longrightarrow H_2SO_2 + 2H^+ + 2e$$

Procedure

A concentration of 0.4070 M $UO_2\ SO_4 \cdot 3H_2O$ saturated with SO_2 was sealed in a pyrex tube and heated at 209° C.

Results

The experiment is still in progress. A considerable amount of a black precipitate formed at the end of three days. The solution is green, which indicates that reduction has taken place and the black material is probably UO_2.

Analytical Data

Reagents	Amounts	Concentrations
$UO_2SO_4 \cdot 3H_2O$, C.P.	85.4950 gms. in 500 ml. of H_2O	0.4070 M
SO_2	Unknown	Saturated
H_2O	5 ml.	--

Starting pH	Temperature of exper.	Pressure of exper.	Time of exper.	Precipitate	Solution
1.21	209° C	Estimated 14 atmos.	Still in progress	Probably UO_2	Green U^{+4}

BULLETIN OF THE AMERICAN ASSOCIATION OF PETROLEUM GEOLOGISTS
VOL. 44, NO. 1 (JANUARY, 1960), PP. 101-106, 6 FIGS.

RELATIONSHIP BETWEEN PRESSURE AND MOISTURE CONTENT OF KAOLINITE, ILLITE, AND MONTMORILLONITE CLAYS[1]

GEORGE V. CHILINGAR[2] AND LARRY KNIGHT[3]
Los Angeles, California

ABSTRACT

High-pressure compaction studies (up to 200,000 psi) were conducted on kaolinite, illite, and montmorillonite clays and a natural organic colloid of Iranian origin, gum tragacanth. The remaining moisture content in per cent (dry weight) was plotted versus the logarithm of pressure in psi. For kaolinite clay there is a straight-line relationship between 40 and 200,000 psi ($M = 33.9 - 5.96 \log P$), and for illite clay the relationship between the moisture content (per cent) and pressure (psi) can be expressed by the formula $M = 50 - 8.7 \log P$. For montmorillonite clay, on the other hand, there is a break in the curve at about 1,000 psi, and from 1,000 to 200,000 psi the curve is a straight line: $M = 104 - 18.06 \log P$. For gum tragacanth, moisture versus pressure curve has a "hyperbolic" shape; and it appears to be harder to squeeze water out of the crystalline clays than it is from the amorphous gel at low pressures. The moisture versus pressure curves of the more plastic (higher swelling) clays have steeper slopes than those of the clays having low plasticity; however, much longer time is needed for the establishment of equilibrium in more plastic clays.

INTRODUCTION

An excellent discussion of the problem of compaction of sediments was presented recently in the articles of Weller (1959), Rubey and Hubbert (1959), and Hubbert and Rubey (1959). These papers also contain a comprehensive bibliography on the subject.

As pointed out by Rubey and Hubbert (1959, p. 174), in geology the problem involves the compaction of clays which are deposited as sediments in the geosynclinal basins; and with the progressive sedimentation the imposed loads could range from zero up to the weight of several miles of superposed sediments. The compaction of clays in response to the tectonically applied huge compressive forces is a related problem. Rubey and Hubbert (1959, p. 174) further state that "The magnitude of the stresses involved, and the degree of compaction produced, is thus in a range far beyond the limits for which laboratory data are available." The review of the Russian literature by the writer, however, revealed that some high-pressure compaction studies (up to 5,000 kg./cm.^{2}) have been made by Lomtadze (1954). It is indeed unfortunate that no description of the apparatus, techniques used, or the mineralogic type of clays used appears in his article. Thus it was impossible to evaluate his results.

In the present work, the writers studied the relationship between the moisture content (in per cent) and the applied pressure from 40 to 200,000 psi for kaolinite, illite, and montmorillonite clays. For comparison, a natural organic colloid of Iranian origin, gum tragacanth No. 11, was also studied, because of the familiarity of the writer with organic colloids (Tchillingarian, 1950).

NATURE OF HYDRATION OF GUMS AND CLAYS

The Einstein equation for the viscosity of dilute dispersions of spherical particles is:

$$\mu_s = \mu_0(1 + 2.5\phi)$$

where μ_s is the viscosity of the dispersed system, μ_0 is the viscosity of the dispersion medium, and ϕ is the ratio of the volume of dispersed phase to the volume of the sol. This equation, however, does not seem to apply to natural organic, hydrophilic colloids. It also does not apply to clays. For example, according to the results obtained by the writers a sol containing 1.2% of gum tragacanth has a viscosity of 37 centipoises, whereas according to the Einstein formula the viscosity should be only 1.03 centipoises

$$\left[\left(1 + 2.5 \times \frac{1.2}{100}\right) \times 1\right].$$

[1] Manuscript received, July 31, 1959.

[2] Associate Professor, Petroleum Engineering Department, University of Southern California.

[3] Graduate student, Petroleum Engineering Department, University of Southern California.

The help extended by H. C. Heard and D. T. Griggs in designing, building, and calibrating the apparatus was indeed invaluable in carrying the present study to completion. The writers also express sincere appreciation to the following scientists for their helpful suggestions: C. M. Beeson, K. O. Emery, R. E. Grim, W. D. Keller, W. Orr, and H. Brandt. The present research would have been impossible without the A.A.P.G. research grant-in-aid.

This discrepancy indicates that the tragacanth particles have taken up large amounts of water, thus increasing the volume of the dispersed phase. The viscosity of the sol usually increases with time, which indicates further swelling and growing of the particles. In accordance with the Einstein equation, in the foregoing case of 37 centipoises viscosity of the sol, it is necessary for the total volume of the particles of the dispersed phase to be about 1,200 times that of the dry tragacanth. It is not known with certainty whether the particles take up the water like a sponge or whether they become surrounded by thick layers of water molecules.

Similarly, a mud sample containing 27 per cent by weight of kaolinite clay had a viscosity of 3 centipoises, showing that the volume of the dispersed phase (hydrated clay) is about 7.3 times that of the dry clay. For a mud containing 2.7 per cent by weight of bentonite, the viscosity was 2.9 centipoises. This indicates that the volume of hydrated bentonite is about 28.2 times that of the volume of dry clay. In the foregoing calculations a specific gravity of 2.5 was assumed for clays. Obviously, the calculated values are not absolute.

In the opinion of Ralph E. Grim (personal communication) the water adsorbed immediately on the surfaces of the clay minerals is composed of oriented water molecules. The distance that such "oriented" water extends from the clay mineral surfaces depends on the nature of the clay mineral, the nature of the adsorbed cations, and, perhaps, on the presence of organic matter. The water present in pores at considerable distances from the surface is not oriented, or in other words it is a "liquid" water. According to Grim (personal communication), in some cases there is a gradual transition from the non-oriented water to oriented water on proceeding toward the clay mineral surface; whereas in the other cases there is a sharp transition in the character of the water. For example, Grim believes that there is a gradual transition in sodium montmorillonite and a more abrupt transition in calcium montmorillonite.

NATURE OF COMPACTION OF CLAYS

The compaction of clays possibly occurs in three stages: (1) squeezing-out of the interstitial water as the grains of clay minerals come in contact, (2) development of closer packing due to the rearrangement of grains, and (3) deformation of grains and further reduction in porosity (Weller, 1959, p. 273).

In as much as the clay particles are very small and flaky in shape, they form spongy aggregates which are easily deformed. Terzaghi and Peck (1948, p. 74) illustrate the mechanism of compaction of clay aggregates by means of a cylindrical vessel with a series of perforated plates, which are separated by springs from one another. The height of the springs between the plates is first unchanged after the application of pressure to the uppermost plate, because the escape of water through the perforations requires some time. At the beginning, therefore, the applied pressure is supported by the interstitial water. As the water escapes, however, the uppermost plate moves downward and the springs begin carrying part of the applied load. Eventually, upon the escape of sufficient water the springs attain their compaction equilibrium and all of the applied load is carried by the springs. At this time the pressure on the water is simply hydrostatic.

As shown by Rubey and Hubbert (1959, p. 173), the load S is supported by the grain-to-grain bearing strength σ of the clay aggregates together with the fluid pressure p. Thus, $\sigma = S - p$. A measure of the degree of compaction of a clay is its remaining moisture content M; and for each value of M there is a maximum value of compressive stress σ which the clay can support without further compaction, namely, $M = \phi(\sigma)$.

APPARATUS AND EXPERIMENTAL PROCEDURE

The apparatus which is shown in Figures 1 and 2 was built, tested, and calibrated by Hugh C. Heard of the Institute of Geophysics, University of California at Los Angeles. In calibrating the apparatus, the force at the top end of the upper piston was measured by a Baldwin SR-4 load having an accuracy of 0.1 per cent. Series of force measurements were taken and calculated to stresses at the piston face. Then they were compared with similar stresses at the bottom of the lower piston as calculated from the product of the gauge pressure and the ram area/piston area ratio. A 10,000 psi U. S. supergauge with an accuracy of ∓ 0.5 per cent of full-scale reading was used as a pressure gauge. The true cylinder pressure was then taken to be the mean value of these two stresses at any given gauge pressure. The friction on each piston is 6 ∓ 1 per cent of the force exerted on either piston for a $\frac{1}{2}$-inch clay sample and for cylinder pressures up to 200,000 psi.

In as much as about 2 months were spent in developing good experimental techniques, a detailed procedure for assembling and operating this apparatus is presented in an outline form.

1. In assembling the apparatus for a high-pressure experiment, the upper cap is screwed off, the cylinder is removed and all parts are thoroughly cleaned with cotton. The walls of the cylinder are then lubricated

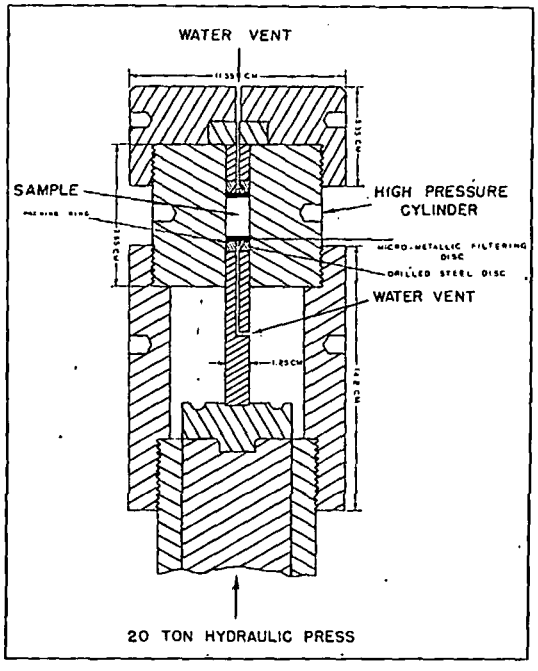

FIG. 1.—Schematic diagram of high-pressure compaction apparatus.

by putting a small amount of lubricating grease on the end of cleaning rod and using it as a swab. In case any of the lubricating compound is rubbed off while introducing clay or cotton, it should be replaced with an additional amount of compound.

2. The cylinder is then turned upside down and the cold rolled steel 45° packing ring, drilled hardened steel disc, and the lower piston are inserted into the cylinder with an aid of a cleaning rod and, if necessary, hammer.

3. Then the Braun stainless steel, micro-metallic filtering disc having an average pore size of 5 microns is introduced on top of the hardened steel disc. These filtering discs become warped upon use; therefore, if they are reused, the concave side should face the clay sample. Otherwise the filtering discs crack when subjected to pressure. A small wad of cotton (about $\frac{1}{8}$ inch in diameter) is packed down with the cleaning rod on top of the filtering disc, and a 2- or 3-cc clay sample is introduced above it. Another (a) cotton wad, (b) filtering disc, (c) ring, (d) steel disc, and (e) upper piston are placed above the clay sample in the order indicated. The cotton should not contain lubricating compound which makes it impermeable to water.

An attempt was made to use layers of sand instead of filtering discs; however, sand is crushed at pressures above and about 3,600 psi. In addition, clay has a tendency to squeeze out into the sand on application of pressure.

4. The cylinder is then placed on the bottom ram so that it pushes against the bottom piston. The cylinder is turned until it is locked in place. Subsequent to that, the cap is replaced.

5. Upon closing the jack valve, the pressure is slowly applied. In the case of plastic clays such as montmorillonite, by-passing (squeezing-out through the water vent hole) presents a problem. A considerable portion of the excess water, however, can be pressed out at low pressures (up to 500 psi) without by-passing. Thus, the subsequent increase of pressure to a desired value does not cause any squeezing-out of the clays.

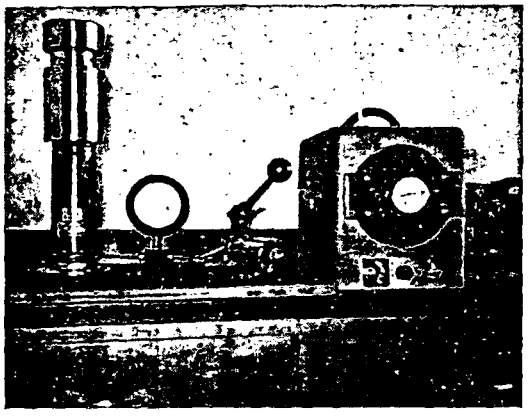

FIG. 2.—Photograph of high-pressure compaction apparatus and electric vacuum oven. Blackhawk hydraulic porto-power jack shown here was obtained from *Blackhawk Manufacturing Company, Milwaukee* Wisconsin.

6. After a certain time interval (the tests at each pressure were repeated until attainment of equilibrium) the pressure is slowly decreased by opening the jack valve slightly in order to prevent bouncing of the gauge needle. It is imperative to remove the excess water present in the water vent opening of the piston with a syringe, because this water can be sucked back into the clay sample upon the release of pressure.

7. Upon removing and weighing the sample, it is cut into small pieces and placed into an electric vacuum oven having a hydraulic thermostat which controls the temperature. The samples are then dried overnight at 100°C. Most of the samples require 6–8 hours of drying; however, in order to insure complete drying the samples are redried for 2 hours and then reweighed.

8. Both rings should be examined for wear after each run, because the worn rings cause scouring inside the cylinder.

The following clay minerals, which are described in the "Preliminary Reports of American Petroleum Institute Research Project 49: Clay-Mineral Standards," were obtained from the Ward's Natural Science Establishment, Inc., 3000 Ridge Road East, Rochester 9, New York.

a. Montmorillonite No. 25, Upton, Wyoming, John C. Lane Tract (bentonite).

b. Illite No. 35, Fithian, Illinois.

c. Kaolinite No. 4, Macon, Georgia, Oneal Pit.

Prior to testing, all clay samples were hydrated in an excess of distilled water for a period of one week.

EXPERIMENTAL RESULTS

Figure 3 shows relationship between the moisture content in per cent (dry weight) and the

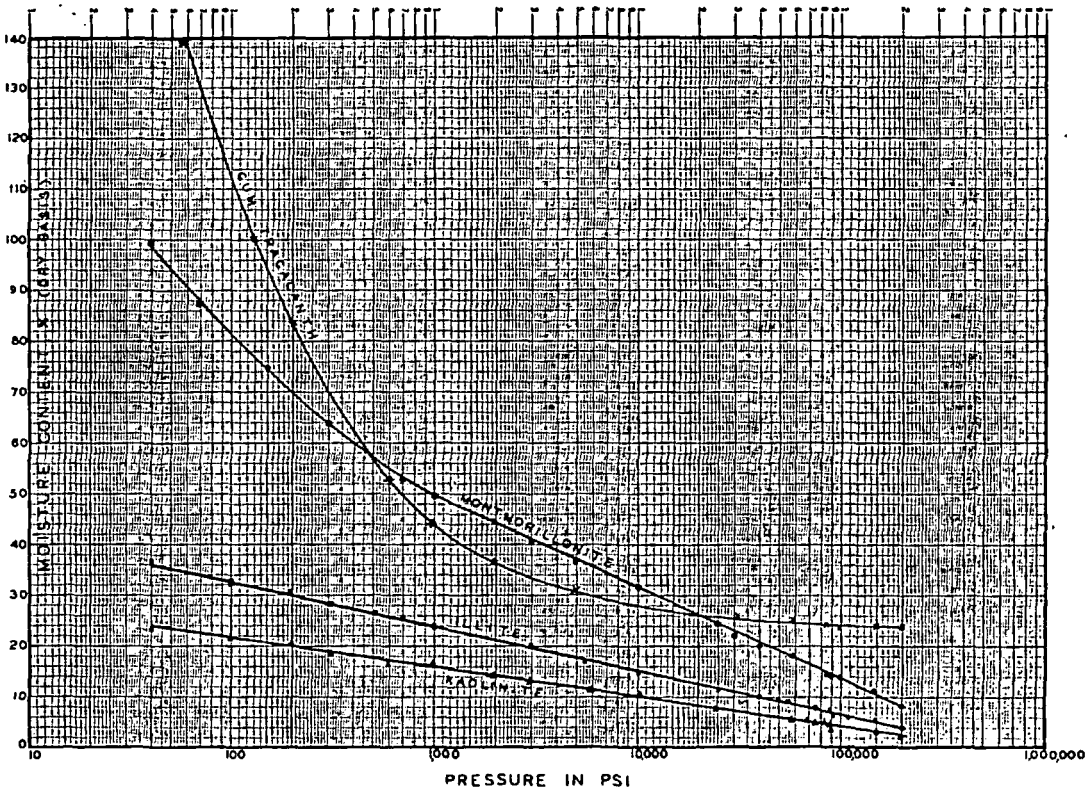

FIG. 3.—Relationship between moisture content (per cent dry weight) and pressure in psi for kaolinite, illite, and montmorillonite clays and gum tragacanth.

logarithm of pressure in psi. For the kaolinite and illite clays this relationship can be expressed by the formulas $M=33.9-5.96 \log P$, and $M=50-8.7 \log P$, respectively. A straight-line relationship between the moisture content and the pressure on semi-logarithmic graph paper (between 40 and 200,000 psi) possibly suggests that compaction is more or less a simple process. In the range indicated, possibly only oriented water is being removed. Or maybe only non-oriented (free) water is being squeezed out? If initially the liquid water and then the oriented water are being removed, then there is indeed a very gradual transition from the oriented to the non-oriented water. Possibly, the curves for kaolinite and illite swing upward, from a straight line, at some pressure less than 40 psi.

For montmorillonite clays a break in the curve is present at 1,000 psi. From 1,000 to 200,000 psi the curve is a straight line following the formula $M=104-18.06 \log P$. Possibly, the relatively loosely held water is lost below the pressure of 1,000 psi. It is also possible that at higher pressures (1,000 to 200,000 psi) the oriented water is being removed.

The steeper slopes of more plastic clays (higher swelling) suggest that it is harder to squeeze a given volume of water out of the less plastic clays; however, the percentage of water remaining in the more plastic clays is still greater.

Figures 4, 5, and 6 show relationship between the moisture content and the time of squeezing. The montmorillonite clay requires more time than illite, and illite, in turn, requires more time than kaolinite for attainment of equilibrium.

On hydrating a sample of illite clay in NaCl solution (5g. NaCl/100 cc. water) instead of distilled water, the moisture content at 10,000 psi was 16.1 per cent as compared with 14.9 per cent. Apparently the flocculated clays do not close-pack as much as deflocculated clays. On the other hand, a sample of kaolinite clay hydrated in NaOH solution (7 M. Mol. NaOH/g. clay) had a moisture content of 17.1 per cent at 200 psi as

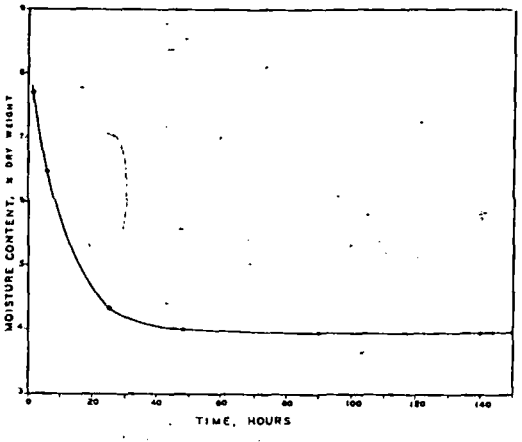

FIG. 4.—Variation in moisture content (per cent dry weight) with time (in hours) for kaolinite clay at 88,500 psi.

compared with 20.2 per cent on using distilled water. The writer (Tchillingarian, 1952) had previously proved that OH^- ions adsorb on the surfaces of kaolinite clay particles. Thus, the presence of OH^- ions on the surface of clay particles seems to result in easier movement of clay particles with respect to each other which causes closer packing.

CONCLUSIONS

The findings of the present study can be summarized as follows.

1. From 40 to 200,000 psi, a straight-line relationship exists between the moisture content (per cent of dry weight) and the logarithm of pressure for kaolinite and illite clays. The curve for illite clay has a steeper slope than that of kaolinite clay. The straight-line relationship possibly suggests that compaction is more or less a simple continuous process in this pressure range.

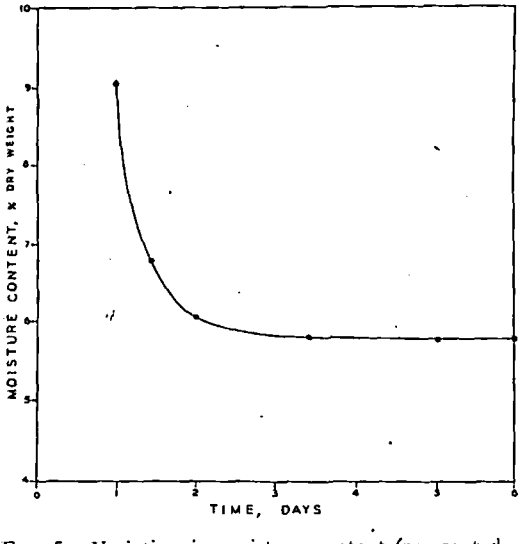

FIG. 5.—Variation in moisture content (per cent dry weight) of illite clay with time (in days) at 91,000 psi.

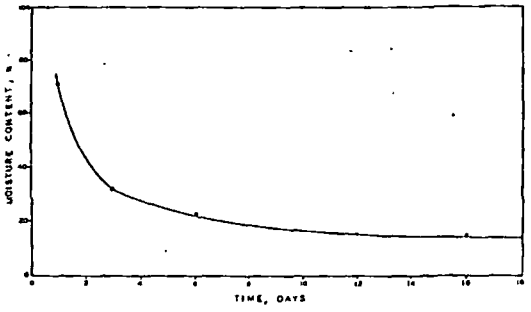

FIG. 6.—Variation in moisture content (per cent dry weight) of montmorillonite clay with time (in days) at 88,500 psi.

2. For montmorillonite clay, a break in the curve is present at about 1,000 psi. Above 1,000 psi, and up to 200,000 psi, the moisture content versus the logarithm of pressure curve is a straight line; however, its slope is steeper than that of either kaolinite or illite. Possibly, up to 1,000 psi a free liquid water is squeezed out, whereas at higher pressures up to 200,000 psi an oriented water is being removed.

3. The natural organic colloid, gum tragacanth, on the other hand, has a "hyperbolic" moisture versus pressure curve. It seems that up to about 3,000 psi it is easier to squeeze water out of the amorphous gel than it is from the crystalline clays. At higher pressures, however, it is very hard to squeeze water out of the gum tragacanth which together with water forms more or less homogeneous plastic mass having a very low permeability.

4. The functional relationship between the moisture content and pressure depends not only on the mineralogic type of clays but also on the type of ions adsorbed on the surfaces of clay particles. It also appears to depend on the degree of flocculation or deflocculation (dispersion) of the clays.

The future line of research suggested by this work is determination of the moisture-pressure curves for different clays, as for example for calcium-montmorillonite and for sodium-montmorillonite. The shapes of the curves and their com-

parison with each other would probably reveal the nature of the removed water and the nature of compaction processes. Obviously, higher pressures (up to 600,000 psi and higher) should be used in order to determine whether straight-line relationship extends beyond the range tested.

Inasmuch as huge amounts of water were squeezed out of muds in the process of their transformation into mudstones, shales, etc., and affected the composition of the ground waters, the mineralization of solutions squeezed out at different stages should also be studied. Preliminary work in this direction has been done by Lomtadze (1954, p. 453).

REFERENCES

HUBBERT, M. K., AND RUBEY, W. W., 1959, "Role of Fluid Pressure in Mechanics of Overthrust Faulting. I. Mechanics of Fluid-Filled Porous Solids and Its Application to Overthrust Faulting," *Bull. Geol. Soc. America*, Vol. 70, No. 2, pp. 115–66.

LOMTADZE, V. D., 1954, "About Role of Compaction Processes of Clayey Deposits in the Formation of Underground Waters," *Dokl. Akad. Nauk SSSR*, Tom 98, No. 3, pp. 451–54.

———, 1955, "Stages in the Formation of Properties of Clayey Rocks during Their Lithification," *ibid.*, Tom 102, No. 4, pp. 819–22.

RUBEY, W. W., AND HUBBERT, M. K., 1959, "Role of Fluid Pressure in Mechanics of Overthrust Faulting. II. Overthrust Belt in Geosynclinal Area of Western Wyoming in Light of Fluid-Pressure Hypothesis," *Bull. Geol. Soc. America*, Vol. 70, No. 2, pp. 167–206.

TCHILLINGARIAN, G., 1950, "A Study of the Properties of Drilling Fluids Containing Certain Natural Organic Colloids of Iranian Origin," *Master of Science Thesis*, Petroleum Engineering Department, University of Southern California.

———, 1952, "Possible Utilization of Electrophoretic Phenomenon for Separation of Fine Sediments into Grades," *Jour. Sed. Petrology*, Vol. 22, No. 1, pp. 29–32.

TERZAGHI, KARL, AND PECK, R. B., 1948, *Soil Mechanics in Engineering Practice*. 566 pp. John Wiley and Sons, Inc., New York.

WELLER, J. M., 1959, "Compaction of Sediments," *Bull. Amer. Assoc. Petrol. Geol.*, Vol. 43, No. 2, pp. 273–310.

BULLETIN OF THE AMERICAN ASSOCIATION OF PETROLEUM GEOLOGISTS
VOL. 44, NO. 1 (JANUARY, 1960), PP. 107-110, 4 FIGS.

GEOLOGICAL NOTES

STRIKE-SLIP FAULT OF CONTINENTAL IMPORTANCE IN BOLIVIA[1]

EMILE ROD[2]
Santa Cruz, Bolivia

From a study of the pertinent literature on the geology of Bolivia, especially Ahlfeld's "Geologia de Bolivia" (1946), combined with 3 months of field work in the region between Cochabamba and Santa Cruz, the following working hypothesis was developed: the northern half of South American has been displaced relative to its southern half toward the west, along a fault zone called here the Ichilo fault.

In the hope of calling attention to the possibility of such a large fault zone and to encourage further research this hypothesis is advanced now, at a time when the geologists of several oil companies are exploring the Subandean Zone west and northwest of Santa Cruz.

[1] Manuscript received, August 28, 1959.

[2] Permanent address: Venezuelan Atlantic Refining Company, Caracas, Venezuela.

Today it is just an idea based on a few scattered observations (Fig. 1) among which should be mentioned: the Chiquitos graben (foso Chiquitano of Ahlfeld, 1946); the very sharp bend of the folds within the Subandean Zone which seems to be due to a very powerful drag; several straight strike-slip faults accompanied by belts of crushed rocks and imbricate structures, cutting through the folds at an acute angle (Tunari fault, Ivirizu fault, Colorado fault); the junction (fractured deflection) of the Andean mountain arcs in central Bolivia at an angle of almost 90°; and finally the block of northern South America (Fig. 2) protruding between the fault zones of the southern Caribbean (Oca, Avila, and El Pilar faults) and the postulated Ichilo fault in a wide arc toward the west.

As central Bolivia is a region of high seismicity,

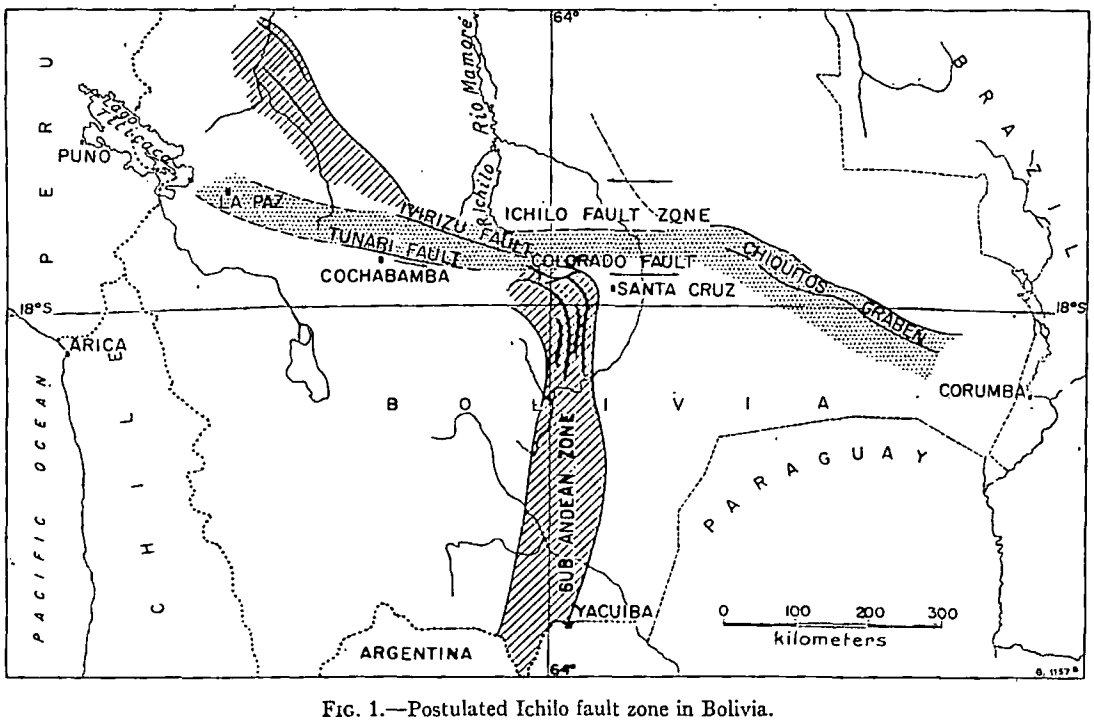

FIG. 1.—Postulated Ichilo fault zone in Bolivia.

[AMERICAN JOURNAL OF SCIENCE, VOL. 275, OCTOBER, 1975, P. 954-983]

REFERENCE FRAMES AND DIFFUSION COEFFICIENTS

JOHN B. BRADY

Department of Geological Sciences, Harvard University,
Cambridge, Massachusetts 02138

ABSTRACT. Diffusion coefficients are empirical constants that express linear relationships between fluxes of chemical components and gradients in composition variables. Component fluxes must be measured with respect to some particular frame of reference, so diffusion coefficients depend on the choice of reference frame as well as the choice of composition gradient. Reference frames based on a mean velocity of all the components, such as the velocity of the center of mass, are particularly convenient, for results obtained using different mean velocity frames may be readily interrelated. Diffusion data is best presented in terms of "standard" diffusion coefficients, D°_{ij}, based on the mean volume reference frame. The continuity equation for a specific reference frame R is given by

$$\left(\frac{\partial \rho_i}{\partial t}\right)_{P,T,x} = -\left[\frac{\partial}{\partial x}\left(J_i^R + \rho_i \bar{v}^{RL}\right)\right]_{P,T,t}$$

where $\bar{v}^{RL}$ is the local velocity of reference frame R with respect to a fixed point not affected by the diffusion process. If there is a volume change during a binary diffusion process in a single crystal, the continuity equation may be solved using a modified distance scale based on appropriate lattice translations in the crystal of interest. Interdiffusion behavior may be predicted on the basis of isotopic self-diffusion measurements; the exact relationship utilized for ionic crystals is not identical to Darken's equation for metallic crystals.

I. INTRODUCTION

The process of diffusion involves the net transfer of atoms due to random thermal motions of atoms initially in a non-random distribution and/or to non-random thermal motions of atoms subject to a driving force. In order to describe and quantify this net movement of atoms, macroscopic measurements must be made with respect to some specific frame of reference, usually consisting of a set of identifiable points. In principle, any set of reference points may be used as long as *all* measurements are made with respect to the same set. In practice, however, it may be inconvenient or impossible to use the same reference frame for all measurements and applications. Since different reference frames lead to different descriptions of diffusion and, therefore, to different diffusion coefficients, it is wise to select for common usage those reference frames that may be readily interrelated. For these reasons, an understanding of the various ways to describe diffusion and to define diffusion coefficients is a prerequisite to the discussion of any diffusion data or diffusion related process.

Extensive discussions of the subject of reference frames may be found in the chemical, physical, and metallurgical literature of the last 25 years. Outstanding papers include those by Darken (1948), Hartley and Crank (1949), Hooyman and others (1953), Hooyman (1956), Kirkwood and others (1960). An excellent summary may be found in a textbook by de Groot and Mazur (1962, p. 239 and following). Summaries may also be found in the texts by Fitts (1962, chap. 8) and Haase (1969, p. 271 and following). In spite of this rather thorough theoretical coverage of the subject, a unified treatment of reference frames is not available. The

several papers listed above u
designed to suit the problem
what follows I will reconside
show how the results of seve
will then show how these res
to problems of diffusion in co

Throughout this paper
logical descriptions of diffusi
by local variations in the che
may be explained, using sim
the transfer of matter of defi
of the system. Hence, one de
chemical components relativ
duce the observed variations
used in the description nece
molecular species and may b
Brady, 1975). For the purpose
used are linearly independen
may be independently varied

The equations presented
dimensional diffusion. To be
fusion coefficients should be
dimensional representation i
and simplifies the already c
three dimensions is straightfo
is moles of component i or g
of quantity simplifies some o
reference frame. Quantities
is specified are written with s
frame, R. The following is a

a	— unit cell param
$A = A^{+a}$	— cation with cha
A_{ij}^{RV}	— parameters usec fluxes in refere
b	— unit cell param
$B = B^{+b}$	— cation with cha
B_i^I	— mobility of con spect to the in unit force (mol
c	— unit cell param
C_i	— any one compo
$D_{ij}^{R,c}$	— practical diffus with respect to j given in terms

several papers listed above utilize a number of different approaches, each designed to suit the problems most often encountered by the authors. In what follows I will reconsider the general topic of reference frames and show how the results of several of the listed authors are interrelated. I will then show how these results may be extended and modified to apply to problems of diffusion in common minerals.

Throughout this paper I consider only macroscopic or phenomenological descriptions of diffusion. Macroscopically, diffusion is manifested by local variations in the chemical composition of a physical system and may be explained, using simple mass balance considerations, in terms of the transfer of matter of definite chemical compositions into and/or out of the system. Hence, one describes diffusion as a motion of quantities of chemical components relative to some reference frame sufficient to produce the observed variations in chemical composition. The components used in the description need not correspond to any moving atomic or molecular species and may be selected on the basis of convenience (see Brady, 1975). For the purposes of this paper I assume that the components used are linearly independent and that the quantity of each component may be independently varied in the systems considered.

The equations presented in the following paragraphs are all for one-dimensional diffusion. To be complete, velocities, fluxes, forces, and diffusion coefficients should be given as tensor quantities. However, a one-dimensional representation is sufficient to convey the important concepts and simplifies the already cumbersome notation. The generalization to three dimensions is straightforward. The unit of quantity used throughout is moles of component i or gram-formula units of i. This choice of unit of quantity simplifies some of the discussion, particularly for the unit cell reference frame. Quantities that have meaning only if a reference frame is specified are written with superscripts to indicate a particular reference frame, R. The following is a list of the symbols used in the text.

NOTATION

a	— unit cell parameter (Å)
$A = A^{+a}$	— cation with charge +a
A_{ij}^{RV}	— parameters used to relate fluxes in reference frame R to fluxes in reference frame V (dimensionless) (3.11)
b	— unit cell parameter (Å)
$B = B^{+b}$	— cation with charge +b
B_i^I	— mobility of component i; velocity of component i with respect to the inert marker reference frame in response to a unit force (mole-cm²/cal-sec) (7.1)
c	— unit cell parameter (Å)
C_i	— any one composition variable for component i
$D_{ij}^{R,C}$	— practical diffusion coefficient; relates flux of component i with respect to reference frame R to gradient of component j given in terms of composition parameter C_j (3.6)

D°_{ij} — "standard" practical diffusion coefficient; relates flux of component i with respect to the mean volume reference frame to gradient in molar density of component j (cm^2/sec) (3.11)

D_i^I — inert marker diffusion coefficient defined in (6.13) and (6.10) (cm^2/sec)

G — Gibbs free energy (cal)

i,j,k,l — dummy subscripts used to represent various components

J_i^R — flux of component i with respect to reference frame R (moles/cm^2-sec) (2.4)

L_{ij}^R — phenomenological diffusion coefficient; relates flux of component i with respect to reference frame R to the force produced by the chemical potential gradient of component j ($mole^2$/cal-cm-sec) (3.1)

L_{ij}^R — phenomenological diffusion coefficient; relates flux of component i to a set of independent forces given in (3.4) ($mole^2$/cal-cm-sec)

M_i — gram formula weight of component i (gm/mole)

n_i — number of moles of component i

n_i^c — number of moles of component i per unit cell

N_i — $\dfrac{n_i}{\sum_{i=1}^{n} n_i}$; mole fraction of component i (dimensionless)

P — pressure (bars)

q_i — charge on species i (esu)

R — gas constant (1.987 cal/mole-deg)

t — time (sec)

T — temperature (°K)

v_i^L — velocity of component i with respect to some laboratory frame L (cm/sec)

$\bar{v}^{RL}$ — a weighted average of the velocities of all components; velocity of mean velocity reference frame R (cm/sec) (2.2)

v_i^R — velocity of component i with respect to mean velocity reference frame R (cm/sec) (2.3)

$\bar{v}^{SR}$ — velocity of reference frame S with respect to reference frame R (cm/sec) (2.6)

V — volume (cm^3)

V_i — $\left(\dfrac{\partial V}{\partial n_i}\right)_{P,T,n_j \neq i}$; partial molar volume ($cm^3$/mole)

$\mathcal{V}$ — $\dfrac{V}{\sum_{i=1}^{n} n_i}$; molar volume of a phase (cm^3/mole)

w_i^R — weight given the velocity of component i in obtaining mean velocity $\bar{v}^{RL}$ (dimensionless) (2.1)

x — distance (cm)

$\chi = Z^{-z}$ — anion or chem

γ_i — activity coeffic

δ_{ik} — $\begin{cases}=0 \text{ if } i \neq k\\ =1 \text{ if } i=k\end{cases}$

μ_i — $\left(\dfrac{\partial G}{\partial n_i}\right)_{P,T,n_j \neq}$ i (cal/mole)

ξ_n^c — modified dista on unit cell ed

ρ_i — molar density

ϕ — electrical pote

Superscripts

C — any one compo

I — inert marker re

K — K*th* componen

L — laboratory refe

M — mean mass refe

N — mean molar ref

R — any one referen

V — mean volume r

* — indicates that t

2. MEAN V

A great number of pape of diffusion that make no m in which the diffusive velocit The authors of nearly all th fluxes and velocities they di identifiable point. This is eq a set of points, each of whic others at all times. I shall cal frame, L, for it is commonly of transport processes. For ex ments are given with respec liquid diffusion experiments, tainer that holds the liquid, frame.

Although laboratory ref vantages, their general utilit Indeed, there are potentially a are laboratories or experime frames may be difficult or im servers of a solid interdiffusio the diffusion couple as the ori overall volume change durin

x — distance (cm)
$\mathcal{A} = \mathcal{A}^{-z}$ — anion or chemical component with charge $-z$
γ_i — activity coefficient for component i (dimensionless)
δ_{ik} — $\left\{\begin{matrix}=0 \text{ if } i \neq k \\ =1 \text{ if } i = k\end{matrix}\right\}$; Kronecker delta function (dimensionless)
μ_i — $\left(\frac{\partial G}{\partial n_i}\right)_{P,T,n_j \neq i}$; chemical potential per mole of component i (cal/mole)
ξ_R^c — modified distance parameter for reference frame R based on unit cell edge c (dimensionless) (5.1)
ρ_i — molar density of component i (moles/cm³)
ϕ — electrical potential (cal/esu)

Superscripts

C — any one composition variable
I — inert marker reference frame (sec. 6)
K — K*th* component reference frame (2.10)
L — laboratory reference frame (sec. 2)
M — mean mass reference frame (2.11)
N — mean molar reference frame (2.8)
R — any one reference frame
V — mean volume reference frame (2.9)
• — indicates that the value is given for a radioactive isotope

2. MEAN VELOCITY REFERENCE FRAMES

A great number of papers have been written on the general subject of diffusion that make no mention whatsoever of the frame of reference in which the diffusive velocities and fluxes discussed are to be measured. The authors of nearly all these papers tacitly assume that the diffusive fluxes and velocities they discuss are measured with respect to a single identifiable point. This is equivalent to using a reference frame based on a set of points, each of which remains in a fixed position relative to the others at all times. I shall call this type of reference frame the laboratory frame, L, for it is commonly used by experimentalists in the description of transport processes. For example, fluxes in solid interdiffusion experiments are given with respect to one end of the sample. Similarly, in liquid diffusion experiments, fluxes are measured with respect to the container that holds the liquid, sometimes called the "cell-fixed" reference frame.

Although laboratory reference frames have obvious practical advantages, their general utility is severely limited by their multiplicity. Indeed, there are potentially as many laboratory reference frames as there are laboratories or experimentalists, and results obtained using such frames may be difficult or impossible to compare. For example, two observers of a solid interdiffusion experiment might pick opposite ends of the diffusion couple as the origin of their laboratory frames. If there is an overall volume change during the diffusion experiment, the two labora-

tory frames chosen would move with respect to one another. This means that two observers of the same experiment would obtain different values for fluxes and velocities of the same components.

These difficulties may be eliminated by reporting motion with respect to a reference frame that is independent of the particular laboratory frame selected by an observer. Such a reference frame can be defined by some weighted average of the velocities of all the chemical components involved, such as the velocity of the center of mass. Whatever laboratory frame is used to measure individual velocities in a given experiment, the same result would be reported by all observers for component velocities relative to the center of mass. This approach has its foundations in classical mechanics and was introduced to describe multicomponent diffusion by Hooyman (1956). Following Hooyman's terminology, I shall call reference frames of this type "mean velocity" reference frames.

Let v_i^L be the velocity of component i as measured by any one observer with respect to any single laboratory frame L at one point in space and at one particular time. Operationally, v_i^L would be a weighted average of the velocities of all the particles that contain component i. Selecting a set of dimensionless weighting factors w_i^R, such as mass fraction, mole fraction, or volume fraction, normalized according to the criteria

$$\sum_{i=1}^{n} w_i^R = 1 \tag{2.1}$$

we may define an average or mean velocity, $\bar{v}^{RL}$, for the n components of a given system as

$$\bar{v}^{RL} \equiv \sum_{i=1}^{n} w_i^R v_i^L \tag{2.2}$$

where the superscript R refers to the reference frame defined by (2.1) and (2.2). Although the magnitude of v_i^L and of the mean velocity $\bar{v}^{RL}$ may vary from observer to observer, the velocity v_i^R of component i with respect to the mean velocity

$$v_i^R \equiv (v_i^L - \bar{v}^{RL}) \tag{2.3}$$

will be the same for all observers. On this basis, then, we may define the flux, J_i^R, of component i with respect to mean velocity reference frame R as

$$J_i^R \equiv \rho_i v_i^R \tag{2.4}$$

where ρ_i is the molar density of i and where the flux, J_i^R, is given in units of moles of i per cm^2 per second. J_i^R will be the same for all observers of the same event.

Comparing equations (
n fluxes in any mean velocit
Indeed, the fluxes are related

Equation (2.5) provides an
R and was used as such by
also pointed out that the flu
may be related using the exp

where $\bar{v}^{SR}$ is the velocity of
frame R. For mean velocity

$$\bar{v}^{SR} = \bar{v}^{SL} -$$

Equations (2.6) and (2.7) poi
reference frames: results fro
interrelated. This fact will b
diffusion coefficient in sectio

Commonly used referen
the following:

1. Mean molar reference

$$w_i^N = N_i =$$

where N_i is the mole fractio
the phase in which the diffus

2. Mean volume referen

$$w_i^V = \rho_i V_i$$

where V_i is the partial molar

3. *Kth* component refer

$$w_i^K = \delta_{ik}$$

where δ_{ik} is the "Kronecker
$\delta_{ik} = 1$ if $i = K$.

Comparing equations (2.1), (2.2), (2.3), and (2.4) it is clear that the n fluxes in any mean velocity reference frame cannot all be independent. Indeed, the fluxes are related by

$$\sum_{i=1}^{n} \frac{w_i^R}{\rho_i} J_i^R = 0 \quad . \tag{2.5}$$

Equation (2.5) provides an alternative definition for the reference frame R and was used as such by Kirkwood and others (1960). These authors also pointed out that the fluxes with respect to *any* two reference frames may be related using the expression

$$J_i^R = J_i^S + \rho_i \bar{v}^{SR} \tag{2.6}$$

where $\bar{v}^{SR}$ is the velocity of reference frame S with respect to reference frame R. For mean velocity reference frames we have

$$\bar{v}^{SR} = \bar{v}^{SL} - \bar{v}^{RL} = \sum_{k=1}^{n} (w_k^S - w_k^R) v_k^L \quad . \tag{2.7}$$

Equations (2.6) and (2.7) point out a very useful feature of mean velocity reference frames: results from various mean velocity frames may be easily interrelated. This fact will be used to advantage in defining a "standard" diffusion coefficient in section 3.

Commonly used reference frames of the mean velocity type include the following:

1. Mean molar reference frame (also called number-fixed frame)

$$w_i^N = N_i = \rho_i \bar{V} \qquad \sum_{i=1}^{n} J_i^N = 0 \tag{2.8}$$

where N_i is the mole fraction of i and where $\bar{V}$ is the molar volume of the phase in which the diffusion occurs.

2. Mean volume reference frame

$$w_i^V = \rho_i V_i \qquad \sum_{i=1}^{n} V_i J_i^V = 0 \tag{2.9}$$

where V_i is the partial molar volume of i.

3. K*th* component reference frame

$$w_i^K = \delta_{iK} \qquad J_K^K = 0 \tag{2.10}$$

where δ_{ik} is the "Kronecker delta" defined such that $\delta_{ik} = 0$ if $i \neq K$ and $\delta_{ik} = 1$ if $i = K$.

4. Mean mass (barycentric) reference frame

$$w_i^M = \tilde{N}_i = \tilde{\rho}_i \tilde{V} \qquad \sum_{i=1}^{n} M_i J_i^M = 0 \qquad (2.11)$$

where $\tilde{N}_i$ is the mass fraction of i, $\tilde{\rho}_i$ is the mass density of i, $\tilde{V}$ is the specific volume, and M_i is the gram-formula weight of i.

Each of these reference frames may be particularly useful for a given set of additional constraints. For example, the mean volume reference frame is most convenient if there is no volume change during the diffusion process. Also, the K*th* component reference frame simplifies the description of a diffusion process in which the K*th* component does not actively participate. Because of their general utility, much of the following discussion will emphasize mean velocity reference frames.

3. FORCES, FLUXES, AND DIFFUSION COEFFICIENTS

The presence of material transport in a system as described by the molar fluxes J_i^R clearly indicates a departure from equilibrium. On a local scale, however, the departure from equilibrium for many transport processes is not great. Therefore, it is a very good approximation to describe the changes of a system in terms of *linear* functions of the forces that tend to restore equilibrium. This linear approximation has withstood the test of countless experiments. It was formulated independently as the "laws" of Darcy, Fick, Fourier, and Ohm which govern specific transport processes. Onsager (1931a, b) unified the various linear laws using a formalism that emphasizes their interrelationships.

Isothermal, isobaric diffusion is a form of material transport linearly related to the force produced by chemical potential gradients. While chemical potential gradients are independent of the choice of reference frame, the molar fluxes J_i^R are not. Thus, the linear relations between fluxes J_i^R and forces $\left(\frac{\partial \mu_i}{\partial x}\right)_{P,T,t}$ given by

$$J_i^R = -\sum_{j=1}^{n} L_{ij}^R \left(\frac{\partial \mu_j}{\partial x}\right)_{P,T,t} \qquad (i = 1,2,\ldots,n) \qquad (3.1)$$

will vary with the choice of reference frame. Equations (3.1) *define* the phenomenological (diffusion) coefficients, L_{ij}^R, for reference frame R. μ_i is the chemical potential per mole of i, and its derivative with respect to distance x is taken at constant pressure P, temperature T, and time t. Note that in general the flux of any component i is linearly related to the chemical potential gradients of *each* of the other components. In other words, the contribution to the diffusion flux from any applied force should be considered. It should also be noted that the degree to which each force contributes to the diffusion flux of a given component

depends directly upon the reference frame selected to describe the diffusion flux.

Equations (3.1) lead to the disturbing conclusion that for an n-component system with r reference frames of interest, there are (r) $(n)^2$ phenomenological coefficients. Fortunately, these coefficients are not all independent. Onsager (1931a, b) has shown that provided the fluxes and forces are properly chosen, the n^2 coefficients for a single reference frame are subject to the relations

$$L_{ij}^{R} = L_{ji}^{R} \tag{3.2}$$

leaving only (n)(n+1)/2 independent coefficients for each reference frame. Hooyman and de Groot (1955) have demonstrated that linear independence of either the fluxes or forces is a sufficient, though not necessary, condition for the Onsager symmetry relations (3.2) to hold. For mean velocity reference frames the fluxes and forces of (3.1) are not independent, being related by (2.5) and the Gibbs-Duhem equation

$$\sum_{i=1}^{n} N_i d\mu_i = 0 \qquad \text{(constant P,T)} \tag{3.3}$$

respectively. The extra terms in (3.1) may be eliminated by using (2.5) and (3.3) and selecting J_n^R and $d\mu_n$ as the dependent variables. The result is an independent set of phenomenological equations for mean velocity frames

$$J_i^R = -\sum_{j=1}^{n-1} L_{ij}^R \left[\sum_{k=1}^{n-1} \left(\delta_{jk} + \frac{w_j^R}{w_n^R} \frac{N_k}{N_j} \right) \left(\frac{\partial \mu_k}{\partial x} \right)_{P,T,t} \right] (i = 1,2,\ldots,n-1) \tag{3.4}$$

as given in de Groot and Mazur (1962, p. 242). Equations (3.4) *define* the phenomenological coefficients L_{ij}^R which express the linear relations between the fluxes J_i^R and a set of independent forces given by the terms enclosed in brackets. The Onsager relations (3.2) become

$$L_{ij}^{R} = L_{ji}^{R} \quad . \tag{3.5}$$

This leaves (n-1)(n)/2 independent coefficients for a given mean velocity frame. And since the various reference frames are related by (2.6), we are left with the task of determining a total of only (n-1)(n)/2 independent phenomenological coefficients.

While chemical potential gradients are theoretically meaningful as the ultimate driving forces for diffusion, they have the unfortunate quality of being difficult to measure. In crystals, they may be found only by calculations based on measurements of composition gradients combined with often-unavailable thermodynamic data. Therefore, it is common practice to describe diffusion processes in terms of "practical"

diffusion coefficients $D_{ij}^{R,C}$ which are *defined* for mean velocity frames by the relations

$$J_i^R = -\sum_{j=1}^{n-1} D_{ij}^{R,C} \left(\frac{\partial C_j}{\partial x}\right)_{P,T,t} \quad (i = 1,2,\ldots,n-1) \tag{3.6}$$

where C_i is some compositional variable. Note that the diffusion coefficients $D_{ij}^{R,C}$ depend *both* on the reference frame R used to describe the fluxes and on the particular composition variable C_i whose gradient is measured. Also, note that as in (3.4) only (n-1) independent fluxes and forces are considered, with J_n^R and dC_n being selected as the dependent variables. The n fluxes are connected through equation (2.5), and the n forces are connected through relations of the type

$$\sum_{i=1}^{n} \alpha_i dC_i = 0 \tag{3.7}$$

which exist for the commonly used compositional variables. The α's are constants for a given composition. For example,

$$\sum_{i=1}^{n} V_i d\rho_i = 0 \qquad \text{(constant P,T)} \tag{3.8}$$

where V_i is the partial molar volume of i and ρ_i is the molar density of i.

Once again with the definitions (3.6) a multiplicity of $(n-1)^2(r)(c)$ diffusion coefficients has been introduced for r reference frames and c compositional variables of interest. As before, these coefficients are not all independent: the various reference frames may be related by (2.6), and relations (perhaps unknown) obviously exist between the various compositional parameters such as mole fractions and molar densities. A maximum of $(n-1)^2$ diffusion coefficients remain. These, however, are not all independent either. Comparing equations (3.4) and (3.6) we may see that the diffusion coefficients $D_{ij}^{R,C}$ are linear functions of the phenomenological coefficients with

$$D_{il}^{R,C} = \sum_{k=1}^{n-1}\sum_{j=1}^{n-1} L_{ij}^R \left[\delta_{jk} + \frac{w_j^R}{w_n^R}\frac{N_k}{N_j}\right]\left(\frac{\partial \mu_k}{\partial C_l}\right)_{P,T,C_i \neq C_l} \quad (i,l = 1,2,\ldots,n-1). \tag{3.9}$$

Since the phenomenological coefficients L_{ij}^R are not independent, but related by the (n-1)(n-2)/2 equations (3.5), only (n)(n-1)/2 of the diffusion coefficients $D_{ij}^{R,C}$ can be independent. The specific relations among the $D_{ij}^{R,C}$ may be found for a given system by solving (3.9) for the L_{ij}^R and

using (3.5). This is only possib

are known. If an equation of st
and (3.9) cannot be used, and (
any event it will not, in genera
such that $D_{ij}^{R,C} = D_{ji}^{R,C}$.

While it is clear that the d
velocity reference frames and co
we are liable to find any of th
The undesirable consequence is
tories may not be directly com
culations. It would seem prefer
and compositional variable C_i t
through which all data would
Following the precedent set by
mean volume reference frame
standard diffusion coefficients D°

$$J_i^V = -\sum_{j=1}^{n-1} D^\circ_{ij}\left(\frac{\partial \rho_j}{\partial x}\right)_{P,T,t}$$

Equations (3.10) reduce to Fick
ponent system. For diffusion w
reference frame R with fluxes J_i

$$J_i^R = \sum_{j=1}^{n-1} A_{ij}^{RV} J_j^V$$

the flux equations become

$$J_i^R = -\sum_{k=1}^{n-1}\left[\sum_{j=1}^{n-1} A_{ij}^{RV} D^\circ_{jk}\right.$$

If a different compositional var

$$J_i^R = -\sum_{l=1}^{n-1}\left[\sum_{k=1}^{n-1}\left(\sum_{j=1}^{n-1} A_{ij}\right.\right.$$

Equations (3.13), which are ide
and Mazur (1962), may be co
multicomponent diffusion.

Equations (3.13) reduce t
ponent systems which may be

using (3.5). This is only possible if the derivatives $\left(\frac{\partial \mu_k}{\partial C_l}\right)_{P,T,C_l \neq C_l}$ are known. If an equation of state is unavailable, then the relations (3.5) and (3.9) cannot be used, and $(n-1)^2$ coefficients must be determined. In any event it will not, in general, be possible to choose fluxes and forces such that $D_{ij}^{R,C} = D_{ji}^{R,C}$.

While it is clear that the diffusion coefficients for the various mean velocity reference frames and compositional variables are interconnected, we are liable to find any of the $(n-1)^2(r)(c)$ possible coefficients in use. The undesirable consequence is that diffusion data from different laboratories may not be directly comparable without performing tedious calculations. It would seem preferable to select a single reference frame R and compositional variable C_i to define a "standard" diffusion coefficient through which all data would be reported and, thus, easily compared. Following the precedent set by Hooyman and others (1953) let us use the mean volume reference frame and the molar densities ρ_i to define the standard diffusion coefficients D°_{ij} with

$$J_i^V = -\sum_{j=1}^{n-1} D^\circ_{ij}\left(\frac{\partial \rho_j}{\partial x}\right)_{P,T,t} \qquad (i = 1,2,\ldots,n-1) \quad . \qquad (3.10)$$

Equations (3.10) reduce to Fick's law at constant volume in a two-component system. For diffusion with respect to a different mean velocity reference frame R with fluxes J_i^R linearly related to fluxes J_i^V by

$$J_i^R = \sum_{j=1}^{n-1} A_{ij}^{RV} J_j^V \qquad (i = 1,2,\ldots,n-1) \qquad (3.11)$$

the flux equations become

$$J_i^R = -\sum_{k=1}^{n-1}\left[\sum_{j=1}^{n-1} A_{ij}^{RV} D^\circ_{jk}\right]\left(\frac{\partial \rho_k}{\partial x}\right)_{P,T,t} \qquad (i = 1,2,\ldots,n-1) \quad . \qquad (3.12)$$

If a different compositional variable C_i is used the flux equations are

$$J_i^R = -\sum_{l=1}^{n-1}\left[\sum_{k=1}^{n-1}\left(\sum_{j=1}^{n-1} A_{ij}^{RV} D^\circ_{jk}\right)\left(\frac{\partial \rho_k}{\partial C_l}\right)_{P,T,C_l \neq C_l}\right]\left[\frac{\partial C_l}{\partial x}\right]_{P,T,t}$$

$$(i = 1,2,\ldots n-1) \quad . \qquad (3.13)$$

Equations (3.13), which are identical to equations (55), p. 243 of de Groot and Mazur (1962), may be considered a generalization of Fick's law to multicomponent diffusion.

Equations (3.13) reduce to particularly simple forms for two component systems which may be described in terms of a single binary (or

interdiffusion) coefficient, since $(n\text{-}1)^2$ equals one. Let us evaluate the A_{ij}^{RV} of (3.11) for a two component system and mean velocity frame R. This may be accomplished by rewriting equation (2.4) using (2.1), (2.2), and (2.3) first for reference frame R

$$J_1^R = \rho_1 v_1^L - \rho_1 \left[w_1^R v_1^L + w_2^R v_2^L \right] \tag{3.14}$$

$$J_1^R = w_2^R \left[\rho_1 (v_1^L - v_2^L) \right] \tag{3.15}$$

and then for reference frame V

$$J_1^V = w_2^V \left[\rho_1 (v_1^L - v_2^L) \right] . \tag{3.16}$$

Comparing (3.15) and (3.16) we see that

$$J_1^R = \frac{w_2^R}{w_2^V} J_1^V = \frac{w_2^R}{\rho_2 V_2} J_1^V . \tag{3.17}$$

Using (3.13) and (3.17) we may give a general definition of the binary diffusion coefficient D° in terms of any mean velocity frame R as

$$J_1^R = -\frac{w_2^R}{\rho_2 V_2} D^\circ \left(\frac{\partial \rho_1}{\partial C_1} \right)_{P,T} \left(\frac{\partial C_1}{\partial x} \right)_{P,T,t} \tag{3.18}$$

taking component 2 as the dependent component (Hooyman and others, 1953). For the mean velocity frames presented above, (3.18) becomes (de Groot and Mazur, 1962, p. 252)

$$J_1^N = -\frac{\bar{V}}{V_2} D^\circ \left(\frac{\partial \rho_1}{\partial x} \right)_{P,T,t} = -\frac{D^\circ}{\bar{V}} \left(\frac{\partial N_1}{\partial x} \right)_{P,T,t} \quad \left(\begin{array}{c} \text{mean molar} \\ \text{frame} \end{array} \right) \tag{3.19}$$

$$J_1^V = -D^\circ \left(\frac{\partial \rho_1}{\partial x} \right)_{P,T,t} \quad \left(\begin{array}{c} \text{mean volume} \\ \text{frame} \end{array} \right) \tag{3.20}$$

$$J_1^2 = -\frac{D^\circ}{\rho_2 V_2} \left(\frac{\partial \rho_1}{\partial x} \right)_{P,T,t} = -\frac{D^\circ}{N_2 \bar{V}} \left(\frac{\partial N_1}{\partial x} \right)_{P,T,t} \quad \left(\begin{array}{c} \text{component 2} \\ \text{frame} \end{array} \right) \tag{3.21}$$

$$J_1^M = -\frac{\tilde{N}_2}{\rho_2 V_2} \left(\frac{\partial \rho_1}{\partial x} \right)_{P,T,t} = -\frac{D^\circ}{M_1 \tilde{V}} \left(\frac{\partial \tilde{N}_1}{\partial x} \right)_{P,T,t} \quad \left(\begin{array}{c} \text{mean mass} \\ \text{frame} \end{array} \right). \tag{3.22}$$

4. THE CONTINUITY EQUATION

The flux equations presented in section 3 involve gradients of chemical potentials or composition variables evaluated at any single time t. Equations (3.4) and (3.13), therefore, are "instantaneous" flux equations. They are valid to describe the process of diffusion only at a given point in space and at one particular time. The one exception is the special case of steady-state diffusion, in which the gradients of chemical potential or composition do not change with time. In general, diffusion is a non-steady-state process and must be described by a form of the continuity equation.

For diffusive mass transfer the equation of continuity is also commonly called the conservation of mass equation or the mass balance equation. It is typically given in terms of fluxes measured with respect to a laboratory reference frame. As discussed in section 2, laboratory reference frames have a number of undesirable features. In addition to those features already mentioned, laboratory frames require the use of more diffusion coefficients than mean velocity frames. Since there is, in general, no equation similar to (2.5) to interrelate laboratory frame fluxes, it will be necessary to determine n^2 diffusion coefficients $D_{ij}^{L,C}$ defined by

$$J_i^L = -\sum_{j=1}^{n} D_{ij}^{L,C}\left(\frac{\partial C_j}{\partial x}\right)_{P,T,t} \qquad (i = 1,2,\ldots,n) \tag{4.1}$$

for any laboratory frame of interest. (The number of diffusion coefficients may be reduced to (n) (n+1)/2 using (3.1) and (3.2) if an equation of state is available.) It will be to our advantage, therefore, to express the continuity equation in terms of mean velocity frame fluxes.

The equation of continuity has been derived numerous times for a multitude of processes, so I will not repeat the derivation here. See Landau and Lifshitz (1959, p. 1-2) for a general derivation. In the notation of this paper the continuity equation for any component i is

$$\left(\frac{\partial \rho_i}{\partial t}\right)_{P,T,x} = -\left[\frac{\partial(\rho_i v_i^L)}{\partial x}\right]_{P,T,t} = -\left(\frac{\partial J_i^L}{\partial x}\right)_{P,T,t} \tag{4.2}$$

Equation (4.2) is strictly applicable only to *conservative* processes in which component i is neither added to nor subtracted from the diffusive system (by reaction, for example). For constant volume diffusion, equation (4.2) has been called Fick's second law. Recalling equation (2.6), we may readily write the continuity equation for any reference frame, R, as

$$\left(\frac{\partial \rho_i}{\partial t}\right)_{P,T,x} = -\left[\frac{\partial}{\partial x}\left(J_i^R + \rho_i \bar{v}^{RL}\right)\right]_{P,T,t} \tag{4.3}$$

where $\bar{v}^{RL}$ is the local velocity of reference frame R with respect to the laboratory frame. The value of $\bar{v}^{RL}$ for a given mean velocity frame R may be expressed in terms of laboratory frame fluxes by using (2.5) as well as (2.6) (see Kirkwood and others, 1960). For the mean molar reference frame, N,

$$\bar{v}^{NL} = \bar{V} \sum_{i=1}^{n} J_i^L \tag{4.4}$$

which upon substitution into (4.3) gives

$$\left(\frac{\partial \rho_i}{\partial t}\right)_{P,T,x} = -\left(\frac{\partial J_i^N}{\partial x}\right)_{P,T,t} - N_i \sum_{k=1}^{n}\left(\frac{\partial J_k^L}{\partial x}\right)_{P,T,t} \tag{4.5}$$

Similarly, for the mean volume reference frame

$$\left(\frac{\partial \rho_i}{\partial t}\right)_{P,T,x} = -\left(\frac{\partial J_i^V}{\partial x}\right)_{P,T,t} - \rho_i \left[\sum_{k=1}^{n} \left(\frac{\partial}{\partial x}(V_k J_k^L)\right)_{P,T,t}\right]. \quad (4.6)$$

We are now in a position to understand some of the problems of treating non-steady-state diffusion. If a laboratory frame and equation (4.2) are used, then a minimum of (n) (n+1)/2 diffusion coefficients must be determined. And even for a two-component system, this would be three diffusion coefficients that must be determined from two simultaneous non-linear differential equations. If a mean velocity frame is used, a minimum of only (n) (n−1)/2 diffusion coefficients are needed: one for a binary system, three for a ternary system. Thus, for a binary system there may be some hope, if a mean velocity frame is used. However, the continuity equation for mean velocity frames (4.3) involves the term $\bar{v}^{RL}$ which complicates the solution.

As a consequence of these considerations, the overwhelming majority of diffusion studies has been restricted to binary systems. Generally, a mean velocity frame is chosen to limit the number of unknown diffusion coefficients to one. In addition, simplifying assumptions are made that lead to the conclusion that $\bar{v}^{RL} = 0$. In such cases the laboratory frame, L, would coincide with the mean velocity frame, R, and the continuity equation is correspondingly simplified to the form of (4.2). The most commonly used assumption is that there is no overall volume change during the diffusion process. This is equivalent to assuming that $\Delta\bar{V}_{mixing} = 0$ or that V_1 and V_2 are constant, which means that $\bar{v}^{VL} = 0$. Assuming constant volume and using (3.20), the continuity equation (4.6) for the binary case becomes

$$\left(\frac{\partial \rho_1}{\partial t}\right)_{P,T,x} = -\left(\frac{\partial J_1^V}{\partial x}\right)_{P,T,t} = \left[\frac{\partial}{\partial x}\left(D^\circ \left[\frac{\partial \rho_1}{\partial x}\right]_{P,T,t}\right)\right]_{P,T,t}. \quad (4.7)$$

Equation (4.7), which is strictly valid only for constant-volume, binary diffusion, has been solved for specific boundary conditions by Matano (1933) using the methods of Boltzmann (1894). The Boltzmann-Matano solution to (4.7), which may be evaluated using a graphical integration, is typically used by experimentalists to determine D° when D° varies with composition.

If D° can be shown to be independent of position x in the diffusion couple, (4.7) simplifies to

$$\left(\frac{\partial \rho_1}{\partial t}\right)_{P,T,x} = D^\circ \left(\frac{\partial^2 \rho_1}{\partial x^2}\right)_{P,T,t} \quad (4.8)$$

which has many solutions for a great variety of boundary conditions (see Carslaw and Jaeger, 1947; or Crank, 1956). The applicability of (4.8)

may be tested for a given set of boundary conditions by comparing the resulting composition profiles with those predicted by the appropriate analytical solution. Diffusion studies using radioactive tracers are correctly described by (4.8) due to the very small composition changes involved. Solutions to the continuity equation (4.3) for three or more components have been given in analytical form only for systems in which the diffusion coefficients D°_{ij} are independent of composition (for example, Fujita and Gosting, 1956; Kirkaldy, 1959; Oishi, 1965). Application of these solutions to ternary diffusion problems may be found in Miller (1959, 1960), Kirkaldy and Brown (1963), Carmen (1968a, 1968b), Cooper and Varshneya (1968), Varshneya and Cooper (1972a, b, and c), and Gupta and Cooper (1971).

5. $\Delta\bar{V}_{mixing}$ AND THE UNIT CELL FRAME

Unfortunately, there are many interesting two-component systems for which there is an overall volume change during a diffusion process. In these cases, (4.7) is strictly incorrect and, though often used, may be a poor approximation (Greskovich and Stubican, 1970). Correct solutions of (4.3) which allow for volume changes have been obtained by several individuals (Prager, 1953; Crank, 1956, p. 236; Balluffi, 1960; and Wagner, 1969). Each of these solutions makes use of the Boltzmann substitution and solves for D°, as defined in this paper ($D^\circ = D$ of Prager and Balluffi; $D^\circ = D^V$ of Crank (11.73); $D^\circ = \tilde{D}$ of Wagner). Balluffi shows how his solution may be evaluated graphically. Of course, in all cases the molar volumes must be known as a function of composition. In addition, all these papers assume there is no change in the cross-sectional area of the sample normal to the diffusion direction. This assumption, while it has some basis in experiment (da Silva and Mehl, 1951; Resnick and Balluffi, 1955) for fcc metals, has been given no general justification.

An alternative approach was proposed by Hartley and Crank (1949) (reprinted in Crank, 1956, p. 219 and following). They suggested that a modified distance scale (and consequent modified concentration scale) be introduced to preserve the continuity equation in the form of (4.7), even when there is a volume change. If the mathematical form of (4.7) is maintained, then the Boltzmann-Matano approach can be used to obtain the correct solution for D°. An interesting feature of the treatment by Hartley and Crank is that the modified distance scales they proposed coincide with the set of points used to define various mean velocity reference frames. For example, their reference frame based on cross sections "fixed with respect to total mass" can be shown to be identical with the mean mass (barycentric) frame of this paper. In the barycentric case, their modified distance parameter, ξ_M, which is "measured so that equal increments of ξ_M always include equal increments of total mass" is clearly consistent with the definition (2.11) of reference points or cross sections across which there is no *net* mass flux.

The approach of Hartley and Crank is perhaps best illustrated using a modified distance scale for crystals based on the length of a unit cell

edge. For example, if there is a volume change during a diffusion process, it should be clear that the individual unit cell dimensions will vary in a manner proportional to the local volume change. Let us restrict the discussion to crystals with orthorhombic or higher symmetry. Then using the appropriate unit cell edge, say c, to define a distance parameter, $\xi_N{}^c$, ensures that equal increments of $\xi_N{}^c$ involve an equal number of unit cells. It is possible, therefore, to derive a continuity equation similar to (4.7) using the distance parameter $\xi_N{}^c$ and a mass balance argument.

The unit cell of a crystal is a particularly convenient frame of reference for conceptualizing the many diffusion problems for which the total number of unit cells is constant. For a unit cell reference frame to be practical, however, it must be possible to relate diffusion coefficients determined using the unit cell frame to the standard diffusion coefficients, D°_{ij}. This will always be possible if the chemical components used in the description are properly selected (Brady, 1975). Specifically, if components are chosen such that the total number of moles of these components per unit cell is constant, then equal increments of $\xi_N{}^c$ will involve equal numbers of moles as well as equal numbers of unit cells. The distance parameter, $\xi_N{}^c$, therefore, would mark the distances between a set of points that may be used to define a mean molar reference frame, N. The flux of component one across a unit cross section identified with a particular $\xi_N{}^c$ would then be given by $J_1{}^N$ evaluated at that $\xi_N{}^c$. The flux across the ab face of a single unit cell is (ab) $(J_1{}^N)$, where a and b are the cell parameters normal to the diffusion direction.

Let us define the distance parameter, $\xi_N{}^c$, as follows

$$d\xi_N{}^c \equiv \frac{dx}{c} \tag{5.1}$$

where c is the length of the unit-cell edge in the diffusion direction. The modified concentration parameter, $n_i{}^c$, in this case defined as the number of moles of component i per unit cell, is simply the mole fraction N_i times the total number of moles per unit cell:

$$n_i{}^c \equiv N_i \frac{(abc)}{\bar{V}} \tag{5.2}$$

Recalling (3.19) and using (5.1) and (5.2), the flux of component one across the unit-cell face ab is given by

$$(ab)J_1{}^N = -\frac{(ab)}{\bar{V}} D^\circ \left(\frac{\partial N_1}{\partial x}\right)_{P,T,t} = -\frac{D^\circ}{c^2}\left(\frac{\partial n_1{}^c}{\partial \xi_N{}^c}\right)_{P,T,t} \tag{5.3}$$

Equation (5.3) is strictly true only if the total number of moles per unit cell is not a function of composition so that $\bar{V}/(abc)$ is constant. The modified continuity equation can be determined by considering the change in content of component one in the unit cell per unit time in

terms of the divergence of the flux of component one across unit-cell faces ab. The modified continuity equation is

$$\left(\frac{\partial n_1^c}{\partial t}\right)_{P,T,\xi_N^c} = -\left[\frac{\partial}{\partial \xi_N^c}\left((ab)J_1^N\right)\right]_{P,T,t} = \left[\frac{\partial}{\partial \xi_N^c}\left(\frac{D^\circ}{c^2}\left[\frac{\partial n_1^c}{\partial \xi_N^c}\right]_{P,T,t}\right)\right]_{P,T,t} \tag{5.4}$$

or using (5.2)

$$\left(\frac{\partial N_1}{\partial t}\right)_{P,T,\xi_N^c} = \left[\frac{\partial}{\partial \xi_N^c}\left(\frac{D^\circ}{c^2}\left[\frac{\partial N_1}{\partial \xi_N^c}\right]_{P,T,t}\right)\right]_{P,T,t} . \tag{5.5}$$

Equation (5.5) is clearly in the same mathematical form as (4.7). It may be evaluated graphically with the usual Boltzmann-Matano procedure using a plot of N_1 versus ξ_N^c. To obtain ξ_N^c for each position $x = X$, equation (5.1) must be integrated to yield

$$\xi_N^c = \int_0^X \frac{dx}{c} \tag{5.6}$$

where $x = 0$ when $\xi_N^c = 0$ which is at the "Matano interface" defined by

$$\int_{N_1(-\infty)}^{N_1(+\infty)} \xi_N^c \, dN_1 = 0 \tag{5.7}$$

or alternatively by

$$\int_{-\infty}^{0} [N_1(-\infty)-N_1] \, d\xi_N^c = \int_0^{+\infty} [N_1-N_1(+\infty)] \, d\xi_N^c \tag{5.8}$$

where N_1 $(+\infty)$ and N_1 $(-\infty)$ correspond to the compositions far removed from the site of diffusion, as specified by the boundary conditions. Using (5.1), (5.8) becomes

$$\int_{-\infty}^{0}\left[\frac{N_1(-\infty)-N_1}{c}\right] dx = \int_0^{+\infty}\left[\frac{N_1-N_1(+\infty)}{c}\right] dx . \tag{5.9}$$

If there is no change in the cross-sectional area of the sample, that is if the product (ab) is constant, then c may be replaced by $\bar{V}$ in equations (5.1) and (5.5) to obtain the result of Cohen, Wagner, and Reynolds (1953, 1954). Thus, using the unit cell reference frame, a solution for D° may be obtained when there is a $\Delta\bar{V}_{mixing}$ by purely graphical means from the composition-distance profile and knowledge of the cell parameter c as a function of composition.

For monoclinic or triclinic crystals, the situation is more complicated. First of all, the diffusion direction should be parallel to one of the "principal" diffusion axes (Nye, 1957) so that the diffusion flux is one-dimensional. The principal diffusion directions generally will not all coincide with the crystal axes, as is the case with crystals of orthorhombic or higher symmetry, so the modified distance parameter would have to utilize a lattice translation which may not correspond to any commonly used unit cell dimension. However, since angular changes as well as volume changes may occur when the composition varies, the diffusion flux across any one crystallographic plane may not be easily determined. Therefore, the simple approach used here is not directly applicable to monoclinic or triclinic crystals if the crystallographic angles α, β, and γ change appreciably with composition.

For some common minerals, though, the variations of lattice angles accompanying compositional changes are small. Since diffusion paths are highly structure sensitive, it is probably valid to assume for these minerals that the variations in orientation of the principal diffusion directions are also small. Thus, it may be a very good approximation to treat these crystals in the manner discussed above, selecting distance parameters based on lattice translations parallel to the principal diffusion directions. The "unit cell" in this case may not correspond to any unit cell normally used. While only an approximation, this approach may yield reasonable results for some otherwise complex monoclinic or triclinic minerals.

6. INERT MARKER REFERENCE FRAME

Observations by Kirkendall (1942), Smiegelskas and Kirkendall (1947), and Hartley (1946) combined with subsequent analyses by Darken (1948) and Hartley and Crank (1949) have led to the definition of a reference frame and associated diffusion coefficients different from any yet considered in this paper. Deeply involved in the definition of this additional reference frame is the question, "What is diffusion?" or "Is all the flux measured in a given reference frame appropriately called 'diffusive flux'?". These questions were raised, and answers were clearly presented by both Darken (1948) and Hartley and Crank (1949). The conclusion reached in both papers was that a distinction should be made between a flux due to "diffusion" of an individual component relative to the others and a flux due to the "bulk flow" of all components at the same rate in the same direction. This distinction is of considerable practical importance, for Hartley's and Kirkendall's experiments demonstrated that if one component diffuses more rapidly than the other in a binary interdiffusion experiment, a bulk flow will occur. As the concept of a bulk flow generated by diffusion can be confusing, I strongly recommend the excellent discussions by Darken (1948) and Hartley and Crank (1949) to any reader who finds this concept unfamiliar.

In order to measure flux due to diffusion only, a reference frame is defined in terms of a set of points, each of which moves with the local bulk flow. Operationally, this would consist of a set of "inert" markers,

which do not participate in the diffusion, but which will move with the bulk flow. For Kirkendall, these inert markers were platinum wires in a copper-brass diffusion couple. We can define, then, inert marker diffusion coefficients, $D_{ij}^{I,C}$, in terms of the fluxes, J_i^I, given with respect to the inert marker reference frame, I, as

$$J_i^I = -\sum_{j=1}^{n} D_{ij}^{I,C} \left(\frac{\partial C_j}{\partial x}\right)_{P,T,t} \qquad (i = 1,2,\ldots,n) \tag{6.1}$$

where C_j is some compositional parameter. As in the case of the laboratory frame (4.1), there is, in general, no relation similar to (2.5) which relates the n independent fluxes of the inert marker frame. Inert marker diffusion coefficients have been called "intrinsic" diffusion coefficients by Hartley and Crank (1949) and others. However, the title inert marker coefficient is to be preferred since the term "intrinsic" is also commonly used to describe diffusion in pure crystals in the absence of "extrinsic" effects due to impurities, grain boundaries, et cetera.

It will be useful to relate the inert marker diffusion coefficients, $D_{ij}^{I,C}$, to the standard diffusion coefficients, D°_{ij}, defined in (3.10). Recalling (2.6) we have

$$J_i^N = J_i^I + \rho_i \bar{v}^{IN} \tag{6.2}$$

Summing both sides of (6.2) over all i and using (2.8), $\bar{v}^{IN}$ may be expressed in terms of the J_i^I. Substituting the results for $\bar{v}^{IN}$ in (6.2) we have

$$J_i^N = J_i^I - N_i \left[\sum_{j=1}^{n} J_j^I\right] . \tag{6.3}$$

For a two component system, then,

$$J_1^N = J_1^I - N_1 (J_1^I + J_2^I) = N_2 J_1^I - N_1 J_2^I \tag{6.4}$$

Substituting for J_1^N from (3.19) and for J_i^I from (6.1), (6.4) becomes

$$\frac{-\bar{V}}{V_2} D^\circ \left(\frac{\partial \rho_1}{\partial x}\right)_{P,T,t} = N_2 \left[-D_{11}^{I,\rho}\left(\frac{\partial \rho_1}{\partial x}\right)_{P,T,t} - D_{12}^{I,\rho}\left(\frac{\partial \rho_2}{\partial x}\right)_{P,T,t}\right] - N_1\left[-D_{21}^{I,\rho}\left(\frac{\partial \rho_1}{\partial x}\right)_{P,T,t} - D_{22}^{I,\rho}\left(\frac{\partial \rho_2}{\partial x}\right)_{P,T,t}\right] \tag{6.5}$$

Using the thermodynamic relation

$$\left(\frac{\partial \rho_2}{\partial \rho_1}\right)_{P,T} = -\frac{V_1}{V_2} \tag{6.6}$$

equation (6.5) leads to

$$\frac{D^\circ \bar{V}}{V_2} = N_2\left[D_{11}^{I,\rho} - \frac{V_1}{V_2} D_{12}^{I,\rho}\right] - N_1\left[D_{21}^{I,\rho} - \frac{V_1}{V_2} D_{22}^{I,\rho}\right]. \tag{6.7}$$

If we then take the traditional approach and neglect $D_{12}^{I,\rho}$ and $D_{21}^{I,\rho}$, we obtain the relation

$$D^\circ = (\rho_2 V_2)D_{11}^{I,\rho} + (\rho_1 V_1)D_{22}^{I,\rho} \tag{6.8}$$

which was given by Hartley and Crank (1949, eq 31) for the case of constant volume, an assumption we have not made. Actually, Hartley and Crank's D^V is equivalent to D° in all respects except their conception of it. They stated that their D^V is meaningless, if there is an overall volume change. However, mathematically their D^V has meaning for all systems. Compare their equation (4) with equation (2.9) of this paper. A relation similar to (6.8) was also obtained by Darken (1948, eq 7)

$$D^\circ = N_2 D_{11}^{I,\rho} + N_1 D_{22}^{I,\rho} \tag{6.9}$$

which follows from (6.8) if $V_1 = V_2 = \bar{V}$.

Although (6.1) is consistent with the classical definition of inert marker diffusion coefficients, I prefer the following alternative definition

$$J_i^I = \sum_{j=1}^{n} \frac{D_{ij}^{I,N}}{\bar{V}} \left(\frac{\partial N_j}{\partial x}\right)_{P,T,t} \tag{6.10}$$

This definition leads to simpler mathematical forms for several important relationships. For example, let us relate the diffusion coefficients $D_{ij}^{I,N}$ to the standard diffusion coefficient D° for a two component system. Using (3.19) and (6.10) equation (6.4) becomes

$$\begin{aligned} -\frac{D^\circ}{\bar{V}}\left(\frac{\partial N_1}{\partial x}\right)_{P,T,t} = {} & N_2\left[\frac{-D_{11}^{I,N}}{\bar{V}} + \frac{D_{12}^{I,N}}{\bar{V}}\right]\left(\frac{\partial N_1}{\partial x}\right)_{P,T,t} \\ & -N_1\left[\frac{-D_{21}^{I,N}}{\bar{V}} + \frac{D_{22}^{I,N}}{\bar{V}}\right]\left(\frac{\partial N_1}{\partial x}\right)_{P,T,t} \end{aligned} \tag{6.11}$$

from which it follows that

$$D^\circ = N_2\,[D_{11}^{I,N} - D_{12}^{I,N}] + N_1[D_{22}^{I,N} - D_{21}^{I,N}] \tag{6.12}$$

If we then define D_1^I and D_2^I as

$$\left.\begin{aligned} D_1^I &\equiv D_{11}^{I,N} - D_{12}^{I,N} \\ D_2^I &\equiv D_{22}^{I,N} - D_{21}^{I,N} \end{aligned}\right\} \tag{6.13}$$

(6.12) may be written as

$$D^\circ = N_2 D_1^I + N_1 D_2^I \tag{6.14}$$

Equation (6.14), which has the simple form of Darken's relation (6.9), is valid even if $V_1 \neq V_2$ and also if $D_{12}^{I,N}$ and $D_{21}^{I,N}$ are not negligible.

In order to obtain the values of the diffusion coefficients D_1^I and D_2^I in (6.14) a measurement of D° is necessary. This is not sufficient, however: a measurement of the velocity, $\bar{v}^{IN}$, of the inert marker frame relative to

Reference f

the mean molar frame is n
(6.3), using also (6.10) and (

$$\bar{v}^{IN} = -\bar{V}\left[\sum_{i=1}^{n} J_i^I\right.$$

$$\bar{v}^{IN} =$$

Darken (1948) derived a fo
$V_2 = \bar{V}$ and, therefore, $\bar{v}^{NL}$
(6.14) to solve for D_1^I and I
of D° (as in the last section)
position and time, the veloc
(relative to the laboratory fr
urements, at several times.
velocity is then compared w
erence frame at the same pos

In a binary interdiffusi
cross sections that define the
in a fashion similar to that
(5.9). Indeed, the Matano in
section. That this is true m
that the $x = 0$, $\xi_N^c = 0$ cross
of atoms across the cross sec
flux of atoms across the cros
sections across which the cu
ance are given by

or

$$\int_{-\infty}^{0}\left[\frac{N_1(-\infty) - N_1}{c}\right.$$

where k is a constant, differ
and (6.18) define an $x = 0$, ξ_N^c
cross section (see fig. 1). Thus,
k for the mean molar refere
the inert marker used to dete
determines $\bar{v}^{NL}$ for the mean
series of calculations at sever
natively, one could use (5.6)

the mean molar frame is needed for the following relation (see (6.2) and (6.3), using also (6.10) and (6.13)):

$$\bar{v}^{IN} = -\bar{V}\left[\sum_{i=1}^{n} J_i^I\right] = D_1^I\left(\frac{\partial N_1}{\partial x}\right)_{P,T,t} + D_2^I\left(\frac{\partial N_2}{\partial x}\right)_{P,T,t} \quad (6.15)$$

$$\bar{v}^{IN} = \left(D_1^I - D_2^I\right)\left(\frac{\partial N_1}{\partial x}\right)_{P,T,t} \quad (6.16)$$

Darken (1948) derived a form of (6.16) for the special case where $V_1 = V_2 = \bar{V}$ and, therefore, $\bar{v}^{NL} = \bar{v}^{VL} = 0$. Equation (6.16) may be used with (6.14) to solve for D_1^I and D_2^I at a given composition from measurements of D° (as in the last section) and $\bar{v}^{IN}$ (as follows). To obtain $\bar{v}^{IN}$ at a single position and time, the velocity of a marker, $\bar{v}^{IL}$, at that position and time (relative to the laboratory frame) must be determined by a series of measurements, at several times, of the position of the marker. The marker velocity is then compared with the velocity, $\bar{v}^{NL}$, of the mean molar reference frame at the same position and time.

In a binary interdiffusion experiment, the location of the points or cross sections that define the mean molar reference frame may be obtained in a fashion similar to that used to locate the "Matano interface" (5.7) or (5.9). Indeed, the Matano interface itself is a mean molar reference cross section. That this is true may be seen from (5.7) or (5.9) which require that the $x = 0$, $\xi_N^c = 0$ cross section be one such that the cumulative flux of atoms across the cross section in one direction equals the cumulative flux of atoms across the cross section in the other direction. Other cross sections across which the cumulative atom fluxes in both directions balance are given by

$$\int_{N_1(-\infty)}^{N_1(+\infty)} \xi_N^c \, dN_1 = k \quad (6.17)$$

or

$$\int_{-\infty}^{0}\left[\frac{N_1(-\infty) - N_1}{c}\right] dx = \int_{0}^{+\infty}\left[\frac{N_1 - N_1(+\infty)}{c}\right] dx + k \quad (6.18)$$

where k is a constant, different for each cross section. Equations (6.17) and (6.18) define an $x = 0$, $\xi_N^c = 0$ plane which is a mean molar reference cross section (see fig. 1). Thus, to evaluate $\bar{v}^{IN}$, one needs to determine the k for the mean molar reference plane which coincides in position with the inert marker used to determine $\bar{v}^{IL}$ at the appropriate time. One then determines $\bar{v}^{NL}$ for the mean molar plane identified with that k by a series of calculations at several times of the position of that plane. Alternatively, one could use (5.6) and (5.9) to locate the plane associated with

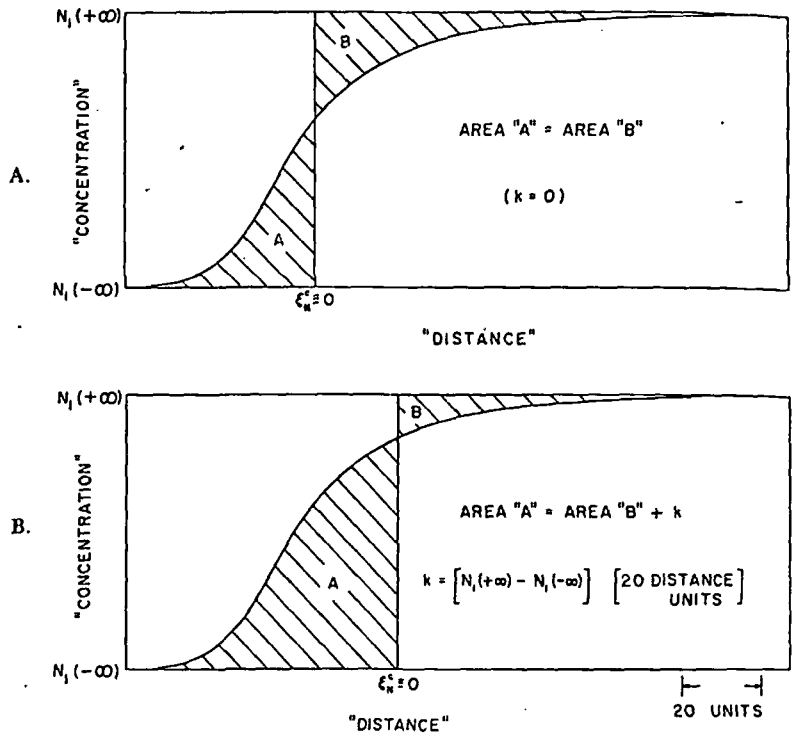

Fig. 1. "Concentration" versus "distance" profile for a binary interdiffusion experiment with the "Matano interface" of equation (5.11) shown in (A) and a mean molar plane k of equation (6.18) shown in (B) with $k = [N_i(+\infty) - N_i(-\infty)] \times$ [20 distance units].

a given ξ_N^c at various times, which would involve more effort than using (6.18).

7. DARKEN'S EQUATION AND TRACER DIFFUSION COEFFICIENTS

There is reason to believe that the inert marker frame coefficients presented above are in some ways more "fundamental" than the mean velocity frame diffusion coefficients; hence, the often used name "intrinsic" diffusion coefficients (suggested by Hartley and Crank, 1949). The argument is based on the assumption that the principal effect of the motion of one component upon the motion of another component is the flux due to bulk flow. Therefore, if the effect of a bulk flow is eliminated by using an inert marker frame, then the flux of a component might be expected to depend only upon gradients of its own chemical potential. In other words, an assumption is made that the off-diagonal terms in the phenomenological equations (3.1) are necessary *only* to account for flux due to bulk flow.

The validity and consequences of the assumption of negligible off-diagonal ($i \neq j$) phenomenological coefficients, L_{ij}^I, for the inert marker frame have been discussed by many individuals (Bardeen and Herring,

Reference

1951; LeClaire, 1953; Mau
Lidiard, 1964; Ziebold an
sensus is that the assumpti
tion for many systems. Ca
nation for "complex Dar
present in more than one
istic approach to demon
correct for diffusion in so
estimated errors that migl
in the inert marker frame
ment on many solids or
mind, it is worthwhile t
sumption.

Two isotopes of the
electron shells surroundi
two isotopes behave ident
it is not unreasonable to
sponse to an identical che
be the same (in the absen
expressed by Darken (19
the velocity of a compone
tion (3.1), B_i^I is defined a

$$J_i^I = -L_i^I \left($$

and Darken's equality wo

where the * refers to a ra

The next step is to
a tracer "self-diffusion"
element) with the inert
relate the mobilities, B_i^I
ing (6.10) for a two com
comparison with (7.1)

$$J_i^I = -B_i^I \left($$

and

$$D_i^I = B_i^I N_i$$

The molar chemical pot

where γ_i is the activity

1951; LeClaire, 1953; Manning, 1961, 1968; Shewmon, 1963; Howard and Lidiard, 1964; Ziebold and Cooper, 1965; Carmen, 1968a, b). The consensus is that the assumption is not correct but may be a good approximation for many systems. Carmen (1968a, b) argues that it is a poor approximation for "complex Darken systems" where a single component may be present in more than one diffusing species. Manning (1968) uses an atomistic approach to demonstrate that the assumption cannot be strictly correct for diffusion in solids by a vacancy mechanism. Nevertheless, the estimated errors that might be caused by neglecting the off-diagonal terms in the inert marker frame are within the range of uncertainty of measurement on many solids or other "simple Darken systems". With this in mind, it is worthwhile to explore a very useful consequence of the assumption.

Two isotopes of the same element are chemically quite similar. The electron shells surrounding each of the slightly different nucleii of the two isotopes behave identically in many interactive situations. Therefore, it is not unreasonable to assume that the motion of either isotope in response to an identical chemical force (chemical potential gradient) would be the same (in the absence of gravitational effects). This assumption was expressed by Darken (1948) as an equality of mobilities, B_i^I, which give the velocity of a component in response to a unit force. In terms of equation (3.1), B_i^I is defined as follows (neglecting the off-diagonal coefficients):

$$J_i^I = -L_i^I \left(\frac{\partial \mu_i}{\partial x}\right)_{P,T,t} = -B_i^I \left(\frac{N_i}{\bar{V}}\right)\left(\frac{\partial \mu_i}{\partial x}\right)_{P,T,t} \tag{7.1}$$

and Darken's equality would be

$$(B_i^I)^* = B_i^I \tag{7.2}$$

where the * refers to a radioactive isotope of component i.

The next step is to compare the diffusion coefficient determined in a tracer "self-diffusion" experiment (mixing of two isotopes of the same element) with the inert marker coefficients (6.13). To do this we must relate the mobilities, B_i^I, to the inert marker diffusion coefficients. Writing (6.10) for a two component system and using (6.13) we obtain upon comparison with (7.1)

$$J_i^I = -B_i^I \left(\frac{N_i}{\bar{V}}\right)\left(\frac{\partial \mu_i}{\partial x}\right)_{P,T,t} = -\frac{D_i^I}{\bar{V}}\left(\frac{\partial N_i}{\partial x}\right)_{P,T,t} \tag{7.3}$$

and

$$D_i^I = B_i^I N_i \left(\frac{\partial \mu_i}{\partial N_i}\right)_{P,T} = B_i^I \left(\frac{\partial \mu_i}{\partial \ln N_i}\right)_{P,T} \tag{7.4}$$

The molar chemical potential, μ_i, is related to the mole fraction, N_i, by

$$\mu_i = \mu_i^\circ + RT \ln N_i \gamma_i \tag{7.5}$$

where γ_i is the activity coefficient necessary to correct for non-ideality.

Using (7.5) to evaluate (7.4) we have:

$$D_1^I = B_1^I RT\left[\frac{\partial \ln(N_1\gamma_1)}{\partial \ln N_1}\right]_{P,T} = B_1^I RT\left[1+\left(\frac{\partial \ln\gamma_1}{\partial \ln N_1}\right)_{P,T}\right]. \quad (7.6)$$

In a tracer "self-diffusion" measurement, there is, ideally, only mixing of isotopes of the same element. For isotopic mixing, which is chemically ideal, (7.6) becomes:

$$(D_1^I)^* = (B_1^I)^* RT \quad . \quad (7.7)$$

Since the mole fraction of the minor isotope in a tracer self-diffusion experiment is very small, the diffusion coefficient measured, D°, will be equal to the intrinsic diffusion coefficient of the tracer, $(D_1^I)^*$, (see 6.14). This is strictly true only in the binary isotopic end member systems. For a detailed phenomenological discussion, see Howard and Lidiard (1964, p. 207 and following). Using (7.2), (7.6), and (7.7), then, we obtain the desired relation

$$D_1^I = (D_1^I)^*\left[1+\left(\frac{\partial \ln\gamma_1}{\partial \ln N_1}\right)_{P,T}\right] \quad . \quad (7.8)$$

Using the identity

$$\left[\frac{\partial \ln\gamma_1}{\partial \ln N_1}\right]_{P,T} = \left[\frac{\partial \ln\gamma_2}{\partial \ln N_2}\right]_{P,T} \quad (7.9)$$

which follows from (7.5) and the Gibbs-Duhem equation (3.3), we may substitute (7.8) into (6.14) to obtain a version of Darken's equation (1948, eq 18)

$$D^\circ = \left[N_2(D_1^I)^* + N_1(D_2^I)^*\right]\left[1+\left(\frac{\partial \ln\gamma_1}{\partial \ln N_1}\right)_{P,T}\right] \quad . \quad (7.10)$$

The practical importance of (7.10) is great indeed. To the extent that (7.10) is correct, measurements of diffusion coefficients using radioactive tracers may be used to predict binary interdiffusion behavior. This is particularly important for those interested in determining diffusion coefficients which are very small, for example, in minerals at metamorphic temperatures. This is a result of the fact that small concentrations of a radioactive isotope may be detected with considerably more precision than small concentrations of non-radioactive species.

8. IONIC CRYSTALS

Crystals that have an appreciable ionic character such as halides, oxides, and silicates present some additional constraints which have not been considered above. Specifically, the strict stoichiometry required to maintain electrical neutrality leads to a coupling of fluxes for an interdiffusion experiment in an ionic crystal. Nevertheless, nearly all the results given above are valid for ionic crystals if the components used in the

Reference fr

description are *actual* comp
ponents of a crystal may be
without destroying the hon
Thompson, 1959; Brady, 19
any actual component of
Therefore, the constraints
automatically satisfied in ar
The results of section 7, h
particular, Darken's equatic
shall now consider.

In ionic crystals either
move, rarely both (Jost, 19
shall consider the motion
results are equally applicat
the anions do not diffuse.
most ionic crystals the iner
unit cell reference frame
judicious choice of compon
sion coefficients (6.13) for
This means that there will
ionic crystals and that the
with the initial crystal-cryst

In section 7 a relation
cients and the standard bi
lating inert marker diffusio
same approach cannot be v
two inert marker coefficient
that the self-diffusion coef
crystal must be equal. Exp
so equation (7.8) must not
steps followed in obtaining
is in error for ionic crystal
has been neglected, the for
ometry. Since the mobility,
to a unit force, (7.1) cannot

It is not unreasonable
chiometry in ionic crystals
would develop if any devi
sponse of a diffusing specie
tional to both its charge,

species i in response to an a

$$J_i^I = -$$

description are *actual* components of the crystal considered. Actual components of a crystal may be both added to and subtracted from a crystal without destroying the homogeneity of that crystal (Gibbs, 1928, p. 64; Thompson, 1959; Brady, 1975). In the absence of external electric fields, any actual component of a given crystal must be electrically neutral. Therefore, the constraints of stoichiometry or electrical neutrality are automatically satisfied in any description, if actual components are used. The results of section 7, however, are not correct for ionic crystals. In particular, Darken's equation (7.10) is subject to modifications, which we shall now consider.

In ionic crystals either the positive ions move or the negative ions move, rarely both (Jost, 1952). Therefore, in the following discussion we shall consider the motion of cations in a network of stationary anions; results are equally applicable to the opposite case of mobile anions. If the anions do not diffuse, then they will behave as inert markers. So for most ionic crystals the inert marker reference frame will coincide with the unit cell reference frame and also with the mean molar frame (for a judicious choice of components). Therefore, the two inert marker diffusion coefficients (6.13) for a binary system must be identical (see 6.16). This means that there will be no "Kirkendall effect" for interdiffusion in ionic crystals and that the Matano (1933) interface will always coincide with the initial crystal-crystal interface, even if there is a $\Delta\bar{V}_{\text{mixing}}$.

In section 7 a relationship (7.10) between tracer self-diffusion coefficients and the standard binary diffusion coefficient was obtained by relating inert marker diffusion coefficients to self-diffusion coefficients. The same approach cannot be valid for ionic crystals, since the equality of the two inert marker coefficients combined with equation (7.8) would imply that the self-diffusion coefficients for the two components of a binary crystal must be equal. Experimentally, this is not the case (Askill, 1970), so equation (7.8) must not be valid for ionic crystals. A scrutiny of the steps followed in obtaining (7.8) will reveal that it is equation (7.1) that is in error for ionic crystals. The reason (7.1) is incorrect is that a force has been neglected, the force that prevents any deviations from stoichiometry. Since the mobility, B_i^I, gives the velocity of diffusion in response to a unit force, (7.1) cannot be correct if all the forces are not considered.

It is not unreasonable to assume that the force that maintains stoichiometry in ionic crystals is the large electrical potential gradient that would develop if any deviations from stoichiometry did occur. The response of a diffusing species to an electrical potential gradient is proportional to both its charge, q_i, and its mobility, B_i^I, so that the flux of species i in response to an applied field $\left(\frac{\partial \phi}{\partial x}\right)_{P,T,t}$ would be

$$J_i^I = -B_i^I \left(\frac{N_i}{\bar{V}}\right) q_i \left(\frac{\partial \phi}{\partial x}\right)_{P,T,t} \qquad (8.1)$$

(Jost, 1952). The flux of species i in response to both an electrical potential gradient and a chemical potential gradient is then

$$J_i^I = -B_i^I \left(\frac{N_i}{\bar{V}}\right)\left[\left(\frac{\partial \mu_i}{\partial x}\right)_{P,T,t} + q_i\left(\frac{\partial \phi}{\partial x}\right)_{P,T,t}\right] \quad . \qquad (8.2)$$

Assuming that (8.2) includes all the appropriate forces we might proceed as in section 7 to find a relationship similar to (7.10). Unfortunately, there is one further stumbling block. The chemical potential gradient indicated in (8.2) must be written for a charged species, since it is only for the motion of a charged species that (8.2) is needed to replace (7.1). However, the chemical potential of a charged species in a stoichiometric ionic crystal is an undefined quantity. This dilemma may be resolved by considering explicitly the possibility of vacancies and nonstoichiometry (see Howard and Lidiard, 1964) or by making a simplifying assumption that will lead to a result that may be tested experimentally. We will take the latter approach here, manipulating the chemical potentials of charged species as if they were meaningful and then expressing the result in terms of measurable quantities.

Let us begin by considering a general binary ionic crystal composed of various combinations of two cations, A^{+a} and B^{+b}, and a single anion or negatively charged component Z^{-z}. We shall explicitly include the charges +a, +b, and −z to allow for the possibility of the cations having different charges. This binary ionic crystal will have actual components $A_z Z_a$ and $B_z Z_b$ where the subscripts indicate the number of moles of the cations and anions in one mole of the component. An alkali feldspar would be an example of a binary "ionic" crystals with $A^{+a} = K^{+1}$, $B^{+b} = Na^{+1}$, $Z^{-z} = (AlSi_3O_8)^{-1}$, and actual components $KAlSi_3O_8$ and $NaAlSi_3O_8$. Wustite would be another example (different in the respect that $+a \neq +b$) with $A^{+a} = Fe^{+2}$, $B^{+b} = Fe^{+3}$, $Z^{-z} = O^{-2}$, and actual components Fe_2O_2 and Fe_2O_3.

If the crystal is in local homogeneous equilibrium, the following relations must be satisfied (Prigogine and Defay, 1954, p. 69)

$$\mu_{A_z Z_a} = z\mu_{A+a} + a\mu_{Z-z} \qquad (8.3)$$

$$\mu_{B_z Z_b} = z\mu_{B+b} + b\mu_{Z-z} \quad . \qquad (8.4)$$

We have also from (3.3)

$$N_{A_z Z_a}\, d\mu_{A_z Z_a} + N_{B_z Z_b}\, d\mu_{B_z Z_b} = 0 \quad . \quad . \quad . \qquad (8.5)$$

If we assume that the chemical potential of Z^{-z} is not a function of composition, then (8.3), (8.4), and (8.5) lead to

$$\left(\frac{\partial \mu_{A+a}}{\partial x}\right)_{P,T,t} = \frac{1}{z}\left(\frac{\partial \mu_{A_z Z_a}}{\partial x}\right)_{P,T,t} = -\left[\frac{N_{B_z Z_b}}{N_{A_z Z_a}}\right]\left(\frac{\partial \mu_{B+b}}{\partial x}\right)_{P,T,t} \quad . \qquad (8.6)$$

The validity of the assumption leading to (8.6) is discussed by Cooper and Heasley (1966). See also Wagner (1930) and Jost (1952, p. 146).

Let us simplify the notation slightly by letting $AZ = A_z Z_a$, $BZ = B_z Z_b$, $A = A^{+a}$, and $B = B^{+b}$. Then using (8.6), (8.2) may be written for the fluxes of A and B, respectively

$$J_A^I = -B_A^I \left(\frac{zN_{AZ}}{\bar{V}}\right)\left[\frac{1}{z}\left(\frac{\partial \mu_{AZ}}{\partial x}\right)_{P,T,t} + a\left(\frac{\partial \phi}{\partial x}\right)_{P,T,t}\right] \quad (8.7)$$

$$J_B^I = +B_B^I \left(\frac{zN_{BZ}}{\bar{V}}\right)\left[\frac{1}{z}\left(\frac{N_{AZ}}{N_{BZ}}\right)\left(\frac{\partial \mu_{AZ}}{\partial x}\right)_{P,T,t} - b\left(\frac{\partial \phi}{\partial x}\right)_{P,T,t}\right] \quad (8.8)$$

where we have used the fact that the density of A is z times the density of AZ. Due to the constraint of electrical neutrality, the fluxes of A and B with respect to the unit cell frame (= inert marker frame) must satisfy the relation

$$aJ_A^I + bJ_B^I = 0 \quad (8.9)$$

Using (8.9), (8.7) and (8.8) may be solved for $\left(\frac{\partial \phi}{\partial x}\right)_{P,T,t}$ yielding

$$\left(\frac{\partial \phi}{\partial x}\right)_{P,T,t} = \left(\frac{N_{AZ}}{z}\right)\frac{(bB_B^I - aB_A^I)}{(a^2 N_{AZ} B_A^I + b^2 N_{BZ} B_B^I)}\left(\frac{\partial \mu_{AZ}}{\partial x}\right)_{P,T,t} \quad (8.10)$$

Substituting (8.10) into (8.7), it follows that

$$J_A^I = -\left(\frac{N_{AZ}}{\bar{V}}\right)\frac{(B_A^I B_B^I)(b)(aN_{AZ} + bN_{BZ})}{[a^2 N_{AZ} B_A^I + b^2 N_{BZ} B_B^I]}\left(\frac{\partial \mu_{AZ}}{\partial x}\right)_{P,T,t} \quad (8.11)$$

In order to express the final results completely in terms of actual components, note that stoichiometry requires

$$J_A^I = zJ_{AZ}^I \quad (8.12)$$

and that (8.3) requires (since $v_A^I = v_{AZ}^I$)

$$B_A^I = zB_{AZ}^I \quad (8.13)$$

Combining (8.11), (8.12), and (8.13) then

$$J_{AZ}^I = -\left(\frac{N_{AZ}}{\bar{V}}\right)\frac{(B_{AZ}^I B_{BZ}^I)(b)(aN_{AZ} + bN_{BZ})}{[a^2 N_{AZ} B_{AZ}^I + b^2 N_{BZ} B_{BZ}^I]}\left(\frac{\partial \mu_{AZ}}{\partial x}\right)_{P,T,t} \quad (8.14)$$

or using (7.2), (7.5), and (7.7) (which are still valid even though (7.1) is not)

$$J_{AZ}^I = \frac{-1}{\bar{V}}\frac{(D_{AZ}^I)^*(D_{BZ}^I)^*(b)(aN_{AZ} + bN_{BZ})}{[a^2 N_{AZ}(D_{AZ}^I)^* + b^2 N_{BZ}(D_{BZ}^I)^*]}\left[1 + \left(\frac{\partial \ln \gamma_{AZ}}{\partial \ln N_{AZ}}\right)_{P,T}\right]\left(\frac{\partial N_{AZ}}{\partial x}\right)_{P,T,t} \quad (8.15)$$

Finally we must note that the mean molar reference frame for components $A_z Z_a$ and $B_z Z_b$ does *not* coincide with the unit cell frame (= inert marker frame), although the mean molar frame for components

$A_{bz}\,Z_{ab}$ and $B_{az}\,Z_{ab}$ does (see sec. 5). Using (3.19) written for these latter components and performing a simple component transformation (Brady, 1975), we obtain

$$J_{AZ}^{I} = \frac{-b}{(aN_{AZ} + bN_{BZ})} \frac{D^{\circ}}{\nabla} \left(\frac{\partial N_{AZ}}{\partial x}\right)_{P,T,t} \quad (8.16)$$

On comparing (8.15) and (8.16) it follows that

$$D^{\circ} = \frac{(D_{AZ}^{I})^{*}\,(D_{BZ}^{I})^{*}\,(aN_{AZ} + bN_{BZ})^{2}}{[a^{2}N_{AZ}\,(D_{AZ}^{I})^{*} + b^{2}N_{BZ}\,(D_{BZ}^{I})^{*}]} \left[1 + \left(\frac{\partial \ln \gamma_{AZ}}{\partial \ln N_{AZ}}\right)_{P,T}\right] \quad (8.17)$$

which is the relation we have been looking for. If a = b then (8.17) reduces to the simple form

$$D^{\circ} = \frac{(D_{AZ}^{I})^{*}\,(D_{BZ}^{I})^{*}}{[N_{AZ}\,(D_{AZ}^{I})^{*} + N_{BZ}\,(D_{BZ}^{I})^{*}]} \left[1 + \left(\frac{\partial \ln \gamma_{AZ}}{\partial \ln N_{AZ}}\right)_{P,T}\right] \quad (8.18)$$

as given in Manning (1968, p. 21).

Equations (8.17) and (8.18) have the potential to perform the same important function for ionic crystals that Darken's equation (7.10) performs for metallic crystals: relating relatively easy to measure self-diffusion coefficients to relatively hard to measure interdiffusion coefficients. Equation (8.17) is only an approximation, though, subject to the validity of (8.6). Unfortunately, I know of no experimental verification of (8.17), so it should be used with caution. Equation (7.10), on the other hand, is clearly incorrect for ionic crystals, although it is commonly used for ionic crystals in the literature (for example, Buening and Buseck, 1973, p. 6856; Wei and Wuensch, 1973, p. 564). Cooper and Heasley (1966) give a relation (their eq 14) similar to equation (8.15) but not identical with it. I believe their equation (14) to be incorrect, and Cooper agrees (personal commun., 1974).

Unfortunately, not all binary ionic crystals are suited to the above analysis. Consider, for example, the binary system of the plagioclase feldspars ($NaAlSi_3O_8$–$CaAl_2Si_2O_8$). Interdiffusion in this system involves the exchange of Na and Si for Ca and Al. While we might measure the tracer diffusion coefficients of Ca or Al, there is no way to ensure that doped Ca and Al remain coupled in a tracer experiment in anorthite as they must in an interdiffusion experiment between anorthite and albite. One simplification, which might be useful in practice, would be to assume that the motion of the coupled pair CaAl is limited by the motion of Al, measure the diffusion of an Al isotope, and proceed as in (8.17).

9. CONCLUDING REMARKS

Several points made in the preceding paragraphs deserve reiteration. (1) Fluxes and diffusion coefficients are meaningless quantities unless referred to a specific reference frame. (2) Certain reference frames are preferred for common usage due to the ease with which they may be interrelated; mean velocity frames are particularly convenient. (3) All diffusion data should be reported in terms of "standard" diffusion coefficients

Refe

based on the mean v
significant in many
crystals using a unit
used to predict inte
crystals is different th

The discussion a
many of the results
frame can be particu
in natural polycryst
generally lack comple
so that a laboratory fr
starting configuration
some of the other refe
Thompson, 1975).

Special thanks be
F. Hays, Alan B. Tho
discussions on diffusi
of the paper were
George W. Fisher. Th
mittee on Experimen

Askill, J., 1970, Tracer di
IFI/Plenum, 107 p.
Balluffi, R. W., 1960, On
sion: Acta Metall., v.
Bardeen, J., and Herring
Atom Movements: Cl
Boltzmann, L., 1894, Zur
coefficienten: Ann. Ph
Brady, J. B., 1975, Chemic
Buening, D. K., and Buse
phys. Research, v. 78,
Carmen, P. C., 1968a, Int
isothermal diffusion,
1712.
———— 1968b, Intrins
thermal diffusion, 1
p. 1713-1721.
Carslaw, H. S., and Jaeg
Univ. Press, 386 p.
Cohen, M., Wagner, C., a
cients when volume
v. 197, p. 1534-1536.
———— 1954, Author's
volume changes occu
Cooper, A. R., and Heasl
fusion in ceramics: An
Cooper, A. R., and Varsh
effective binary diffusi
Crank, J., 1956, The math
Darken, L. S., 1948, Diffu
binary metallic syste
201.

based on the mean volume reference frame. (4) Volume changes may be significant in many diffusion processes and can be handled for single crystals using a unit cell reference frame. (5) Self-diffusion data may be used to predict interdiffusion behavior; the approximation for ionic crystals is different than for metallic crystals.

The discussion above has emphasized diffusion in single crystals, but many of the results are not so restricted. Indeed, selecting a reference frame can be particularly important for geologists considering diffusion in natural polycrystalline materials. For example, metasomatic zones generally lack complete information on the initial distribution of material so that a laboratory frame is unavailable. However, assumptions about the starting configuration and diffusion process may still be evaluated using some of the other reference frames considered in this paper (for example, Thompson, 1975).

ACKNOWLEDGMENTS

Special thanks belong to R. James Kirkpatrick, John M. Ferry, James F. Hays, Alan B. Thompson, and Steven M. Richardson for many helpful discussions on diffusion topics and comments on this paper. Early drafts of the paper were also considerably improved by the suggestions of George W. Fisher. This work is published under the auspices of the Committee on Experimental Geology and Geophysics at Harvard University.

REFERENCES

Askill, J., 1970, Tracer diffusion data for metals, alloys, and simple oxides: New York, IFI/Plenum, 107 p.

Balluffi, R. W., 1960, On the determination of diffusion coefficients in chemical diffusion: Acta Metall., v. 8, p. 871-873.

Bardeen, J., and Herring, C., 1951, Diffusion in alloys and the Kirkendall effect, *in* Atom Movements: Cleveland, Am. Soc. for Metals, p. 87-111.

Boltzmann, L., 1894, Zur Integration der Diffusionsgleichung bei variabeln Diffusionscoefficienten: Ann. Physik, v. 53, p. 959-964.

Brady, J. B., 1975, Chemical components and diffusion: Am. Jour. Sci., v. 275, in press.

Buening, D. K., and Buseck, P. R., 1973, Fe–Mg lattice diffusion in olivine: Jour. Geophys. Research, v. 78, p. 6852-6862.

Carmen, P. C., 1968a, Intrinsic mobilities and independent fluxes in multicomponent isothermal diffusion, I. Simple Darken systems: Jour. Phys. Chemistry, v. 72, p. 1707-1712.

———— 1968b, Intrinsic mobilities and independent fluxes in multicomponent isothermal diffusion, II. Complex Darken systems: Jour. Phys. Chemistry, v. 72, p. 1713-1721.

Carslaw, H. S., and Jaeger, J. C., 1947, Conduction of heat in solids: Oxford, Oxford Univ. Press, 386 p.

Cohen, M., Wagner, C., and Reynolds, J. E., 1953, Calculation of interdiffusion coefficients when volume changes occur: Am. Inst. Mining Metall. Engineers Trans., v. 197, p. 1534-1536.

———— 1954, Author's supplement to calculation of interdiffusion coefficients when volume changes occur: Am. Inst. Mining Metall. Engineers Trans., v. 200, p. 702.

Cooper, A. R., and Heasley, J. H., 1966, Extension of Darken's equation to binary diffusion in ceramics: Am. Ceramic Soc. Jour., v. 49, p. 280-283.

Cooper, A. R., and Varshneya, A. K., 1968, Diffusion in the system K_2O–SrO–SiO_2: I, effective binary diffusion coefficients: Am. Ceramic Soc. Jour., v. 51, p. 103-106.

Crank, J., 1956, The mathematics of diffusion: Oxford, Oxford Univ. Press, 347 p.

Darken, L. S., 1948, Diffusion, mobility and their interrelation through free energy in binary metallic systems: Am. Inst. Mining Metall. Engineers Trans., v. 175, p. 184-201.

Fitts, D. D., 1962, Nonequilibrium thermodynamics: New York, McGraw Hill Book Co., 173 p.

Fujita, H. and Gosting, L. J., 1956, An exact solution of the equations for free diffusion in three-component systems with interacting flows, and its use in evaluation of the diffusion coefficients: Am. Chemical Soc. Jour., v. 78, p. 1099-1106.

Gibbs, J. W., 1928, The collected works of J. Willard Gibbs, vol. I: New Haven, Conn., Yale Univ. Press, 434 p.

Greskovich, C., and Stubican, V. S., 1970, Change of molar volume and interdiffusion coefficients in the system MgO–Cr_2O_3: Am. Ceramic Soc. Jour., v. 53, p. 251-253.

de Groot, S. R., and Mazur, P., 1962, Nonequilibrium thermodynamics: Amsterdam, North Holland Publishing Co., 510 p.

Gupta, P. K., and Cooper, A. R., Jr., 1971, The [D] matrix for multicomponent diffusion: Physica, v. 54, p. 39-59.

Haase, R., 1969, Thermodynamics of irreversible processes: Reading, Mass., Addison Wesley, 509 p.

Hartley, G. S., 1946, Diffusion and swelling of high polymers, I: Faraday Soc. Trans., v. 42B, p. 6-11.

Hartley, G. S., and Crank, J., 1949, Some fundamental definitions and concepts in diffusion processes: Faraday Soc. Trans., v. 45, p. 801-818.

Hooyman, G. J., 1956, Thermodynamics of diffusion in multicomponent systems: Physica, v. 22, p. 751-759.

Hooyman, G. J., and de Groot, S. R., 1955, Phenomenological equations and Onsager relations: Physica, v. 21, p. 73-76.

Hooyman, G. J., Holtan, H., Jr., Mazur, P., and de Groot, S. R., 1953, Thermodynamics of irreversible processes in rotating systems: Physica, v. 19, p. 1095-1108.

Howard, R. E., and Lidiard, A. B., 1964, Matter transport in solids: Rept. on Progress in Physics, v. 27, p. 161-240.

Jost, W., 1952, Diffusion in solids, liquids, gases: New York, Academic Press, Inc., 558 p.

Kirkaldy, J. S., 1959, Diffusion in multicomponent metallic systems IV. A general theorem for construction of multicomponent solutions from solution of the binary diffusion equation: Canadian Jour. Physics, v. 37, p. 30-34.

Kirkaldy, J. S., and Brown, L. C., 1963, Diffusion behavior in ternary multiphase systems: Canadian Metall. Quart., v. 2, p. 89-115.

Kirkendall, E. O., 1942, Diffusion of zinc in alpha brass: Am. Inst. Mining Metall. Engineers Trans., v. 147, p. 104-110.

Kirkwood, J. G., Baldwin, R. L., Dunlop, P. J., Gosting, L. J., and Kegeles, G., 1960, Flow equations and frames of reference for isothermal diffusion in liquids: Jour. Chem. Physics, v. 33, p. 1505-1513.

Landau, L. D., and Lifshitz, E. M., 1959, Fluid mechanics, Course on theoretical physics, v. 6: Reading, Mass., Addison Wesley, 536 p.

LeClaire, A. D., 1953, Diffusion in metals: Progress Metal. Physics, v. 4, p. 265-332.

Manning, J. R., 1961, Diffusion in a chemical concentration gradient: Phys. Rev., v. 124, p. 470-482.

———— 1968, Diffusion kinetics for atoms in crystals: Princeton, N. J., Van Nostrand, 257 p.

Matano, C., 1933, On the relation between the diffusion coefficients and concentrations of solid metals: Japan Jour. Physics, v. 8, p. 109-113.

Miller, D. G., 1959, Ternary isothermal diffusion and the validity of the Onsager reciprocity relations: Jour. Phys. Chemistry, v. 63, p. 570-578.

———— 1960, Thermodynamics of irreversible processes, the experimental verification of the Onsager reciprocal relations: Chem. Rev., v. 60, p. 15-37.

Nye, J. F., 1957, Physical properties of crystals: Oxford, Oxford Univ. Press, 322 p.

Oishi, I., 1965, Analysis of ternary diffusion: solutions of diffusion equations and calculated concentration distribution: Jour. Chem. Physics, v. 43, p. 1611-1620.

Onsager, L., 1931a, Reciprocal relations in irreversible processes, I: Phys. Rev., v. 37, p. 405-426.

———— 1931b, Reciprocal relations in irreversible processes, II: Phys. Rev., v. 38, p. 2265-2279.

Prager, S., 1953, Diffusion in binary systems: Jour. Chem. Physics, v. 21, p. 1344-1347.

Progogine, I., and Defay, R., 1954, Chemical thermodynamics: London, Longmans, Green and Co., Ltd., 543 p.

Resnick, R., and Balluffi, R. W., 1955, Diffusion of zinc and copper in alpha and beta brasses: Am. Inst. Mining Metall. Engineers Trans., v. 203, p. 1004-1010.

Shewmon, P. G., 1963, Diffusion in solids: New York, McGraw Hill Book Co., 203 p.

da Silva, L. C., and Mehl, R. F., 1951, Interface and marker movements in diffusion in solid solutions of metals: Am. Inst. Mining Metall. Engineers Trans., v. 191, p. 155-173.
Kirkendall, E. O., 1947, Zinc diffusion in alpha brass: Am. Inst. Mining Metall. Engineers Trans., v. 171, p. 130-142.
Thompson, A. B., 1975, Calc-silicate diffusion zones between marble and pelitic schist: Jour. Petrology, v. 16, p. 314-346.
Thompson, J. B., Jr., 1959, Local equilibrium in metasomatic processes, *in* Abelson, P. H., ed., Researches in geochemistry: New York, John Wiley & Sons, p. 427-457.
Varshneya, A. K., and Cooper, A. R., 1972a, Diffusion in the system K_2O–SrO–SiO_2: II, cation self-diffusion coefficients: Am. Ceramic Soc. Jour., v. 55, p. 220-223.
———— 1972b, Diffusion in the system K_2O–SrO–SiO_2: III, interdiffusion coefficients: Am. Ceramic Soc. Jour., v. 55, p. 312-317.
———— 1972c, Diffusion in the system K_2O–SrO–SiO_2: IV, mobility model, electrostatic effects, and multicomponent diffusion: Am. Ceramic Soc. Jour., v. 55, p. 418-421.
Wagner, C., 1931, Uber den Zusammenhang zwishen Ionenbeweglichkeit und Diffussionsgschwindigkeit in festen Salzen: Zeitschr. phys. Chemie, v. B11, p. 139-151.
———— 1969, The evaluation of data obtained with diffusion couples of binary single-phase and multiphase systems, Acta Metall., v. 17, p. 99-107.
Wei, G. C. T., and Wuensch, B. J., 1973, Composition dependence of ^{63}Ni diffusion in single-crystal NiO–MgO solid solutions: Am. Ceramic Soc. Jour., v. 56, p. 562-565.
Zeibold, T. O., and Cooper, A. R., Jr., 1965, Atomic mobilities and multicomponent diffusion: Acta Metall., v. 13, p. 465-470.

[AMERICAN JOURNAL OF SCIENCE, VOL. 275, OCTOBER, 1975, P. 954-983]

REFERENCE FRAMES AND DIFFUSION COEFFICIENTS

JOHN B. BRADY

Department of Geological Sciences, Harvard University,
Cambridge, Massachusetts 02138

ABSTRACT. Diffusion coefficients are empirical constants that express linear relationships between fluxes of chemical components and gradients in composition variables. Component fluxes must be measured with respect to some particular frame of reference, so diffusion coefficients depend on the choice of reference frame as well as the choice of composition gradient. Reference frames based on a mean velocity of all the components, such as the velocity of the center of mass, are particularly convenient, for results obtained using different mean velocity frames may be readily interrelated. Diffusion data is best presented in terms of "standard" diffusion coefficients, D°_{ij}, based on the mean volume reference frame. The continuity equation for a specific reference frame R is given by

$$\left(\frac{\partial \rho_i}{\partial t}\right)_{P,T,x} = -\left[\frac{\partial}{\partial x}\left(J_i^R + \rho_i \bar{v}^{RL}\right)\right]_{P,T,t}$$

where $\bar{v}^{RL}$ is the local velocity of reference frame R with respect to a fixed point not affected by the diffusion process. If there is a volume change during a binary diffusion process in a single crystal, the continuity equation may be solved using a modified distance scale based on appropriate lattice translations in the crystal of interest. Interdiffusion behavior may be predicted on the basis of isotopic self-diffusion measurements; the exact relationship utilized for ionic crystals is not identical to Darken's equation for metallic crystals.

1. INTRODUCTION

The process of diffusion involves the net transfer of atoms due to random thermal motions of atoms initially in a non-random distribution and/or to non-random thermal motions of atoms subject to a driving force. In order to describe and quantify this net movement of atoms, macroscopic measurements must be made with respect to some specific frame of reference, usually consisting of a set of identifiable points. In principle, any set of reference points may be used as long as *all* measurements are made with respect to the same set. In practice, however, it may be inconvenient or impossible to use the same reference frame for all measurements and applications. Since different reference frames lead to different descriptions of diffusion and, therefore, to different diffusion coefficients, it is wise to select for common usage those reference frames that may be readily interrelated. For these reasons, an understanding of the various ways to describe diffusion and to define diffusion coefficients is a prerequisite to the discussion of any diffusion data or diffusion related process.

Extensive discussions of the subject of reference frames may be found in the chemical, physical, and metallurgical literature of the last 25 years. Outstanding papers include those by Darken (1948), Hartley and Crank (1949), Hooyman and others (1953), Hooyman (1956), Kirkwood and others (1960). An excellent summary may be found in a textbook by de Groot and Mazur (1962, p. 239 and following). Summaries may also be found in the texts by Fitts (1962, chap. 8) and Haase (1969, p. 271 and following). In spite of this rather thorough theoretical coverage of the subject, a unified treatment of reference frames is not available. The

several papers listed above utilize a number of different approaches, each designed to suit the problems most often encountered by the authors. In what follows I will reconsider the general topic of reference frames and show how the results of several of the listed authors are interrelated. I will then show how these results may be extended and modified to apply to problems of diffusion in common minerals.

Throughout this paper I consider only macroscopic or phenomenological descriptions of diffusion. Macroscopically, diffusion is manifested by local variations in the chemical composition of a physical system and may be explained, using simple mass balance considerations, in terms of the transfer of matter of definite chemical compositions into and/or out of the system. Hence, one describes diffusion as a motion of quantities of chemical components relative to some reference frame sufficient to produce the observed variations in chemical composition. The components used in the description need not correspond to any moving atomic or molecular species and may be selected on the basis of convenience (see Brady, 1975). For the purposes of this paper I assume that the components used are linearly independent and that the quantity of each component may be independently varied in the systems considered.

The equations presented in the following paragraphs are all for one-dimensional diffusion. To be complete, velocities, fluxes, forces, and diffusion coefficients should be given as tensor quantities. However, a one-dimensional representation is sufficient to convey the important concepts and simplifies the already cumbersome notation. The generalization to three dimensions is straightforward. The unit of quantity used throughout is moles of component i or gram-formula units of i. This choice of unit of quantity simplifies some of the discussion, particularly for the unit cell reference frame. Quantities that have meaning only if a reference frame is specified are written with superscripts to indicate a particular reference frame, R. The following is a list of the symbols used in the text.

NOTATION

a	— unit cell parameter (Å)
$A = A^{+a}$	— cation with charge +a
A_{ij}^{RV}	— parameters used to relate fluxes in reference frame R to fluxes in reference frame V (dimensionless) (3.11)
b	— unit cell parameter (Å)
$B = B^{+b}$	— cation with charge +b
B_i^I	— mobility of component i; velocity of component i with respect to the inert marker reference frame in response to a unit force (mole-cm²/cal-sec) (7.1)
c	— unit cell parameter (Å)
C_i	— any one composition variable for component i
$D_{ij}^{R,C}$	— practical diffusion coefficient; relates flux of component i with respect to reference frame R to gradient of component j given in terms of composition parameter C_j (3.6)

D°_{ij} — "standard" practical diffusion coefficient; relates flux of component i with respect to the mean volume reference frame to gradient in molar density of component j (cm^2/sec) (3.11)

D_i^I — inert marker diffusion coefficient defined in (6.13) and (6.10) (cm^2/sec)

G — Gibbs free energy (cal)

i,j,k,l — dummy subscripts used to represent various components

J_i^R — flux of component i with respect to reference frame R ($moles/cm^2\text{-}sec$) (2.4)

L_{ij}^R — phenomenological diffusion coefficient; relates flux of component i with respect to reference frame R to the force produced by the chemical potential gradient of component j ($mole^2/cal\text{-}cm\text{-}sec$) (3.1)

L_{ij}^R — phenomenological diffusion coefficient; relates flux of component i to a set of independent forces given in (3.4) ($mole^2/cal\text{-}cm\text{-}sec$)

M_i — gram formula weight of component i (gm/mole)

n_i — number of moles of component i

n_i^c — number of moles of component i per unit cell

N_i — $\dfrac{n_i}{\sum_{i=1}^{n} n_i}$; mole fraction of component i (dimensionless)

P — pressure (bars)

q_i — charge on species i (esu)

R — gas constant (1.987 cal/mole-deg)

t — time (sec)

T — temperature (°K)

v_i^L — velocity of component i with respect to some laboratory frame L (cm/sec)

$\bar{v}^{RL}$ — a weighted average of the velocities of all components; velocity of mean velocity reference frame R (cm/sec) (2.2)

v_i^R — velocity of component i with respect to mean velocity reference frame R (cm/sec) (2.3)

$\bar{v}^{SR}$ — velocity of reference frame S with respect to reference frame R (cm/sec) (2.6)

V — volume (cm^3)

V_i — $\left(\dfrac{\partial V}{\partial n_i}\right)_{P,T,n_{j\neq i}}$; partial molar volume ($cm^3/mole$)

$\bar{V}$ — $\dfrac{V}{\sum_{i=1}^{n} n_i}$; molar volume of a phase ($cm^3/mole$)

w_i^R — weight given the velocity of component i in obtaining mean velocity $\bar{v}^{RL}$ (dimensionless) (2.1)

x

$Z = Z^{-z}$

γ_i

δ_{ik}

μ_i

ξ_R^c

ρ_i

ϕ

Superscri

C

I

K

L

M

N

R

V

*

A gi
of diffus
in which
The aut
fluxes a
identifia
a set of
others a
frame, l
of trans
ments a
liquid d
tainer (
frame.

Alt
vantage
Indeed,
are lab
frames
servers
the diff
overall

x — distance (cm)
$Z = Z^{-z}$ — anion or chemical component with charge $-z$
γ_i — activity coefficient for component i (dimensionless)
δ_{ik} — $\begin{cases}=0 \text{ if } i \neq k \\ =1 \text{ if } i = k\end{cases}$; Kronecker delta function (dimensionless)
μ_i — $\left(\frac{\partial G}{\partial n_i}\right)_{p,T,n_j \neq i}$; chemical potential per mole of component i (cal/mole)
ξ_{iR}^{c} — modified distance parameter for reference frame R based on unit cell edge c (dimensionless) (5.1)
ρ_i — molar density of component i (moles/cm³)
ϕ — electrical potential (cal/esu)

Superscripts

C — any one composition variable
I — inert marker reference frame (sec. 6)
K — K*th* component reference frame (2.10)
L — laboratory reference frame (sec. 2)
M — mean mass reference frame (2.11)
N — mean molar reference frame (2.8)
R — any one reference frame
V — mean volume reference frame (2.9)
* — indicates that the value is given for a radioactive isotope

2. MEAN VELOCITY REFERENCE FRAMES

A great number of papers have been written on the general subject of diffusion that make no mention whatsoever of the frame of reference in which the diffusive velocities and fluxes discussed are to be measured. The authors of nearly all these papers tacitly assume that the diffusive fluxes and velocities they discuss are measured with respect to a single identifiable point. This is equivalent to using a reference frame based on a set of points, each of which remains in a fixed position relative to the others at all times. I shall call this type of reference frame the laboratory frame, L, for it is commonly used by experimentalists in the description of transport processes. For example, fluxes in solid interdiffusion experiments are given with respect to one end of the sample. Similarly, in liquid diffusion experiments, fluxes are measured with respect to the container that holds the liquid, sometimes called the "cell-fixed" reference frame.

Although laboratory reference frames have obvious practical advantages, their general utility is severely limited by their multiplicity. Indeed, there are potentially as many laboratory reference frames as there are laboratories or experimentalists, and results obtained using such frames may be difficult or impossible to compare. For example, two observers of a solid interdiffusion experiment might pick opposite ends of the diffusion couple as the origin of their laboratory frames. If there is an overall volume change during the diffusion experiment, the two labora-

tory frames chosen would move with respect to one another. This means that two observers of the same experiment would obtain different values for fluxes and velocities of the same components.

These difficulties may be eliminated by reporting motion with respect to a reference frame that is independent of the particular laboratory frame selected by an observer. Such a reference frame can be defined by some weighted average of the velocities of all the chemical components involved, such as the velocity of the center of mass. Whatever laboratory frame is used to measure individual velocities in a given experiment, the same result would be reported by all observers for component velocities relative to the center of mass. This approach has its foundations in classical mechanics and was introduced to describe multicomponent diffusion by Hooyman (1956). Following Hooyman's terminology, I shall call reference frames of this type "mean velocity" reference frames.

Let v_i^L be the velocity of component i as measured by any one observer with respect to any single laboratory frame L at one point in space and at one particular time. Operationally, v_i^L would be a weighted average of the velocities of all the particles that contain component i. Selecting a set of dimensionless weighting factors w_i^R, such as mass fraction, mole fraction, or volume fraction, normalized according to the criteria

$$\sum_{i=1}^{n} w_i^R = 1 \tag{2.1}$$

we may define an average or mean velocity, $\bar{v}^{RL}$, for the n components of a given system as

$$\bar{v}^{RL} \equiv \sum_{i=1}^{n} w_i^R v_i^L \tag{2.2}$$

where the superscript R refers to the reference frame defined by (2.1) and (2.2). Although the magnitude of v_i^L and of the mean velocity $\bar{v}^{RL}$ may vary from observer to observer, the velocity v_i^R of component i with respect to the mean velocity

$$v_i^R \equiv (v_i^L - \bar{v}^{RL}) \tag{2.3}$$

will be the same for all observers. On this basis, then, we may define the flux, J_i^R, of component i with respect to mean velocity reference frame R as

$$J_i^R \equiv \rho_i v_i^R \tag{2.4}$$

where ρ_i is the molar density of i and where the flux, J_i^R, is given in units of moles of i per cm^2 per second. J_i^R will be the same for all observers of the same event.

Comparing equations (2.1), (2.2), (2.3), and (2.4) it is clear that the n fluxes in any mean velocity reference frame cannot all be independent. Indeed, the fluxes are related by

$$\sum_{i=1}^{n} \frac{w_i^R}{\rho_i} J_i^R = 0 \quad . \tag{2.5}$$

Equation (2.5) provides an alternative definition for the reference frame R and was used as such by Kirkwood and others (1960). These authors also pointed out that the fluxes with respect to *any* two reference frames may be related using the expression

$$J_i^R = J_i^S + \rho_i \bar{v}^{SR} \tag{2.6}$$

where $\bar{v}^{SR}$ is the velocity of reference frame S with respect to reference frame R. For mean velocity reference frames we have

$$\bar{v}^{SR} = \bar{v}^{SL} - \bar{v}^{RL} = \sum_{k=1}^{n} (w_k^S - w_k^R) v_k^L \quad . \tag{2.7}$$

Equations (2.6) and (2.7) point out a very useful feature of mean velocity reference frames: results from various mean velocity frames may be easily interrelated. This fact will be used to advantage in defining a "standard" diffusion coefficient in section 3.

Commonly used reference frames of the mean velocity type include the following:

1. Mean molar reference frame (also called number-fixed frame)

$$w_i^N = N_i = \rho_i \bar{V} \qquad \sum_{i=1}^{n} J_i^N = 0 \tag{2.8}$$

where N_i is the mole fraction of i and where $\bar{V}$ is the molar volume of the phase in which the diffusion occurs.

2. Mean volume reference frame

$$w_i^V = \rho_i V_i \qquad \sum_{i=1}^{n} V_i J_i^V = 0 \tag{2.9}$$

where V_i is the partial molar volume of i.

3. K*th* component reference frame

$$w_i^K = \delta_{iK} \qquad J_K^K = 0 \tag{2.10}$$

where δ_{ik} is the "Kronecker delta" defined such that $\delta_{ik} = 0$ if $i \neq K$ and $\delta_{ik} = 1$ if $i = K$.

4. Mean mass (barycentric) reference frame

$$w_i^M = \tilde{N}_i = \tilde{\rho}_i \tilde{V} \qquad \sum_{i=1}^{n} M_i J_i^M = 0 \qquad (2.11)$$

where $\tilde{N}_i$ is the mass fraction of i, $\tilde{\rho}_i$ is the mass density of i, $\tilde{V}$ is the specific volume, and M_i is the gram-formula weight of i.

Each of these reference frames may be particularly useful for a given set of additional constraints. For example, the mean volume reference frame is most convenient if there is no volume change during the diffusion process. Also, the *Kth* component reference frame simplifies the description of a diffusion process in which the *Kth* component does not actively participate. Because of their general utility, much of the following discussion will emphasize mean velocity reference frames.

3. FORCES, FLUXES, AND DIFFUSION COEFFICIENTS

The presence of material transport in a system as described by the molar fluxes J_i^R clearly indicates a departure from equilibrium. On a local scale, however, the departure from equilibrium for many transport processes is not great. Therefore, it is a very good approximation to describe the changes of a system in terms of *linear* functions of the forces that tend to restore equilibrium. This linear approximation has withstood the test of countless experiments. It was formulated independently as the "laws" of Darcy, Fick, Fourier, and Ohm which govern specific transport processes. Onsager (1931a, b) unified the various linear laws using a formalism that emphasizes their interrelationships.

Isothermal, isobaric diffusion is a form of material transport linearly related to the force produced by chemical potential gradients. While chemical potential gradients are independent of the choice of reference frame, the molar fluxes J_i^R are not. Thus, the linear relations between fluxes J_i^R and forces $\left(\frac{\partial \mu_i}{\partial x}\right)_{P,T,t}$ given by

$$J_i^R = -\sum_{j=1}^{n} L_{ij}^R \left(\frac{\partial \mu_j}{\partial x}\right)_{P,T,t} \qquad (i = 1,2,\ldots,n) \qquad (3.1)$$

will vary with the choice of reference frame. Equations (3.1) *define* the phenomenological (diffusion) coefficients, L_{ij}^R, for reference frame R. μ_i is the chemical potential per mole of i, and its derivative with respect to distance x is taken at constant pressure P, temperature T, and time t. Note that in general the flux of any component i is linearly related to the chemical potential gradients of *each* of the other components. In other words, the contribution to the diffusion flux from any applied force should be considered. It should also be noted that the degree to which each force contributes to the diffusion flux of a given component

depends directly upon the reference frame selected to describe the diffusion flux.

Equations (3.1) lead to the disturbing conclusion that for an n-component system with r reference frames of interest, there are (r) $(n)^2$ phenomenological coefficients. Fortunately, these coefficients are not all independent. Onsager (1931a, b) has shown that provided the fluxes and forces are properly chosen, the n^2 coefficients for a single reference frame are subject to the relations

$$L_{ij}^{R} = L_{ji}^{R} \tag{3.2}$$

leaving only (n)(n+1)/2 independent coefficients for each reference frame. Hooyman and de Groot (1955) have demonstrated that linear independence of either the fluxes or forces is a sufficient, though not necessary, condition for the Onsager symmetry relations (3.2) to hold. For mean velocity reference frames the fluxes and forces of (3.1) are not independent, being related by (2.5) and the Gibbs-Duhem equation

$$\sum_{i=1}^{n} N_i d\mu_i = 0 \qquad \text{(constant P,T)} \tag{3.3}$$

respectively. The extra terms in (3.1) may be eliminated by using (2.5) and (3.3) and selecting J_n^R and $d\mu_n$ as the dependent variables. The result is an independent set of phenomenological equations for mean velocity frames

$$J_i^R = -\sum_{j=1}^{n-1} L_{ij}^R \left[\sum_{k=1}^{n-1} \left(\delta_{jk} + \frac{w_j^R}{w_n^R} \frac{N_k}{N_j} \right) \left(\frac{\partial \mu_k}{\partial x} \right)_{P,T,t} \right] (i = 1,2,\ldots,n-1) \tag{3.4}$$

as given in de Groot and Mazur (1962, p. 242). Equations (3.4) *define* the phenomenological coefficients L_{ij}^R which express the linear relations between the fluxes J_i^R and a set of independent forces given by the terms enclosed in brackets. The Onsager relations (3.2) become

$$L_{ij}^R = L_{ji}^R \tag{3.5}$$

This leaves (n-1)(n)/2 independent coefficients for a given mean velocity frame. And since the various reference frames are related by (2.6), we are left with the task of determining a total of only (n-1)(n)/2 independent phenomenological coefficients.

While chemical potential gradients are theoretically meaningful as the ultimate driving forces for diffusion, they have the unfortunate quality of being difficult to measure. In crystals, they may be found only by calculations based on measurements of composition gradients combined with often-unavailable thermodynamic data. Therefore, it is common practice to describe diffusion processes in terms of "practical"

diffusion coefficients $D_{ij}^{R,C}$ which are *defined* for mean velocity frames by the relations

$$J_i^R = -\sum_{j=1}^{n-1} D_{ij}^{R,C} \left(\frac{\partial C_j}{\partial x}\right)_{P,T,t} \quad (i = 1,2,\ldots,n-1) \tag{3.6}$$

where C_i is some compositional variable. Note that the diffusion coefficients $D_{ij}^{R,C}$ depend *both* on the reference frame R used to describe the fluxes and on the particular composition variable C_i whose gradient is measured. Also, note that as in (3.4) only (n-1) independent fluxes and forces are considered, with J_n^R and dC_n being selected as the dependent variables. The n fluxes are connected through equation (2.5), and the n forces are connected through relations of the type

$$\sum_{i=1}^{n} a_i dC_i = 0 \tag{3.7}$$

which exist for the commonly used compositional variables. The a's are constants for a given composition. For example,

$$\sum_{i=1}^{n} V_i d\rho_i = 0 \qquad \text{(constant P,T)} \tag{3.8}$$

where V_i is the partial molar volume of i and ρ_i is the molar density of i.

Once again with the definitions (3.6) a multiplicity of $(n-1)^2(r)(c)$ diffusion coefficients has been introduced for r reference frames and c compositional variables of interest. As before, these coefficients are not all independent: the various reference frames may be related by (2.6), and relations (perhaps unknown) obviously exist between the various compositional parameters such as mole fractions and molar densities. A maximum of $(n-1)^2$ diffusion coefficients remain. These, however, are not all independent either. Comparing equations (3.4) and (3.6) we may see that the diffusion coefficients $D_{ij}^{R,C}$ are linear functions of the phenomenological coefficients with

$$D_{il}^{R,C} = \sum_{k=1}^{n-1}\sum_{j=1}^{n-1} L_{ij}^R \left[\delta_{jk} + \frac{w_j^R}{w_n^R}\frac{N_k}{N_j}\right]\left(\frac{\partial \mu_k}{\partial C_l}\right)_{P,T,C_i \neq C_l} \quad (i,l = 1,2,\ldots,n-1). \tag{3.9}$$

Since the phenomenological coefficients L_{ij}^R are not independent, but related by the (n-1)(n-2)/2 equations (3.5), only (n)(n-1)/2 of the diffusion coefficients $D_{ij}^{R,C}$ can be independent. The specific relations among the $D_{ij}^{R,C}$ may be found for a given system by solving (3.9) for the L_{ij}^R and

using (3.5). This is only possible if the derivatives $\left(\frac{\partial \mu_k}{\partial C_l}\right)_{P,T,C_i \neq C_l}$ are known. If an equation of state is unavailable, then the relations (3.5) and (3.9) cannot be used, and $(n-1)^2$ coefficients must be determined. In any event it will not, in general, be possible to choose fluxes and forces such that $D_{ij}^{R,C} = D_{ji}^{R,C}$.

While it is clear that the diffusion coefficients for the various mean velocity reference frames and compositional variables are interconnected, we are liable to find any of the $(n-1)^2(r)(c)$ possible coefficients in use. The undesirable consequence is that diffusion data from different laboratories may not be directly comparable without performing tedious calculations. It would seem preferable to select a single reference frame R and compositional variable C_i to define a "standard" diffusion coefficient through which all data would be reported and, thus, easily compared. Following the precedent set by Hooyman and others (1953) let us use the mean volume reference frame and the molar densities ρ_i to define the standard diffusion coefficients D°_{ij} with

$$J_i^V = -\sum_{j=1}^{n-1} D^\circ_{ij}\left(\frac{\partial \rho_j}{\partial x}\right)_{P,T,t} \qquad (i = 1,2,\ldots,n-1) \quad . \qquad (3.10)$$

Equations (3.10) reduce to Fick's law at constant volume in a two-component system. For diffusion with respect to a different mean velocity reference frame R with fluxes J_i^R linearly related to fluxes J_i^V by

$$J_i^R = \sum_{j=1}^{n-1} A_{ij}^{RV} J_j^V \qquad (i = 1,2,\ldots,n-1) \qquad (3.11)$$

the flux equations become

$$J_i^R = -\sum_{k=1}^{n-1}\left[\sum_{j=1}^{n-1} A_{ij}^{RV} D^\circ_{jk}\right]\left(\frac{\partial \rho_k}{\partial x}\right)_{P,T,t} \qquad (i = 1,2,\ldots,n-1) \quad . \qquad (3.12)$$

If a different compositional variable C_l is used the flux equations are

$$J_i^R = -\sum_{l=1}^{n-1}\left[\sum_{k=1}^{n-1}\left(\sum_{j=1}^{n-1} A_{ij}^{RV} D^\circ_{jk}\right)\left(\frac{\partial \rho_k}{\partial C_l}\right)_{P,T,C_i \neq C_l}\right]\left[\frac{\partial C_l}{\partial x}\right]_{P,T,t}$$

$$(i = 1,2,\ldots n-1) \quad . \qquad (3.13)$$

Equations (3.13), which are identical to equations (55), p. 243 of de Groot and Mazur (1962), may be considered a generalization of Fick's law to multicomponent diffusion.

Equations (3.13) reduce to particularly simple forms for two component systems which may be described in terms of a single binary (or

interdiffusion) coefficient, since $(n-1)^2$ equals one. Let us evaluate the A_{ij}^{RV} of (3.11) for a two component system and mean velocity frame R. This may be accomplished by rewriting equation (2.4) using (2.1), (2.2), and (2.3) first for reference frame R

$$J_1^R = \rho_1 v_1^L - \rho_1 \left[w_1^R v_1^L + w_2^R v_2^L \right] \tag{3.14}$$

$$J_1^R = w_2^R \left[\rho_1 (v_1^L - v_2^L) \right] \tag{3.15}$$

and then for reference frame V

$$J_1^V = w_2^V \left[\rho_1 (v_1^L - v_2^L) \right] . \tag{3.16}$$

Comparing (3.15) and (3.16) we see that

$$J_1^R = \frac{w_2^R}{w_2^V} J_1^V = \frac{w_2^R}{\rho_2 V_2} J_1^V . \tag{3.17}$$

Using (3.13) and (3.17) we may give a general definition of the binary diffusion coefficient D° in terms of any mean velocity frame R as

$$J_1^R = -\frac{w_2^R}{\rho_2 V_2} D^\circ \left(\frac{\partial \rho_1}{\partial C_1} \right)_{P,T} \left(\frac{\partial C_1}{\partial x} \right)_{P,T,t} \tag{3.18}$$

taking component 2 as the dependent component (Hooyman and others, 1953). For the mean velocity frames presented above, (3.18) becomes (de Groot and Mazur, 1962, p. 252)

$$J_1^N = -\frac{\bar{V}}{V_2} D^\circ \left(\frac{\partial \rho_1}{\partial x} \right)_{P,T,t} = -\frac{D^\circ}{\bar{V}} \left(\frac{\partial N_1}{\partial x} \right)_{P,T,t} \quad \left(\begin{array}{c} \text{mean molar} \\ \text{frame} \end{array} \right) \tag{3.19}$$

$$J_1^V = -D^\circ \left(\frac{\partial \rho_1}{\partial x} \right)_{P,T,t} \quad \left(\begin{array}{c} \text{mean volume} \\ \text{frame} \end{array} \right) \tag{3.20}$$

$$J_1^2 = -\frac{D^\circ}{\rho_2 V_2} \left(\frac{\partial \rho_1}{\partial x} \right)_{P,T,t} = -\frac{D^\circ}{N_2 \bar{V}} \left(\frac{\partial N_1}{\partial x} \right)_{P,T,t} \quad \left(\begin{array}{c} \text{component 2} \\ \text{frame} \end{array} \right) \tag{3.21}$$

$$J_1^M = -\frac{\tilde{N}_2}{\rho_2 V_2} \left(\frac{\partial \rho_1}{\partial x} \right)_{P,T,t} = -\frac{D^\circ}{M_1 \tilde{V}} \left(\frac{\partial \tilde{N}_1}{\partial x} \right)_{P,T,t} \quad \left(\begin{array}{c} \text{mean mass} \\ \text{frame} \end{array} \right) . \tag{3.22}$$

4. THE CONTINUITY EQUATION

The flux equations presented in section 3 involve gradients of chemical potentials or composition variables evaluated at any single time t. Equations (3.4) and (3.13), therefore, are "instantaneous" flux equations. They are valid to describe the process of diffusion only at a given point in space and at one particular time. The one exception is the special case of steady-state diffusion, in which the gradients of chemical potential or composition do not change with time. In general, diffusion is a non-steady-state process and must be described by a form of the continuity equation.

For diffusive mass transfer the equation of continuity is also commonly called the conservation of mass equation or the mass balance equation. It is typically given in terms of fluxes measured with respect to a laboratory reference frame. As discussed in section 2, laboratory reference frames have a number of undesirable features. In addition to those features already mentioned, laboratory frames require the use of more diffusion coefficients than mean velocity frames. Since there is, in general, no equation similar to (2.5) to interrelate laboratory frame fluxes, it will be necessary to determine n^2 diffusion coefficients $D_{ij}^{L,C}$ defined by

$$J_i^L = -\sum_{j=1}^{n} D_{ij}^{L,C}\left(\frac{\partial C_j}{\partial x}\right)_{P,T,t} \qquad (i = 1,2,\ldots,n) \tag{4.1}$$

for any laboratory frame of interest. (The number of diffusion coefficients may be reduced to (n) (n+1)/2 using (3.1) and (3.2) if an equation of state is available.) It will be to our advantage, therefore, to express the continuity equation in terms of mean velocity frame fluxes.

The equation of continuity has been derived numerous times for a multitude of processes, so I will not repeat the derivation here. See Landau and Lifshitz (1959, p. 1-2) for a general derivation. In the notation of this paper the continuity equation for any component i is

$$\left(\frac{\partial \rho_i}{\partial t}\right)_{P,T,x} = -\left[\frac{\partial(\rho_i v_i^L)}{\partial x}\right]_{P,T,t} = -\left(\frac{\partial J_i^L}{\partial x}\right)_{P,T,t} \tag{4.2}$$

Equation (4.2) is strictly applicable only to *conservative* processes in which component i is neither added to nor subtracted from the diffusive system (by reaction, for example). For constant volume diffusion, equation (4.2) has been called Fick's second law. Recalling equation (2.6), we may readily write the continuity equation for any reference frame, R, as

$$\left(\frac{\partial \rho_i}{\partial t}\right)_{P,T,x} = -\left[\frac{\partial}{\partial x}\left(J_i^R + \rho_i \bar{v}^{RL}\right)\right]_{P,T,t} \tag{4.3}$$

where $\bar{v}^{RL}$ is the local velocity of reference frame R with respect to the laboratory frame. The value of $\bar{v}^{RL}$ for a given mean velocity frame R may be expressed in terms of laboratory frame fluxes by using (2.5) as well as (2.6) (see Kirkwood and others, 1960). For the mean molar reference frame, N,

$$\bar{v}^{NL} = \bar{V}\sum_{i=1}^{n} J_i^L \tag{4.4}$$

which upon substitution into (4.3) gives

$$\left(\frac{\partial \rho_i}{\partial t}\right)_{P,T,x} = -\left(\frac{\partial J_i^N}{\partial x}\right)_{P,T,t} - N_i\sum_{k=1}^{n}\left(\frac{\partial J_k^L}{\partial x}\right)_{P,T,t} \tag{4.5}$$

Similarly, for the mean volume reference frame

$$\left(\frac{\partial \rho_i}{\partial t}\right)_{P,T,x} = -\left(\frac{\partial J_i^V}{\partial x}\right)_{P,T,t} - \rho_i \left[\sum_{k=1}^{n} \left(\frac{\partial}{\partial x}\left(V_k J_k^L\right)\right)_{P,T,t}\right]. \quad (4.6)$$

We are now in a position to understand some of the problems of treating non-steady-state diffusion. If a laboratory frame and equation (4.2) are used, then a minimum of (n) (n+1)/2 diffusion coefficients must be determined. And even for a two-component system, this would be three diffusion coefficients that must be determined from two simultaneous non-linear differential equations. If a mean velocity frame is used, a minimum of only (n) (n−1)/2 diffusion coefficients are needed: one for a binary system, three for a ternary system. Thus, for a binary system there may be some hope, if a mean velocity frame is used. However, the continuity equation for mean velocity frames (4.3) involves the term $\bar{v}^{RL}$ which complicates the solution.

As a consequence of these considerations, the overwhelming majority of diffusion studies has been restricted to binary systems. Generally, a mean velocity frame is chosen to limit the number of unknown diffusion coefficients to one. In addition, simplifying assumptions are made that lead to the conclusion that $\bar{v}^{RL} = 0$. In such cases the laboratory frame, L, would coincide with the mean velocity frame, R, and the continuity equation is correspondingly simplified to the form of (4.2). The most commonly used assumption is that there is no overall volume change during the diffusion process. This is equivalent to assuming that $\Delta\bar{V}_{mixing} = 0$ or that V_1 and V_2 are constant, which means that $\bar{v}^{VL} = 0$. Assuming constant volume and using (3.20), the continuity equation (4.6) for the binary case becomes

$$\left(\frac{\partial \rho_1}{\partial t}\right)_{P,T,x} = -\left(\frac{\partial J_1^V}{\partial x}\right)_{P,T,t} = \left[\frac{\partial}{\partial x}\left(D^\circ\left[\frac{\partial \rho_1}{\partial x}\right]_{P,T,t}\right)\right]_{P,T,t}. \quad (4.7)$$

Equation (4.7), which is strictly valid only for constant-volume, binary diffusion, has been solved for specific boundary conditions by Matano (1933) using the methods of Boltzmann (1894). The Boltzmann-Matano solution to (4.7), which may be evaluated using a graphical integration, is typically used by experimentalists to determine D° when D° varies with composition.

If D° can be shown to be independent of position x in the diffusion couple, (4.7) simplifies to

$$\left(\frac{\partial \rho_1}{\partial t}\right)_{P,T,x} = D^\circ \left(\frac{\partial^2 \rho_1}{\partial x^2}\right)_{P,T,t} \quad (4.8)$$

which has many solutions for a great variety of boundary conditions (see Carslaw and Jaeger, 1947; or Crank, 1956). The applicability of (4.8)

may be tested for a given set of boundary conditions by comparing the resulting composition profiles with those predicted by the appropriate analytical solution. Diffusion studies using radioactive tracers are correctly described by (4.8) due to the very small composition changes involved. Solutions to the continuity equation (4.3) for three or more components have been given in analytical form only for systems in which the diffusion coefficients D°_{ij} are independent of composition (for example, Fujita and Gosting, 1956; Kirkaldy, 1959; Oishi, 1965). Application of these solutions to ternary diffusion problems may be found in Miller (1959, 1960), Kirkaldy and Brown (1968), Carmen (1968a, 1968b), Cooper and Varshneya (1968), Varshneya and Cooper (1972a, b, and c), and Gupta and Cooper (1971).

5. $\Delta\bar{V}_{mixing}$ AND THE UNIT CELL FRAME

Unfortunately, there are many interesting two-component systems for which there is an overall volume change during a diffusion process. In these cases, (4.7) is strictly incorrect and, though often used, may be a poor approximation (Greskovich and Stubican, 1970). Correct solutions of (4.3) which allow for volume changes have been obtained by several individuals (Prager, 1953; Crank, 1956, p. 236; Balluffi, 1960; and Wagner, 1969). Each of these solutions makes use of the Boltzmann substitution and solves for D°, as defined in this paper ($D^\circ = D$ of Prager and Balluffi; $D^\circ = D^V$ of Crank (11.73); $D^\circ = \tilde{D}$ of Wagner). Balluffi shows how his solution may be evaluated graphically. Of course, in all cases the molar volumes must be known as a function of composition. In addition, all these papers assume there is no change in the cross-sectional area of the sample normal to the diffusion direction. This assumption, while it has some basis in experiment (da Silva and Mehl, 1951; Resnick and Balluffi, 1955) for fcc metals, has been given no general justification.

An alternative approach was proposed by Hartley and Crank (1949) (reprinted in Crank, 1956, p. 219 and following). They suggested that a modified distance scale (and consequent modified concentration scale) be introduced to preserve the continuity equation in the form of (4.7), even when there is a volume change. If the mathematical form of (4.7) is maintained, then the Boltzmann-Matano approach can be used to obtain the correct solution for D°. An interesting feature of the treatment by Hartley and Crank is that the modified distance scales they proposed coincide with the set of points used to define various mean velocity reference frames. For example, their reference frame based on cross sections "fixed with respect to total mass" can be shown to be identical with the mean mass (barycentric) frame of this paper. In the barycentric case, their modified distance parameter, ξ_M, which is "measured so that equal increments of ξ_M always include equal increments of total mass" is clearly consistent with the definition (2.11) of reference points or cross sections across which there is no *net* mass flux.

The approach of Hartley and Crank is perhaps best illustrated using a modified distance scale for crystals based on the length of a unit cell

edge. For example, if there is a volume change during a diffusion process, it should be clear that the individual unit cell dimensions will vary in a manner proportional to the local volume change. Let us restrict the discussion to crystals with orthorhombic or higher symmetry. Then using the appropriate unit cell edge, say c, to define a distance parameter, $\xi_N{}^c$, ensures that equal increments of $\xi_N{}^c$ involve an equal number of unit cells. It is possible, therefore, to derive a continuity equation similar to (4.7) using the distance parameter $\xi_N{}^c$ and a mass balance argument.

The unit cell of a crystal is a particularly convenient frame of reference for conceptualizing the many diffusion problems for which the total number of unit cells is constant. For a unit cell reference frame to be practical, however, it must be possible to relate diffusion coefficients determined using the unit cell frame to the standard diffusion coefficients, D°_{ij}. This will always be possible if the chemical components used in the description are properly selected (Brady, 1975). Specifically, if components are chosen such that the total number of moles of these components per unit cell is constant, then equal increments of $\xi_N{}^c$ will involve equal numbers of moles as well as equal numbers of unit cells. The distance parameter, $\xi_N{}^c$, therefore, would mark the distances between a set of points that may be used to define a *mean molar reference frame*, N. The flux of component one across a unit cross section identified with a particular $\xi_N{}^c$ would then be given by $J_1{}^N$ evaluated at that $\xi_N{}^c$. The flux across the ab face of a single unit cell is (ab) $(J_1{}^N)$, where a and b are the cell parameters normal to the diffusion direction.

Let us define the distance parameter, $\xi_N{}^c$, as follows

$$d\xi_N{}^c \equiv \frac{dx}{c} \tag{5.1}$$

where c is the length of the unit-cell edge in the diffusion direction. The modified concentration parameter, $n_i{}^c$, in this case defined as the number of moles of component i per unit cell, is simply the mole fraction N_i times the total number of moles per unit cell:

$$n_i{}^c \equiv N_i \frac{(abc)}{\bar{V}} \quad . \tag{5.2}$$

Recalling (3.19) and using (5.1) and (5.2), the flux of component one across the unit-cell face ab is given by

$$(ab)J_1{}^N = -\frac{(ab)}{\bar{V}} D^\circ \left(\frac{\partial N_1}{\partial x}\right)_{P,T,t} = -\frac{D^\circ}{c^2}\left(\frac{\partial n_1{}^c}{\partial \xi_N{}^c}\right)_{P,T,t} \quad . \tag{5.3}$$

Equation (5.3) is strictly true only if the total number of moles per unit cell is not a function of composition so that $\bar{V}/(abc)$ is constant. The modified continuity equation can be determined by considering the change in content of component one in the unit cell per unit time in

terms of the divergence of the flux of component one across unit-cell faces ab. The modified continuity equation is

$$\left(\frac{\partial n_1^c}{\partial t}\right)_{P,T,\xi_N^c} = -\left[\frac{\partial}{\partial \xi_N^c}\left((ab)J_1^N\right)\right]_{P,T,t} = \left[\frac{\partial}{\partial \xi_N^c}\left(\frac{D^\circ}{c^2}\left[\frac{\partial n_1^c}{\partial \xi_N^c}\right]_{P,T,t}\right)\right]_{P,T,t} \tag{5.4}$$

or using (5.2)

$$\left(\frac{\partial N_1}{\partial t}\right)_{P,T,\xi_N^c} = \left[\frac{\partial}{\partial \xi_N^c}\left(\frac{D^\circ}{c^2}\left[\frac{\partial N_1}{\partial \xi_N^c}\right]_{P,T,t}\right)\right]_{P,T,t} . \tag{5.5}$$

Equation (5.5) is clearly in the same mathematical form as (4.7). It may be evaluated graphically with the usual Boltzmann-Matano procedure using a plot of N_1 versus ξ_N^c. To obtain ξ_N^c for each position $x = X$, equation (5.1) must be integrated to yield

$$\xi_N^c = \int_0^X \frac{dx}{c} \tag{5.6}$$

where $x = 0$ when $\xi_N^c = 0$ which is at the "Matano interface" defined by

$$\int_{N_1(-\infty)}^{N_1(+\infty)} \xi_N^c \, dN_1 = 0 \tag{5.7}$$

or alternatively by

$$\int_{-\infty}^{0} [N_1(-\infty)-N_1] \, d\xi_N^c = \int_0^{+\infty} [N_1-N_1(+\infty)] \, d\xi_N^c \tag{5.8}$$

where N_1 $(+\infty)$ and N_1 $(-\infty)$ correspond to the compositions far removed from the site of diffusion, as specified by the boundary conditions. Using (5.1), (5.8) becomes

$$\int_{-\infty}^{0}\left[\frac{N_1(-\infty)-N_1}{c}\right] dx = \int_0^{+\infty}\left[\frac{N_1-N_1(+\infty)}{c}\right] dx \quad . \tag{5.9}$$

If there is no change in the cross-sectional area of the sample, that is if the product (ab) is constant, then c may be replaced by $\bar{V}$ in equations (5.1) and (5.5) to obtain the result of Cohen, Wagner, and Reynolds (1953, 1954). Thus, using the unit cell reference frame, a solution for D° may be obtained when there is a $\Delta\bar{V}_{mixing}$ by purely graphical means from the composition-distance profile and knowledge of the cell parameter c as a function of composition.

For monoclinic or triclinic crystals, the situation is more complicated. First of all, the diffusion direction should be parallel to one of the "principal" diffusion axes (Nye, 1957) so that the diffusion flux is one-dimensional. The principal diffusion directions generally will not all coincide with the crystal axes, as is the case with crystals of orthorhombic or higher symmetry, so the modified distance parameter would have to utilize a lattice translation which may not correspond to any commonly used unit cell dimension. However, since angular changes as well as volume changes may occur when the composition varies, the diffusion flux across any one crystallographic plane may not be easily determined. Therefore, the simple approach used here is not directly applicable to monoclinic or triclinic crystals if the crystallographic angles α, β, and γ change appreciably with composition.

For some common minerals, though, the variations of lattice angles accompanying compositional changes are small. Since diffusion paths are highly structure sensitive, it is probably valid to assume for these minerals that the variations in orientation of the principal diffusion directions are also small. Thus, it may be a very good approximation to treat these crystals in the manner discussed above, selecting distance parameters based on lattice translations parallel to the principal diffusion directions. The "unit cell" in this case may not correspond to any unit cell normally used. While only an approximation, this approach may yield reasonable results for some otherwise complex monoclinic or triclinic minerals.

6. INERT MARKER REFERENCE FRAME

Observations by Kirkendall (1942), Smiegelskas and Kirkendall (1947), and Hartley (1946) combined with subsequent analyses by Darken (1948) and Hartley and Crank (1949) have led to the definition of a reference frame and associated diffusion coefficients different from any yet considered in this paper. Deeply involved in the definition of this additional reference frame is the question, "What is diffusion?" or "Is all the flux measured in a given reference frame appropriately called 'diffusive flux'?". These questions were raised, and answers were clearly presented by both Darken (1948) and Hartley and Crank (1949). The conclusion reached in both papers was that a distinction should be made between a flux due to "diffusion" of an individual component relative to the others and a flux due to the "bulk flow" of all components at the same rate in the same direction. This distinction is of considerable practical importance, for Hartley's and Kirkendall's experiments demonstrated that if one component diffuses more rapidly than the other in a binary interdiffusion experiment, a bulk flow will occur. As the concept of a bulk flow generated by diffusion can be confusing, I strongly recommend the excellent discussions by Darken (1948) and Hartley and Crank (1949) to any reader who finds this concept unfamiliar.

In order to measure flux due to diffusion only, a reference frame is defined in terms of a set of points, each of which moves with the local bulk flow. Operationally, this would consist of a set of "inert" markers,

which do not participate in the diffusion, but which will move with the bulk flow. For Kirkendall, these inert markers were platinum wires in a copper-brass diffusion couple. We can define, then, inert marker diffusion coefficients, $D_{ij}^{I,C}$, in terms of the fluxes, J_i^I, given with respect to the inert marker reference frame, I, as

$$J_i^I = -\sum_{j=1}^{n} D_{ij}^{I,C} \left(\frac{\partial C_j}{\partial x}\right)_{P,T,t} \qquad (i = 1,2,\ldots,n) \tag{6.1}$$

where C_j is some compositional parameter. As in the case of the laboratory frame (4.1), there is, in general, no relation similar to (2.5) which relates the n independent fluxes of the inert marker frame. Inert marker diffusion coefficients have been called "intrinsic" diffusion coefficients by Hartley and Crank (1949) and others. However, the title inert marker coefficient is to be preferred since the term "intrinsic" is also commonly used to describe diffusion in pure crystals in the absence of "extrinsic" effects due to impurities, grain boundaries, et cetera.

It will be useful to relate the inert marker diffusion coefficients, $D_{ij}^{I,C}$, to the standard diffusion coefficients, D°_{ij}, defined in (3.10). Recalling (2.6) we have

$$J_i^N = J_i^I + \rho_i \bar{v}^{IN} \quad . \tag{6.2}$$

Summing both sides of (6.2) over all i and using (2.8), $\bar{v}^{IN}$ may be expressed in terms of the J_i^I. Substituting the results for $\bar{v}^{IN}$ in (6.2) we have

$$J_i^N = J_i^I - N_i \left[\sum_{j=1}^{n} J_j^I\right] \quad . \tag{6.3}$$

For a two component system, then,

$$J_1^N = J_1^I - N_1 (J_1^I + J_2^I) = N_2 J_1^I - N_1 J_2^I \quad . \tag{6.4}$$

Substituting for J_i^N from (3.19) and for J_i^I from (6.1), (6.4) becomes

$$\begin{aligned}\frac{-\bar{V}}{V_2} D^\circ \left(\frac{\partial \rho_1}{\partial x}\right)_{P,T,t} = N_2 &\left[-D_{11}^{I,\rho}\left(\frac{\partial \rho_1}{\partial x}\right)_{P,T,t} - D_{12}^{I,\rho}\left(\frac{\partial \rho_2}{\partial x}\right)_{P,T,t}\right] \\ -N_1 &\left[-D_{21}^{I,\rho}\left(\frac{\partial \rho_1}{\partial x}\right)_{P,T,t} - D_{22}^{I,\rho}\left(\frac{\partial \rho_2}{\partial x}\right)_{P,T,t}\right]\end{aligned} \tag{6.5}$$

Using the thermodynamic relation

$$\left(\frac{\partial \rho_2}{\partial \rho_1}\right)_{P,T} = -\frac{V_1}{V_2} \tag{6.6}$$

equation (6.5) leads to

$$\frac{D^\circ \bar{V}}{V_2} = N_2 \left[D_{11}^{I,\rho} - \frac{V_1}{V_2} D_{12}^{I,\rho}\right] - N_1 \left[D_{21}^{I,\rho} - \frac{V_1}{V_2} D_{22}^{I,\rho}\right]. \tag{6.7}$$

If we then take the traditional approach and neglect $D_{12}^{I,\rho}$ and $D_{21}^{I,\rho}$, we obtain the relation

$$D^\circ = (\rho_2 V_2)D_{11}^{I,\rho} + (\rho_1 V_1)D_{22}^{I,\rho} \tag{6.8}$$

which was given by Hartley and Crank (1949, eq 31) for the case of constant volume, an assumption we have not made. Actually, Hartley and Crank's D^V is equivalent to D° in all respects except their conception of it. They stated that their D^V is meaningless, if there is an overall volume change. However, mathematically their D^V has meaning for all systems. Compare their equation (4) with equation (2.9) of this paper. A relation similar to (6.8) was also obtained by Darken (1948, eq 7)

$$D^\circ = N_2 D_{11}^{I,\rho} + N_1 D_{22}^{I,\rho} \tag{6.9}$$

which follows from (6.8) if $V_1 = V_2 = \bar{V}$.

Although (6.1) is consistent with the classical definition of inert marker diffusion coefficients, I prefer the following alternative definition

$$J_1^I = \sum_{j=1}^{n} \frac{D_{1j}^{I,N}}{\bar{V}} \left(\frac{\partial N_j}{\partial x}\right)_{P,T,t} \tag{6.10}$$

This definition leads to simpler mathematical forms for several important relationships. For example, let us relate the diffusion coefficients $D_{ij}^{I,N}$ to the standard diffusion coefficient D° for a two component system. Using (3.19) and (6.10) equation (6.4) becomes

$$\begin{aligned} -\frac{D^\circ}{\bar{V}}\left(\frac{\partial N_1}{\partial x}\right)_{P,T,t} = {} & N_2\left[\frac{-D_{11}^{I,N}}{\bar{V}} + \frac{D_{12}^{I,N}}{\bar{V}}\right]\left(\frac{\partial N_1}{\partial x}\right)_{P,T,t} \\ & -N_1\left[\frac{-D_{21}^{I,N}}{\bar{V}} + \frac{D_{22}^{I,N}}{\bar{V}}\right]\left(\frac{\partial N_1}{\partial x}\right)_{P,T,t} \end{aligned} \tag{6.11}$$

from which it follows that

$$D^\circ = N_2\,[D_{11}^{I,N} - D_{12}^{I,N}] + N_1[D_{22}^{I,N} - D_{21}^{I,N}] \tag{6.12}$$

If we then define D_1^I and D_2^I as

$$\left.\begin{aligned} D_1^I &\equiv D_{11}^{I,N} - D_{12}^{I,N} \\ D_2^I &\equiv D_{22}^{I,N} - D_{21}^{I,N} \end{aligned}\right\} \tag{6.13}$$

(6.12) may be written as

$$D^\circ = N_2 D_1^I + N_1 D_2^I \tag{6.14}$$

Equation (6.14), which has the simple form of Darken's relation (6.9), is valid even if $V_1 \neq V_2$ and also if $D_{12}^{I,N}$ and $D_{21}^{I,N}$ are not negligible.

In order to obtain the values of the diffusion coefficients D_1^I and D_2^I in (6.14) a measurement of D° is necessary. This is not sufficient, however; a measurement of the velocity, $\bar{v}^{IN}$, of the inert marker frame relative to

the mean molar frame is needed for the following relation (see (6.2) and (6.3), using also (6.10) and (6.13)):

$$\bar{v}^{IN} = -\bar{V}\left[\sum_{i=1}^{n} J_i^I\right] = D_1^I\left(\frac{\partial N_1}{\partial x}\right)_{P,T,t} + D_2^I\left(\frac{\partial N_2}{\partial x}\right)_{P,T,t} \quad (6.15)$$

$$\bar{v}^{IN} = \left(D_1^I - D_2^I\right)\left(\frac{\partial N_1}{\partial x}\right)_{P,T,t} . \quad (6.16)$$

Darken (1948) derived a form of (6.16) for the special case where $V_1 = V_2 = \bar{V}$ and, therefore, $\bar{v}^{NL} = \bar{v}^{VL} = 0$. Equation (6.16) may be used with (6.14) to solve for D_1^I and D_2^I at a given composition from measurements of D° (as in the last section) and $\bar{v}^{IN}$ (as follows). To obtain $\bar{v}^{IN}$ at a single position and time, the velocity of a marker, $\bar{v}^{IL}$, at that position and time (relative to the laboratory frame) must be determined by a series of measurements, at several times, of the position of the marker. The marker velocity is then compared with the velocity, $\bar{v}^{NL}$, of the mean molar reference frame at the same position and time.

In a binary interdiffusion experiment, the location of the points or cross sections that define the mean molar reference frame may be obtained in a fashion similar to that used to locate the "Matano interface" (5.7) or (5.9). Indeed, the Matano interface itself is a mean molar reference cross section. That this is true may be seen from (5.7) or (5.9) which require that the $x = 0$, $\xi_N^c = 0$ cross section be one such that the cumulative flux of atoms across the cross section in one direction equals the cumulative flux of atoms across the cross section in the other direction. Other cross sections across which the cumulative atom fluxes in both directions balance are given by

$$\int_{N_1(-\infty)}^{N_1(+\infty)} \xi_N^c \, dN_1 = k \quad (6.17)$$

or

$$\int_{-\infty}^{0}\left[\frac{N_1(-\infty) - N_1}{c}\right] dx = \int_{0}^{+\infty}\left[\frac{N_1 - N_1(+\infty)}{c}\right] dx + k \quad (6.18)$$

where k is a constant, different for each cross section. Equations (6.17) and (6.18) define an $x = 0$, $\xi_N^c = 0$ plane which is a mean molar reference cross section (see fig. 1). Thus, to evaluate $\bar{v}^{IN}$, one needs to determine the k for the mean molar reference plane which coincides in position with the inert marker used to determine $\bar{v}^{IL}$ at the appropriate time. One then determines $\bar{v}^{NL}$ for the mean molar plane identified with that k by a series of calculations at several times of the position of that plane. Alternatively, one could use (5.6) and (5.9) to locate the plane associated with

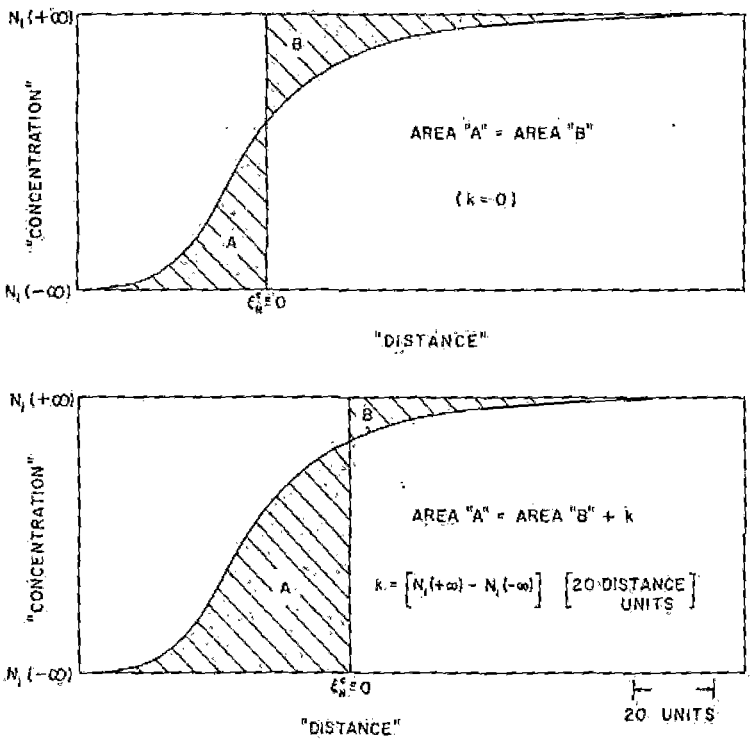

Fig. 1. "Concentration" versus "distance" profile for a binary interdiffusion experiment with the "Matano interface" of equation (5.11) shown in (A) and a mean molar plane k of equation (6.18) shown in (B) with $k = [N_1(+\infty) - N_1(-\infty)] \times$ [20 distance units].

a given ξ_N^c at various times, which would involve more effort than using (6.18).

7. Darken's Equation and Tracer Diffusion Coefficients

There is reason to believe that the inert marker frame coefficients presented above are in some ways more "fundamental" than the mean velocity frame diffusion coefficients; hence, the often used name "intrinsic" diffusion coefficients (suggested by Hartley and Crank, 1949). The argument is based on the assumption that the principal effect of the motion of one component upon the motion of another component is the flux due to bulk flow. Therefore, if the effect of a bulk flow is eliminated by using an inert marker frame, then the flux of a component might be expected to depend only upon gradients of its own chemical potential. In other words, an assumption is made that the off-diagonal terms in the phenomenological equations (3.1) are necessary *only* to account for flux due to bulk flow.

The validity and consequences of the assumption of negligible off-diagonal ($i \neq j$) phenomenological coefficients, L_{ij}^I, for the inert marker frame have been discussed by many individuals (Bardeen and Herring,

1951; LeClaire, 1953; Manning, 1961, 1968; Shewmon, 1963; Howard and Lidiard, 1964; Ziebold and Cooper, 1965; Carmen, 1968a, b). The consensus is that the assumption is not correct but may be a good approximation for many systems. Carmen (1968a, b) argues that it is a poor approximation for "complex Darken systems" where a single component may be present in more than one diffusing species. Manning (1968) uses an atomistic approach to demonstrate that the assumption cannot be strictly correct for diffusion in solids by a vacancy mechanism. Nevertheless, the estimated errors that might be caused by neglecting the off-diagonal terms in the inert marker frame are within the range of uncertainty of measurement on many solids or other "simple Darken systems". With this in mind, it is worthwhile to explore a very useful consequence of the assumption.

Two isotopes of the same element are chemically quite similar. The electron shells surrounding each of the slightly different nuclei of the two isotopes behave identically in many interactive situations. Therefore, it is not unreasonable to assume that the motion of either isotope in response to an identical chemical force (chemical potential gradient) would be the same (in the absence of gravitational effects). This assumption was expressed by Darken (1948) as an equality of mobilities, B_i^I, which give the velocity of a component in response to a unit force. In terms of equation (3.1), B_i^I is defined as follows (neglecting the off-diagonal coefficients):

$$J_i^I = -L_i^I \left(\frac{\partial \mu_i}{\partial x}\right)_{P,T,t} = -B_i^I \left(\frac{N_i}{\bar{V}}\right)\left(\frac{\partial \mu_i}{\partial x}\right)_{P,T,t} \tag{7.1}$$

and Darken's equality would be

$$(B_i^I)^* = B_i^I \tag{7.2}$$

where the * refers to a radioactive isotope of component i.

The next step is to compare the diffusion coefficient determined in a tracer "self-diffusion" experiment (mixing of two isotopes of the same element) with the inert marker coefficients (6.13). To do this we must relate the mobilities, B_i^I, to the inert marker diffusion coefficients. Writing (6.10) for a two component system and using (6.13) we obtain upon comparison with (7.1)

$$J_1^I = -B_1^I \left(\frac{N_1}{\bar{V}}\right)\left(\frac{\partial \mu_1}{\partial x}\right)_{P,T,t} = -\frac{D_1^I}{\bar{V}}\left(\frac{\partial N_1}{\partial x}\right)_{P,T,t} \tag{7.3}$$

and

$$D_1^I = B_1^I N_1 \left(\frac{\partial \mu_1}{\partial N_1}\right)_{P,T} = B_1^I \left(\frac{\partial \mu_1}{\partial \ln N_1}\right)_{P,T} . \tag{7.4}$$

The molar chemical potential, μ_1, is related to the mole fraction, N_1, by

$$\mu_1 = \mu_1^\circ + RT\ln N_1\gamma_1 \tag{7.5}$$

where γ_1 is the activity coefficient necessary to correct for non-ideality.

Using (7.5) to evaluate (7.4) we have:

$$D_i^I = B_i^I RT\left[\frac{\partial \ln(N_1\gamma_1)}{\partial \ln N_1}\right]_{P,T} = B_i^I RT\left[1+\left(\frac{\partial \ln\gamma_1}{\partial \ln N_1}\right)_{P,T}\right]. \quad (7.6)$$

In a tracer "self-diffusion" measurement, there is, ideally, only mixing of isotopes of the same element. For isotopic mixing, which is chemically ideal, (7.6) becomes:

$$(D_i^I)^* = (B_i^I)^* RT \quad . \quad (7.7)$$

Since the mole fraction of the minor isotope in a tracer self-diffusion experiment is very small, the diffusion coefficient measured, D^o, will be equal to the intrinsic diffusion coefficient of the tracer, $(D_i^I)^*$, (see 6.14). This is strictly true only in the binary isotopic end member systems. For a detailed phenomenological discussion, see Howard and Lidiard (1964, p. 207 and following). Using (7.2), (7.6), and (7.7), then, we obtain the desired relation

$$D_1^I = (D_1^I)^*\left[1+\left(\frac{\partial \ln\gamma_1}{\partial \ln N_1}\right)_{P,T}\right] \quad . \quad (7.8)$$

Using the identity

$$\left[\frac{\partial \ln\gamma_1}{\partial \ln N_1}\right]_{P,T} = \left[\frac{\partial \ln\gamma_2}{\partial \ln N_2}\right]_{P,T} \quad (7.9)$$

which follows from (7.5) and the Gibbs-Duhem equation (3.3), we may substitute (7.8) into (6.14) to obtain a version of Darken's equation (1948, eq 18)

$$D^o = \left[N_2(D_1^I)^* + N_1(D_2^I)^*\right]\left[1+\left(\frac{\partial \ln\gamma_1}{\partial \ln N_1}\right)_{P,T}\right] \quad . \quad (7.10)$$

The practical importance of (7.10) is great indeed. To the extent that (7.10) is correct, measurements of diffusion coefficients using radioactive tracers may be used to predict binary interdiffusion behavior. This is particularly important for those interested in determining diffusion coefficients which are very small, for example, in minerals at metamorphic temperatures. This is a result of the fact that small concentrations of a radioactive isotope may be detected with considerably more precision than small concentrations of non-radioactive species.

8. IONIC CRYSTALS

Crystals that have an appreciable ionic character such as halides, oxides, and silicates present some additional constraints which have not been considered above. Specifically, the strict stoichiometry required to maintain electrical neutrality leads to a coupling of fluxes for an interdiffusion experiment in an ionic crystal. Nevertheless, nearly all the results given above are valid for ionic crystals if the components used in the

description are *actual* components of the crystal considered. Actual components of a crystal may be both added to and subtracted from a crystal without destroying the homogeneity of that crystal (Gibbs, 1928, p. 64; Thompson, 1959; Brady, 1975). In the absence of external electric fields, any actual component of a given crystal must be electrically neutral. Therefore, the constraints of stoichiometry or electrical neutrality are automatically satisfied in any description, if actual components are used. The results of section 7, however, are not correct for ionic crystals. In particular, Darken's equation (7.10) is subject to modifications, which we shall now consider.

In ionic crystals either the positive ions move or the negative ions move, rarely both (Jost, 1952). Therefore, in the following discussion we shall consider the motion of cations in a network of stationary anions; results are equally applicable to the opposite case of mobile anions. If the anions do not diffuse, then they will behave as inert markers. So for most ionic crystals the inert marker reference frame will coincide with the unit cell reference frame and also with the mean molar frame (for a judicious choice of components). Therefore, the two inert marker diffusion coefficients (6.13) for a binary system must be identical (see 6.16). This means that there will be no "Kirkendall effect" for interdiffusion in ionic crystals and that the Matano (1933) interface will always coincide with the initial crystal-crystal interface, even if there is a $\Delta\bar{V}_{mixing}$.

In section 7 a relationship (7.10) between tracer self-diffusion coefficients and the standard binary diffusion coefficient was obtained by relating inert marker diffusion coefficients to self-diffusion coefficients. The same approach cannot be valid for ionic crystals, since the equality of the two inert marker coefficients combined with equation (7.8) would imply that the self-diffusion coefficients for the two components of a binary crystal must be equal. Experimentally, this is not the case (Askill, 1970), so equation (7.8) must not be valid for ionic crystals. A scrutiny of the steps followed in obtaining (7.8) will reveal that it is equation (7.1) that is in error for ionic crystals. The reason (7.1) is incorrect is that a force has been neglected, the force that prevents any deviations from stoichiometry. Since the mobility, $B_i{}^I$, gives the velocity of diffusion in response to a unit force, (7.1) cannot be correct if all the forces are not considered.

It is not unreasonable to assume that the force that maintains stoichiometry in ionic crystals is the large electrical potential gradient that would develop if any deviations from stoichiometry did occur. The response of a diffusing species to an electrical potential gradient is proportional to both its charge, q_i, and its mobility, $B_i{}^I$, so that the flux of species i in response to an applied field $\left(\frac{\partial\phi}{\partial x}\right)_{P,T,t}$ would be

$$J_i{}^I = -B_i{}^I\left(\frac{N_i}{\bar{V}}\right) q_i \left(\frac{\partial\phi}{\partial x}\right)_{P,T,t} \qquad (8.1)$$

(Jost, 1952). The flux of species i in response to both an electrical potential gradient and a chemical potential gradient is then

$$J_i^I = -B_i^I \left(\frac{N_i}{\bar{V}}\right)\left[\left(\frac{\partial \mu_i}{\partial x}\right)_{P,T,t} + q_i\left(\frac{\partial \phi}{\partial x}\right)_{P,T,t}\right] \quad . \qquad (8.2)$$

Assuming that (8.2) includes all the appropriate forces we might proceed as in section 7 to find a relationship similar to (7.10). Unfortunately, there is one further stumbling block. The chemical potential gradient indicated in (8.2) must be written for a charged species, since it is only for the motion of a charged species that (8.2) is needed to replace (7.1). However, the chemical potential of a charged species in a stoichiometric ionic crystal is an undefined quantity. This dilemma may be resolved by considering explicitly the possibility of vacancies and nonstoichiometry (see Howard and Lidiard, 1964) or by making a simplifying assumption that will lead to a result that may be tested experimentally. We will take the latter approach here, manipulating the chemical potentials of charged species as if they were meaningful and then expressing the result in terms of measurable quantities.

Let us begin by considering a general binary ionic crystal composed of various combinations of two cations, A^{+a} and B^{+b}, and a single anion or negatively charged component Z^{-z}. We shall explicitly include the charges +a, +b, and −z to allow for the possibility of the cations having different charges. This binary ionic crystal will have actual components $A_z Z_a$ and $B_z Z_b$ where the subscripts indicate the number of moles of the cations and anions in one mole of the component. An alkali feldspar would be an example of a binary "ionic" crystals with $A^{+a} = K^{+1}$, $B^{+b} = Na^{+1}$, $Z^{-z} = (AlSi_3O_8)^{-1}$, and actual components $KAlSi_3O_8$ and $NaAlSi_3O_8$. Wustite would be another example (different in the respect that $+a \neq +b$) with $A^{+a} = Fe^{+2}$, $B^{+b} = Fe^{+3}$, $Z^{-z} = O^{-2}$, and actual components Fe_2O_2 and Fe_2O_3.

If the crystal is in local homogeneous equilibrium, the following relations must be satisfied (Prigogine and Defay, 1954, p. 69)

$$\mu_{A_zZ_a} = z\mu_{A^{+a}} + a\mu_{Z^{-z}} \qquad (8.3)$$

$$\mu_{B_zZ_b} = z\mu_{B^{+b}} + b\mu_{Z^{-z}} \quad . \qquad (8.4)$$

We have also from (3.3)

$$N_{A_zZ_a}\, d\mu_{A_zZ_a} + N_{B_zZ_b}\, d\mu_{B_zZ_b} = 0 \quad . \qquad (8.5)$$

If we assume that the chemical potential of Z^{-z} is not a function of composition, then (8.3), (8.4), and (8.5) lead to

$$\left(\frac{\partial \mu_{A^{+a}}}{\partial x}\right)_{P,T,t} = \frac{1}{z}\left(\frac{\partial \mu_{A_zZ_a}}{\partial x}\right)_{P,T,t} = -\left[\frac{N_{B_zZ_b}}{N_{A_zZ_a}}\right]\left(\frac{\partial \mu_{B^{+b}}}{\partial x}\right)_{P,T,t} \quad . \qquad (8.6)$$

The validity of the assumption leading to (8.6) is discussed by Cooper and Heasley (1966). See also Wagner (1930) and Jost (1952, p. 146).

Let us simplify the notation slightly by letting $AZ = A_z Z_a$, $BZ = B_z Z_b$, $A = A^{+a}$, and $B = B^{+b}$. Then using (8.6), (8.2) may be written for the fluxes of A and B, respectively

$$J_A^I = -B_A^I \left(\frac{zN_{AZ}}{\bar{V}}\right)\left[\frac{1}{z}\left(\frac{\partial \mu_{AZ}}{\partial x}\right)_{P,T,t} + a\left(\frac{\partial \phi}{\partial x}\right)_{P,T,t}\right] \quad (8.7)$$

$$J_B^I = +B_B^I \left(\frac{zN_{BZ}}{\bar{V}}\right)\left[\frac{1}{z}\left(\frac{N_{AZ}}{N_{BZ}}\right)\left(\frac{\partial \mu_{AZ}}{\partial x}\right)_{P,T,t} - b\left(\frac{\partial \phi}{\partial x}\right)_{P,T,t}\right] \quad (8.8)$$

where we have used the fact that the density of A is z times the density of AZ. Due to the constraint of electrical neutrality, the fluxes of A and B with respect to the unit cell frame (= inert marker frame) must satisfy the relation

$$aJ_A^I + bJ_B^I = 0 \quad (8.9)$$

Using (8.9), (8.7) and (8.8) may be solved for $\left(\frac{\partial \phi}{\partial x}\right)_{P,T,t}$ yielding

$$\left(\frac{\partial \phi}{\partial x}\right)_{P,T,t} = \left(\frac{N_{AZ}}{z}\right)\frac{(bB_B^I - aB_A^I)}{(a^2 N_{AZ} B_A^I + b^2 N_{BZ} B_B^I)}\left(\frac{\partial \mu_{AZ}}{\partial x}\right)_{P,T,t} \quad (8.10)$$

Substituting (8.10) into (8.7), it follows that

$$J_A^I = -\left(\frac{N_{AZ}}{\bar{V}}\right)\frac{(B_A^I B_B^I)(b)(aN_{AZ} + bN_{BZ})}{[a^2 N_{AZ} B_A^I + b^2 N_{BZ} B_B^I]}\left(\frac{\partial \mu_{AZ}}{\partial x}\right)_{P,T,t} \quad (8.11)$$

In order to express the final results completely in terms of actual components, note that stoichiometry requires

$$J_A^I = zJ_{AZ}^I \quad (8.12)$$

and that (8.3) requires (since $v_A^I = v_{AZ}^I$)

$$B_A^I = zB_{AZ}^I \quad (8.13)$$

Combining (8.11), (8.12), and (8.13) then

$$J_{AZ}^I = -\left(\frac{N_{AZ}}{\bar{V}}\right)\frac{(B_{AZ}^I B_{BZ}^I)(b)(aN_{AZ} + bN_{BZ})}{[a^2 N_{AZ} B_{AZ}^I + b^2 N_{BZ} B_{BZ}^I]}\left(\frac{\partial \mu_{AZ}}{\partial x}\right)_{P,T,t} \quad (8.14)$$

or using (7.2), (7.5), and (7.7) (which are still valid even though (7.1) is not)

$$J_{AZ}^I = \frac{-1}{\bar{V}}\frac{(D_{AZ}^I)^*(D_{BZ}^I)^*(b)(aN_{AZ} + bN_{BZ})}{[a^2 N_{AZ}(D_{AZ}^I)^* + b^2 N_{BZ}(D_{BZ}^I)^*]}\left[1 + \left(\frac{\partial \ln \gamma_{AZ}}{\partial \ln N_{AZ}}\right)_{P,T}\right]\left(\frac{\partial N_{AZ}}{\partial x}\right)_{P,T,t} \quad (8.15)$$

Finally we must note that the mean molar reference frame for components $A_z Z_a$ and $B_z Z_b$ does *not* coincide with the unit cell frame (= inert marker frame), although the mean molar frame for components

$A_{bz}\,Z_{\hat{a}b}$ and $B_{az}\,Z_{\hat{a}b}$ does (see sec. 5). Using (3.19) written for these latter components and performing a simple component transformation (Brady, 1975), we obtain

$$J_{AZ}^{I} = \frac{-b}{(aN_{AZ} + bN_{BZ})} \frac{D^{\circ}}{\bar{V}} \left(\frac{\partial N_{AZ}}{\partial x}\right)_{P,T,t} \tag{8.16}$$

On comparing (8.15) and (8.16) it follows that

$$D^{\circ} = \frac{(D_{AZ}^{I})^{*}\,(D_{BZ}^{I})^{*}\,(aN_{AZ} + bN_{BZ})^{2}}{[a^{2}N_{AZ}\,(D_{AZ}^{I})^{*} + b^{2}N_{BZ}\,(D_{BZ}^{I})^{*}]} \left[1 + \left(\frac{\partial \ln \gamma_{AZ}}{\partial \ln N_{AZ}}\right)_{P,T}\right] \tag{8.17}$$

which is the relation we have been looking for. If $a = b$ then (8.17) reduces to the simple form

$$D^{\circ} = \frac{(D_{AZ}^{I})^{*}\,(D_{BZ}^{I})^{*}}{[N_{AZ}\,(D_{AZ}^{I})^{*} + N_{BZ}\,(D_{BZ}^{I})^{*}]} \left[1 + \left(\frac{\partial \ln \gamma_{AZ}}{\partial \ln N_{AZ}}\right)_{P,T}\right] \tag{8.18}$$

as given in Manning (1968, p. 21).

Equations (8.17) and (8.18) have the potential to perform the same important function for ionic crystals that Darken's equation (7.10) performs for metallic crystals: relating relatively easy to measure self-diffusion coefficients to relatively hard to measure interdiffusion coefficients. Equation (8.17) is only an approximation, though, subject to the validity of (8.6). Unfortunately, I know of no experimental verification of (8.17), so it should be used with caution. Equation (7.10), on the other hand, is clearly incorrect for ionic crystals, although it is commonly used for ionic crystals in the literature (for example, Buening and Buseck, 1973, p. 6856; Wei and Wuensch, 1973, p. 564). Cooper and Heasley (1966) give a relation (their eq 14) similar to equation (8.15) but not identical with it. I believe their equation (14) to be incorrect, and Cooper agrees (personal commun., 1974).

Unfortunately, not all binary ionic crystals are suited to the above analysis. Consider, for example, the binary system of the plagioclase feldspars ($NaAlSi_3O_8$–$CaAl_2Si_2O_8$). Interdiffusion in this system involves the exchange of Na and Si for Ca and Al. While we might measure the tracer diffusion coefficients of Ca or Al, there is no way to ensure that doped Ca and Al remain coupled in a tracer experiment in anorthite as they must in an interdiffusion experiment between anorthite and albite. One simplification, which might be useful in practice, would be to assume that the motion of the coupled pair CaAl is limited by the motion of Al, measure the diffusion of an Al isotope, and proceed as in (8.17).

9. CONCLUDING REMARKS

Several points made in the preceding paragraphs deserve reiteration. (1) Fluxes and diffusion coefficients are meaningless quantities unless referred to a specific reference frame. (2) Certain reference frames are preferred for common usage due to the ease with which they may be interrelated; mean velocity frames are particularly convenient. (3) All diffusion data should be reported in terms of "standard" diffusion coefficients

based on the mean volume reference frame. (4) Volume changes may be significant in many diffusion processes and can be handled for single crystals using a unit cell reference frame. (5) Self-diffusion data may be used to predict interdiffusion behavior; the approximation for ionic crystals is different than for metallic crystals.

The discussion above has emphasized diffusion in single crystals, but many of the results are not so restricted. Indeed, selecting a reference frame can be particularly important for geologists considering diffusion in natural polycrystalline materials. For example, metasomatic zones generally lack complete information on the initial distribution of material so that a laboratory frame is unavailable. However, assumptions about the starting configuration and diffusion process may still be evaluated using some of the other reference frames considered in this paper (for example, Thompson, 1975).

ACKNOWLEDGMENTS

Special thanks belong to R. James Kirkpatrick, John M. Ferry, James F. Hays, Alan B. Thompson, and Steven M. Richardson for many helpful discussions on diffusion topics and comments on this paper. Early drafts of the paper were also considerably improved by the suggestions of George W. Fisher. This work is published under the auspices of the Committee on Experimental Geology and Geophysics at Harvard University.

REFERENCES

Askill, J., 1970, Tracer diffusion data for metals, alloys, and simple oxides: New York, IFI/Plenum, 107 p.

Balluffi, R. W., 1960, On the determination of diffusion coefficients in chemical diffusion: Acta Metall., v. 8, p. 871-873.

Bardeen, J., and Herring, C., 1951, Diffusion in alloys and the Kirkendall effect, *in* Atom Movements: Cleveland, Am. Soc. for Metals, p. 87-111.

Boltzmann, L., 1894, Zur Integration der Diffusionsgleichung bei variabeln Diffusionscoefficienten: Ann. Physik, v. 53, p. 959-964.

Brady, J. B., 1975, Chemical components and diffusion: Am. Jour. Sci., v. 275, in press.

Buening, D. K., and Buseck, P. R., 1973, Fe–Mg lattice diffusion in olivine: Jour. Geophys. Research, v. 78, p. 6852-6862.

Carmen, P. C., 1968a, Intrinsic mobilities and independent fluxes in multicomponent isothermal diffusion, I. Simple Darken systems: Jour. Phys. Chemistry, v. 72, p. 1707-1712.

———— 1968b, Intrinsic mobilities and independent fluxes in multicomponent isothermal diffusion, II. Complex Darken systems: Jour. Phys. Chemistry, v. 72, p. 1713-1721.

Carslaw, H. S., and Jaeger, J. C., 1947, Conduction of heat in solids: Oxford, Oxford Univ. Press, 386 p.

Cohen, M., Wagner, C., and Reynolds, J. E., 1953, Calculation of interdiffusion coefficients when volume changes occur: Am. Inst. Mining Metall. Engineers Trans., v. 197, p. 1534-1536.

———— 1954, Author's supplement to calculation of interdiffusion coefficients when volume changes occur: Am. Inst. Mining Metall. Engineers Trans., v. 200, p. 702.

Cooper, A. R., and Heasley, J. H., 1966, Extension of Darken's equation to binary diffusion in ceramics: Am. Ceramic Soc. Jour., v. 49, p. 280-283.

Cooper, A. R., and Varshneya, A. K., 1968, Diffusion in the system K_2O–SrO–SiO_2: I, effective binary diffusion coefficients: Am. Ceramic Soc. Jour., v. 51, p. 103-106.

Crank, J., 1956, The mathematics of diffusion: Oxford, Oxford Univ. Press, 347 p.

Darken, L. S., 1948, Diffusion, mobility and their interrelation through free energy in binary metallic systems: Am. Inst. Mining Metall. Engineers Trans., v. 175, p. 184-201.

Fitts, D. D., 1962, Nonequilibrium thermodynamics: New York, McGraw Hill Book Co., 173 p.

Fujita, H. and Gosting, L. J., 1956, An exact solution of the equations for free diffusion in three-component systems with interacting flows, and its use in evaluation of the diffusion coefficients: Am. Chemical Soc. Jour., v. 78, p. 1099-1106.

Gibbs, J. W., 1928, The collected works of J. Willard Gibbs, vol. 1: New Haven, Conn., Yale Univ. Press, 434 p.

Greskovich, C., and Stubican, V. S., 1970, Change of molar volume and interdiffusion coefficients in the system MgO–Cr_2O_3: Am. Ceramic Soc. Jour., v. 53, p. 251-253.

de Groot, S. R., and Mazur, P., 1962, Nonequilibrium thermodynamics: Amsterdam, North Holland Publishing Co., 510 p.

Gupta, P. K., and Cooper, A. R., Jr., 1971, The [D] matrix for multicomponent diffusion: Physica, v. 54, p. 39-59.

Haase, R., 1969, Thermodynamics of irreversible processes: Reading, Mass., Addison Wesley, 509 p.

Hartley, G. S., 1946, Diffusion and swelling of high polymers, I: Faraday Soc. Trans., v. 42B, p. 6-11.

Hartley, G. S., and Crank, J., 1949, Some fundamental definitions and concepts in diffusion processes: Faraday Soc. Trans., v. 45, p. 801-818.

Hooyman, G. J., 1956, Thermodynamics of diffusion in multicomponent systems: Physica, v. 22, p. 751-759.

Hooyman, G. J., and de Groot, S. R., 1955, Phenomenological equations and Onsager relations: Physica, v. 21, p. 73-76.

Hooyman, G. J., Holtan, H., Jr., Mazur, P., and de Groot, S. R., 1953, Thermodynamics of irreversible processes in rotating systems: Physica, v. 19, p. 1095-1108.

Howard, R. E., and Lidiard, A. B., 1964, Matter transport in solids: Rept. on Progress in Physics, v. 27, p. 161-240.

Jost, W., 1952, Diffusion in solids, liquids, gases: New York, Academic Press, Inc., 558 p.

Kirkaldy, J. S., 1959, Diffusion in multicomponent metallic systems IV. A general theorem for construction of multicomponent solutions from solution of the binary diffusion equation: Canadian Jour. Physics, v. 37, p. 30-34.

Kirkaldy, J. S., and Brown, L. C., 1963, Diffusion behavior in ternary multiphase systems: Canadian Metall. Quart., v. 2, p. 89-115.

Kirkendall, E. O., 1942, Diffusion of zinc in alpha brass: Am. Inst. Mining Metall. Engineers Trans., v. 147, p. 104-110.

Kirkwood, J. G., Baldwin, R. L., Dunlop, P. J., Gosting, L. J., and Kegeles, G., 1960, Flow equations and frames of reference for isothermal diffusion in liquids: Jour. Chem. Physics, v. 33, p. 1505-1513.

Landau, L. D., and Lifshitz, E. M., 1959, Fluid mechanics, Course on theoretical physics, v. 6: Reading, Mass., Addison Wesley, 536 p.

LeClaire, A. D., 1953, Diffusion in metals: Progress Metal. Physics, v. 4, p. 265-332.

Manning, J. R., 1961, Diffusion in a chemical concentration gradient: Phys. Rev., v. 124, p. 470-482.

———— 1968, Diffusion kinetics for atoms in crystals: Princeton, N. J., Van Nostrand, 257 p.

Matano, C., 1933, On the relation between the diffusion coefficients and concentrations of solid metals: Japan Jour. Physics, v. 8, p. 109-113.

Miller, D. G., 1959, Ternary isothermal diffusion and the validity of the Onsager reciprocity relations: Jour. Phys. Chemistry, v. 63, p. 570-578.

———— 1960, Thermodynamics of irreversible processes, the experimental verification of the Onsager reciprocal relations: Chem. Rev., v. 60, p. 15-37.

Nye, J. F., 1957, Physical properties of crystals: Oxford, Oxford Univ. Press, 322 p.

Oishi, I., 1965, Analysis of ternary diffusion: solutions of diffusion equations and calculated concentration distribution: Jour. Chem. Physics, v. 43, p. 1611-1620.

Onsager, L., 1931a, Reciprocal relations in irreversible processes, I: Phys. Rev., v. 37, p. 405-426.

———— 1931b, Reciprocal relations in irreversible processes, II: Phys. Rev., v. 38, p. 2265-2279.

Prager, S., 1953, Diffusion in binary systems: Jour. Chem. Physics, v. 21, p. 1344-1347.

Progogine, I., and Defay, R., 1954, Chemical thermodynamics: London, Longmans, Green and Co., Ltd., 543 p.

Resnick, R., and Balluffi, R. W., 1955, Diffusion of zinc and copper in alpha and beta brasses: Am. Inst. Mining Metall. Engineers Trans., v. 203, p. 1004-1010.

Shewmon, P. G., 1963, Diffusion in solids: New York, McGraw Hill Book Co., 203 p.

da Silva, L. C., and Mehl, R. F., 1951, Interface and marker movements in diffusion in solid solutions of metals: Am. Inst. Mining Metall. Engineers Trans., v. 191, p. 155-173.

Smigelskas, A. D., and Kirkendall, E. O., 1947, Zinc diffusion in alpha brass: Am. Inst. Mining Metall. Engineers Trans., v. 171, p. 130-142.

Thompson, A. B., 1975, Calc-silicate diffusion zones between marble and pelitic schist: Jour. Petrology, v. 16, p. 314-346.

Thompson, J. B., Jr., 1959, Local equilibrium in metasomatic processes, *in* Abelson, P. H., ed., Researches in geochemistry: New York, John Wiley & Sons, p. 427-457.

Varshneya, A. K., and Cooper, A. R., 1972a, Diffusion in the system K_2O–SrO–SiO_2: II, cation self-diffusion coefficients: Am. Ceramic Soc. Jour., v. 55, p. 220-223.

———— 1972b, Diffusion in the system K_2O–SrO–SiO_2: III, interdiffusion coefficients: Am. Ceramic Soc. Jour., v. 55, p. 312-317.

———— 1972c, Diffusion in the system K_2O–SrO–SiO_2: IV, mobility model, electrostatic effects, and multicomponent diffusion: Am. Ceramic Soc. Jour., v. 55, p. 418-421.

Wagner, C., 1931, Uber den Zusammenhang zwishen Ionenbeweglichkeit und Diffussionsgschwindigkeit in festen Salzen: Zeitschr. phys. Chemie, v. B11, p. 139-151.

———— 1969, The evaluation of data obtained with diffusion couples of binary single-phase and multiphase systems, Acta Metall., v. 17, p. 99-107.

Wei, G. C. T., and Wuensch, B. J., 1973, Composition dependence of ^{63}Ni diffusion in single-crystal NiO–MgO solid solutions: Am. Ceramic Soc. Jour., v. 56, p. 562-565.

Zeibold, T. O., and Cooper, A. R., Jr., 1965, Atomic mobilities and multicomponent diffusion: Acta Metall., v. 13, p. 465-470.

Contrib. Mineral. Petrol. 55, 127–130 (1976)

Contributions to Mineralogy and Petrology

Short Communication

The Reaction Sillimanite + Biotite + Quartz ⇌ Cordierite + K-Feldspar + H_2O and Partial Melting in the System $K_2O-FeO-MgO-Al_2O_3-SiO_2-H_2O$

E. Hoffer

Mineralogisch-Petrologisches Institut, Universität Göttingen, D-3400 Göttingen, Federal Republic of Germany

The reaction

$$\text{biotite} + \text{sillimanite} + \text{quartz} \rightleftharpoons \text{cordierite} + \text{K-feldspar} + H_2O \quad (1)$$

is observed in many high grade metamorphic terrains. It was studied by standard hydrothermal methods for $P_s = P_{H_2O}$. Equilibrium conditions (reversed experiments) have been determined at the following points:

650° C at 2,500 bars P_{H_2O}
680° C at 3,000 bars P_{H_2O}
710° C at 3,500 bars P_{H_2O}

The errors of the P and T conditions are better than ± 100 bars and $\pm 10°$ C, respectively. A curve representing the data in a $P-T$ diagram is shown in Fig. 1. The starting materials for this and for the subsequently described reaction (2) were natural minerals: sillimanite, biotite, and cordierite (Damara Orogen, SW Africa); K-feldspar (Adularia ($Or_{90}Ab_{10}$), St. Gotthard, Switzerland); quartz (Mandt). Biotite and cordierite were separated from the same rock specimen. Detailed chemical investigations show that cordierite and biotite are in exchange equilibrium with respect to Mg and Fe. The molar ratio $X_{Mg} = Mg/Mg + Fe^{2+}$ of the biotite is 0.50 and for the cordierite it is 0.66. The partial pressure of oxygen correspond to that of the quartz-magnetite-fayalite buffer.

The equilibrium curve of reaction (1) is terminated at higher temperatures by the intersection (II) with the melting reaction.

$$\text{biotite} + \text{K-feldspar} + \text{quartz} + \text{sillimanite} + H_2O \rightleftharpoons \text{liquid} \quad (2)$$

This reaction was studied at 7 and 10 kb $P_s = P_{H_2O}$. The first melt is generated

at 703° C and 7,000 bars P_{H_2O}
685° C and 10,000 bars P_{H_2O}.

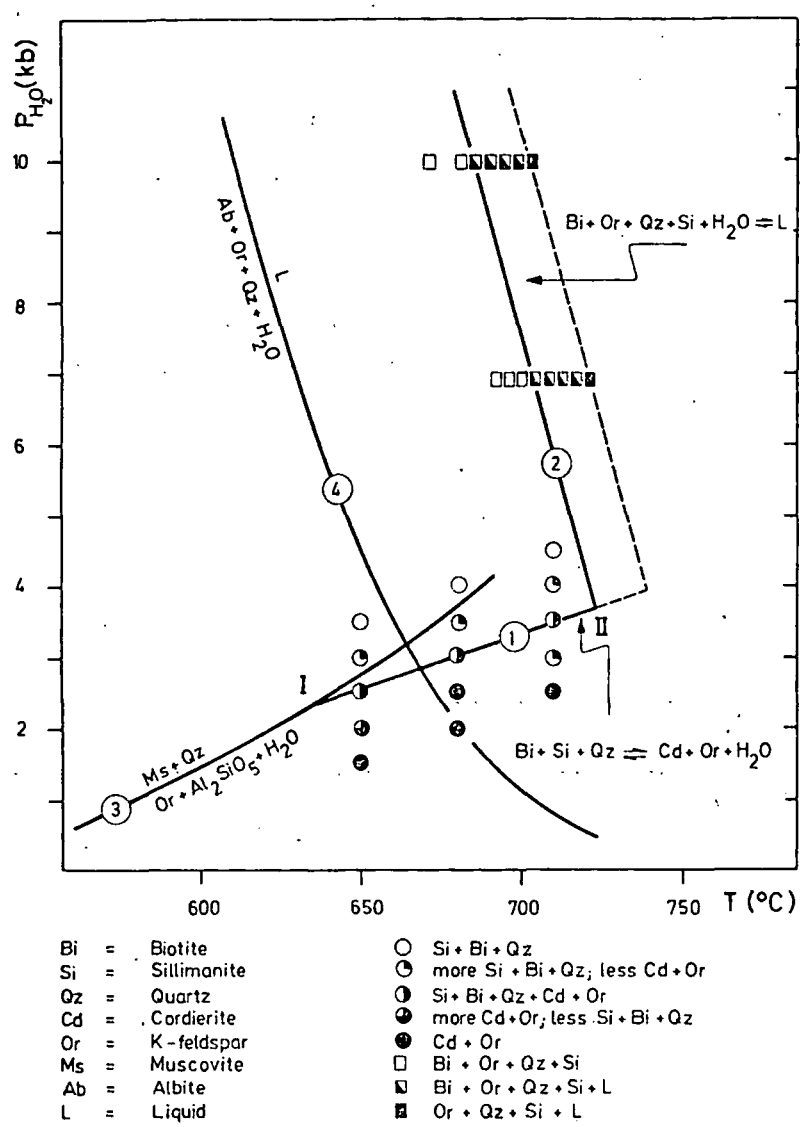

Fig. 1. Pressure-temperature diagram with the experimental results of the reactions

biotite + sillimanite + quartz ⇌ cordierite + K-feldspar + H_2O; (1)

biotite + K-feldspar + quartz + sillimanite + H_2O ⇌ liquid. (2)

The equilibrium curves of the reactions

muscovite + quartz ⇌ K-feldspar + Al_2SiO_5 + H_2O (3)

(Althaus *et al.*, 1970) and

albite + K-feldspar + quartz + H_2O ⇌ liquid (4)

(Tuttle and Bowen, 1958; Merrill *et al.*, 1970) are quoted from the literature

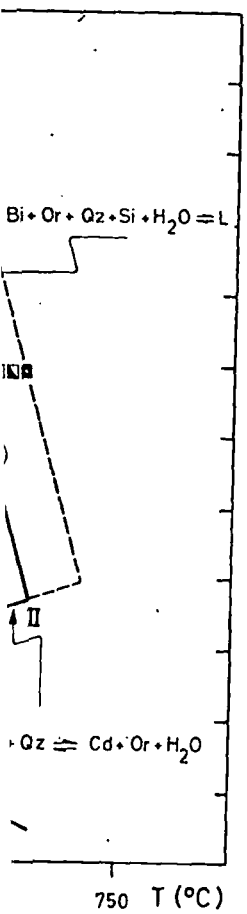

; less Cd + Or
Or
Si + Bi + Qz

+ L

ults of the reactions

O; (1)

(2)

(3)

(4)

ie literature

The melting occurs within a temperature interval of approximately 15–20° C in which melt coexists with biotite + K-feldspar + quartz + sillimanite + H_2O. The width of this interval is probably determined by the incongruent melting of the biotite and the alkali feldspar. Towards lower temperatures, the equilibrium curve of reaction (1) is terminated at the intersection point (I) by the reaction

$$\text{muscovite} + \text{quartz} \leftrightharpoons \text{K-feldspar} + Al_2SiO_5 + H_2O \quad (3)$$

which has been studied by several authors (Evans, 1965; Althaus *et al.*, 1970; Day, 1973; Chatterjee and Johannes, 1974).

When the data for reaction (3), according to Althaus *et al.* (1970), are used (which are approximate intermediate between those given by Chatterjee *et al.* and by Day, respectively), the coordinates in the $P-T$ diagram for the intersection points I and II are as follows:

I 640° C at 2,500 bars P_{H_2O}
II 723° C at 3,750 bars P_{H_2O}.

If, in a first approximation, Mg and Fe would be considered as one component the system K_2O-(FeO + MgO) $- Al_2O_3 - SiO_2 - H_2O$ could be treated as a five-component system. In this system the intersection points I and II would be invariant points for a given Mg : Fe ratio of the system. According to the phase theory, the following additional reactions (neglecting the quartz- and H_2O-absent reactions) must pass through point I:

$$\text{cordierite} + \text{muscovite} \rightleftharpoons \text{biotite} + \text{sillimanite} + \text{quartz} + H_2O \quad (4)$$

$$\text{biotite} + \text{muscovite} + \text{quartz} \rightleftharpoons \text{cordierite} + \text{K-feldspar} + H_2O, \quad (5)$$

and through point II

$$\text{biotite} + \text{sillimanite} + \text{quartz} \rightleftharpoons \text{liquid} + \text{cordierite} + H_2O \quad (6)$$

$$\text{K-feldspar} + \text{cordierite} + H_2O \rightleftharpoons \text{liquid} + \text{biotite} + \text{quartz} \quad (7)$$

$$\text{K-feldspar} + \text{sillimanite} + \text{cordierite} + \text{quartz} + H_2O \rightleftharpoons \text{liquid}. \quad (8)$$

Reaction (4) was determined in the system $K_2O - MgO - Al_2O_3 - SiO_3 - H_2O$ by Seifert (1970). The invariant point I in the Fe-free system lies at about 695° C and 5 kbars (Schreyer & Seifert, 1969). The present study shows clearly that point I is shifted to appreciably lower temperature and pressure if Fe is present.

It is important for petrogenetic conclusions from these experiments that reaction (1) occurs in a very narrow range of $P-T$ conditions. Furthermore, one has to take into consideration that pelitic rocks generally contain plagioclase (usually oligoclase); therefore, the melting conditions involving plagioclase, K-feldspar, and quartz are important also. The curve of the reaction albite + K-feldspar + quartz + $H_2O \leftrightharpoons$ liquid after Tuttle and Bowen (1958) and Merrill *et al.* (1970) intersects that of reaction (1) at approximately 665° C and 2.8 kbars.

Therefore, reaction (1) can be expected only in the small temperature range from about 640°–665° C and at pressures of about 2.5–3 kbars, because metapelites that contain plagioclase besides K-feldspar and quartz will undergo anatexis beyond about 665° C/2.8 kb and therefore reaction (1) is impossible.

In spite of these restrictions for reaction (1) to occur, it is a fact that the paragenesis which is due to reaction (1) has been observed in Nature in several places, e.g. the Moldanubian crystalline areas, Bavaria (Schreyer, 1966) and Gananoque area, Ontario (Reinhardt, 1968).

Acknowledgements. This work forms part of the research program of the Sonderforschungsbereich 48 "Entwicklung, Bestand und Eigenschaften der Erdkruste, insbesondere der Geosynklinalräume", University of Göttingen, Federal Republic of Germany. Funds for this work were provided by the Deutsche Forschungsgemeinschaft. The author wishes to express his cordial thanks to Prof. H.G.F. Winkler and Prof. P. Metz for stimulating discussions and reviewing the manuscript.

References

Althaus, E., Karotke, E., Nitsch, K.-H., Winkler, H.G.F.: An experimental re-examination of the upper stability limit of muscovite plus quartz. Neues Jahrb. Mineral. Monatsh. 1970, 325–336 (1970)

Chatterjee, N.D., Johannes, W.: Thermal Stability and Standard thermodynamic of Synthetic "M_1-Muscovite" $K\,Al_2[AlSi_3O_{10}(OH)_2]$. Contrib. Mineral. Petrol. **48**, 89–114 (1974)

Day, A.W.: The high temperature stability of muscovite plus quartz. Am. Mineralogist **58**, 255–262 (1973)

Evans, B.W.: Application of a reaction-rate method to the breakdown equilibria of muscovite and muscovite plus quartz. Am. J. Sci. **263**, 647–667 (1965)

Merrill, R.B., Robertson, J.K., Wyllie, P.J.: Melting reactions in the system $NaAlSi_3O_8-KAlSi_3O_8-SiO_2-H_2O$ to 20 kilobars compared with results for other feldspar-quartz-H_2O and rock-H_2O systems. J. Geol. **78**, 558–569 (1970)

Reinhardt, E.W.: Phase relations in cordierite-bearing gneisses from the Gananoque area, Ontario. Canadian Jour. Earth Sci. **5**, 455–482 (1968)

Schreyer, W.: Metamorpher Übergang Saxothuringikum – Moldanubikum östlich Tirschenreuth Obpf., nachgewiesen durch phasenpetrologische Analyse. Geol. Rundschau **55**, 481–509 (1966)

Schreyer, W., Seifert, F.: Compatibility relations of the aluminum silicates in the system $MgO-Al_2O_3-SiO_2-H_2O$ and $K_2O-MgO-Al_2O_3-SiO_2-H_2O$ at high pressures. Am. J. Sci. **267**, 371–388 (1969)

Seifert, F.: The low-temperature compatibility relations of cordierites in haplopelites of the system $K_2O-MgO-Al_2O_3-SiO_2-H_2O$. J. Petrol. **11**, 73–99 (1970)

Tuttle, O.F., Bowen, N.L.: Origin of granite in the light of experimental studies in the system $NaAlSi_3O_8-KAlSi_3O_8-SiO_2-H_2O$. Geol. Soc. Am. Mem. **74**, 153 (1958)

Received December 12, 1975 / Accepted December 16, 1975

Reprinted from
Economic Geology
Vol. 64, 1969, pp. 459–461

SCIENTIFIC COMMUNICATIONS

THE STABILITY OF ARGENTOPYRITE AND STERNBERGITE[1]

GERALD K. CZAMANSKE

L. Taylor of Lehigh University and I began independent studies of the Ag-Fe-S system in 1965. A common problem was the inability to synthesize any of the reported natural ternary sulfides (the German "Silberkiesgruppe," Ramdohr, 1955). A note confirming the chemical identity (dimorphic relation) of the two best documented "silberkies" minerals, argentopyrite and sternbergite, is currently in press (Czamanske and Larson, 1969). The present note reports the results of heating experiments on natural materials and a calculation of approximate thermodynamic values for the $AgFe_2S_3$ phases based on these experiments.

For the study, free-standing crystals from samples furnished by John White, of the United States National Museum (Washington, D. C.), were used: argentopyrite from Andreasberg, Harz, Germany (USNM R9630) and sternbergite from Jachymov, Bohemia, Czechoslovakia (USNM 85115). Mineralographic, X-ray, and chemical studies served to establish these as representative samples, with identical formula $AgFe_2S_3$ (Czamanske and Larson, 1969).

Heating experiments, conducted in evacuated silica tubes, show that both minerals are stable only at low temperatures and break down on heating to form an intergrowth of argentite, pyrite, and pyrrhotite. Both phases broke down in less than 7 days at 200° C, but apparently were unreacted after 8 months at 150° C. At 175° C no breakdown was detected after 2 days, whereas both phases had broken down completely after 30 days. After 8 days at 175° C the argentopyrite had begun to break down, whereas the sternbergite had not. This behavior may indicate a somewhat greater thermal stability for sternbergite or may represent a kinetic effect; the likelihood of the latter possibility is reduced by the fact that the breakdown products are identical. The notably slow nucleation of pyrite is involved in each instance. (The same order of breakdown is confirmed by Taylor (1967) who reports that at 150° C argentopyrite broke down nearly completely in 221 days and sternbergite only partially in 405 days. On this basis, Taylor suggests that argentopyrite is a lower temperature polymorph.)

[1] Publication authorized by the Director, U. S. Geological Survey.

The initial break-down products of each mineral are highly magnetic monoclinic pyrrhotite, argentite, and pyrite. Pyrrhotite and argenite are the dominant phases and occur in an intimate, graphic eutectoid-type intergrowth. Small grains of pyrite are irregularly distributed. As indicated in Figures 1 and 2, this assemblage is metastable at 150° C because the tie-line switch from the high-temperature assemblage, argentite-pyrrhotite-pyrite, to the low-temperature assemblage, silver-pyrrhotite-pyrite, takes place at 248 ± 8° C (Taylor, 1967). With continued annealing, argentite and pyrrhotite react slowly to form native silver and additional pyrite, and the stable assemblage is approached.

Calculations

Because it has been impossible to synthesize any of the ternary Ag-Fe-S phases, thermochemical values for the natural phases must be estimated. The principal difficulties with the calculations stem from the fact that the observed initial breakdown is to a metastable assemblage and the fact that the thermal data for monoclinic pyrrhotite have considerable errors as-

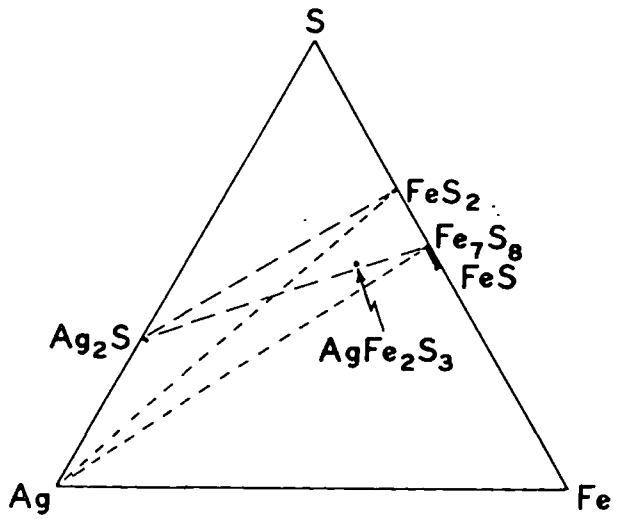

FIG. 1. Ternary diagram showing the principal minerals in the Ag-Fe-S system (plotted on the basis of mole percentages). The dashed lines indicate three phase assemblages stable at temperatures above (long dashes) and below (short dashes) 248 ± 8° C. (The solid bar represents the range of natural pyrrhotite compositions.)

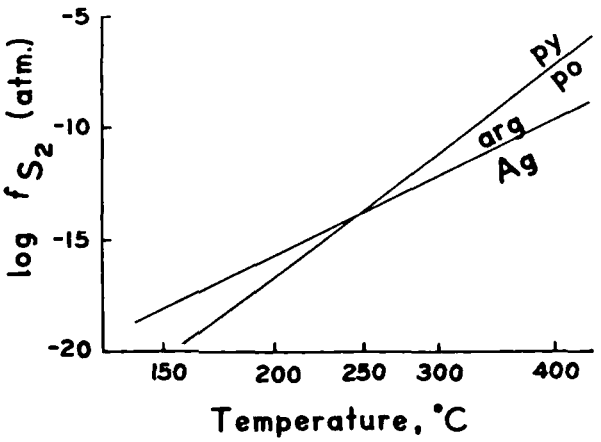

FIG. 2. Plot of 1/T vs log f_{S_2} (atm) showing the stability fields of the minerals Ag, argentite, pyrite, and pyrrhotite. The intersection of the schematic equilibrium curves at 248 ± 8° C (Taylor, 1967) precludes the stable coexistence of argentite and pyrrhotite at lower temperatures.

sociated with them and values must be estimated at the reaction temperature. Pertinent data are summarized by Freeman (1962) and Robie (1968). Low-temperature specific heats and entropies at 298.5° K of monoclinic pyrrhotite ($Fe_{0.877}S$) and troilite (FeS) were measured by Grønvold and Westrum (1959), and the entropy of argentite was determined by Walsh et al. (1962).

The most direct approach to a free energy of formation ($\Delta G°_{f423}$) value for $AgFe_2S_3$ is to assume that 150° C is the true equilibrium temperature for the observed reaction

$$4AgFe_2S_3 = 2Ag_2S + 8Fe_{0.877}S + FeS_2 \quad (1)$$

i.e., that $\Delta G°_{423} = 0$ for this reaction. Because reaction (1) involves a metastable breakdown assemblage, $\Delta G°_{423}$ should be negative for the reaction

$$6AgFe_2S_3 = 6Ag + 8Fe_{0.877}S + 5FeS_2, \quad (2)$$

involving the stable assemblage. Interpolation at 423° K (150° C) of values for the free energy functions of the compounds involved in reaction (1) permits calculation of the value −61,550 ± 2,200 cal. for $\Delta G°_{f423}$ of $AgFe_2S_3$. This value differs by only a few hundred calories from a value calculated in like manner for an assumed equilibrium breakdown temperature as low as 127° C (400° K). Through combination of reactions (1) and (2), $AgFe_2S_3$ may be eliminated and a value of −4,430 cal. can be calculated for reaction (2) using available free energy data for Ag_2S, $Fe_{0.877}S$, and FeS_2. As noted, a negative value is required by the actual stability of the silver-bearing assemblage relative to the Ag_2S-bearing assemblage.

Standard conventions allow other data to be roughly estimated. Cp_{298} for $AgFe_2S_3$ is calculated to be about 37.8 cal/deg on the assumption that ΔCp for reaction (1) is approximately zero (the Neumann-Kopp rule). The several methods available for estimating a value of $S°_{298}$ for $AgFe_2S_3$ give poor agreement. Estimations based on typical chalcogenide entropy contributions for the constituent elements result in a value of 48.6 cal/deg if the method of Latimer (1951) is used and 44 cal/deg if that proposed by Grønvold and Westrum (1962) is employed. The common method of estimation, involving the assumption that $\Delta S°_{298} = 0$ for a reaction forming the compound, results in values of 49.4 and 40.1 cal/deg when applied to reactions (1) and (2), using Walsh et al.'s (1962), Grønvold and Westrum's (1962), and Robie's (1968) values of $S°_{298}$

Table 1.--Comparison of estimated values of $S°_{298}$ for $AgFe_2S_3$ and dependent thermodynamic values.

Method of estimating $S°_{298}$	Estimated value of $S°_{298}$ for $AgFe_2S_3$	Resultant value of $\Delta S°_{298}$ for reaction (1)	Resultant value of $\Delta H°_{298}$ for reaction (1)	Resultant value of $\Delta H°_{f_{298}}$ for $AgFe_2S_3$[a/]	Resultant value of $\Delta G°_{f_{298}}$ for $AgFe_2S_3$[a/]
(1) Latimer (1951)	48.6 cal/deg.	3.05 cal/deg.	1,290 cal.	-60,438 cal.	-61,184 cal.
(2) Grønvold and Westrum (1962)	44	21.45	9,073	-62,383	-61,759
(3) $\Delta S°_{298} = 0$ for reaction (1)	49.4	0	0	-60,115	-61,089
(4) $\Delta S°_{298} = 0$ for reaction (2)	40.1	37.05	15,672	-64,033	-62,247
(5) Average of 1-3	47.3	8.25	3,490	-60,988	-61,347

[a/] Values of $\Delta H°_{f_{298}}$ and $\Delta G°_{f_{298}}$ for Ag_2S and FeS_2 from Robie (1968). Value of $\Delta H°_{f_{298}}$ for $Fe_{0.877}S$ from Freeman (1962). Value of $\Delta G°_{f_{298}}$ for $Fe_{0.877}S$ calculated from free energy function data (Robie, 1968, and Grønvold and Westrum, 1959).

for Ag_2S, $Fe_{0.877}S$, and FeS_2, respectively. In order to calculate recommended values of $\Delta H°_{f298}$ and $\Delta G°_{f298}$ for the compound $AgFe_2S_3$ a preferred entropy value of 47.3 cal/deg was taken; the average of the first 3 values listed in Table 1. The value obtained by setting $\Delta S°_{298} = 0$ for reaction (2) was not considered because the state of the ions in the reactants is not representative of their state in $AgFe_2S_3$; specifically, the silver is not combined with sulfur and over 56% of the reactant sulfur is contained in pyrite as $S_2^=$.

$\Delta H°_{298}$ values for reaction (1) can be calculated by using the estimated entropy values and a simplified form of the Gibbs-Helmholtz equation.

$$\Delta G_T = \Delta H_{298} - T\Delta S_{298}. \qquad (3)$$

$\Delta H°_{f298}$ values for $AgFe_2S_3$ may then be estimated by using the calculated $\Delta H°_{298}$ values for reaction (1), and known heats of formation for the remaining phases, in conjunction with an expression of the form $\Delta H°_{Reaction} = \sum_i \nu_i H°_{f_i}$, where ν_i is the stoichiometric coefficient. The calculated values of $\Delta H°_{298}$ for reaction (1) may be reinserted in equation (3) to derive values of $\Delta G°_{298}$ for reaction (1). Finally these values of $\Delta G°_{298}$ may be used in conjunction with available values of $\Delta G°_{f298}$ for Ag_2S, $Fe_{0.877}S$, and FeS_2 to derive values of $\Delta G°_{f298}$ for AgF_2S_3.

The results of these several estimations and calculations are summarized in Table 1. Recommended thermochemical values for $AgFe_2S_3$ are shown in Table 2. Error estimations are based on root mean square consideration of independent error sources.

The infrequent and minor occurrence of sternbergite and argentopyrite results primarily from the fact that they require sulfur fugacities near those associated with pyrite-pyrrhotite equilibrium, whereas geologic environments seldom provide such low values for f_{S_2} at low temperatures with an availability of abundant silver. Furthermore, argentopyrite and sternbergite are ordered ternary compounds which are only a few thousand calories per gram formula weight more stable than an assemblage of binary minerals; at temperatures below 150° C there is relatively little thermal energy available to overcome ordering thresholds.

TABLE 2.—*Recommended thermochemical values for* $AgFe_2S_3$

$\Delta G°_{f298} = -61{,}350 \pm 2{,}500$ cal.	$Cp_{298} \simeq 37.8$ cal/deg.
$\Delta G°_{f423} = -61{,}550 \pm 2{,}200$ cal.	$S°_{298} \simeq 47.3$ cal/deg.
$\Delta H°_{f298} = -61{,}000 \pm 2{,}500$ cal.	

Acknowledgments

I gratefully acknowledge the interest and constructive criticism of Paul B. Barton, Jr., who suggested study of the system Ag-Fe-S, and the cooperation of Larry Taylor, who shared his experimental results.

U. S. GEOLOGICAL SURVEY,
MENLO PARK, CALIF.

Dec. 27, 1968

REFERENCES

Czamanske, G. K., and Larson, R. R., 1969, The chemical identity and formula of argentopyrite and sternbergite: Am. Mineralogist, v. 54.

Freeman, R. D., 1962, Thermo dynamic properties of binary sulfides: Oklahoma Univ., Chem. Dept., Research Found. Rept. No. 60.

Grønvold, F., and Westrum, E. F., Jr., 1959, Heat capacities and thermodynamic properties of the pyrrhotites FeS and $Fe_{0.877}S$ from 5 to 350° K: Jour. Chem. Physics, v. 30, p. 528–531.

Grønvold, F., and Westrum, E. F., Jr., 1962, Heat capacities and thermodynamic functions of iron disulfide (pyrite), iron diselenide, and nickel diselenide from 5 to 350° K. The estimation of standard entropies of transition metal chalcogenides: Inorg. Chemistry, v. 1, p. 36–48.

Latimer, W. M., 1951, Methods of estimating the entropies of solid compounds: Jour. American Chem. Soc., v. 73, p. 1480–1482.

Ramdohr, Paul, 1955, Die Erzmineralien und ihre Verwachsungen: Akademie-Verlag, Berlin, 875 p.

Robie, R. A., and Waldbaum, D. R., 1968, Thermodynamic properties of minerals and related substances at 298.15° K (25.0° C) and one atmosphere (1.013 bars) pressure and at higher temperatures: U. S. Geol. Survey Bull. 1259, 256 p.

Taylor, L. A., 1967, Phase relationships in the system Ag-Fe-S: Geol. Soc. American Ann. Mtg., New Orleans, La., 1967, Program, p. 221–222.

Walsh, P. N., Art, E. W., and White, D., 1962, The heat capacity of the silver chalcogenides, $Ag_{1.99}S$, $Ag_{1.99}Se$, and $Ag_{1.88}Te$ from 16 to 300° K: Jour. Phys. Chemistry, v. 66, p. 1546–1549.

Reprinted from
Economic Geology
Vol. 64, 1969, pp. 462–468

DISCUSSIONS

COPPER MINERALIZATION IN THE UPPER PART OF THE COPPER HARBOR CONGLOMERATE AT WHITE PINE, MICHIGAN—A REPLY

Sir: In my paper concerning copper mineralization in the upper part of the Copper Harbor Conglomerate at White Pine, Michigan, I concluded that the native copper is diagenetic (2, p. 886). Ohle (3) and Brecke (1) in discussions of my paper have suggested that the copper mineralization is post-diagenetic.

Ohle has questioned the diagenetic origin on four main points, which can be summarized as follows: (1) the spatial association of the White Pine fault and copper mineralization in the Upper Sandstone (First Lode), Lower Sandstone (Second Lode), and the Third Lode indicate that the mineralization is fault controlled; (2) hydrocarbon, which controls the distribution of native copper, migrated to its present location in the sandstone through the White Pine fault system; (3) native copper, which typically occurs surrounding interstitial hydrocarbon, replaced the hydrocarbon; and (4) the origin of the chloritic facies at White Pine, which is closely tied to the origin of the native copper, may be due to a reducing environment imposed by the hydrocarbon. I will discuss these four points in order.

(1) There is a spatial association of fault and ore, which Ohle states can be reconciled with a diagenetic age for the copper only if there is a coincidental location of the favorable lithology with the fault. I have stated (2, p. 899) that "The apparent relationship between sandstone mineralization and structure seems only fortuitous."

As I have pointed out, copper mineralization is associated with cross-stratified, chloritic, carbonaceous sandstone (2, p. 897, Figs. 7 and 8). But in detail, the mineralization departs from exact correspondence with the cross-stratification. The irregular distribution of native copper is closely controlled by the irregular distribution of carbonaceous material, which in turn seems to be controlled by irregular sorting along individual cross-laminae. Thus, the favorable lithology occurs as small lenses and pods along individual cross-laminations and not as a continuous unit. Detailed examination of cores shows that these favorable lenses and pods are less abundant away from the fault in both the northeast and southwest blocks, particularly in the northeast block.

Also, it is an exaggeration to state, as Ohle has (3, p. 190), that Lower Sandstone ore is restricted to a zone within 1,000 feet of the White Pine Fault. White and Wright (4, p. 707) show three holes containing more than 5 foot-percent copper located 3,000–4,000 feet from the White Pine fault. These holes are located near where sections 10, 11, 14 and 15 meet. Southwest of the fault, drill hole N61 (NW¼, NW¼, sec. 16) is 3,300 feet from the fault and contains 6.2 foot-percent copper, and drill hole N12 (NE¼ SW¼, sec. 6) is 5,500 feet from the fault and contains 13.8 foot-percent copper in the Lower Sandstone.

The Third Lode mineralization occurs in the same type of favorable lithology as the Lower Sandstone mineralization. Ohle states that "near the fault, the greater thickness and closer stratigraphic spacing of the favorable, greenish-gray, bleached beds with scattered traces of copper led to continuation of the holes, and thus to the original discovery of the Third Lode ore zone" (3, p. 190). Holes away from the fault were stopped in the top few feet of the sand when it became red.

In all cases where there is Third Lode mineralization, there is some red sandstone separating the Lower Sandstone from the Third Lode. Thus, the presence of red sandstone below chloritic sandstone near the fault did not result in stopping the holes. It appears that the reasoning used in stopping the holes away from the fault without testing for Third Lode mineralization was based on the theory that the mineralization is fault-controlled. Thus, because of a lack of drilling away from the fault, there is no real proof that Third Lode mineralization exists only near the fault.

Ohle states that all known ore occurrences in the Upper Sandstone are close to the White Pine fault or one of its branches (3, p. 190). He mentions an exposure in the White Pine mine where the Upper Sandstone, exposed as a result of faulting, contains a 10-foot long concentration of native copper, which tapers from two feet to zero in that distance. I have not seen this exposure, but it appears from Ohle's discussion that the Upper Sandstone on the upthrown block is not exposed. It would be interesting to know if copper also occurs in that block.

Ohle does not comment on a nearly identical occurrence of native copper in the Lower Sandstone in the Southwest mine, which I have pictured (2, p.

Reprinted from
Economic Geology
Vol. 64, 1969, pp. 459–461

SCIENTIFIC COMMUNICATIONS

THE STABILITY OF ARGENTOPYRITE AND STERNBERGITE [1]

GERALD K. CZAMANSKE

L. Taylor of Lehigh University and I began independent studies of the Ag-Fe-S system in 1965. A common problem was the inability to synthesize any of the reported natural ternary sulfides (the German "Silberkiesgruppe," Ramdohr, 1955). A note confirming the chemical identity (dimorphic relation) of the two best documented "silberkies" minerals, argentopyrite and sternbergite, is currently in press (Czamanske and Larson, 1969). The present note reports the results of heating experiments on natural materials and a calculation of approximate thermodynamic values for the $AgFe_2S_3$ phases based on these experiments.

For the study, free-standing crystals from samples furnished by John White, of the United States National Museum (Washington, D. C.), were used: argentopyrite from Andreasberg, Harz, Germany (USNM R9630) and sternbergite from Jachymov, Bohemia, Czechoslovakia (USNM 85115). Mineralographic, X-ray, and chemical studies served to establish these as representative samples, with identical formula $AgFe_2S_3$ (Czamanske and Larson, 1969).

Heating experiments, conducted in evacuated silica tubes, show that both minerals are stable only at low temperatures and break down on heating to form an intergrowth of argentite, pyrite, and pyrrhotite. Both phases broke down in less than 7 days at 200° C, but apparently were unreacted after 8 months at 150° C. At 175° C no breakdown was detected after 2 days, whereas both phases had broken down completely after 30 days. After 8 days at 175° C the argentopyrite had begun to break down, whereas the sternbergite had not. This behavior may indicate a somewhat greater thermal stability for sternbergite or may represent a kinetic effect; the likelihood of the latter possibility is reduced by the fact that the breakdown products are identical. The notably slow nucleation of pyrite is involved in each instance. (The same order of breakdown is confirmed by Taylor (1967) who reports that at 150° C argentopyrite broke down nearly completely in 221 days and sternbergite only partially in 405 days. On this basis, Taylor suggests that argentopyrite is a lower temperature polymorph.)

[1] Publication authorized by the Director, U. S. Geological Survey.

The initial break-down products of each mineral are highly magnetic monoclinic pyrrhotite, argentite, and pyrite. Pyrrhotite and argenite are the dominant phases and occur in an intimate, graphic eutectoid-type intergrowth. Small grains of pyrite are irregularly distributed. As indicated in Figures 1 and 2, this assemblage is metastable at 150° C because the tie-line switch from the high-temperature assemblage, argentite-pyrrhotite-pyrite, to the low-temperature assemblage, silver-pyrrhotite-pyrite, takes place at 248 ± 8° C (Taylor, 1967). With continued annealing, argentite and pyrrhotite react slowly to form native silver and additional pyrite, and the stable assemblage is approached.

Calculations

Because it has been impossible to synthesize any of the ternary Ag-Fe-S phases, thermochemical values for the natural phases must be estimated. The principal difficulties with the calculations stem from the fact that the observed initial breakdown is to a metastable assemblage and the fact that the thermal data for monoclinic pyrrhotite have considerable errors as-

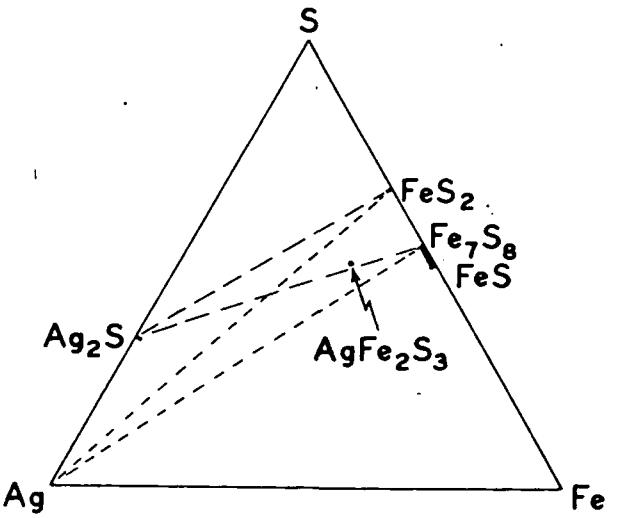

FIG. 1. Ternary diagram showing the principal minerals in the Ag-Fe-S system (plotted on the basis of mole percentages). The dashed lines indicate three phase assemblages stable at temperatures above (long dashes) and below (short dashes) 248 ± 8° C. (The solid bar represents the range of natural pyrrhotite compositions.)

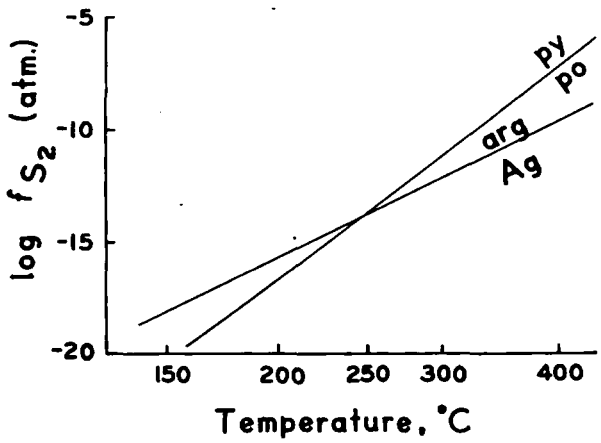

FIG. 2. Plot of 1/T vs log f_{S_2} (atm) showing the stability fields of the minerals Ag, argentite, pyrite, and pyrrhotite. The intersection of the schematic equilibrium curves at 248 ± 8° C (Taylor, 1967) precludes the stable coexistence of argentite and pyrrhotite at lower temperatures.

sociated with them and values must be estimated at the reaction temperature. Pertinent data are summarized by Freeman (1962) and Robie (1968). Low-temperature specific heats and entropies at 298.5° K of monoclinic pyrrhotite ($Fe_{0.877}S$) and troilite (FeS) were measured by Grønvold and Westrum (1959), and the entropy of argentite was determined by Walsh et al. (1962).

The most direct approach to a free energy of formation ($\Delta G°_{f423}$) value for $AgFe_2S_3$ is to assume that 150° C is the true equilibrium temperature for the observed reaction

$$4AgFe_2S_3 = 2Ag_2S + 8Fe_{0.877}S + FeS_2 \quad (1)$$

i.e., that $\Delta G°_{423} = 0$ for this reaction. Because reaction (1) involves a metastable breakdown assemblage, $\Delta G°_{423}$ should be negative for the reaction

$$6AgFe_2S_3 = 6Ag + 8Fe_{0.877}S + 5FeS_2, \quad (2)$$

involving the stable assemblage. Interpolation at 423° K (150° C) of values for the free energy functions of the compounds involved in reaction (1) permits calculation of the value −61,550 ± 2,200 cal. for $\Delta G°_{f423}$ of $AgFe_2S_3$. This value differs by only a few hundred calories from a value calculated in like manner for an assumed equilibrium breakdown temperature as low as 127° C (400° K). Through combination of reactions (1) and (2), $AgFe_2S_3$ may be eliminated and a value of −4,430 cal. can be calculated for reaction (2) using available free energy data for Ag_2S, $Fe_{0.877}S$, and FeS_2. As noted, a negative value is required by the actual stability of the silver-bearing assemblage relative to the Ag_2S-bearing assemblage.

Standard conventions allow other data to be roughly estimated. Cp_{298} for $AgFe_2S_3$ is calculated to be about 37.8 cal/deg on the assumption that ΔCp for reaction (1) is approximately zero (the Neumann-Kopp rule). The several methods available for estimating a value of $S°_{298}$ for $AgFe_2S_3$ give poor agreement. Estimations based on typical chalcogenide entropy contributions for the constituent elements result in a value of 48.6 cal/deg if the method of Latimer (1951) is used and 44 cal/deg if that proposed by Grønvold and Westrum (1962) is employed. The common method of estimation, involving the assumption that $\Delta S°_{298} = 0$ for a reaction forming the compound, results in values of 49.4 and 40.1 cal/deg when applied to reactions (1) and (2), using Walsh et al.'s (1962), Grønvold and Westrum's (1962), and Robie's (1968) values of $S°_{298}$

Table 1.--Comparison of estimated values of $S°_{298}$ for $AgFe_2S_3$ and dependent thermodynamic values.

Method of estimating $S°_{298}$	Estimated value of $S°_{298}$ for $AgFe_2S_3$	Resultant value of $\Delta S°_{298}$ for reaction (1)	Resultant value of $\Delta H°_{298}$ for reaction (1)	Resultant value of $\Delta H°_{f298}$ for $AgFe_2S_3$[a/]	Resultant value of $\Delta G°_{f298}$ for $AgFe_2S_3$[a/]
(1) Latimer (1951)	48.6 cal/deg.	3.05 cal/deg.	1,290 cal.	-60,438 cal.	-61,184 cal.
(2) Grønvold and Westrum (1962)	44	21.45	9,073	-62,383	-61,759
(3) $\Delta S°_{298} = 0$ for reaction (1)	49.4	0	0	-60,115	-61,089
(4) $\Delta S°_{298} = 0$ for reaction (2)	40.1	37.05	15,672	-64,033	-62,247
(5) Average of 1-3	47.3	8.25	3,490	-60,988	-61,347

[a/] Values of $\Delta H°_{f298}$ and $\Delta G°_{f298}$ for Ag_2S and FeS_2 from Robie (1968). Value of $\Delta H°_{f298}$ for $Fe_{0.877}S$ from Freeman (1962). Value of $\Delta G°_{f298}$ for $Fe_{0.877}S$ calculated from free energy function data (Robie, 1968, and Grønvold and Westrum, 1959).

for Ag_2S, $Fe_{0.877}S$, and FeS_2, respectively. In order to calculate recommended values of $\Delta H°_{f298}$ and $\Delta G°_{f298}$ for the compound $AgFe_2S_3$ a preferred entropy value of 47.3 cal/deg was taken; the average of the first 3 values listed in Table 1. The value obtained by setting $\Delta S°_{298} = 0$ for reaction (2) was not considered because the state of the ions in the reactants is not representative of their state in $AgFe_2S_3$; specifically, the silver is not combined with sulfur and over 56% of the reactant sulfur is contained in pyrite as $S_2^=$.

$\Delta H°_{298}$ values for reaction (1) can be calculated by using the estimated entropy values and a simplified form of the Gibbs-Helmholtz equation.

$$\Delta G_T = \Delta H_{298} - T\Delta S_{298}. \qquad (3)$$

$\Delta H°_{f298}$ values for $AgFe_2S_3$ may then be estimated by using the calculated $\Delta H°_{298}$ values for reaction (1), and known heats of formation for the remaining phases, in conjunction with an expression of the form $\Delta H°_{Reaction} = \sum_i^1 \nu_i H°_{fi}$, where ν_i is the stoichiometric coefficient. The calculated values of $\Delta H°_{298}$ for reaction (1) may be reinserted in equation (3) to derive values of $\Delta G°_{298}$ for reaction (1). Finally these values of $\Delta G°_{298}$ may be used in conjunction with available values of $\Delta G°_{f298}$ for Ag_2S, $Fe_{0.877}S$, and FeS_2 to derive values of $\Delta G°_{f298}$ for AgF_2S_3.

The results of these several estimations and calculations are summarized in Table 1. Recommended thermochemical values for $AgFe_2S_3$ are shown in Table 2. Error estimations are based on root mean square consideration of independent error sources.

The infrequent and minor occurrence of sternbergite and argentopyrite results primarily from the fact that they require sulfur fugacities near those associated with pyrite-pyrrhotite equilibrium, whereas geologic environments seldom provide such low values for f_{S_2} at low temperatures with an availability of abundant silver. Furthermore, argentopyrite and sternbergite are ordered ternary compounds which are only a few thousand calories per gram formula weight more stable than an assemblage of binary minerals; at temperatures below 150° C there is relatively little thermal energy available to overcome ordering thresholds.

TABLE 2.—*Recommended thermochemical values for $AgFe_2S_3$*

$\Delta G°_{f298} = -61{,}350 \pm 2{,}500$ cal.	$Cp_{298} \simeq 37.8$ cal/deg.
$\Delta G°_{f423} = -61{,}550 \pm 2{,}200$ cal.	$S°_{298} \simeq 47.3$ cal/deg.
$\Delta H°_{f298} = -61{,}000 \pm 2{,}500$ cal.	

Acknowledgments

I gratefully acknowledge the interest and constructive criticism of Paul B. Barton, Jr., who suggested study of the system Ag-Fe-S, and the cooperation of Larry Taylor, who shared his experimental results.

U. S. GEOLOGICAL SURVEY,
MENLO PARK, CALIF.
Dec. 27, 1968

REFERENCES

Czamanske, G. K., and Larson, R. R., 1969, The chemical identity and formula of argentopyrite and sternbergite: Am. Mineralogist, v. 54.

Freeman, R. D., 1962, Thermo dynamic properties of binary sulfides: Oklahoma Univ., Chem. Dept., Research Found. Rept. No. 60.

Grønvold, F., and Westrum, E. F., Jr., 1959, Heat capacities and thermodynamic properties of the pyrrhotites FeS and $Fe_{0.877}S$ from 5 to 350° K: Jour. Chem. Physics, v. 30, p. 528–531.

Grønvold, F., and Westrum, E. F., Jr., 1962, Heat capacities and thermodynamic functions of iron disulfide (pyrite), iron diselenide, and nickel diselenide from 5 to 350° K. The estimation of standard entropies of transition metal chalcogenides: Inorg. Chemistry, v. 1, p. 36–48.

Latimer, W. M., 1951, Methods of estimating the entropies of solid compounds: Jour. American Chem. Soc., v. 73, p. 1480–1482.

Ramdohr, Paul, 1955, Die Erzmineralien und ihre Verwachsungen: Akademic-Verlag, Berlin, 875 p.

Robie, R. A., and Waldbaum, D. R., 1968, Thermodynamic properties of minerals and related substances at 298.15° K (25.0° C) and one atmosphere (1.013 bars) pressure and at higher temperatures: U. S. Geol. Survey Bull. 1259, 256 p.

Taylor, L. A., 1967, Phase relationships in the system Ag-Fe-S: Geol. Soc. American Ann. Mtg., New Orleans, La., 1967, Program, p. 221–222.

Walsh, P. N., Art, E. W., and White, D., 1962, The heat capacity of the silver chalcogenides, $Ag_{1.98}S$, $Ag_{1.99}Se$, and $Ag_{1.96}Te$ from 16 to 300° K: Jour. Phys. Chemistry, v. 66, p. 1546–1549.

Reprinted from
Economic Geology
Vol. 64, 1969, pp. 462–468

DISCUSSIONS

COPPER MINERALIZATION IN THE UPPER PART OF THE COPPER HARBOR CONGLOMERATE AT WHITE PINE, MICHIGAN—A REPLY

Sir: In my paper concerning copper mineralization in the upper part of the Copper Harbor Conglomerate at White Pine, Michigan, I concluded that the native copper is diagenetic (2, p. 886). Ohle (3) and Brecke (1) in discussions of my paper have suggested that the copper mineralization is post-diagenetic.

Ohle has questioned the diagenetic origin on four main points, which can be summarized as follows: (1) the spatial association of the White Pine fault and copper mineralization in the Upper Sandstone (First Lode), Lower Sandstone (Second Lode), and the Third Lode indicate that the mineralization is fault controlled; (2) hydrocarbon, which controls the distribution of native copper, migrated to its present location in the sandstone through the White Pine fault system; (3) native copper, which typically occurs surrounding interstitial hydrocarbon, replaced the hydrocarbon; and (4) the origin of the chloritic facies at White Pine, which is closely tied to the origin of the native copper, may be due to a reducing environment imposed by the hydrocarbon. I will discuss these four points in order.

(1) There is a spatial association of fault and ore, which Ohle states can be reconciled with a diagenetic age for the copper only if there is a coincidental location of the favorable lithology with the fault. I have stated (2, p. 899) that "The apparent relationship between sandstone mineralization and structure seems only fortuitous."

As I have pointed out, copper mineralization is associated with cross-stratified, chloritic, carbonaceous sandstone (2, p. 897, Figs. 7 and 8). But in detail, the mineralization departs from exact correspondence with the cross-stratification. The irregular distribution of native copper is closely controlled by the irregular distribution of carbonaceous material, which in turn seems to be controlled by irregular sorting along individual cross-laminae. Thus, the favorable lithology occurs as small lenses and pods along individual cross-laminations and not as a continuous unit. Detailed examination of cores shows that these favorable lenses and pods are less abundant away from the fault in both the northeast and southwest blocks, particularly in the northeast block.

Also, it is an exaggeration to state, as Ohle has (3, p. 190), that Lower Sandstone ore is restricted to a zone within 1,000 feet of the White Pine Fault. White and Wright (4, p. 707) show three holes containing more than 5 foot-percent copper located 3,000–4,000 feet from the White Pine fault. These holes are located near where sections 10, 11, 14 and 15 meet. Southwest of the fault, drill hole N61 (NW¼, NW¼, sec. 16) is 3,300 feet from the fault and contains 6.2 foot-percent copper, and drill hole N12 (NE¼ SW¼, sec. 6) is 5,500 feet from the fault and contains 13.8 foot-percent copper in the Lower Sandstone.

The Third Lode mineralization occurs in the same type of favorable lithology as the Lower Sandstone mineralization. Ohle states that "near the fault, the greater thickness and closer stratigraphic spacing of the favorable, greenish-gray, bleached beds with scattered traces of copper led to continuation of the holes, and thus to the original discovery of the Third Lode ore zone" (3, p. 190). Holes away from the fault were stopped in the top few feet of the sand when it became red.

In all cases where there is Third Lode mineralization, there is some red sandstone separating the Lower Sandstone from the Third Lode. Thus, the presence of red sandstone below chloritic sandstone near the fault did not result in stopping the holes. It appears that the reasoning used in stopping the holes away from the fault without testing for Third Lode mineralization was based on the theory that the mineralization is fault-controlled. Thus, because of a lack of drilling away from the fault, there is no real proof that Third Lode mineralization exists only near the fault.

Ohle states that all known ore occurrences in the Upper Sandstone are close to the White Pine fault or one of its branches (3, p. 190). He mentions an exposure in the White Pine mine where the Upper Sandstone, exposed as a result of faulting, contains a 10-foot long concentration of native copper, which tapers from two feet to zero in that distance. I have not seen this exposure, but it appears from Ohle's discussion that the Upper Sandstone on the upthrown block is not exposed. It would be interesting to know if copper also occurs in that block.

Ohle does not comment on a nearly identical occurrence of native copper in the Lower Sandstone in the Southwest mine, which I have pictured (2, p.

Earth and Planetary Science Letters, 25 (1975) 385-397

SEAWATER–BASALT INTERACTION AT 200°C AND 500 BARS: IMPLICATIONS FOR ORIGIN OF SEA-FLOOR HEAVY-METAL DEPOSITS AND REGULATION OF SEAWATER CHEMISTRY

JAMES L. BISCHOFF*
Department of Geological Sciences, University of Southern California, Los Angeles, Calif. (USA)

and

FRANK W. DICKSON
Geology Department, Stanford University, Stanford, Calif. (USA)

Received November 5, 1974
Revised version received January 23, 1975

Seawater reacted with basalt at 200°C and 500 bars for 4752 hours changed chemically from an original slightly basic Na–Mg–SO_4–Cl solution to slightly acid dominantly Na–Ca–Cl solution. Mg and SO_4 decreased to near the limit of detection, and SiO_2 rose to near-saturation with amorphous silica. Ca dropped initially because of anhydrite precipitation, then rose to twice its initial value. K rose quickly to a steady level. Acidity at room conditions changed from the original pH of 7.9 to 3.9 at 72 hours, but subsequently increased to about 4.9. Fe and Mn passed through a maximum of 35 ppm at 1000 hours and steadily dropped thereafter to about 5 ppm. Low but significant levels of Ni and Cu entered the solution. The major solid products were anhydrite and montmorillonite. A small amount of glass decomposed during the experiment.

Conclusions based on the seawater–basalt reaction are: aqueous composition and alteration minerals were similar to those in the Iceland geothermal fields; sufficient heavy metals were solubilized to account for the deep-sea heavy-metal deposits; and the reaction provides a capacity for an adequate sink for Mg and SO_4, as well as potential source of H^+ needed for the geochemical balance of the oceans.

1. Introduction

Recent geochemical and geophysical work along active ocean ridge systems has led to the hypothesis that seawater continuously circulates through and interacts with basaltic rocks in the upper part of layer II.

This process was first suggested in an attempt to explain the observed patterns of heat flow of ocean ridge systems [1–3]. The average apparent heat flow over the ridge crest is less than half that anticipated if heat is transferred by conduction. Many areas within the crestal region are characterized by anomalously low heat flow. These facts led to the suggestion that most heat is being transferred by the penetration of seawater to several kilometers below the sea floor. Areas of low heat flow were explained as overlying zones of downward convection of seawater.

Calculations concerning permeability and flow rates showed that such convective flow most likely takes place on a scale adequate to account for the observed heat flow [2,4].

Geochemical, petrographic and isotopic studies on many weathered and metasomatized basalts from ridge crests and ophiolite sequences on land have provided evidence that seawater has acted as a metasomatic fluid at the temperatures ranging from 2°C

* Present address: U.S. Geological Survey, Menlo Park, Calif. 94025

(submarine weathering conditions) to 400°C (metamorphic conditions leading to the albite–epidote–actinolite assemblage) [4–11]. Seawater–basalt metasomatism has been suggested as a possible regulatory mechanism of the levels of certain components in seawater, namely Na, K, Mg, SO_4, and HCO_3 [4,9,12]. Although the data are still inadequate, known sinks for these components in the sedimentary environments appear to be inadequate to balance the annual supplies brought to the oceans by the rivers [13–15]. Hart [9] has suggested that seawater–basalt interaction takes place in three different catagories with gradations between them, as follows: (a) sea-floor weathering, with the formation of K-rich smectite (K removed from seawater); (b) retrograde greenschist metamorphism with formation of chlorite (Mg removed from seawater); and (c) primary greenschist metamorphism with formation of albite–actinolite (Na removed from seawater).

In addition, the suggestion has been made that seawater may leach significant amounts of heavy metals from basalts. Reprecipitation of heavy metals as hydroxides and silicates from basalt-reacted seawater that has re-entered the sea has been thought to be a possible mode of formation of both ancient and modern ferromanganoan sediments of the type recently found along the east Pacific Rise [7,12,16–18]. Boström [19], however, who has studied these deposits in great detail, came to the conclusion that seawater–basalt interaction could not produce such deposits; he pointed out that they are deficient in Al, and he felt that seawater should transport and precipitate significant amounts of Al along with the heavy metals.

The occurrence of fluids with modified seawater characteristics in the Reykjanes geothermal system of Iceland is direct evidence that seawater circulation can be effective in active ridge segments [20–22]. Subsurface temperatures reach 290°C at 1 km depth where basaltic glass has altered to anhydrite, calcite and montmorillonite in the upper parts and to chlorite, epidote and prehnite in the lower parts of rocks penetrated by 1 km deep drill holes. The seawater has lost most of its Mg and SO_4 and gained significant concentrations of Ca, K and SiO_2 [22]. Little work, however, has been carried out on the heavy-metal content of the geothermal fluids.

With the exception of the Iceland geothermal system, the hypothesis of seawater–basalt interaction on a large scale has been based on geophysical and petrological data and not on the basis of experimental knowledge. Our objective, therefore, was to experimentally react seawater with basalt under controlled conditions and to observe changes which took place in the seawater and the basalt. We wished to ascertain whether sufficient heavy metals would be solubilized for seawater to act as a transport medium and whether significant amounts of Na, K, Mg or SO_4 would be removed from the seawater or H^+ added, for the process to qualify as a regulatory mechanism for the steady-state composition of seawater.

2. Experimental procedures

Experimental conditions were chosen that approximated those found at 1/2 to 1 km below a typical active ocean ridge crest in the open ocean, with a geothermal gradient equivalent to the higher gradients observed for the Reykjanes geothermal area [22], namely 200°C and 500 bars. Three hundred grams of standard Copenhagen seawater were reacted with 30 g of tholeiite basalt ground to <100 mesh. The basalt is the U.S. Geological Survey standard rock BCR-1 [23] and Table 1).

The powdered basalt was suspended in Copenhagen seawater overnight before use, as a means to avoid adsorption and ion-exchange effects. Preliminary experiments were conducted using experimental apparatus which required quenching prior to separation of the seawater. These gave non-reproducible results, suggesting that partial back-reactions took place between the seawater and the basalt during quenching. Therefore, the experiment was conducted in such a way that seawater samples could be extracted from the system without disturbing the pressure of temperature of the experiment.

The hydrothermal solution equipment used was designed to avoid such difficulties [24]. In essence, the equipment consists of a 300-ml bottle-shaped sample cell of tetrafluorethylene resin (teflon), held in a stainless steel pressure vessel. Teflon was used because of its chemical inertness and its easy deformability. The sample cell is isloated from the interior of the steel pressure vessel and is provided with an exit tube through which liquid may be withdrawn or injected.

TABLE 1
Chemical and mineralogical composition of U.S. Geological Survey standard basalt, BCR-1 (from data compiled and averaged by Flanagan [23])

Major constituents (%)	
SiO_2	54:48
Al_2O_3	13.65
Fe_2O_3	3.68
FeO	8.91
MgO	3.28
CaO	6.95
Na_2O	3.31
K_2O	1.68
H_2O	1.59
TiO_2	2.23
MnO	0.17
P_2O_5	0.36
CO_2	0.03
S	0.03
Sum	100.35
Selected trace elements (ppm)	
Cu	22
Ni	15
Zn	132
Pb	18
Co	35
Cr	16
Ba	790

Petrographic description
BCR-1 is characterized as an aphanitic, hypocrystalline basalt with an intersertal texture consisting of randomly oriented plagioclase laths (An_{56}) with interstitial angite, brown glass, and iron oxides

A teflon filter is located at the lower end of the exit tube at the top of the cell. The basic principle of the equipment is simple: the sample cell changes shape in response to a pressure change in fluid surrounding it, thus allowing the internal pressure to become equal to the external pressure. The equipment provides an inert environment of teflon for the experimental mixtures; it allows essentially constant temperature and pressure to be maintained during sampling by the pumping of fluid into the steel pressure vessel at the same rate that liquid is withdrawn from the sample cell; it provides for internal filtering; in addition, it provides for mixing solids and liquids by continuous mechanical oscillation of the entire bomb housing.

Samples can be taken at arbitrary time intervals. The number of samples is limited only by the minimum volume to which the cell can be deformed without rupture, about 150 ml.

The seawater–basalt reaction was conducted for 4752 hours, during which time 19 samples of 6 ml each of the seawater were extracted at arbitrary intervals for chemical analysis.

Sample handling, dilution and analysis for pH, alkalinity and major ions follow those developed earlier for studies of interstitial water of marine sediments [16]. Na was determined by difference. Al, Fe, Mn, Zn, Ni, Cu and Pb contents of acidified aliquots were determined by both flame and flameless atomic absorption spectroscopy. Of these, Al, Zn and Pb were at or below the level of contamination from storage vials and added reagents, of approximately 0.03–0.05 ppm for all samples.

2.1. Control experiment

In addition, one control experiment was conducted to assess the changes that take place in seawater with basalt not present, on taking the seawater to 200 °C, 500 bars. The control experiment provided a means to recognize possible contamination and to provide data for comparison with the effect of basalt in subsequent experiments. In the control experiment, the seawater was held at conditions for only 305 hours, sufficiently long in view of the lack of changes observed after 48 hours.

The data indicate (Table 2) that simple heating causes decreases in Ca, SO_4, alkalinity and pH, suggesting that calcium sulfate and carbonate become supersaturated and precipitate. Anhydrite was found in the teflon cell after quenching, but no calcium carbonate was detected. The corroded nature of the anhydrite crystals (20 micron length) suggested that resolution took place during the quenching process, which required about 2 hours.

2.2. Basalt–seawater reaction

Major components. The changes which took place in the seawater in contact with basalt was profound (Figs. 1 and 2, Table 2). Mg continuously decreased (Fig. 1) during the course of the experiment, and 98% of the original Mg was removed. Ca displayed an initial decrease within the first 48 hours, presumably a re-

TABLE 2
Concentration of selected dissolved species in standard seawater before and during interaction with basalt

Sample	Parts per thousand (per mil)					Parts per million (ppm)		pH*	Alkalinity (meq./kg)
	Mg	Ca	K	SO_4	SiO_2	Fe	Mn		
Standard seawater, 25°C	1.29	0.41	0.40	2.70	0.01	< 0.05	< 0.05	7.9	2.6
Seawater at 200°C, 500 bars (by itself) 305 hr	1.28	0.14	0.40	2.21	0.01	< 0.05	< 0.05	6.2	0.5
Seawater reacted with basalt at 200°C; 500 bars									
0 hr	1.18	0.41	0.40	2.61	0.2	< 0.05	< 0.05	5.2	0.3
24 hr	0.96	0.10	0.44	1.26	0.3	15	10	3.2	< 0.3
71 hr	0.83	0.15	0.49	0.92	0.5	31	10	3.9	< 0.3
90 hr	0.76	0.15	0.47	0.78	(–)	31	13	4.0	< 0.3
142 hr	0.71	0.21	0.52	0.58	(–)	37	20	4.2	< 0.3
212 hr	0.64	0.28	0.53	0.39	(–)	35	25	4.2	< 0.3
262 hr	0.60	0.33	0.53	0.33	(–)	29	25	4.2	< 0.3
335 hr	0.50	0.36	0.53	0.29	0.5	32	28	4.2	< 0.3
426 hr	0.48	0.41	0.55	0.25	(–)	32	33	4.5	< 0.3
552 hr	0.43	0.47	0.55	0.22	(–)	29	35	4.4	< 0.3
738 hr	0.36	0.52	0.55	0.20	0.78	34	32	4.4	< 0.3
785 hr	0.35	0.55	0.55	0.17	0.79	33	32	4.7	< 0.3
1576 hr	0.19	0.81	0.55	0.12	0.67	24	23	4.7	< 0.3
2328 hr	0.12	0.95	0.58	0.10	0.88	17	23	4.7	< 0.3
2928 hr	0.08	0.95	0.58	0.10	0.87	16	17	4.9	< 0.3
3576 hr	0.06	0.95	0.55	0.06	0.80	12	11	4.9	< 0.3
4176 hr	0.05	0.90	0.54	0.06	–	8	8	(–)	< 0.3
4752 hr	0.03	0.90	0.53	0.06	0.80	5	5	4.9	< 0.3

* Measured at room temperature under nitrogen atmosphere. (–) not analyzed.

sult of initial precipitation of anhydrite, followed by a continuous increase to a factor of two greater than the original concentration. K increased to approximately 35% greater than the original concentration within the first 70 hours, and remained at that concentration for the duration of the experiment. pH, which was measured after the seawater sample was allowed to cool to 25°C in isolation from air, showed an initial decrease to 3.9 followed by a gradual increase to 4.9, a value considerably lower than the original pH of 7.9.

SO_4 continuously decreased to less than 3% of its original composition (Fig. 2). Dissolved SiO_2, in contrast, became a major species, and after 700 hours attained concentrations near saturation for amorphous silica [25]. Na and Cl decreased slightly and continuously during the experiment, most likely resulting from gentle dilution accompanying slow, osmotically-driven diffusion of pure water into the saline fluid inside the teflon bottle. The decreases in Na and Cl concentration, therefore, do not reflect interaction with the basalt.

The composition of the seawater changed from a slightly alkaline Na, Mg, Cl, SO_4 solution to a slightly acid Na, Ca, Cl solution.

Heavy elements. The reacted seawater was significantly enriched in some heavy elements (Fig. 3). Fe and Mn had almost identical patterns and concentration; they reached a maximum of approximately 35 ppm at 1000 hours, and thereafter slowly decreased to 5 ppm by the end of the experiment. Of the remaining elements looked for, Cu and Ni displayed

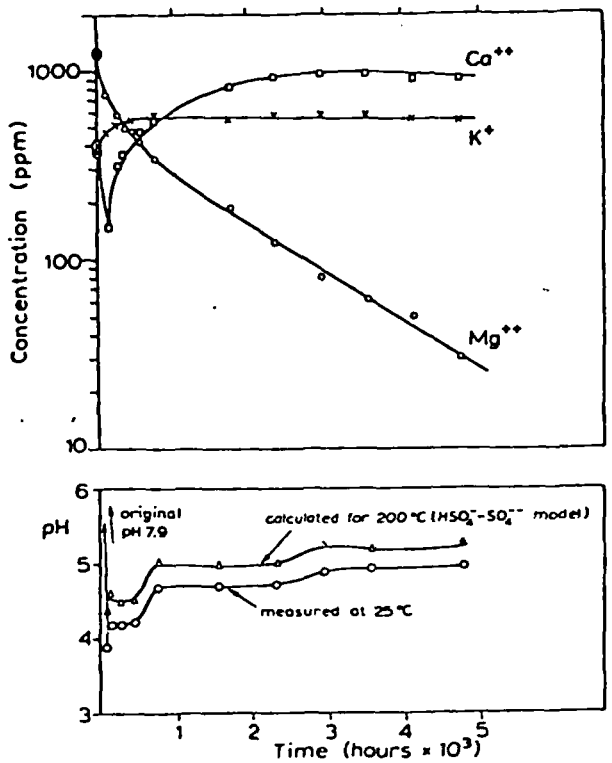

Fig. 1. pH and concentrations of Ca, Mg and K in Copenhagen seawater during interaction with basalt powder (BCR-1) at 200°C, 500 bars.

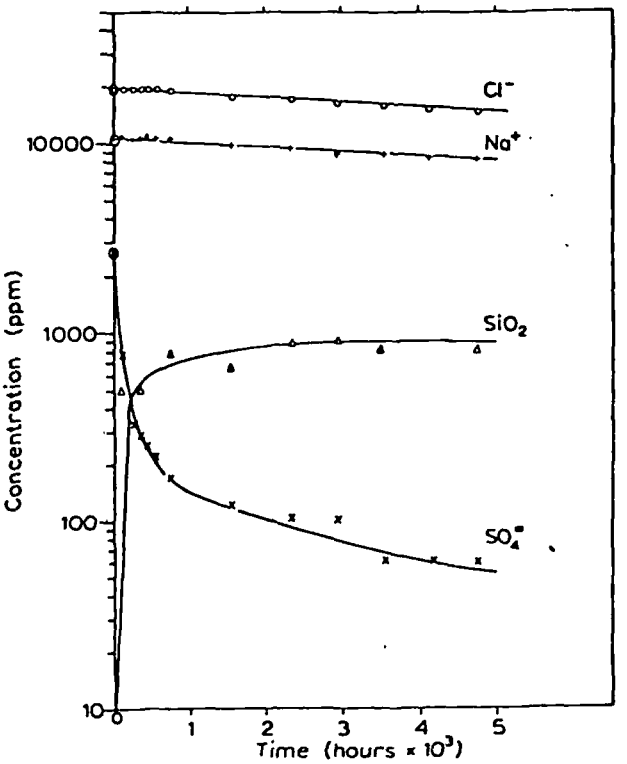

Fig. 2. Concentration of SO_4, dissolved SiO_2, Na and Cl in Copenhagen seawater during interaction with basalt powder (BCR-1) at 200°C and 500 bars.

concentrations above detection limits, reaching 0.2 ppm by the end of the experiment. The concentrations of Fe, Mn, Cu and Ni, therefore, were 2 to 3 orders of magnitude enriched over normal seawater and are above the theoretical minimum concentration for metal concentration of ore fluids [26].

Solid phases. At the close of the experiment the solid phase was examined. The rock powder had formed a slightly lithified, crudely stratified cake, but it otherwise had not changed much in appearance. The powder had apparently fallen out of suspension during the times that rocking had been temporarily stopped for sampling and maintenance purposes. Some of the cementing agent was anhydrite, which was dispersed throughout the solid cake as well as on outer portions of the cake and inner surfaces of the sample cell. Petrographic and X-ray diffraction studies revealed that a small fraction of the glass phase had been altered to a montmorillonite. We could find no evidences that the plagioclase or pyroxene crystals had reacted, either by dissolving or by development of overgrowths. The montmorillonite displayed usual behavior upon glycolation and heating. X-ray examination of the clay revealed an 060 spacing at 1.49 Å, indicating a dominantly dioctahedral nature. A less distinct spacing at 1.53 Å suggested that a co-existing trioctahedral montmorillonite may have been present in small amounts. The mean refractive index of the clay was 1.58, indicating a significant iron content [27].

We were unsuccessful in attempts to separate the montmorillonite cleanly from the glass phase, and, therefore, we were unable to determine the stoichiometric composition of the clay. Lacking this information we could not reconstruct the details of the alteration reaction.

3. Discussion

3.1. Aqueous species

Calculations. To estimate in-situ pH, degree of

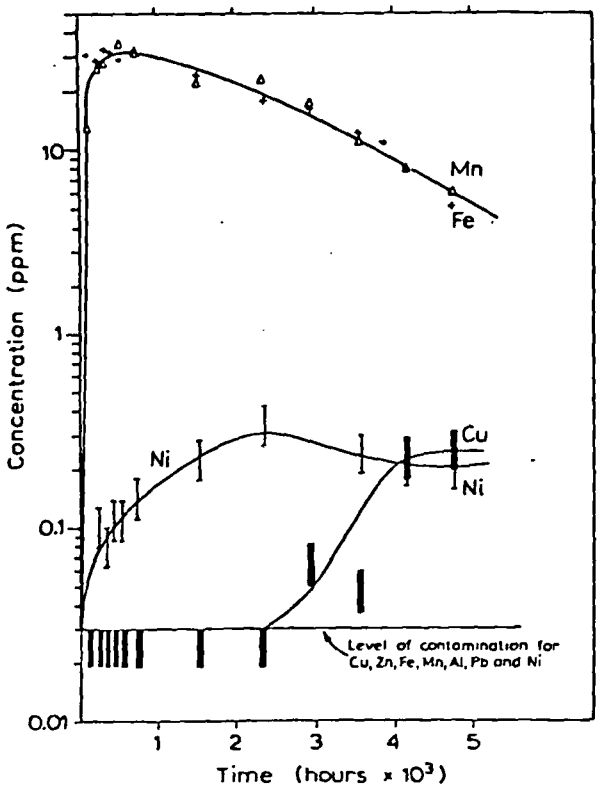

Fig. 3. Concentration of various dissolved metals in Copenhagen seawater during interaction with basalt powder (BCR-1) at 200°C and 500 bars. The contamination levels of approximately 0.03 ppm for these elements is that caused by the reagent grade HNO_3 used to acidify the samples, and that from the glass vials used for storage of the samples. Note that Al, Zn and Pb remain at or below this level during the entire experiment. Vertical bars for Ni and Cu indicate precision of analyses.

complexing, and degree of saturation by certain minerals, a calculation of the distribution of ionic species was performed, following the general procedures developed by Garrels and Thompson [28] for seawater at 25°C. Our solution at the experimental conditions differed from normal seawater in that carbonate species were absent, and ion pairs such as $NaCl^0$ and HCl^0 become important because of the elevated temperature. Mass-balance relations were derived to relate analyzed components to the various species (Table 3). To relate measured pH at room temperature to pH at 200°C, a hydrogen ion mass balance (eq. 7, Table 3) was constructed. This relation assumes that species which significantly associates with hydrogen ion at higher temperatures (e.g., HSO_4^- and HCl^0), rapidly dissociate upon cooling, and that the pH measured at room temperature is a sum of their hydrogen ion equivalents plus the free hydrogen ion that had existed at 200°C. Values for dissociational equilibria (Table 3) are for 200°C and 15 bars, not the 500 bars of the experiment [29]. In the absence of partial molar volume data for the ion pairs, pressure corrections cannot be made. For comparison, however, a pressure increase of 500 bars increases the solubility of anhydrite in NaCl solutions at 200°C by about 20% [30]. We have made the approximation that ion pair stability was affected in as minimal a degree. The uncertainty introduced is about the same as our analytical uncertainty for SO_4 for the latter half of the experiment, during which SO_4 concentration became very low. Activity coefficients were estimated using the expanded Debye–Hückel relation with equation parameters for 200°C.

TABLE 3

Dissociational equilibria and mass-balance relations used to calculate distribution of ionic species in seawater at 200°C

Mass-balance relation	Dissociational equilibria	
	reaction	log $K_{200°C}$**
(1) $m_{Ca^{2+}}(\text{total}) = m_{Ca^{2+}} + m_{CaSO_4^0}$	(1) $CaSO_4^0 \rightleftharpoons Ca^{2+} + SO_4^{2-}$	−3.6
(2) $m_{Mg^{2+}}(\text{total}) = m_{Mg^{2+}} + m_{MgSO_4^0}$	(2) $MgSO_4^0 \rightleftharpoons Mg^{2+} + SO_4^{2-}$	−4.0
(3) $m_{K^+}(\text{total}) = m_{K^+} + m_{KSO_4^-}$	(3) $KSO_4^- \rightleftharpoons K^+ + SO_4^{2-}$	−1.94
(4) $m_{Na^+}(\text{total}) = m_{Na^+} + m_{NaCl^0}$	(4) $NaCl^0 \rightleftharpoons Na^+ + Cl^-$	0.42
(5) $m_{SO_4^{2-}}(\text{total}) = m_{SO_4^{2-}} + m_{HSO_4^-} + m_{CaSO_4^0} + m_{MgSO_4^0} + m_{KSO_4^-}$	(5) $HSO_4^- \rightleftharpoons H^+ + SO_4^{2-}$	−3.15
(6) $m_{Cl^-}(\text{total}) = m_{Cl^-} + m_{NaCl^0} + m_{HCl^0}$	(6) $HCl^0 \rightleftharpoons H^+ + Cl^-$	0.06
(7) $m_{H^+}(25°C) = m_{H^+}(200°C) + m_{HSO_4^-} + m_{HCl^0}$*		

* This relation is derived on the basis that $M_{HSO_4^-}$ and M_{HCl^0} are negligible at 25°C in comparison with 200°C.
** Data taken from [29] and references therein.

An iterative procedure was used to perform the calculation by computer [28]. Successive approximations were made of ionic strength, and in turn, individual ion activity coefficients, and dissolved species until successive iterations resulted in insignificant change. This calculation resulted in a list of concentrations for each free and complexed ion, for each sample taken during the experiment.

Distribution of species. A condensed summary of results for a few selected samples are compared with unreacted seawater in Table 4. Increased complexing as a result of increased temperature is apparent from the decrease in ionic strength, and the decrease in the fraction of free Mg^{2+} and SO_4^{2-}. The pH would be expected to be higher at 200°C than at 25°C because of the hydrolysis of SO_4^{2-} to HSO_4^-. Actually, the pH at 200°C was near neutrality (neutral = 5.6). For pH to drop in this manner requires that extra hydrogen ion be created during interaction with the basalt. The degree of Ca^{2+} ion complexing was not changed significantly, nor was more than 1% of Na^+ or K^+ present as complex ions (data for Na^+ and K^+ not shown).

Anhydrite saturation. Calculation of the ion activity product (IAP) for anhydrite from these data (Table 4) indicate that the seawater was near saturation with respect to anhyrdite, with an average log IAP of −7.5 compared to log K_{sp} of −7.2 reported by other workers [29]. The slight, but systematic difference probably reflects our analytical uncertainty of approximately ±10% for sulfate, and to unassessed pressure effects on the equilibrium constants. In spite of these uncertainties, the close agreement suggests that the solution was essentially saturated with anhydrite throughout the experiment. Anhydrite precipitated continuously throughout the experiment by reaction of SO_4 in solution with Ca released from the rock. The precipitation of anhydrite continued until SO_4 was almost quantitatively removed from the seawater.

Iron-phase reactions. Before undertaking the experiment we had postulated that during seawater–basalt interaction, dissolved O_2 would likely be removed by oxidation of magnetite to hematite by the well-known reaction:

$$\tfrac{1}{2}O_2 + 2Fe_3O_4 \rightleftharpoons 3Fe_2O_3$$

Log K is 18.95 for this reaction at 200°C [29]. This indicates that magnetite transforms to hematite until the fugacity of oxygen declines to $10^{-37.9}$ (this represents less than 4×10^{-40} ppm dissolved oxygen. Moreover, only an insignificant mass of magnetite need transform to hematite to buffer the dissolved oxygen in this manner. In our experiment, for example, which utilized a 10/1 ratio of seawater to basalt, only 0.01 g of hematite would have formed in the 30 g of rock powder, an amount too small to be detected.

Is our system in equilibrium with magnetite–hematite? If this reaction controls the concentration of dissolved oxygen, it likely would control dissolved ferrous iron, as follows:

$$Fe^{2+} + H_2O + Fe_2O_3 \rightleftharpoons Fe_3O_4 + 2H^+$$

the equilibrium constant, $K = a^2_{H^+}/a_{Fe^{2+}}$ is $10^{-3.48}$ at 200°C [29]. Values for $a^2_{H^+}/a_{Fe^{2+}}$ for our experiment, calculated from the distribution of species data (Table 4) averaged $10^{-5.33}$. Taken at face value, this would indicate that there was more dissolved ferrous iron than would be expected at the observed pH's and therefore the system is not in equilibrium with magnetite–hematite. This suggests, therefore, that ferrous iron was being supplied by a silicate or glass phase and that the system was even more reducing than had been anticipated. The oxidized phase in this case is likely a nontronite component within the montmorillonite alteration product. Although the gross trends of pH and Fe with time were similar, equilibrium was not attained with regard to Fe contribution to and subtraction from solution during the course of the reaction.

3.2. Overall reaction

The following sequence of events can be constructed for the reaction of seawater with basalt. Initially, anhydrite precipitates in response to increased temperature. This is followed by the alteration of some of the glass phase to montmorillonite, releasing in the process Ca, SiO_2, Fe, Mn, Cu, and Ni. As Ca continues to build up in solution, anhydrite continues to precipitate until essentially all sulfate is consumed. That Mg plays a major kinetic role in the formation of montmorillonite alteration product was noted by Hawkins and Roy [31]. Mg^{2+}, the most reactive cation in seawater is likely incorporated into the montmorillonite, and is probably accompanied by OH^- from seawater to preserve electrical neutrality. This provides a mechanism for the observed pH lowering, which in turn

TABLE 4
Selected solution parameters derived from distribution of ionic species calculation

	Ionic strength	pH	Mg^{2+} (% free ion)	Ca^{2+} (% free ion)	SO_4^{2-} (% free ion)	$\log m_{SO_4^{2-}}/m_{HSO_4^-}$	$\log a_{Ca^{2+}}/a_{SO_4^{2-}}$ **	$\log a_H^2/a_{Fe^{2+}}$ ***
Standard seawater, 25°C, 1 bar *	0.70	8.11	87	91	54	6.9	−5.3	–
Seawater at 200°C, 500 bars								
305 hr	0.57	6.8	63	97	3	3.1	−7.6	–
Seawater reacted with basalt at 200°C, 500 bars								
71 hr	0.55	4.4	74	98	4	0.6	−7.7	−4.7
335 hr	0.55	4.5	87	99	6	0.8	−7.7	−4.9
785 hr	0.54	4.9	89	99	8	1.3	−7.6	−5.7
1576 hr	0.50	5.0	88	99	12	1.3	−7.4	−5.8
3576 hr	0.45	5.1	88	99	21	1.4	−7.4	−5.7
4752 hr	0.42	5.2	83	96	31	1.5	−7.2	−5.2

* Taken from Garrels and Thompson model of seawater [16].
** These figures should be compared to $\log K_{sp}$ anhydrite of −4.7 at 25°C and −7.2 at 200°C, as given by Helgeson [29].
*** These figures should be compared to $\log K$ of −3.48 at 200°C for the reaction $Fe^{2+} + H_2O + Fe_2O_3 \rightarrow Fe_3O_4 + 2H^+$, derived from data in [29].

accelerates the alteration process. As the seawater Mg is used up, the pH begins to increase, thereby slowing the rate of montmorillonite formation. Al, Fe^{2+}, Fe^{3+}, contained in the montmorillonite structure came from the basalt and perhaps some Mg as well.

In the absence of knowledge of stoichiometric compositions of the glass and montmorillonite phases, the overall reaction can be expressed only as follows with unspecified coefficients:

(a) glass + Mg^{2+} + H_2O ⇌ montmorillonite + Ca^{2+}

+ K^+ + H_4SiO_4 + H^+ + Fe^{2+} + Mn^{2+}

(b) Ca^{2+} + SO_4^{2-} ⇌ anhydrite

The pH lowering, however, would be partially offset by H^+ attack on glass and anhydrous silicates.

Montmorillonite continues to form while Mg^{2+} is actively being removed from solution. Eventually, the pH then begins to rise as hydrolysis reactions become increasingly more important. Fe and Mn concentrations decrease in response to the increasing pH, probably by entering the montmorillonite or by formation of Fe and Mn oxides.

Only a small fraction of the glass phase in the sample altered to montmorillonite; the capacity of the rock to consume Mg^{2+} (OH^-?) from the seawater by reaction of all the glass, therefore, is much larger than shown in our experiment. Presumably, if Mg^{2+} were continuously supplied by fresh seawater, all glass might eventually be converted to montmorillonite.

3.3. Anhydrite–pyrite problem

Our experimental results are consistent with alteration products and chemistry of the modified seawater of the Reykjanes geothermal field in Iceland, as mentioned earlier [22]. The alteration assemblage anhydrite–montmorillonite, which was noted in the upper portions of the rock sequence, was likely formed roughly under the conditions of our experiment. However, anhydrite has not been reported in altered basaltic rocks from the sea floor, although montmorillonite phases are common. Basalts cored during DSDP leg 34 in the Nasca plate, for example, displayed veinlets of montmorillonite, calcite and pyrite [32–34]. These minerals contained stable isotopes that suggested that they formed at about 7°C [34,35], by reaction with waters too cool to permit $CaSO_4$ phases to form.

Pyrite is a common mineral in many basalts that presumably have been altered by seawater. The presence of pyrite in ophiolitic rocks of Italy led Spooner and Fyfe [12] to suggest that seawater SO_4 may be reduced during reaction with basalt, as follows:

$$11Fe_2SiO_4 + 2SO_4^{2-} + 4H^+ = 7Fe_3O_4 + FeS_2 + 11SiO_2 + 2H_2O$$

in which Fe_2SiO_4 is representative for the ferrous silicate component in olivine, pyroxene or glass.

Anhydrite formed readily and rapidly in our experiment as it apparently has in the Reykjanes geothermal system. Perhaps anhydrite commonly forms early in the seawater–basalt reaction, and it may be reduced completely to form pyrite given sufficient time. To examine this possibility, Spooner and Fyfe's reaction can be modified by substituting $CaSO_4$ for SO_4^{2-}, yielding:

$$11Fe_2SiO_4 + 2CaSO_4 + 4H^+ = 7Fe_3O_4 + FeS_2 + 11SiO_2 + 2H_2O + 2Ca^{2+}$$

The equilibrium constant for this reaction, $a_{Ca^{2+}}/a_{H^+}^2$, calculated for 200°C [29] is very much larger than the experimental value of $a_{Ca^{2+}}/a_{H^+}^2$ (Fig. 4), indicating a strong thermodynamic potential for the reaction to proceed as written. This suggests, therefore, that

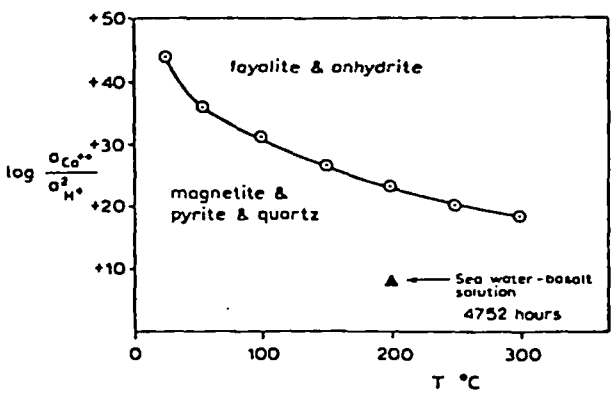

Fig. 4. Log $a_{Ca^{2+}}/a_{H^+}^2$ (which is 1/2 log K) plotted versus temperature for the reaction $11Fe_2SiO_4 + 2CaSO_4 + 4H^+ \rightarrow 7Fe_3O_4 + FeS_2 + 11SiO_2 + 2H_2O + 2Ca^{2+}$. Calculated from thermodynamic data given in [29].

anhydrite formed and persisted as a metastable phase in our experiments. However, unbuffered solutions such as seawater need react only with a negligible amount of solid phase to adjust acidity to the equilibrium value. The limited capacity of water to furnish H^+ is the reason that only a trivial amount of pyrite would form.

Modifying Spooner and Fyfe's reaction in another way, by substituting seawater Mg^{2+} for H^+, gives:

$$2H_2O + 11Fe_2SiO_4 + 2Mg^{2+} + 2SO_4^{2-}$$

$$= Mg_2Si_3O_6(OH)_4 + FeS_2 + 8SiO_2 + 7Fe_3O_4$$

in which $Mg_2Si_3O_6(OH)_4$ (sepiolite) represents the magnesium component of a secondary montmorillonite. This reaction does not require H^+, and it consumes Mg^{2+} and SO_4^{2-} in a 1/1 ratio. However, the reaction does not transform anhydrite; rather it removes SO_4 directly from solution. To better represent a reaction with anhydrite, a source of Ca is required on the left and a sink for Ca is needed on the right, possibly a zeolite. The number of interdependent reactions possible in this multicomponent system is very large, and an exact solution is not possible in the present state of knowledge.

The absence of anhydrite in submarine rocks, therefore, may be a consequence of a slow transformation of early-formed anhydrite, possibly at elevated temperatures. Alternatively, anhydrite might be removed by the dissolving action of late cool seawater. Even so, some remnants of early anhydrite should be found, judging from the persistence of other metastable minerals in low-temperature and marine environments. The absence of anhydrite in altered submarine basalts, therefore, is puzzling.

3.4. Removal of major components from seawater

Mg and SO_4. Our experimental results indicate that seawater–basalt interaction at 200°C, has the capacity to provide a removal mechanism for Mg and SO_4, two components for which adequate removal mechanisms could not be found in sedimentary environments [14,15].

The annual global flux of seawater in basaltic terrains, a critical unknown in assessing the adequacy of the process, cannot at present be estimated. Our experiments show that seawater–basalt reaction has the potential capacity to regulate these two components. We observed that, during the alteration of a small fraction of the glass phase to montmorillonite, Mg and SO_4 were nearly completely removed from a mass of seawater 10 times that of the rock. Although it is impossible to calculate the exact efficiency of a basalt acting on seawater in nature, it is possible that basalt can remove Mg and SO_4 from much more seawater than we used in the experiment, perhaps by a factor of 10 or more.

Na and K. What are the controls on the elements Na and K? Independent experiments, carried out concurrently with our study, by Mottl et al. [36] and by Hajash [37] at temperatures from 200 to 500°C, indicated that Na is partially removed from the seawater at the higher temperatures. They also found, however, that K was leached from the basalt, in some cases almost quantitatively, at the higher temperatures. Results from Mottl et al.'s experiment at 200°C correspond well with ours, both in alteration products and in the general changes in the seawater chemistry, although they did not report analyses for SO_4 or heavy metals other than Fe and Mn.

Low-temperature changes. Preliminary experiments in our laboratory indicate that basalt can remove up to 30% dissolved K from seawater at 25°C. These results support field observations [11] that under low-temperature conditions basalt alters to a K-rich montmorillonite.

Depending on the temperature, therefore, seawater–basalt interaction can provide a removal mechanism for Mg, SO_4, K and Na.

3.5. Controls on Fe and Mn concentrations

During the experiment, sufficient Fe and Mn were solubilized for the fluid to act as an ore fluid. Mn and Fe displayed almost identical behavior, both in their concentrations and in the changes with time. A problem is posed by two factors: the ratio of Fe/Mn in the basalt is approximately 75, which contrasts greatly to the solution ratio of 1/1; and dissolved Fe easily separates from Mn because Fe^{2+} oxidizes more quickly and tends to form insoluble Fe^{3+} compounds. The identical behavior of Fe and Mn, with regard to both level and trend, is puzzling. We have no explanation as to why their respective concentration should be so similar, but the fact that they both increase in the

same manner with time and increasing pH suggest that both are incorporated in an alteration product in the divalent state. Otherwise we would expect dissimilar behavior during precipitation.

Inasmuch as no other alteration phases were detected, we suggest that dissolved iron and manganese are incorporated and controlled by the dioctahedral component of the montmorillonite; however, some Fe and Mn may have formed oxides either amorphous or in such small quantity that they were not detected. At any rate, the total amount of ferric iron that could have been produced by the original dissolved oxygen in the seawater amounts to about 0.2% of the total ferrous iron originally in the rock. During the course of the experiment, 0.15–0.02% of the original ferrous iron was in the solution phase at any one time, but we cannot judge how much actually went through the solution phase to be incorporated as ferrous iron in the alteration product.

3.6. *Precipitation reactions*

What processes will take place as a modified seawater, such as produced in these experiments, ascends and finally discharges on the sea floor? Obviously much depends on the flow rate and contact time. As the solution rises and cools, dissolved SiO_2 might slowly and continuously precipitate, probably as amorphous silica. During such cooling, the concentration of dissolved Fe and Mn should not change very much. A sharp, almost catastrophic change would take place when the fluid encounters oxygen-rich bottom waters. At this point, Fe^{2+} initially will become oxidized to Fe^{3+}, followed by the oxidation of Mn^{2+} to higher valences; the oxidized metals would precipitate as colloidal hydroxy-hydrates along with remnant dissolved SiO_2. Ni and Cu would presumably coprecipitate on the colloids. Some of the dissolved SiO_2, however, might precipitate as sepiolite, extracting Mg^{2+} from the seawater and producing H^+ as follows:

$$2Mg^{2+} + 3SiO_2(aq) + 4H_2O = Mg_2Si_3O_6(OH)_4(\text{sepiolite}) + 4H^+$$

Sepiolite apparently provides a limit on the solubility of dissolved SiO_2 in the pore waters of marine sediments [16]. Such a mixture would closely resemble, both physically and chemically, the siliceous heavy-metal muds found along the east Pacific Rise [17]. If such a solution were to discharge on the sea floor under near-shore reducing conditions, such as along the spreading centers in the Gulf of California, the abundant biogenic H_2S in the sediment would preferentially precipitate dissolved Fe and Cu as sulfides, but Mn would be able to pass through the system. SiO_2 would likewise precipitate in the same environment, and the resulting material would resemble sulfide-rich deposits of the Red Sea geothermal system [38] and some of the stratiform copper deposits on land.

3.7. *Production of hydrogen ions*

Note that for both circumstances mentioned above, the precipitation reactions produce hydrogen ions. For each Fe^{2+} that is precipitated, two hydrogen ions are created, and for each Mn^{2+}, either two or four are created, depending on the oxidation state of the precipitate. For each 3 moles of dissolved SiO_2 precipitated as sepiolite, four moles of H^+ are produced.

In addition, it is conceivable that the precipitation of $CaCO_3$, resulting from mixing of Ca-rich fluid with the bicarbonate-rich seawater could produce additional H^+. Such a process would act as a source of hydrogen ions to the oceans that would help balance excess HCO_3^-. If about 5 ppm Mn and Fe, along with as as 25 ppm SiO_2, were to precipitate as hydrat ides and sepiolite from a unit volume of bas fied seawater emerging on the sea floor, t of hydrogen ion produced would be eq ing an equal volume of solution with Clearly, a capacity for producing s of hydrogen ion in the oceans e ed with basalt.

4. Summary

We feel the ex ing conclusions (1) Durin seawater l from a s slightl

(2) Alteration of the basalt was restricted to a small fraction of the glass phase, which altered to montmorillonite. Anhydrite was produced as a response to heating and by reaction of Ca released from the glass with SO_4 in seawater.

(3) Basalt–seawater interaction at 200°C has the potential to remove Mg and SO_4 in seawater, as well as to be a source for H^+ needed for the geochemical balance in the seas. We make no speculations, however, whether the amount of seawater interacting with basalt on a world-wide and annual basis is adequate to effect this balance.

(4) Heavy metals, such as Fe, Mn, Ni, and Cu, are solubilized during seawater–basalt interaction at 200 °C in amounts sufficiently large to permit altered seawater to transport them to the sea bottom where they can be incorporated in submarine sediments of the kind that occur along the East Pacific Rise.

Acknowledgement

We are grateful to the following persons at the University of Southern California for technical assistance: to Wayne Shanks for carrying out some preliminary experiments which helped define a need for the final experimental technique; to Robert Rosenbauer for carrying out a large portion of the analyses; to William Seyfried for clay mineral analysis; and to Thomas O'Niel for programming the calculation of the distribution of aqueous species.

We are pleased to acknowledge valuable criticisms and suggestions which greatly improved the manuscript by A.J. Ellis, DSIR, New Zealand; W.S. Fyfe, University of Western Ontario; R.M. Garrels, Northwestern University; A. Hajash, Texas A and M University; H.D. Holland and M.J. Mottl, Harvard University; Y. Kajiwara, Tokyo Kyoiku University; W.G. Melson, Smithsonian Institute; H. Sakai, Okayama University; and E.B. Spooner, Oxford University.

This research was supported by NSF grants GA 495 and ID 074-12880.

2 C.R.B. Lister, On the thermal balance of a mid-ocean ridge, R. Astron. Soc. Geophys. J. 26 (1972) 515–535.
3 R.N. Anderson, Petrologic significance of low heat flow on the flanks of slow-spreading mid-ocean ridges, Geol. Soc. Am. Bull. 83 (1972) 2947–2956.
4 K.S. Deffeyes, The axial valley: a steady-state feature of the terrain, in: The Megatectonics of Continents and Oceans, H. Johnson and B. Smith, eds. (New Brunswick, N.J., 1970) 194–222.
5 W.G. Melson, G. Thompson and Tj.H. van Andel, Volcanism and metamorphism in the Mid-Atlantic Ridge, 22°N latitude, J. Geophys. Res. 73 (1968) 5925–5941.
6 S.R. Hart, K, Rb, Cs contents and K/Rb, K/Cs ratios of fresh and altered submarine basalts, Earth Planet. Sci. Letters 6 (1969) 295–303.
7 J.B. Corlis, The origin of metal-bearing submarine hydrothermal solutions, J. Geophys. Res. 76 (1971) 8128–8138.
8 K. Muehlenbacks and R.N. Clayton, Oxygen isotope geochemistry of submarine greenstones, Can. J. Earth Sci. 9 (1972) 5: 471–478.
9 R. Hart, A model for chemical exchange in the basalt–seawater system of ocean layer II, Can. J. Earth Sci. 10 (1973) 799–816.
10 W.G. Melson and G. Thompson, Glassy abyssal basalts, Atlantic sea floor near St. Pauls rocks: petrography and composition of secondary clay minerals, Geol. Soc. Am. Bull. 84 (1973) 703–716.
11 G. Thompson, A geochemical study of the low-temperature interaction of seawater and oceanic igneous rocks, Trans. Am. Geophys. Union 54 (1973) 1015–1019.
12 E.T.C. Spooner and W.S. Fyfe, Sub-sea floor metamorphism, heat and mass transfer, Contrib. Mineral. Petrol. 42 (1973) 287–304.
13 R.M. Garrels and F.G. Mackenzie, Evolution of Sedimentary Rocks (W.W. Norton, New York, 1971).
14 J. Drever, The magnesium problems, in: The Sea, 5, E. Goldberg, ed. (John Wiley and Sons, New York, 1974) 337–357.
15 R.A. Berner, Sulfate reduction, pyrite formation and the oceanic sulfur budget, in: The Changing Chemistry of the Oceans, D. Dyrssen and D. Jagner, eds. (John Wiley and Sons, New York, 1972) Nobel Symp. 20: 347–361.
16 J.L. Bischoff and F.L. Sayles, Pore fluid and mineralogical studies of recent marine sediments; Bauer Depression region of East Pacific Rise, J. Sediment. Petrol. 42 (1972) 711–724.
17 F.L. Sayles and J.L. Bischoff, Ferromanganoan sediments in the equatorial East Pacific, Earth Planet. Sci. Letters 19 (1973) 330–336.
18 J. Dymond, J.B. Corliss, G.R. Heath, C.W. Field, E.J. Dasch and H.H. Veeh, Origin of metalliferous sediments from the Pacific Ocean, Geol. Soc. Am. Bull. 84 (1973) 3355–3372.
19 K. Boström, The origin and fate of ferromanganoan active ridge sediments, Stockholm Contrib. Geol. 24 (1973) 2: 149–243.

...s

...On heat flow in Iceland in relation to the ...idge in: Iceland and Mid-ocean Ridges, S. ... Soc. Sci. Islandica 38 (1967) 111–127.

Economic Geology
Vol. 69, 1974, pp. 826–842

Sulfur and Carbon Isotopes and Ore Genesis: A Review

ROBERT O. RYE AND HIROSHI OHMOTO

Abstract

Important new developments in carbon and sulfur isotope geochemistry are reviewed with reference to a number of hydrothermal ore deposits that represent a considerable range in age, temperature of deposition, mineralogy, and mode of occurrence. Recent carbon and sulfur isotope studies that have made important contributions to our understanding of ore genesis emphasize that for meaningful interpretation investigations must be coupled with detailed geologic, mineralogic, and other geochemical studies. Under equilibrium conditions, the $\delta^{34}S$ and $\delta^{13}C$ of hydrothermal minerals are determined by the physical chemical conditions of the hydrothermal fluids (T, pH, f_{O_2}) as well as the isotopic composition of sulfur and carbon ($\delta^{34}S_{\Sigma S}$ and $\delta^{13}C_{\Sigma C}$) in the ore fluids. These variables, along with the f_{S_2}, $m_{\Sigma S}$, f_{CO_2} and $m_{\Sigma C}$ of the fluids and the possible mechanism of ore deposition, have been determined in several deposits by combining isotopic and other geochemical data.

The important sources of sulfur in ore deposits are deep-seated sources (mantle or homogenized crust), local country rocks, and sea water or marine evaporites. The important sources of carbon are deep-seated sources (mantle or homogenized crust), marine limestones, and organic matter in sedimentary rocks. Discussions of the origin of sulfur and carbon in ore deposits must be based on accurate determinations of $\delta^{34}S_{\Sigma S}$ and $\delta^{13}C_{\Sigma C}$ values which can be greatly different from the $\delta^{34}S$ and $\delta^{13}C$ values of individual minerals in these deposits.

In shallow environments where boiling, mixing of fluids, or redox reactions occurred, sulfur isotopic equilibrium may not have been established among hydrothermal minerals and between fluids and minerals. The occurrence of isotopic disequilibrium in such environments, however, may help elucidate the history of hydrothermal fluids.

Bacteriogenic sulfide deposits involving bacteriologic reduction of sea water sulfate can be recognized by their occurrence in nonvolcanic sedimentary environments, by nonequilibrium distribution of sulfur isotopes between coexisting minerals, and by the time-space relationships of their $\delta^{34}S$ (and $\delta^{13}C$) values, but not necessarily by the statistical distribution of their $\delta^{34}S$ values. Bacteria need not be involved in the reduction of sea water sulfate in volcanic environments inasmuch as sulfate may readily be reduced by deep circulation into high-temperature rocks and precipitated as sulfides at lower temperatures in or near sedimentary basins.

Preliminary data on metamorphosed stratiform deposits suggest that original large-scale sulfur and carbon isotope distributions are generally preserved during metamorphism making it possible to determine the origin of sulfur and carbon in such deposits. However, minor changes in the sulfur and carbon isotope systematics that reflect the metamorphic event are often superimposed on the original isotope distributions.

Introduction

THE application of sulfur and carbon isotope data to the study of ore deposits has undergone a remarkable transformation since 1968. As a result, recent sulfur and carbon isotope studies have contributed much to our understanding of some of the processes of ore deposition. The purpose of this paper is to discuss the relatively new principles of application of sulfur and carbon isotopic data to problems of ore genesis rather than to provide an extensive review of the literature. To illustrate these principles, the authors have drawn largely from their own studies with various investigators and a from a few other studies where sulfur or carbon isotope investigations have been accompanied by detailed geologic, mineralogic, and other geochemical data. The review does not give equal weight to all types of ore deposits. It is devoted largely to hydrothermal deposits, although short sections cover bacteriogenic and metamorphosed deposits.

Sulfur Isotopes and Ore Genesis

$\delta^{34}S$ variations in hydrothermal deposits

The total ranges of $\delta^{34}S$[1] values of sulfide and sulfate minerals from a number of hydrothermal ore

[1] The $\delta^{34}S$ or the $\delta^{13}C$ value of a species i is defined as:

$$\delta^{34}S_i(‰) = \frac{(^{34}S/^{32}S)_i - (^{34}S/^{32}S)_{std}}{(^{34}S/^{32}S)_{std}} \times 1{,}000,$$

deposits that have been the subject of detailed studies are shown in Figure 1. These deposits cover a considerable range in age, temperature of mineralization, mineralogy, and mode of occurrence (see references in Fig. 1). For example, ages of mineralization range from late Tertiary at Casapalca through Hercynian at Panasqueira to Precambrian at Echo Bay. Temperatures of ore deposition range from 100°C or less at Pine Point to nearly 500°C at Bluebell. The majority of deposits studied contain lead-zinc and minor silver and copper mineralization. Pasto Bueno contains tungsten; Panasqueira is a tin and tungsten deposit; Cortez is a disseminated gold deposit; and Echo Bay is a U-Ni-Ag-Cu deposit. Some of these deposits, such as Providencia, Casapalca, and Pasto Bueno, are vein types; others, such as Mogul, the Kuroko deposits, and Pine Point, are stratiform types (*sensu lato*).

Certain deposits, such as Providencia, Casapalca, and Creede, exhibit a narrow range of $\delta^{34}S$ values that average near 0 per mil. Others, such as Bluebell, Cortez, Pine Point, and Black Hills Tertiary deposits, have a narrow range of positive $\delta^{34}S$ values. Still others, such as Mogul and Echo Bay, have a very wide range of $\delta^{34}S$ values which include both positive and negative values. Deposits such as Panasqueira have a wide range of values only when very late stage sulfides are included. In some deposits sulfate minerals are present and all these are isotopically heavier with respect to sulfur than the sulfides from the same deposit. It is obvious from Figure 1 that one cannot classify the types of ore deposits or say very much about their genesis on the basis of sulfur isotope values alone. In certain cases, sulfides of apparently similar types of deposits, such as the stratiform Mogul and Pine Point deposits, have greatly different sulfur isotope values. In other cases, sulfides of greatly different types of deposits, like the Darwin replacement ores and the stratiform Kuroko ores, have very similar sulfide sulfur isotope values.

Under a previous system of interpretation, the sulfur of any deposit that contained a narrow range of $\delta^{34}S$ values was considered to be of magmatic origin, whereas the sulfur of a deposit that had a wide range of $\delta^{34}S$ values was considered to be biogenic (e.g., Jensen, 1959, 1967). The following discussion, however, demonstrates that sulfides which precipitated from magmatic sulfur can exhibit a wide range of $\delta^{34}S$ values (e.g., Mogul deposits). On the other hand, sulfides precipitated from nonmagmatic sulfur, such as sea water, can have a modest range of $\delta^{34}S$ values near 0 per mil (e. g., the Kuroko deposits).

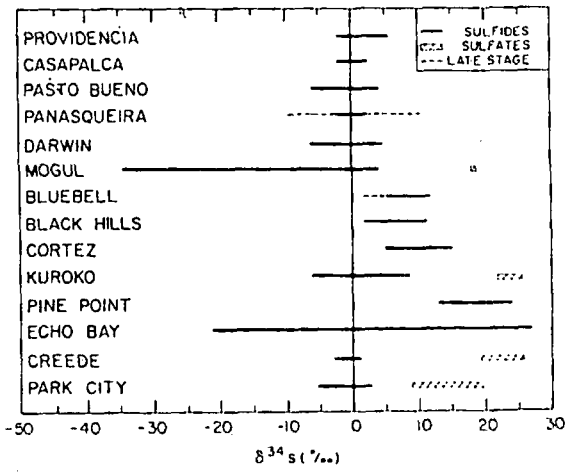

FIG. 1. Range of $\delta^{34}S$ values of sulfides and sulfates from various hydrothermal ore deposits. Sources of data: Providencia, Mexico (Rye, 1974, and unpub. data); Casapalca, Peru (Rye and Sawkins, 1974); Pasto Bueno, Peru (Landis and Rye, 1974); Panasqueira, Portugal (R. O. Rye and W. C. Kelly, unpub. data); Darwin, southern California (Rye et al., 1974b); Mogul, Ireland (Greig et al., 1971); Bluebell, British Columbia (Ohmoto, unpub. data; Ohmoto and Rye, 1970); Tertiary deposits of Black Hills, South Dakota (Rye and Rye, 1974); Cortez, Nevada (Rye et al., 1974a); Kuroko deposits, Shakanai, Japan (Ohmoto et al., 1970); Pine Point, N. W. T. (Sasaki and Krouse, 1969); Creede, Colorado (Bethke et al., 1973), Park City, Utah (R. O. Rye and J. T. Nash, unpub. data).

Temperature significance of $\delta^{34}S$ variations among coexisting minerals

The range of sulfur isotope values for pyrite, sphalerite, and galena for various hydrothermal deposits is shown in Figure 2. It can be seen that a considerable portion of the range of $\delta^{34}S$ values at a given deposit reflects typical differences in the isotopic composition of common sulfide minerals. Note that for most deposits the average $\delta^{34}S$ for sphalerite is larger than that for galena. In fact, in some of these deposits, such as Providencia, Casapalca, Pasto Bueno, and Darwin, there is complete separation of $\delta^{34}S$ values for these two minerals. The range of $\delta^{34}S$ values for pyrite, on the other hand, often overlaps that for sphalerite and in some cases even overlaps that for galena. We will see in

---

or

$$\delta^{13}C_i(‰) = \frac{(^{13}C/^{12}C)_i - (^{13}C/^{12}C)_{stnd}}{(^{13}C/^{12}C)_{stnd}} \times 1{,}000,$$

in which $(^{34}S/^{32}S)_{stnd}$ is the sulfur isotopic composition of troilite of the Cañon Diablo meteorite, 0.0450045 (Macnamara and Thode, 1950; Ault and Jensen, 1963), and $(^{13}C/^{12}C)_{stnd}$ is the carbon isotopic composition of the Chicago standard (PDB), 0.0112372 (Craig, 1957).

The isotopic fractionation factor between species A and B is defined as

$$\alpha_B^A = \frac{R_A}{R_B} = \frac{1{,}000 + \delta_A}{1{,}000 + \delta_B},$$

in which R is the isotopic ratio, $(^{34}S/^{32}S)$ or $(^{13}C/^{12}C)$.

It should be noted that

$$1{,}000 \ln\alpha_B^A \simeq \delta^{34}S_A - \delta^{34}S_B = \Delta^{34}S_{A-B}.$$

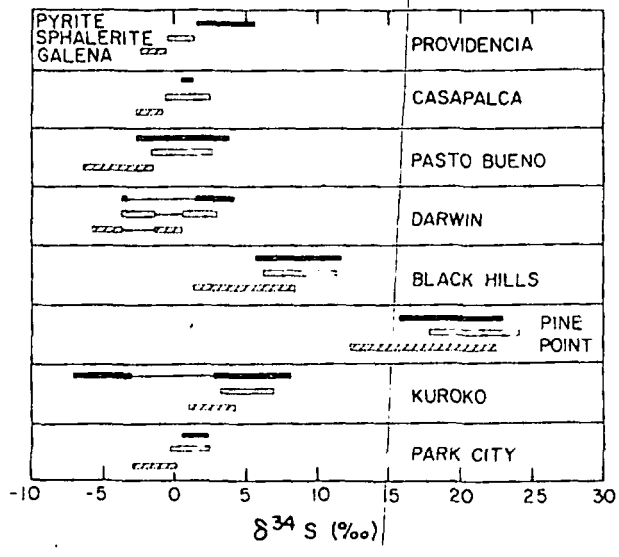

FIG. 2. Range of $\delta^{34}S$ values in pyrite, sphalerite, and galena in various hydrothermal deposits. Tie lines join early and late periods of mineralization.

the following discussion that these distributions of $\delta^{34}S$ values in pyrite, sphalerite, and galena have an important bearing on the use of sphalerite-galena and pyrite-galena mineral pairs in sulfur isotope geothermometry.

Sulfur isotope geothermometry is based on the equilibrium sulfur isotope fractionations between coexisting sulfur-bearing compounds. The sulfur isotopic fractionations among important sulfur species in hydrothrmal solutions and sulfur-bearing minerals are given in Figure 3. For example, the sulfur isotope fractionation at 200°C between pyrite and galena is about 4.6 per mil. Likewise the fractionation between sphalerite and galena at 200°C is a little over 3 per mil. These curves are based on experimental and theoretical data and there are some differences between the curves produced by various laboratories that have yet to be worked out (see Czamanske and Rye, 1974). However, the relative position of the curves among the minerals will not change and from Figure 3 one can predict which mineral pairs are most useful as sulfur isotope geothermometers. The larger the separation of the curves for any two minerals, the more sensitive will the mineral pair be as an isotopic thermometer; i.e., the order of sensitivity of sulfur isotope fractionations to temperature among mineral pairs is: sulfate-sulfide >> pyrite-galena > sphalerite (or pyrrhotite)-galena > pyrite-chalcopyrite > pyrite-sphalerite (see Fig. 3). The analytical precision in the $\delta^{34}S$ value for a mineral is usually better than ±0.1 per mil and better than ±0.2 per mil for the $\Delta\delta^{34}S$ value relating to a mineral pair. At a temperature of 250°C, this analytical uncertainty causes an uncertainty in the sulfur isotopic temperatures of about ±10°C for a pyrite-galena pair, ±15°C for a sphalerite-galena pair, and ±40°C for a pyrite-chalcopyrite pair.

The successful application of any sulfur isotope thermometer to a particular deposit depends upon the suitability of the samples. Ideally, one would like to have contemporaneous samples that crystallized in equilibrium with each other. However, for most mineral pairs it is very difficult to sample each mineral in such a manner that the samples represent the same period of time in the evolution of the hydrothermal fluids. Fortunately, mineral pairs may give geologically reasonable temperatures as long as the two minerals were formed in equilibrium with solutions which were uniform in temperature and in chemical states (e.g., $\delta^{34}S_{\Sigma S}$, pH, and f_{O_2}). Conversely, if a mineral pair gives a geologically reasonable isotopic temperature that correlates with other available temperature data, the two minerals may be assumed to have formed from solutions of uniform temperature and chemistry. The fact that sphalerite-galena pairs in many deposits give reasonable temperatures even when these minerals do not appear to be contemporaneous suggests that the depositional mechanisms and conditions of sphalerite

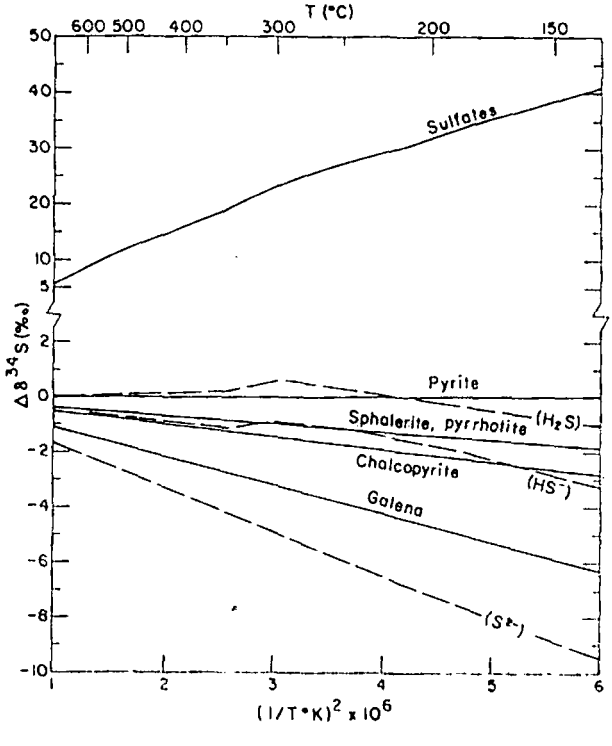

FIG. 3. Sulfur isotope fractionations among sulfur species and hydrothermal minerals plotted with respect to pyrite. Dashed lines indicate species in solution. Solid lines indicate minerals. (For sources of data see Ohmoto, 1972, and Robinson and Ohmoto, 1973.)

and galena formation were similar. In contrast, pyrite-galena pairs seldom give good temperatures, apparently due to the fact that pyrite tends to precipitate over a much larger part of the paragenesis than galena, allowing a greater chance that the minerals formed under different conditions or from distinctly different solutions (note, Fig. 2).

The sphalerite-galena sulfur isotope geothermometer has been applied successfully to several deposits (see, for example, Rye, 1974; Rye et al., 1974b). With suitable sulfide pairs and careful sampling, temperatures of deposition or metamorphism can usually be determined to within ±40°C, even taking into account the uncertainty in the fractionation factors. The sphalerite-galena sulfur isotope geothermometer is especially useful on massive or metamorphosed deposits where it is difficult to determine temperatures by other means, such as filling temperature measurements of fluid inclusions.

Significance of $\delta^{34}S$ variations in time and space

The previous discussion concerns the significance of $\delta^{34}S$ variations among coexisting minerals. In this section we consider the significance of the variation of $\delta^{34}S$ values of minerals that occur in time and space in hydrothermal ore deposits. Figure 4 is a schematic diagram showing such changes in average $\delta^{34}S$ values of sulfide minerals for various deposits. These generalized trends are based on large numbers of analyses for each deposit.

Based on these investigations, it is evident that generalizations about the time-space variations of $\delta^{34}S$ values in all hydrothermal deposits are impossible. The $\delta^{34}S$ values can be relatively constant in time and space with a value of near 0 per mil, as at Casapalca, Providencia, and Pasto Bueno, or constant with a value of about 20 per mil, as at Pine Point. The $\delta^{34}S$ values can increase with time or space as at the Echo Bay deposit or decrease with time or space as with the Kuroko, Mogul, and Darwin deposits. During late-stage mineralization they may reverse direction as at Bluebell or scatter as at Panasqueira. It should be obvious from Figure 4 that it is imperative to know the time and space relationships of samples in order to interpret properly the sulfur isotope data. The following is a discussion of the factors that control the $\delta^{34}S$ variations in time and space and what these variations tell us about ore deposition.

The turning point in sulfur isotope geochemical research on ore deposits occurred in 1968 when Sakai (1968) suggested that the sulfur isotope composition of minerals could be controlled by the chemistry of the ore solutions. In publications in 1970 and 1972, Ohmoto evaluated quantitatively the

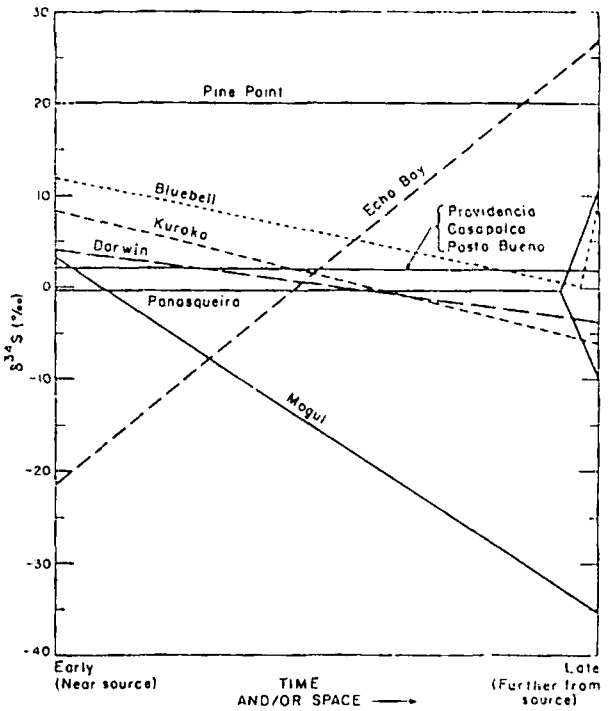

FIG. 4. Generalized trends of sulfide $\delta^{34}S$ values in time and/or space for various hydrothermal ore deposits. (See references in Fig. 1 for sources of data.)

effects of the chemical nature of ore-forming solutions on the sulfur isotopic composition of hydrothermal minerals. The basis of their contributions is the recognition of large isotopic fractionations among various sulfur species, particularly between oxidized and reduced forms of sulfur, in hydrothermal solutions (see Fig. 3). For example, at a temperature of 200°C, the sulfur isotopic fractionation between SO_4^{-2} and H_2S is about 32 per mil.

An illustration of how the sulfur isotopic compositions of precipitating mineral phases are affected by the chemistry of ore fluids is shown in Figure 5. Suppose the sulfur in an ore fluid is distributed between H_2S and SO_4^{-2}, the sulfur isotopic composition of the fluid system ($\delta^{34}S_{\Sigma S}$ value) is 0 per mil, T = 200°C, and the H_2S/SO_4^{-2} ratio changes from 1/9 to 9/1. As long as isotopic equilibrium is established between the species, the $\delta^{34}S$ value of each aqueous sulfur species varies depending on the H_2S/SO_4^{-2} ratio (e.g., $\delta^{34}S_{H_2S}$ shifts from −28.8 to −16 to −3.2 per mil, according to the change in the H_2S/SO_4^{-2} ratio from 1/9 to 9/1). If sulfide minerals, such as sphalerite and galena, precipitate from these solutions, and if the amount of sulfur taken out from the solutions is negligible, $\delta^{34}S$ values for the sulfide minerals will also change with the change in the H_2S/SO_4^{-2} ratio (see Fig. 5). Note that the differences in the $\delta^{34}S$ value among the coexisting

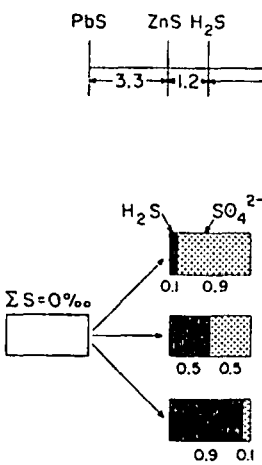

	$\delta^{34}S$			
	H_2S	SO_4^{2-}	ZnS	PbS
	-28.8	+3.2	-30.0	-33.3
	-16.0	+16.0	-17.2	-20.5
	-3.2	+28.8	-4.4	-7.7

FIG. 5. Variation of $\delta^{34}S$ of sulfate (ion or mineral), H_2S, and sulfide minerals with variation in H_2S/SO_4^{-2} of the hydrothermal solution at T = 200°C, $\delta^{34}S_{\Sigma S} = 0$ per mil.

sulfur-bearing species are constant in each case, because the $\delta^{34}S$ values are dependent only on temperature.

In the environment of ore deposition there are other aqueous sulfur species which may become important (e.g., HSO_4^-, KSO_4^-, $NaSO_4^-$, and HS^-). However, it can be shown that the major factors which control the sulfur isotopic composition of hydrothermal minerals are: (1) temperature, which determines the fractionations between sulfur-bearing species; (2) $\delta^{34}S_{\Sigma S}$, which is controlled by the source of sulfur; and (3) the proportions of oxidized and reduced sulfur species in solution. Because the proportions of oxidized and reduced sulfur species in fluids can be evaluated in terms of T, pH, and f_{O_2} of hydrothermal fluids, we can also evaluate the variation of $\delta^{34}S$ values of minerals in terms of T, pH, and f_{O_2}.

Figure 6 shows an example of the effect of pH and f_{O_2} variation on the sulfur isotopic composition of minerals at 250°C, as constructed by Ohmoto (1972). The solid curves and their dashed extensions are $\delta^{34}S$ contours which indicate the sulfur isotopic compositions of pyrite in brackets and coexisting barite in parentheses. The $\delta^{34}S$ values of other sulfide minerals could be contoured by using the appropriate fractionation factors shown in Figure 3. The heavy dashed lines show the stability fields for minerals in the Fe-S-O system with total sulfur concentration ($m_{\Sigma S}$) of 0.1 and 0.001 mole/kg H_2O. Notice that the stability fields of minerals are sensitive to ΣS concentration but the sulfur isotope contours are not. These pH-f_{O_2} diagrams that combine sulfur isotope contours and stability fields for minerals at a given temperature, $\delta^{34}S_{\Sigma S}$, and $m_{\Sigma S}$ can be very valuable in the interpretation of sulfur isotope data for hydrothermal deposits and the interested reader should refer to Ohmoto (1972) for details of their construction. Similar diagrams could be constructed using other variables (e.g., f_{O_2}-f_{S_2}, f_{O_2}-T) and these could have application in certain instances.

It should be noted that $\delta^{34}S$ values for pyrite can range from about +5 to −27 per mil and for barite from about 0 to +32 per mil within geologically reasonable limits of pH and f_{O_2} when $\delta^{34}S_{\Sigma S} = 0$ per mil and T = 250°C. In the low f_{O_2} and pH region of the pyrite stability field, sulfide $\delta^{34}S$ values can be similar to $\delta^{34}S_{\Sigma S}$ and can be rather insensitive to pH and f_{O_2} changes. Whereas in the region of high f_{O_2} values, near the pyrite-magnetite and pyrite-hematite boundaries, where the proportion of sulfate aqueous species becomes significantly large compared to reduced sulfur aqueous species, sulfide $\delta^{34}S$ values can be greatly different from $\delta^{34}S_{\Sigma S}$ and small changes in pH or f_{O_2} may result in large changes in $\delta^{34}S$ values of the minerals. Some examples of how these pH-f_{O_2} diagrams have been applied to detailed

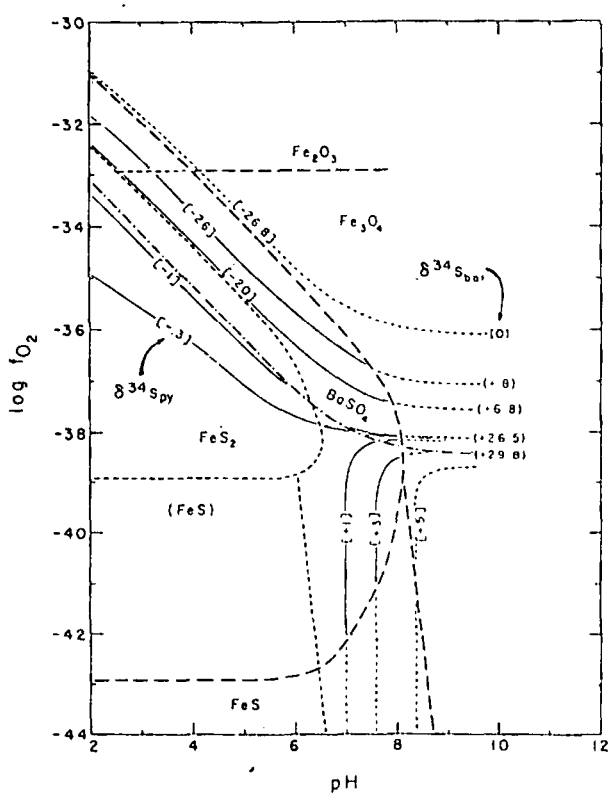

FIG. 6. Comparison of the positions of $\delta^{34}S$ contours with the stability fields of Fe-S-O minerals and barite at T = 250°C, $\delta^{34}S_{\Sigma S} = 0$ per mil (reproduced from Ohmoto, 1972). Solid line: $\delta^{34}S$ contours. Values in [ ] and ( ) are, respectively, for pyrite and barite at $\delta^{34}S_{\Sigma S} = 0$ per mil. Dashed line: Fe-S-O mineral boundaries at ΣS = 0.1 moles/kg H_2O. Small dashed line: Fe-S-O mineral boundaries at ΣS = 0.001 moles/kg H_2O. Dash and dot line: Barite soluble/insoluble boundary at $m_{Ba^{2+}} \cdot m_{\Sigma S} = 10^{-4}$.

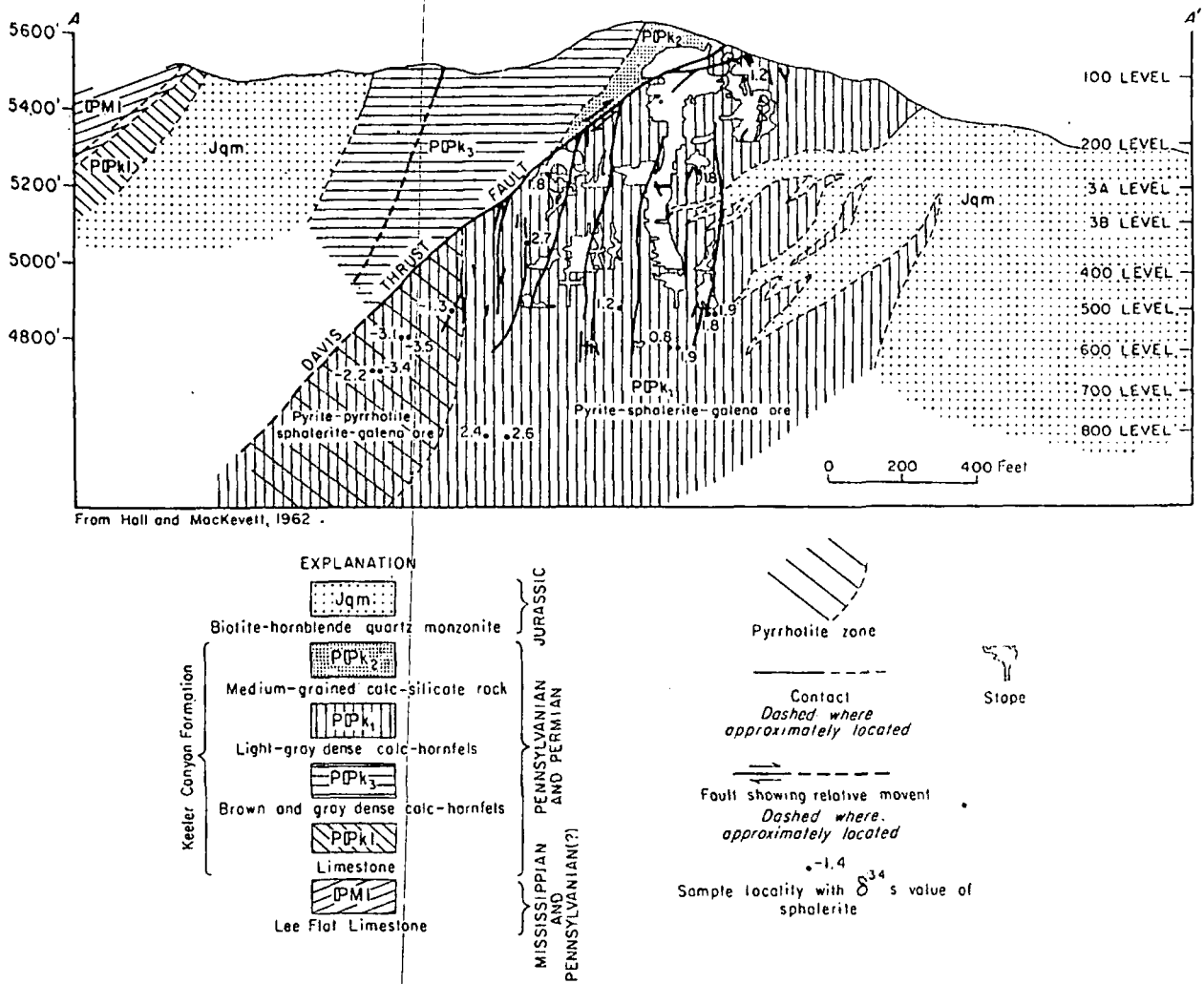

FIG. 7. Cross section section of the Darwin, California, Ag-Pb-Zn-Cu deposit showing $\delta^{34}S$ values of sphalerite (from Rye et al., 1974b).

sulfur isotope studies of specific ore deposits are presented in the succeeding discussion.

A cross section of the Darwin Ag-Pb-Zn-Cu deposit in southern California is shown in Figure 7. The ore occurs as a massive replacement of heavily calc-silicated limestone adjacent to a granodiorite stock. Near the granodiorite, pyrite is the dominant iron sulfide, coexisting with sphalerite and galena. To the west, away from the intrusive and near the thrust fault, the iron mineral assemblage which coexists with sphalerite and galena is pyrite-pyrrhotite-magnetite. The $\delta^{34}S$ values of the sulfide minerals in the pyrite-pyrrhotite-magnetite ore are about 5 per mil lower than for the corresponding minerals in the pyrite ores (Rye et al., 1974b).

A pH-f_{O_2} diagram which shows the chemical environment of ore deposition at Darwin as determined from a study of the wall rock and ore mineral assemblage is shown in Figure 8. In this case, the $\delta^{34}S$ contours show the isotopic composition of sphalerite when $\delta^{34}S_{\Sigma S} = 3$ per mil and the temperature is 350° ± 55°C, as indicated by sphalerite-galena sulfur isotope data. The heavy lines outline the stability fields for the minerals pyrite, pyrrhotite, and magnetite at different sulfur concentrations.

There are two pH regions shown in Figure 8: the first indicates the range of pH of the Darwin hydrothermal solutions in equilibrium with the quartz-K-feldspar-sericite assemblage in the granodiorite; the second indicates the pH range of fluids in equilibrium with the calc-silicate assemblages. The distribution of the calc-silicate minerals and iron minerals, namely the occurrence of pyrite near the stock and pyrite-pyrrhotite-magnetite farther from the stock, suggests that the pH of the ore-forming fluids increased along the path suggested in Figure 8 as the solutions moved

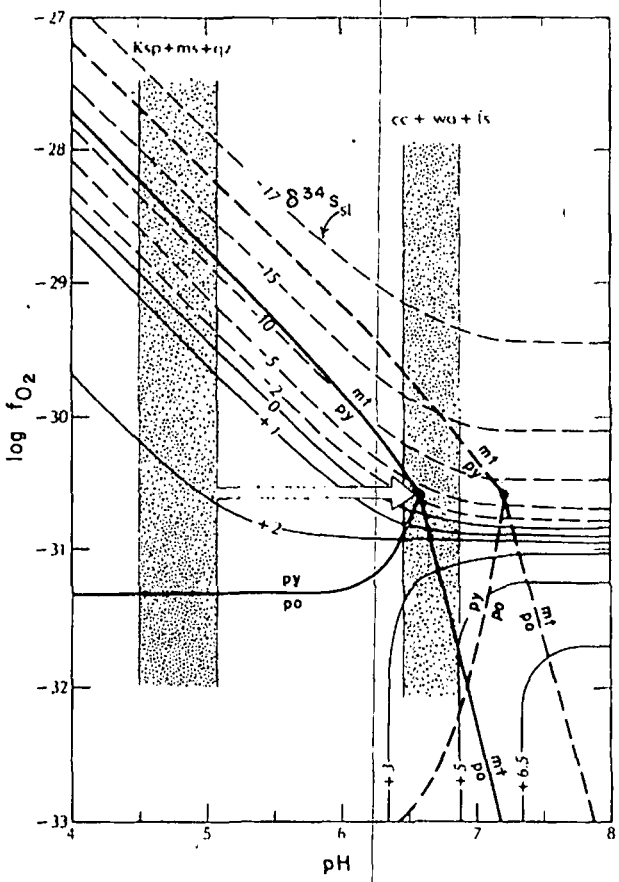

FIG. 8. Composite diagram showing the pH-f_{O_2} relationships between the stability fields of hydrothermal minerals and the sulfur isotopic composition of sulfide minerals at 350°C (from Rye et al., 1974b). Shaded areas: (1) pH fields of solutions in equilibrium with the assemblage K-feldspar (Ksp) + muscovite (ms) + quartz (qz) under a condition of $\Sigma KCl = 0.5$–0.3 moles/kg H_2O. (2) pH of solutions in equilibrium with the assemblage calcite (cc) + wollastonite (wo) + alkali feldspar (fs). Heavy solid lines: Mineral stability boundaries among pyrite (py), pyrrhotite (po), and magnetite (mt) in solutions with $\Sigma S = 0.01$ moles/kg H_2O. Heavy dashed lines: Mineral stability boundaries among pyrite, pyrrhotite, and magnetite in solutions with $\Sigma S = 0.1$ moles/kg H_2O. Thin lines: $\delta^{34}S$ contours for sphalerite under a condition of $\delta^{34}S_{\Sigma S} = +3$ per mil. The same contours can be applied to other sulfides. For example, add −2 per mil for galena or add +0.7 per mil for pyrite.

away from the stock. It can be seen from the relationship between the $\delta^{34}S$ contours and the stability fields in Figure 8 that the pH increase could readily account for the 5 per mil shift observed in the $\delta^{34}S$ values of the sulfides between the pyrite and the pyrite-pyrrhotite-magnetite ores, if ΣS was around 0.01 molal. In this case, the sulfur isotope data, when used in conjunction with mineral stability fields, can actually indicate the $m_{\Sigma S}$ of hydrothermal fluids. It should be noted that the pH increase could also have been an effective mechanism of precipitation of sulfide minerals from the hydrothermal solutions at Darwin (see Rye et al., 1974b).

A cross section of the lead-zinc deposits at Mogul, Ireland (Greig et al., 1971), is shown in Figure 9. They consist of a lower ore body in a steeply dipping fault near red beds and an upper ore body which is a stratiform, massive replacement of carbonate rocks.

The $\delta^{34}S$ values for the sulfide minerals at Mogul show a very wide range. The $\delta^{34}S$ values of pyrite, for example, range from about +4 to −34.5 per mil. Two barites have $\delta^{34}S$ values of about +18 per mil. From the sequence of locations on Figure 9, it is clear that the $\delta^{34}S$ values show a pronounced trend whereby they become progressively more negative upward along the fault and away from the fault in the stratiform zone.

A pH-f_{O_2} diagram for the Mogul deposits is shown in Figure 10 (Greig et al., 1971). Filling temperature measurements on fluid inclusion and $\delta^{34}S$ values of coexisting sulfide minerals indicate that the temperature of deposition for the Mogul deposits was about 250°C. The $\delta^{34}S$ contours are drawn for $\delta^{34}S_{\Sigma S} = 0$ per mil and indicate the isotopic composition of pyrite and barite. Stability fields for pyrite, pyrrhotite, magnetite, and hematite at $\Sigma S = 0.01$ m are also shown. The shaded areas indicate the probable initial and final chemical environments of the ore fluids at Mogul as indicated by the changes in wall rock and ore mineral assemblages. The observed trend of $\delta^{34}S$ values in the minerals can readily be explained by increases in pH and f_{O_2} in the hydrothermal fluids as they reacted with the red beds and the carbonate host rocks in the upper ore body. If this interpretation is correct, $\delta^{34}S_{\Sigma S}$ appears to have remained constant near 0 per mil, in spite of the large variation of $\delta^{34}S$ values of the sulfides.

Sulfur isotope data from the Shakanai mine, one of the Kuroko deposits in the Hokuroku district, Japan, are summarized in Figure 11 (Ohmoto et al., 1970; Kajiwara, 1971). These deposits, which are associated with submarine volcanic activity, have a unique stratigraphy and mineral zonation. Disseminated pyrite ores in the footwall (siliceous ore) are followed in ascending sequence by pyrite-chalcopyrite (yellow ore), sphalerite-galena (black ore), and hematite-rich ores. The $\delta^{34}S$ values of pyrite decrease rather systematically from about +8 to −6 per mil from the lower to upper levels in the ore body.

Figure 12 is basically the same as the other pH-f_{O_2} diagrams, except that f_{S_2} contours and the stability field for additional minerals have been added (Ohmoto et al., 1970). The $\delta^{34}S$ contours for pyrite are drawn for $\delta^{34}S_{\Sigma S} = 20$ per mil, which is the value of sea water and T = 250°C as indicated by

sulfur isotope data for coexisting sphalerite and galena. As shown by the arrow, the observed trend in the data can readily be explained if the source of sulfur was sea-water sulfate and if the f_{O_2} and pH of the solutions changed in the late stages of the mineral sequence. For more discussion on the Kuroko deposits see Ohmoto and Rye (1974).

Examples could be given for several other deposits in which changes in the chemical environment of ore fluids apparently account for widespread variation in sulfur isotope compositions of hydrothermal sulfides. It should be obvious from the above examples that any meaningful interpretation of sulfur isotope data must be tied into detailed geologic, mineralogic, and geochemical studies. When such studies are available, sulfur isotope data may help to define the temperature, pH, f_{O_2}, f_{S_2}, $m_{\Sigma S}$, and $\delta^{34}S_{\Sigma S}$ of the hydrothermal fluids as well as possible mechanisms of ore deposition.

Source of sulfur in hydrothermal ore deposits

The origin of sulfur in ore deposits can be discussed only on the basis of the calculated isotopic composition of the total sulfur in solution ($\delta^{34}S_{\Sigma S}$). Figure 13 summarizes $\delta^{34}S_{\Sigma S}$ data for 15 hydrothermal ore deposits as determined by the principles discussed in the preceding section. The $\delta^{34}S_{\Sigma S}$ values fall into three groups. One group has slightly positive $\delta^{34}S_{\Sigma S}$ values, the second has values between 5 and 15 per mil, and the third has average values near 20 per mil. These groups reflect the three major sources of sulfur in hydrothermal ore deposits.

Deposits such as Providencia and Casapalca that have $\delta^{34}S_{\Sigma S}$ values near 0 per mil are associated with felsic igneous rocks. Their sulfur was probably derived from igneous sources, which include sulfur released from silicate melts and sulfur leached from sulfides in igneous rocks. Igneous sulfur must be derived either from the upper mantle or from the homogenization of large volumes of deeply buried or subducted crustal material.

Deposits such as Kuroko, Echo Bay, and Pine Point have $\delta^{34}S_{\Sigma S}$ values close to that of sea-water sulfates. The sulfur in these deposits was most likely derived either from ocean water, as at the Kuroko and Echo Bay deposits, or from marine

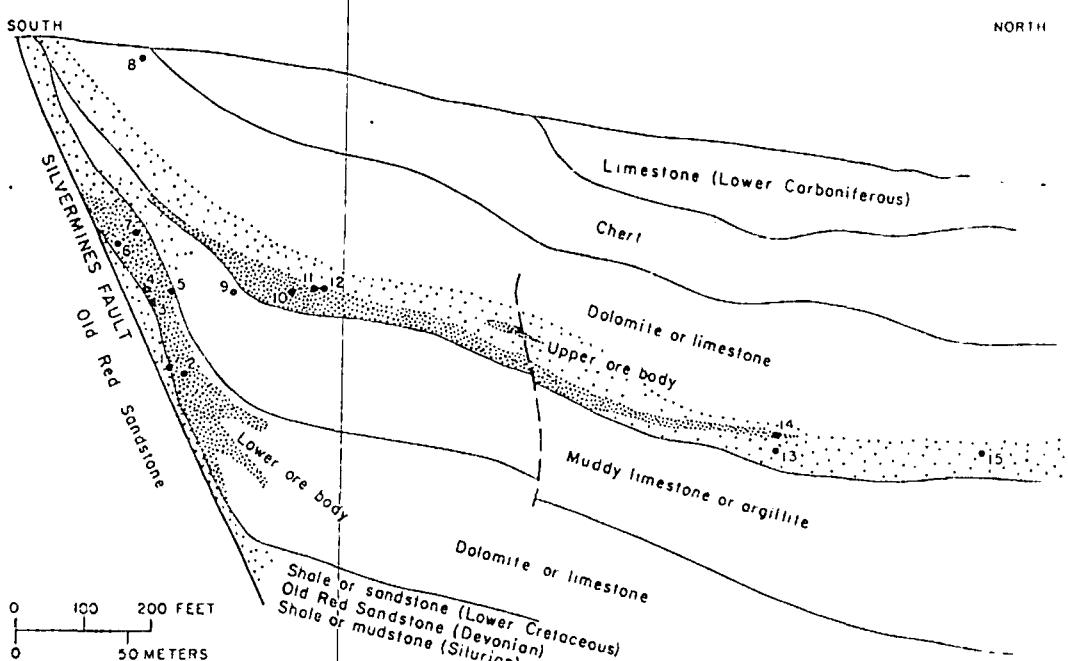

Location	1	2	3	4	5	6	7	8	9	10	11	12	13	14	15
$\delta^{34}S$ (‰) Pyrite	----	----	+4.2	----	----	----	----	-20.2	----	-22.2	-8.1	-15.6	-----	-34.8	-33.6
Sphalerite	-0.9	-1.0	-0.1	-0.9	-0.7	-3.1	-5.2	-----	-8.9	-----	----	-----	-----	-----	-----
Galena	-3.6	-3.7	----	----	-5.1	-5.3	-6.6	-----	----	-18.7	----	-----	-----	-29.6	-17.0
Barite	----	----	----	----	----	----	----	+18.0	----	-----	----	-----	+18.4	-----	-----

FIG. 9. Cross section of the consolidated Mogul mine, Ireland, showing the distribution of mineral $\delta^{34}S$ values. Ore bodies are indicated by the stippled pattern (modified from Greig et al., 1971).

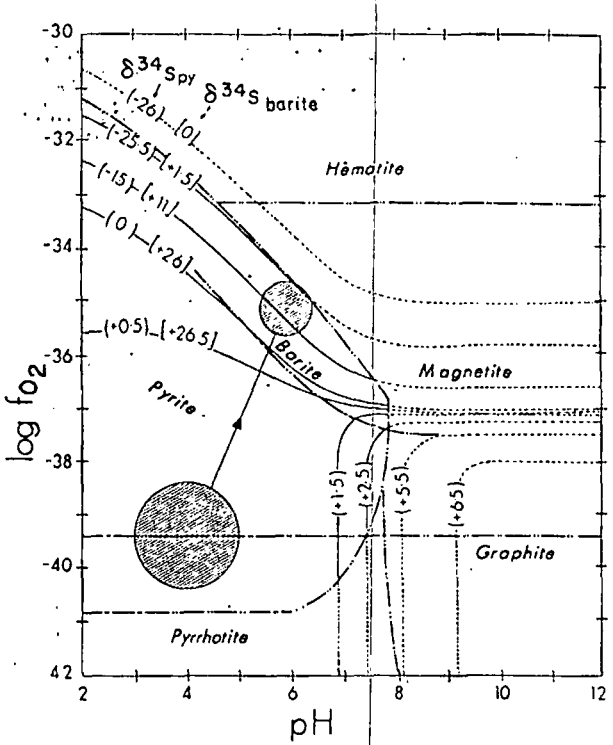

FIG. 10. pH-f_{O_2} diagram for the Mogul, Ireland, deposits. Sulfur isotope contours (fine solid lines and dashed extensions) are drawn for $\delta^{34}S_{\Sigma S} = 0$ per mil, T = 250°C, ionic strength = 1, and $m_{K^+} = 0.1$ m. The broken lines indicate the stability fields of minerals when $\Sigma S = 0.01$ m and $f_{CO_2} =$ 1 atm. The barite field is calculated from the solubility data of Holland (1965) and $m_{Ba^{++}}$ concentration of 0.01–0.001 m. The shaded areas show the initial and the final states of the fluids related to ore deposition at the Mogul deposits (modified from Greig et al., 1971).

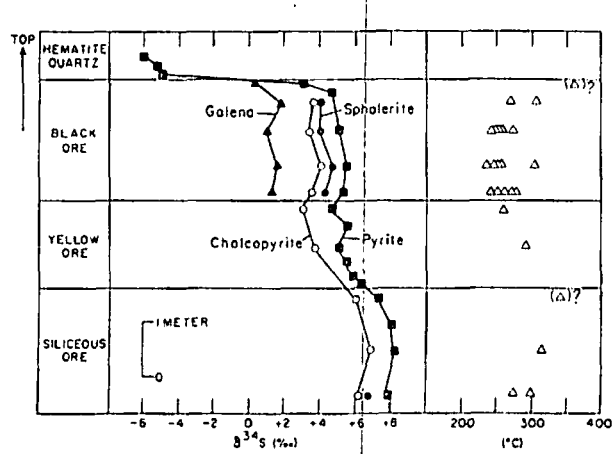

FIG. 11. Sulfide $\delta^{34}S$ values and sulfur isotope temperatures for Shakanai deposit (Kuroko type), Japan. Triangle indicates sulfur isotopic temperature. Triangle in parentheses with a question mark indicates higher than average temperatures. Mineral zones are arranged in order of stratigraphic occurrence (data from Ohmoto et al., 1970, and Kajiwara, 1971).

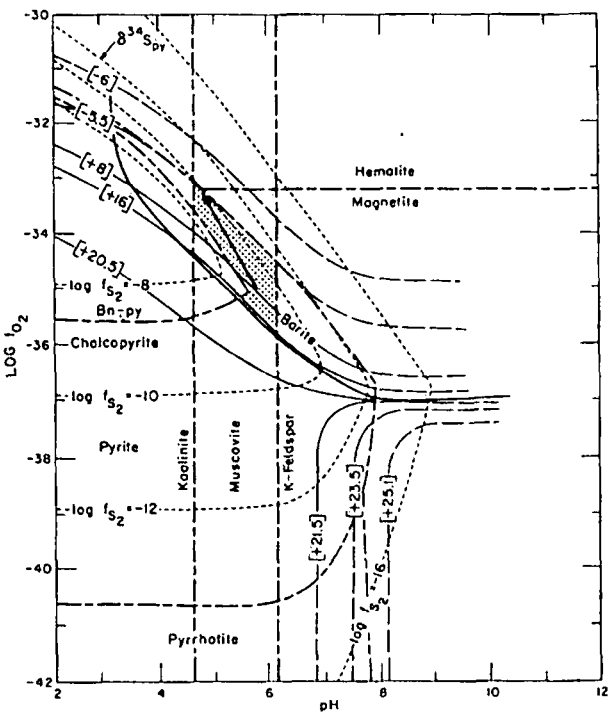

FIG. 12. pH and f_{O_2} diagram showing depositional environment of the Shakanai deposit (Kuroko ores), Japan, as suggested by the mineral associations (shaded area). T = 250°C, ionic strength = 1, $m_{K^+} = 0.01$, and $\Sigma S = 0.01$ m. The broken lines indicate mineral stability fields and the dotted lines indicate f_{S_2} contours. The chalcopyrite ≥ bornite-pyrite (Bn-py) line is taken from Barton and Skinner (1967). The boundary for barite is calculated from the solubility data summarized by Holland (1965) with a value of $m_{Ba^{++}} = 0.001$. The stability fields of silicate minerals (with excess quartz present) are calculated from Hemley (1959). The solid lines indicate $\delta^{34}S$ values of pyrite precipitated from solutions in which $\delta^{34}S_{\Sigma S}$ is +20 per mil. The arrow represents the range and sequence of $\delta^{34}S_{py}$ values at the Shakanai mine (Ohmoto et al., 1970).

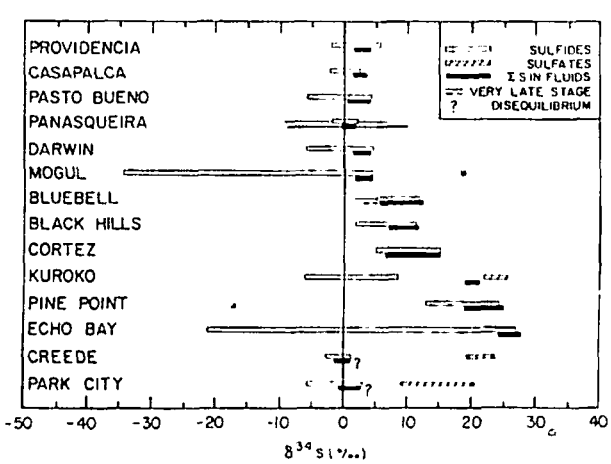

FIG. 13. $\delta^{34}S$ values of sulfides, sulfates, and $\delta^{34}S_{\Sigma S}$ for various hydrothermal ore deposits (see Fig. 1).

evaporites, as at Pine Point.

Deposits such as Cortez and the Black Hills Tertiary deposits whose fluids have intermediate $\delta^{34}S_{\Sigma S}$ values probably got their sulfur from local country rocks—from either disseminated sulfides or older ore deposits. The sulfur in the Bluebell deposit was probably a mixture of sulfur from evaporites and sedimentary sulfides. The interpreted source of sulfur in each of these deposits was determined by the relationship of the time and space distribution of their $\delta^{34}S$ values to geologic details. The range of $\delta^{34}S_{\Sigma S}$ values in deposits where sulfur is derived from sedimentary or mixed sources can be large or small depending on the extent to which the sulfur was homogenized by the ore-generating event. The reasonably narrow range of $\delta^{34}S_{\Sigma S}$ values for the Bluebell fluids indicates that the different sulfur components were fairly well mixed in the hydrothermal solutions.

Sulfur isotope disequilibrium in hydrothermal environments

The previous discussion has been based on the assumption of chemical and isotopic equilibrium among sulfur species in solutions and precipitating mineral phases. The close agreement of temperatures and chemical environments estimated from sulfur isotopic data with those suggested from other geochemical data (e.g., fluid inclusions, trace element distribution, mineral assemblages) indicates that in many deposits isotopic and chemical equilibrium was established between sulfur species in fluids and between species in fluids and the precipitating minerals. Under equilibrium conditions, the $\delta^{34}S$ values of the minerals respond readily to changes in the chemical environment of ore deposition as indicated by ore and wall-rock mineral assemblages.

The data on the lead-zinc deposits at Creede, Colorado, appear to illustrate the type of $\delta^{34}S$ distributions that may result when sulfur disequilibrium occurs during hydrothermal ore deposition. Figure 14 is a pH-f_{O_2} diagram for the Creede deposit. Sulfur isotope contours are drawn for $\delta^{34}S_{\Sigma S} = 0$ per mil and $T = 250°C$. The shaded region indicates the approximate chemical environment for most of the ore fluids at Creede as indicated by ore and wall-rock assemblages. From the sulfur isotope contours one would expect that the sulfides which precipitated over the range of f_{O_2} values in this environment would have a large range of $\delta^{34}S$ values. The sulfides, however, have a very narrow range of $\delta^{34}S$ values that average near 0 per mil (see Figs. 1 and 13). Under the conditions of disequilibrium at Creede, the $\delta^{34}S$ values did not respond to changes in the chemical environment of ore deposition. Even though the f_{O_2} range for the ore fluids was quite

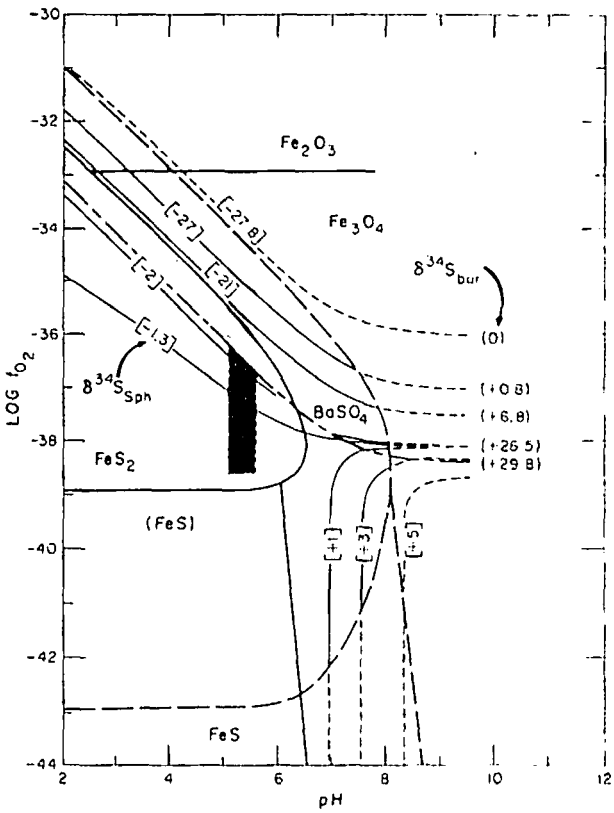

FIG. 14. pH-f_{O_2} diagram for the Creede, Colorado, Pb-Zn deposit. Sulfur isotope contours are drawn for $\delta^{34}S_{\Sigma S} = 0$ per mil and $T = 250°C$. The Fe-S-O mineral boundaries are shown for $\Sigma S = 0.1$ moles/kg H_2O, short dashed lines, and $\Sigma S = 0.001$ moles/kg H_2O, solid lines. The barite soluble/insoluble boundary is for $m_{Ba^{2+}} \cdot m_{\Sigma S} = 10^{-4}$, long and short dashed line. The rectangle region shows the approximate chemical environment for the Creede ore fluids (Bethke et al., 1973). The dark shaded region of the rectangle shows the approximate range of chemical environment indicated by the $\delta^{34}S$ values for sphalerite which precipitated over the entire f_{O_2} range of the ore fluids.

large, the sulfide $\delta^{34}S$ values reflect only a limited portion of this range, as indicated by the dark shaded region. For more discussion of sulfur isotope disequilibrium at Creede, see Bethke et al. (1973).

A similar situation has been observed for the base metal deposit at Park City, Utah (R. O. Rye and J. T. Nash, unpub. data). The only thing that seems to be peculiar about the Creede and Park City deposits is that they are shallow deposits and that boiling, mixing of fluids, and redox reactions probably occurred very near the site of ore deposition. If we are interpreting the data correctly, the indications are that sulfur isotope and/or chemical disequilibrium can occur even at fairly high temperatures in shallow deposits when there is a short time span between an event in the hydrothermal fluid, such as a redox reaction, and the precipitation of ore.

Available data on isotopic exchange experiments suggest that isotopic and chemical reactions between reduced and oxidized sulfur species can be extremely slow below about 200°C (see reference in Ohmoto, 1972, p. 576). With the aid of experimental studies, it may eventually be possible to comment specifically on the conditions that lead to disequilibrium in this type of deposit.

An example of how sulfur isotope disequilibrium can elucidate hydrothermal fluid histories is provided by some of the thermal areas in Yellowstone National Park. Sulfur occurs in several forms in the acid hot springs areas in Yellowstone. It occurs as H_2S and SO_4^{-2} in hot springs and as native sulfur and SO_4^{-2} in the soil around fumaroles. Studies by Schoen and Rye (1970) have shown that most of the sulfate in the thermal springs in the acid areas is initially produced by surficial oxidation of H_2S in the soil around the fumaroles. It is then leached from the soil and added to the hot springs by percolating ground water. Coexisting H_2S, S, and SO_4^{-2} have nearly identical $\delta^{34}S$ values (Fig. 15), which is a gross disequilibrium situation. The fact that there is little evidence of isotope exchange between H_2S and SO_4^{-2} in the hot springs is interpreted to indicate that the SO_4^{-2} does not circulate to great depths in the acid areas. In the Mammoth Hot Springs area, fumaroles are rare and SO_4^{-2} in the hot springs is derived from a solution of a deeply buried, marine evaporite. H_2S and SO_4^{-2} in the springs are in apparent isotopic equilibrium at a temperature of about 300°C based on the H_2S-SO_4^{-2} sulfur isotope fractionation. Apparently H_2S and SO_4^{-2} did equilibrate at considerable depth at the Mammoth area.

Bacteriogenic sulfides

The classical example of sulfur isotope disequilibrium occurs during bacteriogenic reduction of sulfate.

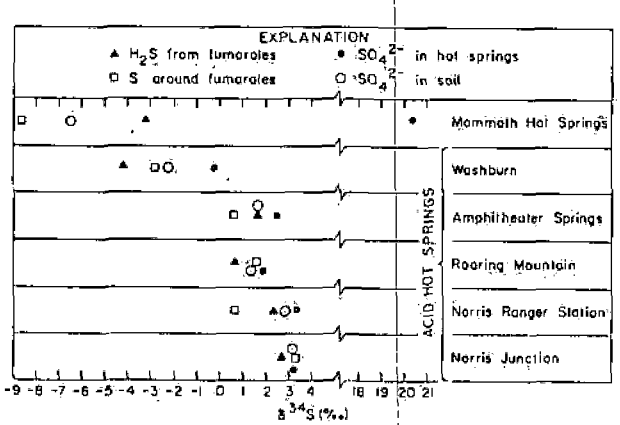

FIG. 15. Distribution of $\delta^{34}S$ values of H_2S, S, SO_4^{-2} in acid hot springs areas and Mammoth Hot Springs, Yellowstone National Park (data from Schoen and Rye, 1970).

In surficial, low-temperature environments the only known means of reducing sulfate to H_2S and precipitating sulfides is by the life processes of sulfur-reducing bacteria. These bacteria are ubiquitous in low-temperature environments and it seems likely that they have played an important role in many stratiform deposits which occur in nonvolcanic environments. Bacteriogenic sulfide deposits may also occur in ocean basins in volcanic environments. However, sea water sulfate may readily be reduced by deep circulation into rocks of high temperature and syngenetic and/or epigenetic sulfides may precipitate from the inorganically reduced sulfur at lower temperatures on or near the ocean floor. This is the probable mechanism for reduction of sulfate in Kuroko deposits and perhaps for many massive sulfide deposits associated with volcanic environments throughout geologic time (Ohmoto et al., 1970; Ohmoto, J. F. Whelan, and R. O. Rye, unpub. data).

In our opinion, reevaluation is needed for some deposits that have been designated as bacteriogenic. It should be obvious, from the previous discussion, that a deposit cannot be proven to be bacteriogenic on the basis of the range or statistical distribution of $\delta^{34}S$ values alone. Heretofore this has been the major criterion for recognizing bacteriogenic sulfide ore deposits (see Jensen, 1967; Marowsky, 1970; Burnie et al., 1972). Caution is required because some deposits perviously considered bacteriogenic on this basis have been shown, on reexamination with careful attention to geologic and geochemical details, to have notable sulfur isotope systematics that can be a result of inorganic processes. An excellent example is the roll-type uranium deposit of Wyoming (Granger and Warren, 1969; Warren, 1972). Bacteriogenic base metal ore deposits can be unequivocally recognized only on the basis of geologic occurrence and time-space distribution of $\delta^{34}S$ values.

Schwarcz and Burnie (1973) have reviewed the $\delta^{34}S$ data of sulfides in modern and ancient clastic, nonvolcanic sedimentary rocks and have attempted to evaluate the environmental significance of the data in the light of available experimental data. It should be noted that $\delta^{34}S$ distributions in bacteriogenic deposits can be large or small depending upon whether the sedimentary environment is an open or closed system. The $\delta^{34}S$ values of bacteriogenic deposits should not be amenable to the type of approach we have discussed for the hydrothermal deposits because kinetic factors are always involved in the bacteriogenic reduction of sea-water sulfate. The $\delta^{34}S$ values may vary drastically over a small distance, sulfur isotope disequilibrium may be very common among coexisting sulfides, and overall $\delta^{34}S$ variations should be related to paleogeographic trends rather than to the lithology of the host rocks.

$\delta^{34}S$ variations in metamorphosed deposits

The previous discussion has dealt with the principles of application of sulfur isotope data to undisturbed ore deposits. In this section we will consider what happens to sulfur isotope distributions in sulfide minerals during metamorphism. There have been several detailed studies on metamorphosed stratiform deposits and two principles of sulfur isotope distribution during metamorphism of these deposits are beginning to emerge:

(1) Large-scale, premetamorphic $\delta^{34}S$ variations are generally preserved. The average $\delta^{34}S$ for sulfides in major units such as formations are generally not changed.

(2) Small-scale sulfur isotope changes are in many cases superimposed upon the original sulfur isotope distribution during metamorphism. These include: (a) redistribution of sulfur isotopes among coexisting minerals that define the temperature of metamorphism, and (b) local $\delta^{34}S$ variations which reflect the structural or chemical metamorphic history.

The principles can be illustrated from the data for the Homestake, South Dakota, gold deposit (Rye and Rye, 1974). A generalized cross section of the Homestake deposit is shown in Figure 16. The ore occurs as conformable replacement bodies in dilatant zones of the highly deformed Precambrian Homestake formation and is associated with arsenopyrite and pyrrhotite in chlorite-rich cummingtonite schist of cherty carbonate iron-formation. Sulfides are also present in the overlying Ellison and the underlying Poorman formations. The grade of metamorphism is upper green schist or lower amphibolite. (Stratigraphic nomenclature for the Homestake deposit is from Hosted and Wright, 1923.)

Each formation has a distinct lithology and a distinct $\delta^{34}S$ distribution (Fig. 16). The stratigraphic dependence of the $\delta^{34}S$ values for this deposit indicates a syngenetic origin for the sulfur. It is important to note that it is possible to determine the origin of the sulfur in these formations only because the original sulfur isotope distribution was not unduly distorted by the metamorphic event. Stratigraphic dependence of $\delta^{34}S$ values in metamorphosed sulfide deposits has also been observed in the massive sulfide deposits at Bathurst, New Brunswick (Lusk, 1972), and Ducktown, Tennessee (Mauger, 1972). The fact that original large-scale $\delta^{34}S$ distributions were retained in these deposits indicates that large amounts of sulfur were not added to and not subtracted from the system during metamorphism and that remobilization

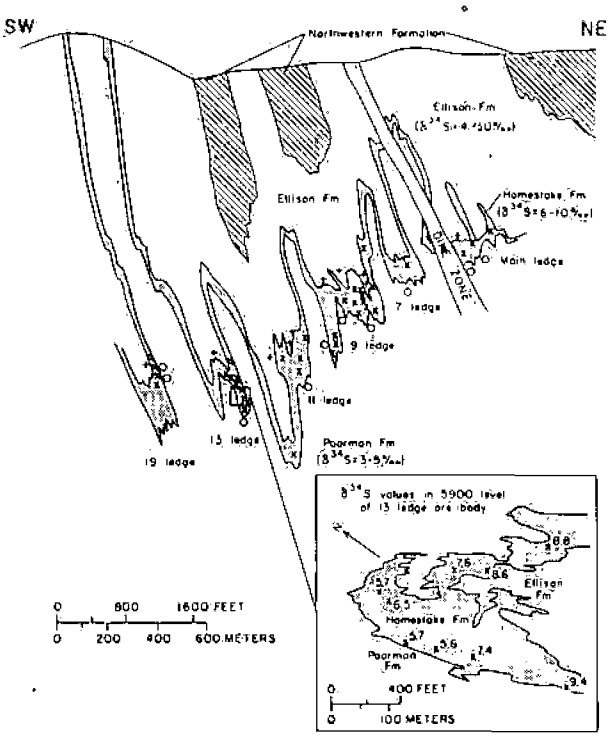

FIG. 16. Generalized cross section of the Homestake, South Dakota, gold deposit showing sample locations and average $\delta^{34}S$ values for sulfides in each formation and a sketch map of one of the dilatant zones of the Homestake formation showing distribution of $\delta^{34}S$ values for pyrrhotite and arsenopyrite (from Rye and Rye, 1974). Stratigraphic nomenclature shown in the figure is from Hosted and Wright (1923). Symbols show sample locations in the Homestake formation (X), Poorman formation (O), and Ellison formation (+).

of sulfur was restricted to a small scale during metamorphism.

Although there is apparently little migration of sulfur across formational boundaries during metamorphism, there may be significant redistribution of sulfur within formations which reflects some aspects of the metamorphic history. In the Bathurst deposit, for example, the sphalerite-galena sulfur isotope fractionations apparently reflect the temperature of metamorphism (Lusk and Crocket, 1969). In the Homestake deposit, $\delta^{34}S$ values for sulfide minerals in a single ore body in one of the dilatant zones of the Homestake formation range systematically from about 5.7 per mil in the dilatant zone where sulfide concentrations are high to about 9.4 per mil in the stretched limbs where sulfide concentrations are low (Fig. 16). This trend is a consistent feature of the Homestake ore zones (Rye and Rye, 1974). The Fe/Mg ratios of the wall rocks also decrease in the ore zones. Available data indicate that during metamorphism pyrite was broken down into pyrrhotite plus sulfur and that the excess sulfur was taken into solution by the metamorphic fluids. These fluids

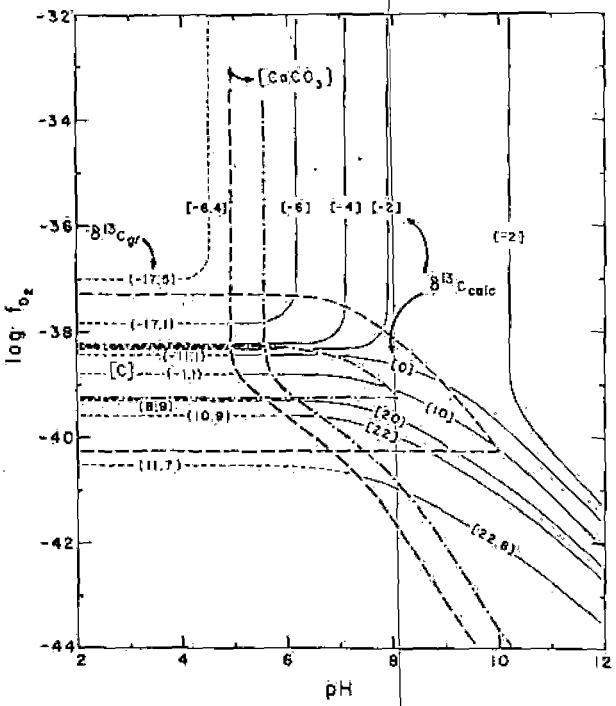

FIG. 17. pH-f_{O_2} diagram comparing the position of $\delta^{13}C$ contours with the stability fields of calcite and graphite. $T = 250°C$ and $\delta^{13}C_{\Sigma C} = -5$ per mil (from Ohmoto, 1972). Solid line: $\delta^{13}C$ contours. Values in [ ] and ( ) are, respectively, for calcite and graphite. Dashed line: Stability boundaries for calcite and graphite at $\Sigma C = 1$ mole/kg H_2O. Dash and dot line: Stability boundaries for calcite and graphite at $\Sigma C = 0.1$ moles/kg H_2O.

migrated into the dilatant zones where sulfur reacted with the wall rocks to produce iron-rich sulfides. The $\delta^{34}S$ distribution resulted from the fractional distillation of sulfides in the limbs as the sulfides broke down and as excess sulfur was removed by the metamorphic fluids. When detailed sulfur isotope data are combined with other geochemical data on metamorphosed deposits, it should be possible to determine the chemical environments of metamorphism as has been done for hydrothermal deposits.

Carbon Isotopes and Ore Genesis

$\delta^{13}C$ variations in hydrothermal deposits

The principles of the application of carbon isotope data to hydrothermal ore deposits are similar to those for sulfur. The $\delta^{13}C$ values of carbon-bearing minerals are also controlled by the physical-chemical conditions within the hydrothermal fluids. Carbon in hydrothermal fluids can be present in a number of forms but occurs primarily as CO_2 or CH_4. As in the case of sulfur, there are large isotopic fractionations between reduced and oxidized carbon species and the abundance of these species in solution is largely a function of temperature, pH, and f_{O_2} (Ohmoto, 1972).

The variations in $\delta^{13}C$ values for calcite and graphite as a function of pH and f_{O_2} are shown in Figure 17 for the case when $T = 250°C$ and $\delta^{13}C_{\Sigma C} = -5$ per mil (Ohmoto, 1972). The fine solid lines and their dashed extensions are $\delta^{13}C$ contours. The two sets of heavy dashed curves show the stability fields for calcite and graphite when the carbon concentrations in the fluid ($m_{\Sigma C}$) are 1 and 0.1 molal. In the high f_{O_2} region, $\delta^{13}C$ values of carbonates are similar to those of the total carbon in fluids ($\delta^{13}C_{\Sigma C}$); in regions of low f_{O_2} or high pH, $\delta^{13}C$ values of carbonates can be much larger than $\delta^{13}C_{\Sigma C}$. Thus, for a meaningful interpretation, carbon isotope data, like sulfur isotope data, must be tied in with detailed geologic and geochemical studies. Carbon isotope fractionations among coexisting carbon-bearing minerals such as graphite and carbonates may be used as a geothermometer (e.g., Bottinga, 1969). Carbon fractionation among aqueous carbon species also may

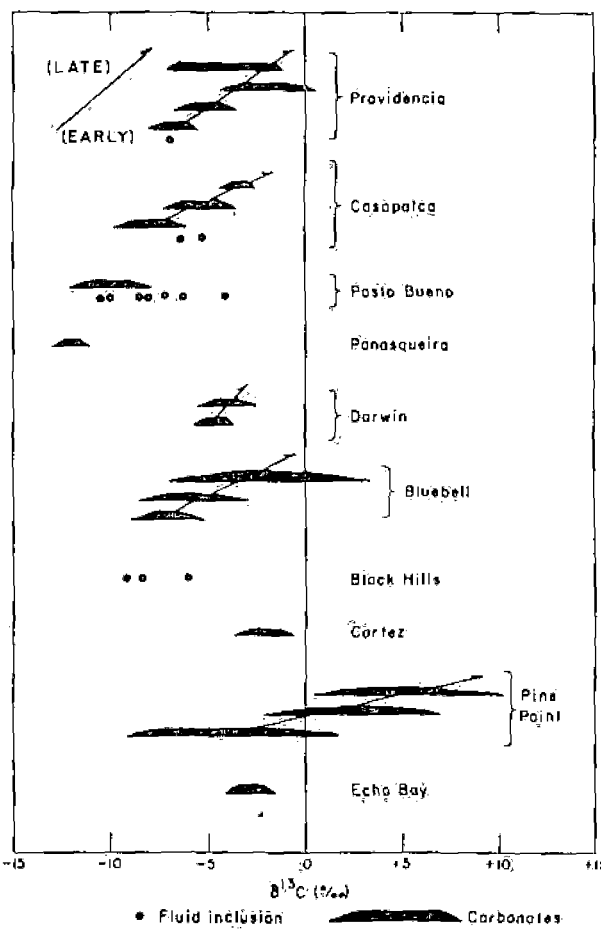

FIG. 18. $\delta^{13}C$ values of carbonates and CO_2 in fluid inclusions from various hydrothermal ore deposits. Different generations of carbonates are arranged from early to late as indicated by the arrows. Sources of data same as for Figure 1.

be used to indicate temperatures in hydrothermal systems (e.g., Hulston and McCabe, 1962).

Figure 18 shows the variation of $\delta^{13}C$ values of carbonate gangue minerals and for CO_2 in fluid inclusions for a number of hydrothermal ore deposits. In many hydrothermal deposits there are several generations of carbonate minerals that have a definite paragenetic sequence. For each deposit the different generations are indicated by bars and are arranged from early to late, as shown by the arrows in Figure 18. The earliest generation is invariably a rhombohedral carbonate, which is followed by other crystal varieties. The temperatures of deposition of the carbonates vary for each deposit but are typically between 350° and 100°C. Important points to note about the carbon isotopic data on the carbonates (Fig. 18) are that these deposits sometimes occur in limestone environments and that the carbonates are usually late in the paragenesis and are often of postsulfide deposition. Because sulfide deposition from hydrothermal fluids in limestone environments may have been associated with the dissolution of limestone and the consequent increase in $\delta^{13}C_{\Sigma C}$ in the hydrothermal solutions, late-stage carbonate-forming fluids may not have the same carbon isotopic composition as the original ore-forming fluids. In order to determine the carbon isotope composition of the fluids from which ores actually precipitated, one needs to have $\delta^{13}C$ analyses of total carbon (usually CO_2) in fluid inclusions in main-stage minerals. Available analyses for $\delta^{13}C$ in CO_2 in fluid inclusions range from about -4 to -12 per mil. In these samples $\delta^{13}C_{CO_2} \simeq \delta^{13}C_{\Sigma C}$, so the data reflect the carbon isotopic composition of the hydrothermal fluids.

Generalized trends of carbon isotope data of the carbonates in these deposits versus paragenetic time are plotted in Figure 19. Also shown are the ranges of $\delta^{13}C$ values for the major reservoirs of carbon in hydrothermal systems. These are: (1) marine limestones, which have average $\delta^{13}C$ values near 0 per mil; (2) deep-seated carbon, which has an average $\delta^{13}C$ value of about -7 per mil as indicated by analyses of carbonatites; and (3) reduced or organic carbon in sediments which normally has $\delta^{13}C$ values of less than -15 per mil. Early carbonates in all deposits except Panasqueira have $\delta^{13}C$ values between -6 and -9 per mil. In all the deposits studied, the f_{O_2} values for fluid from which the early carbonates formed were such that $\delta^{13}C_{carb} \simeq \delta^{13}C_{CO_2} \simeq \delta^{13}C_{\Sigma C}$. When these values for $\delta^{13}C_{\Sigma C}$ are considered, it is hard to escape the conclusion that the carbon in the early fluids in *most* of these deposits was probably derived from a deep-seated source. Such $\delta^{13}C_{\Sigma C}$ values do not necessarily prove a deep-seated source for hydrothermal carbon. At the Bluebell deposit, for example, the $\delta^{13}C_{\Sigma C}$ value of -7 per mil probably resulted from high-temperature exchange of the carbon in the hydrothermal fluids with graphite in the country rocks.

The carbonates at Panasqueira have $\delta^{13}C$ values averaging about -14 per mil, indicating that much of the hydrothermal carbon was probably derived from a graphitic source.

Late-stage carbonates in all deposits except Panasqueira show an increase in $\delta^{13}C$ values. This increase can be caused by several factors, which must be evaluated for a specific deposit. A decrease in the oxidation state of the fluids seems to have caused the increase in $\delta^{13}C$ at Pine Point. In this deposit $\delta^{13}C_{\Sigma C}$ apparently remained constant during ore deposition, but carbonates with large positive $\delta^{13}C$ values were probably precipitated as a result of increasing CH_4 in the late fluids. Increasing carbon fractionation between fluids and carbonates with decreasing temperature is apparently reflected in the carbonate paragenesis Providencia. Finally, a change in $\delta^{13}C_{\Sigma C}$ of the fluid as a result of an increasing contribution of carbon from limestone sources is suggested for the Bluebell, Darwin, and Casapalca deposits.

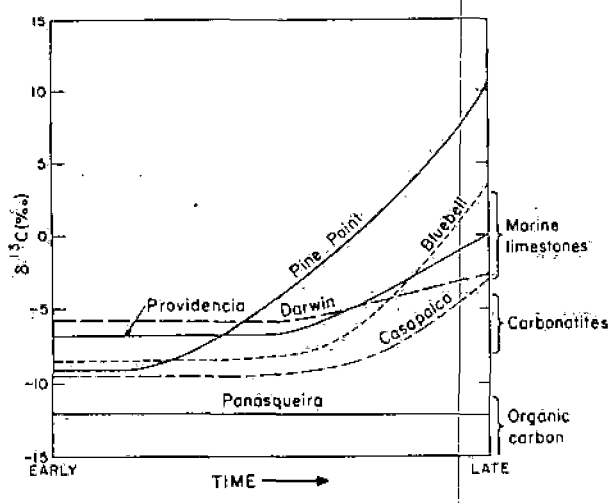

FIG. 19. Generalized trends of average $\delta^{13}C$ values of carbonates versus paragenetic time for a number of hydrothermal ore deposits. Sources of data same as for Figure 1.

Bacteriogenic carbonates

In low-temperature environments where bacteriogenic sulfides are produced, anaerobic bacteria also produce CO_2 and CH_4 from the associated organic matter which they consume as an energy source (Cheney and Jensen, 1965). Depending upon the depositional environment and the proportion of carbonate derived from CO_2 and CH_4, precipitated carbonates may show a wide and random spread of

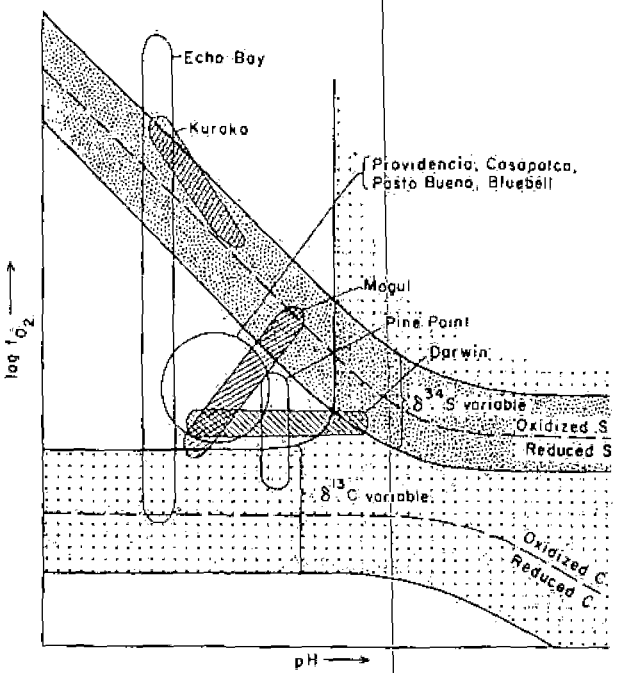

FIG. 20. Schematic pH-f_{O_2} diagram showing reconstructed depositional environments of nine hydrothermal deposits. Dashed lines separate environments of predominantly reduced and oxidized carbon and reduced and oxidized sulfur. The stippled zones indicate environment where carbon and sulfur isotope values in carbonates and sulfides will be strongly influenced by change in pH and f_{O_2}. Encircled areas indicate environments of ore deposition.

variations in $\delta^{13}C$ values, including some large negative values. Very large negative $\delta^{13}C$ values, however, can also be produced in syngenetic carbonates in volcanic environments by the refluxing of organic carbon from restricted ocean basins, and a wide range of $\delta^{13}C$ values can be produced in the carbonates by changes in the f_{O_2} of the depositional environment or by mixing of refluxed organic carbon with marine or deep-seated carbon (Rye and Rye, 1974).

$\delta^{13}C$ variations in metamorphic deposits

Carbon and oxygen isotope exchange in carbonates occur primarily during recrystallization, when the carbonate is dissolved and reprecipitated. Even when extensive recrystallization in carbonate occurs, extensive carbon isotope exchange will not take place unless good permeability allows penetration by CO_2-rich fluids (see Pinckney and Rye, 1972).

Preliminary carbon isotope data for the Precambrian iron carbonates in the Homestake gold deposit indicate that no significant change in average $\delta^{13}C$ values of major units occurred during metamorphism (Rye and Rye, 1974). Detailed studies of marbles representative of a wide range of metamorphic grades, including marbles in anatectic granites, indicate that $\delta^{13}C$ values of carbonates are, in general, little changed during regional metamorphism even when the metamorphic fluid/rock ratios are high and the fluids are CO_2-rich. Exceptions may occur where the marbles have been decarbonated (Rye and Schuiling, in press). Host rock carbonates occasionally show $\delta^{13}C$ variations away from vein systems, but these are usually quite limited in extent and apparently occur because the rocks maintain an appreciable permeability during recrystallization in the presence of CO_2-rich fluids (Rye, unpub. data on Providencia; Pinckney and Rye, 1972; Rye et al., 1974b). Hydrothermal carbonates are extremely resistant to carbon isotope exchange and their $\delta^{13}C$ values are "frozen in" as the carbonates crystallize. We are not aware of any published evidence where $\delta^{13}C$ values of early hydrothermal carbonates have been altered by exchange with later hydrothermal fluids.

Sulfur and Carbon Isotopes and the Chemical Environments of Hydrothermal Ore Deposition

A schematic pH-f_{O_2} diagram (Fig. 20) shows how carbon and sulfur isotope data can be combined to define the depositional environments of hydrothermal deposits. The encircled areas in Figure 20 indicate the environments of ore deposition of nine hydrothermal deposits. The ore fluids in these deposits had a variety of pH and oxidation states that are reflected in various ways by sulfur and carbon isotopic data on the minerals.

The pH and f_{O_2} environments for the ore fluids at Providencia, Casapalca, Pasto Bueno, and Bluebell were such that changes in these variables were not reflected by significant variations in $\delta^{34}S$ and $\delta^{13}C$ values of the minerals. The ore fluids at Echo Bay appear to have changed their oxidation state over a wide range, as indicated by the wide range of sulfide $\delta^{34}S$ values. Very low oxidation states are indicated by large positive $\delta^{13}C$ values in carbonates at Pine Point. Isotope data indicate that the fluids for deposits such as Darwin apparently underwent considerable change of pH, while fluids for the Kuroko deposits and Mogul changed both pH and oxidation state during the course of ore deposition.

The pH increase in the ore fluids at Darwin was a possible cause of the precipitation of ore (Rye et al., 1974b). The f_{O_2} decrease in the ore fluids probably played an important role in the precipitation of ore at Echo Bay (Robinson and Ohmoto, 1973). Because combined sulfur and carbon isotope studies can often help define the pH and f_{O_2} as well as other important variables of hydrothermal fluids (e.g., T, $m_{\Sigma S}$, $m_{\Sigma C}$, f_{S_2}, f_{CO_2}), it seems likely that such studies will become increasingly integrated with theoretical and experimental studies of base metal solubilities

and mineral stabilities in discussions of the mechanisms of ore deposition at specific ore deposits.

Acknowledgments

For permission to quote unpublished data the authors are indebted to J. T. Nash, U. S. Geological Survey (Park City, Utah), and W. C. Kelley, University of Michigan (Panasqueira, Portugal). A National Science Foundation Grant GA-3190 to Ohmoto is gratefully acknowledged. We are grateful to F. J. Sawkins, University of Minnesota; D. M. Rye, Yale University; H. D. Holland, Harvard University; and G. K. Czamanske, U. S. Geological Survey, for reviewing this paper.

R. O. R.
U. S. Geological Survey
Federal Center
Denver, Colorado 80225
H. O.
Department of Geosciences
Pennsylvania State University
University Park, Pennsylvania 16802

REFERENCES

Ault, W. V., and Jensen, M. L., 1963, Summary of sulfur isotope standards, *in* Jensen, M. L., ed., Biogeochemistry of sulfur isotopes: Natl. Sci. Found., Symposium Proc., Yale Univ., April 12–14.

Barton, P. B., Jr., and Skinner, B. J., 1967, Sulfide mineral stabilities, Chap. 7, *in* Barnes, H. L., ed., Geochemistry of hydrothermal ore deposits: New York, Holt, Rinehart and Winston, Inc., p. 236–333.

Bethke, P. M., Rye, R. O., and Barton, P. B., 1973, Hydrogen, oxygen, and sulfur isotopic compositions of ore fluids in the Creede district, Mineral County, Colorado: Geol. Soc. America, Abs. with Program, v. 2, no. 7, p. 549.

Bottinga, Y., 1969, Calculated fractionation factors for carbon and hydrogen isotopic exchange in the system, calcite-carbon dioxide-graphite-methane-hydrogen-water vapor: Geochim. et Cosmochim. Acta, v. 33, p. 41–64.

Burnie, S. W., Schwarcz, H. P., and Crocket, J. H., 1972, A sulfur isotopic study of the White Pine mine, Michigan: Econ. Geol., v. 67, p. 895–914.

Cheney, E. S., and Jensen, M. L., 1965, Stable carbon isotopic composition of biogenic carbonates: Geochim. et Cosmochim. Acta, v. 29, p. 1331–1346.

Craig, Harman, 1957, Isotopic standards for carbon and oxygen and correction factors for mass-spectrometric analysis of carbon dioxide: Geochim. et Cosmochim. Acta, v. 12, p. 133–149.

Czamanske, G. K., and Rye, R. O., 1974, Experimentally determined sulfur isotope fractionations between sphalerite and galena in the temperature range 600°C to 275°C: Econ. Geol., v. 69, p. 17–25.

Granger, H. C., and Warren, C. G., 1969, Unstable sulfur compounds and the origin of roll type uranium deposits: Econ. Geol., v. 64, p. 160–171.

Greig, J. A., Baadsgaard, H., Cumming, G. L., Folinsbee, R. E., Krouse, H. R., Ohmoto, H., Sasaki, A., and Smejkal, V., 1971, Lead and sulfur isotopes of the Irish base metal mines in Carboniferous carbonate host rocks: Soc. Mining Geologists Japan, Spec. Issue 2 Proc. (IMA-IAGOD Mtgs. 1970, Joint Symp. Vol.), p. 84–92.

Hemley, J. J., 1959, Some mineralogical equilibria in the system K_2O-Al_2O_3-SiO_2-H_2O: Am. Jour. Sci., v. 257, p. 241–270.

Holland, H. D., 1965, Some applications of thermochemical data to problems of ore deposits. II. Mineral assemblages and the composition of ore-forming fluids: Econ. Geol., v. 60, p. 1101–1166.

Hosted, J. O., and Wright, L. B., 1923, Geology of the Homestake ore bodies and the lead area, South Dakota: Eng. Mining Jour. v. 115, p. 793–799, 836–843.

Hulston, J. R., and McCabe, W. J., 1962, Mass spectrometer measurements in the thermal areas of New Zealand: Part I—Carbon dioxide and residual gas analyses; Part II—Carbon isotopic ratios: Geochim. et Cosmochim. Acta, v. 26, p. 383–410.

Jensen, M. L., 1959, Sulfur isotopes and hydrothermal mineral deposits: Econ. Geol., v. 54, p. 374–394.

—— 1967, Sulfur isotopes and mineral genesis, Chap. 5, *in* Barnes, H. L., ed., Geochemistry of hydrothermal ore deposits: New York, Holt, Rinehart and Winston, Inc., p. 143–165.

Kajiwara, Yoshimichi, 1971, Sulfur isotope study of the Kuroko-ores of the Shakanai No. 1 deposit: Akita Prefecture, Japan: Geochem. Jour., v. 4, p. 157–181.

Landis, G. P., and Rye, R. O., 1974, Geologic, fluid inclusion, and stable isotope studies of the Pasto Bueno tungsten-base metal ore deposits, Northern Peru: Econ. Geol., v. 69, (in press).

Lusk, John, 1972, Examination of volcanic-exhalative and biogenic origins for sulfur in the stratiform massive sulfide deposits of New Brunswick: Econ. Geol., v. 67, p. 169–183.

—— and Crocket, J. H., 1969, Sulfur isotope fractionation in coexisting sulfides from the Heath-Steele B-1 ore body, New Brunswick, Canada: Econ. Geol., v. 64, p. 147–155.

Macnamara, J., and Thode, H. G., 1950, Comparison of the isotopic constitution of terrestrial and meteoric sulfur: Phys. Rev., v. 78, p. 307–308.

Marowsky, G., 1970, Schwefel-Kohlenstoff-und Sauerstoff Isotopenuntersuchungen am Kuperschiefer as Beitrog zur genetischen Deutung: Contr. Mineralogy Petrology, v. 22, p. 290–334.

Mauger, R. L., 1972, A sulfur isotope study of the Ducktown, Tennessee, district, U.S.A.: Econ. Geol., v. 67, p. 497–510.

Ohmoto, Hiroshi, 1970, Influence of pH and f_{O_2} of hydrothermal fluids on the isotopic composition of sulfur species: Geol. Soc. America, Abs. with Program, v. 2, no. 7, p. 640.

—— 1972, Systematics of sulfur and carbon isotopes in hydrothermal ore deposits: Econ. Geol., v. 67, p. 551–578.

—— Kajiwara, Yoshimichi, and Date, Jiro, 1970, The Kuroko ores in Japan: Products of sea water?: Geol. Soc. America, Abs. with Program, v. 2, no. 7, p. 640–641.

Ohmoto, Hiroshi, and Rye, R. O., 1970, The Bluebell mine, British Columbia—[Pt.] I, Mineralogy, paragenesis, fluid inclusions, and the isotopes of hydrogen, oxygen, and carbon: Econ. Geol., v. 65, p. 417–437.

—— 1974, Hydrogen and oxygen isotopic compositions of fluid inclusions in the Kuroko deposits, Japan: Econ. Geol., v. 69, p. 947–953.

Pinckney, D. M., and Rye, R. O., 1972, Variation of O^{18}/O^{16}, C^{13}/C^{12}, texture, and mineralogy in altered limestone in the Hill mine Cave-in-Rock district, Illinois: Econ. Geol., v. 67, p. 1–18.

Robinson, B. W., and Ohmoto, H., 1973, Mineralogy, fluid inclusions, and stable isotopes of the Echo Bay U-Ni-Ag-Cu deposits, Northwest Territories, Canada: Econ. Geol., v. 68, p. 635–656.

Rye, D. M., and Rye, R. O., 1974, Homestake gold mine, South Dakota: I. Stable isotope studies: Econ. Geol., v. 69, p. 293–317.

Rye, R. O., 1966, The carbon, hydrogen, and oxygen isotopic composition of the hydrothermal fluids responsible for the lead-zinc deposits at Providencia, Zacatecas, Mexico: Econ. Geol., v. 61, p. 1399–1427.

—— 1974, A comparison of sphalerite-galena sulfur isotope temperatures with filling temperatures of fluid inclusions: Econ. Geol., v. 69, p. 26–32.

—— Doe, B. R., and Wells, J. D., 1974a, Stable isotope and lead isotope studies of the Cortez, Nevada, gold deposit

and surrounding area: U. S. Geol. Survey Jour. Research, v. 2, p. 13–23.
Rye, R. O., Hall, W. E., and Ohmoto, H., 1974b, Carbon, hydrogen, oxygen, and sulfur isotope study of the Darwin lead-silver-zinc deposit, southern California: Econ. Geol., v. 69, p. 468–481.
Rye, R. O., and Sawkins, F. J., 1974, Fluid inclusions and stable isotope studies in the Casapalca Ag-Pb-Zn-Cu deposit, Central Andes, Peru: Econ. Geol., v. 69, p. 181–205.
Rye, R. O., and Schuiling, R. D., in press, Preliminary carbon, hydrogen, and oxygen isotope studies of the regional metamorphic complex at Naxos, Greece.
Sakai, H., 1968, Isotopic properties of sulfur compounds in hydrothermal processes: Geochem. Jour., v. 2, p. 29–49.
Sasaki, Akira, and Krouse, H. R., 1969, Sulfur isotopes and the Pine Point lead-zinc mineralization: Econ. Geol., v. 64, p. 718–730.
Schoen, Robert, and Rye, R. O., 1970, Sulfur isotope distribution in solfataras, Yellowstone National Park: Science, v. 170, p. 1082–1084.
Schwarcz, H. P., and Burnie, S. W., 1973, Influence of sedimentary environments on sulfur isotope ratios in clastic rocks—A Review: Mineralium Deposita, v. 8, p. 264–277.
Warren, C. G., 1972, Sulfur isotopes as a clue to the genetic geochemistry of a roll-type uranium deposit: Econ. Geol., v. 67, p. 759–767.

STABILITY CONSTANTS

of Metal-ion Complexes,
with Solubility Products of Inorganic Substances

Compiled by JANNIK BJERRUM,
GEROLD SCHWARZENBACH, and LARS GUNNAR SILLÉN

Under the Auspices of
THE INTERNATIONAL UNION OF PURE & APPLIED CHEMISTRY

PART II: INORGANIC LIGANDS

with Solubility Products of Inorganic Substances

Compiled from the literature
up to the middle of 1957

With collaboration by

CLARA BERECKI-BIEDERMANN, LORENS MALTESEN,
SVEND ERIK RASMUSSEN, and FRANCIS J. C. ROSSOTTI

Specialist Editor : K. W. SYKES

Special Publication No. 7

LONDON: THE CHEMICAL SOCIETY, BURLINGTON HOUSE, W.1
1958

Metal	Method	Temp.	Medium	Log of equilibrium constant, remarks	Ref.
	cal	25	0 corr	$\Delta H_6[Ca^{2+}(H_2L^-)_2H_2O] = -3$ to -4	43
	sol, gl	25	0 corr	$K_6[Ca^{2+}HL^{2-}(H_2O)_2] -6{\cdot}57$ [$K_{12}(H^+)$ 7·19]	43a
Ce^{3+}	i ex	25	0 corr	K_1 18·53 [$\beta_{13}(H^+)$ 23·30]	44
Th^{4+}	dist	25	2 ($NaClO_4$)	$\beta(Th^{4+}H_3L)$ 1·89, $\beta(Th^{4+}H^+_{-1}H_3L)$ 2·18, $\beta(Th^{4+}H^+_{-2}(H_3L)_2)$ 3·90, $\beta(Th^{4+}H^+_{-1}(H_3L)_2)$ 4·15	45
	sol	19—20	var	$K_{so}(Th^{4+}{}_3L^{3-}{}_4) -78{\cdot}59$ or $-57{\cdot}61$?	45a
				$K_6[Th^{4+}(HL^{2-})_2] -21{\cdot}04$ or $-19{\cdot}92$	45a
	pol	25	→ 0	$K_{so} -24{\cdot}1$	46
Cr^{3+}	sol, qh	18—20	var	$K_{so} -22{\cdot}62$(green), $-17{\cdot}00$(violet), (H^+: K_1 12·44, K_{12} 6·71, K_{13} 1·96)	37
	i ex, ani ex	40	var	ev $CrHL^+$, CrL_2^{3-}	47
	i ex, ani ex		1 H_3L	ev $CrHL^+$, ani cpx, $Cr(HL)_2^-$?, form slowly	47a
Cr^{VI}	sp	25	0·25 ($NaClO_4$)	$K(HCrO_4^- + H_2PO_4^- \rightleftharpoons HCrPO_7^{2-} + H_2O)$ 0·48	48
				$K(HCrO_4^- + H_3PO_4 \rightleftharpoons H_2CrPO_7^- + H_2O)$ 0·95	
Mo^{VI}	kin	22—23	0·48	$K(H_2MoO_4 + H_3L \rightleftharpoons MoO_2L^- + H^+ + 2H_2O)$ 1·02	49
				$K(H_2MoO_4 + 2H_3L \rightleftharpoons MoO_2L_2^{4-} + 4H^+ + 2H_2O)$ 2·64	49
U^{4+}	sol	35	var	ev $UAl_6(HL)_8^{6+}$ or $UAl_8(HL)_8^{12+}$	50
UO_2^{2+}	sp	25	1 $HClO_4$	$K[UO_2^{2+} + H_3L \rightleftharpoons UO_2H_{1+x}L^{x+} + (2-x)H^+]$ 1·58	51a
	sol	25	1 $HClO_4$	$K[UO_2^{2+} + H_3L \rightleftharpoons UO_2H_{1+x}L^{x+} + (2-x)H^+]$ 1·57	51b, 51c,
				$x = 1$ or 2	cf. 51c
			1 $HClO_4$?	$K[UO_2^{2+} + 2H_3L \rightleftharpoons UO_2(H_2L)_2 + 2H^+]$ 1·18	
			1 $HClO_4$?	$K[UO_2^{2+} + 3H_3L \rightleftharpoons UO_2(H_2L)_2H_3L + 2H^+]$ 2·30	
			1 $HClO_4$	$K_6[UO_2HL(s) + 2H^+ \rightleftharpoons UO_2^{2+} + H_3L] -2{\cdot}85$	
			1 $HClO_4$	$K_6[UO_2HL(s) + xH^+ \rightleftharpoons UO_2H_{1+x}L^{x+}] -1{\cdot}29$, $x = 1$ or 2	
			H_3L var	$K_6[UO_2HL(s) + H_3L \rightleftharpoons UO_2(H_2L)_2] -1{\cdot}7$	
			H_3L var	$K_6[UO_2HL(s) + 2H_3L \rightleftharpoons UO_2(H_2L)_2H_3L] -0{\cdot}55$	
			H_3L dil	$K_6[(UO_2)_3L_2(s) + 6H^+ \rightleftharpoons 3UO_2^{2+} + 2H_3L] -6{\cdot}15$	
			H_3L dil	$K_6[(UO_2)_3L_2(s) + H_3L + 3H^+ \rightleftharpoons 3UO_2H_2L^+] -2{\cdot}40$	
			H_3L dil	$K_6[(UO_2)_3L_2(s) + 4H_3L \rightleftharpoons 3UO_2(H_2L)_2] -2{\cdot}89$	
			H_3L dil	$K_6[(UO_2)_3L_2(s) + 7H_3L \rightleftharpoons 3UO_2(H_2L)_2H_3L] 0{\cdot}53$	
				solid: "$UO_2HL(s)$" = $UO_2HPO_4(H_2O)_4(s)$	
	sol	25	var	ev $UO_2H_2L^+$, $UO_2H_3L^{2+}$, $UO_2(H_2L)_2$	52a, 52b
	ani ex	20	0 corr	H_3L^-: K_1 3·00, K_2 2·43, K_3 1·90, H_3L: $K_1 < 1{\cdot}88$, β_2 3·88, β_3 5·23, $K_a[UO_2(H_3L)_3^{2+}] -0{\cdot}53, -2{\cdot}27, -1{\cdot}48$, $K_a[UO_2(H_3L)_2^{2+}] -1{\cdot}52, -1{\cdot}18$, ($H^+$: K_{13} 2·12)	53
	sol	19—20	var	$K_6(UO_2^{2+}NH_4^+L^{3-}) -26{\cdot}36$, $K_6(UO_2^{2+}K^+L^{3-}) -23{\cdot}11$, $K_6(UO_2^{2+}HL^{2-}) -10{\cdot}67$, ($H^+$: K_1 12·44, K_{12} 6·71, K_{13} 1·96)	45a
	sp	25	var	ev $UO_2H_2L^+$, $UO_2H_3L^{2+}$, $UO_2(H_2L)_2$, $UO_2H_6L_2^+$	54

(43) E. P. Egan, jun., B. B. Luff, and Z. T. Wakefield, *J. Amer. Chem. Soc.*, 1957, **79**, 2696
(43a) B. S. Strates, W. F. Neuman, and G. J. Levinskas, *J. Phys. Chem.*, 1957, **61**, 279
(44) S. W. Mayer and S. D. Schwartz, *J. Amer. Chem. Soc.* 1950, **72**, 5166
(45) E. L. Zebroski, H. W. Alter, and F. K. Heumann, *ibid.*, 1951, **73**, 5646
(45a) V. G. Chukhlantsev and S. I. Stepanov, *Zhur. neorg. Khim.*, 1956, **1**, 478
(46) V. I. Zolotavin and V. K. Kuznetsova, *ibid.*, p. 2257
(47) R. F. Jameson and J. E. Salmon, *J. Chem. Soc.*, 1955, 360
(47a) A. Holroyd and J. E. Salmon, *J. Chem. Soc.*, 1956, 269
(48) F. Holloway, *J. Amer. Chem. Soc.*, 1952, **74**, 224
(49) K. B. Yatsimirskii and I. I. Alekseeva, *Zhur. neorg. Khim.*, 1956, **1**, 952
(50) E. Strandell, *Acta Chem. Scand.*, 1957, **11**, 105
(51a) C. F. Baes, jun., J. M. Schreyer, and J. M. Lesser, ORNL-Y-12, ORNL-1577, 1953
(51b) J. M. Schreyer and C. F. Baes, jun., ORNL-Y-12, ORNL-1578, 1953
(51c) C. F. Baes, jun., and J. M. Schreyer, ORNL-1579, 1953
(52a) J. M. Schreyer and C. F. Baes, jun., *J. Amer. Chem. Soc.*, 1954, **76**, 354
(52b) *Idem*, *J. Phys. Chem.*, 1955, **59**, 1179
(53) Y. Marcus, Diss., Hebrew Univ. Jerusalem, 1955, p. 17
(54) C. F. Baes, jun., *J. Phys. Chem.*, 1956, **60**, 878

[continued overleaf

Metal	Method	Temp.	Medium	Log of equilibrium constant, remarks	Ref.
Cr^{3+}	cond	25—100	dil	ev $Cr_2(OH)_2L^{2+}$, $Cr_2(OH)_2L_3^{2-}$	75, 76
	?	25	1 ($NaClO_4$)	K_1^{out} 1·34	77
CrO_4^{2-}	sp		H_2SO_4 var	ev cpx	78
MoO_4^{2-}	sp			ev $MoO_3SO(OH)_3^+$	79
U^{4+}	dist	25	2 ($HClO_4$)	$*K_1$ 2·53, $*K_2$ −0·13	80
		25	2 ($HClO_4$)	$*K_1$ 2·41, $*K_2$ 1·32	80, cf. 8.
		25	2 ($HClO_4$)	K_1 3·24, K_2 2·18 ($K_1(H^+)$ 1·125) (?)	80, cf. 8.
	dist	10	2 (Na)ClO_4, 1 H^+	$*K_1$ 2·63, $*K_2$ 1·34	82
	dist	25	2 (Na)ClO_4, 1 H^+	$*K_1$ 2·52, $*K_2$ 1·35, $\Delta H_1 = -3·2$, $\Delta H_2 = 0·9$, $\Delta S_1 = 0·7$, $\Delta S_2 = 9·3$	82
	dist	40	2 (Na)ClO_4, 1 H^+	$*K_1$ 2·38, $*K_2$ 1·38	82
UO_2^{2+}	sp	25	2·65($NaClO_4$), 2 H^+	$*K_1$ 0·70	83
		25	3·5(?), 2 H^+	K_1 1·83 [$K_1(H^+)$ 1·125]	83, cf. 7
	qh	20	1 ($NaClO_4$)	K_1 1·70, K_2 0·84, K_3 0·86, $\beta(UO_2^{2+}L^{2-}Ac^-)$ 3·78, $\beta(UO_2^{2+}L^{2-}{}_2Ac^-)$ 4·60	84
	sp	20	1 ($NaClO_4$)	K_1 1·75, K_2 0·90	84
	cond	25	0 corr	K_1 3·23?	85
	dist	10	2 ($NaClO_4$)	K_1 1·80, K_2 0·96 [$K_1(H^+)$ 1·01]	86
	dist	25	2 ($NaClO_4$)	K_1 1·88, K_2 0·97 [$K_1(H^+)$ 1·08], $\Delta H_1 = 2·3$, $\Delta H_2 = -0·9$, $\Delta S_1 = 16$, $\Delta S_2 = 2$	86
	dist	40	2 ($NaClO_4$)	K_1 1·98, K_2 0·93 [$K_1(H^+)$ 1·17]	86
	ani ex		var	ev $UO_2L_3^{4-}$, $U_2O_5L_3^{4-}$	87a
	ani ex	25	var	ev UO_2L, $UO_2L_2^{2-}$, $UO_2L_3^{4-}$, $U_2O_5L_3^{4-}$	87b
	sp	25	→ 0	K_1 2·96, K_2 ~1	87c
Np^{4+}	dist	10·2	2 ($NaClO_4$)	$*K_1$ 2·47, $*K_2$ 0·91	88
	dist	25·2	2 ($NaClO_4$)	$*K_1$ 2·43, $*K_2$ 1·04 [$K_1(H^+)$ 1·08]	88
	dist	35·3	2 ($NaClO_4$)	$*K_1$ 2·40, $*K_2$ 1·14	88
		25	2 ($NaClO_4$)	$\Delta H_1 = 4·0$, $\Delta H_2 = 6·22$, $\Delta S_1 = 29·5$, $\Delta S_2 = 41·0$	88
Pu^{3+}	kin	25	2 ($NaClO_4$)	(K_1 1·0), K_2 0·62	89
Pu^{4+}	red	25	1 $HClO_4$	K_1 3·66 [$K_1(H^+)$ 0·62]	15
Am^{3+}	sp, tp		var	ev ani cpx	91
AmO_2^{2+}	sp		var	ev cpx	90
	sp		25	ev cpx	91
Mn^{2+}	cond	25	0 corr	K_1 2·28	92
Fe^{2+}	kin	30·5	~1·1 ($NaClO_4$)	K_1 0·04	94
Fe^{3+}	kin	18	0·066($NaClO_4$)	K_1 3·02	95
		18	0 corr	K_1 4·18	95
	i ex	28	1 H(ClO_4)	K_1 1·98, K_2 0·97 [$K_1(H^+)$ 1·125]	74
	sp	27	1 H(ClO_4)	K_1 2·03	74

(75) A. Küntzel, H. Erdmann, and H. Spahrkäs, *Das Leder*, 1952, 3, 73
(76) H. Erdmann, *Angew. Chem.*, 1952, 64, 500
(77) R. E. Connick and M. S. Tsao, *Amer. Chem. Soc.*, 1953, 123rd meeting, Abs. 4P
(78) K. B. Yatsimirskii and V. N. Vasil'eva, *Zhur. neorg. Khim.*, 1956, 1, 1983
(79) F. Chauveau, *Compt. rend.*, 1956, 242, 2154
(80) R. H. Betts and R. M. Leigh, *Canad. J. Res.*, 1950, 28, *B*, 514
(81) J. C. Sullivan and J. C. Hindman, *J. Amer. Chem. Soc.*, 1952, 74, 6091
(82) R. A. Day, jun., R. N. Wilhite, and F. D. Hamilton, *ibid.*, 1955, 77, 3180
(83) R. H. Betts and R. K. Michels, *J. Chem. Soc.*, 1949, S286
(84) S. Ahrland, *Acta Chem. Scand.*, 1951, 5, 1151
(85) R. D. Brown, W. B. Bunger, W. L. Marshall, and C. E. Secoy, *J. Amer. Chem. Soc.*, 1954, 76, 1532
(86) R. A. Day, jun., and R. M. Powers, *ibid.*, p. 3895
(87a) T. V. Arden and G. A. Wood, *J. Chem. Soc.*, 1956, 1596
(87b) T. V. Arden and M. Rowley, *ibid.*, 1957, 1709
(87c) E. W. Davies and C. B. Monk, *Trans. Faraday Soc.*, 1957, 53, 442
(88) J. C. Sullivan and J. C. Hindman, *J. Amer. Chem. Soc.*, 1954, 76, 5931
(89) T. W. Newton and F. B. Baker, *J. Phys. Chem.*, 1956, 60, 1417
(90) L. B. Asprey, S. E. Stephanou, and R. A. Penneman, *J. Amer. Chem. Soc.*, 1951, 73, 5715
(91) G. N. Yakovlev and V. N. Kosyakov, Proc. Internat. Conference Geneva, 1955, Vol. VII, 363
(92) J. C. James, Thesis, London, 1947
(93) T. O. Denney and C. B. Monk, *Trans. Faraday Soc.*, 1951, 47, 992
(94) R. E. Huffman and N. Davidson, *J. Amer. Chem. Soc.*, 1956, 78, 4836
(95) K. W. Sykes, *J. Chem. Soc.*, 1952, 124

[continued

Metal	Method
	sp
	sp
	sp
Co^{3+}	cond
	dial
	dial
	gl, Bi, sol
	lit
	fp
	cond
Co^{3+}	kin
$Co(NH_3)_5^{3+}$	sp, kin
	sp
	sp
	Kis
$Co(NH_3)_6^{3+}$	sol
	cond
	sp
	sp
$Co(NH_3)_5Cl^{2+}$	sp
$Co\ en_3^{3+}$	cond
$Co\ pn_3^{3+}$	cond
Ni^{2+}	cond
	dial
	dial
	gl, Bi, sol
	lit
	fp
	fp
	cond
Cu^{2+}	cond
	dial
	dial
	cond
	cond
	Cu–Hg
	sp

(96) K. W. Sykes, Chem. S
(97) M. W. Lister and D. 83, 1591, 1603
(98) E. Franke, *Z. phys. C*
(99) H. Brintzinger and H.
(99a) Á. von Kiss and V.
(100) G. N. Dobrokhotov,
(101) Ya. A. Fialkov and 1, 1238

Metal	Method	Temp.	Medium	Log of equilibrium constant, remarks	Ref.
	dist	25	0·5	$*K_1$ 4·63, $*K_2$ 2·86	41
				$*4{\cdot}2\,\beta(Th^{4+}F^-NO_3^-)$ $*\beta(Th^{4+}F^-{}_2NO_3^-)$ 6·9	
	dist	25	0·5 ($NaClO_4$)	$*K_1$ 4·70, $*K_2$ 2·76	42
VO^{2+}	gl?	25?	0 corr	K_1 3·15, ev higher cpx	13b
Cr^{3+}	sp		var	ev CrF^{2+}	43
	sp	25	0·5 ($NaClO_4$)	$*K_1$ 1·42, $*K_2$ 0·40, $*K_3$ −0·46,	44
				K_1 4·36, K_2 3·34, K_3 2·48 [$K_1(H^+)$ 2·94]	
		25	0 corr	K_1 5·20	44, cf. 32
	est	25	0 corr	$\Delta*H_1 = -0{\cdot}6$, $\Delta*H_2 = -0{\cdot}1$	15
U^{4+}	dist	25	2 ($NaClO_4$),1H^+	$*K_1 \geqslant 6$, $*\beta_2 \geqslant 8$	45
UO_2^{2+}	ani ex	25	HCl var	$*K_1$ 1·18	46
				K_1 4·32	46, cf. 47
	sp		var	K_1 5·5, $\beta_4 \sim 8$	47
	fp	~0	UO_2F_2 var	$\dagger K_{42}[2UO_2F_2 \rightleftharpoons (UO_2F_2)_2]$ 0·18	48
	qh	20	1 ($NaClO_4$)	K_1 4·59, K_2 3·34, K_3 2·56, K_4 1·36 [$K_1(H^+)$ 2·94]	18
	cond	25	0 corr	$K_2 \sim 4{\cdot}4$, ev other cpx	49
	dist	10—40	2 ($NaClO_4$)	$*K_1$ 1·74(10°), 1·42(25°), 1·32(40°)	50
		25	2 ($NaClO_4$)	$\Delta*H_1 = -5{\cdot}4$, $\Delta*S_1 = -12$	50
	dist	25	C($NaClO_4$)	$*K_1$ 1·42($C = 2$), 1·43($C = 1$), 1·38($C = 0{\cdot}5$), 1·57($C = 0{\cdot}25$), 1·71($C = 0{\cdot}05$)	50
	cfug	0—30	UO_2F_2 var	$\dagger K_{42}$ 0·48(0°), 0·85(30°)	51
	qh	20	1 (Na)ClO_4	K_1 4·54, K_2 3·34, K_3 2·57, K_4 1·34	18, 23,
				[$K_1(H^+)$ 2·93], no ev polyn cpx for <0·1M-UO_2^{2+}	cf. 23
Pu^{4+}	sp	25	1 HNO_3	K_1 6·77 [$K_1(H^+)$ 3·14]	52
	red	25	2 HCl	ev PuF_2^{2+}	52
		25	0 corr	K_1 7·94	52, cf. 32
Mn^{2+}	ani ex	25—30	KF var	no ev ani cpx in 10M-KF	54
Mn^{3+}	kin	25·2	2 ($HClO_4$)	$*K_1$ 2·51	53
	sp, Pb, tp			ev MnF_6^{3-}	43
Re^{4+}	*X*-ray		solid	ev ReF_6^{2-} in K_2ReF_6(s)	55
Re^{5+}	*X*-ray		solid	ev ReF_6^- in $NaReF_6$(s) etc	55a
Fe^{2+}	fp		var	$K_1 < 1{\cdot}5$	56, cf. 40
	red	25	0·53 KNO_3	no ev cpx	57, 58
	ani ex	25—30	KF var	no ev ani cpx in 1M-KF	54
Fe^{3+}	red	20	dil	K_1 5·52	59
	red	25	0·53 KNO_3	K_1 5·15, K_3 4·00 [$K_1(H^+)$ 2·94]	60, 57, 58
	sp	?	var	K_1 5·30	61
	hyp	?	var	K_3 4·46, K_2 3·22, K_4 2·00, K_5 0·36	61
	red	25	0·5 ($NaClO_4$)	$*K_1$ 2·28, $*K_2$ 1·02, $*K_3$ −0·24,	40
				(H^+: K_1 3·38, K_2 1·52)	
		25	0·5 ($NaClO_4$)	K_1 5·21, K_2 3·95, K_3 2·70 [$K_1(H^+)$ 2·93]	40, cf. 17
	sp	25?	0 corr	K_1 4·90, $\Delta H_1 = 7{\cdot}5$, $\Delta S_1 = 49$	62
	red	15	0·5 ($NaClO_4$)	K_1 5·13, K_2 3·91, K_3 2·85 [$K_1(H^+)$ 2·85]	14, 19, 22
	red	25	0·5 ($NaClO_4$)	$*K_1$ 2·21, $*K_2$ 1·05, $*K_3$ −0·20	28
	red	25	0·5 ($NaClO_4$)	K_1 5·17, K_2 3·92, K_3 2·91 [$K_1(H^+)$ 2·91]	34, 22

(41) R. A. Day, jun., and R. W. Stoughton, *ibid.*, 1950, **72**, 5662
(42) E. L. Zebroski, H. W. Alter, and F. K. Heumann, *ibid.*, 1951, **73**, 5646
(43) E. R. Scheffer and E. M. Hammaker, *ibid.*, 1950, **72**, 2575
(44) A. S. Wilson and H. Taube, *ibid.*, 1952, **74**, 3509
(45) R. A. Day, jun., R. N. Wilhite, and F. D. Hamilton, *ibid.*, 1955, **77**, 3180
(46) G. E. Moore and K. A. Kraus, ORNL-795, 1950
(47) C. A. Blake, R. S. Lowrie, and K. B. Brown, AECD-3212, 1951
(48) J. S. Johnson and K. A. Kraus, *J. Amer. Chem. Soc.*, 1952, **74**, 4436
(49) R. D. Brown, W. B. Bunger, W. L. Marshall, and C. H. Secoy, *ibid.*, 1954, **76**, 1580
(50) R. A. Day, jun., and R. M. Powers, *ibid.*, p. 3895
(51) J. S. Johnson, K. A. Kraus, and T. F. Young, *ibid.*, p. 1436
(52) C. K. McLane, *Nat. Nuclear Energy Ser.*, 1949, IV-14B, 414
(53) H. Taube, *J. Amer. Chem. Soc.*, 1948, **70**, 3928
(54) G. B. Kauffman, Thesis, Univ. Florida, 1956, Univ. Microfilms 16358
(55) R. D. Peacock, *Chem. and Ind.*, 1955, 1453
(55a) R. D. Peacock, *J. Chem. Soc.*, 1957, 467
(56) R. Peters, *Z. phys. Chem.*, 1898, **26**, 193
(57) C. Brosset, Diss., Stockholm, 1942
(58) C. Brosset and B. Gustaver, *Svensk kem. Tidskr.*, 1942, **54**, 183
(59) F. Lindstrand, Diss., Lund, 1939
(60) C. Brosset, *Naturwiss.*, 1941, **29**, 455
(61) A. K. Babko and K. E. Kleiner, *Zhur. obshchei Khim.*, 1947, **17**, 1259
(62) M. G. Evans and M. Uri, *Symp. Soc. Exp. Biol.*, 1951, **5**, 139

[continued

Metal	Method	Te
	red	
	kin	
	sp	
	red	
	red	
	red	
	ani ex	
	ani ex	
Co^{2+}	ani ex	25
Ni^{2+}	qh	
	ani ex	25
Pt^{2+}	prep	
Cu^{2+}	red	15
	qh	
Ag^+	Ag	
	Ag	15
Zn^{2+}	red	15
	qh	
	ani ex	25
Cd^{2+}	Cd–Hg	
	Cd–Hg	
Hg_2^{2+}	Hg	
Hg^{2+}	red	15
B^{III}	H	
	anal	25
	anal	20
	anal, kin	
	kin	

(63) G. Saini, *Gazzetta*, 1953, 83, 6
(64) S. Ahrland and K. Rosen
10, 727
(64a) T. P. Perros, W. F. Sager, *Chem. Soc.*, 1957, 79, 13
(65) I. Leden and L. E. Marthén
(66) I. Leden, Diss., Lund, 1943

American Mineralogist, Volume 58, pages 195-202, 1973

Sulfides in Eclogite Nodules from a Kimberlite Pipe, South Africa, with Comments on Violarite Stoichiometry[1]

GEORGE A. DESBOROUGH
U.S. Geological Survey, Denver, Colorado 80225
GERALD K. CZAMANSKE
U.S. Geological Survey, Menlo Park, California 94025

Abstract

An unusual assemblage composed of four sulfides of Fe, Ni, and Cu occurs in rounded eclogite nodules which were inclusions in the kimberlite pipe at the Roberts Victor diamond mine, 45 miles ENE of Kimberley, South Africa. The polymineralic sulfide aggregates commonly are spherical and are composed of similar proportions of individual phases; they are interpreted to have developed from an immiscible liquid phase.

Electron microprobe, X-ray diffraction, and reflectivity data indicate that the dominant sulfide phase in the aggregates is a new mineral, approximate formula $(Fe, Ni)_9S_{11}$, typically containing 2.4 to 3.2 wt percent Ni; the higher Ni concentrations occur in 1 mm wide lamellae. Additional phases are Ni-bearing pyrite, a new, violarite-like, $(Fe, Ni)_9S_{11}$ phase, and stoichiometric chalcopyrite.

The complex sulfide assemblage, considered to have developed on cooling from a homogeneous liquid, is apparently metastable because it contains phases not reported in synthetic studies of the Cu-Fe-Ni-S system.

Introduction

Examination of 18 eclogite nodules[2] from the Roberts Victor diamond mine, South Africa, showed that a few specimens have sulfide accessory minerals. Specimen USNM 110607 contains the freshest, abundant sulfide. This nodule is essentially bimineralic, consisting of about 60 percent subhedral garnet grains 0.5-6 mm in diameter which occur as solitary grains or clots of grains, intergrown with coarser omphacite. Subsequent study by Dr. George Switzer (oral communication, 1969), indicating that this specimen contains the freshest omphacite, is in agreement with our impression that secondary processes may be responsible for alteration and removal of sulfides from more altered material.

Unpublished analyses of the dominant silicate phases in USNM 110607 are reported in Table 1. A. T. Anderson (oral communication, 1969), in an earlier study of similar Roberts Victor samples, found no ilmenite or magnetite, but did find accessory chromite having compositions (wt percent) in the range $MgAl_2O_4$, 2.6-16.1; $MgCr_2O_4$, 42.5-47.3; $FeCr_2O_4$, 25.9-36.0; Fe_2TiO_4, 1.8-5.6; and Fe_3O_4, 7.4-10.6.

In all sulfide-containing specimens examined, the sulfide occurs as aggregates which are mostly semirounded and elongated blebs between silicate grains, and also as nearly spherical inclusions within single crystals of garnet, omphacite, and phlogopite. Sulfides constitute about 0.2 percent by volume of specimen 110607. Individual aggregates are from 0.05 to 1 mm in greatest dimension and invariably consist of at least four phases, listed in order of decreasing abundance: (1) $(Fe,Ni)_9S_{11}$, with 2.4 to 3.2 wt percent Ni; (2) an isotropic, violarite-like mineral, also of $(Fe,Ni)_9S_{11}$ stoichiometry, with 21.5 to 30.0 wt percent Ni; (3) stoichiometric chalcopyrite, and (4) pyrite containing 0.6 to 4.8 wt percent Ni. Secondary alteration in the rock has resulted in deposition of minor amounts of Ni-free pyrite which is restricted to areas interstitial to the silicates and shows no apparent relationship to the four-phase sulfide assemblage.

Because of its strong magnetism and appearance in polished section, the major $(Fe,Ni)_9S_{11}$ phase can easily be misidentified as pyrrhotite. The intergrowth of this phase with the subordinate high-Ni $(Fe,Ni)_9S_{11}$ mineral of higher reflectivity is also similar to some pyrrhotite-pentlandite intergrowths or to replacement of pyrrhotite by marcasite (Fig. 1).

[1] Publication authorized by the Director, U.S. Geological Survey.

[2] The nodules are in the collection of Dr. George Switzer, U.S. National Museum, Washington, D. C.

TABLE 1. Chemical Analyses of Omphacite and Garnet from Roberts Victor Eclogite, USNM 110607

Omphacite					Garnet				
Oxide	Wt.%[a]	Cation	Proportion[b]		Oxide	Wt.%[c]	Cation	Proportion[b]	
SiO_2	55.42	Si	1.97	2.00	SiO_2	40.7	Si	5.86	5.90
TiO_2	0.37	Al	0.03		TiO_2	0.4	Ti	0.04	
Al_2O	8.89	Al	0.34		Al_2O_3	23.9	Al	4.07	4.07
Fe_2O_3	1.35	Ti	0.01		FeO[d]	16.3	Fe^{2+}	1.97	
FeO	3.41	Fe^{3+}	0.04	1.10	MnO	0.4	Mn	0.05	6.15
MnO	0.10	Mg	0.61		MgO	15.7	Mg	3.44	
MgO	11.57	Fe^{2+}	0.10		CaO	4.5	Ca	0.69	
CaO	13.75	Na	0.35	0.87	Sum	101.9			
Na_2O	5.00	Ca	0.52						
K_2O	0.15								
		Components:					Components:		
$H_2O(+)$	n.d.								
		Acmite		4			Pyrope		55.9
$H_2O(-)$	0.02	Jadeite		31			Almadine		32.0
		Tschermakite		3			Spessartine		0.1
		Hedenbergite		10			Grossular		12.0
Sum	100.03	Diopside		50					

a/ Wet chemical analysis by E. Jarosewich.
b/ Calculated on the basis of six and 24 oxygens for omphacite and garnet, respectively.
c/ Microprobe analysis by George Switzer using close standards, corrected for background and drift.
d/ Fe = 12.6; all Fe assumed to be Fe^{2+}.

We (Czamanske and Desborough, 1968) have previously suggested the formula $(Fe,Ni)_3S_4$ for the dominant, low-Ni phase, but now believe that this formula is incorrect.

Microprobe analyses of sulfides in eclogitic material have been made by White (1966) and Meyer and Brookins (1971). For a compositionally zoned sulfide grain in an ultramafic inclusion in Hawaiian basalt, White reported (Table 8a and p. 293): Fe, 48.5-50.9; Ni, 12.8-10.8; and S, 37.9-38.0. Meyer and Brookins (1971) report finding chalcopyrite, pyrrhotite, and apparent pentlandite from the Stockdale Kimberlite, Kansas.

Four-Sulfide Assemblage Mineralogy

Aggregate blebs contain fairly uniform proportions of the four phases, and the phases are everywhere distributed in a characteristic pattern (Fig. 1a). At the center of each bleb is the low-Ni, $(Fe,Ni)_9S_{11}$ phase which comprises 60 to 80 percent of the whole. Peripheral to, and as marginal lamellae within this phase is the violarite-like, high-Ni $(Fe,Ni)_9S_{11}$ phase. Within both of these phases, Ni-bearing pyrite is found as subhedral grains as large as 25 μm across. Chalcopyrite, in small amounts, is typically found only at the margin of blebs (Fig. 1a).

Quantitative electron microprobe analyses were performed on these phases in the U.S. Geological Survey laboratories in Washington, D. C., and Denver, Colorado. Ten synthetic sulfides of appropriate composition were used as reference standards. Appropriate standards were occupied both before and after analysis of the samples. Weight percentages of elements in our unknown phases were calculated by the USGS B-890 computer program.

Low-Ni, $(Fe,Ni)_9S_{11}$. Quantitative microprobe analysis was difficult due to problems of surface imperfections and beam overlap onto lamellae of a more Ni-rich phase (see Fig. 1). However, our best analyses of this phase have shown satisfying concordance for three distinct analytical efforts on two microprobes. We reanalyzed this phase carefully on three occasions because of shortcomings in our early analyses in which the three principal elements could not be measured simultaneously, and because of concern over suggesting 9:11 stoichiometry.

Our ultimate analysis of the low-Ni phase is presented in Table 2; the formula $(Fe,Ni)_3S_4$, with comparable Ni content, would require 43.3 wt percent sulfur (*cf* Table 5). Therefore we were in error in reporting our early data as evidence of a new $(Fe,Ni)_3S_4$ phase. Simultaneous determinations of Fe and Ni consistently show a lesser standard deviation for the sums of these two elements than for the individual elements, clearly indicating mutual substitution over a small range.

A maximum of 7.9 wt percent Ni was measured on marginal, fine lamellae of the major low-Ni $(Fe,Ni)_9S_{11}$ phase which projected into the high Ni-phase; the scattering of X-rays from the high-Ni phase may be partially responsible for this high value, but the extent of this contribution is unknown. As is shown below, the concentration of Co in these lamellae shows them to be atypical.

As much as 1.3 wt percent Co was measured in the lamellae of the major low-Ni $(Fe,Ni)_9S_{11}$ phase which project into the high-Ni, violarite-like phase. In general the highest Co values were obtained on areas adjacent to the violarite-like phase. Among 25 determinations on central areas of four grains, only 11 indicated Co above 0.1 wt percent, and only four contained more than 0.4 wt percent Co. From 0.2-0.6 wt percent Cu is present in the major low-Ni phase. Probably neither Cu nor Co is essential to the structure of $(Fe,Ni)_9S_{11}$.

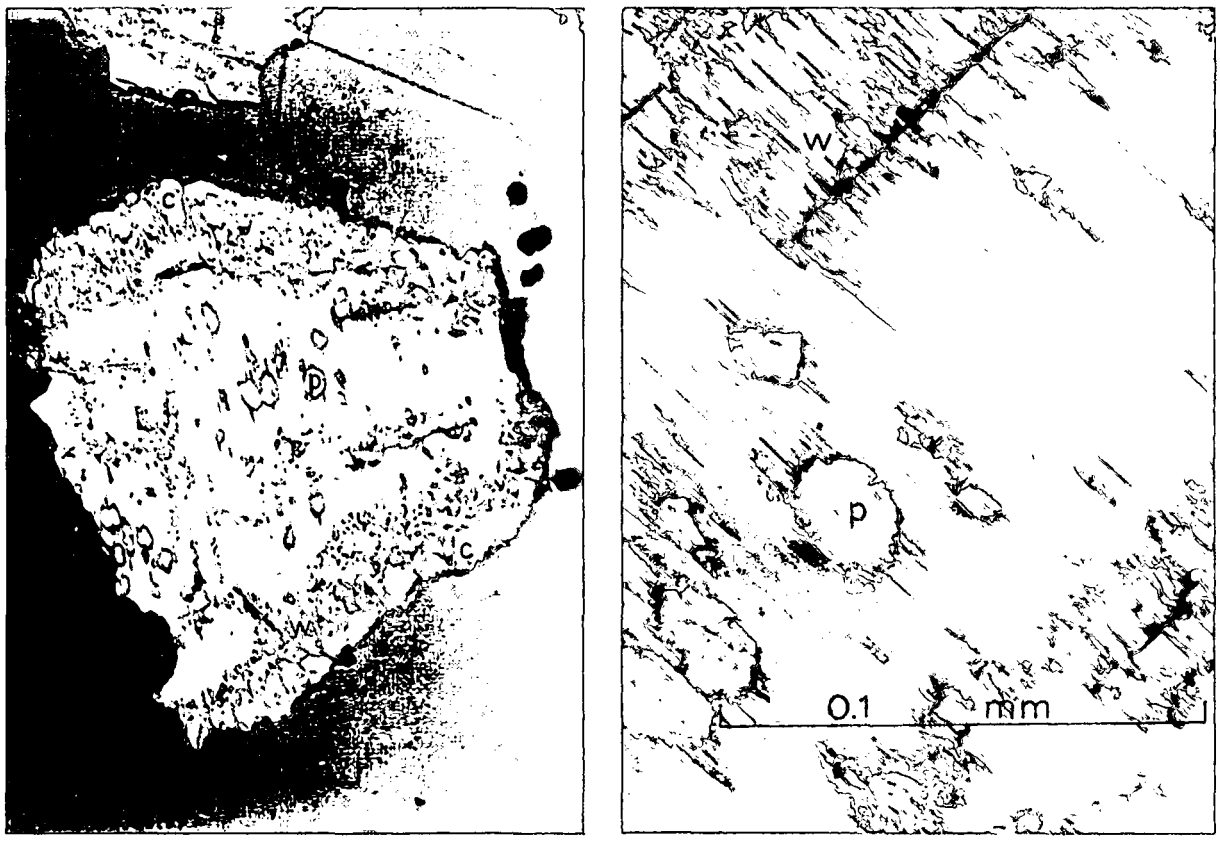

(a) (b)

FIG. 1. (a) Typical polymineralic grain from eclogite mounted in epoxy (reflected light). Pyrite and similar high-relief central grains = p, chalcopyrite and similar grains = c, white, high-Ni, $(Fe,Ni)_9S_{11}$ and continuous submarginal fractured material = w; the major central phase is low-Ni, $(Fe,Ni)_9S_{11}$.

(b) Enlarged portion of grain in (a) showing parallel 1μm wide lamellae in major low-Ni, $(Fe,Ni)_9S_{11}$. (Nomarski objective, reflected light.)

TABLE 2. Electron Microprobe Analyses (in weight percent)[a] and Calculated Formulas for Low- and High-Nickel 9:11 Phases

	Low-Nickel Phase		High-Nickel Phase	
	Range[b]	Mean	Range[c]	Mean
Fe	55.2-56.4	55.5(9)	29.2-40.5	32.3(29)
Ni	2.4-3.2	2.8(6)	21.5-30.0	27.4(22)
Fe+Ni	--	58.3(5)	57.4-61.2	59.7(12)
S	40.1-41.6	40.9(7)	39.1-41.6	40.8(7)
Total		99.2		100.5
Formula[d]	$(Fe_{8.575}Ni_{0.414})_{8.989}S_{11}$		$(Fe_{4.999}Ni_{4.035})_{9.034}S_{11}$	

a/ Estimated standard deviations (enclosed in parentheses) refer to the last decimal place cited. Thus 32.3(29) indicates an estimated standard deviation of 2.9. This convention will also be followed in the text and in subsequent tables.
b/ Eighteen determinations on 10 grains.
c/ Fifteen determinations on five grains.
d/ Totals normalized to 100.0

Unfortunately, the small size and finely intergrown mineralogy of the sulfide blebs have made it impossible to obtain completely satisfactory X-ray, reflectivity, and hardness data for even the major low-Ni phase. Judging from its polishing characteristics relative to the other sulfides present, it is apparently about the same hardness as pyrrhotite. Its color and anisotropism also may best be described as indistinguishable from those of monoclinic pyrrhotite.

Reflectivity data on this new phase were measured by B. F. Leonard in plane-polarized light by means of a Reichert photoelectric microphotometer. The U.S. primary germanium standard calibrated by the National Physical Laboratory, Teddington, England, was used as the standard for comparison. Values for the germanium standard are 47.0, 51.3, and 52.0 percent at 470, 546, and 589 nm. Values for the mineral, determined on three grains of suitable size and polish, are:

	470	546	589 nm
Rg'	38.1	40.5	41.1
Rm	—	37.4	—
Rp'	31.0	35.9	36.9
Rg'-Rp'	7.1	4.6	4.2
$\bar{R}$	34.6	37.7	38.6

The probable values for Rg and Rp are indicated by primes because one cannot be certain that these few grains truly show principal reflectivities. Values for $\bar{R}$, the midrange of all values for apparent maximum and minimum reflectivity at the standard wavelengths, are reproducible with a precision of 0.1–0.2 percent. Reconnaissance in the critical part of the spectrum suggests that the reflectivity curves have a single broad peak at or very close to 589 nm. Reflectivity at 650 nm was not determined, owing to the insensitivity of the photoreceptor at that wavelength. These reflectivity values are slightly higher than those for hexagonal pyrrhotite, but distinctly lower than those reported by Nickel and Harris (1971) for smythite of similar stoichiometry from Cobalt, Ontario. Reflectivity data for well-documented monoclinic pyrrhotite are not available.

At the three standard wavelengths, Rp' is parallel to the trace of elongate exsolution(?) bodies of both the higher Ni (*i.e.*, 7.0 wt percent) lamellae and the white, isotropic Ni-Fe sulfide; Rg' is perpendicular thereto. The presence of a nearly constant intermediate value of reflectivity, corresponding to Rm, shows that the mineral is optically biaxial.

X-ray powder diffraction investigation of several grains of this material was conducted utilizing Mn-filtered Fe radiation and also Fe-filtered Co radiation. The intimate nature of the intergrowth with the isotropic, high-Ni phase precluded extraction of a single phase. However, the fine-grain size and preferred orientation of the intergrowth aided in discrimination of the powder lines of each phase. The symmetry of the dominant, low-Ni, $(Fe,Ni)_9S_{11}$ phase could not be deduced from X-ray powder data. Attempts at indexing the X-ray powder lines for a hexagonal or tetragonal model were unsuccessful; the phase is thus either orthorhombic, monoclinic, or triclinic, as we later determined also from the quantitative reflectivity data.

X-ray powder lines of the minerals in the polymineralic sulfide assemblage are shown in Table 3. A powder pattern of the entire sulfide assemblage is shown in the second column. The third column lists powder lines obtained from a microprobe-analyzed, single crystal fragment extracted from the polished surface. (The data are representative of those obtained from several additional mounts and films.) This crystal was chiefly low-Ni, $(Fe,Ni)_9S_{11}$ with minor amounts of the intergrown white, high-Ni, $(Fe,Ni)_9S_{11}$ sulfide. The spottiness of the film lines associated with the major phase contrast with the smooth lines of the minor fine-grained phase to permit discrimination of these minerals. Column one of Table 3 lists powder lines of material containing neither chalcopyrite nor pyrite, and consisting entirely of the low-Ni and high-Ni sulfides. The major, low-Ni, $(Fe,Ni)_9S_{11}$ phase is indicated in the line-identity column of Table 3 by triple asterisks. The strongest lines of this phase are distinctive enough to permit identification and have *d*-values of 1.73Å, 2.56Å, 2.24Å, 1.98Å, and 1.90Å.

Numerous attempts by Howard T. Evans, U.S. Geological Survey, to produce interpretable single crystal photographs by both X-ray and electron dif-

TABLE 3. X-Ray Powder Camera Data for Sulfides in Eclogite

$(Fe,Ni)_9S_{11}$ plus White Ni-Fe sulfide spindle 3, Co/Fe[2]		Sulfide aggregate capillary tube, Fe/Mn[3]		$(Fe,Ni)_9S_{11}$ plus White Ni-Fe sulfide spindle 2, Fe/Mn[3]		
d(Å)[4]	I	d(Å)[4]	I	d(Å)[4]	I	Line Identity[5]
5.47	w	5.45	mw	----		WNiFeS
3.33	m	3.32	s	3.35	w	WNiFeS
----		3.12	w	----		py
----		3.03	s	----		cpy
2.989	m	2.99	w	2.99	w	***
2.847	m	2.84	vs	2.85	m	WNiFeS
2.810	m	----		----		***
----		2.70	m	----		py
2.561	ms	2.55	mw	2.56	m	***
2.466	w	2.47	w	----		***
----		2.42	mw	----		py
2.362	mw	2.36	s	2.37	w	WNiFeS
2.244	m	2.25	vw	2.23	w	***
----		2.21	mw	----		***
2.150	m	2.15	w	2.16	w	***
----		2.01	w	2.02	w	***
1.981	m	1.98	m	1.98	w	***
1.901	m	1.92	mw	1.905	w	***
----		1.85	w	----		cpy
1.818	vw	1.818	m	----		WNiFeS
1.730	vs	[6]1.730	m	1.730	s	***
1.666	mw	1.668	ms	----		WNiFeS
----		1.635	mw	----		py
----		1.590	vw	----		cpy
1.548	vw	1.562	vw	1.567	w	***
----		1.502	w	----		***
----		1.450	w	----		***
----		1.423	w	----		***
1.303	w	----		----		***
1.275	vw	[6]1.260	w	----		***
1.200	vw	[6]1.210	vw	----		***
1.181	vw	[6]1.183	mw	----		WNiFeS
1.100	ms	[6]1.102	w	----		***
----		[6]1.091	vw	----		***
----		[6]1.043	mw	----		py
----		[6]1.007	w	----		py
----		[6]0.999	w	----		py(?)
0.9852	w	[6]0.986	w	----		***

1/ 114.6 mm diameter powder camera. Relative intensities of lines are visual estimates where w = weak, m = medium, s = strong.
2/ Co/Fe = Fe filtered $Co_{K\alpha}$ radiation.
3/ Fe/Mn = Mn filtered $Fe_{K\alpha}$ radiation.
4/ Corrected for film shrinkage.
5/ WNiFeS = white, isotropic Ni, Fe sulfide intergrown with $(Fe,Ni)_9S_{11}$; cpy = chalcopyrite; py = pyrite; *** = $(Fe,Ni)_9S_{11}$.
6/ Very broad line due to large spindle diameter.

fraction techniques were unsuccessful, due to the presence of small domains and more than one phase.

Taylor (1970) and Nickel and Harris (1971) have reported on smythite from Cobalt, Ontario, which has a chemical composition almost identical to that of our low-Ni $(Fe,Ni)_9S_{11}$ phase (see also last section of the present report and Table 5). We emphasize that Buerger precession patterns obtained by Evans in one of the original descriptions of smythite (Erd *et al,* 1957), and from *both* Taylor's (1970) smythite and our low-Ni $(Fe,Ni)_9S_{11}$ phase clearly show that our phase is not smythite.

High-Ni, $(Fe,Ni)_9S_{11}$. This white, isotropic phase occurs chiefly as a sub-marginal rim (Fig. 1a), separating the dominant, low-Ni phase from the host silicate or chalcopyrite. The high-Ni phase has a distinctly higher reflectivity than the other sulfides and appears to be fractured on a fine scale (Fig. 1b), but this feature may be due to plucking during polishing. The high-Ni phase commonly projects into the low-Ni $(Fe,Ni)_9S_{11}$ phase as lamellae, 2-10μm wide (Fig. 1), that are similar in texture to some pyrrhotite-pentlandite intergrowths, or to the replacement of pyrrhotite by marcasite.

Microprobe analyses for Fe, Ni, and S were conducted simultaneously and the results are shown in Table 2. Measured variations in Fe, Ni, and S are shown on Figure 2; cobalt is not considered in this figure because its concentration is less than 1 wt percent. The average composition of this phase, like that of the low-Ni phase, corresponds most closely to $(Fe,Ni)_9S_{11}$, with variations in Fe and Ni due to mutual substitution. Some of the variability may be due to electron beam placement on the fine intergrowths.

Because of the slight difference in atomic weight between Fe and Ni, a $(Fe,Ni)_3S_4$ phase containing 27 wt percent Ni will have an S content of 42.8 wt percent. When normalized to totals of 100 percent, the microprobe analyses for the high- and low-Ni phases show the expected weight percentage changes in Ni+Fe and S values as a function of Ni content.

The high-Ni, $(Fe,Ni)_9S_{11}$ phase is always in contact with the low-Ni, $(Fe,Ni)_9S_{11}$ phase, but never adjacent to Ni-bearing pyrite. We believe this to indicate that the high-Ni phase did not react directly with the grains of Ni-bearing pyrite which were protected in the low-Ni phase. This interpretation is consistent with the fact that the sulfur contents of the two phases differ only to the extent required by their differing Fe:Ni ratios.

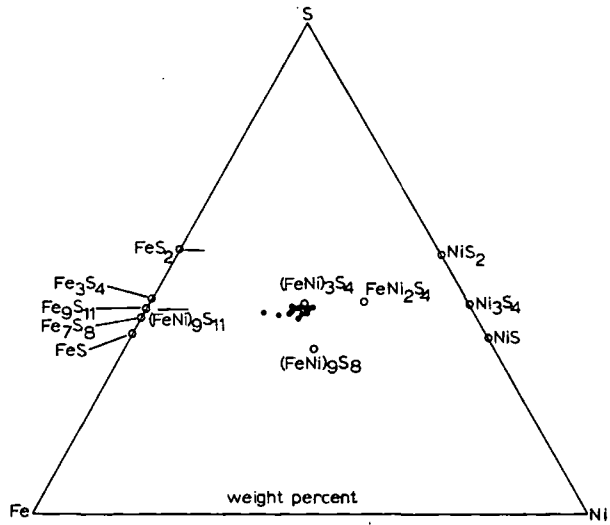

FIG. 2. Some of the stable phases in the Fe-Ni-S system. The new low-Ni, $(Fe,Ni)_9S_{11}$ phase and the coexisting Ni-pyrite are plotted with their compositional ranges shown by short horizontal lines. Small filled circles represent the white, isotropic high-Ni, $(Fe,Ni)_9S_{11}$ sulfide which is similar in structure to violarite.

The intimate intergrowth of high-Ni, $(Fe,Ni)_9S_{11}$ with the low-Ni $(Fe,Ni)_9S_{11}$ phase and with chalcopyrite prohibited unequivocal elucidation of its X-ray powder pattern. However, the seven lines labeled in Table 3 as white, isotropic Ni,Fe sulfide (WNiFeS) correspond closely to the strongest X-ray powder lines of violarite (Berry and Thompson, 1962). It is noteworthy that although both the structure and composition are very similar to those of violarite, this phase does not correspond to a known phase in the Fe-Ni-S system (Fig. 2).

Ni-bearing pyrite and chalcopyrite. The pyrite disseminated in $(Fe,Ni)_9S_{11}$ as subhedral to euhedral grains (Fig. 1) ranges in Ni content from 0.6 to 4.9 wt percent and in Co content from less than 0.1 to 0.55 wt percent; the average Ni content determined for 16 pyrite grains is 2.1 wt percent. Simultaneous analyses of Fe and Ni for 14 grains distributed among five separate polymineralic sulfide aggregates demonstrates that Ni is substituting for Fe. Nine of 16 grains contained less than 0.1 wt percent Co, the limit of detection for the conditions of analysis. Cobalt values greater than 0.1 wt percent were found only in pyrite grains with more than 1.5 wt percent Ni; however, there is no linear correlation between Ni and Co contents of pyrite.

The chalcopyrite at the sulfide bleb-silicate interface has been determined by microprobe analysis to be of stoichiometric composition.

Distribution of S, Fe, Ni, and Cu. To supplement our detailed mineralogical study, we have also attempted to determine the sulfur and sulfide-bound metal content of eclogite USNM 110607 and of a somewhat less sulfide-rich specimen, USNM 110586. Sulfur determinations by X-ray fluorescence on bulk powders gave respective values of 0.20 and 0.10 percent for these specimens. Sulfide-bound metal analyses were made by treating ground eclogite with bromine water (Czamanske and Ingamells, 1970) and analyzing the resulting solution for metals by atomic absorption techniques. Specimen 110607 was leached twice to check the efficiency of the leaching process. Values presented in Table 4 show that more than 97 percent of three sulfide-bound metals were extracted by the initial leach and give a picture of the overall transition-metal distribution in the nodules. Total sulfide-bound metals determined on the initial leach were 2,340 ppm for USNM 110607 and 709 ppm for USNM 110586. Metal proportions were, respectively, Fe:Ni:Cu—63.5:27.0:9.5 and Fe:Ni:Cu—61.0:24.1:14.9. All analyses on specimen 110607 are considered superior because it is less altered than specimen 110586; nevertheless, there is general agreement of ratios between the two.

Discussion

Carter and MacGregor (1969) reported trace element data for coexisting garnets and clinopyroxenes from Roberts Victor eclogites. Their values (in ppm) from eclogites of the 110607 type are for garnet Ni, 44 to 155; Cu, 0.1 to 22; Co, 55 to 134; and for omphacite Ni, 122 to 1,000; Cu, 1.2 to 39; Co, 32 to 51. On the basis of our work, we believe that their analyses are probably upper limits for metal concentrations in the silicate phases because of possible sulfide inclusions; they did not note sulfides.

There is thus the suggestion, in comparing our best data (USNM 110607) with those of Carter and MacGregor (1969), that where S is present under conditions of eclogite formation, the chalcophile metals are quantitatively to be found as sulfides. John Gurney (1971, written communication) indicates that a search for sulfides among 500 samples from Roberts Victor revealed them in nearly all specimens. Systematic investigation of the presence and nature of sulfides in a broad spectrum of materials of deep origin should be made.

TABLE 4. Distribution of Fe, Ni, Cu, and Co in Two Roberts Victor Eclogite Nodules on the Basis of Parts per Million in the Whole Rock

	USNM 110607				USNM 110586			
	Whole Rock	First Leach	Second Leach	Leached Rock	Whole Rock	First Leach	Second Leach	Leached Rock
Fe	—	1480	33	--	--	430	--	--
Ni	680	630	14	25	390	170	—	230
Cu	240	220	8	12	120	105	--	11
Co	N.D.	10	0.5	N.D.	N.D.	4	--	N.D.
Total		2340	55.5			709		

* Analyst, Neil Elsheimer. N.D. signifies "not detected" and -- indicates "not analyzed for."

The roundness, distribution, and similar relative proportions of phases of the sulfide aggregates suggest an origin by liquid immiscibility within a silicate melt. Both the sulfur and sulfur-bound metal values that we have obtained for these aggregates indicate sulfur contents for sulfides in excess of those for sulfide associated with sulfide immiscibility in basalts under surface conditions (Desborough *et al.*, 1968; Skinner and Peck, 1969). In marked contrast to the sulfides in basalts reported by Desborough *et al* (1968) and Skinner and Peck (1969), these eclogite sulfides lack an iron oxide phase and posses higher Ni content.

The effects of pressure on sulfur solubility and fractionation, the sulfur content of the mantle, and the metal-sulfur redistribution associated with possible eclogite-to-basalt transitions are topics of considerable interest toward which we are here able to contribute only meager data. Eclogite nodule USNM 110607 shows strong fractionation of the typical chalcophile elements, Co, Ni, and Cu, toward the sulfide fraction, and the sulfidation state of the minerals described is not minimal. In particular, the exsolution of pyrite is somewhat surprising and indicates a sulfide liquid richer in sulfur than would be expected for a typical surficial mafic rock with appreciable concentrations of chalcophile elements. It seems likely that the rather high sulfur and sulfur-bound metal values which we report can be explained in terms of lower oxygen fugacities during crystallization than are associated with crystallization of previously described mafic-sulfide occurrences (see MacLean, 1969). The absence of iron oxide phases from our material supports this theory.

Because of the unknown effect of pressure on the Fe-Ni-Cu-S system and our observation of two phases unknown in extensive synthetic studies, it seems pointless to try to follow a crystallization history for the four-phase assemblage we report. We believe that the four phases have evolved from an originally homogeneous sample of immiscible sulfide liquid.

Comments on Violarite Stoichiometry

The apparent departure of the composition of our sulfides from $(Fe,Ni)_3S_4$ warrants discussion of the problem of the composition of violarite-like minerals.

At least two other investigators have reported iron sulfides with apparent 9:11 stoichiometry. Taylor (1970) and Nickel and Harris (1971) report analyses of smythite from Cobalt, Ontario, as $Fe_{3.25}S_4$. Their analyses are compared in Table 5 with ideal 3:4 and 9:11 stoichiometry.

On the basis of Craig's (1971) study, Czamanske sulfidized homogeneous Mss (monosulfide solid solutions) ranging in composition from $Fe_{61.0}S_{39.0}$ to $Fe_{20.45}Ni_{43.00}S_{36.56}$. We attempted 3:4 and 9:11 syntheses at four low-Ni compositions, plus a composition of Fe,Ni content equivalent to violarite. We experimented at 200° and 296°C in runs to 6 months in length. Reactions in the low-Ni experiments produced considerable pyrite and yielded no phases suitable for microprobe examination.

We have analyzed our own synthetic violarite-like materials, a synthetic violarite supplied by Craig, and a natural violarite from Sudbury, Ontario (USNM, R-699), furnished by B. F. Leonard. All have an X-ray pattern typical of violarite, although the first three of our materials listed in Table 6 show traces of Mss as well.

The material provided by Craig and considered to be synthetic $FeNi_2S_4$ contains traces of both unreacted Mss and pyrite (or $(Fe,Ni)S_2$) which are visible microscopically at 1625 magnifications using an oil immersion objective. Electron microprobe analysis of the major phase, presumably $FeNi_2S_4$, gives a sulfur content of 41.8(4) wt percent, instead of 42.5 wt percent as expected for stoichiometric $FeNi_2S_4$.

Microscopic study of the four violarite-like materials analyzed for sulfur (Table 6) revealed the presence of unreacted Mss in the interior of virtually all grains. Traces of pyrite and/or $(Fe,Ni)S_2$, as well as a gray phase within the reaction rim, were also detected.

The accuracy of our analytical method for the determination of sulfur content may be evaluated in Table 6. For Runs I, II, and III, all values for sulfur in the cores (Mss) are within one standard deviation of the starting composition—*i.e.*, 36.56 wt percent sulfur. The product of Run IV contains only very small remnants of Mss plus some very small but conspicuous pyrite grains; these factors may have contributed to poor electron beam placement on Mss and thus the slightly higher results for sulfur. None of the sulfur contents determined for the prepared products are within one standard deviation of either $FeNi_2S_4$ or $Fe_3Ni_6S_{11}$, which have S contents of 42.54 and 40.42, respectively. However, the value 41.6(5), which includes all of our data in Table 6 for reacted material, is identical to that obtained for Craig's presumed synthetic $FeNi_2S_4$.

TABLE 5. Comparison of Cobalt Smythite (Taylor, 1970, and Nickel and Harris, 1971) with Theoretical Stoichiometry

	Cobalt Smythite		Fe_3S_4	Fe_9S_{11}
	Taylor	Nickel and Harris		
Fe	58.3	58.6	56.64	58.76
Ni	0.45	0.1	...	...
S	41.2	41.5	43.36	41.24

Natural violarite from Sudbury, Ontario, as shown by 20 analyses on 10 grains of the material, contains only 41.0(3) wt percent sulfur. This value is not directly comparable with the value 40.8(7) wt percent sulfur obtained for our high-Ni $(Fe,Ni)_9S_{11}$ phase, but it is intriguing that the sulfur values for the two natural phases are distinctly lower than those for the synthetic materials.

The analytical sulfur data for materials which have the X-ray diffraction pattern of violarite, including natural violarite, synthetic violarite provided by Craig, and our synthetic violarites, force us to conclude that "violarite" is generally not stoichiometric $FeNi_2S_4$.

Additional evidence supporting this conclusion is found in reports on the Marbridge ore bodies, Quebec, by Buchan and Blowes (1968) and Graterol and Naldrett (1971). Both papers report several

TABLE 6. Microprobe Analysis of Sulfur on Synthetic Fe–Ni–S Products, Using Two Spectrometers Simultaneously*

Run No.	Temperature and intended product	Sulfur content (wt. percent, std. dev.) Margins of grains		Monosulfide solid solution in core of grains	
		Spectrometer		Spectrometer	
		1	2	1	2
I	200°C, $Fe_3Ni_6S_{11}$	41.3(6)	41.4(6)	36.3(5)	36.4(4)
II	296°C, $Fe_3Ni_6S_{11}$	41.1(4)	41.8(5)	36.4(4)	36.3(3)
III	200°C, $FeNi_2S_4$	41.8(3)	42.0(4)	36.2(4)	36.3(9)
IV	296°C, $FeNi_2S_4$	41.7(5)	42.1(7)	37.1(3)	37.6(7)

* Analyst G. A. Desborough using two spectrometers simultaneously at 6 kV according to the method of Desborough et al. (1971). Estimated standard deviations (in parenthesis) are in terms of the last decimal place cited.

analyses of "violarites," all of which have a metal: sulfur ratio greater than 3:4. Specifically, Buchan and Blowes identify three types of "violarite" with an average metal:sulfur ratio of 3.24:4 or 8.91:11. Graterol and Naldrett report four analyses averaging 3.35:4 or 9.22:11 (excluding one apparently inferior analysis with S = 37.1 wt percent, 3.28:4 or 8.96:11). In each of these studies, the authors ascribe deviations from 3:4 stoichiometry to difficulties in polishing and resolving fine "violarite" intergrowths. We believe that this explanation is erroneous and obscures the fact that "violarite" is not strictly a 3:4 compound. Clearly, a problem arises concerning the proposed solid solution between violarite and polydymite (*e.g.*, Graterol and Naldrett, Fig. 8). On the basis of our study, that of Graterol and Naldrett, and that of Buchan and Blowes (see their Fig. 6), it seems more reasonable to propose an extensive solid solution series that contains throughout a proportion of sulfur more clearly corresponding to 9:11 than 3:4 stoichiometry and ranges from compositions richer in Fe than violarite toward polydymite (compositions richer in Ni than violarite).

We propose that synthetic material previously assumed to be synthetic $FeNi_2S_4$ contained traces of pyrite and/or traces of $(Ni,Fe)S_2$, a suggestion compatible with the phase diagram of Craig (1968) at temperatures below 450°C. Trace quantities of these two additional phases, as well as traces of unreacted Mss cores, would change the sulfur content of presumed violarite. Such small quantities are not detected in routine X-ray diffraction studies of a bulk product and may go unnoticed in microscopic investigations unless extreme care is taken. Furthermore, only the most careful microprobe study, with well-known, homogeneous standards of close composition, is able to document unequivocally the observed deviation from stoichiometry.

In any case, the nickel-rich violarite-like material we report in eclogite contains 40.8(7) wt percent sulfur but is apparently indistinguishable from the mineral referred to as violarite. It has the X-ray pattern reported for violarite, but does not have M_3S_4 stoichiometry.

Acknowledgments

We thank A. T. Anderson for bringing this unusual sulfide occurrence to our attention and George Switzer for providing material. We appreciate greatly the reflectivity data obtained by B. F. Leonard and the metal and sulfur analyses provided by Neil Elsheimer and B. P. Fabbi.

References

BERRY, L. G., AND R. M. THOMPSON (1962) X-ray powder data for ore minerals. The Peacock Atlas, *Geol. Soc. Amer. Mem.* **85**, 281 pp.

BUCHAN, R., AND J. H. BLOWES (1968) Geology and mineralogy of a millerite nickel ore deposit. *Can. Mineral. Met. Bull.* **61**, 529–534.

CARTER, J. L., AND I. D. MACGREGOR (1969) Trace and minor element chemistry of coexisting garnets and clinopyroxenes from Roberts Victor eclogites (abstr.). *Trans. Amer. Geophys. Union*, **50**, 342.

CHAMBERLAIN, J. A. (1967) Sulfides in the Muskox intrusion. *Can. J. Earth Sci.* **4**, 105–153.

CRAIG, J. R. (1968) The Fe-Ni-S System, Pt. 1. Violarite stability relations. *Carnegie Inst. Washington Year Book* **66**, 434–436.

———, (1971) Violarite stability relations. *Amer. Mineral.* **56**, 1303–1311.

CZAMANSKE, G. K., AND G. A. DESBOROUGH (1968) Primary Fe-Ni-Cu sulfides in eclogite nodules in South African kimberlite (abstr.). *Geol. Soc. Amer. Abstr. 1967*, p. 41.

———, AND C. O. INGAMELLS (1970) Selective chemical dissolution of sulfide minerals: A method of mineral separation. *Amer. Mineral.* **55**, 2131–2134.

DESBOROUGH, G. A., A. T. ANDERSON, AND T. L. WRIGHT (1968) Mineralogy of sulfides from certain Hawaiian basalts. *Econ. Geol.* **63**, 636–644.

———, R. H. HEIDEL, AND G. K. CZAMANSKE (1971) Improved quantitative electron microprobe analysis of sulfur in some common sulfides using low operating voltage. *Amer. Mineral.* **56**, 2136–2141.

ERD, R. C., H. T. EVANS, JR., AND D. H. RICHTER (1957) Smythite, a new iron sulfide, and associated pyrrhotite from Indiana. *Amer. Mineral.* **42**, 309–333.

GRATEROL, M., AND A. J. NALDRETT (1971) Mineralogy of the Marbridge No. 3 and No. 4 nickel-iron sulfide deposits with some comments on low temperature equilibration in the Fe-Ni-S system. *Econ. Geol.* **66**, 886–901.

MACLEAN, WALLACE H. (1969) Liquidus phase relations in the FeS-FeO-Fe_3O_4-SiO_2 system, and their application in geology. *Econ. Geol.* **64**, 865–884.

MEYER, H. O. A., AND D. G. BROOKINS (1971) Eclogite xenoliths from Stockdale Kimberlite, Kansas. *Contrib. Mineral. Petrology*, **34**, 60–72.

NICKEL, E. H., AND D. C. HARRIS (1971) Reflectance and microhardness of smythite. *Amer. Mineral.* **56**, 1464–1469.

SKINNER, B. J., AND D. L. PECK (1969) An immiscible sulfide melt from Hawaii. *Econ. Geol. Monogr.* **4**, 310–322.

TAYLOR, L. A. (1970) Smythite, $Fe_{3+x}S_4$ and associated minerals from the Silverfields Mine, Cobalt, Ontario. *Amer. Mineral.* **55**, 1650–1658.

WHITE, R. W. (1966) Ultramafic inclusions in basaltic rocks from Hawaii. *Contrib. Mineral. Petrology* **12**, 245–314.

Manuscript received, December 10, 1971; accepted for publication, September 28, 1972.

Scapolites, granulites, and volatiles in the lower crust

Address as Retiring President of the Geological Society of America, Salt Lake City, Utah, October 1975

JULIAN R. GOLDSMITH *Department of the Geophysical Sciences, University of Chicago, Chicago, Illinois 60637*

INTRODUCTION

I would like to consider a little-understood and sometimes maligned family of minerals and its relationship to an ill-defined type of rock. The mineral is scapolite, the rock is granulite, and both are probably more important than some of us think. Before going further, however, I would like to make it clear that the work reported here was done in cooperation with my colleague, Robert C. Newton, and although more detailed and extensive versions complete with data will appear elsewhere under joint authorship, the bylaws of the Geological Society of America do not permit "co-presidents." I hope that this address does not become as well known as the one Lincoln gave at Gettysburg, for my conscience would suffer the more. This concern would be unnecessary if presidential addresses could be seen and not heard, or even better, looked at without being read. This latter would permit reprinting of the same piece for each President, and editorial and typesetting costs could be eliminated. Or, if they must be heard and read, each president could be assigned to one of a limited number of addresses, and could work it over, add new data as necessary and available, inject or interpret new ideas, polish, hone, modify to conform to the existing zeitgeist, and hopefully do so in an area reasonably close to whatever his specialty may be. This approach would not only be instructional for the retiring officer, but it could conceivably eliminate random and rambling papers, and provide us all with current and noncontroversial review articles.

One current very hot subject is the Earth's mantle, and recent interest is not limited to geophysicists, geochemists, and petrologists, for interrelationships with global tectonics bring it before almost every kind of earth scientist. Not very many years ago, the mantle was cloaked in obscurity by the crust, and very few geologists gave it any thought, although it provided a ray path for seismologists and an intellectual home for a few geophysicists.

The first meeting of the Society I attended was in Chicago in 1946, and my mentor, N. L. Bowen, held forth in his usual delightful and erudite way on magmatism and granitization, pontiffs, and soaks (Bowen, 1947). This was the heyday of the granite controversy, and with the crust presenting so much food for thought, who cared about the mantle? The new global tectonics has introduced a new snobbishness, and a "downward drift" has taken place; the mantle is "in," and much of the crust is viewed not as food for thought, but as potentially subductible nutrient for the upper mantle. The disdain for the visible and more familiar can have sociological as well as scientific overtones; that great conman, "Yellow Kid" Weil, commenting about his marks, said "The upper crust is composed mostly of crumbs." The upper crust we see. We are reasonably sure that we see fragments of the upper mantle brought up as exotics in deep volcanoes and kimberlite pipes. Rather few geologists have attempted to characterize the lower crust, however, and it is my impression that it currently carries a larger element of the unknown than any other region of the Earth; at the same time, it is not a popular area of speculation. This may be due to an assumed high degree of complexity, variability, or inhomogeneity.

Some of my acquaintances feel that I have not been field oriented, yet I am aware of the fact that there are aspects of our understanding of the Earth that require observations of rocks and minerals in their natural habitat. In order to do anything like field work in the deep crust however, one has to be a "trash man" of sorts. Our best samples of deep crustal as well as mantle material are the fragments ripped out of place by the rising magma in the above-mentioned volcanoes, and by the kimberlitic and other deep-seated pipes; this deep-earth trash, a litter of xenoliths, is picked up at or near the surface by the combination field man and refuse collector. This kind of field work appeals to me.

Collecting these nodules has become scientifically a very profitable enterprise, particularly for those working with the (presumed) mantle material. Rather little attention has been given to the more siliceous nodules, although a number of authors have noted the presence of crustal material, particularly granulites. Lovering and White (1964) have worked on material from the Delegate pipes in eastern Australia and called attention to the presence of apparently primary scapolite in granulites included in these breccia- and basalt-filled pipes. Scapolite has also been noted in similar occurrences in South Africa and Siberia (Bobrievich and Sobolev, 1957; Sobolev, 1959; Dawson, 1964, 1968, 1971; Cox and others, 1973; Verhoogen, 1938), although as indicated by Bobrievich and Sobolev (1957) and by Misch (1964), the scapolite in metamorphic occurrences is generally viewed as secondary, after plagioclase, with no clear mechanism for or time of the scapolitization suggested. This statement could be made about most descriptions of scapolite terranes or occurrences to be found in the literature. Lovering and White stated that the scapolite in the Australian pipes is primary, and that the granulite xenoliths containing it come from the deep crust.

It is difficult to speculate on the genesis of a mineral if nothing is known about the conditions for stability and the interrelations of composition and stability of the species. As I attempt to demonstrate in this paper, much of the haziness about the role of scapolite in a variety of parageneses has been due to lack of information and in part to misconceptions about the nature of the scapolite minerals. Accordingly, an investigation was begun to clarify at least some of the compositional uncertainties and at the same time to learn something about the stability regions of the various compositions. It turns out that P. M. Orville had been working on the scapolites containing carbonate and chloride as anions; his experiments, carried out at lower temperatures and pressures, supplement our data.

SCAPOLITE RELATIONS

Up until this year, almost all of our knowledge of scapolites has come from the examination of natural materials, and Shaw (1960a, 1960b) and Evans and others (1969) have examined many scapolites and summarized the data on them. The designated end mem-

Geological Society of America Bulletin, v. 87, p. 161–168, 9 figs., February 1976, Doc. no. 60201.

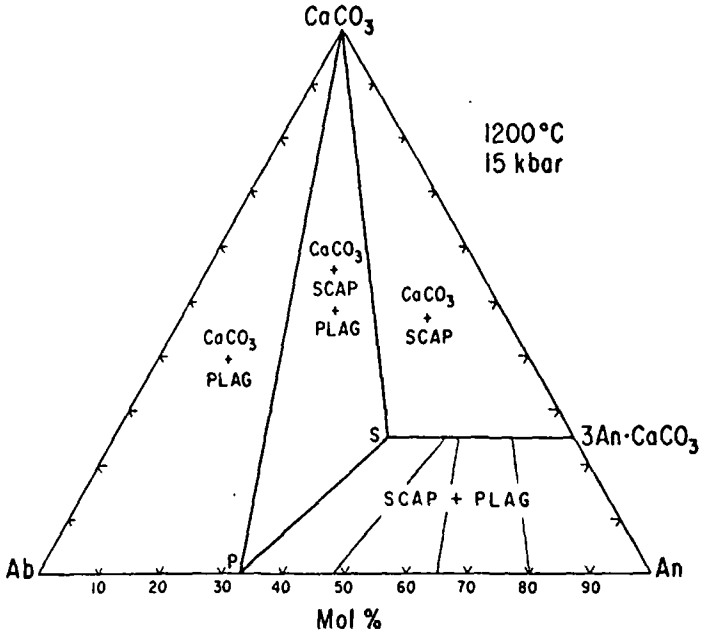

Figure 1. The system Ab-An-$CaCO_3$ at 1200°C and 15 kbar. $3An \cdot CaCO_3$ is the scapolite meionite, and the range of scapolite solid solutions stable at this temperature and pressure is from point S, the most sodic, to the meionite end member. Four experimentally determined tie lines are shown in the field of scapolite + plagioclase, the limiting one being the line SP, in which a scapolite of the composition S is in equilibrium with a plagioclase of composition P. In the sodic portion of the system, calcite can coexist with a plagioclase of any composition between An_0 and An_{33}.

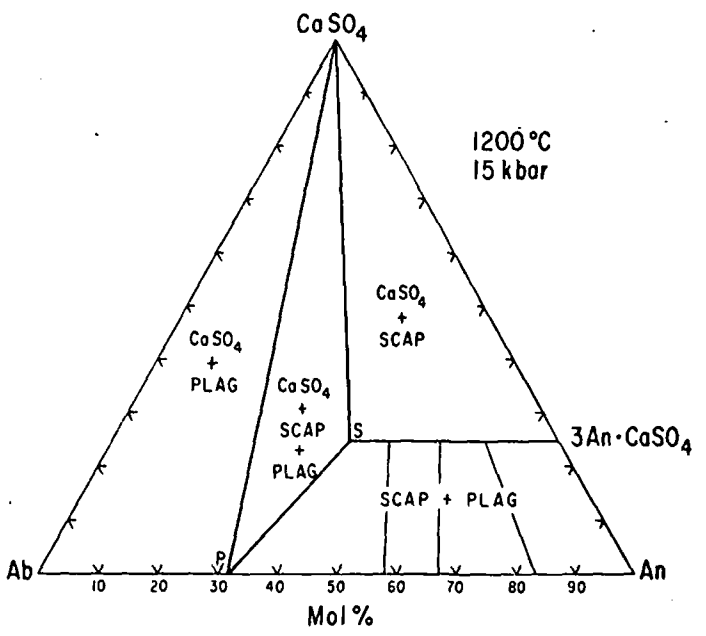

Figure 2. The system Ab-An-$CaSO_4$ at 1200°C and 15 kbar. The range of scapolite solid solutions stable at this temperature and pressure is from the sulfate meionite end member $3An \cdot CaSO_4$ to the composition S. Four experimentally determined tie lines in the field of scapolite + plagioclase are shown, the limiting one being the line SP, in which sulfate scapolite of the composition S is in equilibrium with a plagioclase of the composition P. In the sodic portion of the system, anhydrite can coexist with a plagioclase of any composition between An_0 and An_{33}.

bers are marialite, $3NaAlSi_3O_8 \cdot NaCl$ and meionite, $3CaAl_2Si_2O_8 \cdot CaCO_3$, easily remembered as 3 albite + NaCl and 3 anorthite + $CaCO_3$. Speaking as one who has spent a good deal of time on feldspars and carbonates, I think that meionite in particular has a friendly feel about it. Analyzed scapolites run from approximately 80 percent marialite to approximately 90 percent meionite, although almost all of the analyses cluster between 30 percent (70 percent marialite) and 80 percent meionite (Evans and others, 1969). Evans and others (1969) showed that these intermediate compositions do not lie on a simple binary join between the end members, and Papike (1964) indicated that the anion site can be filled with CO_3 at approximately 80 percent Me or, according to Evans and others (1969), Ca/(Ca+Na) = 0.75. Orville (1975) demonstrated that if Cl^- is present, the classic marialite-meionite join can exist. The Cl^- and $CO_3^=$ ions reside in equivalent cavities within the silicate structure, which is based on an Al-Si framework with tetragonal symmetry. The details and subtleties of the structure are still being investigated by several workers, and although complex and interesting, need not be considered for our present purposes.

Some scapolites contain quite a lot of sulfur, now known to be present as $SO_4^=$. We have synthesized and determined the stability relations of the end member scapolites $3NaAlSi_3O_8 \cdot NaCl$ (marialite), $3CaAl_2Si_2O_8 \cdot CaCO_3$ (meionite), and $3CaAl_2Si_2O_8 \cdot CaSO_4$ (sulfate meionite), and have determined the isothermal stability relations in the systems Ab-An-$CaCO_3$, Ab-An-$CaSO_4$, and the hybrid system arbitrarily containing one-half carbonate and one-half sulfate, all at 15 kbar and temperatures in the range 1000° to 1300°C (15 kbar is equivalent to a depth of about 50 km). In this temperature and pressure range, the Ca–end member scapolites $3An \cdot CaCO_3$ (meionite) and $3An \cdot CaSO_4$ (sulfate meionite) are stable, and phase relations at 1200°C and 15 kbar are shown in Figures 1 through 3.

Figure 1 is the system Ab-An-$CaCO_3$ at 1200°C and 15 kbar. The end member meionite is shown as $3An \cdot CaCO_3$. The horizontal line from this end member to point S represents the range of scapolite compositions that are stable under these conditions, point S being the most sodic composition. Thus, at 1200°C and 15 kbar, chlorine-free $CaCO_3$-scapolites are stable with Na/Ca ratios up to the equivalent of an $Ab_{40}An_{60}$ plagioclase. The three-phase triangle outlines the regions where calcite, plagioclase of the composition P, and the limiting scapolite S are in equilibrium. Bulk compositions to the left of this triangle do not produce scapolite, but calcite coexists with plagioclases from Ab_{100} to $Ab_{67}An_{33}$. The upper field on the calcic side of the three-phase triangle contains coexisting calcite and scapolite. Tie lines could be drawn in this field, radiating from the $CaCO_3$ apex to all of the scapolite compositions; the same could be done in the two-phase field of calcite and plagioclase.

The most interesting field in the diagram is that representing the coexistence of scapolite and plagioclase. Four experimentally determined tie lines in this region are shown, the limiting one to the left also being one side of the three-phase triangle. These tie lines connect the composition of scapolite in equilibrium with plagioclase.

The scapolites at 1200°C range in composition from pure meionite, which can only be in equilibrium with pure anorthite, to one represented by point S. Tie lines connect these scapolites with the appropriate plagioclase, ranging from An_{100} to $Ab_{70}An_{30}$. It is apparent that at this temperature a large range of scapolite solid solutions can exist in the absence of chlorine, or without substitution of the marialite end member as such. These data uphold the views of Evans and others (1969) and the observations of Orville (1975).

Figure 2 shows the system Ab-An-$CaSO_4$ at 1200°C and 15 kbar. The configuration of the diagram is very much like that in the

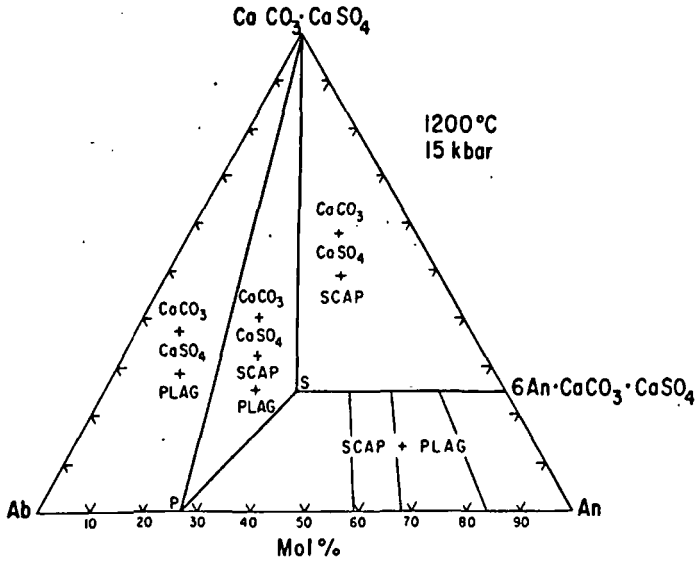

Figure 3. The system Ab-An-$CaCO_3$·$CaSO_4$ ($CaCO_3$ and $CaSO_4$ in equimolar proportions) at 1200°C and 15 kbar. The range of scapolite solid solutions stable at this temperature and pressure is from the end member 6An·$CaCO_3$·$CaSO_4$ to the composition S. Four experimentally determined tie lines in the field of scapolite + plagioclase are shown, the limiting one being the line SP, in which a hybrid scapolite of the composition S is in equilibrium with a plagioclase of the composition P. In the sodic portion of the system, calcite and anhydrite can coexist with a plagioclase of any composition between An_0 and An_{27}.

carbonate system, but sulfate-scapolites cover an even larger range of solid solutions. Point S, the limiting scapolite composition at 1200°C, has a plagioclase equivalent of $Ab_{47}An_{53}$. The sulfate scapolite can take even more albite component in solid solution without the need for Cl than can the carbonate scapolite. Three experimentally determined tie lines plus the limiting tie line S-P are shown. The range of compositions of plagioclase in equilibrium with the sulfate scapolites is also slightly larger than in the carbonate system.

The system containing one-half carbonate and one-half sulfate was investigated because of the observed association of these anions in subequal proportions in several analyzed scapolites (Knorring and Kennedy, 1958; Lovering and White, 1964). Figure 3 is the system Ab-An-$CaCO_3$·$CaSO_4$ at 1200°C and 15 kbar. The combination of anions produces a range of solid solutions that is somewhat greater than that for either the carbonate or sulfate scapolites; point S is at a plagioclase equivalent of $Ab_{52}An_{48}$, more than one-half of the distance along the join. Again, three experimentally determined tie lines plus the limiting tie line are shown.

The effect of temperature on the extent of the scapolite solid solutions and on the scapolite-plagioclase equilibria (tie lines) in these three systems has been examined at 1000°, 1100°, 1200°, and 1300°C. The solid-solution limits are difficult to determine and hence poorly known in the sulfate and hybrid system at 1000° and 1100°C; reaction rates are slower than in the pure carbonate system. Nevertheless, at least from 1100° to 1300°C, the range of solid solution is extended toward more sodic compositions with decreasing temperatures. This may not be a simple unidirectional effect, however. The effect of temperature on the scapolite-plagioclase equilibrium is of greater interest. Rather than show a series of isothermal diagrams such as those in Figures 1 through 3, the data can be more conveniently plotted as the ratio Na/Na+Ca in the plagioclase component of the scapolite against the same ratio in the plagioclase. This distribution of Na and Ca between scapolite and plagioclase in fact defines the tie lines as shown in Figures 1 through 3.

Figures 4 through 6 illustrate the effect of temperature on the scapolite-plagioclase equilibrium at 15 kbar. Figure 4 is for the carbonate-scapolites, Figure 5 for the sulfate scapolites, and Figure 6 for the 50:50 $CaCO_3$·$CaSO_4$ hybrid. The number of points is meager; generally four tie-line determinations at each temperature were carried out. The scatter is such that dashed curves are drawn, as the best estimate of the Na-Ca distribution. There is, however, a consistent trend; the scapolite becomes more sodic relative to the plagioclase with decreasing temperature. Thus the tie lines tend to "lean" more to the left as the temperature decreases. This effect is apparent in all three of the scapolite systems. The Na-Ca distribution between coexisting scapolite and plagioclase can thus be treated as a geologic thermometer, at least in the case of the more calcic plagioclases and essentially Cl-free scapolites. More precise determinations of these equilibria are desirable, and the effect of pressure should be evaluated, although more will be said about pressure shortly. Point D represents the composition of a scapolite

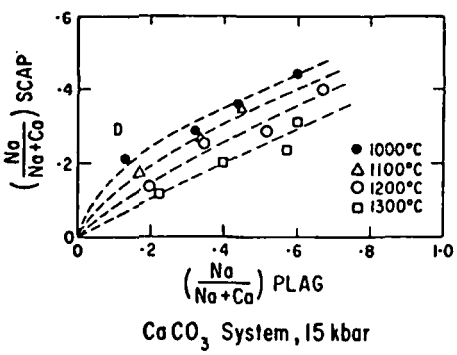

Figure 4. Plot of the ratio Na/Na+Ca in the plagioclase component of the carbonate scapolite against the same ratio in the plagioclase, for temperatures of 1000°, 1100°, 1200°, and 1300°C, at 15 kbar. The letter D represents the scapolite-plagioclase pair in the two-pyroxene granulite inclusions in the Delegate pipes, Australia (Lovering and White, 1964).

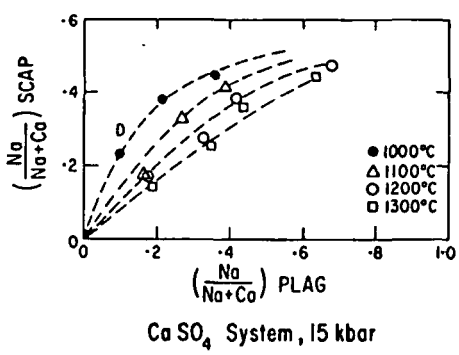

Figure 5. Plot of the ratio Na/Na + Ca in the plagioclase component of the sulfate scapolite against the same ratio in the plagioclase for temperatures of 1000°, 1100°, 1200°, and 1300°C, at 15 kbar. The letter D represents the scapolite-plagioclase pair in the two-pyroxene granulite inclusions in the Delegate pipes, Australia (Lovering and White, 1964).

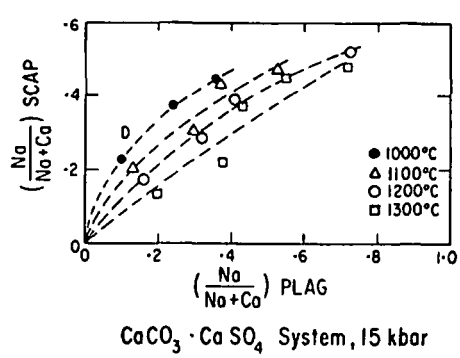

Figure 6. Plot of the ratio Na/Na+Ca in the plagioclase component of the hybrid carbonate-sulfate scapolite against the same ratio in the plagioclase, for temperatures of 1000°, 1100°, 1200°, and 1300°C, at 15 kbar. The letter D represents the scapolite-plagioclase pair in the two-pyroxene granulite inclusions in the Delegate pipes, Australia (Lovering and White, 1964).

coexisting with plagioclase in a 2-pyroxene granulite nodule from the Delegate pipes of Australia described by Lovering and White, which also will be considered shortly.

STABILITY RELATIONS OF THE END-MEMBER SCAPOLITES

There are a number of metamorphic localities in which almost pure anorthite coexists with calcite (Wenk, 1962; Misch, 1964). This would indicate that under the particular metamorphic conditions, the end-member meionite is not stable. Orville (1975) has recently published on the stability of scapolite in the system Ab-An-$CaCO_3$-NaCl at 750°C and 4 kbar. His results suggest that under these conditions pure meionite is unstable relative to anorthite and calcite, but that scapolite is stabilized by the presence of Na in the system. Figure 7 is taken from Orville's work and indicates that in the absence of Cl, a scapolite of limited range of compositions (about Ab-2An-$CaCO_3$; Orville uses the old term mizzonite for this composition) is in equilibrium with plagioclases from approximately $Ab_{60}An_{40}$ to $Ab_{15}An_{85}$. The field data (and Orville's results) thus indicate that pure meionite is unstable at moderate to low temperatures. Newton and Goldsmith (1975) have shown that the end member meionite is stable at temperatures of 1000°C, and remains so up to the melting curve which exceeds 1500°C at 20 kbar. The high-pressure breakdown to grossular, kyanite, quartz, and calcite in the range 25 to 30 kbar was also demonstrated by Newton and Goldsmith. We now have additional data showing that meionite becomes unstable relative to anorthite and calcite at between 850° and 900°C at 15 kbar and between 825° and 850°C at 8 kbar. The volume change of the reaction is quite small, and the equilibrium curve is steep. Thus, meionite is unstable at temperatures below 800°C, and in any geological range of pressures, scapolite can be produced in the reaction 3An + $CaCO_3 \rightleftharpoons$ meionite only at temperatures somewhat greater than 800°C. These relations are shown in Figure 8, where the field of meionite is outlined by the limiting stability curve to the left, the melting curve to the right, and the high-pressure breakdown of meionite to grossular, kyanite, quartz, and calcite at the top. It is apparent that meionite is a high-temperature mineral, and one capable of existing at rather high pressures, as well.

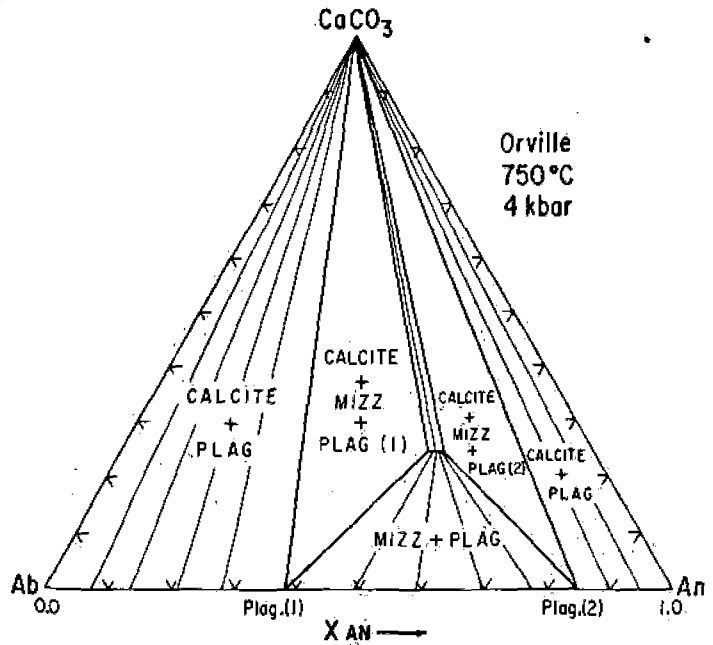

Figure 7. The system Ab-An-$CaCO_3$ at 750°C and 4 kbar, according to Orville (1975). The end member meionite is unstable under these conditions, and Orville's data indicate that the range of stable Cl-free scapolite compositions is quite limited and in the mizzonite region of the scapolite solid-solution series.

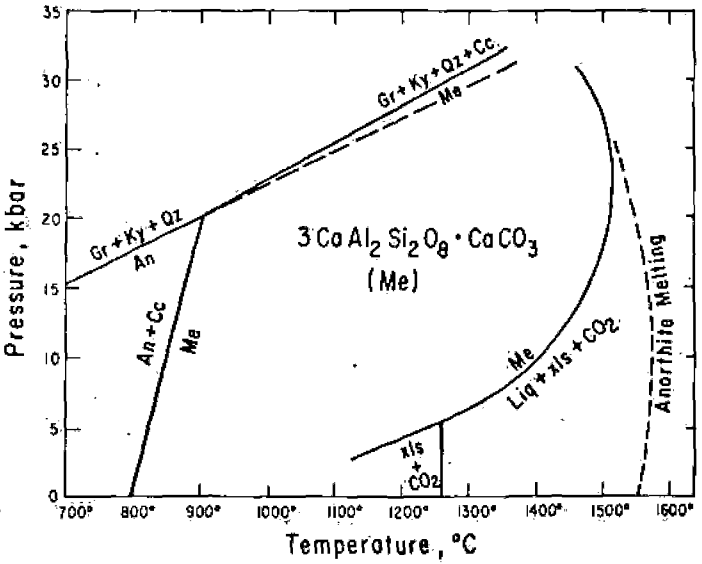

Figure 8. The stability relations of meionite, $3CaAl_2Si_2O_8 \cdot CaCO_3$. The continuous subsolidus-breakdown and melting curves are taken from Newton and Goldsmith (1976), as is the curve representing the reaction Me $\rightleftharpoons$ Gr+ Ky + Qz + Cc, the upper pressure limit of meionite. The steep curve for the reaction An + Cc $\rightleftharpoons$ Me is based on reversed reactions at 8 and 15 kbar. Me = meionite, Gr = grossularite, Ky = kyanite, Qz = quartz, Cc = calcite, An = anorthite.

The pure sulfate-meionite also has interesting properties, and its *P-T* region of stability is shown in Figure 9. It is quite refractory, and at pressures above about 20 kbar, melts at higher temperatures than anorthite. The steeply rising melting curve is shown to the right, crossing the anorthite melting curve. At these high temperatures and pressures, $CaSO_4$ is present along the melting curve — a long way from sedimentary and evaporite conditions! The stability curve separating sulfate scapolite from the assemblage anorthite + anhydrite is the lower curve shown in Figure 9, with a negative slope. The stability curves for scapolites in Figures 8 and 9 were determined with the use of "reversed" reactions, that is, the reactions were made to run in both directions, and thus are true equilibrium boundaries. The melting curve projected to low pressures and projected stability curve intersect at approximately 2 kbar and 1530°C; thus at any temperature, sulfate meionite is stable only at elevated pressures and is unusual in that it is also favored by increasing temperature as well as pressure. The calculated curve for the high-pressure breakdown of sulfate meionite to grossular, kyanite, quartz, and $CaSO_4$ is shown at the top of the diagram. The shape of the stability field of the end member sulfate meionite indicates that the minimum temperature of existence of the scapolite is approximately 775°C at 17 kbar, and that sulfate-rich meionite could only be expected to exist under rather deep-seated and high-temperature conditions. Although generally metamorphic minerals, the Ca-rich scapolites are obviously stable in a temperature range high enough to crystallize as primary magmatic phases at depth, assuming an adequate supply of CO_2 and sulfate.

Textbooks of mineralogy and petrology, if they mention scapolites at all, generally leave the impression that although typically metamorphic minerals, they are formed by metasomatic activity, pneumatolytic alteration, or for the most part by secondary or retrogressive processes. Barth, in the 1952 edition of his book *Theoretical Petrology* (p. 283-284) stated, "It is expedient to re-

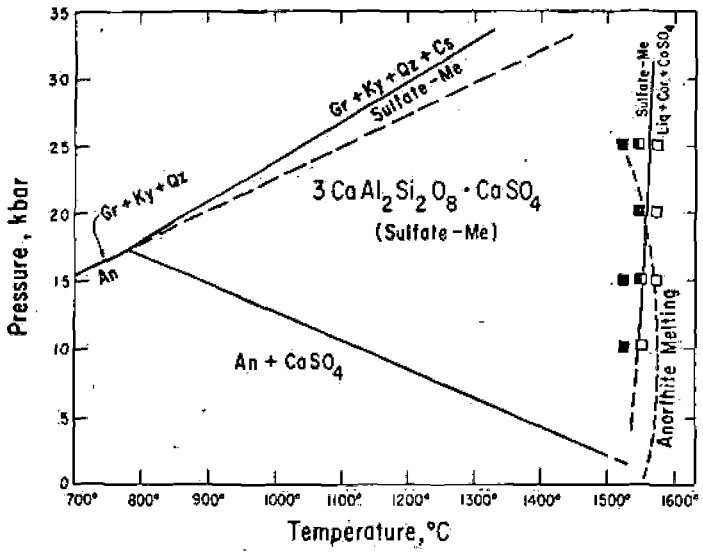

Figure 9. The stability relations of sulfate-meionite, $3CaAl_2Si_2O_8 \cdot CaSO_4$. The steep melting curve is from data of Newton and Goldsmith (1976). The dashed curve for the melting of anorthite is taken from unpublished data of Newton and Goldsmith. The curve for the upper pressure limit of sulfate-meionite, the reaction sulfate Me $\rightleftharpoons$ Gr + Ky + Qz + $CaSO_4$ is from Newton and Goldsmith (1976). The flat curve with the negative slope represents the reaction An + $CaSO_4 \rightleftharpoons$ sulfate Me. Me = meionite, Gr = grossularite, Ky = kyanite, Qz = quartz, An = anorthite, Cs = calcium sulfate.

gard meionite and marialite as the low-temperature 'modifications' of anorthite and albite, respectively." He developed a diagram that geometrically resembles the plagioclase melting loop, with plagioclases on the top curve and scapolites on the bottom. It was suggested that any stable plagioclase, on cooling in the presence of carbonate-bearing solutions, will thus break up into a more calcic scapolite and a more sodic plagioclase. Interestingly, the entire discussion of scapolites was omitted from the 1962 revision (Barth, 1962). Similarly, Fyfe and Turner (in Fyfe and others, 1958), in agreement with Barth, present a hypothetical scapolite stability diagram, in which scapolite is shown to be on the low-temperature side of the curve that represents the reaction scapolite $\rightleftharpoons$ anorthite + calcite. These and other authors had little information with which to operate. No one had data indicating that the equilibrium relationship has the opposite sense — that scapolite is the stalwart or that scapolite takes over from the weaker combination when things get hot.

If this is an unexpected result, it points up the importance of experimental petrology as an adjunct to field and theoretical approaches. It is another example of Bowen's (1938) plea for "Mente et Malleo Atque Carino," for here both field observations and theorizing led to the wrong conclusion. I should hasten to add, however, that sloppy experimental work, particularly that in which little care is exercised in the attainment of equilibrium, can make unreserved fools of experimentalists.

Our very recent experiments have shown that marialite is stable relative to albite plus NaCl in a high-temperature range down to at least 800°C, a fact not anticipated by Orville (1975) in his work at 750°C but not at variance with it. We have not been able to determine the lower-temperature stability boundary of marialite by our methods. Our data, in conjunction with those of Orville (1975) would place a boundary between 750° and 800°C in the pressure range 0 to 8 kbar, with a steep dP/dT slope. Thus, the general appearance of the marialite stability diagram would be very similar to that of meionite. This matter will not be pursued further because of the fact that chlorine has been found to be present only in trace amounts in the scapolites of deep-seated origin considered here. We have already seen that scapolite can contain rather large amounts of the sodic component without needing chloride ions, and furthermore chlorides are not abundant in the lower crust. Marialite scapolites are probably most prevalent in metamorphosed sediments containing halite (Hietanen, 1967) or rocks in which chlorides have been metasomatically introduced (Edwards and Baker, 1953). If scapolites were to form in association with the common native minerals of the lower crust, one would expect rather calcic scapolites containing carbon (carbonate) and sulfur (sulfate), if only on the basis of the elements that are available.

The only experimental data on the stability of the intermediate Na-Ca scapolites are the limited data of Orville (1975), as shown in Figure 7. Orville (1975) has shown that the sodic component stabilizes the carbonate scapolite to lower temperatures, and one might assume a similar effect in the case of the Na-Ca sulfate scapolites, but that would be guesswork. Although we have investigated the tie lines in the $CaCO_3$-$CaSO_4$ hybrid system, nothing has been done on the effect of a varying $CaCO_3$-$CaSO_4$ ratio on the P-T relations on the scapolite stability field. It is not too difficult, however, to imagine states intermediate between those shown in Figures 8 and 9, representing intermediate compositions. Another unknown is the effect Na may have on stabilizing the sulfate-scapolite to lower pressures, although it is not unreasonable to expect it to do so. This multicomponent system with both P and T as variables has hardly been touched.

ROLE OF SCAPOLITES IN CRUST

We have seen that the lime-rich compositions are very refractory — perhaps surprisingly so, considering that they contain what we usually think of as volatile substances. Goldsmith and others (1974) showed that a marialite with nitrate in place of chloride was stable to fairly high temperatures at elevated pressures. At elevated temperatures and pressures, calcic feldspar is unstable in the presence of carbonate and (or) sulfate (or CO_2 or oxidized sulfur), and Ca-rich scapolite is formed. Figures 8 and 9 show that for both the carbonate and sulfate end members, the temperature must be greater than 800°C for scapolite to form. As we have seen, the presence of Na will stabilize scapolite at lower temperatures, and calcite plus a plagioclase containing some albite will react at temperatures well below 800°C.

Lovering and White (1964), using as a basis their analysis of the scapolite occurrences in granulite nodules from the Delegate pipes in Australia, suggested that the lower crust beneath Australia may contain as much as 5 percent scapolite as a primary phase. Dawson (1964, 1968, 1971) has noted the presence of scapolite in calc-silicate granulites in kimberlite diatremes, and stated (1971), "... it is a possibility that the granulite xenoliths in kimberlites were perhaps derived from lenses or layers of granulite at the base of the crust or in the extreme upper levels of the upper mantle." As indicated above, scapolite has now been observed in granulite inclusions from three continents and may be more common than the published record shows, for there is a tendency to preferentially collect and examine the more basic xenoliths, presumed to have come from the mantle. It is fair to say that the extent to which meionitic scapolite exists in the lower crust is largely dependent on the availability of carbonate and sulfate as well as on the distribution of basic plagioclase.

The words scapolite and granulite are associated in the title of this address. It appears to me that most of the Ca-rich scapolites occur in granulites or related high-grade rocks; Fyfe and others (1958) have suggested that scapolite is a granulite-facies mineral. Several considerations that relate composition and P-T stability to this association favor a hypothesis that granulites are the typical lower-crustal rocks of much of the continental areas. More about this follows.

The Delegate pipe material is one of the few documented examples of analyzed scapolite from the deep earth. Is it possible to draw some conclusions as to the pressure and temperature conditions of its formation? Lovering and White (1964) report a high sulfur content, as much as 72 percent of the carbon (in carbonate) replaced by S (now known to be sulfate) in the scapolite of one of the two types of granulites they have examined. A plagioclase of An_{89} is associated with the scapolite. This material is plotted as the letter *D* in Figures 4 through 6; from our tie-line data, we must conclude that this scapolite-plagioclase pair equilibrated at a temperature below 1000°C. Thus it is unlikely that this pair is a primary igneous association directly related to the magmatism which carried it close to the surface. It is more likely that the scapolite is a primary metamorphic constituent of an assemblage which may be quite representative of the constitution of much of the lower crust of eastern Australia. Irving (1974) also made this interpretation of the scapolite-bearing, two-pyroxene granulites from the Delegate occurrence on the basis of textures and trace elements. This use of the scapolite-plagioclase pair as a geothermometer assumes no significant pressure correction; it has been investigated only at 15 kbar.

There is little doubt that much of the carbonate in the deep-seated scapolites comes from the mantle. Newton and Sharp (1975) present evidence against the presence of free CO_2 in the upper mantle, for the assemblage $MgCO_3 + MgSiO_3$ is stable relative to Mg_2SiO_4 and CO_2, at least under subcontinental environments. Whether the carbonate groups in scapolite came from gaseous CO_2 or from CO_2 in solution in a melt or even as a solid carbonate would make little difference to the scapolite, however; in any case, there is certainly oxidized carbon in the upper mantle. Touret (1971) stated that CO_2 is given off by the crystallization of deep-seated basic intrusions containing CO_2 in solution, and that the CO_2 permeates the metamorphic terrane in a wave of dry regional granulite metamorphism. If, however, the intrusions crystallize at the level of the lower crust, the CO_2 would crystallize in primary igneous scapolite, and the scapolite would re-equilibrate with plagioclase as the intrusion cooled.

We have seen in Figure 9 that the pure sulfate-meionite is a true high-pressure mineral favored by both high pressures and high temperatures. The sulfate content of scapolite thus has the potential of yielding information on the pressure of crystallization or equilibration. Before it can be useful as a geobarometer, however, it must be calibrated as a function of composition. The effect of the CO_3/SO_4 ratio and of the Na/Ca ratio on the slope of the stability boundary must be known. This is a large order, and it means working out the *P-T* stability relations in the 4-component system Ab-An-$CaCO_3$-$CaSO_4$. It is not likely, however, that the substitution of Na will have a great effect on the *slope* of the stability boundary, for the volume change with substitution is small. It will shift the equilibrium to lower temperatures, however, and the reaction will become divariant. In the Na-free system, as sulfate replaces carbonate, the steep stability curve of meionite (Fig. 8) must steepen even more, become vertical, then become negative and approach the flat negative slope of the sulfate end member. Thus, the sulfate-rich meionites are potentially excellent geobarometers, assuming that the presence of Na and the development of divariancy does not drastically alter the shape of things.

The Delegate scapolite has nearly a 4:1 Ca/Na ratio, and the sulfate substitution of 70 percent or more is large enough to make tempting the claim for a deep-seated origin, even if no ancillary evidence were available and with no data on the effect of Na. This view is strengthened by the published analyses of scapolites (Shaw, 1960a; Deer and others, 1963); those with high sulfur content all appear to be from deep-seated sources.

Is sulfur always available at depth? Brimstone is surely associated with volcanic fires, but little attention has been given to the abundance and state of sulfur in the mantle. Presumed upper-mantle rocks contain sulfur in sulfides, and I am not aware of any report of sulfate in kimberlites and peridotites; if it *were* to be noted, it might well be passed off as an alteration product. Is the sulfate in scapolite derived from reaction with sulfides or other forms of reduced sulfur from the mantle? Very probably so, and it is likely that oxidation takes place by a ferrous-ferric equilibrium with deep crustal minerals, and with no transfer of oxygen or need for other oxidizing agents. A bare-bones simplification, with ions pulled out of their silicate and oxide context would be:

$$\underset{\text{(in sulfide)}}{S^{=}} + \underset{\text{(in magnetite)}}{4\ Fe_2O_3} \rightleftharpoons \underset{\text{(in scapolite)}}{SO_4^{=}} + \underset{\text{(in silicate)}}{8\ FeO}$$

We do see sulfur as well as carbon brought in one form or another to the surface. Sulfur, SO_2, SO_3, or even sulfate are associated with volcanism; we must assume that in basaltic volcanoes, it has been rather quickly brought up from the mantle with little chance for oxidation. Carbon also acts as a traveler in the crust, explosively rammed through in kimberlite diatremes. Aside from diamonds, which may be residents of the mantle, but surely transients in the crust, carbon as carbonate or CO_2 should react with plagioclase in the deep crust and assume residential status as scapolite. The sulfur that becomes oxidized should do the same, and the existence of sulfate-bearing scapolite in deep-crustal xenoliths is good evidence that this is what takes place.

We have seen the need for a deep, hot situation for Ca-rich scapolite. Just as the sulfate-rich scapolites come from depths, the meionites also come from hot spots; the most Ca-rich known is from Monta-Somma, a pyrometamorphic occurrence. In fact, the *P-T* conditions (especially *T*) for nearly pure meionite are so stringent that they surely cannot be met along a normal geothermal gradient but could only be satisfied by such a locally hot situation. A reasonable amount of Na in the system lowers the temperature needed for stability, and more sodic scapolites settle for less severe conditions. The granulite facies represents the highest grade of regional metamorphism in the crust, and may well offer the minimal conditions needed for the Ca- and S-rich scapolites, at least. It is unlikely that scapolite exists in the eclogite facies, for we have seen that the upper pressure limit, where scapolites break down to isochemical assemblages containing garnet, kyanite, quartz (Figs. 8 and 9), and presumably jadeite if Na is present, is close to that of the equivalent feldspar. Granulites are thought of in terms of regional metamorphism — but where is the "region"? Is metamorphism always the result of an "event"? Many insinuate that it is, yet is it not more reasonable to assume that this type of regional metamorphism is a normal form of subcontinental deep-crustal behavior? This view is a throwback to the concept of successive depth zones, the catazone being the home of granulites and related rocks. Granulites are from deeply eroded Precambrian gneissic areas — from where else should they come but the lower crust? Their variability is an expression of crustal inhomogeneity, and metamorphic grade may be related to a "local" geothermal gradient, strongly affected by intrusion of molten material from the mantle.

Granulites are known as dry rocks. Bowen (1947), in arguing against a high water content in basaltic magma at depth and pointing out the dry nature of deep-zone metamorphic rocks, said, "One possible interpretation of this situation is that the temperature in the deeper zones is too high for the formation of the hydrous minerals even at the high pressure there prevailing; but a more probable interpretation is that the principal source of water for rocks is at the surface or at shallow depths, and the mechanical barriers to the penetration of such water to great depths are al-

together effective." We now know that hydrous minerals are stable in the deeper zones; granulites *are* dry because of the absence of water. One might also argue that granulites are granulites and not amphibolites, at least in part because of this reason (Gjelsvik, 1952; Yoder, 1952; Poldervaart, 1953; Thompson, 1955; Buddington, 1963; Misch, 1964, p. 354; Touret, 1971). Furthermore, Bowen was unaware of the mechanism of carrying water to deep rocks by subduction. It is quite possible that a revealing geographic restriction can be placed on granulites — might they be indicators of relatively stable regions of the deep continental crust removed from those areas in which subduction has taken place? A listing of the classic granulite localities reads like a recitation of such ancient and stable areas of the world.

The role of water in the structure of scapolites and its relations to the stability of these minerals become important with respect to the anhydrous nature of granulites. Many of the scapolite analyses show H_2O to be present, but one is hard put to avoid contamination. Shaw (1960a) states that the water seen in the analyses is of uncertain significance, but the possibility of structurally bound water is not discounted. Zoisite and meionite have chemical compositions that differ only with respect to the anionic group:

scapolite: $3CaAl_2Si_2O_8 \cdot CaCO_3$

zoisite: $3CaAl_2Si_2O_8 \cdot Ca(OH)_2$

We have found that in the experimental runs made on meionite at temperatures of approximately 900°C or below, great pains had to be taken to avoid the crystallization of zoisite at the expense of the scapolite. Not only was it necessary to thoroughly dry the reactants before welding shut the platinum capsule that contained them, but the entire assembly had to be baked out. Any source of H_2O within the capsule or of hydrogen in the external setup, including that formed from the decomposition of H_2O at elevated temperature, must be avoided. H_2 readily diffuses through the platinum, reduces the carbonate to carbon, and the water thus formed reacts with the charge to produce zoisite. Here is still another system that needs study, for the equilibrium relations between zoisite and meionite are functions of P, T, and the partial pressures of CO_2 and H_2O. It is apparent that zoisite and scapolite have an antithetical relationship and that water would hardly be expected to be a component of meionite. It is most probable, however, that as Na enters the scapolite structure, the need for large CO_2/H_2O ratios becomes less stringent. The existence of Na-containing scapolites in epidote-amphibolite rocks and even in the greenschist facies (Hietanen, 1967) would indicate that increasing Na permits a tolerance for water, as does the recent experiment of Milhollen (1974), in which a scapolite of the composition 2An + 1Ab + $CaCO_3$ was formed in the presence of a liquid in a nepheline syenite melt, with vapor rich in CO_2 and H_2O at pressures above 3 kbar. Hietanen (1967) points out the increased Na content of scapolite and the accompanying progressive decrease in metamorphic grade with distance from the Idaho batholith, in the St. Joe–Clearwater region, Idaho. This effect is analogous to the breakdown of plagioclase in the presence of water to form zoisite (epidote). Calcic plagioclase reacts to form zoisite and an albitic plagioclase, and the more sodic plagioclases are more resistant to this alteration at low temperatures.

A hot, dry environment is what a lime-rich scapolite wants, and that is just what a granulite has. Touret (1975) considers granulites to be catazonal rocks in which metamorphism takes place in the presence of a water-free and CO_2-rich fluid phase, the CO_2 presumably coming from the upper mantle. Touret noted that high-density, CO_2-rich fluid inclusions are abundant in granulite facies rocks from all over the world. From the location and features of these rocks, he modeled the distribution of fluids within the continental crust and suggested that CO_2 is concentrated in the lower crust, between the Conrad and Mohorovičić discontinuities. Our data suggest that Touret's picture of volatiles in the lower crust should be modified. Mafic compositions surely have prevailed at Earth levels equivalent to the present lower crust, and this region must have acted as a trap for oxidized carbon and sulfur. CO_2 would not be in the form of included fluids, but would be locked up as scapolite. Much of the work done on fluid inclusions by Touret has been in acidic quartz-feldspathic rocks with which CO_2 could not react. Figures 1 through 3 show that in the absence of chlorine, scapolites are not stable in the Na- and Si-rich portions of the systems.

Those parts of the present lower crust that are appropriately basic must still be acting as a "getter" for sulfur and CO_2 coming from the deeper earth. The lower crust could be a principal place of residence for these volatile elements, and, in the case of sulfur, might be one of the more important repositories in the Earth. Deep continental drilling in selected sites might give us some insight into these and other aspects of the lower crust, although justifying such activity for scientific purposes is not an easy thing to do.

The carbon and sulfur are readily freed to the upper crust and atmosphere, and ultimately to the biosphere by any activity that takes scapolite out of its field of stability. If calcic scapolite is carried upward by diastrophic or volcanic processes, it will ultimately decompose at the elevated temperatures and low pressures. If water is carried down to it by subduction, it may also decompose, depending upon the Na content and H_2O/CO_2+SO_3 ratio. In general, with respect to Ca-rich varieties, the retrogressive processes that are commonly considered to produce scapolite (see, for example, Misch, 1964) are probably the very processes that destroy it. It is not too far fetched to assume that most of the CO_2 (and SO_2) of the air we breathe and therefore the carbon of our bodies has at one time been in scapolite. It is unlikely that the carbon cycle operates as deeply as the lower crust, and although subduction may carry quantities of carbon into the mantle and thus recycle some of us, we, the crumbs of the upper crust, are hardly in equilibrium with scapolites of the nether regions.

ACKNOWLEDGMENTS

This research was supported by the Earth Science Section, National Science Foundation, Grants DES74-22851 and DES72-01535. I would also like to acknowledge the general support of the Materials Research Laboratory of the National Science Foundation. Robert C. Newton was a partner in all of the research reported here. I am also indebted to Robert C. Newton, J. V. Smith, and Lelde Kalmite for suggesting changes that have materially improved the manuscript.

Note Added In Proof: My attention has been called to several publications by A. F. Wilson that contain views quite similar to some presented here. At this time, only one of these publications is available to me (Wilson, A. F., 1969, Problems of exploration for metals in granulite terrains, with particular reference to Australian localities: Geol. Soc. Australia, Spec. Pubs. No. 2, p. 375–376). Wilson calls attention to the very high sulfur content of some of the scapolites from the Musgrave Ranges of central Australia and states that "although granulites are normally considered to be very 'dry' rocks, chemical analyses show that large amounts of normal 'volatile substances' that are involved in hydrothermal mineralisation are fixed in many granulites." He also states that "scapolite is much more widespread in granulites than is generally recognized. It is superficially like plagioclase." He further indicates, referring to Lovering and White (1964), that portions of the deep crust may contain large amounts of sulfur in the scapolite structure and that retrograde metamorphism must release sulfur which could be available for reaction with metals that are released from pyroxenes to form minerals of economic interest.

REFERENCES CITED

Barth, T.F.W., 1952, Theoretical petrology: New York, John Wiley & Sons, Inc., 387 p.

——1962, Theoretical petrology (2nd ed.): New York, John Wiley & Sons, Inc., 416 p.

Bobrievich, A. P., and Sobolev, V. S., 1957, Eclogitization of the pyroxene crystalline schists of the Archean complex [in Russian]: Zap. Vses. Mineralog. Obschestva, V. Ser., v. 86, p. 3–17.

Bowen, N. L., 1938, Mente et malleo atque catino: Am. Mineralogist, v. 23, p. 123–130.

——1947, Magmas: Geol. Soc. America Bull., v. 58, p. 263–280.

Buddington, A. F., 1963, Isograds and the role of H_2O in metamorphic facies of orthogneisses of the northwest Adirondack area, New York: Geol. Soc. America Bull., v. 74, p. 1155–1182.

Cox, K. G., Gurney, J. J., and Harte, B., 1973, Xenoliths from the Matsoku pipe, *in* Nixon, P. H., ed., Lesotho kimberlites: Maseru, Lesotho Natl. Devel. Corp., p. 76–100.

Dawson, J. B., 1964, Carbonate tuff cones in northern Tanganyika: Geol. Mag., v. 101, p. 129–137.

——1968, Recent researches in kimberlite and diamond geology: Econ. Geology, v. 63, p. 504–511.

——1971, Advances in kimberlite geology: Earth-Sci. Rev., v. 7, p. 187–214.

Deer, W. A., Howie, R. A., and Zussman, J., 1963, Rock-forming minerals: Vol. 4, Framework silicates: London, Longman Group Ltd., 435 p.

Edwards, A. B., and Baker, G., 1953, Scapolitization in the Cloncurry district, northwestern Queensland: Geol. Soc. Australia Jour., v. 1, p. 1–33.

Evans, B. W., Shaw, D. M., and Haughton, D. R., 1969, Scapolite stoichiometry: Contr. Mineralogy and Petrology, v. 24, p. 293–305.

Fyfe, W. S., Turner, F. J., and Verhoogen, J., 1958, Metamorphic reactions and metamorphic facies: Geol. Soc. America Mem. 73, 259 p.

Gjelsvik, T., 1952, Metamorphosed dolerites in the gneiss area of Sunnmøre on the west coast of southern Norway: Norsk Geol. Tiddskr., v. 30, p. 33–134.

Goldsmith, J. R., Newton, R. C., and Moore, P. B., 1974, Silicate-nitrate compounds: High-pressure synthesis and stability of a nitrate scapolite: Am. Mineralogist, v. 59, p. 768–774.

Hietanen, A., 1967, Scapolite in the Belt series in the St. Joe–Clearwater region, Idaho: Geol. Soc. America Spec. Paper 86, 56 p.

Irving, A. J., 1974, Geochemical and high pressure experimental studies of garnet pyroxenite and pyroxene granulite xenoliths from the Delegate basaltic pipes, Australia: Jour. Petrology, v. 15, p. 1–40.

Knorring, O. von, and Kennedy, W. Q., 1958, The mineral paragenesis and metamorphic status of garnet-hornblende-pyroxene-scapolite gneiss from Ghana (Gold Coast): Mineralog. Mag., v. 31, p. 846–859.

Lovering, J. F., and White, A.J.R., 1964, The significance of primary scapolite in granulitic inclusions from deep-seated pipes: Jour. Petrology, v. 5, p. 195–218.

Milhollen, G. L., 1974, Synthesis of scapolite under magmatic conditions: Am. Mineralogist, v. 59, p. 618–620.

Misch, P., 1964, Stable association wollastonite-anorthite and other calc-silicate assemblages in amphibolite facies crystalline schists of Nanga Parbat, northwest Himalayas: Beitr. Mineralogie u. Petrographie, v. 10, p. 315–356.

Newton, R. C., and Goldsmith, J.R., 1975, Stability of the scapolite meionite ($CaAl_2Si_2O_8 \cdot CaCO_3$) at high pressures and storage of CO_2 in the deep crust: Contr. Mineralogy and Petrology, v. 49, p. 49–62.

——1976, Stability of the end-member scapolites: $3NaAlSi_3O_8 \cdot NaCl$, $3CaAl_2Si_2O_8 \cdot CaCO_3$, $3CaAl_2Si_2O_8 \cdot CaSO_4$: Zeitschr. Kristallographie (in press).

Newton, R. C., and Sharp, W. E., 1975, Stability of forsterite + CO_2 and its bearing on the role of CO_2 in the mantle: Earth and Planetary Sci. Letters, v. 26, p. 239–244.

Orville, P. M., 1975, Stability of scapolite in the system Ab-An-NaCl-$CaCO_3$ at 4 kb and 750°C: Geochim. et Cosmochim. Acta, v. 39, p. 1091–1105.

Papike, J. J., 1964, The crystal chemistry and crystal structure of scapolite [Ph.D. thesis]: Minneapolis, Univ. Minnesota.

Poldervaart, A., 1953, Metamorphism of basaltic rocks, a review: Geol. Soc. America Bull., v. 64, p. 259–274.

Shaw, D. M., 1960a, The geochemistry of scapolite: Pt. I. Previous work and general mineralogy: Jour. Petrology, v. 1, p. 218–260.

——1960b, The geochemistry of scapolite: Pt. II. Trace elements, petrology and general geochemistry: Jour. Petrology, v. 1, p. 261–285.

Sobolev, V. S., ed., 1959, The diamond deposits of Yakutia: Moscow, 527 p.

Thompson, J. B., Jr., 1955, The thermodynamic basis for the mineral facies concept: Am. Jour. Sci., v. 253, p. 65–103.

Touret, J., 1971, Le faciès granulite en Norvège meridionale. Pts. I and II: Lithos, v. 4, p. 239–249, 423–436.

——1975, Faciès granulite et fluids carbonique, *in* Belliére, J., and Duchesne, J. C., eds., Geologie des Domaines Cristallins: Liege, Soc. Géol. Belgique, p. 267–287.

Verhoogen, J., 1938, Les pipes de kimberlite de Katanga: Annales Services Mines, Comité Special du Katanga, v. 9, p. 3–46.

Wenk, E., 1962, Plagioklas als indexmineral in den zentralalpen: Schweizer. Mineralog. u. Petrog. Mitt., v. 42, p. 139–152.

Yoder, H. S., Jr., 1952, The MgO-Al_2O_3-SiO_2-H_2O system and the related metamorphic facies: Am. Jour. Sci. (Bowen volume), p. 569–627.

MANUSCRIPT RECEIVED BY THE SOCIETY SEPTEMBER 26, 1975

Printed in U.S.A.

Scapolites, granulites, and volatiles in the lower crust

Address as Retiring President of the Geological Society of America, Salt Lake City, Utah, October 1975

JULIAN R. GOLDSMITH *Department of the Geophysical Sciences, University of Chicago, Chicago, Illinois 60637*

INTRODUCTION

I would like to consider a little-understood and sometimes maligned family of minerals and its relationship to an ill-defined type of rock. The mineral is scapolite, the rock is granulite, and both are probably more important than some of us think. Before going further, however, I would like to make it clear that the work reported here was done in cooperation with my colleague, Robert C. Newton, and although more detailed and extensive versions complete with data will appear elsewhere under joint authorship, the bylaws of the Geological Society of America do not permit "co-presidents." I hope that this address does not become as well known as the one Lincoln gave at Gettysburg, for my conscience would suffer the more. This concern would be unnecessary if presidential addresses could be seen and not heard, or even better, looked at without being read. This latter would permit reprinting of the same piece for each President, and editorial and typesetting costs could be eliminated. Or, if they must be heard and read, each president could be assigned to one of a limited number of addresses, and could work it over, add new data as necessary and available, inject or interpret new ideas, polish, hone, modify to conform to the existing zeitgeist, and hopefully do so in an area reasonably close to whatever his specialty may be. This approach would not only be instructional for the retiring officer, but it could conceivably eliminate random and rambling papers, and provide us all with current and noncontroversial review articles.

One current very hot subject is the Earth's mantle, and recent interest is not limited to geophysicists, geochemists, and petrologists, for interrelationships with global tectonics bring it before almost every kind of earth scientist. Not very many years ago, the mantle was cloaked in obscurity by the crust, and very few geologists gave it any thought, although it provided a ray path for seismologists and an intellectual home for a few geophysicists.

The first meeting of the Society I attended was in Chicago in 1946, and my mentor, N. L. Bowen, held forth in his usual delightful and erudite way on magmatism and granitization, pontiffs, and soaks (Bowen, 1947). This was the heyday of the granite controversy, and with the crust presenting so much food for thought, who cared about the mantle? The new global tectonics has introduced a new snobbishness, and a "downward drift" has taken place; the mantle is "in," and much of the crust is viewed not as food for thought, but as potentially subductible nutrient for the upper mantle. The disdain for the visible and more familiar can have sociological as well as scientific overtones; that great conman, "Yellow Kid" Weil, commenting about his marks, said "The upper crust is composed mostly of crumbs." The upper crust we see. We are reasonably sure that we see fragments of the upper mantle brought up as exotics in deep volcanoes and kimberlite pipes. Rather few geologists have attempted to characterize the lower crust, however, and it is my impression that it currently carries a larger element of the unknown than any other region of the Earth; at the same time, it is not a popular area of speculation. This may be due to an assumed high degree of complexity, variability, or inhomogeneity.

Some of my acquaintances feel that I have not been field oriented, yet I am aware of the fact that there are aspects of our understanding of the Earth that require observations of rocks and minerals in their natural habitat. In order to do anything like field work in the deep crust however, one has to be a "trash man" of sorts. Our best samples of deep crustal as well as mantle material are the fragments ripped out of place by the rising magma in the above-mentioned volcanoes, and by the kimberlitic and other deep-seated pipes; this deep-earth trash, a litter of xenoliths, is picked up at or near the surface by the combination field man and refuse collector. This kind of field work appeals to me.

Collecting these nodules has become scientifically a very profitable enterprise, particularly for those working with the (presumed) mantle material. Rather little attention has been given to the more siliceous nodules, although a number of authors have noted the presence of crustal material, particularly granulites. Lovering and White (1964) have worked on material from the Delegate pipes in eastern Australia and called attention to the presence of apparently primary scapolite in granulites included in these breccia- and basalt-filled pipes. Scapolite has also been noted in similar occurrences in South Africa and Siberia (Bobrievich and Sobolev, 1957; Sobolev, 1959; Dawson, 1964, 1968, 1971; Cox and others, 1973; Verhoogen, 1938), although as indicated by Bobrievich and Sobolev (1957) and by Misch (1964), the scapolite in metamorphic occurrences is generally viewed as secondary, after plagioclase, with no clear mechanism for or time of the scapolitization suggested. This statement could be made about most descriptions of scapolite terranes or occurrences to be found in the literature. Lovering and White stated that the scapolite in the Australian pipes is primary, and that the granulite xenoliths containing it come from the deep crust.

It is difficult to speculate on the genesis of a mineral if nothing is known about the conditions for stability and the interrelations of composition and stability of the species. As I attempt to demonstrate in this paper, much of the haziness about the role of scapolite in a variety of parageneses has been due to lack of information and in part to misconceptions about the nature of the scapolite minerals. Accordingly, an investigation was begun to clarify at least some of the compositional uncertainties and at the same time to learn something about the stability regions of the various compositions. It turns out that P. M. Orville had been working on the scapolites containing carbonate and chloride as anions; his experiments, carried out at lower temperatures and pressures, supplement our data.

SCAPOLITE RELATIONS

Up until this year, almost all of our knowledge of scapolites has come from the examination of natural materials, and Shaw (1960a, 1960b) and Evans and others (1969) have examined many scapolites and summarized the data on them. The designated end mem-

Geological Society of America Bulletin, v. 87, p. 161–168, 9 figs., February 1976, Doc. no. 60201.

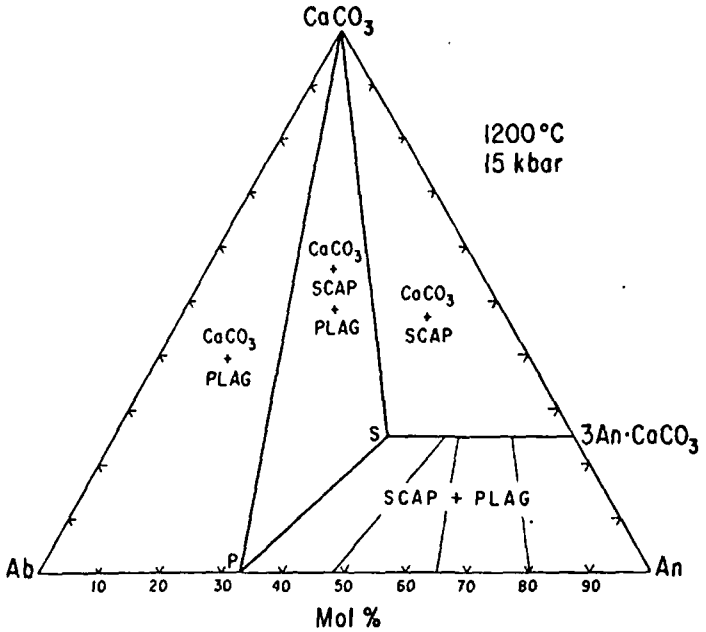

Figure 1. The system Ab-An-$CaCO_3$ at 1200°C and 15 kbar. $3An \cdot CaCO_3$ is the scapolite meionite, and the range of scapolite solid solutions stable at this temperature and pressure is from point S, the most sodic, to the meionite end member. Four experimentally determined tie lines are shown in the field of scapolite + plagioclase, the limiting one being the line SP, in which a scapolite of the composition S is in equilibrium with a plagioclase of composition P. In the sodic portion of the system, calcite can coexist with a plagioclase of any composition between An_0 and An_{33}.

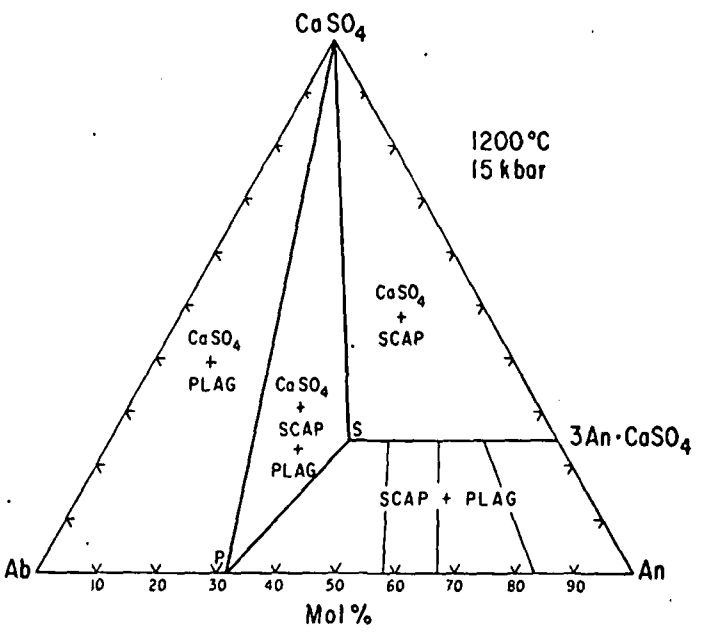

Figure 2. The system Ab-An-$CaSO_4$ at 1200°C and 15 kbar. The range of scapolite solid solutions stable at this temperature and pressure is from the sulfate meionite end member $3An \cdot CaSO_4$ to the composition S. Four experimentally determined tie lines in the field of scapolite + plagioclase are shown, the limiting one being the line SP, in which sulfate scapolite of the composition S is in equilibrium with a plagioclase of the composition P. In the sodic portion of the system, anhydrite can coexist with a plagioclase of any composition between An_0 and An_{32}.

bers are marialite, $3NaAlSi_3O_8 \cdot NaCl$ and meionite, $3CaAl_2Si_2O_8 \cdot CaCO_3$, easily remembered as 3 albite + NaCl and 3 anorthite + $CaCO_3$. Speaking as one who has spent a good deal of time on feldspars and carbonates, I think that meionite in particular has a friendly feel about it. Analyzed scapolites run from approximately 80 percent marialite to approximately 90 percent meionite, although almost all of the analyses cluster between 30 percent (70 percent marialite) and 80 percent meionite (Evans and others, 1969). Evans and others (1969) showed that these intermediate compositions do not lie on a simple binary join between the end members, and Papike (1964) indicated that the anion site can be filled with CO_3 at approximately 80 percent Me or, according to Evans and others (1969), Ca/(Ca+Na) = 0.75. Orville (1975) demonstrated that if Cl^- is present, the classic marialite-meionite join can exist. The Cl^- and $CO_3^=$ ions reside in equivalent cavities within the silicate structure, which is based on an Al-Si framework with tetragonal symmetry. The details and subtleties of the structure are still being investigated by several workers, and although complex and interesting, need not be considered for our present purposes.

Some scapolites contain quite a lot of sulfur, now known to be present as $SO_4^=$. We have synthesized and determined the stability relations of the end member scapolites $3NaAlSi_3O_8 \cdot NaCl$ (marialite), $3CaAl_2Si_2O_8 \cdot CaCO_3$ (meionite), and $3CaAl_2Si_2O_8 \cdot CaSO_4$ (sulfate meionite), and have determined the isothermal stability relations in the systems Ab-An-$CaCO_3$, Ab-An-$CaSO_4$, and the hybrid system arbitrarily containing one-half carbonate and one-half sulfate, all at 15 kbar and temperatures in the range 1000° to 1300°C (15 kbar is equivalent to a depth of about 50 km). In this temperature and pressure range, the Ca–end member scapolites $3An \cdot CaCO_3$ (meionite) and $3An \cdot CaSO_4$ (sulfate meionite) are stable, and phase relations at 1200°C and 15 kbar are shown in Figures 1 through 3.

Figure 1 is the system Ab-An-$CaCO_3$ at 1200°C and 15 kbar. The end member meionite is shown as $3An \cdot CaCO_3$. The horizontal line from this end member to point S represents the range of scapolite compositions that are stable under these conditions, point S being the most sodic composition. Thus, at 1200°C and 15 kbar, chlorine-free $CaCO_3$-scapolites are stable with Na/Ca ratios up to the equivalent of an $Ab_{40}An_{60}$ plagioclase. The three-phase triangle outlines the regions where calcite, plagioclase of the composition P, and the limiting scapolite S are in equilibrium. Bulk compositions to the left of this triangle do not produce scapolite, but calcite coexists with plagioclases from Ab_{100} to $Ab_{67}An_{33}$. The upper field on the calcic side of the three-phase triangle contains coexisting calcite and scapolite. Tie lines could be drawn in this field, radiating from the $CaCO_3$ apex to all of the scapolite compositions; the same could be done in the two-phase field of calcite and plagioclase.

The most interesting field in the diagram is that representing the coexistence of scapolite and plagioclase. Four experimentally determined tie lines in this region are shown, the limiting one to the left also being one side of the three-phase triangle. These tie lines connect the composition of scapolite in equilibrium with plagioclase.

The scapolites at 1200°C range in composition from pure meionite, which can only be in equilibrium with pure anorthite, to one represented by point S. Tie lines connect these scapolites with the appropriate plagioclase, ranging from An_{100} to $Ab_{70}An_{30}$. It is apparent that at this temperature a large range of scapolite solid solutions can exist in the absence of chlorine, or without substitution of the marialite end member as such. These data uphold the views of Evans and others (1969) and the observations of Orville (1975).

Figure 2 shows the system Ab-An-$CaSO_4$ at 1200°C and 15 kbar. The configuration of the diagram is very much like that in the

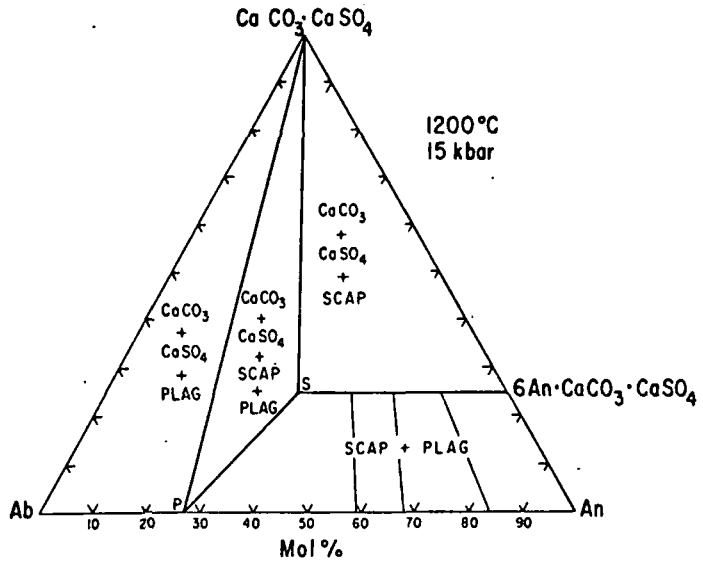

Figure 3. The system Ab-An-$CaCO_3$·$CaSO_4$ ($CaCO_3$ and $CaSO_4$ in equimolar proportions) at 1200°C and 15 kbar. The range of scapolite solid solutions stable at this temperature and pressure is from the end member 6An·$CaCO_3$·$CaSO_4$ to the composition S. Four experimentally determined tie lines in the field of scapolite + plagioclase are shown, the limiting one being the line SP, in which a hybrid scapolite of the composition S is in equilibrium with a plagioclase of the composition P. In the sodic portion of the system, calcite and anhydrite can coexist with a plagioclase of any composition between An_0 and An_{27}.

carbonate system, but sulfate-scapolites cover an even larger range of solid solutions. Point S, the limiting scapolite composition at 1200°C, has a plagioclase equivalent of $Ab_{47}An_{53}$. The sulfate scapolite can take even more albite component in solid solution without the need for Cl than can the carbonate scapolite. Three experimentally determined tie lines plus the limiting tie line S-P are shown. The range of compositions of plagioclase in equilibrium with the sulfate scapolites is also slightly larger than in the carbonate system.

The system containing one-half carbonate and one-half sulfate was investigated because of the observed association of these anions in subequal proportions in several analyzed scapolites (Knorring and Kennedy, 1958; Lovering and White, 1964). Figure 3 is the system Ab-An-$CaCO_3$·$CaSO_4$ at 1200°C and 15 kbar. The combination of anions produces a range of solid solutions that is somewhat greater than that for either the carbonate or sulfate scapolites; point S is at a plagioclase equivalent of $Ab_{52}An_{48}$, more than one-half of the distance along the join. Again, three experimentally determined tie lines plus the limiting tie line are shown.

The effect of temperature on the extent of the scapolite solid solutions and on the scapolite-plagioclase equilibria (tie lines) in these three systems has been examined at 1000°, 1100°, 1200°, and 1300°C. The solid-solution limits are difficult to determine and hence poorly known in the sulfate and hybrid system at 1000° and 1100°C; reaction rates are slower than in the pure carbonate system. Nevertheless, at least from 1100° to 1300°C, the range of solid solution is extended toward more sodic compositions with decreasing temperatures. This may not be a simple unidirectional effect, however. The effect of temperature on the scapolite-plagioclase equilibrium is of greater interest. Rather than show a series of isothermal diagrams such as those in Figures 1 through 3, the data can be more conveniently plotted as the ratio Na/Na+Ca in the plagioclase component of the scapolite against the same ratio in the plagioclase. This distribution of Na and Ca between scapolite and plagioclase in fact defines the tie lines as shown in Figures 1 through 3.

Figures 4 through 6 illustrate the effect of temperature on the scapolite-plagioclase equilibrium at 15 kbar. Figure 4 is for the carbonate-scapolites, Figure 5 for the sulfate scapolites, and Figure 6 for the 50:50 $CaCO_3$·$CaSO_4$ hybrid. The number of points is meager; generally four tie-line determinations at each temperature were carried out. The scatter is such that dashed curves are drawn, as the best estimate of the Na-Ca distribution. There is, however, a consistent trend; the scapolite becomes more sodic relative to the plagioclase with decreasing temperature. Thus the tie lines tend to "lean" more to the left as the temperature decreases. This effect is apparent in all three of the scapolite systems. The Na-Ca distribution between coexisting scapolite and plagioclase can thus be treated as a geologic thermometer, at least in the case of the more calcic plagioclases and essentially Cl-free scapolites. More precise determinations of these equilibria are desirable, and the effect of pressure should be evaluated, although more will be said about pressure shortly. Point D represents the composition of a scapolite

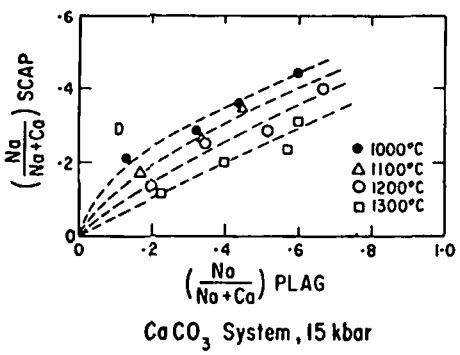

Figure 4. Plot of the ratio Na/Na+Ca in the plagioclase component of the carbonate scapolite against the same ratio in the plagioclase, for temperatures of 1000°, 1100°, 1200°, and 1300°C, at 15 kbar. The letter D represents the scapolite-plagioclase pair in the two-pyroxene granulite inclusions in the Delegate pipes, Australia (Lovering and White, 1964).

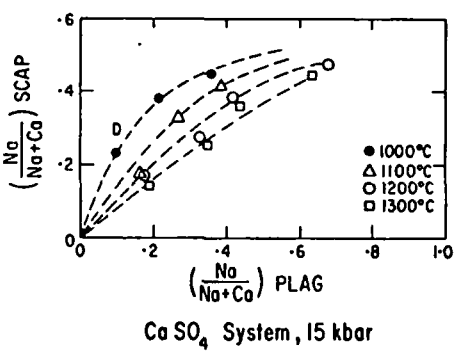

Figure 5. Plot of the ratio Na/Na + Ca in the plagioclase component of the sulfate scapolite against the same ratio in the plagioclase for temperatures of 1000°, 1100°, 1200°, and 1300°C, at 15 kbar. The letter D represents the scapolite-plagioclase pair in the two-pyroxene granulite inclusions in the Delegate pipes, Australia (Lovering and White, 1964).

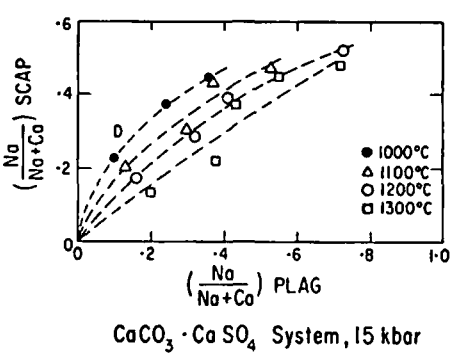

Figure 6. Plot of the ratio Na/Na+Ca in the plagioclase component of the hybrid carbonate-sulfate scapolite against the same ratio in the plagioclase, for temperatures of 1000°, 1100°, 1200°, and 1300°C, at 15 kbar. The letter D represents the scapolite-plagioclase pair in the two-pyroxene granulite inclusions in the Delegate pipes, Australia (Lovering and White, 1964).

coexisting with plagioclase in a 2-pyroxene granulite nodule from the Delegate pipes of Australia described by Lovering and White, which also will be considered shortly.

STABILITY RELATIONS OF THE END-MEMBER SCAPOLITES

There are a number of metamorphic localities in which almost pure anorthite coexists with calcite (Wenk, 1962; Misch, 1964). This would indicate that under the particular metamorphic conditions, the end-member meionite is not stable. Orville (1975) has recently published on the stability of scapolite in the system Ab-An-$CaCO_3$-NaCl at 750°C and 4 kbar. His results suggest that under these conditions pure meionite is unstable relative to anorthite and calcite, but that scapolite is stabilized by the presence of Na in the system. Figure 7 is taken from Orville's work and indicates that in the absence of Cl, a scapolite of limited range of compositions (about Ab-2An-$CaCO_3$; Orville uses the old term mizzonite for this composition) is in equilibrium with plagioclases from approximately $Ab_{60}An_{40}$ to $Ab_{15}An_{85}$. The field data (and Orville's results) thus indicate that pure meionite is unstable at moderate to low temperatures. Newton and Goldsmith (1975) have shown that the end member meionite is stable at temperatures of 1000°C, and remains so up to the melting curve which exceeds 1500°C at 20 kbar. The high-pressure breakdown to grossular, kyanite, quartz, and calcite in the range 25 to 30 kbar was also demonstrated by Newton and Goldsmith. We now have additional data showing that meionite becomes unstable relative to anorthite and calcite at between 850° and 900°C at 15 kbar and between 825° and 850°C at 8 kbar. The volume change of the reaction is quite small, and the equilibrium curve is steep. Thus, meionite is unstable at temperatures below 800°C, and in any geological range of pressures, scapolite can be produced in the reaction 3An + $CaCO_3$ ⇌ meionite only at temperatures somewhat greater than 800°C. These relations are shown in Figure 8, where the field of meionite is outlined by the limiting stability curve to the left, the melting curve to the right, and the high-pressure breakdown of meionite to grossular, kyanite, quartz, and calcite at the top. It is apparent that meionite is a high-temperature mineral, and one capable of existing at rather high pressures, as well.

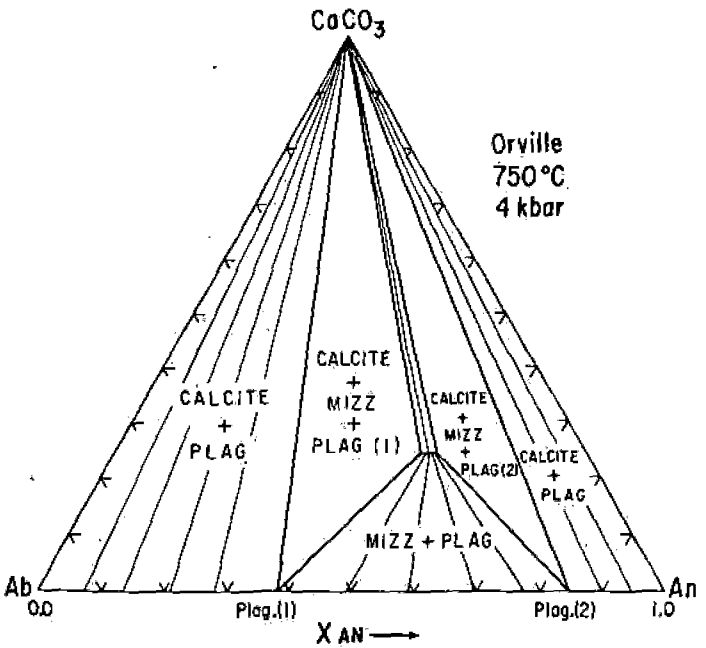

Figure 7. The system Ab-An-$CaCO_3$ at 750°C and 4 kbar, according to Orville (1975). The end member meionite is unstable under these conditions, and Orville's data indicate that the range of stable Cl-free scapolite compositions is quite limited and in the mizzonite region of the scapolite solid-solution series.

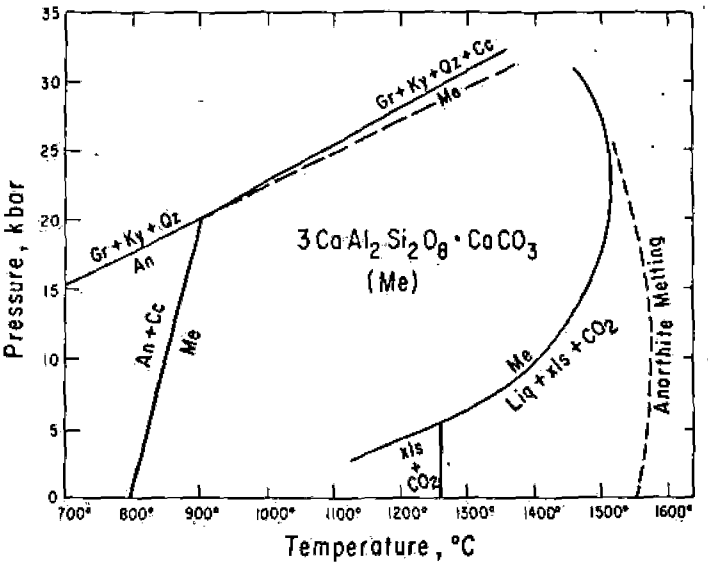

Figure 8. The stability relations of meionite, $3CaAl_2Si_2O_8 \cdot CaCO_3$. The continuous subsolidus-breakdown and melting curves are taken from Newton and Goldsmith (1976), as is the curve representing the reaction Me ⇌ Gr + Ky + Qz + Cc, the upper pressure limit of meionite. The steep curve for the reaction An + Cc ⇌ Me is based on reversed reactions at 8 and 15 kbar. Me = meionite, Gr = grossularite, Ky = kyanite, Qz = quartz, Cc = calcite, An = anorthite.

The pure sulfate-meionite also has interesting properties, and its *P-T* region of stability is shown in Figure 9. It is quite refractory, and at pressures above about 20 kbar, melts at higher temperatures than anorthite. The steeply rising melting curve is shown to the right, crossing the anorthite melting curve. At these high temperatures and pressures, $CaSO_4$ is present along the melting curve — a long way from sedimentary and evaporite conditions! The stability curve separating sulfate scapolite from the assemblage anorthite + anhydrite is the lower curve shown in Figure 9, with a negative slope. The stability curves for scapolites in Figures 8 and 9 were determined with the use of "reversed" reactions, that is, the reactions were made to run in both directions, and thus are true equilibrium boundaries. The melting curve projected to low pressures and projected stability curve intersect at approximately 2 kbar and 1530°C; thus at any temperature, sulfate meionite is stable only at elevated pressures and is unusual in that it is also favored by increasing temperature as well as pressure. The calculated curve for the high-pressure breakdown of sulfate meionite to grossular, kyanite, quartz, and $CaSO_4$ is shown at the top of the diagram. The shape of the stability field of the end member sulfate meionite indicates that the minimum temperature of existence of the scapolite is approximately 775°C at 17 kbar, and that sulfate-rich meionite could only be expected to exist under rather deep-seated and high-temperature conditions. Although generally metamorphic minerals, the Ca-rich scapolites are obviously stable in a temperature range high enough to crystallize as primary magmatic phases at depth, assuming an adequate supply of CO_2 and sulfate.

Textbooks of mineralogy and petrology, if they mention scapolites at all, generally leave the impression that although typically metamorphic minerals, they are formed by metasomatic activity, pneumatolytic alteration, or for the most part by secondary or retrogressive processes. Barth, in the 1952 edition of his book *Theoretical Petrology* (p. 283-284) stated, "It is expedient to re-

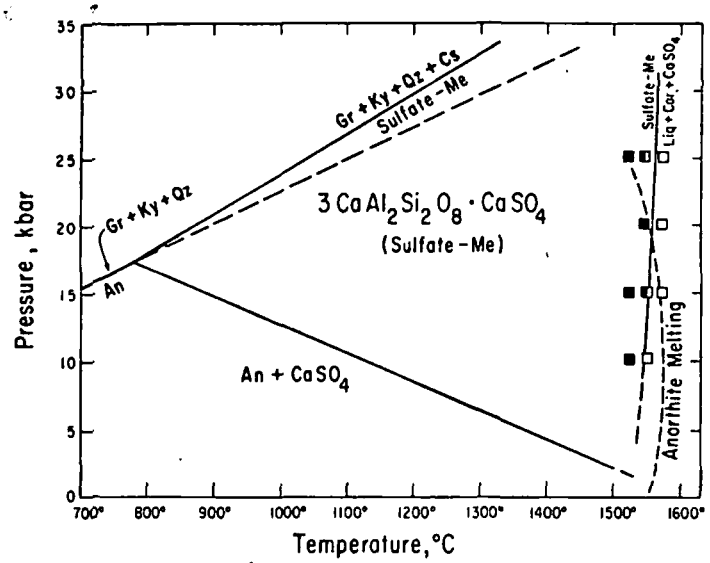

Figure 9. The stability relations of sulfate-meionite, $3CaAl_2Si_2O_8 \cdot CaSo_4$. The steep melting curve is from data of Newton and Goldsmith (1976). The dashed curve for the melting of anorthite is taken from unpublished data of Newton and Goldsmith. The curve for the upper pressure limit of sulfate-meionite, the reaction sulfate Me $\rightleftharpoons$ Gr + Ky + Qz + $CaSO_4$ is from Newton and Goldsmith (1976). The flat curve with the negative slope represents the reaction An + $CaSO_4 \rightleftharpoons$ sulfate Me. Me = meionite, Gr = grossularite, Ky = kyanite, Qz = quartz, An = anorthite, Cs = calcium sulfate.

gard meionite and marialite as the low-temperature 'modifications' of anorthite and albite, respectively." He developed a diagram that geometrically resembles the plagioclase melting loop, with plagioclases on the top curve and scapolites on the bottom. It was suggested that any stable plagioclase, on cooling in the presence of carbonate-bearing solutions, will thus break up into a more calcic scapolite and a more sodic plagioclase. Interestingly, the entire discussion of scapolites was omitted from the 1962 revision (Barth, 1962). Similarly, Fyfe and Turner (in Fyfe and others, 1958), in agreement with Barth, present a hypothetical scapolite stability diagram, in which scapolite is shown to be on the low-temperature side of the curve that represents the reaction scapolite $\rightleftharpoons$ anorthite + calcite. These and other authors had little information with which to operate. No one had data indicating that the equilibrium relationship has the opposite sense — that scapolite is the stalwart or that scapolite takes over from the weaker combination when things get hot.

If this is an unexpected result, it points up the importance of experimental petrology as an adjunct to field and theoretical approaches. It is another example of Bowen's (1938) plea for "Mente et Malleo Atque Catino," for here both field observations and theorizing led to the wrong conclusion. I should hasten to add, however, that sloppy experimental work, particularly that in which little care is exercised in the attainment of equilibrium, can make unreserved fools of experimentalists.

Our very recent experiments have shown that marialite is stable relative to albite plus NaCl in a high-temperature range down to at least 800°C, a fact not anticipated by Orville (1975) in his work at 750°C but not at variance with it. We have not been able to determine the lower-temperature stability boundary of marialite by our methods. Our data, in conjunction with those of Orville (1975) would place a boundary between 750° and 800°C in the pressure range 0 to 8 kbar, with a steep dP/dT slope. Thus, the general appearance of the marialite stability diagram would be very similar to that of meionite. This matter will not be pursued further because of the fact that chlorine has been found to be present only in trace amounts in the scapolites of deep-seated origin considered here. We have already seen that scapolite can contain rather large amounts of the sodic component without needing chloride ions, and furthermore chlorides are not abundant in the lower crust. Marialite scapolites are probably most prevalent in metamorphosed sediments containing halite (Hietanen, 1967) or rocks in which chlorides have been metasomatically introduced (Edwards and Baker, 1953). If scapolites were to form in association with the common native minerals of the lower crust, one would expect rather calcic scapolites containing carbon (carbonate) and sulfur (sulfate), if only on the basis of the elements that are available.

The only experimental data on the stability of the intermediate Na-Ca scapolites are the limited data of Orville (1975), as shown in Figure 7. Orville (1975) has shown that the sodic component stabilizes the carbonate scapolite to lower temperatures, and one might assume a similar effect in the case of the Na-Ca sulfate scapolites, but that would be guesswork. Although we have investigated the tie lines in the $CaCO_3 \cdot CaSO_4$ hybrid system, nothing has been done on the effect of a varying $CaCO_3$-$CaSO_4$ ratio on the P-T relations on the scapolite stability field. It is not too difficult, however, to imagine states intermediate between those shown in Figures 8 and 9, representing intermediate compositions. Another unknown is the effect Na may have on stabilizing the sulfate-scapolite to lower pressures, although it is not unreasonable to expect it to do so. This multicomponent system with both P and T as variables has hardly been touched.

ROLE OF SCAPOLITES IN CRUST

We have seen that the lime-rich compositions are very refractory — perhaps surprisingly so, considering that they contain what we usually think of as volatile substances. Goldsmith and others (1974) showed that a marialite with nitrate in place of chloride was stable to fairly high temperatures at elevated pressures. At elevated temperatures and pressures, calcic feldspar is unstable in the presence of carbonate and (or) sulfate (or CO_2 or oxidized sulfur), and Ca-rich scapolite is formed. Figures 8 and 9 show that for both the carbonate and sulfate end members, the temperature must be greater than 800°C for scapolite to form. As we have seen, the presence of Na will stabilize scapolite at lower temperatures, and calcite plus a plagioclase containing some albite will react at temperatures well below 800°C.

Lovering and White (1964), using as a basis their analysis of the scapolite occurrences in granulite nodules from the Delegate pipes in Australia, suggested that the lower crust beneath Australia may contain as much as 5 percent scapolite as a primary phase. Dawson (1964, 1968, 1971) has noted the presence of scapolite in calc-silicate granulites in kimberlite diatremes, and stated (1971), "... it is a possibility that the granulite xenoliths in kimberlites were perhaps derived from lenses or layers of granulite at the base of the crust or in the extreme upper levels of the upper mantle." As indicated above, scapolite has now been observed in granulite inclusions from three continents and may be more common than the published record shows, for there is a tendency to preferentially collect and examine the more basic xenoliths, presumed to have come from the mantle. It is fair to say that the extent to which meionitic scapolite exists in the lower crust is largely dependent on the availability of carbonate and sulfate as well as on the distribution of basic plagioclase.

The words scapolite and granulite are associated in the title of this address. It appears to me that most of the Ca-rich scapolites occur in granulites or related high-grade rocks; Fyfe and others (1958) have suggested that scapolite is a granulite-facies mineral. Several considerations that relate composition and P-T stability to this association favor a hypothesis that granulites are the typical lower-crustal rocks of much of the continental areas. More about this follows.

The Delegate pipe material is one of the few documented examples of analyzed scapolite from the deep earth. Is it possible to draw some conclusions as to the pressure and temperature conditions of its formation? Lovering and White (1964) report a high sulfur content, as much as 72 percent of the carbon (in carbonate) replaced by S (now known to be sulfate) in the scapolite of one of the two types of granulites they have examined. A plagioclase of An_{89} is associated with the scapolite. This material is plotted as the letter *D* in Figures 4 through 6; from our tie-line data, we must conclude that this scapolite-plagioclase pair equilibrated at a temperature below 1000°C. Thus it is unlikely that this pair is a primary igneous association directly related to the magmatism which carried it close to the surface. It is more likely that the scapolite is a primary metamorphic constituent of an assemblage which may be quite representative of the constitution of much of the lower crust of eastern Australia. Irving (1974) also made this interpretation of the scapolite-bearing, two-pyroxene granulites from the Delegate occurrence on the basis of textures and trace elements. This use of the scapolite-plagioclase pair as a geothermometer assumes no significant pressure correction; it has been investigated only at 15 kbar.

There is little doubt that much of the carbonate in the deep-seated scapolites comes from the mantle. Newton and Sharp (1975) present evidence against the presence of free CO_2 in the upper mantle, for the assemblage $MgCO_3 + MgSiO_3$ is stable relative to Mg_2SiO_4 and CO_2, at least under subcontinental environments. Whether the carbonate groups in scapolite came from gaseous CO_2 or from CO_2 in solution in a melt or even as a solid carbonate would make little difference to the scapolite, however; in any case, there is certainly oxidized carbon in the upper mantle. Touret (1971) stated that CO_2 is given off by the crystallization of deep-seated basic intrusions containing CO_2 in solution, and that the CO_2 permeates the metamorphic terrane in a wave of dry regional granulite metamorphism. If, however, the intrusions crystallize at the level of the lower crust, the CO_2 would crystallize in primary igneous scapolite, and the scapolite would re-equilibrate with plagioclase as the intrusion cooled.

We have seen in Figure 9 that the pure sulfate-meionite is a true high-pressure mineral favored by both high pressures and high temperatures. The sulfate content of scapolite thus has the potential of yielding information on the pressure of crystallization or equilibration. Before it can be useful as a geobarometer, however, it must be calibrated as a function of composition. The effect of the CO_3/SO_4 ratio and of the Na/Ca ratio on the slope of the stability boundary must be known. This is a large order, and it means working out the *P-T* stability relations in the 4-component system Ab-An-$CaCO_3$-$CaSO_4$. It is not likely, however, that the substitution of Na will have a great effect on the *slope* of the stability boundary, for the volume change with substitution is small. It will shift the equilibrium to lower temperatures, however, and the reaction will become divariant. In the Na-free system, as sulfate replaces carbonate, the steep stability curve of meionite (Fig. 8) must steepen even more, become vertical, then become negative and approach the flat negative slope of the sulfate end member. Thus, the sulfate-rich meionites are potentially excellent geobarometers, assuming that the presence of Na and the development of divariancy does not drastically alter the shape of things.

The Delegate scapolite has nearly a 4:1 Ca/Na ratio, and the sulfate substitution of 70 percent or more is large enough to make tempting the claim for a deep-seated origin, even if no ancillary evidence were available and with no data on the effect of Na. This view is strengthened by the published analyses of scapolites (Shaw, 1960a; Deer and others, 1963); those with high sulfur content all appear to be from deep-seated sources.

Is sulfur always available at depth? Brimstone is surely associated with volcanic fires, but little attention has been given to the abundance and state of sulfur in the mantle. Presumed upper-mantle rocks contain sulfur in sulfides, and I am not aware of any report of sulfate in kimberlites and peridotites; if it *were* to be noted, it might well be passed off as an alteration product. Is the sulfate in scapolite derived from reaction with sulfides or other forms of reduced sulfur from the mantle? Very probably so, and it is likely that oxidation takes place by a ferrous-ferric equilibrium with deep crustal minerals, and with no transfer of oxygen or need for other oxidizing agents. A bare-bones simplification, with ions pulled out of their silicate and oxide context would be:

$$\underset{\text{(in sulfide)}}{S^{=}} + \underset{\text{(in magnetite)}}{4\ Fe_2O_3} \rightleftharpoons \underset{\text{(in scapolite)}}{SO_4^{=}} + \underset{\text{(in silicate)}}{8\ FeO}$$

We do see sulfur as well as carbon brought in one form or another to the surface. Sulfur, SO_2, SO_3, or even sulfate are associated with volcanism; we must assume that in basaltic volcanoes, it has been rather quickly brought up from the mantle with little chance for oxidation. Carbon also acts as a traveler in the crust, explosively rammed through in kimberlite diatremes. Aside from diamonds, which may be residents of the mantle, but surely transients in the crust, carbon as carbonate or CO_2 should react with plagioclase in the deep crust and assume residential status as scapolite. The sulfur that becomes oxidized should do the same, and the existence of sulfate-bearing scapolite in deep-crustal xenoliths is good evidence that this is what takes place.

We have seen the need for a deep, hot situation for Ca-rich scapolite. Just as the sulfate-rich scapolites come from depths, the meionites also come from hot spots; the most Ca-rich known is from Monta-Somma, a pyrometamorphic occurrence. In fact, the *P-T* conditions (especially *T*) for nearly pure meionite are so stringent that they surely cannot be met along a normal geothermal gradient but could only be satisfied by such a locally hot situation. A reasonable amount of Na in the system lowers the temperature needed for stability, and more sodic scapolites settle for less severe conditions. The granulite facies represents the highest grade of regional metamorphism in the crust, and may well offer the minimal conditions needed for the Ca- and S-rich scapolites, at least. It is unlikely that scapolite exists in the eclogite facies, for we have seen that the upper pressure limit, where scapolites break down to isochemical assemblages containing garnet, kyanite, quartz (Figs. 8 and 9), and presumably jadeite if Na is present, is close to that of the equivalent feldspar. Granulites are thought of in terms of regional metamorphism — but where is the "region"? Is metamorphism always the result of an "event"? Many insinuate that it is, yet is it not more reasonable to assume that this type of regional metamorphism is a normal form of subcontinental deep-crustal behavior? This view is a throwback to the concept of successive depth zones, the catazone being the home of granulites and related rocks. Granulites are from deeply eroded Precambrian gneissic areas — from where else should they come but the lower crust? Their variability is an expression of crustal inhomogeneity, and metamorphic grade may be related to a "local" geothermal gradient, strongly affected by intrusion of molten material from the mantle.

Granulites are known as dry rocks. Bowen (1947), in arguing against a high water content in basaltic magma at depth and pointing out the dry nature of deep-zone metamorphic rocks, said, "One possible interpretation of this situation is that the temperature in the deeper zones is too high for the formation of the hydrous minerals even at the high pressure there prevailing; but a more probable interpretation is that the principal source of water for rocks is at the surface or at shallow depths, and the mechanical barriers to the penetration of such water to great depths are al-

together effective." We now know that hydrous minerals are stable in the deeper zones; granulites *are* dry because of the absence of water. One might also argue that granulites are granulites and not amphibolites, at least in part because of this reason (Gjelsvik, 1952; Yoder, 1952; Poldervaart, 1953; Thompson, 1955; Buddington, 1963; Misch, 1964, p. 354; Touret, 1971). Furthermore, Bowen was unaware of the mechanism of carrying water to deep rocks by subduction. It is quite possible that a revealing geographic restriction can be placed on granulites — might they be indicators of relatively stable regions of the deep continental crust removed from those areas in which subduction has taken place? A listing of the classic granulite localities reads like a recitation of such ancient and stable areas of the world.

The role of water in the structure of scapolites and its relations to the stability of these minerals become important with respect to the anhydrous nature of granulites. Many of the scapolite analyses show H_2O to be present, but one is hard put to avoid contamination. Shaw (1960a) states that the water seen in the analyses is of uncertain significance, but the possibility of structurally bound water is not discounted. Zoisite and meionite have chemical compositions that differ only with respect to the anionic group:

scapolite: $3CaAl_2Si_2O_8 \cdot CaCO_3$

zoisite: $3CaAl_2Si_2O_8 \cdot Ca(OH)_2$

We have found that in the experimental runs made on meionite at temperatures of approximately 900°C or below, great pains had to be taken to avoid the crystallization of zoisite at the expense of the scapolite. Not only was it necessary to thoroughly dry the reactants before welding shut the platinum capsule that contained them, but the entire assembly had to be baked out. Any source of H_2O within the capsule or of hydrogen in the external setup, including that formed from the decomposition of H_2O at elevated temperature, must be avoided. H_2 readily diffuses through the platinum, reduces the carbonate to carbon, and the water thus formed reacts with the charge to produce zoisite. Here is still another system that needs study, for the equilibrium relations between zoisite and meionite are functions of P, T, and the partial pressures of CO_2 and H_2O. It is apparent that zoisite and scapolite have an antithetical relationship and that water would hardly be expected to be a component of meionite. It is most probable, however, that as Na enters the scapolite structure, the need for large CO_2/H_2O ratios becomes less stringent. The existence of Na-containing scapolites in epidote-amphibolite rocks and even in the greenschist facies (Hietanen, 1967) would indicate that increasing Na permits a tolerance for water, as does the recent experiment of Milhollen (1974), in which a scapolite of the composition 2An + 1Ab + $CaCO_3$ was formed in the presence of a liquid in a nepheline syenite melt, with vapor rich in CO_2 and H_2O at pressures above 3 kbar. Hietanen (1967) points out the increased Na content of scapolite and the accompanying progressive decrease in metamorphic grade with distance from the Idaho batholith, in the St. Joe–Clearwater region, Idaho. This effect is analogous to the breakdown of plagioclase in the presence of water to form zoisite (epidote). Calcic plagioclase reacts to form zoisite and an albitic plagioclase, and the more sodic plagioclases are more resistant to this alteration at low temperatures.

A hot, dry environment is what a lime-rich scapolite wants, and that is just what a granulite has. Touret (1975) considers granulites to be catazonal rocks in which metamorphism takes place in the presence of a water-free and CO_2-rich fluid phase, the CO_2 presumably coming from the upper mantle. Touret noted that high-density, CO_2-rich fluid inclusions are abundant in granulite facies rocks from all over the world. From the location and features of these rocks, he modeled the distribution of fluids within the continental crust and suggested that CO_2 is concentrated in the lower crust, between the Conrad and Mohorovičić discontinuities. Our data suggest that Touret's picture of volatiles in the lower crust should be modified. Mafic compositions surely have prevailed at Earth levels equivalent to the present lower crust, and this region must have acted as a trap for oxidized carbon and sulfur. CO_2 would not be in the form of included fluids, but would be locked up as scapolite. Much of the work done on fluid inclusions by Touret has been in acidic quartz-feldspathic rocks with which CO_2 could not react. Figures 1 through 3 show that in the absence of chlorine, scapolites are not stable in the Na- and Si-rich portions of the systems.

Those parts of the present lower crust that are appropriately basic must still be acting as a "getter" for sulfur and CO_2 coming from the deeper earth. The lower crust could be a principal place of residence for these volatile elements, and, in the case of sulfur, might be one of the more important repositories in the Earth. Deep continental drilling in selected sites might give us some insight into these and other aspects of the lower crust, although justifying such activity for scientific purposes is not an easy thing to do.

The carbon and sulfur are readily freed to the upper crust and atmosphere, and ultimately to the biosphere by any activity that takes scapolite out of its field of stability. If calcic scapolite is carried upward by diastrophic or volcanic processes, it will ultimately decompose at the elevated temperatures and low pressures. If water is carried down to it by subduction, it may also decompose, depending upon the Na content and H_2O/CO_2+SO_3 ratio. In general, with respect to Ca-rich varieties, the retrogressive processes that are commonly considered to produce scapolite (see, for example, Misch, 1964) are probably the very processes that destroy it. It is not too far fetched to assume that most of the CO_2 (and SO_2) of the air we breathe and therefore the carbon of our bodies has at one time been in scapolite. It is unlikely that the carbon cycle operates as deeply as the lower crust, and although subduction may carry quantities of carbon into the mantle and thus recycle some of us, we, the crumbs of the upper crust, are hardly in equilibrium with scapolites of the nether regions.

ACKNOWLEDGMENTS

This research was supported by the Earth Science Section, National Science Foundation, Grants DES74-22851 and DES72-01535. I would also like to acknowledge the general support of the Materials Research Laboratory of the National Science Foundation. Robert C. Newton was a partner in all of the research reported here. I am also indebted to Robert C. Newton, J. V. Smith, and Lelde Kalmite for suggesting changes that have materially improved the manuscript.

Note Added In Proof: My attention has been called to several publications by A. F. Wilson that contain views quite similar to some presented here. At this time, only one of these publications is available to me (Wilson, A. F., 1969, Problems of exploration for metals in granulite terrains, with particular reference to Australian localities: Geol. Soc. Australia, Spec. Pubs. No. 2, p. 375–376). Wilson calls attention to the very high sulfur content of some of the scapolites from the Musgrave Ranges of central Australia and states that "although granulites are normally considered to be very 'dry' rocks, chemical analyses show that large amounts of normal 'volatile substances' that are involved in hydrothermal mineralisation are fixed in many granulites." He also states that "scapolite is much more widespread in granulites than is generally recognized. It is superficially like plagioclase." He further indicates, referring to Lovering and White (1964), that portions of the deep crust may contain large amounts of sulfur in the scapolite structure and that retrograde metamorphism must release sulfur which could be available for reaction with metals that are released from pyroxenes to form minerals of economic interest.

REFERENCES CITED

Barth, T.F.W., 1952, Theoretical petrology: New York, John Wiley & Sons, Inc., 387 p.

——1962, Theoretical petrology (2nd ed.): New York, John Wiley & Sons, Inc., 416 p.

Bobrievich, A. P., and Sobolev, V. S., 1957, Eclogitization of the pyroxene crystalline schists of the Archean complex [in Russian]: Zap. Vses. Mineralog. Obschestva, V. Ser., v. 86, p. 3–17.

Bowen, N. L., 1938, Mente et malleo atque catino: Am. Mineralogist, v. 23, p. 123–130.

——1947, Magmas: Geol. Soc. America Bull., v. 58, p. 263–280.

Buddington, A. F., 1963, Isograds and the role of H_2O in metamorphic facies of orthogneisses of the northwest Adirondack area, New York: Geol. Soc. America Bull., v. 74, p. 1155–1182.

Cox, K. G., Gurney, J. J., and Harte, B., 1973, Xenoliths from the Matsoku pipe, *in* Nixon, P. H., ed., Lesotho kimberlites: Maseru, Lesotho Natl. Devel. Corp., p. 76–100.

Dawson, J. B., 1964, Carbonate tuff cones in northern Tanganyika: Geol. Mag., v. 101, p. 129–137.

——1968, Recent researches in kimberlite and diamond geology: Econ. Geology, v. 63, p. 504–511.

——1971, Advances in kimberlite geology: Earth-Sci. Rev., v. 7, p. 187–214.

Deer, W. A., Howie, R. A., and Zussman, J., 1963, Rock-forming minerals: Vol. 4, Framework silicates: London, Longman Group Ltd., 435 p.

Edwards, A. B., and Baker, G., 1953, Scapolitization in the Cloncurry district, northwestern Queensland: Geol. Soc. Australia Jour., v. 1, p. 1–33.

Evans, B. W., Shaw, D. M., and Haughton, D. R., 1969, Scapolite stoichiometry: Contr. Mineralogy and Petrology, v. 24, p. 293–305.

Fyfe, W. S., Turner, F. J., and Verhoogen, J., 1958, Metamorphic reactions and metamorphic facies: Geol. Soc. America Mem. 73, 259 p.

Gjelsvik, T., 1952, Metamorphosed dolerites in the gneiss area of Sunnmøre on the west coast of southern Norway: Norsk Geol. Tiddskr., v. 30, p. 33–134.

Goldsmith, J. R., Newton, R. C., and Moore, P. B., 1974, Silicate-nitrate compounds: High-pressure synthesis and stability of a nitrate scapolite: Am. Mineralogist, v. 59, p. 768–774.

Hietanen, A., 1967, Scapolite in the Belt series in the St. Joe–Clearwater region, Idaho: Geol. Soc. America Spec. Paper 86, 56 p.

Irving, A. J., 1974, Geochemical and high pressure experimental studies of garnet pyroxenite and pyroxene granulite xenoliths from the Delegate basaltic pipes, Australia: Jour. Petrology, v. 15, p. 1–40.

Knorring, O. von, and Kennedy, W. Q., 1958, The mineral paragenesis and metamorphic status of garnet-hornblende-pyroxene-scapolite gneiss from Ghana (Gold Coast): Mineralog. Mag., v. 31, p. 846–859.

Lovering, J. F., and White, A.J.R., 1964, The significance of primary scapolite in granulitic inclusions from deep-seated pipes: Jour. Petrology, v. 5, p. 195–218.

Milhollen, G. L., 1974, Synthesis of scapolite under magmatic conditions: Am. Mineralogist, v. 59, p. 618–620.

Misch, P., 1964, Stable association wollastonite-anorthite and other calc-silicate assemblages in amphibolite facies crystalline schists of Nanga Parbat, northwest Himalayas: Beitr. Mineralogie u. Petrographie, v. 10, p. 315–356.

Newton, R. C., and Goldsmith, J.R., 1975, Stability of the scapolite meionite ($CaAl_2Si_2O_8 \cdot CaCO_3$) at high pressures and storage of CO_2 in the deep crust: Contr. Mineralogy and Petrology, v. 49, p. 49–62.

——1976, Stability of the end-member scapolites: $3NaAlSi_3O_8 \cdot NaCl$, $3CaAl_2Si_2O_8 \cdot CaCO_3$, $3CaAl_2Si_2O_8 \cdot CaSO_4$: Zeitschr. Kristallographie (in press).

Newton, R. C., and Sharp, W. E., 1975, Stability of forsterite + CO_2 and its bearing on the role of CO_2 in the mantle: Earth and Planetary Sci. Letters, v. 26, p. 239–244.

Orville, P. M., 1975, Stability of scapolite in the system Ab-An-NaCl-$CaCO_3$ at 4 kb and 750°C: Geochim. et Cosmochim. Acta, v. 39, p. 1091–1105.

Papike, J. J., 1964, The crystal chemistry and crystal structure of scapolite [Ph.D. thesis]: Minneapolis, Univ. Minnesota.

Poldervaart, A., 1953, Metamorphism of basaltic rocks, a review: Geol. Soc. America Bull., v. 64, p. 259–274.

Shaw, D. M., 1960a, The geochemistry of scapolite: Pt. I. Previous work and general mineralogy: Jour. Petrology, v. 1, p. 218–260.

——1960b, The geochemistry of scapolite: Pt. II. Trace elements, petrology and general geochemistry: Jour. Petrology, v. 1, p. 261–285.

Sobolev, V. S., ed., 1959, The diamond deposits of Yakutia: Moscow, 527 p.

Thompson, J. B., Jr., 1955, The thermodynamic basis for the mineral facies concept: Am. Jour. Sci., v. 253, p. 65–103.

Touret, J., 1971, Le faciès granulite en Norvège meridionale. Pts. I and II: Lithos, v. 4, p. 239–249, 423–436.

——1975, Faciès granulite et fluids carbonique, *in* Belliére, J., and Duchesne, J. C., eds., Geologie des Domaines Cristallins: Liege, Soc. Géol. Belgique, p. 267–287.

Verhoogen, J., 1938, Les pipes de kimberlite de Katanga: Annales Services Mines, Comité Special du Katanga, v. 9, p. 3–46.

Wenk, E., 1962, Plagioklas als indexmineral in den zentralalpen: Schweizer. Mineralog. u. Petrog. Mitt., v. 42, p. 139–152.

Yoder, H. S., Jr., 1952, The MgO-Al_2O_3-SiO_2-H_2O system and the related metamorphic facies: Am. Jour. Sci. (Bowen volume), p. 569–627.

MANUSCRIPT RECEIVED BY THE SOCIETY SEPTEMBER 26, 1975

Printed in U.S.A.

VOLUME 70 NUMBER 2

THE JOURNAL OF GEOLOGY

March 1962

SILICA SOLUBILITY, 0°–200° C., AND THE DIAGENESIS OF SILICEOUS SEDIMENTS[1]

RAYMOND SIEVER
Harvard University, Cambridge, Massachusetts

ABSTRACT

The data on solubility of amorphous silica and quartz at low temperatures are reviewed. Determinations of the metastable equilibrium solubility of amorphous silica at 25° C. in distilled water and artificial sea water give values of about 140 p.p.m., in agreement with earlier workers' results. Solubility in simulated oil-field brines of 30,000 and 50,000 p.p.m. is about the same. Solubility was drastically reduced in peat waters, presumably due to adsorption of organic material on free silica surfaces. Quartz solubility was determined between 125° and 181° C. in sealed bombs; the results interpolate well between the lower temperature data of Van Lier and the higher temperature data of Kennedy. The solubility of quartz under directed stress at 95° C. approximates that of amorphous silica at the same temperature.

Diagenetic changes in silica content of sediments, in particular the origin of chert and silica cementation of sandstones, are explained by the metastability of amorphous silica, the dissolution of biogenic amorphous silica, the effects of increased ionic strength of subsurface formation waters on silica and carbonate solubility, the equilibria between clay minerals of differing Si/Al ratios, the action of clays as semipermeable membranes, and the effects of pressure and temperature increase on burial.

A large number of papers on the solubility of silica have appeared in the past decade, and attempts have been made to relate these fundamental data to the occurrence of primary and secondary silica in sedimentary rocks. It is the purpose of this paper to summarize and integrate this information, to add to the data on solubility of silica below 200° C., and to examine carefully the bearing these data have on the precipitation of various forms of silica in sediments after deposition. In the discussion, I shall draw on the pertinent general geologic and petrographic information.

I. Silica Solubility

In the discussion of solubility one must distinguish between the different silica polymorphs, for they do not have the same solubility. Because this paper is concerned only with sedimentary rocks, the two silica species that are of interest are ordinary low quartz and amorphous silica. In the range of temperature under consideration, 0°–200° C., low quartz is the stable form of SiO_2. In this range amorphous silica is metastable, but because of the sluggishness of the inversion to quartz at low temperatures, it may be characterized by a metastable equilibrium solubility. Included as amorphous silicas are the different varieties of hydrated and dehydrated silica gels, silica glass, siliceous sinters, opals, and the skeletal remains of silica-secreting organisms, such as diatoms, radiolaria, and siliceous sponges. A more complete discussion of the forms of solid silica found in sediments can be found in an earlier paper (Siever, 1957).

Amorphous silica solubility

The metastable equilibrium solubility of amorphous silica in the range 0°–200° C. is

[1] Published under the auspices of the Committee on Experimental Geology and Geophysics and the Department of Geological Sciences at Harvard University. Manuscript received April 4, 1961.

now fairly well known. It has been established that there is a definite solubility value and that this value differs only slightly from one kind of amorphous silica to another. Iler (1955) has summarized the literature on this subject up to 1954. Since that time papers have appeared (by Krauskopf [1956, 1959], White, Brannock, and Murata [1956], Okamoto [1957], and Greenberg [1957]) that have confirmed and extended conclusions reached earlier. The solubility of amorphous silica is fairly well known up to 200° C. but

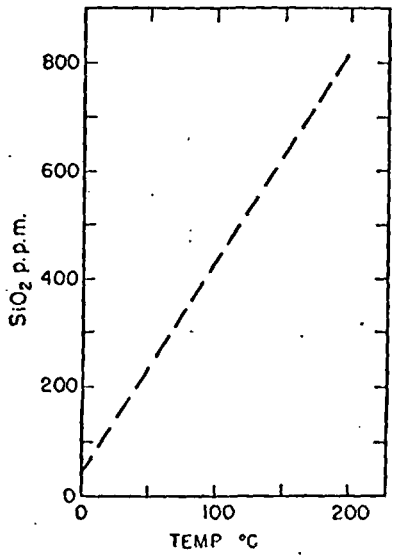

FIG. 1.—The solubility of amorphous silica as a function of temperature (after Alexander *et al.*, 1954).

less well known above that point. Using silica glass, Kennedy (1950) gives some data for higher temperatures. The curve for temperature versus solubility is given in figure 1.

The solubility of amorphous silica at 25° C. as a function of pH has been measured by a number of workers and, in the past, has been the subject of some dispute. Although Correns (1941) found that the solubility steadily increases with higher pH above pH5, later workers have confirmed the work of Alexander *et al.* (1954), which indicated that the solubility of amorphous silica as monomeric silicic acid, H_4SiO_4, was independent of pH from pH values 2 to about 9.5. At higher pH values the solubility does increase, mainly as a result of ionization of H_4SiO_4. It is not clear wherein the discrepancy between Correns' and the others' data lies, but repeated experiments with many different starting materials, approaching equilibrium from both under- and supersaturated solutions, indicate that Alexander *et al.* are correct.

QUARTZ SOLUBILITY

The solubility of quartz below 200° C. has been little studied, mainly because the rate of dissolution is so slow at these temperatures. An additional difficulty is the fact that quartz does not precipitate readily from low-temperature solutions so that solubility values cannot be easily demonstrated to be equilibrium figures by precipitating from supersaturated solutions as well as dissolving from undersaturated ones. The lowest-temperature runs made by Kennedy (1950) were at 160° and 182° C. Figures were reported by Gardner (1938) and Lenher (1921) as 6 and 30 p.p.m., respectively. Van Lier (1959) carefully and systematically measured the solubility of quartz between 60° and 100° C. Fournier (1960) has reported data at 84° and 165° C.

EXPERIMENTAL METHODS

Quartz used for solubility studies reported here was prepared by hand picking optically clear quartz crystals (Hot Springs, Ark.) then crushing and grinding them to appropriate sizes. Very fine sizes were prepared by settling in glass cylinders. Coarser grades were prepared by sieving after first running a throw-away sample through the sieves to reduce the possibility of contamination. Different sized samples were then treated with 1 *N* hydrofluoric acid for one minute to remove any disordered surface layers of amorphous silica produced in the grinding and crushing process. Powders were then washed with dilute alkali, followed by three successive distilled water washings.[2] A size check on the fine powders

[2] This preparation, similar to the one used by van Lier (1959), is absolutely necessary if all traces of amorphous silica, Na^+, and F^- ions, which affect the solubility, are to be removed from the samples.

showed no appreciable decrease in size after the HF treatment.

Amorphous silica powders were prepared by running sodium silicate solutions (prepared from reagent grade sodium silicate) through an ion-exchange column of Nalcite HCR resin in order to remove all sodium, and then evaporating to dryness. Synthetic opal was prepared by making a supersaturated silica sol free of Na and by drying very slowly. The product was a glassy clear, hard, brittle solid that gave an amorphous silica X-ray diffraction pattern (Warren and Biscoe, 1938).

Long-term solubility runs at room temperatures were made in polyethylene bottles, with periodic checks made of water loss by transpiration through the polyethylene. Such loss was negligible except in runs that ran longer than six months. Higher-temperature runs were made in reaction vessels, machined from a nickel stainless steel, and were heated for 24 hours at 400° C. in order to form an oxide coating (Kennedy, 1950). Teflon O-rings were first used and then rejected, because of contamination of solutions by F^- ion. Neoprene O-rings proved satisfactory. Several blanks were run with each vessel; these showed no contamination with materials that might affect quartz solubility. The design of the reaction vessels is shown in figure 2, *a* and *b*. Vessel B proved more satisfactory for the runs between 150° and 200° C., and all later runs were made with this vessel. No attempt was made to control pressure—rather, the systems were completely closed after filling to one-half capacity and so under autogenous water-vapor pressure.

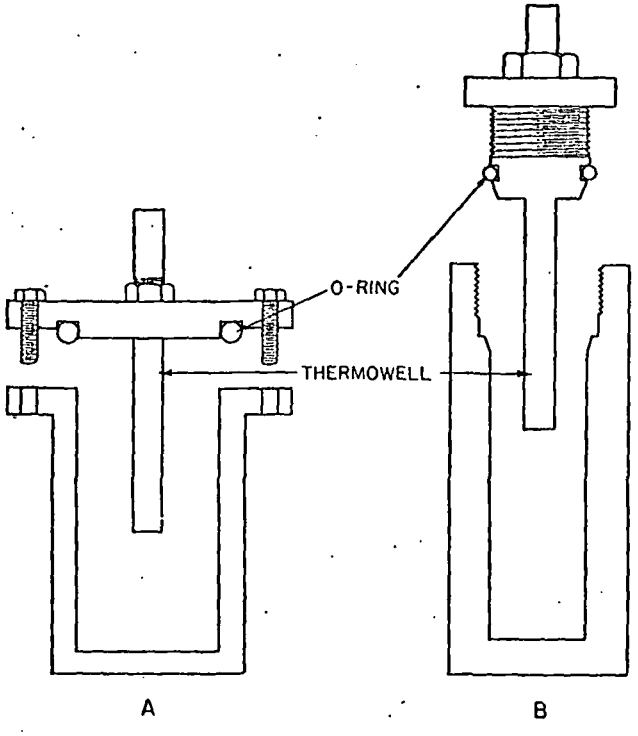

FIG. 2.—Pressure vessels used in solubility determinations

Temperature was controlled by immersing the vessels completely in a stirred high-temperature wax bath with thermostatic control. The temperatures in the bath and in the thermowell in the vessels were measured by calibrated mercury thermometers. Temperature excursion of the sample in the wax bath was less than $1\frac{1}{2}$° C. Temperature gradients within the vessel were negligible.

At the conclusion of each run the vessel was rapidly quenched, the sample of solution was centrifuged, and analysis for dissolved silica was made immediately. Weight loss of the solid was used as a check only in the highest-temperature runs where the solubility was sufficiently high to be judged by this method. Highly supersaturated silica solutions, which formed in some high-temperature runs, started polymerizing almost immediately after quenching and formed gelatinous precipitates. Because of this rapid polymerization, some of which may have taken place before the vessel could be opened, there was some doubt regarding the accuracy of these runs, and they were not used.

The analysis of the solutions was made by the silicomolybdate, yellow colorimetric determination, using the same techniques as Alexander, Heston, and Iler (1954). The optical density was determined with a Beckman DU spectrophotometer at 400 mμ. Prepared solutions of known silica concentration were used to calibrate $KCrO_4$ secondary standards. All analyses are given directly in terms of parts per million (p.p.m.) in table 1. Samples with high amounts of dissolved salts were corrected for the salt effect on the color development (Chow and Robinson, 1953). Samples were diluted by different amounts to keep the optical density low enough to insure good sensitivity. The determinations are accurate to 2 per cent of the amount of silica present.

The determination with the silicomolybdate yellow was made so that the amount of monomeric silicic acid could be determined in addition to the total silica (Alexander *et al.*, 1954). In all cases where the solubility of amorphous silica at room temperature was not exceeded, all silica present was as the monomer, $Si(OH)_4$. Except where otherwise noted, the pH of the starting solution was between 6 and 7.

Several experiments were run in which EDTA (ethylene dinitriloacetic acid) disodium salt was added to the solutions to chelate metals that might complex with silicic acid. Runs with and without EDTA showed negligible differences.

RATES OF DISSOLUTION AND ATTAINMENT OF EQUILIBRIUM

Samples run at room temperatures were checked periodically to follow the rate of dissolution, the sample bottle being resealed after a pipetted sample was removed. The course of dissolution of the higher-temperature runs was followed by immersing four vessels in the same bath, using splits of the same powdered sample and removing them after different lengths of time. The rates of solution show roughly the same picture for quartz and amorphous silica that have been given by van Lier (1959), Krauskopf (1957), Okamoto (1957), and others. There is a rapid increase in dissolved silica in the beginning of the run and leveling off at a presumed equilibrium value. In the high-temperature runs attainment of equilibrium was judged (1) by the point at which dissolved silica showed no change in two successive time intervals and (2) by duplicate runs at the same temperature.

The rate of attainment of equilibrium is strongly dependent on the particle size of the sample powder and the temperature of the run, as well as on the nature of the starting material. For reasons of time, most samples were sized to 2 × 5 microns. Other size grades, in particular 60–80 mesh, were run, but these coarse sizes were not considered to have reached equilibrium except at the highest temperatures. Amorphous silica reached equilibrium more quickly than the synthetic opal, and both were much quicker than quartz. In fact no values for quartz are reported below 95° C. because of lack of certainty that equilibrium was reached. Quartz samples at 25° C. did not show measurable dissolution after three years!

DISCUSSION OF RESULTS

The samples of various kinds of amorphous silicas all showed about the same solubility at 25° C., between 120 and 140 p.p.m. The synthetic opals were on the low end of the range at 120 and 122 p.p.m. The finely powdered gels were at the high end at 135 and 145 p.p.m. Room-temperature solubility of amorphous silica in artificial sea water (Lyman and Fleming, 1940) was approxi-

mately the same as in distilled water, about 140 p.p.m., checking Krauskopf's (1956) conclusions that ionic strength, at least up to the concentration of sea water, had little effect on the solubility.

Room-temperature runs of amorphous silica in two concentrated brines prepared to approximate the composition of some deep oil-field brines (Meents *et al.*, 1952) also showed a lack of effect of ionic strength on solubility. There is no discrepancy here with the conclusions of Greenberg (1957), who found the solubility reduced a little less than 10 per cent in neutral 1 *N* sodium chloride

TABLE 1

SOLUBILITY DATA*

Sample Description	Temperature (° C.)	SiO_2 (p.p.m.)
Amorphous silica:		
Gel, distilled H_2O	25	135
Gel, distilled H_2O	25	136
Gel, distilled H_2O	25	142
Gel, distilled H_2O	25	145
Gel, distilled H_2O, stirred constantly	25	132
Gel, distilled H_2O, stirred constantly	25	145
Powdered dried gel, distilled H_2O	25	135
Powdered dried gel, distilled H_2O	25	148
Synthetic opal, distilled H_2O	25	120
Synthetic opal, distilled H_2O	25	122
Gel, artificial sea water	25	132
Gel, artificial sea water	25	135
Gel, artificial sea water	25	145
Gel, artificial sea water+calcite, pH 8.5	25	140
Gel, artificial sea water+calcite, pH 8.5	25	150
Synthetic opal, artificial sea water	25	120
Gel, brine (30,000 p.p.m.)†	25	140
Gel, brine (30,000 p.p.m.)†	25	142
Gel, brine (50,000 p.p.m.)†	25	138
Gel, raw peat water, pH 4.8	25	14
Gel, filtered peat water, pH 5.2	25	23
Gel, peat+distilled H_2O, pH 4.6	25	15
Gel, EDTA+distilled H_2O	25	130
Gel, EDTA+distilled H_2O	25	148
Gel, EDTA+distilled H_2O	95	420
Quartz:		
Quartz crystal, crushed, washed, 2–5 μ, distilled H_2O	125	94
Quartz crystal, crushed, washed, 2–5 μ, distilled H_2O	125	100
Quartz crystal, crushed, washed, 2–5 μ, distilled H_2O	125	103
Quartz crystal, crushed, washed, 2–5 μ, distilled H_2O	125	104
Quartz crystal, crushed, washed, 2–5 μ, distilled H_2O	140	125
Quartz crystal, crushed, washed, 2–5 μ, distilled H_2O	140	127
Quartz crystal, crushed, washed, 2–5 μ, distilled H_2O	140	128
Quartz crystal, crushed, washed, 2–5 μ, distilled H_2O	140	132
Quartz crystal, crushed, washed, 2–5 μ, distilled H_2O, pH 8.5, adjusted with KOH	161	167
Quartz crystal, crushed, washed, 2–5 μ, distilled H_2O, pH 8.5, adjusted with KOH	161	176
Quartz crystal, crushed, washed, 2–5 μ, distilled H_2O, pH 8.5, adjusted with KOH	161	176
Quartz crystal, crushed, washed, 2–5 μ, distilled H_2O, pH 8.5, adjusted with KOH	161	181
Quartz crystal, crushed, washed, 2–5 μ, distilled H_2O, pH 8.5, adjusted with KOH	181.5	195
Quartz crystal, crushed, washed, 2–5 μ, distilled H_2O, pH 8.5, adjusted with KOH	181.5	196
Quartz crystal, crushed, washed, 2–5 μ, distilled H_2O, pH 8.5, adjusted with KOH	181.5	203
Quartz crystal, crushed, washed, 2–5 μ, distilled H_2O, pH 8.5, adjusted with KOH	181.5	205
St. Peter sandstone 100×200 mesh, washed, under pressure, fluid at 1 atmosphere, distilled H_2O	95	380
St. Peter sandstone 100×200 mesh, washed, under pressure, fluid at 1 atmosphere, distilled H_2O	95	395
St. Peter sandstone 100×200 mesh, washed, under pressure, fluid at 1 atmosphere, distilled H_2O	95	395
St. Peter sandstone 100×200 mesh, washed, under pressure, fluid at 1 atmosphere, distilled H_2O	95	430

* All runs at 25° C. checked for two years.

† Brines made up by mixing NaCl, KCl, $MgSO_4$, $CaCl_2$, $MgCl_2$ to approximate typical formation waters as given by Meents *et al.* (1952).

solutions while finding no appreciable effect of 0.0001–0.10 *N* sodium chloride and 0.005–0.20 *N* sodium sulfate solutions; the brines used for the runs reported here are less concentrated than equivalent 1 *N* sodium chloride solutions. Greenberg's data imply that silica solubility in those brines which are more concentrated than 1 *N* should continue to fall off as the ionic strength increases.

Amorphous silica solubility in several humic acid solutions appears to be greatly reduced over that in distilled water. Samples of peat and peat water were collected from a bog (Tophet swamp, Lexington, Mass.), and some of the peat water was filtered. Solubility determinations were made of amorphous silica in raw peat water (14 p.p.m.), filtered peat water (23 p.p.m.), and distilled water mixed with raw, wet peat (15 p.p.m.). In these determinations the blanks were the same solutions without silica added in order to eliminate the effect of the humic acid color on the colorimetric determination. The peat waters were mixed with solutions of known silica content and were found to have no effect on the development of the silicomolybdate complex. The raw peat water as collected contained less than 1 p.p.m. dissolved silica; the solid peat contained minute quantities of silt-sized quartz.

The solubility values in the peat solutions were attained as quickly as in distilled water. No change was observed after six weeks up to two years. Without more extensive work, it is difficult to judge whether the results are equilibrium values. The simplest explanation for the anomalously low results is that colloidal organic compounds in the peat and peat water were adsorbed on the free silica gel surface and prevented that surface from fully saturating the solution.

The results of the quartz solubility determinations fit well with the interpolation made by van Lier (1959) between his data below 100° and Kennedy's (1950) data at 200° and above. The lowest temperature runs of Kennedy, those at 160° and 182,° are lower than values obtained here. As noted above, particle size strongly affects the rate of solution, and it seems likely that even with the long duration of his runs equilibrium was not reached with the large single crystal oscillator plates used. From his data, van Lier derived an empirical equation for the solubility of quartz as a function of temperature:

$$-\log C = -0.151 + 1.162 \cdot \frac{1}{T} \cdot 10^3,$$

where C is concentration in moles/liter and T is in degrees Kelvin. Using a combination of the data of van Lier, Fournier, Kennedy (excluding the figures at 160° and 182°), and the present report, a revised equation was calculated by the method of least squares:

$$\log c = 4.829 - 1.132 \cdot \frac{1}{T} \cdot 10^3,$$

where c is concentration in parts per million and T is degrees Kelvin. With appropriate conversion factors for the different concentration units used, the two equations are in good agreement.[3] Extrapolation of the revised equation to 25° C. gives a solubility of 10.8 p.p.m., in fair agreement with estimates of solubility from free-energy data (Siever, 1957). The standard heat of dissolution, $\Delta H°$, can be calculated from the solubility equation as 5.18 Kcal/mole, again not very different from van Lier's value of 5.32 Kcal/mole.

Several quartz solubility runs at 95° C. were made to estimate the magnitude of "pressure solution," a term used by Heald (1956) for dissolution of solid particles under higher pressure than the water solutions surrounding them. The quartz used was 100 × 200 mesh St. Peter sandstone, carefully washed with hydrofluoric acid, alkali, and distilled water as were the other samples. The solid was put under pressure by means of a solid steel rod when the vessel was sealed, while the fluid remained unconfined. With this crude device it was impossible to estimate the pressure on the solid. The quartz grains were examined under a petrographic microscope before and after

[3] Using p.p.m. as concentration units, van Lier's equation becomes $\log c = 4.929 - 1.162 \cdot 1/T \cdot 10^3$.

runs and showed no visible evidence of fracturing and breaking of grains. The solution was at one atmosphere pressure.

The average of the results of four runs, plotted on figure 3, lies close to the solubility curve for amorphous silica. It would appear that granulation and submicroscopic fracturing at grain contacts effectively produced some amorphous silica in much the same way that grinding of quartz does. Although it would be inappropriate to use these data directly in interpreting the magnitude of "pressure solution" in the geologic case of compaction of sandstones, it is not unreasonable to speculate that this mechanism does operate in nature. If so, pore waters in compacting sandstones might reach saturation with respect to amorphous silica even though only quartz was present originally.

The solubility-temperature curves of amorphous silica and quartz (fig. 3) appear to converge at higher temperatures and presumably would meet at some temperature close to the critical temperature of water if they were extrapolated. In fact, at high temperatures the concept of metastable equilibrium of amorphous silica breaks down because above 200° C. quartz can be precipitated easily from solution. As amorphous silica dissolves, the more stable solid, quartz, precipitates, and all the amorphous silica is converted to quartz, the silica in solution being that in equilibrium with quartz rather than amorphous silica. This is not true at lower temperatures because of the difficulty with which quartz precipitates, in harmony with the geologic occurrence of amorphous silica being restricted to low-temperature deposits.

Natural waters.—Extrapolation of the temperature-solubility curves to 5° C. indicates that quartz would have a solubility of about 5.7 p.p.m. and amorphous silica, about 60 p.p.m. The great bulk of the oceans is between 2–5° C., where average SiO_2 concentrations are very low, usually less than 1 p.p.m. and with a maximum of 4 p.p.m. Thus those parts of the ocean with higher dissolved silica concentrations, between 1 and 4 p.p.m., are only slightly undersaturated with respect to quartz, although something like 1/10 saturation with respect to amorphous silica. As pointed out in an earlier paper (Siever, 1957), it is organisms which undoubtedly keep the oceans so low in dissolved silica; for it is apparent that quartz precipitation is too slow near 0° C., even in special situations in the oceans where the water is slightly supersaturated.

If the oceans of the geologic past were somewhat warmer, as deduced from paleotemperatures based on O^{18}/O^{16} ratios (Urey *et al.*, 1951) and paleontologic and paleobotanic evidence and if the silica-secreting organisms maintained the same low concentration of dissolved silica in the sea as at present, the oceans presumably would have been more greatly undersaturated as the solubility increased as a function of temperature. The magnitude of solubility increase with just a few degrees rise in ocean temperature is small; its importance is that it is even more unlikely that in most of the geologic past there was any significant amount of inorganic precipitation of silica from sea water.

The experimental work reported here confirms statements by Iler (1955) that the external form of amorphous silica seems to matter little and that the solubilities of glasses, sols, and powders are all much the same except for opals, both natural and synthetic, which appear to be somewhat lower. Iler (1955) has presented an argument that amorphous silica increases in solubility as a function of particle size only when the particle diameters are reduced to less than 50 mμ. Lewin (1961) gives 123 and 89 m^2/g for the specific surface (measured by nitrogen adsorption) of two diatom species, values that correspond to the specific surface of hollow spheres of about 4 μ diameter. But electron micrographs of diatoms show that the internal surface of the small delicate forms may be so great that the effective particle size is less than 50 mμ. This may explain why diatoms dissolve and reprecipitate as ordinary amorphous silica gel of lower specific surface area and therefore lower

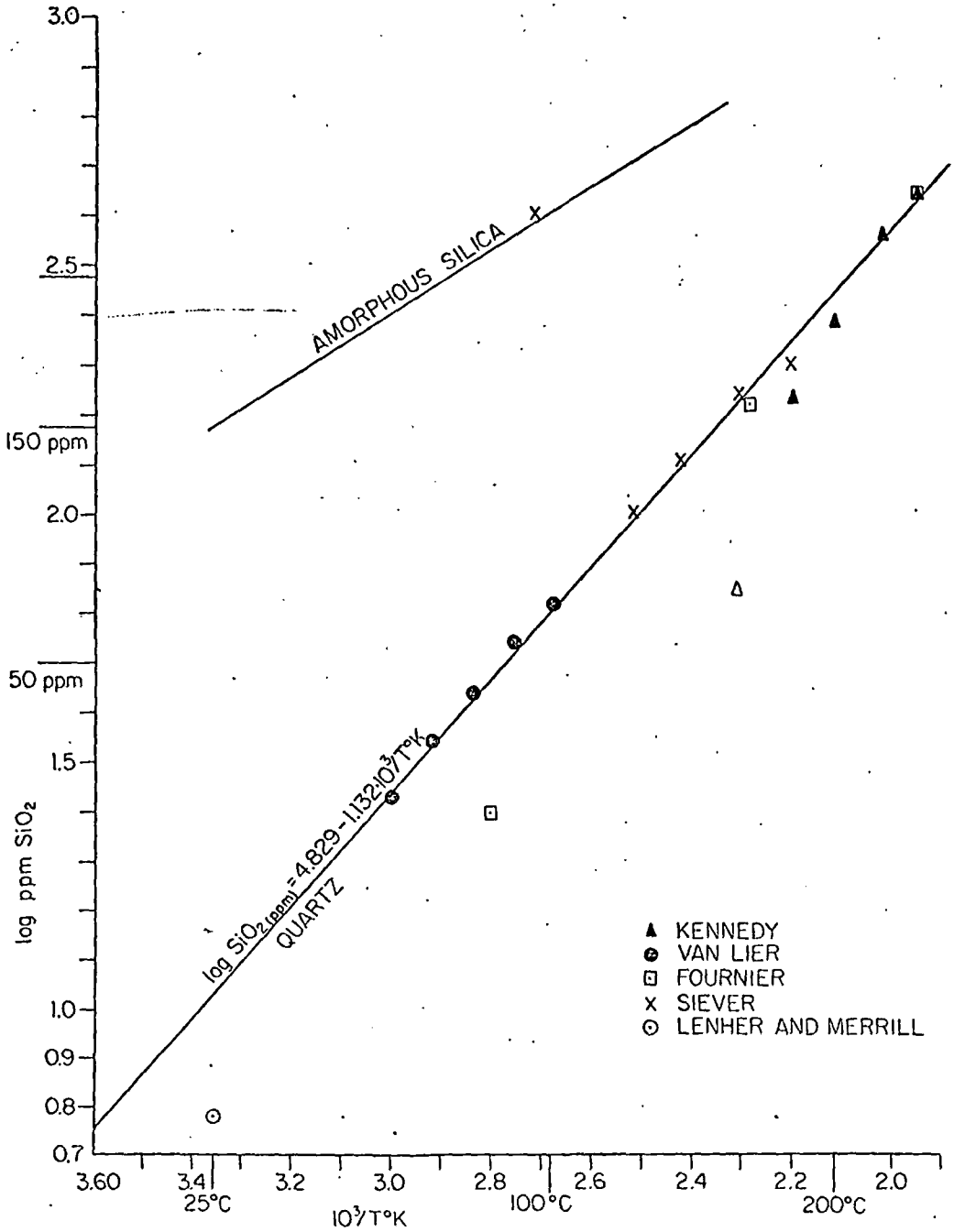

FIG. 3.—The solubility of quartz and amorphous silica as a function of temperature

solubility. If this were so, there should be a correspondence between fragility and delicacy of the diatom structure and its preservation. In fact at present it is commonly the more robust forms that are preserved in deep sea oozes.

The question of rate of equilibration in nature has not been answered by the study of equilibrium solubilities. It is clear that quartz-water solutions in the laboratory at low temperatures are very slow to react, so slow that rates of dissolution and precipitation are probably best measured in geologic times. It is also apparent that the amorphous silica-water system is relatively quick to come to equilibrium. Some forms of amorphous silica will equilibrate at room temperature in a matter of a few weeks; only a few kinds of amorphous silica, such as fused silica glass, do not equilibrate in six months. Thus we expect to find natural waters that are not in equilibrium with quartz but do not expect to find such waters in contact with solid amorphous silica that are not in equilibrium with it.

If we consider a sediment containing both quartz and amorphous silica, we may expect that the amorphous silica will gradually dissolve and the quartz will precipitate. Inasmuch as the rate of dissolution of amorphous silica is much faster than the rate of precipitation of quartz, any natural water in contact with the sediment should be saturated with respect to amorphous silica and not quartz. But this does not always seem to be the case in nature.

Reports of silica concentrations in interstitial waters made by Bezrukov (1955), Bruevitch (1953), and Emery and Rittenberg (1952) show that, although the waters are more concentrated than the sea water overlying the sediment, they are normally below saturation values as determined in the laboratory. The low values are not to be explained by lack of sufficient solid amorphous silica to keep the water saturated, for amorphous silica skeletal materials are present.

In this, as in so many other natural situations, we reach the conclusion that major factors to be considered are (1) that the behavior of natural materials in the geologic environment cannot be precisely judged by comparison with pure materials in the laboratory and (2) that other chemical components may be affecting the equilibria. The equilibrium solubility of biogenic amorphous silica (diatoms, radiolaria, etc.) may be more or less than that of the pure prepared silicas used in the laboratory. The rate of solution of biogenic amorphous silica in sea water or interstitial waters similar to sea water in composition may be much slower than that measured in the laboratory, so much slower that they may take geologically significant times to saturate a solution. One cannot neglect the unlikely possibility that in the natural environment the rate of precipitation of quartz is speeded up so that it is almost the same as the rate of dissolution of amorphous silica; then the solution would take a long time to become saturated with respect to amorphous silica.

Recent work on diatom dissolution by Lewin (1961) shows that in many cases the behavior of the diatoms may be causing the apparently anomalous situation. She found that rates of dissolution of diatoms vary greatly, depending on such factors as the kind of metal ions in solution (Al being most important) and the way in which the diatoms died (chemical destruction, deprivation of light for photosynthesis). It is not certain that all species of diatoms have the same solubility; it may vary with the kinds and amounts of metal ions and organic material bound to the silica.

That organic matter may play an important role in the dissolution of amorphous silica is suggested by the solubility determinations in peat solutions. If the lowered solubility is the result of organic adsorbates on the silica surface, we may expect that the silica will not come to equilibrium with the surrounding waters until the organic matter has been removed by bacterial decay and oxidation. On the other hand, some organic compounds may form organic-silica complexes (Siever and Scott, 1961) and increase the solubility. At present, not enough is known of the occurrence of these complexes in nature to warrant any definite conclusions.

Answers to many of the problems posed above may come in the study of solubilities and the rates of solution of the biogenic silicas found in natural environments in relation to variations in trace elements, specific surface area, and interaction with organic materials. It is also necessary to have much more data on the amount of dissolved SiO_2 in interstitial sediment waters in diatom and radiolarian oozes to see what supposed saturation values are.

Effect of other components.—Thus far we have considered only the silica-water system and its controls on silica precipitation. If other components are added, in particular, aluminum, the alkalies, and the alkaline earths, the precipitation of silica may be governed by equilibria with aluminosilicates. At low temperatures and pressures the minerals of most concern are the clay minerals. Alteration of one clay type to another with different silica/alumina ratios will lead to silica liberation to or absorption from the surroundings (Siever, 1957). The reactions of greatest interest are those involving transformations of montmorillonite to muscovite, illite, or kaolinite—all of which result in the release of silica.

If we take the montmorillonite formula given by Ross and Hendricks (1945) and write the appropriate equations for transformations to muscovite, kaolinite, and illite (formula given by Yoder and Eugster, 1955), the relative amounts of silica can be calculated.

$$1.2[\underset{\text{Montmorillonite}}{Na_{0.66}Al_{3.34}Mg_{0.66}Si_8O_{20}(OH)_4 \cdot nH_2O}] + 6.4\,H^+ = 2\,\underset{\text{Kaolin}}{Al_2Si_2O_5\,(OH)_4} + 5.6\,SiO_2 + 0.79\,Na^+ + 0.79\,Mg^{++} + (1.2n + 3.6)\,H_2O. \quad (1)$$

$$1.8\,[Na_{0.66}Al_{3.34}Mg_{0.66}Si_8O_{20}\,(OH)_4 \cdot nH_2O] + 1.6\,H^+ + 2\,K^+ = \underset{\text{Muscovite}}{2KAl_3Si_3O_{10}\,(OH)_2} + 8.4\,SiO_2 + 1.19\,Na^+ + 1.19\,Mg^{++} + (1.8n + 2.4)\,H_2O. \quad (2)$$

$$1.78\,[Na_{0.66}Al_{3.34}Mg_{0.66}Si_8O_{20}\,(OH)_4 \cdot nH_2O] + 3.7\,H^+ + 1.33\,K^+ + 4.82\,Mg^{++} = \underset{\text{Illite}}{K_{1.33}Al_{5.33}Mg_6Si_{6.67}O_{20}\,(OH)_4} + 7.63\,SiO_2 + 1.18\,Na^+ + (1.78n + 3.4)\,H_2O. \quad (3)$$

If we compute the relative amounts of silica and clay mineral products of these reactions, we find that for (1) 1 gm. silica is produced for 1.53 gm. kaolinite; for (2) 1 gm. silica is produced for 1.57 gm. muscovite; and for (3), 1 gm. silica is produced for 2 gm. illite.

Garrels and Christ (unpublished manuscript) have calculated equilibrium constants for many of the reactions between clay minerals, feldspars, and aqueous solutions by estimating the standard free energies of formation of the minerals involved. From the equilibrium constants, it is possible to calculate amounts of silica in equilibrium with montmorillonite, kaolinite, and muscovite in aqueous solutions with various amounts of cations. The calculations can be approximate only, for appreciable error is introduced in estimating the free energies of formation of the minerals involved. From the calculations it appears that, if the waters are in equilibrium with kaolinite, the silica concentrations will vary from 20 to 60 p.p.m. when the Na^+/H^+ ratio ranges from 5 to 8. Higher concentrations of silica would lead to the formation of Na-montmorillonite. Similar calculations can be carried out for the muscovite-orthoclase pair, which is dependent on the K^+/H^+ ratio and silica concentration (Garrels and Howard, 1957).

Abrasion solution.—Abnormally high silica concentrations in waters in contact with quartz have been produced by Fournier (1960), who tumbled quartz in polyethylene vessels for over a year and found that the solution increased steadily to a maximum of 300 p.p.m. dissolved silica, vastly supersaturated with respect to amorphous silica.

The mechanism of abrasion solution seems to be one of disordering and hydrating

the surface layers of quartz by continued impacts of other grains to produce a finely divided amorphous silica. Indeed, it is the production of this surface layer that is troublesome when pure quartz is wanted from a grinding operation. Van Lier (1959) has calculated that there is a disturbed layer about 300 A. thick on 2–5 μ quartz grains produced by grinding.

II. Diagenesis of Silica

Silica in the sedimentary environment

Before the when and where of silica dissolution and precipitation during diagenesis can be specified, the silica available and precipitated in the sedimentary environment must be evaluated (Siever, 1957). In the discussion, I shall use the word "primary" to indicate the material which is precipitated from the free water of the environment, including the biogenic component of the sediment, before any burial takes place. It would also include any detrital material as finally deposited (after any mechanical reworking). Thus both a precipitate forming while detritus is being deposited and a precipitate added to the surface layer of a sediment after final mechanical deposition would qualify as "primary." This usage is dictated by the impossibility of operationally establishing a reasonable differentiation between "during deposition" and "already deposited but not yet buried."

I shall use the work "diagenesis" in a loose sense for any process after initial burial of a layer by the next deposited layer of sediment, recognizing that there is no real boundary between diagenesis and metamorphism, on the one hand, and diagenesis and weathering, on the other.

The open ocean.—Amorphous silica is precipitated in the oceans by organisms: diatoms, radiolaria, siliceous sponges, and silicoflagellates. No substantiated occurrence of quartz being precipitated at the present time is known; nor is there any definite record of primary amorphous silica being precipitated in the sea at present by any nonbiological processes, although Bien *et al.* (1959) have indicated that dissolved silica in Mississippi River water may be adsorbed on suspended matter in and around the delta. Open sea water is undersaturated with respect to both quartz and amorphous silica, and so non-biogenic precipitation as free silica is ruled out, although silicates may precipitate by reaction of silica with alumina or aluminosilicates.

This is not to say that biogenic removal of silica from the sea is not conditioned by changes in silica content of the water. Local diatom blooms may occur as a result of high silica concentrations from the alteration of volcanic materials. The productivity of diatoms is determined by many organic and inorganic nutrients, among them silica (Harvey, 1957). But their use of silica is dependent on the amount of silica in the water. This is especially illustrated by fresh water diatoms that live in lakes of varying SiO_2 content, where, other things being equal, there is a direct relation between the size of diatom populations and available silica. Silica-deficient shells are produced in cultures grown in low silica nutrient solutions (Harvey, 1957). The diatoms can precipitate silica from solution even at very low concentrations, less than 1 p.p.m., but they cannot be abundant unless there is enough SiO_2 in solution to support the population. Thus a higher productivity of diatoms and siliceous sediments resulting therefrom is the consequence of a greater quantity of dissolved SiO_2 supplied to the environment rather than the converse. We know most about the diatoms; available knowledge of present and past patterns of sedimentation suggest that the radiolaria and siliceous sponges act in the same way. Fundamentally, it is the contribution from inorganic sources that determines the presence or absence or amount of siliceous sediment.

The diatoms extend back in time only to the Mesozoic; the radiolaria to the early Paleozoic. The siliceous sponges extend back to the beginning of the Paleozoic, but we are unsure whether they existed during the Precambrian. The silicoflagellates' evolutionary pattern is poorly known, but they extend

back to the Upper Cretaceous. By a line of reasoning fully explored in an earlier paper (Siever, 1957), it was concluded that silica sedimentation in the later Precambrian must have been much like today, that is, primarily biogenic, for there is no essential difference between later Precambrian sedimentary sections and younger rocks insofar as siliceous rocks are concerned. This implies the existence during the Precambrian of silica-secreting organisms even though the direct fossil evidence is missing.

It is worthwhile to consider silica precipitation in earlier Precambrian seas in which no silica-secreting organisms had yet evolved. The simplest analysis of the pure silica-water system would lead us to conclude that the rate of supply of silica to the oceans and the time available would have led to saturation with respect to amorphous silica, for quartz would have been as slow to precipitate in the earlier Precambrian as today. As additional dissolved silica was supplied by rivers, the excess would have been precipitated as a silica gel, later to be altered to chert or microcrystalline quartz. The quantity of siliceous sediment deposited in this early ocean would have been solely a function of supply from the weathering of continental rocks. If Archean rocks represent the later part of this time, then we should expect sedimentary sections with a more or less constant component of silica. But Pettijohn (1943) has marshalled a great deal of evidence to show that Archean sedimentation was the same as in later times, and, in particular, he pointed out that the origin of Precambrian chert must have been the same as for later cherts, at least for those bedded cherts associated with the geosynclinal graywacke suite. This implies that either silica-secreting organisms evolved very early indeed or that this variety of chert is not dependent on organisms. A third but unlikely alternative is that montmorillonite was formed by reaction of silica with kaolin or illite, and this reaction kept the early oceans undersaturated with respect to amorphous silica. This reaction is not possible in the present oceans because of low silica concentrations caused by organisms, but it would have been possible before the silica secreters had evolved.

Speculation on the origin of life in the early ocean (Oparin, 1953) has led to the hypothesis that an organic-rich "soup" was the raw material that was converted by some form of energy (electrical discharge, ultraviolet radiation, etc.) into amino acids and then protein molecules. This would have led to the adsorption of organic compounds on free silica surfaces and thus to the prevention of silica dissolving to saturation. In addition, the number and variety of organic compounds present in the early seas may have made more probable the wholesale complexing of dissolved silica, thus increasing the solubility and lessening the likelihood of saturation.

Restricted environments.—We may ask what would happen in restricted parts of the sea with poor mixing with the open ocean reservoir. If in such environments the supply of non-siliceous nutrients necessary to support sizable populations of silica-secreters is low (so that biogenic precipitation cannot keep silica concentrations in the water low) and there is an abundant supply of silica by weathering or volcanism, it is possible for local supersaturation and precipitation to take place non-biogenically. This is more likely to have happened before the evolution of the diatoms, for at present this kind of environment normally has sufficient nutrients to support a population of diatoms adequate to keep silica concentrations below saturation levels.

If a restricted environment becomes the site of extensive evaporation so that soluble salts are precipitated, there is the possibility that, after sufficient concentration of the bittern, silica will precipitate. If we take 1 p.p.m. as a somewhat liberal estimate for dissolved silica in sea water, then that water would have to be reduced in volume over 100 times before saturation with respect to amorphous silica is reached. This same magnitude of reduction of volume is necessary for KCl to precipitate, and so in those salt deposits where KCl is found, amorphous

silica (perhaps now recrystallized to quartz) should be found. However, the amount of SiO_2 is small compared to KCl and so would be present in minor amounts. This obviously is not the place to look for siliceous sediments or a source of silica.

Lakes.—Some lakes, in particular the sodium carbonate lakes, may have high concentrations of dissolved silica. Some are highly supersaturated as, for example, Owens Lake, California, with 300 p.p.m. dissolved silica (Clarke, 1924). Deposits formed in such lakes are expected to show appreciable silica. Whether the silica is biogenic or not depends on the available nutrients and also on other conditions, such as pH, that may affect the viability of diatoms. In some soda lake deposits that are very alkaline and aluminum rich, the dissolved silica may combine with aluminate ion and form an alkali aluminosilicate precipitate such as analcite or montmorillonite.

Abrasion solution during re-working.—Experimental work with tumbling barrels and observations of rounding and size decrease in natural streams has led sedimentary petrologists (Pettijohn, 1957, p. 533–540) to the conclusion that purely mechanical abrasion is very slow to change angular quartz particles into rounded ones or to reduce their size. The abrasion involved in an average distance of transport in one sedimentary cycle is apparently insufficient to account for any significant rounding or size decrease. Yet there are many well-rounded quartz sandstones in the geologic column. The discrepancy has been explained by assuming either multiple cycles of transport or constant re-working in a beach or near-shore environment during one cycle to permit sufficient abrasion to accomplish the rounding. It may be equally well explained by the fact that quartz particles may dissolve chemically more quickly under abrasion conditions—such dissolution almost certainly resulting in greater rounding of the particles. As noted earlier, Fournier's (1960) experiments indicated that abrasion may produce supersaturated solutions. His work, taken together with the arguments on rounding of quartz particles, raises the possibility that in those sedimentary environments in which sands are constantly being shifted and abraded, such as beaches, bars, and near-shore littoral areas, dissolved silica may reach high concentrations.

Here one must distinguish between two types of transport—suspended load and bed load. In suspended-load transport, abrasion solution will release silica to the open waters of the environment, which are well mixed by the currents competent to transport sand. As a rule, the waters of these environments are undersaturated, and, because of rapid mixing, the silica concentration of the reservoir will not be built up to any significant extent. The sole result may be decrease in grain size and rounding of the particles.

In bed-load transport, the entire upper part of the bed may be in transit, with attendant impacts and mutual abrasion of grains. The water within the bed is not always well mixed with the overlying water, and it is conceivable that dissolved silica concentrations could build up locally to give solutions supersaturated with respect to quartz and possibly even with respect to amorphous silica. The high silica concentrations in the interstitial waters of the moving bed would not be reduced by the activities of organisms, for this is not the ecological niche of the siliceous sponges, and the other siliceous organisms are pelagic.

Is it possible that this mechanism is responsible for those rounded sands cemented by silica, in which petrographic evidence shows that the cementation took place before appreciable compaction (Siever, 1959)? Fournier (1960) reported that his high supersaturation values were eventually reduced, presumably first by amorphous silica and then by quartz precipitation. Here is experimental evidence that quartz may be precipitated at room temperatures, given enough time and enough quartz grains to act as nuclei. A test for this hypothesis is to take sands presumably formed in these environments and see whether there is any positive correlation between cementation and roundness. Another test would be the

careful measurement of silica concentrations in interstitial waters of sands in the appropriate modern environments.

EARLY DIAGENESIS

By early diagenesis I shall mean that stage in the history of sediment during which it is buried only up to a few tens of feet. During this stage the sediment is not yet compacted greatly and has a high porosity and water content and may be moderately permeable. It has been established that bacteria may be active in this soft sediment and instrumental in promoting chemical reactions. A further characteristic of this stage is the passage of water expressed by compaction upward through the sediment. The greater the gradient of compaction in the uppermost few feet of sediment, the greater the flow through of water.

Dissolution of organisms.—During early diagenesis any siliceous organisms trapped in the sediment should slowly dissolve if the interstitial waters, essentially trapped sea water, are undersaturated in silica. Thus in the case of a marine sediment containing diatoms, the diatom walls, protected from dissolution during life, will slowly corrode, releasing dissolved silica to the interstitial waters.

The rate of solution depends, among other factors, on the concentration of silica in solution and will be expected to slow as the concentration builds up. The rate of flow through of water expressed by compaction fundamentally depends on the rate of accumulation of sediment overburden. Rates of sedimentation are slow; even in areas of relatively rapid deposition, they may reach only 0.1 mm/yr averaged over long geologic times. The rate of dissolution, of diatoms, up to 50 mg/l for the first month (Lewin, 1961), is more than sufficient to saturate the water squeezed out by compaction as it passes through the sediment. Then we may anticipate a buildup of silica in solution if any siliceous organisms are present. If such organisms are not present in excess, they may dissolve, leaving no relic behind. The analyses of interstitial waters of some southern California modern sediments by Emery and Rittenberg (1952) that show increases in dissolved silica below the sediment surface are good evidence for this buildup. Interstitial waters of some Atlantic Ocean sediments analyzed in the writer's laboratory show the same kind of increase.

As mentioned earlier, the high surface areas of some diatoms may give rise to abnormally high solubilities and rates of solution that might lead to supersaturation and consequent precipitation of a gel. One may think of this as a simple process of recrystallization or digestion of a precipitate from a state of higher surface area to a state of lower surface area, the decrease in surface energy being the driving force of the transformation.

There is also the possibility that the interstitial waters enriched in silica by the dissolution of organisms will relieve their supersaturation with respect to quartz by precipitation as quartz crystals or overgrowths. Quartz crystallization may depend on the presence of nuclei in the form of quartz sand or silt grains.

Alteration of volcanic glass.—Volcanic glass is unstable in sea water and will hydrolyze and release silica to solution. Depending on the concentration of dissolved silica in equilibrium with the particular glass in sea water, the interstitial waters may become supersaturated and amorphous silica may precipitate. Even if saturation with respect to amorphous silica is not reached, quartz may precipitate. The association of volcanic glass and secondary opal in ash falls has been noted frequently and seems to be a fairly common occurrence. Also common is the association of a silicified zone with bentonites. The marine alteration of volcanic glass has been studied by Zen (1959*b*) in some modern sediments from the Peru-Chile trench. Zen noted devitrification at all levels in most of the forty cores studied, and, from index of refraction measurements on fresh glass, he deduced a dominantly basaltic composition. Some beds had such an abundance of glass that they could be considered ash beds. The amount of silica re-

leased by the devitrification of a marine ash bed is probably a significant source of diagenetic silica.

ORIGIN OF CHERT

Most of the silica in chert consists of microcrystalline quartz (Midgley, 1951; Folk and Weaver, 1952). The very fine crystal size of the quartz, the occurrence of opal in recent cherts, the abundance of water-filled cavities (Folk and Weaver, 1952), and the evidence that there may be an admixture of amorphous silica between quartz fibers in chalcedony (Sosman, 1927; Correns and Nagelschmidt, 1933; Donnay, 1936)—all suggest that most, if not all, cherts were originally precipitated as amorphous silica rather than quartz. This does not necessarily mean that the precipitate was a low-density, high-water content, soft gel. Gels can be precipitated in a wide variety of water contents, particle sizes, and states of aggregation (Iler, 1955, p. 127–134). Opal is a dense form of amorphous silica, and gels with similar characteristics can be made easily in the laboratory without resort to extreme conditions of temperature and pressure. The fact that some chert nodules have shown resistance to compaction greater than the surrounding carbonate sediment supports the conclusion that this silica was no soft gel but a hard opaloid precipitate.

The alternative to amorphous silica precipitation is that chert was originally precipitated as microcrystalline quartz, and its extremely fine particle size is due to the lack of nuclei of larger crystals of quartz in the form of silt or sand grains or lack of quartz nuclei formed spontaneously. Supporting this suggestion is the fact that microcrystalline quartz precipitates are obtained in high-temperature quartz synthesis experiments when nuclei are absent or precipitation is too rapid. Militating against this argument is the fact that chert has been observed as cement between quartz grains in sandstones (and in sandy limestones), where presumably some of the abundant quartz grains would have acted as nuclei.

Bedded chert.—I will not attempt here to summarize the literature on this problem; that has been done ably by Pettijohn (1957). Recent contributions include those of Goldstein (1959) and Bissell (1959), who have discussed the geologic occurrence and origin of bedded cherts in the Ouachita and Cordillera belts, respectively. The weight of the evidence supports the primary or early diagenetic origin of bedded chert, but there is no general agreement on whether it originates from biogenic precipitation or alteration of volcanics. The petrographic and geologic arguments reduce to a question of whether siliceous fossil remains can be found in the chert or the chert beds are associated with volcanic rocks in the near vicinity. Either or both have been described in various bedded cherts. The cherts of unknown origin are those that contain no recognizable siliceous fossil remains and are not associated with volcanic rocks.

The argument that the sea water of the environment became supersaturated by alteration of volcanic materials and so precipitated silica non-biogenically assumes either (1) that silica-secreting organisms could not reduce concentrations as rapidly as solutions were supersaturated or (2) that the diatoms and silicoflagellates did not exist before the Cretaceous, and the radiolaria and siliceous sponges were not efficient in reducing silica supersaturation. The first asssumption, at least so far as the diatoms are concerned, is not justified from studies of modern sediments and environments, in which the organisms are able to keep up with the supply. If the second assumption were so, sea waters generally would have become saturated early in geologic history, after which there would have been precipitated a relatively constant component of silica to all marine sediments; this has not been observed. In addition, there is no evidence from the literature that pre-Cretaceous cherts are generally different from younger ones. The assumptions (1) and (2) are not justified; therefore the original statement lacks basis.

The best argument in favor of non-biogenic precipitation from supersaturated sea

water is that the bedded cherts were deposited in restricted basins (Pettijohn, 1957) in which the supply of nutrients other than silica was restricted and so could not support a silica-secreting population. This would be particularly true of those stagnant basins with stable density stratifications; bottom waters rich in nutrients would not mix with surface waters, and the latter would become depleted and not be able to support large planktonic populations. In these basins, because of lack of vertical mixing, the bottom waters might become enriched in silica as a result of the inability of sponges to live on a deoxygenated bottom and the lack of communication with surface waters where the diatoms, silicoflagellates, and radiolaria live.

Any disruption of the stable stratification that would lead to vertical circulation and regeneration of nutrients in the surface waters would make possible a flourishing of planktonic populations and abundant biogenic precipitation of silica. Periodic overturn alternating with stable stratification could lead to alternation of biogenic and non-biogenic siliceous deposits.

The origin of bedded chert as an early diagenetic product of the alteration of volcanic materials is implied by the observations on devitrification and alteration of volcanic glass in modern sediments. Zen (1959*a*) has described the association of calcite and kaolinite as alteration products of devitrified glass. A chert formed in this way would be expected to show, in addition to quartz, mineral assemblages, such as calcite-kaolinite, calcite-chlorite-kaolinite, calcite-dolomite-chlorite, and others, depending on the number of components and phases in the system. Obviously, only the impure argillaceous and carbonate-rich bedded cherts would fit with this origin. The siliceous Mowry shale (Rubey, 1929) may have originated in this way.

An explanation for the pure bedded cherts that have no siliceous organisms preserved may be sought in the relation of the rate of sedimentation to the rate of dissolution of the organisms during early diagenesis. According to this view, the organisms, given enough time, will dissolve and reprecipitate as structureless amorphous silica gel in early stages of diagenesis, before compaction and lithification. If, however, the siliceous ooze is rapidly buried and compacted after only partical dissolution and reprecipitation of the organisms, the individual shells may become "frozen in" and protected from dissolution by lack of pore space and fluid in which to dissolve, analogous to the exquisite preservation of calcium carbonate shells showing original structures and composition in some argillaceous limestones and marls. Then cherts like the Monterey (Bramlette, 1946), in which diatoms are preserved, would represent high rates of sedimentation, and cherts in which no fossils are preserved resulted from low rates.

Nodular cherts.—The weight of petrographic evidence is in favor of most chert nodules, most often associated with marine limestones, being postconsolidation, epigene replacement deposits. The main evidence for this has been summarized by Pettijohn (1957). On the other hand, the differential compaction of limestone around and the lack of compression of fossils within some chert nodules point to some silica emplacement at early stages of compaction before much interstitial water had been squeezed out by the weight of overlying sediments.

For simplicity we shall take the case of small, discontinuous nodules distributed along a bedding plane in a limestone, in which there is petrographic evidence for replacement origin. A model of origin that will be consistent with our knowledge of silica chemistry and explain such an occurrence must fulfil three major requirements. It must explain (1) how supersaturated silica solutions are produced that enable precipitation of amorphous silica or microcrystalline quartz, (2) the conditions for replacement under which carbonate is dissolved as silica is precipitated, and (3) the distribution as discontinuous nodules instead of a uniform bed.

The source of the silica and the mechanism by which supersaturated solutions are produced is probably the least difficult of the

three requirements. Siliceous organisms have been present at least since the early Paleozoic, and their remains are to be found in many limestones and chert nodules. As discussed above, we may expect a high proportion of these organisms to dissolve in the interstitial waters after death and burial. The almost exclusive association of nodules with biogenic carbonate rocks is circumstantial evidence that it is the organisms that are the primary source of the material, for here we have little or no detrital material as a supply, and silica does not precipitate from normal sea water non-biogenically. Another important support for this hypothesis is the occurrence of siliceous sponge spicules in the chert nodules and the lack of siliceous spicules in the limestone away from the nodules, as reported from several localities (Lowenstam, 1948; Newell *et al.*, 1953; Pittman, 1959). Finally, it is the dissolution of organisms that is most likely to result in supersaturated solutions because of the fine structure of the siliceous skeletal materials. Even very fine-grained quartz silt particles would not dissolve beyond equilibrium.

If volcanic glass were associated with the deposit, its devitrification would also contribute to silica in solution. Still another source of silica is the transformation of montmorillonite to illite during diagenesis, a hypothesis that is supported by the relative decrease in abundance of montmorillonite in older sedimentary rocks.

No better answer to the problem of getting supersaturated solutions is given by hypothesizing mass transfer of supersaturated solution into the bed from elsewhere, for this just compounds the difficulty by imposing the necessity for explaining the how and why of the mass transfer as well as still requiring that supersaturated solutions be built up someplace.

The laboratory conditions under which carbonate is dissolved and silica precipitated are fairly well known, although no one has demonstrated actual replacement. It is convenient to discuss carbonate solubility in terms of pH, although, in fact, the dominant independent variable in geologic situations is the activity of CO_2, pH being the dependent variable and not the controlling factor. Carbonate dissolves in acid and precipitates in alkaline solutions, the precise value of pH at the point of precipitation depending on the activity of CO_2, Ca^{++}, and CO_3^{--}, pressure, and temperature.

The relationship of silica solubility to pH is not at all similar to that of carbonate. As pointed out earlier in this paper, all the recent work has shown that solubility is independent of pH between 2 and 9 and increases greatly only in alkaline solutions of pH 9.5 and higher. Therefore, the appealing relationship expounded by Correns (1950)—wherein at lower pH values silica precipitates as carbonate dissolves, while at higher pH values silica dissolves as carbonate precipitates—is not validly based on experimental data on equilibrium solubilities, at least for that range of pH values found in the vast majority of natural environments (Baas-Becking *et al.*, 1960).

Whether or not pH has anything to do with silica precipitation, the conditions for replacement of carbonate can be related to localized areas in which the pH is lowered at an early diagenetic stage. This situation is readily explained by the addition of CO_2 to the system by bacterial decomposition of organic matter. This effect has been noted in modern sediments by Emery and Rittenberg (1952), van Andel and Postma (1954), and Siever *et al.* (1961). The localization of the increase in CO_2 may be explained by the irregular distribution and clumping of organic matter. At these sites of organic decay the carbonate would dissolve, increasing the concentration of HCO_3^- and Ca^{++} (plus Mg^{++} if dolomite or magnesian calcite is present). This would set up a concentration gradient between the sites and surrounding areas where no CO_2 was added, making possible diffusion of dissolved carbonate away from the sites of organic decay. This explains the disappearance of carbonate from the site but not the appearance of silica.

The appearance of silica at the site of organic decay cannot be ascribed to the influence of pH change on silica solubility. Nor

can one explain it by the effect of pH on rate of polymerization of supersaturated solutions (Iler, 1955, p. 45–48), for in strong electrolyte solutions such as sea water the rate of polymerization is high regardless of pH. But clay mineral-silica reactions are strongly affected by pH; lowered alkalinity would displace the montmorillonite-kaolinite reaction toward the production of kaolinite and silica. The argillaceous cherts may owe their origin to this reaction.

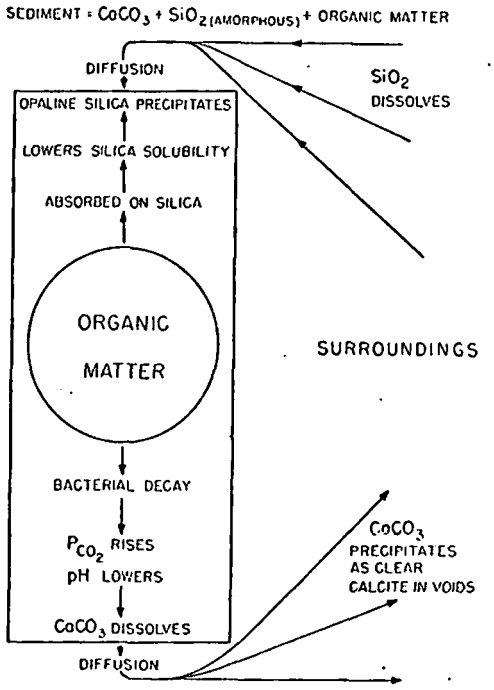

FIG. 4.—Possible mode of formation of early diagenetic chert nodules as related to the presence of organic matter.

Emery and Rittenberg (1952) have suggested that what may happen at the site of organic decay is the lowering of solubility of silica by adsorption on organic matter, whether originally deposited or produced as the metabolic products of bacteria. In addition, the adsorption of organic matter on silica, for which we have ample evidence, may have its effect. This would act in the following way. What siliceous organisms there were at the site would dissolve very slowly and slightly because of organic adsorption, whereas the siliceous organisms in the surrounding areas without organic adsorbates would be free to dissolve. A concentration gradient of dissolved silica would be set up, making possible diffusion from the surroundings into the site where organic material would continue to immobilize the silica by producing insoluble organic silica complexes. The process would continue, as in figure 4, carbonate dissolving and silica precipitating at the site until the organic matter was either completely oxidized by bacteria or complexed with silica, or until the bacterial activity that produced CO_2 ceased.

The test of the above hypothesis would be to demonstrate more clearly the role of organic matter in complexing silica, the presence of secondarily precipitated clear calcite in the surroundings of the chert nodule, and the already noted difference in preservation of siliceous organisms in and surrounding the nodules.

The mechanism proposed above would not account for the more abundant postconsolidation nodules, for at this stage bacterial activity and oxidation of organic matter would have ceased. Here also, local pH variations could not be used for an explanation, for we know of no reason why pH should be heterogeneous in a consolidated rock other than random minor fluctuations. The answer should be sought in variations in solubility of carbonate and silica related to changes in pore-water composition, pressure, or temperature, or any combination of the three.

Pressure and temperature increase with depth of burial, the pressure increasing by the weight of overburden and the temperature increasing along the geothermal gradient. The effect of temperature and pressure on silica solubility reinforce each other and make silica much more soluble at higher temperatures and pressures. The effect of temperature is much greater than that of pressure (Kennedy, 1950). Thus we expect silica to dissolve as the rock gets deeply buried and the pore waters in equilibrium with that rock to get more concentrated with dissolved silica. The amount of silica dissolved depends on the depth of burial and the amount of pore water available.

The effects of pressure and temperature on carbonate solubility are more complicated, for inextricably tied up with carbonate solubility is the activity of CO_2, and CO_2 solubility in water is strongly affected by temperature and pressure. If CO_2 pressure is constant, carbonate solubility increases with greater pressure and decreases with higher temperature (Miller, 1952; Ellis, 1959). If, however, we specify the more appropriate geologic situation in which a certain amount of CO_2 is trapped initially and then the system is sealed so that CO_2 pressure also varies with temperature and pressure, the solubility changes in a different way. Weyl (1959*a*) measured the solubility as a function of temperature in this way, but no data are available as a function of pressure. Owen and Brinkley (1941) used partial molal volumes to calculate the change in carbonate equilibrium constants with pressure, and we can use these figures and Weyl's to roughly calculate the magnitude of the change in solubility with increasing temperature and pressure along earth crustal gradients (Siever, R., and Garrels, R. M., unpublished Ms.). Somewhat surprisingly, the results are that the solubility is practically unchanged or very slightly decreased with burial, the effects of pressure and temperature almost exactly balancing each other.

The above analysis shows that pressure and temperature changes associated with burial cannot be used to account for silica replacement of carbonate, for carbonate solubility is not very responsive to temperature and pressure. It could conceivably have some slight importance in the filling of open-pore spaces by silica, associated with uplift, lowering of temperature and pressure, and consequent lowering of silica solubility.

Changes in pore-water composition are left as the driving force behind replacement of carbonate by silica. We know that the major long-term change attendant on burial is increase in salinity up to 150,000 p.p.m. and more (Meents *et al.*, 1952; Chave, 1960). The salinity increases with depth in a basin and thus also with age. Although the composition of the waters is somewhat different from concentrated sea water, the over-all aspect of the average brine is a concentrated NaCl solution, generally similar in relative proportions to sea water. The pH of brines appears to be slightly reduced over that of sea water, but it is difficult to trust the measurements as being the same as that in the *in situ* fluid.

The dominant effect of the change in brine composition is that of increasing ionic strength and its effect on the solubility of silica and carbonate. The increased ionic strength, up to 1.5, decreases the activity coefficients of Ca^{++}, CO_3^{--}, and HCO_3^- (Harned and Owens, 1950; Garrels *et al.*, 1961) and thus effectively increases the concentration of the dissolved species and the equilibrium solubility of carbonates. On the other hand, Greenberg's (1957) data show that silica solubility decreases in NaCl solutions of high ionic strength. Here, then, is an effect which may explain the simultaneous solution of carbonate and precipitation of silica in a postlithification stage, which is presumably associated with moderate to deep burial. It now remains to examine this concept quantitatively to see whether it can account for the volumes of silica precipitated.

It is obvious that, if there is no movement of pore fluid through the rock, only minute amounts of carbonate and silica can be dissolved and precipitated, respectively. Let us take the case of 1 cc. of limestone with 25 per cent porosity, the pores filled with a silica-saturated brine. A reduction of silica solubility of 15 per cent would mean that at a depth of 10,000 feet, corresponding to a temperature of about 110° C. and a pressure of about 600 atmospheres, the solubility of amorphous silica would be reduced from about 500 p.p.m. to 425 p.p.m. and the brine would be supersaturated by 75 p.p.m., or about 0.075 mg/cc. Further, assuming that quartz (density = 2.65) was precipitated, this would amount to 0.0000283 cc. of quartz precipitated per cc. of solution. With 25 per cent porosity the amount of quartz precipitated would be only 0.0000071 cc. per cc. of rock. This would amount to 1 chert nodule 7 cc. in volume in 1 cubic meter

of rock. This certainly corresponds to the lower limit of volume of chert observed. Most cherty limestones contain far more than this; a typical occurrence might contain a thousand times the amount calculated, and many rocks include far more than that. Clearly, if the replacement were to be quantitatively significant, there must be greater quantities of solution circulating through the rock and continually dissolving carbonate and precipitating silica.

Ample demonstration has been given of the fact of circulation through rocks, even in formations thousands of feet deep; a recent summary and analysis of this phenomenon is given by Hubbert (1953). Aside from the direct evidence of water-column heights in drill holes, there is the indirect evidence given by increase in density of shales with depth (Athy, 1930; Hedberg, 1936), a fact which implies increasing compaction and movement of water upward in the column over a long period of time. The rate of compaction is exponential with time, and so water movement would be greater initially than for long times afterward. We may inquire as to the effects of this movement.

A much merited explanation for the increasing concentration of brines with depth is that proposed by DeSitter (1947), who reasoned that, as shales became compacted, they would act as semipermeable membranes, letting water through but retarding ions. This effect has recently been noted in laboratory experiments (McKelvey and Milne, 1960) and implied by determinations of salinities in modern sediment interstitial waters (Siever *et al.*, 1961). We can represent this situation by a simple model as in figure 5, in which water is passing through a semipermeable membrane. As a salt solution passes through, the fluid becomes more concentrated beneath the membrane and less concentrated above the membrane. If dissolved silica, H_4SiO_4, does not pass through the membrane as the ionic strength increases below the membrane, the silica becomes less soluble, eventually builds up to supersaturation and precipitates, while carbonate becomes more soluble below and dissolves. Above the membrane the solutions are undersaturated and only solution can take place. The dissolution of carbonate below the membrane can continue only until the solution becomes so concentrated that calcium carbonate also becomes supersaturated and starts precipitating along with the silica. It is difficult to evaluate this effect quantitatively because so little data are available on the magnitude of the retardation of ions as a function of compaction of shales; but a comparison of the general increase in brine salinity and compaction with depth suggests that there is more than enough water enriched in silica passing upward through the section to account for the amount of chert observed.

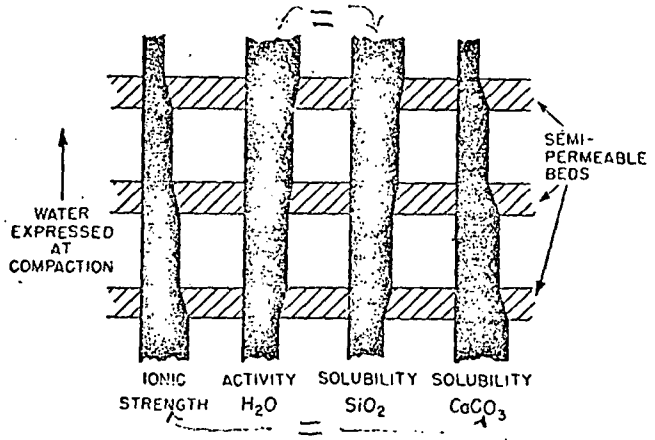

FIG. 5.—Changes in composition of pore waters as a result of water of compaction passing through semipermeable membranes.

If the effect of ionic strength is reinforced

by the slight temperature and pressure effects on solubility, the possibilities are improved; if we further hypothesize that much of the source is amorphous silica from organisms and silica released by the alteration of montmorillonite, there is certainly enough material that can be emplaced.

The question of the cause of the distribution of the nodules would then be answered by noting that, in essence, the replacement is determined by permeability distributions, which exhibit many seemingly random irregularities within beds and between beds that are complex functions of the fabric of the rock, including porosity, permeability, and tortuosity of flow channels. A sophisticated analysis of the probable distribution patterns of this kind of replacement phenomena has yet to be made.

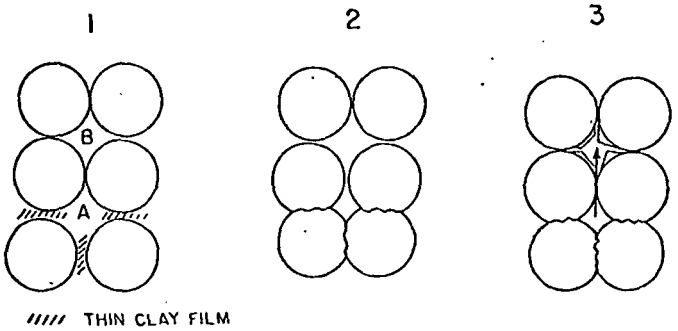

FIG. 6.—Sequence of stages in the development of sand grains cemented by pressure solution. In stage *1* the two beds differ only in the presence of interstitial clay. In stage *2* pressure solution has begun, decreasing the volume of pore space *A*. In stage *3* some fluid from *A* escapes to *B*, reduces pressure, and precipitates quartz.

SILICA CEMENTATION OF SANDSTONES

Most of the reasoning on origin of silica cementation of sandstones has been based on petrographic observations. Much of the literature has been summarized in Pettijohn (1957), Siever (1959), and Thomson (1959). Although there is no general agreement on a single mode of origin for all silica cement, there is arising a consensus (Heald, 1955, 1956; Siever, 1959; Thomson, 1959; Weyl, 1959*b*) that "pressure solution" at points of contact of quartz sand grains is responsible for cementation of sands showing interpenetrating detrital quartz grains. The evidence is both petrographic (Heald, 1956) and theoretical (Weyl, 1959*b*). Results of pressure solution experiments given in Part I above are in accord with their conclusions. Thermodynamic approaches to the problem, as related to change in preferred orientation of quartz crystals, have been given by MacDonald (1957), Kamb (1959), and Brace (1960).

The origin of silica cement in sandstones that show no interpenetration of grains is not so clear. In a general way, one can make the statement that the supersaturated solutions produced by pressure solution may migrate into a rock with little pressure solution and precipitate there. The validity of this statement depends in part on a plausible mechanism for movement of supersaturated pore waters from one horizon to another. Consideration of a model that is in accord with the facts of petrography leads to such a mechanism.

Let us take two sandstone beds, *A* and *B*, as shown in figure 6. Initially the only difference between the two beds is the small amount of interstitial clay present in *A* and absent in *B*. The relation of small amounts of clay to pressure solution was first pointed out by Heald (1956), and that relationship was analyzed in detail by Weyl (1959*b*) on a theoretical basis. In stage II, pressure solution has started in *A* because of the clay content but has not proceeded at all in *B*. As a result of the pressure solution, the grains of *A* have become slightly interpenetrated and the pore space has been reduced. As a result

of the pressure solution, the pore waters in *A* have become supersaturated, and as a consequence of pore-volume reduction, the pressure on the pore water in *A* has increased. In response to the pressure increase some of the pore waters migrate away from *A* to regions of lower pressure, such as at *B*, where pore volume has not been reduced by pressure solution. In stage III interpenetration is more advanced at *A* and the supersaturated pore waters, in part originally from *A* and now in *B* precipitate quartz cement in *B*. The process may be expected to continue until equilibrium has been reached over a very long period of time with both *A* and *B* completely cemented—*A* by interpenetration ("welding") and *B* by precipitation of introduced silica.

The natural situation is more complex, but the mechanism proposed allows for more or less pressure solution depending on the amount of interstitial clay, the depth of burial, and the time. The movement of the dissolved silica may be over short distances or long ones, for we have seen that solutions supersaturated with respect to quartz may persist for long times at low temperatures. It is easy to see why cementation may not be at all uniform in a sedimentary section, either vertically or laterally.

We have not yet accounted for all the sandstones that show quartz cement, for silica-cemented sandstones have been described that were cemented very early in their history. Examples studied by the author come from the Pennsylvanian of the northeastern United States. The evidence for the early origin is the presence of quartz cemented pebbles of a lower sandstone found in a calcite-cemented conglomerate, where the pebble is much better cemented than the conglomerate. This cement could not have come from pressure solution, for much time and depth of burial is needed for that process. Since the occurrences noted are far from any evidence of volcanism, there is no possibility of deriving the cement from glass. Possibilities that remain are the dissolution of siliceous organisms and reprecipitation as quartz and the concentration of silica in solution by the action of clay membranes, as was pointed out in the section on chert.

Conclusion

It appears that most of the occurrences of silica that give evidence of having formed in the postdepositional history of rocks are explicable in terms of (1) the metastability of amorphous silica at low temperatures; (2) the temperature and pressure coefficients of silica solubility, including pressure solution at points of contact; and (3) the effects of clay and shale beds acting as semipermeable membranes.

The metastability of amorphous silica leads to widespread production of solutions supersaturated with respect to quartz that will, given enough time, precipitate that mineral. The source of primary amorphous silica appears to be dominantly the silica-secreting organisms that keep the oceans depleted in dissolved silica far below saturation levels. It is not yet known by what biochemical mechanism the organisms are able to accomplish the precipitation.

Experimental determinations by many workers have established the dependence of quartz and amorphous silica solubility on temperature and pressure. Pressure solution at points of contact has been established both observationally and experimentally. The changes in solubility are of such magnitude that they could account for the quantities of silica that must have moved through rocks. The assumption of movement of silica-bearing solutions through rocks is made necessary by the abundance of silica of replacement origin which could not have been contained in static pore waters. The role of clay membranes as concentrators of dissolved materials has been demonstrated experimentally and by implication from observations on modern sediment waters and ancient rock brines and connate waters.

Acknowledgments.—I am indebted to many of my colleagues for stimulating discussions of the problems, both theoretical and experimental, that developed during the course of the work. Robert M. Garrels and I explored almost every different aspect of this work at one time or another. Clifford Frondel was helpful in

discussions of mineralogy and crystal chemistry. Francis Birch helped in the design of some of the experimental equipment. I have had the benefit of several thought-provoking talks with Peter K. Weyl of the Shell Development Company. While J. A. van Lier was at the Massachusetts Institute of Technology, we had many interesting conversations and compared notes. Garrels and Birch were kind enough to read the manuscript and made valuable suggestions. Harold Ames made the bombs for the higher-temperature solubility determinations, and Mahmoud Otooni helped with a portion of the experimental work.

The work was started while I was a National Science Foundation Senior Postdoctoral Fellow at Harvard in 1956–57. Later, much of the cost of the experimental work was met by a grant from the Shell Development Company. Additional support was received from the Committee on Experimental Geology and Geophysics, Harvard University.

REFERENCES CITED

ALEXANDER, G. B., HESTON, W. M., and ILER, R. K., 1954, The solubility of amorphous silica in water: Jour. Phys. Chemistry, v. 58, p. 453–455.

ANDEL, TJ. H. VAN, and POSTMA, H., 1954, Recent sediments of the Gulf of Paria, v. 1: Amsterdam, North-Holland Pub. Co., 245 p.

ATHY, L. F., 1930, Density, porosity and compaction of sedimentary rocks: Am. Assoc. Petroleum Geologists Bull., v. 14, p. 1–24.

BAAS-BECKING, L. G. M., KAPLAN, I. R., and MOORE, D., 1960, Limits of the natural environment in terms of pH and oxidation-reduction potentials: Jour. Geology, v. 68, p. 243–284.

BEZRUKOV, P. L., 1955, Distribution and rate of sedimentation of silica silts in the Sea of Okhotsk: Doklady Akad. Nauk S.S.S.R., v. 103, p. 473–476.

BIEN, G. S., CONTOIS, D. E., and THOMAS, N. H., 1959, The removal of soluble silica from fresh water entering the sea. *In:* Silica in sediments: Soc. Econ. Paleontologists & Mineralogists Special Pub. 7, p. 20–35.

BISSELL, H. J., 1959, Silica in sediments of the Upper Paleozoic of the Cordilleran area. *In:* Silica in sediments: Soc. Econ. Paleontologists & Mineralogists Special Pub. 7, p. 150–185.

BRACE, W. F., 1960, Orientation of anisotropic minerals in a stress field: Discussion: Geol. Soc. Am. Mem. 79, p. 9–20.

BRAMLETTE, M. N., 1946, The Monterey formation of California and the origin of its siliceous rocks: U.S. Geol. Survey Prof. Paper 212, 57 p.

BRUEVITCH, S. V., 1953, Geochemistry of silicon in the sea: Izvest. Akad. Nauk S.S.S.R., Ser. Geol., no. 4, p. 67–69.

CHAVE, K. E., 1960, Evidence of history of sea water from chemistry of deeper subsurface waters of ancient basins: Am. Assoc. Petroleum Geologists Bull., v. 44, p. 357–370.

CHOW, D. T. W., and ROBINSON, R. J., 1953, Forms of silicate available for colorimetric determination: Anal. Chemistry, v. 25, p. 646–648.

CLARKE, F. W., 1924, The data of geochemistry: U.S. Geol. Survey Bull. 770, 841 p.

CORRENS, C. W., 1941, Über die Löslichkeit von Kieselsäure in schwach sauren und alkalischen Lösungen: Chemie der Erde, v. 13, p. 92–96.

——— 1950, Zur Geochimie der Diagenese: Geochim. et Cosmochim. Acta, v. 1, p. 49–54.

——— and NAGELSCHMIDT, G., 1933, Über Faserbau und optische Eigenschaften von Chalzedon: Zeitschr. Kristallographie, v. 85, p. 199–213.

DESITTER, L. U., 1947, Diagenesis of oil-field brines: Am. Assoc. Petroleum Geologists Bull., v. 31, p. 2030–2040.

DONNAY, J. D. H., 1936, La birefringence de forme dans la calcédoine: Soc. géol. de Belgique Ann., v. 59, p. 289–302.

ELLIS, A. J., 1959, The solubility of calcite in carbon dioxide solutions: Am. Jour. Sci., v. 257, p. 354–365.

EMERY, K. O., and RITTENBERG, S. C., 1952, Early diagenesis of California basin sediments in relation to origin of oil: Am. Assoc. Petroleum Geologists Bull., v. 36, p. 735–806.

FOLK, R. L., and WEAVER, C. E., 1952, A study of the texture and composition of chert: Am. Jour. Sci., v. 250, p. 498–510.

FOURNIER, R. O., 1960, Solubility of quartz in water in the temperature interval from 25° C. to 300° C.: Geol. Soc. America Bull., v. 71, p. 1867–1868.

GARDNER, L. U., 1938, Reaction of the living body to different types of mineral dusts: Am. Inst. Mining & Metall. Eng., Tech. Pub. 929, p. 1–15.

GARRELS, R. M., 1960, Mineral equilibrium: New York, Harper & Bros., 254 p.

———, THOMPSON, M. E., and SIEVER, R., 1961, Control of carbonate solubility by carbonate complexes: Am. Jour. Sci., v. 259, p. 24–45.

GOLDSTEIN, A., JR., 1959, Cherts and novaculites of Ouachita facies. *In:* Silica in sediments: Soc. Econ. Paleontologists & Mineralogists Special Pub. 7, p. 135–149.

GREENBERG, S. A., and PRICE, E. W., 1957, The solubility of silica in solutions of electrolytes: Jour. Phys. Chem., v. 61, p. 1539–1541.

HARNED, H. S., and OWEN, B. B. 1950, The physical chemistry of electrolytic solutions: New York, Reinhold Pub. Corp., 645 p.

HARVEY, H. W., 1957, The chemistry and fertility of sea waters: London, Cambridge Univ. Press, 234 p.

HEALD, M. T., 1955, Stylolites in sandstones: Jour.

Geology, v. 63, p. 101–114.

——— 1956, Cementation of Simpson and St. Peter sandstones in parts of Oklahoma, Arkansas, and Missouri: *ibid.*, v. 64, p. 16–30.

HEDBERG, H. D., 1936, Gravitational compaction of clays and shales: Am. Jour. Sci., v. 31, p. 241–297.

HUBBERT, M. K., 1953, Entrapment of petroleum under hydrodynamic conditions: Am. Assoc. Petroleum Geologists Bull., v. 37, p. 1954–2026.

ILER, R. K., 1955, The colloid chemistry of silica and silicates: Ithaca, Cornell Univ. Press, 324 p.

KAMB, W. B., 1959, Theory of preferred crystal orientation developed by crystallization under stress: Jour. Geology, v. 67, p. 153–170.

KENNEDY, G. C., 1950, A portion of the system silica-water: Econ. Geology, v. 45, p. 629–653.

KRAUSKOPF, K. B., 1956, Dissolution and precipitation of silica at low temperatures: Geochim. et Cosmochim. Acta, v. 10, p. 1–26.

——— 1959, The geochemistry of silica in sedimentary environments. *In:* Silica in sediments: Soc. Econ. Paleontologists & Mineralogists Special Pub. 7, p. 4–19.

LENHER, V., 1921, Silicic acid: Jour. Am. Chem. Soc., v. 43, p. 391–396.

LEWIN, J. C., 1961, The dissolution of silica from diatom walls: Geochim. et Cosmochim. Acta, v. 21, p. 182–198.

LIER, J. A., VAN, 1959, The solubility of quartz: Utrecht, Kemink en Zoon, 54 p.

LOWENSTAM, H. A., 1948, Biostratigraphic studies of the Niagaran inter-reef formation in northeastern Illinois: Illinois State Museum Sci. Papers, v. 4.

LYMAN, J., and FLEMING, R. H., 1940, Composition of sea water: Jour. Marine Research, v. 3, p. 134–146.

MACDONALD, G. J. F., 1957, Thermodynamics of solids under non-hydrostatic stress with geological applications: Am. Jour. Sci., v. 255, p. 266–281.

MCKELVEY, J. G., and MILNE, I. H., 1960, The flow of salt solutions through compacted clay: Proc. Natl. Clay Conference (in press).

MEENTS, W. F., BELL, A. H., REES, O. W., and TILBURY, W. G., 1952, Illinois oil-field brines, their geologic occurrence and chemical composition: Illinois Geol. Survey, Illinois Petroleum 66, 37 p.

MIDGLEY, H. G., 1951, Chalcedony and flint: Geol. Mag., v. 88, p. 179–184.

MILLER, J. P., 1952, A portion of the system calcium carbonate-carbon dioxide-water, with geologic implications: Am. Jour. Sci., v. 250, p. 161–203.

NEWELL, N. D., RIGBY, J. K., FISCHER, A. G., WHITEMAN, A. J., HICKOX, J. E., and BRADLEY, J. S., 1953, The Permian reef complex of the Guadalupe Mountains region, Texas and New Mexico: San Francisco, W. H. Freeman & Co., 236 p.

OKAMOTO, G., OKURA, T., and GOTO, K., 1957, Properties of silica in water. Geochim. et Cosmochim. Acta, v. 12, p. 123–132.

OPARIN, A. I., 1953, The origin of life: New York, Dover Publishers, Inc., 270 p.

OWEN, B. B., and BRINKLEY, S. R., 1941, Calculation of the effect of pressure upon ionic equilibrium in pure water and in salt solutions: Chem. Rev., v. 29, p. 461–474.

PETTIJOHN, F. J., 1943, Archean sedimentation: Geol. Soc. America Bull., v. 54, p. 925–972.

——— 1957, Sedimentary rocks: New York, Harper & Bros., 718 p.

ROSS, C. S., and HENDRICKS, S. B., 1945, Minerals of the Montmorillonite group: U.S. Geol. Survey Prof. Paper 205B, p. 23–77.

RUBEY, W. W., 1929, Origin of the siliceous Mowry shale of the Black Hills region: U.S. Geol. Survey Prof. Paper 154, p. 153–170.

SIEVER, R., 1957, The silica budget in the sedimentary cycle: Am. Mineralogist, v. 42, p. 821–841.

——— 1959, Petrology and geochemistry of silica cementation in some Pennsylvanian sandstones. *In:* Silica in sediments: Soc. Econ. Paleontologists & Mineralogists Special Pub. 7, p. 55–79.

———, GARRELS, R. M., KANWISHER, J., and BERNER, R. A., 1961, Interstitial waters of recent marine muds off Cape Cod: Science, v. 133, p. 1071–1072.

——— and SCOTT, R. A., 1961, Organic geochemistry of silica. *In:* BREGER, I. A. (ed.), Organic geochemistry: London, Pergamon Press (in press).

SOSMAN, R. B., 1927, The properties of silica: Am. Chem. Soc. Mon. Ser. No. 37: New York: Chemical Catalogue Co.

THOMSON, A., 1959, Pressure solution and porosity. *In:* Silica in sediments: Soc. Econ. Paleontologists & Mineralogists Special Pub. 7, p. 92–110.

UREY, H. C., LOWENSTAM, H. A., EPSTEIN, S., and MCKINNEY, C. R., 1951, Measurement of paleotemperatures and temperatures of the Upper Cretaceous of England, Denmark, and the Southeastern United States: Geol. Soc. America Bull., v. 62, p. 399–416.

WARREN, B. E., and BISCOE, J., 1938, The structure of silica glass by X-ray diffraction studies: Jour. Am. Ceramic Soc., v. 21, p. 49–54.

WEYL, P. K., 1959*a*, Change in solubility of calcium carbonate with temperature and carbon dioxide content: Geochim. et Cosmochim. Acta, v. 17, p. 214–225.

——— 1959*b*, Pressure solution and the force of crystallization—a phenomenological theory: Jour. Geophys. Research, v. 64, p. 2001–2025.

WHITE, D. E., BRANNOCK, W. W., and MURATA, K. J., 1956, Silica in hot-spring waters: Geochim. et Cosmochim. Acta, v. 10, p. 27–59.

YODER, H. S., and EUGSTER, H. P., 1955, Synthetic and natural muscovites: Geochim. et Cosmochim. Acta, v. 8, p. 225–280.

ZEN, E-AN, 1959*a*, Clay mineral-carbonate relations in sedimentary rocks: Am. Jour. Sci., v. 257, p. 29–43.

——— 1959*b*, Mineralogy and petrography of marine bottom sediment samples off the coast of Peru and Chile: Jour. Sed. Petrology, v. 29, p. 513–539.

Economic Geology
Vol. 73, 1978, pp. 21-28

Sourcelines, Sourceregions, and Pathlines for Fluids in Hydrothermal Systems Related to Cooling Plutons

DENIS NORTON

Abstract

Simulation of hydrothermal systems by numerical methods permits computation of the initial positions (sources) of all fluids in the system. The locus of these positions, which are sourcelines, defines an essential link between the theories of irreversible mass transfer and those of thermally driven fluid flow. The concept of a fluid sourceline is introduced to facilitate the quantitative description of the initial composition of fluids which ultimately circulate through rocks in the vicinity of hot plutons.

The mathematical definition of fluid sourcelines and pathlines for hydrothermal systems permits the quantitative prediction of the initial position and, hence, initial compositions of all fluids which circulate through rocks in the vicinity of an igneous intrusion and the variations in temperature, pressure, and rock type along flow paths and, hence, the changes in composition of the fluid as it flows from its source to a position of interest in the system.

Examples of fluid sourcelines, sourceregions, and pathlines defined for inert fluids in an idealized hydrothermal system indicate the predominant source of fluids flowing through permeable hot plutons is from host rock environments adjacent to and above the pluton. These sourceregions in two dimensions include rocks from a 50-km² region as far as 5.5 km away from a 2.7-km-wide and 4.5-km-tall pluton.

Introduction

FLUID convection appears to be a universal process related to igneous and volcanic activity in the upper crust. Furthermore, the flow of fluids from one geologic environment into another is suggested by observations of active geothermal systems (Lapwood, 1948; Elder, 1965; Wooding, 1957; Donaldson, 1962), stable-light isotope data (Taylor, 1974), gains and losses of major and minor components from host rocks, and changes in mineralogy (Meyer, 1950; Villas, 1975). Also, calculations which simulate interactions between fluids and rocks (Helgeson, 1970; Norton, 1971) and fluid convection around cooling plutons (Norton and Knight, 1977) indicate that thorough redistribution of large masses of fluids is a natural feature of these environments.

Fluids in the Wairakei geothermal system are estimated to have circulated through permeable rocks for distances of tens of kilometers during the active thermal history of this region (Elder, 1965; Grindley, 1965). Similarly, meteoric water circulation to depths of several kilometers is called upon to account for the oxygen isotope values measured in numerous plutons (Taylor, 1974). The circulation paths of meteoric water through various host rock environments, at moderate temperatures without significant isotopic changes, ultimately flow into many plutons, where exchange reactions result in the depletion of the ^{18}O content of the igneous rocks.

There are numerous references in the literature to rock alteration associated with plutons emplaced into both the upper continental and oceanic crusts; however, only a few typical examples are mentioned herein. Compositional and mineralogical changes in carbonate and noncarbonate rocks around plutons have been noted several kilometers away from the plutons (Cooper, 1957; Brown and Ellis, 1970), as well as in the plutons themselves (Nielson, 1968; Gustafson and Hunt, 1975). Extensive alterations of rock composition clearly occur as a consequence of the large masses of reactive fluids circulating through the rocks.

The simulation of rock alteration processes, using reasonable estimates of initial fluid compositions, further supports the concept of extensive fluid circulation and reactions between fluids and rocks in the temperature range from 25° to 350°C (Helgeson, 1970). Analogous studies of the circulation process have described the style of fluid motion (Wooding, 1957; Ribando et al., 1976; Norton and Cathles, in press; Henley, 1973) and have provided some notion of the masses of fluid in the hydrothermal systems. The description of actual fluid flow paths and effective fluid : rock ratios related to cooling plutons has provided quantitative heuristic models of these systems (Norton and Knight, 1977). The process of fluid circulation and concomitant reaction with rocks is, however, not well enough understood to enable ore deposit geologists either to test hypotheses regarding the sources of fluids and ore-forming com-

ponents or to predict the occurrence of subsurface ore deposits on the basis of limited surface or drill hole data.

The purpose of this communication is to describe the concepts that permit quantitative description of the sources and flow paths of inert fluids which circulate in the vicinity of cooling plutons. These concepts permit the quantitative description of the initial positions of all fluids which ultimately circulate through rocks in the vicinity of an igneous intrusion and the paths along which the fluids flow (including the temperature, pressure, and compositional variations of the path) from the fluid source to any position of interest in the system. Quantitative description of reactive circulation and mineral zoning in hydrothermal systems follows simply from the concepts presented below, when they are coupled with those of irreversible mass transfer between fluids and rocks (Helgeson, 1970). The sources and redistribution of the chemical components in reactive fluids will form the basis of a future communication.

Fluid Circulation around Cooling Plutons

Hydrothermal fluid flow is caused by lateral density perturbations in the fluids confined within the flow porosity of rocks. Fluid density anomalies resulting from thermal and concentration effects are relatively common in upper crustal rocks, especially the large thermal perturbations which occur in pluton environments. Therefore, it is reasonable to expect fluid circulation to be a characteristic feature of these environments, if the rock permeability is sufficiently large.

Fluid circulation in natural systems is not easily studied by direct observation since even the most thoroughly explored geothermal systems are a small sample of the total system and the duration of field studies represents only a small fraction of the time duration of the thermal anomalies. The lack of a quantitative understanding of fluid circulation is, therefore, not surprising.

However, the fluid flow in pluton environments can be effectively scaled and represented by partial differential equations which describe the conservation of mass, momentum, and energy for the fluid-rock system (Norton and Knight, 1977):

$$\gamma \frac{\partial T}{\partial t} + \bar{q} \cdot \bar{\nabla} \bar{H} = \bar{\nabla} \cdot \kappa \bar{\nabla} \bar{T}$$

(conservation of energy) (1)

and

$$\frac{\nu}{k} \bar{\nabla} \cdot \frac{\nu}{k} \bar{\nabla} \bar{\Psi} = R \frac{\partial \rho}{\partial y}$$

(conservation of momentum) (2)

where T is the temperature; Ψ the scalar streamfunction; $\bar{q}$ the fluid flux; H, ρ, and ν are the enthalpy, density, and viscosity of the fluid; k is the permeability of the rock; κ the thermal conductivity and γ the volumetric heat capacity of the fluid saturated media; R the Rayleigh number; t the time; ∇ the gradient operator; and y the horizontal distance in the two-dimensional section to which these equations apply. The conservation of mass is explicitly included in equations (1) and (2). Equations (1) and (2) are approximated by finite difference numerical equations which permit the computation of the values of the dependent variables at discrete points in the domain from the initial and boundary values specified for the system.

The physical meaning of equations (1) and (2) is apparent if one considers that the fluid density gradients, on the right-hand side of equation (2), resulting from a thermal anomaly cause fluid circulation; e.g., they define gradient values of the streamfunction and, therefore, fluid flux since $q_z = -\partial\Psi/\partial y$ and $q_y = \partial\Psi/\partial z$. The fluid flux, $\bar{q}$, in turn transports heat away from the thermal anomaly, i.e., the second term on the left of equation (1); at the same time, thermal energy is conducted away from the thermal anomaly, the right-hand side in equation (1). Both of these processes give rise to a decrease in temperature with respect to time and, therefore, decrease the horizontal fluid density gradients; and, consequently, the thermal anomaly is decreased by the combined convective and conductive heat transfer. The coupled solution of (1) and (2) is achieved by a series of steady-state computations at explicitly stable time steps, thereby defining the temperature and fluid flux as a function of time. The pressure is in turn computed at each steady-state step by integration of the Darcy equation,

$$\bar{q} = -\frac{k}{\nu} [\bar{\nabla} \bar{P} + \rho \bar{g}], \qquad (3)$$

in which the fluid properties, ν and ρ, are expressed as a function of temperature and pressure, P, and the gravitational force vector, $\bar{g}$, is constant. Fluid velocities are then determined from

$$\bar{V} = \bar{q}/\rho. \qquad (4)$$

Numerical simulation of the equations quantitatively predicts the nature of hydrothermal fluid flow and provides the ore deposit geologist with a key to understanding how these processes operated in the past. The reliability of these computations and their applicability to specific locations is a direct function of the degree to which those parameters that affect heat and mass transport in the hydrothermal system (e.g., permeability, flow porosity, heat source geome-

try, and transport properties of the fluid and rock) are known. The permeability of fossil hydrothermal systems is poorly known and difficult to estimate but is requisite knowledge for understanding the ore-forming process. As a consequence of the inadequate data base, especially with regard to permeability, computer stimulation requires estimation of these data; numerical results are therefore obtained for geologically reasonable ranges of parameters. The reliability of the computations for a given set of transport parameters depends directly on the number of discrete points used and on the convergence and stability of the numerical algorithm.

Analysis of idealized pluton environments using the above procedure indicates that in systems where permeabilities are greater than 10^{-14} cm^2 convective fluid circulation accounts for 10 percent or more of the total heat transport. Permeabilities of this order are realized in fractured rocks where the fracture frequency is on the order of one fracture per meter and the fracture aperture is ~ 2 μm. The abundance of fractures commonly observed in pluton environments suggests that many of these rocks are host to extensive fluid circulation. The most significant aspect of these computer experiments for the subsequent discussion is that the fluid flux and velocity (of inert fluids, e.g., fluid approximated by the H_2O system) can be quantitatively determined for idealized pluton environments.

The Sourceline Concept in Hydrothermal Systems

Fluid velocities may be computed for thermal or solute perturbations that cause fluid flow in geologic systems for which rock permeabilities are known or can be estimated. These fluid velocities in turn permit the quantitative description of fluid pathlines. Consider a fluid packet of some arbitrary position in the system, then the fluid path is defined by

$$d\bar{l} = \bar{V}dt, \qquad (5)$$

where $\bar{V}$ is the Darcy velocity and $d\bar{l}$ is the incremental distance along the path traveled during time interval, dt. Since the velocity is known as a function of time from equations (1), (2), and (4), equation (5) may be integrated for the n*th* such fluid packet during time interval $t - t_0$ in the system,

$$\bar{l}_n = \int_{t_0}^{t} \bar{V}_n(t)dt, \qquad (6)$$

where $\bar{V}_n(t)$ is the average velocity of the n*th* particle during the discrete time interval Δt (Fig. 1). Along the n*th* such path, variations in temperature and pressure are also defined from the transport equations (1) and (2), and variations in the rock environment are determined by geologic data. Therefore, the reaction history of each fluid packet may be explicitly determined on the basis of its initial composition and subsequent flow path. However, as a packet moves from one position to another it flows through rocks which may have already reacted with fluid which flowed through earlier and probably altered the initial composition or mineralogy of the rock. This requires, then, a concept by which to simulate the flow-reaction processes at discrete points in the system instead of following the fluid circulation.

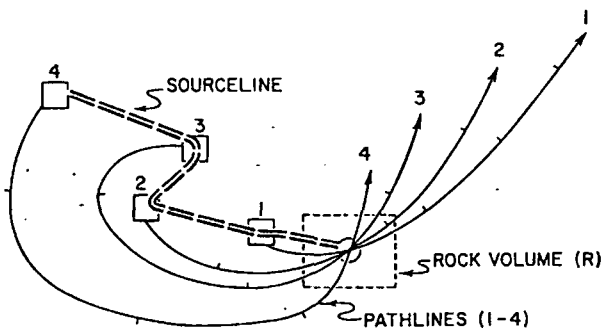

FIG. 1. A schematic of fluid pathlines and sourcelines. Pathlines are defined by equation (6) for $n = 4$ fluid packets where the box indicates the initial position, $\bar{l}_n = 0$, of each fluid packet at time = 0, and their respective positions are indicated by tic marks which represent equal elapsed times. The variation in distance between the tics along a pathline reflects the fluid velocity variations. The fluid packets flow sequentially through a common rock volume in this schematic example; however, this is a special case. The line connecting the original positions, boxes, of this special set of pathlines defines the fluid sourceline for the rock volume, R. The sourceline may be computed directly from equation (9) for $n = 4$. Note that the sourceline for the rock volume defines the fluid source, but the sourceline is significantly different from the paths followed by the fluids from their sources to the rock volume. Since tht simulation is computed in two dimensions, the rock volume has an arbitrary unit depth.

The concept of a fluid sourceline is introduced in order to study the circulation-reaction process with respect to fixed positions in the system. A fluid sourceline is the locus of points of all fluid packets whose pathline intersect a fixed position of interest in the system. Consider such a position in a rock volume, R (Fig. 1). The position vector $\bar{S}_{ij}$, of a fluid sourceline for this position is defined in terms of the individual fluid packet position vectors:

$$\bar{S}_{ij} = \bar{r}_i + [\bar{r}_{i+1} - \bar{r}_i]\xi_j, \quad 0 \le \xi_j \le 1, \quad i = 1, N-1 \qquad (7)$$

where $\bar{r}_i$ and $\bar{r}_{i+1}$ are the position vectors for the fluid packets at an initial time, t_0, which flow through the rock volume, and ξ_j is an interpolation factor which varies continuously from 0 to 1 as j increases. The individual vectors are in turn defined by equation (6), but since we are tracing back along the flow

path, the integration limits are reversed with respect to equation (6):

$$\bar{r}_i = \int_{t_i}^{t_0} \bar{V}_i(t)dt, \qquad (8)$$

where t_i is the time at which particle i was at the position of interest, R. The sourceline position vector in equation (7) becomes

$$\bar{S}_{ij} = \int_{t_i}^{t_0} [\bar{V}_i(t) + (\bar{V}_{i+1}(t) - \bar{V}_i(t))\xi_i]dt. \qquad (9)$$

The definition of a sourceline, for an arbitrary time interval prior to the end of a thermal event, follows directly from equation (9) (Fig. 1).

A fluid sourceline may be defined at each discrete point in the system at which the variation in fluid velocity is known for the elapsed time interval of interest. Since hydrothermal fluid velocities around cooling plutons typically vary over several orders of magnitude throughout the cooling event, sourcelines may accordingly be very sinuous lines.

Examples of Sourcelines and Pathlines

Fluid pathlines and sourcelines for a hydrothermal system in the region of a cooling pluton which was emplaced into a stratified permeable host rock environment have been calculated. Although the concept of sourcelines and pathlines is quite independent of extenuating geologic circumstances, the extension of this concept to natural systems is not. Therefore, the following example is merely a first approximation to nature. One natural analog to this system is the stratified host rock environment in southeastern Arizona that many plutons have intruded (Fig. 2A). The thermal history of this system, for a period of $\sim 2 \times 10^5$ years, has been simulated by the methods summarized above. The details of this analysis are thoroughly described in Norton and Knight (1977). Those aspects of the system relevant to this discussion are the initial and boundary conditions (Fig. 2B) and the time variation of the pluton permeability (Fig. 3). The fluid velocities computed at discrete time intervals permit the calculation of fluid pathlines and sourcelines of the inert fluid assumed to be in the system.

First we examine examples of pathlines in the system and the temperature-pressure variations encountered along the flow paths. Pathlines for fluid packets (Fig. 4), 1, which occurs in the relatively permeable rocks and is initially several kilometers away laterally and above the pluton, 2, which is adjacent to the pluton near the contact between low and high permeability rocks, and 3, which is adjacent to the pluton in the low permeability rocks near the pluton side contact and deep in the system,

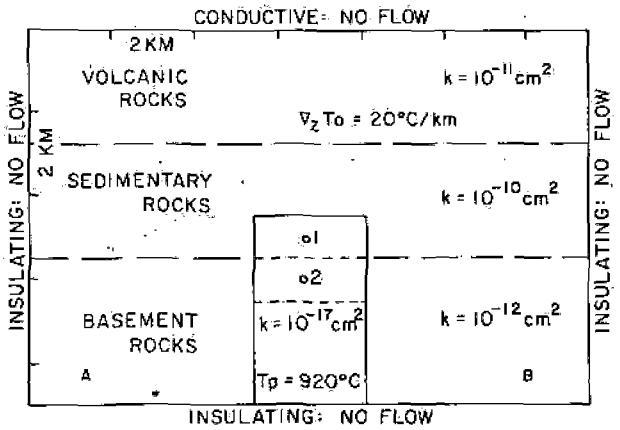

FIG. 2. A two-dimensional cross section of pluton environment. A. Hypothetical geologic units representing stratified host rocks around magma initially at 920°C. B. Initial and boundary conditions appropriate for an idealized system for which host rock permeabilities were assigned on the basis of estimates, Norton and Knapp (1977). The level of emplacement of the pluton was selected by an analog to Tertiary plutons which occur in southeastern Arizona. The bottom boundary conditions for flow and energy simulate decreases in permeability and increases in temperature with depth, and the conditions at the top of the system simulate conductive energy loss and no loss of fluid to surface hot springs. Side boundaries are selected for convenience and do not significantly affect the results discussed herein. Pluton permeability is 10^{-17} cm^2, or effectively zero, in order to represent an initially unfractured magma. The domain is symmetrical with respect to a vertical centerline through the pluton. The domain was discretized into 144 points for the numerical solution of equations, resulting in a spatial error on the order of 5 percent of the system height. Discrete time steps were computed such that the computations converge to within approximately ten percent of the true value defined by the differential equations.

are considered. The length and shape of these circulation paths are directly related to the spatial and temporal variation in the fluid velocities. The fluid

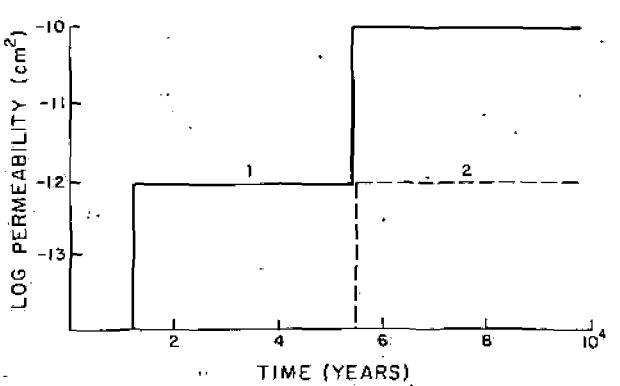

FIG. 3. Permeability variations with respect to time in the upper portion of the pluton, Figure 1, points 1 and 2. Values of $k = 10^{-11}$ cm^2 are equivalent to a millidarcy. Instantaneous permeability variations were used to simulate fracturing of pluton as it crystallizes and cools to below solidus temperatures, circa 800°C. These variations are in accord with the observation that plutons in these types of systems are thoroughly fractured.

paths are initially through host rock environments then into the pluton, where packet 3 remains for the 2×10^5-year duration of the event while 1 and 2 move out the pluton top and through host rocks again. The Darcy velocities of the fluids along their respective paths range from an average of 10^{-6} cm/sec for packet 2 to $< 10^{-8}$ cm/sec for packet 3.

Representing the path of the fluid packets through temperature-pressure space with respect to the phases in the H_2O system permits quantitative prediction of the solution properties of the circulating fluid packets (Fig. 5). Packet 1 flows downward along a nearly normal temperature-pressure gradient, then its temperature increases at constant pressure as it flows into the pluton. The pluton temperature by this time has decreased to $\sim 200°C$. This packet then flows out the pluton top and upward into overlying host rocks subparallel to a nearly normal gradient. Packets 2 and 3 have similar paths except that they are initially at higher pressures than they subsequently encounter along their paths. The solution properties of liquid and supercritical fluid along these types of paths vary in a manner that undoubtedly has a profound affect on fluid-rock reactions along the path (Helgeson and Kirkham, 1974a, 1974b).

Sourcelines for fluids which flow through positions 1 and 2 in the pluton indicate that during the initial 5,000- to 15,000-year cooling period fluid sources occurred entirely within the solidified and permeable pluton, but that at times $> 10^4$ years fluids were derived from the surrounding host rocks (Fig. 6A). An implicit assumption in the computation is that the fractures which form in the pluton are

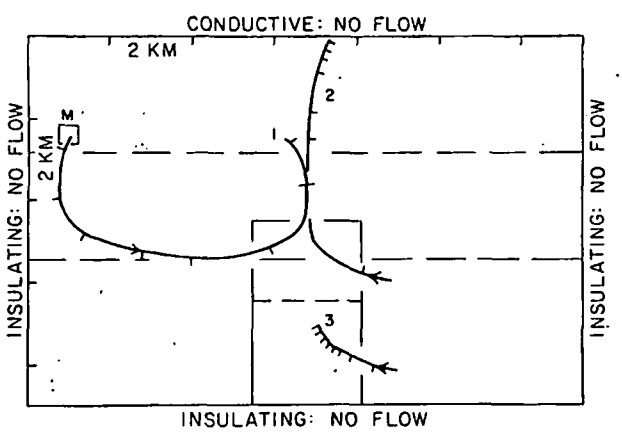

FIG. 4. Fluid pathlines 1–3 after 2×10^5-years elapsed time: 1, for fluids whose initial positions are in relatively permeable host rocks and far away from the pluton; 2, in low permeability host rocks, near the side contact of the pluton and adjacent to the portion of the pluton which has time dependent permeability; and 3, near the base of the system adjacent to the pluton. Tic intervals along the pathlines are at 25,000-year increments, and arrows represent the direction of fluid packet motion.

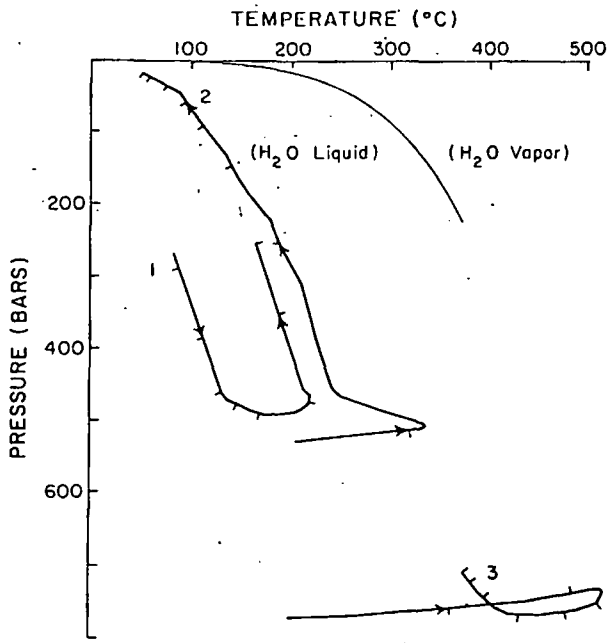

FIG. 5. Fluid pathlines after 2×10^5-years elapsed time, 1–3, from Figure 4 projected onto a temperature-pressure section of the H_2O system, illustrating variations in conditions encountered along flow paths with respect to the liquid-vapor surface. Arrows represent direction of flow and tic marks represent 25,000-year time increments.

filled with fluids derived from the magma crystallization process. These fluids are analogous to magmatic fluids but are approximated by the H_2O system. Relatively large concentrations, > 15 weight percent, of dissolved components in this fluid phase might temporarily alter the flow pattern as a result of the higher density of these fluids with respect to lower concentrations in the surrounding host rock fluids. The important point here is that during the cooling period fluids derived from the host rock environments are the predominant fluids which flow through the pluton. Fluid sources within the host rocks, however, occur as far as 2 km above and 5 km laterally away from the pluton (Fig. 6A, sourceline 1, source point M) but are dominantly from within the 2.7-km-thick permeable layer. The inflections in sourceline 1 between position (1) and the tic mark at 25,000 years reflect both the fracture of the pluton, simulated by a sudden increase in its permeability, and the shift in the fluid density perturbation upward as the rocks and fluids above the pluton become heated.

Sets of sourcelines defined for the pluton describe a sourceregion from which all fluids circulating through the pluton for some time interval were derived. The sourceregion in the host rocks for fluids which flowed through the example pluton extends over a ~ 50 km^2 cross-sectional area (Fig.

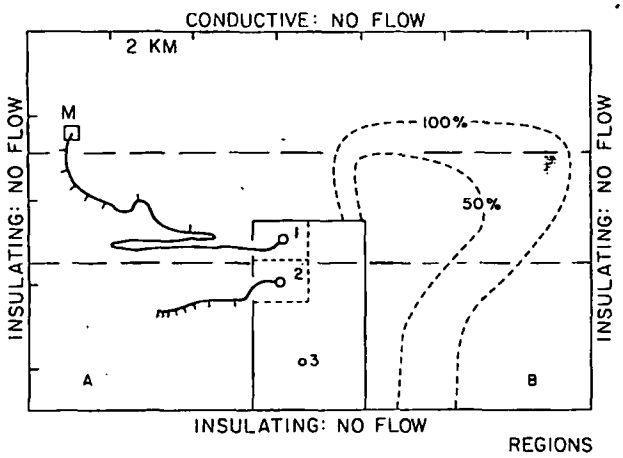

FIG. 6. Sourcelines and sourceregions for fluids which flow through the pluton. A. Sourcelines for positions 1 and 2 for the system in Figure 2, for all fluids which flow through these positions in 2×10^5 years elapsed time. Tic marks on the sourcelines are at 2.5×10^4-year intervals, starting at the end of the line marked with the position number. Position 3 represents a region of effectively zero permeability and therefore cools predominantly by conductive heat transfer for comparison with 1 and 2. The box, M. represents the fluid source farthest from position 1 and coincides with M in Figure 4 on pathline 1. Note the difference between the sourcelines and the actual pathlines that fluids flow along. The regions around the positions (indicated by dashed lines) denote the effective volume (1.25 km² and 1 cm deep) used in computing mass flux in the vicinity of a respective position. B. Sourceregions for all fluids flowing through the pluton. Regions are delimited by contours depicting 100 and 50 percent of those fluids whose source are in the host rocks and were defined by 25 independent sourcelines.

6B). During the initial 5×10^4-year cooling period the fluid mass that circulates through the pluton from host rock sources is derived entirely from between the 50 percent contour and the pluton margins, Figure 6B. The fluid from these sources amounts to approximately 95 percent of the fluid flowing through the upper 2 km of the pluton during the 5×10^4-year time interval; the other 5 percent of the fluid flowing through the upper 2 km of the pluton was derived from sources within the pluton. At an elapsed time of 2×10^5 years, only 2 percent of the fluid was derived from sources within the pluton, and 98 percent was derived from between the 100 percent host rock contour value and the pluton margins. Also, more than 75 percent of the fluid flowing through the upper 2 km of the pluton was derived from the permeable stratigraphic unit in the host rocks.

Sourcelines for fluids which flow through positions in the host rocks are considerably more diversified than for fluids through positions in the pluton. At positions in the relatively permeable host rocks, typified by 4, Figure 7, a considerable amount of fluid recirculation is evident, even to the degree that fluid originating in the vicinity of 4 circulates back through 4 in 4×10^5 years. This recirculation is characteristic of horizontally stratified host rocks within confined permeable units. Positions directly above the pluton, 5, 6, and 8, have sourcelines which indicate a portion of the fluids were derived from sources within the pluton; however, a predominance of these fluids is from sources within host rocks. Because of the thorough redistribution of fluids from host rocks adjacent to the pluton to regions above the pluton, the effect of fluids from magmatic sources is probably obscured.

Sources for hydrothermal fluids in natural systems analogous to the model system analyzed herein are predicted to be predominantly from the host rocks adjacent to and above the pluton. These sourceregions encompass rocks up to 5.5 km away from the side of the pluton. A portion of the fluids is derived from within the pluton, but it only accounts for less than a few weight percent of the total fluid mass that ultimately circulates through the pluton. The compositions of these fluids are a function of conditions at their sources prior to pluton emplacement, as well as temperature-pressure variations and the compositions of fluids and rocks along their pathlines.

The nature of fluid sourcelines in other types of systems, such as those with uniformly permeable host rocks, vertical fracture zones over the pluton, impermeable plutons, and boundary conditions open to flow, have been examined. The sourcelines in these systems are similar to the model systems discussed. However, in systems with impermeable plutons, $k < 10^{-14}$ cm², a minor amount of fluids circulate through the hot plutons. Variations in boundary conditions, permeabilities (for values $> 10^{-14}$ cm²), and pluton geometry result in variations in the shape of the sourcelines and pathlines, but the over-

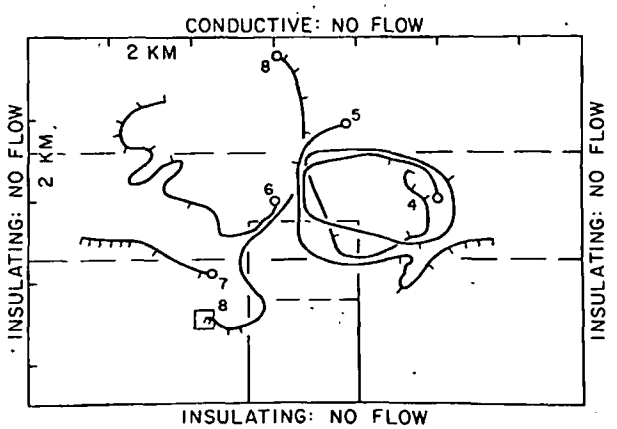

FIG. 7. Sourcelines for fluids which flow through host rocks. The sourcelines for positions 4–8, marked by small circles, indicate a diversity of sourcelines and sourceregions in the domain and a thorough mixing of fluids. Tic marks occur at every 2.5×10^4 years.

all conclusions discussed above are not significantly different for other systems.

The nature of fluid-rock reactions may be predicted if the temperature, pressure, fluid velocity, and amount of fluid flowing through the positions of interest are known. Therefore, these variables were defined for regions in the pluton coincident with sourcelines positions, as represented in Figure 6A. The temperature variation with time at position 3 in the pluton is included since it is analogous to a pluton which cools by simple conduction, whereas the variations at positions 1 and 2 are affected by the large convective heat transport (Fig. 8A). At position 1, Figure 6A, temperatures decrease rapidly to 250°C at $\sim 6 \times 10^3$ years, coincident with a second fracture event. At position 2 temperatures decrease to < 400°C at $> 3 \times 10^4$ years, suggesting that relatively low temperatures are common for the major portion of the cooling time in relatively permeable plutons (Fig. 8A). In general, the increase in pluton permeability to $\geq 10^{-12}$ cm^2 results in the rapid cooling of the upper portion of the pluton to a few tens of degrees above the regional temperature at the corresponding depth. Pressure does not vary significantly during the cooling event and tends to remain at about hydrostatic pressure. However, the fluid velocity increases rapidly in response to the initial conditions and the permeability changes. Darcy velocity maximums of 5×10^{-5} cm/sec and 5×10^{-6} cm/sec are realized at positions 1 and 2, respectively, Figure 8B. A subsequent decrease in velocity follows this initial peak and then a gradual increase to a second maxima. This second maxima in velocities occurs at $\sim 3 \times 10^4$ years, as a consequence of fluid transport properties (Norton and Knight, 1977). As a consequence of these large velocities, 60 percent of the fluid which circulates through these regions does so in $\sim 10^5$ years elapsed time (Fig. 8C).

Conclusions

The redistribution of fluids in hydrothermal systems can be effectively estimated on the basis of numerical solutions to partial differential equations which simulate the cooling of a pluton. The amount and velocity of the fluid flowing through a reference position in the system can also be simulated. The source and flow path of all the fluid which flows through the reference position can be quantitatively determined from the numerical data and the concept of fluid pathlines and sourcelines. These concepts are applicable in any environment where fluids circulate through rocks but appear particularly useful in studies of hydrothermal systems. A detailed approximation of the sourcelines in real systems obviously requires estimations of bulk rock permeability, a geometric description of the geologic units,

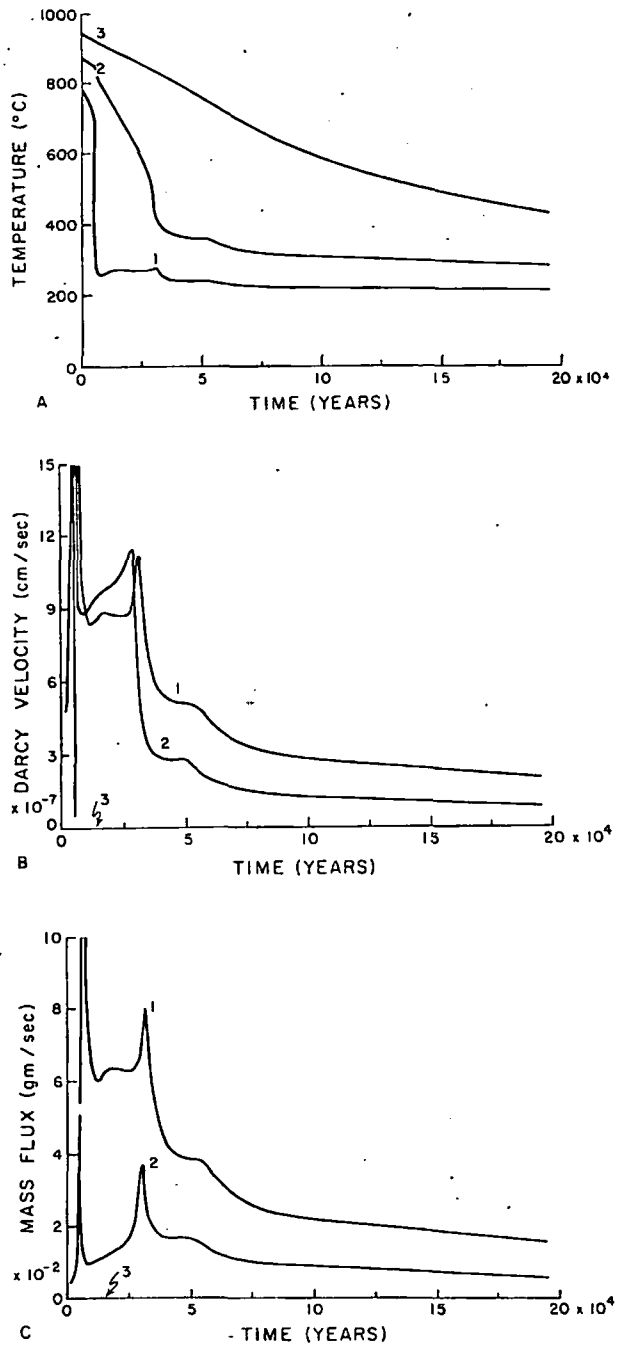

FIG. 8. Transient values for transport variables in the region around sourceline positions 1, 2, and 3 in the pluton. Figure 6A; note tic marks on the ordinate occur at 2.5×10^4-year increments, similar to sourceline tics. A, temperature, B, Darcy velocity, and C, mass flux as a function of time through a 1.25 km^2 area around a respective position. The velocity and mass flux for position 3 plot along the ordinate at the scale of these plots. The maxima on the velocity and mass flux plots near 3×10^3 years result from the emplacement of the pluton. The subsequent decrease is a result of the permeability increase of the pluton. The maxima around 3×10^4 years are the result of the system evolving to temperature-pressure conditions at which the transport properties of the fluid are optimized. Mass flux is computed for 1 cm depth extent into cross section.

and equations of state for saline fluids. There appears to be ample qualitative evidence to suggest that permeabilities in natural systems exceed the 10^{-14} cm^2 minimum in many instances, but by how much is unknown. The scanty data on saline fluids suggest that, as the concentrations of salts approach ~3 molal, significant variations in circulation patterns may be expected, but these effects are highly dependent on the initial distribution of the fluids. The importance of obtaining data on the transport properties of natural systems is clear from the theoretical considerations discussed above.

The example pluton system analyzed suggests that many notions regarding the source of fluid in hydrothermal systems can be quantitatively tested. In particular, the quantity of fluid derived from outside the plutons which cool in permeable host rocks and are themselves permeable appears to be even greater than has been indicated by stable isotope data. Perhaps this is because these data clearly indicate where fluid is not in equilibrium with the rocks it flows through, but once fluid and rock are in isotopic equilibrium the isotopes are no longer a viable tracer.

A definition of the fluid sources and the initial compositions of fluids together with their flow paths are necessary conditions required to simulate the mass transfer of components between fluids and rocks. The previous reaction history of rocks with earlier packets of fluid is then sufficient to define the conditions that prevail during fluid-rock reactions in a hydrothermal system.

Acknowledgments

This research was supported by NSF-GA41136 and its continuation, EAR74-03515 A01. The topic of this manuscript has enjoyed the critique of several colleagues, particularly R. Beane, S. R. Titley, and R. Capuano. I am grateful to J. Knight, R. Knapp, and B. Moskowitz for their thorough discussions and numerous contributions and to L. McLean for her editorial assistance in preparing the manuscript.

Department of Geosciences
University of Arizona
Tucson, Arizona 85721
August 31, 1976; February 23, 1977

REFERENCES

Browne, P. R. L., and Ellis, A. J., 1970, The Okaki-Broadlands hydrothermal area, New Zealand: Mineralogy and related geochemistry: Am. Jour. Sci., v. 268, p. 97–131.

Cooper, John R., 1957, Metamorphism and volume losses in carbonate rocks near Johnson Camp, Cochise County, Arizona: Geol. Soc. America Bull., v. 68, p. 577–610.

Donaldson, I. G., 1962, Temperature gradients in the upper layers of the earth's crust due to convective water flows: Jour. Geophys. Research, v. 67, p. 28–48.

Elder, J. W., 1965, Physical processes in geothermal areas, chap. 8, *in* Lee, W. H. K., ed., Terrestrial heat flows: Geophys. Mon. Ser. No. 8, Baltimore, Am. Geophys. Union, 276 p.

Grindley, G. W., 1965, The geology, structure, and exploitation of the Wairakei geothermal field, Taupo, New Zealand: New Zealand Geol. Survey Bull. 75, p. 131.

Gustafson, L. B., and Hunt, John P., 1975, The porphyry copper deposit at El Salvador, Chile: Econ. Geol., v. 70, p. 857–912.

Helgeson, H. C., 1970, A chemical and thermodynamic model of ore deposition in hydrothermal systems: Mineralog. Soc. America Spec. Paper 3, p. 155–186.

Helgeson, H. C., and Kirkham, D. H., 1974a, Theoretical behavior of aqueous electrolytes at high pressures and temperatures: I. Summary of thermodynamic/electronic properties of the solvent: Am. Jour. Sci., v. 274, p. 1089–1198.

—— 1974b, Theoretical behavior of aqueous electrolytes at high pressures and temperatures: II. Debye-Hückel parameters for activity coefficients and relative partial molal properties: Am. Jour. Sci., v. 274, p. 1199–1261.

Henley, R. W., 1973, Some fluid dynamics and ore genesis: Inst. Mining Metallurgy Trans., v. 2, sec. B, p. B1–B8.

Lapwood, E. R., 1948, Convection of a fluid in a porous medium: Cambridge Philos. Soc. Proc., v. 44, p. 508–521.

Meyer, Charles, 1950, Hydrothermal wall rock alteration at Butte, Montana: Unpub. Ph.D. thesis, Harvard Univ. 329 p.

Nielson, R. L., 1968, Hypogene texture and mineral zoning in a copper-bearing granodiorite porphyry stock, Santa Rita, New Mexico: Econ. Geol., v. 63, p. 37–50.

Norton, D., 1971, Concepts relating anhydrite deposition to solution flow in hydrothermal systems: Internat. Geol. Cong., 24*th* Montreal, sec. 10, p. 237–244.

Norton, D., and Cathles, L., in press, Thermal aspects of ore formation, *in* Barnes, H. L., ed., Geochemistry of hydrothermal ore deposits: New York, John Wiley and Sons Inc.

Norton, D., and Knapp, R., 1977, Transport phenomena in hydrothermal systems: Nature of porosity: Am. Jour. Sci., v. 277, p. 913–936.

Norton, D., and Knight, J., 1977, Transport phenomena in hydrothermal systems: Cooling plutons: Am. Jour. Sci., v. 277, p. 937–981.

Ribando, R. J., Torrance, K. B., and Turcotte, D. L., 1976, Numerical models for hydrothermal circulation in the oceanic crust: Jour. Geophys. Research, v. 81, p. 3007–3012.

Taylor, Hugh P., Jr., 1974, The application of oxygen and hydrogen isotope studies to problems of hydrothermal alteration and ore deposition: Econ. Geol., v. 69, p. 843–883.

Villas, Netuno R., 1975, Fracture analysis, hydrodynamic properties, and mineral abundance in altered igneous rocks at the Mayflower mine, Park City district, Utah: Unpubl. Ph.D. thesis, Univ. Utah.

White, D. E., 1974, Diverse origins of hydrothermal ore fluids: Econ. Geol., v. 69, p. 954–973.

Wooding, R. A., 1957, Steady state free thermal convection of liquid in a saturated permeable medium: Jour. Fluid Mech., v. 2, p. 273–285.

[AMERICAN JOURNAL OF SCIENCE, VOL. 269, SUMMER 1970, P. 97-131]

American Journal of Science

SUMMER 1970

THE OHAKI-BROADLANDS HYDROTHERMAL AREA, NEW ZEALAND: MINERALOGY AND RELATED GEOCHEMISTRY

P. R. L. BROWNE* and A. J. ELLIS**

ABSTRACT. Deep drilling in the Ohaki-Broadlands geothermal area, New Zealand, with mineralogical examination of hydrothermally altered volcanic rocks at levels down to 7000 ft (2134 m) and the chemical analysis of coexisting fluids, shows that hydrothermal mineral alteration at temperatures of 230 to 290° at deep levels in permeable rocks tends to an equilibrium assemblage of K-mica, K-feldspar, albite, chlorite, calcite, and quartz (and occasionally wairakite). The deep waters are dilute (~ 1200 ppm Cl^-) chloride-bicarbonate solutions containing appreciable carbon dioxide ($m_{CO_2} = 0.15$). Individual minerals and their occurrences are discussed briefly, and stability diagrams are developed to correlate observed rock alteration mineralogy with water chemistry. Changes in water composition caused by boiling off steam and CO_2 can be related to changes in mineral assemblages, such as calcite precipitation and adularia and epidote formation. Variations in mineralogy are discussed in terms of temperature, permeability, water composition, and carbon dioxide concentrations, and a comparison is made with alteration at Wairakei where the carbon dioxide concentration is lower. Pyrite, pyrrhotite, chalcopyrite, sphalerite, and galena occur at depth in some Broadlands altered rocks and are mentioned briefly.

INTRODUCTION

The natural hydrothermal activity in the Ohaki-Broadlands area consists of a large, near-boiling spring (Ohaki Pool) on the west side of the Waikato River (fig. 1), together with minor outflows of lower temperature, more dilute chloride water on the nearby river banks, and also 3 km to the southeast near drillholes 7 and 16 (fig. 1). Before drilling investigations, the Ohaki pool had a 10 l/sec outflow of near-neutral pH, chloride-bicarbonate water at 95°C. It had a well-developed silica sinter margin and produced an antimony-arsenic sulphide precipitate rich in trace metals such as gold, thallium, and silver (Weissberg, 1969). Spring water analyses are shown in table 1. The waters are all of a similar composition, varying mainly in their degree of dilution by surface waters. The high boron and bicarbonate concentrations relative to chloride are the major features.

During a geothermal exploration program, deep drillholes on both sides of the Waikato River tapped high temperature chloride water at depths varying from 2500 to 7000 ft (762 to 2134 m). Maximum temperatures are usually in the range 270° to 290°C, and mass outflows from holes vary from almost zero to 250 metric tons per hour. In this paper an outline is given of the geological structure revealed by drilling and of the chemistry of the drillhole discharges. The hydrothermal alteration

* Geology Department, Victoria University of Wellington, New Zealand and Staff member, New Zealand Geological Survey, Box 30368, Lower Hutt, New Zealand.

** Chemistry Division, Department Scientific Industrial Research, Private Bag, Petone, New Zealand.

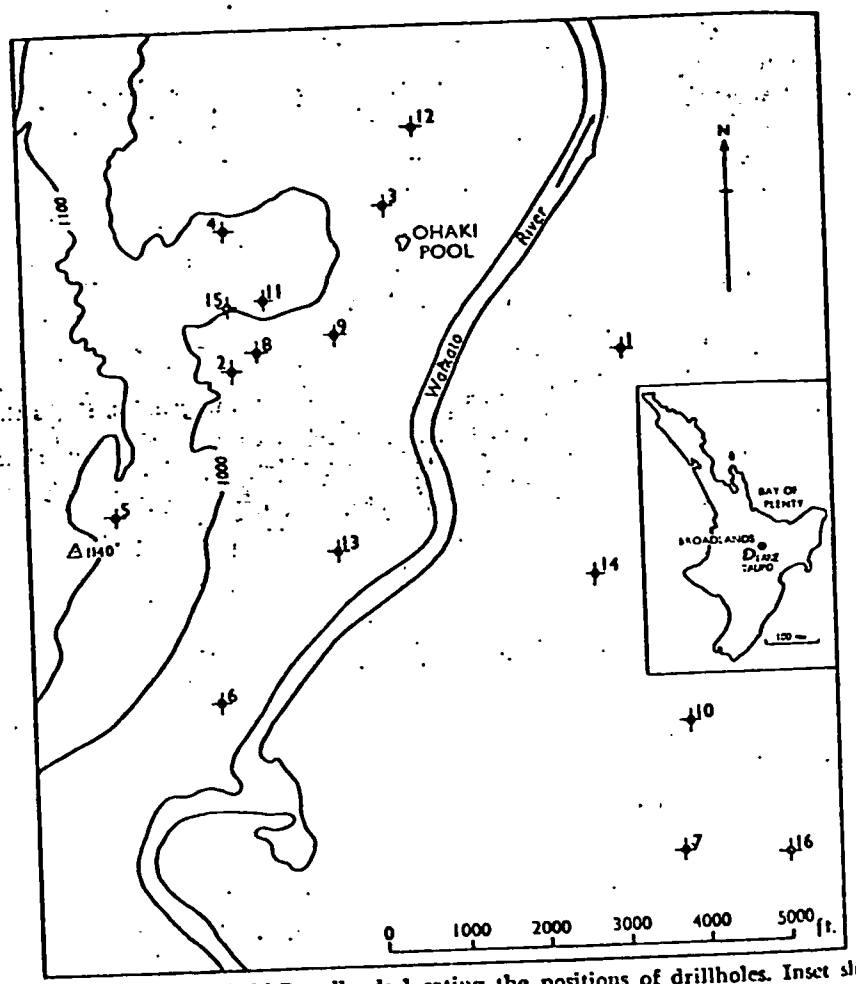

Fig. 1. Map of Ohaki-Broadlands locating the positions of drillholes. Inset shows position of Ohaki-Broadlands in the North Island, New Zealand.

of the rocks at various depths is described in detail, and a correlation made between mineral stabilities and the temperatures and compositions of the fluids.

GEOLOGY

Rocks exposed in the Taupo Volcanic Zone include a series of rhyolitic airfall and ashflow tuffs, water-deposited volcanic sediments, several rhyolite domes, and rare basalt (Grindley, 1960 and 1961). Exposures around the Broadlands area however are poor, and information on the subsurface geology of the field is based almost entirely upon the examination of cores and cuttings recovered during drilling.

The geology of the field has been described in unpublished (open file DSIR) reports by Healy (ms, 1968a; ms, 1968b) and Grindley and Browne (ms). The rocks penetrated by the drillholes consist mainly of Quaternary horizontal and near-horizontal airfall, ashflow, and water-

ons of drillholes. Inset shows
r Zealand.

detail, and a correlation
atures and compositions

one include a series of
ited volcanic sediments
ley, 1960 and 1961). Ex-
re poor, and information
almost entirely upon the
ing drilling.
d in unpublished (oper-
968b) and Grindley and
illholes consist mainly of
fall, ashflow, and water-

TABLE 1

Compositions of waters from springs and drillholes

Source		pH (20°)	Concentrations in mg/kg in water discharged to atmosphere													Atomic ratios				
			Li^+	Na^+	K^+	Rb^+	Cs^+	Ca^{2+}	Mg^{2+}	F^-	Cl^-	SO_4^{2-}	B	SiO_2	NH_3	HCO_3^- + CO_3^{2-}	of Cl to B	of Cl to F	of Cl to Cs	of Na to Li	of Na to K
Drillhole	1	8.3	10.9	1065	152	0.6	0.6	4.6	—	6.2	1700	43	48	565	12	230	10.8	147	11000	30	11.9
"	2	8.2	11.7	1050	224	2.2	1.7	2.2	—	7.3	1743	8	48	805	2.1	178	11.0	128	8800	27	8.0
"	3	8.0	12.2	1045	218	—	—	5.0	—	6.1	1800	6	55	750	4	174	10.0	160	—	26	8.3
"	4	8.35	11.8	1075	218	—	—	3.0	—	4.5	1850	29	56	880	2.3	282	10.0	220	—	28	8.4
"	5	9.1	4.9	1400	146	—	—	—	—	—	1142	—	—	—	0.2	1410	14.8	—	—	86	16.3
"	8	7.9	11.3	1040	246	—	—	0.0	—	8.6	1186	4	53	795	2.3	160	10.8	117	—	28	7.2
"	9	8.45	12.7	930	203	—	—	2	—	8.0	1709	4	44	805	—	140	11.8	114	—	22	7.8
"	10	8.6	9.5	910	143	1.1	1.4	1.1	0.05	6.2	1244	12	55	635	1.2	553	6.9	107	3300	29	10.8
"	11	8.25	12.2	1020	219	1.7	1.4	7.3	—	6.4	1794	10	49	803	1.4	78	11.1	150	4800	25	7.9
"	13	8.6	12.6	980	200	2.2	1.3	2.4	0.02	4.5	1668	7	48	750	1.9	162	10.6	198	4800	24	8.3
Spring 1 (95°) (Ohaki Pool)		7.05	7.4	860	82	0.1	1.2	2.5	—	5.2	1060	160	32	338	3.8	680	10.1	109	3300	35	17.8
Spring 3 (25°)		2.6	4.6	440	44	—	—	30	—	—	680	530	19	280	5.8	0	10.9	—	—	29	17.2
Spring 4 (75°)		8.05	3.6	430	32	—	—	28	—	2.2	525	132	14.5	280	0.1	322	11.0	128	—	36	23
Spring 7 (42°)		7.3	4.0	500	21	—	—	7	—	4.2	638	185	23.5	232	1.1	188	8.2	81	—	38	41

lkid tuffs and breccias, interbedded with rhyolite and dacite flows unconformably overlying the Mesozoic graywacke and argillite basement surface (Grindley, 1961) (see fig. 2). The hydrological sequence effectively consists of a series of alternating permeable and impermeable formations locally disrupted by faults and dikes.

Rocks considered to be part of the Mesozoic graywacke and argillite basement, which crops out 18 miles (29 km) southeast of the field (Grindley, 1960), were penetrated below 3000 ft (914 m) by three eastern drillholes, Br-7, Br-10 and Br-16 (fig. 2). These rocks have low porosity, (4–8 percent), poorly defined bedding, and are likely to be permeable only where brecciated.

Locally overlying the basement and with a maximum thickness of about 900 ft (274 m) is a sequence of crystal-rich ignimbrites, thinly bedded sandstone, basement derived conglomerate, coarse tuffs, and non-volcanic sandstone. (These ignimbrites have been found only in Br-1 and therefore are not shown in figure 2.) This group of rocks, with the possible exception of the tuff, are of low porosity and, as shown by the absence of extensive hydrothermal alteration in spite of high temperature, are relatively impermeable to geothermal fluids except where fractured.

A quartz-plagioclase ignimbrite containing volcanic rock fragments in places is probably composed of several ash flows. It has been penetrated by most deep drillholes. It varies from 100 to 1400 ft (30-427 m) in thickness and is important in controlling the hydrology of the field. The degree of welding varies with its thickness, and in the most highly welded zone, it has shards (originally glass) that are so elongated that its texture is undistinguishable from a flow-banded rhyolite. In the upper zone it is unwelded (above 3500 ft (1068 m) in Br-9), and the groundmass and feldspar phenocrysts of the ignimbrite are extensively altered. At greater depth the degree of welding increases (and porosity decreases), and the amount of alteration decreases until, in places, it is almost fresh despite a measured temperature of 287°. Below 4000 ft (1219 m) the degree of welding again decreases, and the porosity and extent of hydrothermal alteration increases.

Above the ignimbrite, and occurring in all drillholes, is a heterogeneous formation of tuff-breccia and tuffs (between 600 and 900 ft (183-274 m) thick) which are of major hydrological importance. They occur below a depth of 2400 ft (732 m) and typically are poorly sorted and composed of quartz and feldspar crystals and abundant lithic fragments (predominantly pumice, pumiceous rhyolite, and rhyolite). In places the tuffs have a well developed unwelded vitroclastic texture. Their texture, high porosity, and susceptibility to hydrothermal alteration indicate that this formation functions as an aquifer, and it is, in fact, the main production zone for drillholes 13 and 14 as well as contributing to production from drillholes 2, 3, 4, 7 and 9.

Thin beds (0-250 ft (0-76 m) thick) of relatively impermeable siltstone locally overlie the tuffs and tuff-breccia and, in turn, are overlain in the west by thick (0-1500 ft (0-457 m)) dense, impermeable plagioclase-

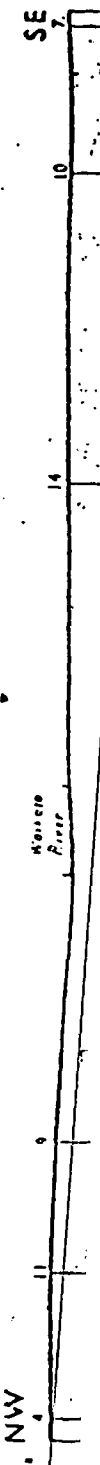

and dacite flows un-
d argillite basement
l sequence effectively
ermeable formations

ywacke and argillite
t of the field (Grind-
y three eastern drill-
ve low porosity, (4–
o be permeable only

ximum thickness of
ignimbrites, thinly
oarse tuffs, and non-
found only in Br-1
p of rocks, with the
nd, as shown by the
of high temperature,
pt where fractured.
anic rock fragments
has been penetrated
(30-427 m) in thick-
of the field. The de-
most highly welded
ated that its texture
n the upper zone it
the groundmass and
y altered. At greater
decreases), and the
almost fresh despite
19 m) the degree of
nt of hydrothermal

llholes, is a hetero-
600 and 900 ft (183-
ortance. They occur
orly sorted and com-
nt lithic fragments
olite). In places the
ture. Their texture.
ration indicate that
fact, the main pro-
ributing to produc-

y impermeable silt-
n turn, are overlain
meable plagioclase-

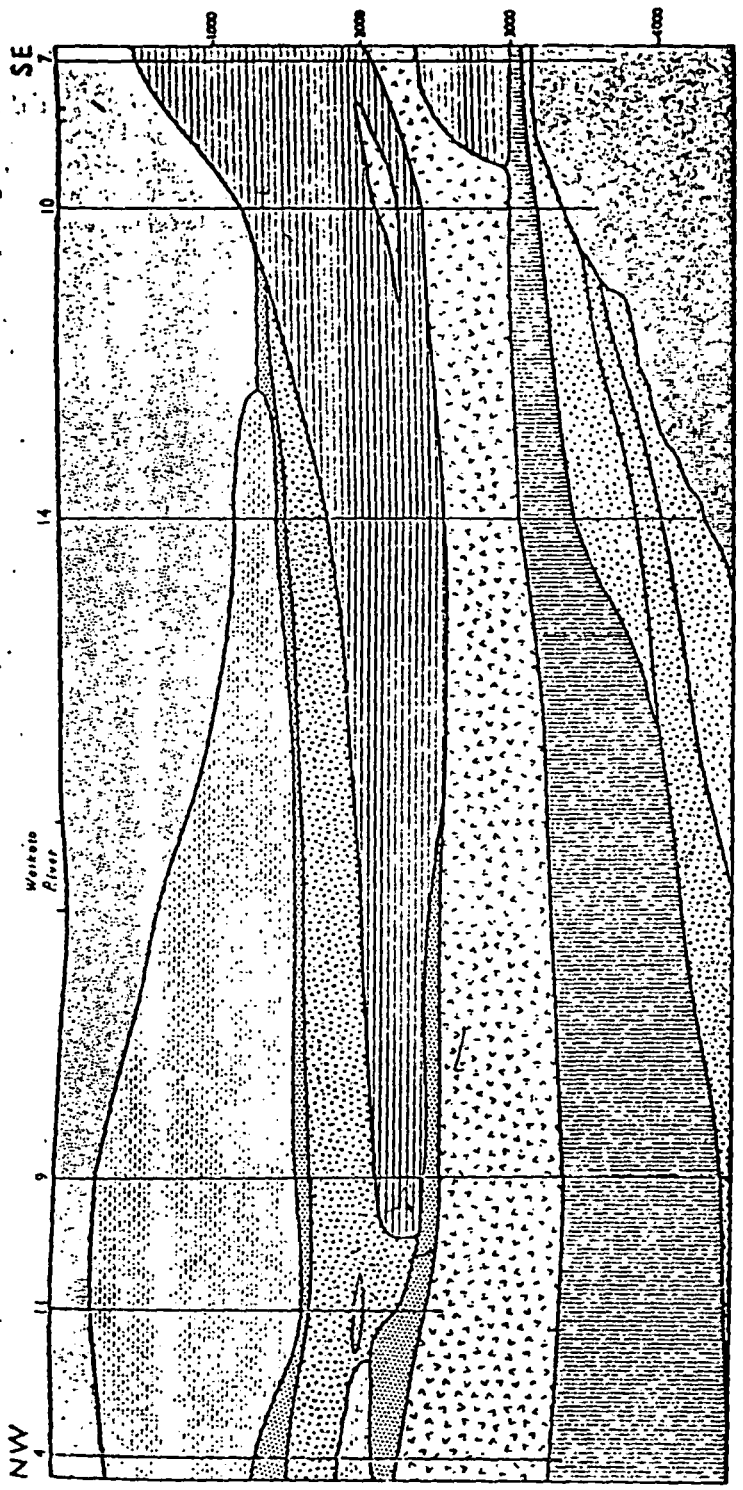

Fig. 2. Diagram of subsurface geology of Ohaki-Broadlands geothermal field. Not a cross section, but relative positions of drillholes 2, 7, 9, 10, and 14 are shown.

bearing rhyolite of low porosity and east of the river by dacite from [illegible] to 1400 ft (30-427 m) in thickness. These formations act primarily as a caprock and are permeable only along fracture zones; consequently they have seldom altered to an equilibrium mineral assemblage. However, in places the dacite occurs as a breccia, and this has apparently allowed access of water to the upper flows, resulting in the formation of abundant clays.

A water-laid pumiceous tuff-breccia formation which thickens to the west from 0 to 900 ft (0-274 m) overlies the lavas. It is of high porosity and permeability and serves as the upper steam and water aquifer, as demonstrated by its high susceptibility to alteration. It is the main source of fluid production for drillholes 2, 4, 8, 9, and 11 and is usually capped by about 40 ft (12 m) of impermeable mudstone and 0 to 1400 ft (0-426 m) of hornblende–biotite–quartz–andesine rhyolite. This formation is of variable porosity, permeability, and degree of alteration, for example, in Br-5 it is unaltered but where fractured in drillholes 2, 4, 8, and 11 contains abundant secondary quartz and adularia.

Tuffs (in places pisolitic), tuffaceous siltstones and sandstones, lacustrine sediments, gravels, and ash extend over the entire field and in the vicinity of Br-10 are up to 1100 ft (335 m) thick but are of little importance for geothermal production and are seldom extensively altered above a low temperature assemblage.

FEED CHANNELS

Grindley and Browne (ms), on the basis of the fractured and sheared nature of some recovered cores, suggested that several faults occur in the Ohaki-Broadlands field, although they have little surface expression. Faulting is common in the region however (Grindley, 1961 and 1965) and Grindley and Browne (ms) suggested that faults, for example in the zone intersected by Br-2, provide permeable channels for geothermal fluid and allow upflow into the two main aquifers. Healy (ms, 1965) however, considers that rupture zones formed by the intrusion of rhyolite dikes would be more likely upflow centers. The trends and outputs of the drillholes are consistent with the presence of a natural flow channel in the vicinity of drillholes 2, 8, and 11.

CHEMISTRY OF DRILLHOLE DISCHARGES

Only essential points of the geochemistry of the Ohaki-Broadlands area are given here, as this will be the subject of a detailed publication. Table 1 gives the compositions of water tapped by the drillholes, expressed as mg/kg of constituents in waters separated from the mixed steam and water discharges at local atmospheric pressure (boiling point about 99°C).

With the exceptions of drillholes 5 and 6 on the cool margins of the area, the general chemistry of the deep waters is similar throughout the field. However, the waters of the eastern and western zones differ in their Cl/B and Cl/HCO_3 ratios, and this difference can be explained by additional boron and carbon dioxide being liberated by the interaction

of hot water with graywacke sediments found at the base of the eastern drillholes (fig. 2). All the waters had pH values in the region of 7.5 to 8.5 after collection and cooling. The close association between the source of spring and drillhole waters can be seen in terms of Cl/B, Cl/Cs, and Na/Li ratios. The very low magnesium concentrations are typical of high temperature, dilute, natural water systems (Ellis, 1969). Bicarbonate ion concentrations in the highest temperature deep waters are about 10 times those found in the Wairakei geothermal area but are similar in magnitude to those in the deep hot water at Kawerau and Waiotapu, New Zealand. For equal ionic strengths and temperatures, the bicarbonate concentration at depth in natural high temperature waters is proportional to the carbon dioxide concentration (Ellis, 1969).

Br-5 is on the southern margin of the field where chloride water has become cooled by conduction and dilution, and the lower temperatures have allowed high bicarbonate concentrations to develop through reaction of carbon dioxide with rhyolite rock. Br-6 taps a low-chloride ground water which has probably been warmed by steam (and carbon dioxide) migrating from the main hot system.

Proportions of steam and water in a drillhole discharge depend on the heat content of the deep inflow and the pressure at which the observation is made. Drillholes that tap water alone at the average Broadlands inflow temperature of 260°C discharge 32 percent steam and 68 percent water at 99°C to the atmosphere. This type of production, however, is sustained only in zones of high rock permeability. In impermeable zones local pressure drawdown occurs in the country rocks, the water boils, and drillholes may tap an inflow of steam and water. Consequently, the outflow has a higher proportion of steam (high enthalpy discharge) than is expected from the deep water temperature. This is a common feature with Broadlands drillholes, for example Br-7 in the eastern side of the field discharges nearly dry steam.

TABLE 2

Gas content and composition in steam

Drillhole no.	Enthalpy (Btu/lb)	Steam collection pressure (psig)	Total gas in steam (mole %)	Total gas in original water (mole %)	Composition of gas (mole %)				
					CO_2	H_2S	$\overline{HC}$*	H_2	$N_2 + A$
1	1150	20	2.77	—	95.0	0.5	2.1	0.2	2.2
2	530	60	0.94	0.26	94.4	1.6	2.2	0.2	1.5
7	—	—	—	—	92.4	0.8	3.8	0.6	2.4
9	550	40	0.70	0.22	93.5	1.8	3.0	0.15	1.6
11	525	168	1.07	0.22	95.0	2.1	1.2	0.2	1.5

*$\overline{HC}$ = total hydrocarbon gases

TABLE 3

Depth and temperature information on minerals in cores from Broadlands geothermal drillholes

Depths in ft; Temp in °C

Mineral	Bore no. / 1st core depth (ft)	1 100 4585	2 183 3397	3 188 2997	4 188 3351	5 167 4436	6 188 3556	7 196 3677	8 388 2550	9 185 4493	10 232 3572	11 228 2498	12 180 4497	13 182 3549
Biotite	greatest depth	1388	<390	<390	<288	1888	888	N.P.	<388	786	N.P.	<341	1143	1491
	highest temp	170	<194	<170	<140	99	76		<149	172		<112	78	164
Hornblende	greatest depth	581	<390	<390	<288	888	888	N.P.	<388	<337	N.P.	<341	1143	<941
	highest temp	75	<194	<170	<140	73	76		<149	<171		<112	78	<135
Pyroxene	greatest depth	581	<390	<390	<288	1368	888	N.P.	<388	<337	N.P.	<341	N.P.	N.P.
	highest temp	75	<194	<170	<140	46	76		<149	<171		<112		
Magnetite	greatest depth	581	<390	<390	<288	1368	N.P.	N.P.	<388	<337	N.P.	<341	N.P.	N.P.
	highest temp	75	<194	<170	<140	46			<149	<171		<112		
Glass	greatest depth	792	<390	<390	<288	1788	2503	1258	<388	<337	242	<341	1446	182
	highest temp	108	<194	<170	<140	86	120	190	<149	<171	69	<112	106	51
Andesine	greatest depth	2688	688	1180	<288	2400	3556	1560	<388	3970	2263	<341	1838	1732
	highest temp	241	240	246	<140	73	160	228	<149	289	245	<112	122	204
Cristobalite	shallowest depth	671	N.P.	N.P.	N.P.	688	593	N.P.	N.P.	493	232	N.P.	330	693
	lowest temp	88				46	95			176	68		50	148
	greatest depth	884				2272	2503				288		1990	1491
	highest temp	119				143	120				76		130	164
Siderite	shallowest depth	N.P.	N.P.	N.P.	N.P.	N.P.	2203	N.P.	N.P.	N.P.	232	N.P.	180	182
	lowest temp						49				68		37	51
	greatest depth						2613				242		1990	1186
	highest temp						98				69		130	130
Calcite	shallowest depth	581	183	588	288	1014	288	338	2089	185	268	228	1548	485
	lowest temp	75	120	160	140	46	98	80	265	147	76	75	108	105
	greatest depth	4585	3397	2898	3151	3715	3556	3677	—	4493	3071	2498	4497	3549
	highest temp	275	285	278	270	230	160	290	—	292	258	271	274	256
Pyrite	shallowest depth	1179	288	692	188	1545	188	196	388	337	588	341	1294	1884
	lowest temp	152	156	180	120	56	58	42	149	166	152	112	98	218
	greatest depth	3988	3397	2997	3145	2981	2914	3243		3749	3071	2498	4039	3549
	highest temp	266	285	280	270	200	160	276		292	258	271	258	258
Pyrrhotite	shallowest depth	1688	N.P.	N.P.	2341	2400	N.P.	2758	N.P.	N.P.	N.P.	N.P.	2590	1601
	lowest temp	198			263	152		272					166	188
	greatest depth	4178			3351	2715							3887	2189
	highest temp	268			268	230							249	237
Base metal sulphides	shallowest depth	N.P.	N.P.	N.P.	N.P.	N.P.	N.P.	2628	N.P.	N.P.	3130	N.P.	N.P.	N.P.
	lowest temp							271			272			
	greatest depth							3138			3428			

	greatest depth	4585	3397	2898	3151	3715	3556	3677	—	4493				
	highest temp	275	285	278	270	230	160	290	—	292	258			
Pyrite	shallowest depth	1179	288	692	188	1545	188	196	388	337	588	81		
	lowest temp	152	156	180	120	56	58	42	149	166	152	112	93	
	greatest depth	3983	3397	2997	3145	2981	2914	3243		3749	3071	2498	4039	3
	highest temp	266	285	280	270	200	160	276		292	258	271	258	258
	shallowest depth	1688	N.P.	N.P.	2341	2400	N.P.	2758	N.P.	N.P.	N.P.	N.P.	2590	1601
Pyrrhotite	lowest temp	198			265	152		272					166	183
	greatest depth	4178			3351	2715							3887	2169
	highest temp	268			268	230							249	237

Base metal sulphides	shallowest depth	N.P.	N.P.	N.P.	N.P.	N.P.	N.P.	2628	N.P.	N.P.	5130	N.P.	N.P.	N.P.
	lowest temp							271			272			
	greatest depth							3138			3428			
	highest temp							275			277			
Ptilolite	shallowest depth	N.P.	N.P.	390	N.P.	1688	388	N.P.	N.P.	N.P.	N.P.	N.P.	633	941
	lowest temp			170		73	69						59	135
	greatest depth			—		—	2708						1838	1180
	highest temp			—		—	152						122	130
Wairakite	shallowest dept	N.P.	N.P.	N.P.	N.P.	N.P.	N.P.	N.P.	N.P.	2032	1500	N.P.	N.P.	2189
	lowest temp									270	232			237
	greatest depth									2932	—			—
	highest temp									276	—			—
Kaolin	shallowest depth	N.P.	N.P.	N.P.	N.P.	1688	1035	N.P.	N.P.	N.P.	N.P.	N.P.	1294	N.P.
	lowest temp					73	49						93	
	greatest depth					2189	2503						1990	
	highest temp					134	120						130	
Montmorillonite	shallowest depth	941	183	188	188	1545	188	196		185	232	228	180	182
(or as interlayered	lowest temp	125	120	95	120	56	90	42	N.P.	147	68	75	37	51
illite/montmorillonite)	greatest depth	—	288	1381	1290	2487	2914	1788		1242	2063	1994	1850	1732
	highest temp	—	156	251	248	161	160	252		176	244	264	122	204
Illite (or interlayered	shallowest depth	1794	338	390	500	1545	388	328	388	185	588	228	1990	788
illite/montmorillonite)	lowest temp	206	176	170	183	56	90	80	149	147	152	75	130	155
	greatest depth	4585	1586	2898	3313	3715	3556	3677	2089	4493	3572	2498	4497	3549
	highest temp	275	266	278	270	230	160	290	265	292	280	271	274	258
Chlorite	shallowest depth	2186	183	993	1088	1688	188	671	2550	185	438	1429	3591	1186
	lowest temp	230	120	195	238	73	88	145	272	147	100	258	230	130
	greatest depth	2288	3397	2997	3313	3498	3556	3677		4493	3572	1605	4497	3549
	highest temp	232	285	280	270	223	160	290		292	280	259	274	258
Albite	shallowest depth	2793	1090	1778	1728	2487	2808	1788	2550	2516	1500	2104	2590	2342
	lowest temp	242	259	257	259	161	122	252	272	279	232	267	166	244
	greatest depth	4585	3397	2997	3351	3715	3338	3677	—	4493	3572	2498	4497	3549
	highest temp	275	285	280	270	230	152	290	—	292	280	271	274	258
Adularia	shallowest depth	N.P.	738	390	698	N.P.	N.P.	2262	785	2516	916	228	3591	2342
	lowest temp		248	170	205			270	215	279	212	75	230	244
	greatest depth		3397	2997	3351			2860	2550	3518	3572	2498	4497	3559
	highest temp		285	280	263			273	272	280	280	271	274	258

The steam discharged from the drillholes was collected for analysis from tappings on the discharge pipes and separated from the liquid by a small cyclone operating at the pressure in the pipe. The composition of steam from several holes is given in table 2. Where drillholes have a liquid inflow, that is, a combined outflow enthalpy that corresponds to that for water at the underground temperature,[1] the deep water composition can be calculated from the analyses of steam and water. For example, for non-volatile constituents the concentration factor for water at 260° through steam flashing to atmospheric pressure is 1.47. Gas concentrations in the original deep water can also be calculated and are shown in table 2 for drillholes 2, 9, and 11, which at the times of collection were the only holes supplied by a single liquid phase. The deep water in the western zone contains about 0.20 to 0.25 moles carbon dioxide and about 0.005 to 0.006 moles hydrogen sulphide per 100 moles water.

The pH of the deep water before steam separation can be calculated from the integrated analyses of steam and water collected at the surface (Ellis, 1967). Knowledge is required of the ionization constants of the various weak acids and bases in the water at the high temperature. As an example the pH of deep water at 260° in the western area is estimated to be about 6.0 to 6.2, which is very slightly alkaline with respect to the neutral pH of water (5.7) at this temperature.

The partial pressure of gases dissolved in the original deep water can be calculated for holes such as 2, 9, and 11 from steam analyses, the discharge enthalpy, and through knowing the solubility of the various gases in water at high temperatures (Ellis, 1967). The approximate partial pressures in atmospheres at 260° are as follows:

$$CO_2 = 12;\ H_2S = 0.1;\ H_2 = 0.1;\ CH_4 = 0.5;\ N_2 = 1.0.$$

An estimate of the depth of first boiling for water rising in a permeable zone, such as near holes 2, 8, and 11, can be obtained by balancing the steam and gas pressure against hydrostatic pressures. At Broadlands this would be at about 2000 ft (609 m) for water at 260° and at about 3000 ft (915 m) for water at 285°.

HYDROTHERMAL ALTERATION IN INDIVIDUAL DRILLHOLES

The identification of hydrothermal alteration minerals in cores is based on a combination of petrography, differential thermal analysis, quantitative infra-red spectroscopy, and semi-quantitative X-ray diffraction analysis using a technique similar to that described by Talbot (1966) and also used by Muffler and White (1969). Clay minerals were mainly identified by X-ray diffraction of a separated clay fraction before and after treatment with ethylene glycol, and the Na_2O and K_2O concentrations in the rocks were determined by flame photometry. Table 5 summarizes the range of distribution of the common minerals in the Ohaki-Broadlands geothermal field, and figures 3 to 6 show the mineralogy of holes 2, 4, 6, and 9. These figures are intended to illustrate

[1] The gas composition of the discharge provides an extra check on the close matching of enthalpy through a mixed steam + water intake to the drillhole.

was col' ior analysis
rate· he liquid by
ie composition
rillholes have a
it corresponds to
ep water composi-
ater. For example,
for water at 260°
Gas concentrations
l are shown in table
collection were the
ie deep water in the
on dioxide and about
les water.
ration can be calculated
collected at the surface
zation constants of the
igh temperature. As an
estern area is estimated
line with respect to the

original-deep water can
steam analyses, the dis-
lity of the various gases
e approximate partial

0.5; $N_2 = 1.0$.

water rising in a per-
be obtained by balanc-
e pressures. At Broad-
water at 260° and at

. DRILLHOLES

minerals in cores is
tial thermal analysis,
titative X-ray diffrac-
lescribed by Tatlock
. Clay minerals were
l clay fraction before
Na_2O and K_2O con-
photometry. Table 3
non minerals in the
o 6 show the miner-
ntended to illustrate

ra check on the chang
the drillhole.

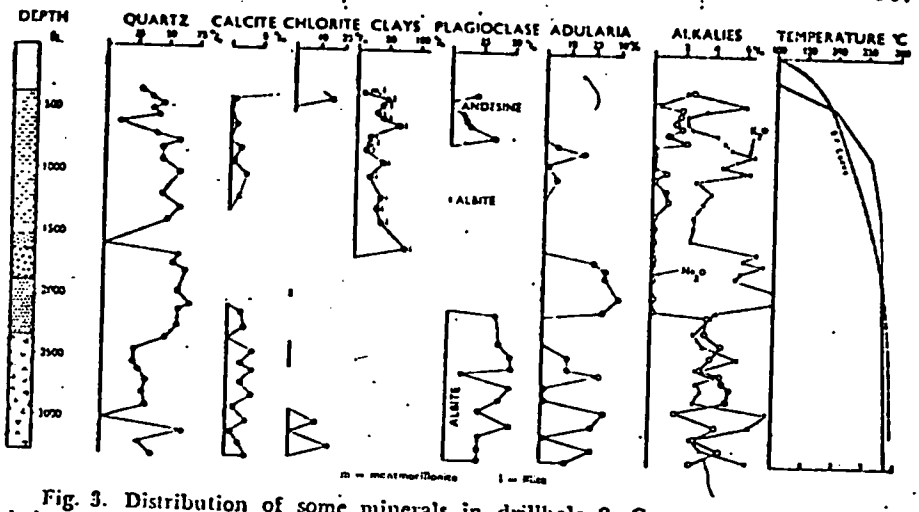

Fig. 3. Distribution of some minerals in drillhole 2. Cores are represented by circles and straight lines have arbitrarily been drawn between circles. Not shown is the distribution of epidote which occurs in traces in deeper parts of the hole and a small amount of gypsum at a depth of 390 ft (119 m). The geological column at the left uses the same stratigraphic symbols as those shown in figure 2. Hole is cased to 1367 ft (416 m).

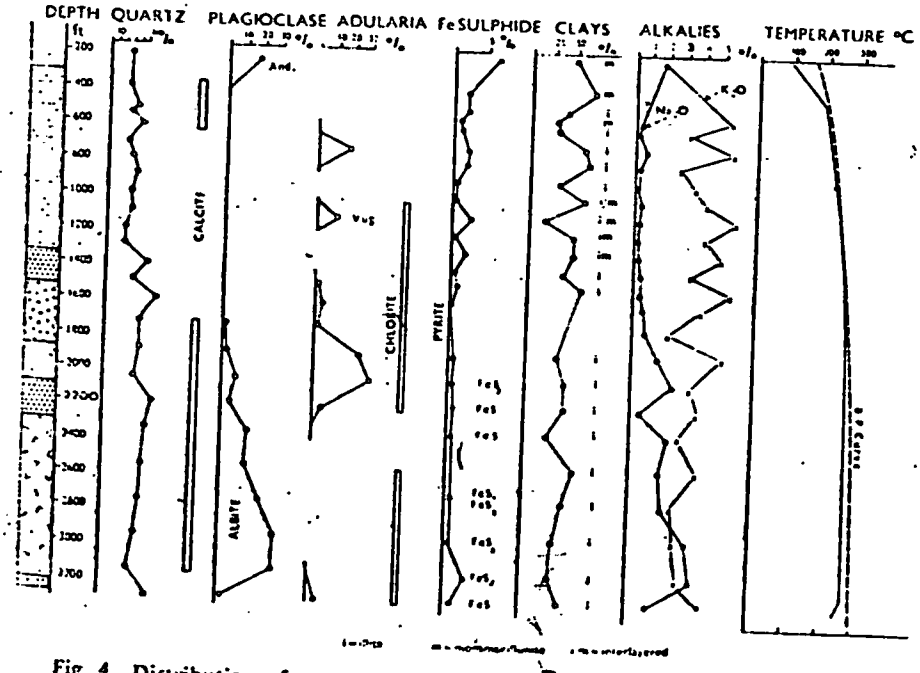

Fig. 4. Distribution of some minerals in drillhole Br-4. Hole is cased to 1697 ft (517 m).

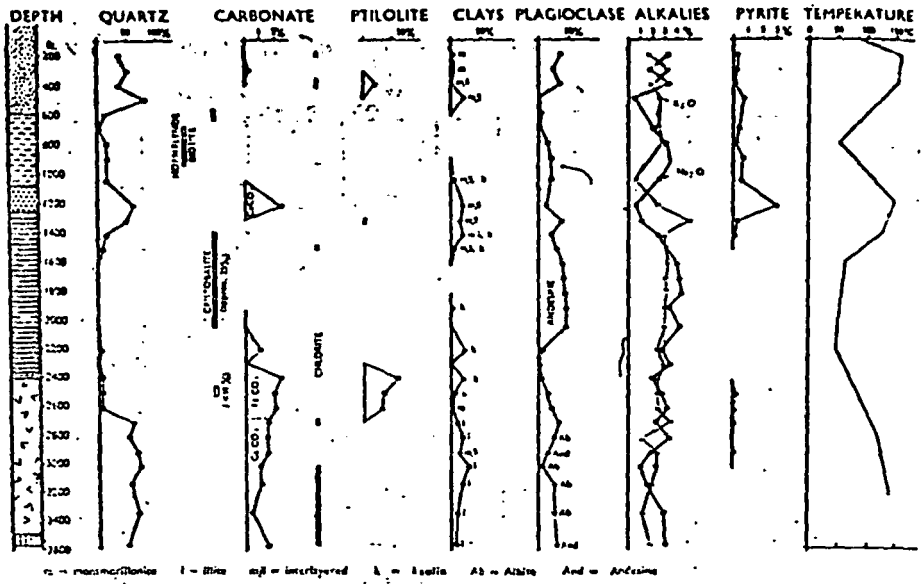

Fig. 5. Distribution of some minerals in drillhole Br-6. Hole is cased to 2762 ft (842 m).

changes in mineral abundance with depth and temperature, and a high degree of accuracy is not claimed. In particular it is possible for the quantities of adularia and clay to be in error by several percent. Not shown is the distribution of leucoxene, sphene, gypsum, and epidote which are all of limited distribution or else not present in sufficient quantity to detect by instrumental methods. A further point is that cores were usually taken at between 50 and 250 ft (15 and 76 m) intervals, and it is therefore difficult to know how representative they are.

A simplified geological column and the measured downhole temperatures in the bore holes are also shown in figures 3 to 6. Temperatures were measured several times between drilling and initial discharge, but the readings made immediately before discharge are considered closest to the undisturbed subsurface temperature (N.D. Dench, personal commun.). Drillholes 3, 7, and 11 were discharged before sufficient time had elapsed to estimate the steady-state temperatures accurately, and they may be in error by several degrees.

It may be noted from figures 3 to 6 that there is some correlation between the albite and Na_2O contents of the cores, because albite is the only hydrothermal sodium mineral, whereas potassium is present in both adularia and illite.

STABILITY OF PRIMARY MINERALS

Before alteration most of the rocks of the Ohaki-Broadlands field contained quartz, andesine, and groundmass (glassy or devitrified), often with minor hornblende, biotite, hypersthene, and magnetite. Of these, only quartz is unaffected during alteration.

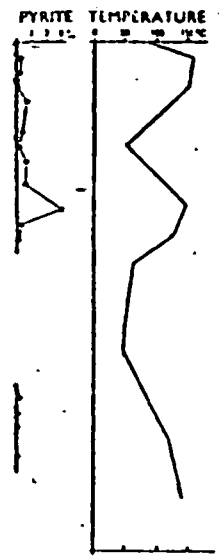

is cased to 2762 ft

ture, and a high
possible for the
ral percent. Not
m, and epidote
ent in sufficient
er point is that
1 76 m) intervals,
ey are.
wnhole tempera-
6. Temperatures
al discharge, but
onsidered closest
h, personal com-
fficient time had
rately, and they

some correlation
use albite is the
s present in both

Broadlands field
levitrified), often
netite. Of these.

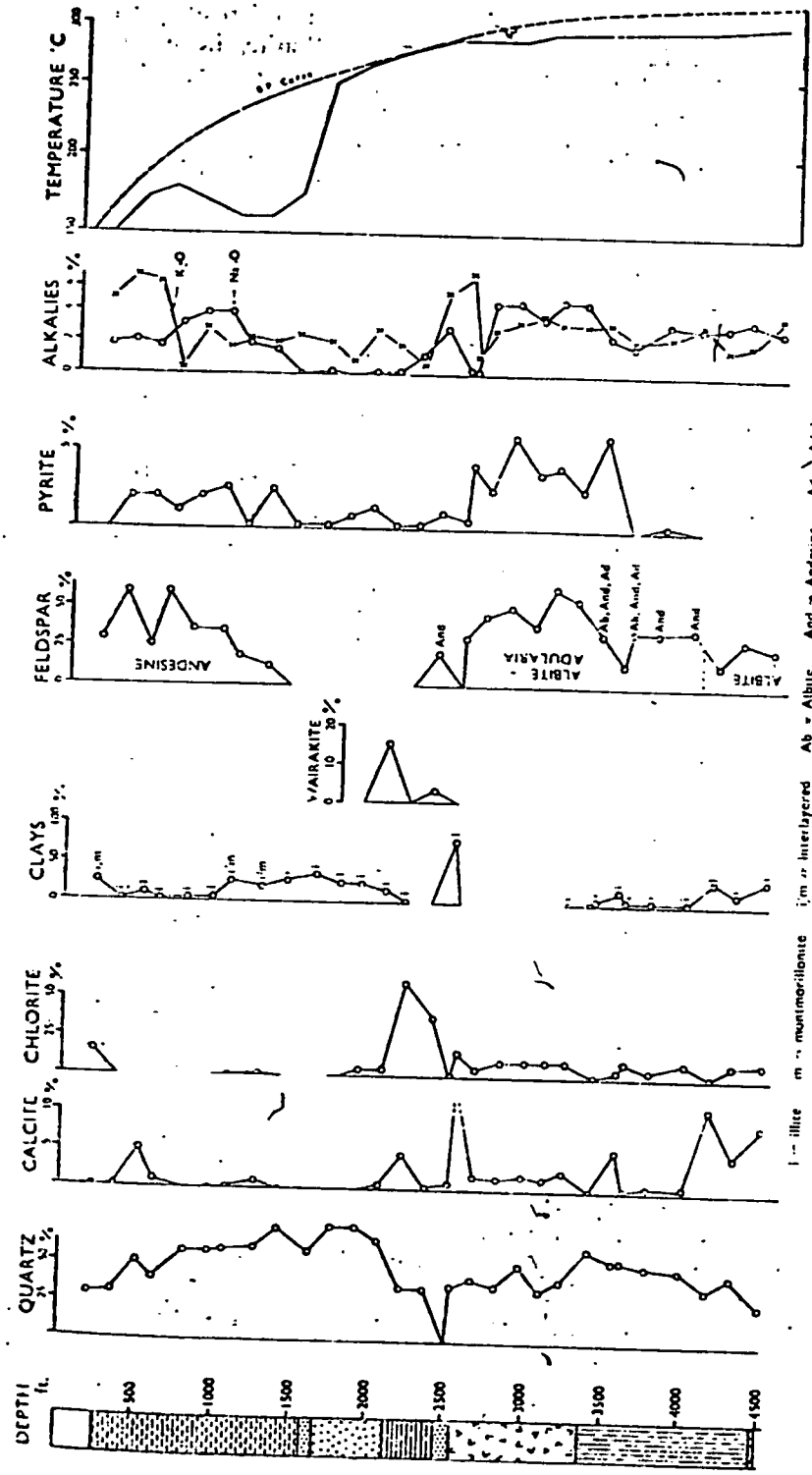

Ad = Adularia
And = Andesine
Ab = Albite
i/m = interlayered
i = illite
m = montmorillonite

Fig. 6. Distribution of some minerals in drillhole Br-9. Hole is cased to 1639 ft (500 m).

Volcanic glass is very susceptible to alteration and readily alters at temperatures below 120° (table 3) to montmorillonite, illite, and less commonly, chlorite, calcite, siderite, K-feldspar, and quartz. Magnetite is also relatively sensitive to alteration and generally alters either to pyrite or leucoxene at temperatures as low as 80°.

Hypersthene, hornblende, and biotite alter at progressively higher temperatures and are generally replaced by chlorite, illite, calcite, quartz, or pyrite. Andesine is less readily altered than biotite at Ohaki-Broadlands, in contrast to Wairakei (Steiner, 1968), and its stability and reaction products are particularly influenced by temperature, permeability, and fluid composition. Under conditions of very low permeability, andesine may persist to temperatures in excess of 285°. In the Salton Sea drillhole I.I.D. No. 1, calcic plagioclase was present in intensely altered rocks below 5000 ft (1524 m) and above a temperature of 323°C, but this was considered by Muffler and White (1969) to be due to the exceptionally high Ca content of the associated geothermal brine. In Ohaki-Broadlands, andesine may be replaced by one or more of the following: adularia, albite, calcite, illite, wairakite, epidote, or quartz.

HYDROTHERMAL MINERALS

Zeolites.—These have only a limited distribution and are not as common at Ohaki-Broadlands as at Wairakei, mainly because of differences in water composition. Neither heulandite nor laumontite have been positively identified in the cores, although both are present at Wairakei (Coombs and others, 1959). However, ptilolite is present in several cores where measured temperatures are between 60° and 170° (table 3). These temperatures are comparable with those for its occurrence at Wairakei (Steiner, 1953 and 1968) where it forms between 60° and 160° and in Iceland where it occurs at 120° (Sigvaldason, 1963) but lower than temperatures reported by Coombs and others (1959). Ellis (1960) crystallized ptilolite (possibly metastably) from obsidian at 230° during exposure to natural hydrothermal solutions. In cores from Ohaki-Broadlands, ptilolite occurs as small, fibrous crystals, which have been deposited directly from solution in pumice or rhyolite cavities, and it does not appear to form directly from glass hydration or devitrification.

The other zeolite present at Ohaki-Broadlands is wairakite, which occurs in only a few cores. Measured temperatures are between 232° and 276° (table 3), which compare with temperatures from 142° to 250° at Wairakei (Steiner, 1953 and 1968; Coombs and others, 1959), and 222° to 260° in the Tauhara geothermal field, New Zealand. Generally the wairakite occurs as twinned, weakly birefrigent, euhedral crystals up to 3 mm in diameter lining fractures, where they have been deposited from solution. It only rarely replaces plagioclase.

Both ptilolite and wairakite are high-silica zeolites. Their distribution conforms with the established pattern of the more hydrated species forming at the lower temperature. At Ohaki-Broadlands, temperature and water composition (particularly pH, Ca content, and silica activity)

appear to be the main factors affecting zeolite stability, although the formation of ptilolite is favored by the presence of glass in the host rock.

Quartz.—Quartz is abundant both as a primary constituent of most rocks and as product of devitrification and hydrothermal alteration. It is possible to distinguish origins only by using a microscope. Figures 3 to 6 therefore show the total quartz in the cores. In common with rocks in other New Zealand geothermal fields, primary quartz remains unaffected during contact with the silica-saturated geothermal water. Hydrothermal quartz is also widespread both as a replacement mineral and as clear, inclusion free, euhedral crystals up to several millimeters in length, lining cavities and fractures. It is particularly common as a replacement of pumice, plagioclase, and glass and forms at depths where temperatures are above about 100° but is most abundant in zones of good steam production.

Cristobalite.—α-cristobalite (X-ray peak at 4.05Å) is present in several holes but is most abundant in holes 5 and 6, where some cores contain up to 25 percent. It occurs as round, near-isotopic spherules less than 0.1 mm in diameter, between temperatures of 46° and 176°, and to a maximum depth of 2503 ft (763 m). At higher temperatures it probably changes to quartz. Its origin is uncertain, but the low temperature of occurrence, its abundance, and occasional association with montmorillonite suggest that it is possibly a metastable, first alteration product of volcanic glass. However, cristobalite is commonly considered to be a high temperature devitrification product, and this is also its origin in drillhole Y-1, Yellowstone National Park (Honda and Muffler, in press). It may also have originated this way at Ohaki-Broadlands, but it was not reported by Ewart (1966) in surface rocks of the region.

Chlorite.—Chlorite is a common mineral in all drillholes and may constitute up to 40 percent of the rocks. It is usually formed from groundmass or pumice alteration but may be an alteration product of primary ferromagnesian minerals or occasionally plagioclase. More rarely, it is deposited directly from solution. Typically, the chlorite is green, slightly pleochroic, weakly birefringent, and of variable crystallinity. Infra-red and X-ray diffraction data show it to be an iron-rich, trioctohedral nonswelling type, similar to that commonly found at Wairakei (Steiner, 1968). The distribution of chlorite indicates that its stability is largely independent of depth, permeability, and temperature (table 3), and its abundance appears to be related to the initial iron content of the unaltered rocks (MgO content <0–3 percent in unaltered rocks). In places however, there has also been addition of iron to the rocks to form chlorite or pyrite.

Kaolin.—Surface hydrothermal activity at Ohaki-Broadlands is minor compared with that at Wairakei, and therefore supergene kaolin, opal, and alunite are virtually absent even in shallow cores. However, several cores from Br-5, Br-6, and Br-12 contain kaolinite which has formed as an alteration product of volcanic glass. Measured temperatures here are

low (table 3), and these drillholes have the poorest production in the field. The presence of kaolinite may be due to one of the following reasons:

A. It represents buried zones of superficial acid alteration.

B. It was formed by an inflow of oxygenated ground water, causing acid conditions by sulphide oxidation.

C. At low temperatures, kaolin is a stable phase in waters of Broadlands composition.

The third explanation is preferred because the kaolinite is locally associated with small amounts of both carbonate and pyrite, implying non-acid, reducing conditions, and its comparatively broad vertical distribution in the rhyolite in drillhole Br-6 (fig. 5) suggests that it is not fossil alteration. Extrapolated experimental data (see later) indicate that at a temperature of about 100° the kaolinite-mica phase boundaries for waters of Broadlands composition would be at about pH 7.

Illite, interlayered illite-montmorillonite, and montmorillonite.—These minerals are widespread and abundant at Ohaki-Broadlands and constitute more than half of some recovered cores. With increasing temperature and depth, there is a general sequence of montmorillonite→interlayered illite-montmorillonite (rich in montmorillonite)→interlayered illite (rich in illite)→illite, although local reversals are not uncommon, and in places, illite and montmorillonite may coexist, without interlayering. The amount of the illite component in the interlayered illite-montmorillonite generally increases with temperature, but, unlike Wairakei (Steiner, 1968), clay mineral type appears to be unrelated to fault-fissures. Clay minerals form from the alteration of plagioclase, ferromagnesian minerals, and particularly pumice fragments but in places, where the rocks are fractured, may also be deposited directly from solution.

Montmorillonite occurs in the calcium form, usually as minute, weakly birefringent grains with an 001 reflection about 14Å, although this decreases with increasing illite interlayering. In places, for example, Br-7 at 2758 ft (841 m), the illite is comparatively coarse grained, has sharp basal reflections, a high birefringence, does not have a low temperature D.T.A. endothermic peak, and may be more correctly called sericite (Taboadela and Ferrandis, 1957). In the later discussion the terms illite, sericite, and K-mica are considered synonymous. Steiner (1968) gave evidence that illite forms from silicic volcanic glass via the sequence: montmorillonite→mixed-layer illite-montmorillonite deficient in interstratified illite→mixed-layer illite-montmorillonite with dominant illite →illite. Although a similar assemblage and sequence is also found at Ohaki-Broadlands, the evidence would be consistent with contemporaneous formation of clays, with distribution and type dominantly a function of temperature. In some places, predominantly sedimentary rocks at depth contain illite that has not been derived from glass, and as previously mentioned illite may be deposited directly from solution.

Montmorillonite, illite, and interlayered illite-montmorillonite distribution is similar to that at Salton Sea, where Muffler and White (1969) found that montmorillonite existed at surface temperature but disappeared as a discrete phase at about 100°C, and illite-montmorillonite converted to K-mica at about 210°.

Albite.—Albite is present in varying amounts in cores from all drillholes. With the exception of a small amount in Br-2 at 1090 ft (332 m) albite does not occur above a depth of 1500 ft (457 m) (table 3)—in contrast to Wairakei and Waiotapu where it forms at depths as shallow as 280 ft (86 m) (Steiner, 1953 and 1968) and 200 ft (61 m) in Steamboat Springs drillhole GS-3 (Schoen and White, 1965).

Table 3 shows that the albite may form at temperatures as low as 122° (in Br-6), but in holes with geothermal gradients more typical of the area, it generally forms first between temperatures of 232° and 279°. This compares with its occurrence at temperatures of 230° to 250° at Wairakei (Coombs and others, 1959). Typically it forms twinned, unzoned, clouded crystals, in places together with adularia, replacing, or partly replacing, primary plagioclase. Albite is seldom pure. As shown by refractive indices and infra-red spectra, it varies in composition up to about An_{15}, although most seems to be in the range An_3 to An_{10}. The reason for the variable calcium content is not known but may be a result of incomplete reaction between the water and the primary plagioclase. In the later discussion the term albite refers to all secondary plagioclase regardless of composition. The clouded appearance of the albite crystals contrasts with the clear, inclusion-free andesine and adularia and suggests that the inclusions formed during the alteration processes. These minute inclusions probably consist of iron oxide and indicate that iron is less soluble in sodic plagioclase than in either K-feldspar or more calcic plagioclase, a conclusion consistent with the work of Ribbe and Smith (1966).

At Ohaki-Broadlands, albite formation appears to be particularly affected by temperature and depth but not by permeability, since it is present in cores from all holes. Its formation also requires that plagioclase be present in the unaltered rock.

Potash feldspar.—Secondary monoclinic potash feldspar, referred to as adularia) is an important hydrothermal mineral at Ohaki-Broadlands, because its presence and abundance is related to the measured output of individual drillholes (Browne, in preparation). It has three modes of occurrence:

A. Commonly it replaces primary plagioclase in a manner similar to albite with which it may coexist in equilibrium. These crystals are clear and generally structurally complex.

B. In the groundmass of cores from several holes, particularly the upper thousand feet of drillholes 2, 8, and 11, it occurs as minute, diamond-shaped crystals. These must be formed by major potash infusion, since some cores from Br-11 contain as much as 11 per-

cent K_2O, and this cannot be accounted for by glass devitrification alone. It appears that this type of adularia may form at lower temperatures than that formed by replacement of andesine.

C. More rarely, it occurs as euhedral crystals lining cavities and core fractures (for example, Br-4 at 1093 ft (333 m) and Br-7, 2758 ft (840 m)) where it has been deposited directly from solution in response to change of pH and loss of CO_2 during boiling. This is a rapid non-equilibrium process.

Adularia is abundant in some cores from drillholes 2, 4, 7, 8, and 11 and is a minor constituent of drillholes 3, 9, 10, 12, and 13, where it usually coexists with albite. Though in Br-11 it has formed at a depth of only 228 ft (69 m) where the temperature is 75°, it commonly occurs below about 800 ft (244 m) and above about 220°, which compares with Wairakei where it is found below 1263 ft (385 m) and above 230° (Steiner, 1968; Coombs and others, 1959). Adularia appears to form in places where there is good permeability, but its stability is markedly affected by changes in water composition (figs. 8, 11, and 12).

Epidote.—Epidote is an uncommon mineral at Ohaki-Broadlands but is abundant at Wairakei (Steiner, 1953) and the Salton Sea (Muffler and White, 1969). At Ohaki-Broadlands it is present in concentrations below about 1 percent.

Epidote is most abundant in a core from Br-13 at 3540 ft (1079 m), where it occurs as euhedral, slightly pleochroic crystals in thin (1 mm wide) veins and in vugs together with calcite. In rare instances it appears that calcite has been deposited directly on top of epidote. An electron microprobe examination of a crystal showed it to be an iron-rich variety (approx 13 percent Fe; C. P. Wood, personal commun.).

The formation of epidote at Ohaki-Broadlands is probably restricted because of high underground carbon dioxide concentrations which favor the formation of calcite (see later), but it does not seem to form below a temperature of about 260°. This compares with measured minimum formation temperatures of 290° at Salton Sea (Muffler and White, 1969) and about 250° at both Wairakei (Steiner, 1968) and in the Tauhara field. However, it is considerably higher than Iceland where epidote occurs at about 225° at Hveragerdi and only 130° at Reykjavik (White and Sigvaldason, 1963). Muffler and White (1969) noted that at Salton Sea a decrease in calcite complemented an increase of epidote which they considered due to incorporation of Ca into epidote following the breakdown of calcite, but this does not seem to have been the case at Ohaki-Broadlands. Its distribution is not shown in table 3 because of its low abundance in recovered cores.

Calcite.—This is a common and important mineral at Ohaki-Broadlands, present in all drillholes. It is usually most abundant below a depth of about 2000 ft (610 m), but it also occurs at shallower depths (table 3) and at temperatures below 100°.

It forms as a replacement, or partial replacement, of andesine together with secondary albite, adularia, or quartz but also occurs as irregular grains in the groundmass of some rocks. Less commonly it has been deposited as scaly crystals filling or lining fractures and cavities and is occasionally ejected during initial bore discharges as white rhombohedral crystals up to 1.5 cm long. Typically it is white, inclusion free, and nearly pure $CaCO_3$ in composition (C. P. Wood, personal commun.).

Its formation at Ohaki-Broadlands is little affected by temperature, but it is particularly sensitive to changes in water and gas composition, caused, for example, by boiling.

Siderite.—Siderite is an uncommon mineral at Ohaki-Broadlands but is present in amounts of up to 10 percent, in cores from Br-6, Br-10, and Br-12. It occurs either as minute spherules or larger irregular grains up to 0.1 mm long in the groundmass of some rocks, but, unlike calcite, it does not replace plagioclase. Siderite from Br-12 at 1850 ft (564 m) (temp 122°), which apparently coexists in equilibrium with calcite, was examined by electron microprobe and found to contain about 6 percent CaO and detectable MgO and MnO (C. P. Wood, personal commun.), whereas the calcite contains less than 2 percent FeO. Siderite occurs at temperatures between 37° and 130° (table 3). This compares with slightly higher temperatures at the Salton Sea (about 135°, Muffler and White, 1969), but it does not occur at the depths of base metal sulphides, in contrast to several hydrothermal ore deposits where it is often associated with base-metal sulphide veins (for example, Shaw, 1959). In drillhole 6, Wairakei, it also occurs at low temperatures at a depth of only 90 ft (27 m) (Steiner, 1953). It does not coexist with magnetite and seldom with pyrite, suggesting that some of the iron is derived from the alteration of magnetite, probably under relatively high P_{CO_2} and low P_{O_2} conditions (Garrels and Christ, 1965).

Iron sulphides.—The iron sulphides present are pyrite and pyrrhotite. Marcasite has not been identified at Ohaki-Broadlands. Pyrite in amounts of up to 10 percent is the most common sulphide and is present in cores from all drillholes. In most places it forms evenly distributed, euhedral crystals up to 2 mm in diameter or small irregular and occasionally "doughnut-shaped" grains, but it also occurs in thin veins and small vugs. Pyrite crystals from Br-4 analyzed spectrochemically by W. C. Tennant, Chemistry Division, contain up to 1000 ppm arsenic, but as local concentrations of arsenic could not be detected under the electronmicroprobe (G. A. Challis, personal commun.) it appears that this element does not form a discrete mineral. Pyrrhotite is much less abundant than pyrite, but it occurs in 6 drillholes (table 3) below 1600 ft (488 m), commonly as magnetic brown-black pseudohexagonal crystals (composition near Fe_7S_8, by X-ray diffraction) up to 4 mm in diameter, and usually in evenly distributed clusters. A small amount of yellow monoclinic (?) pyrrhotite occurs at a depth of about 2758 ft (840 m) in

hole Br-7 (Browne, 1969). Pseudohexagonal pyrrhotite was also present in a scaly deposit on the slotted liners removed from Br-1.

Pyrite and pyrrhotite may form from the alteration of magnetite and ferromagnesian minerals, but the abundance of pyrite and its presence in veins and vugs suggest most must have been deposited from solution by addition of iron and sulphur. Pyrite forms readily at temperatures below 100°, but pyrrhotite is present only above 152° (table 3) and under the lower P_{H_2S}/P_{H_2} conditions that may occur in more impermeable zones. It may be significant that pseudohexagonal pyrrhotite is present in cores from drillholes that are all poor steam producers. The formation of pyrrhotite is also favored by the presence of organic matter, and this seems to have been the case in some fine-grained sediments from Br-12.

Both iron sulphides coexist, apparently in equilibrium, in a core from 2189 ft (667 m), Br-13, where the measured temperature is 237°. Pyrite is common at Wairakei and Waiotapu (Steiner, 1953; 1963), but pyrrhotite has not been found in the latter geothermal field and is only a minor constituent at Wairakei (Steiner, personal commun.). In the Salton Sea area, pyrite occurs in the I.I.D. No. 1 and Sportsman No. 1 drillholes below a depth of 2000 ft (610 m) and above a temperature of 200° (Muffler and White, 1969), but pyrrhotite is a minor phase.

Base-metal sulphides.—Small quantities of sphalerite, galena, and chalcopyrite were found in cores and cuttings from 5 drillholes (7, 10, 14, 15, 16) and are of interest because textural evidence suggests they are in equilibrium with one another, with other hydrothermal minerals, and with the fluid discharged (Browne, 1969). They are most abundant in drillholes 7 and 16, where they occur in silicified rhyolites and tuffs, and are less common in the other holes where the host rocks are conglomerates and tuffs. Sphalerite is generally the most abundant, but locally galena and rarely chalcopyrite may predominate. The waters associated with these sulphides are of low salinity (table 1) and have low concentrations (few ppb of copper, lead, and zinc), which indicate that base-metal sulphides may deposit from solutions of quite a different character from the metal-rich, saline brines as found at Salton Sea or in the Red Sea deeps. A precipitate rich in Sb, As, Tl, Au, and Ag which was deposited from the Ohaki Pool, some 200 yards from bore Br-3 and from the Br-2 discharge was discussed by Weissburg (1969). Water from the pool has a similar composition to that discharged from the drillholes. A crude metalliferous zoning process exists with Cu–Pb–Zn predominating at between 140° to 300° and As, Sb, Tg, Tl, and Au near 100° (Ellis, 1969; and Browne, in preparation).

FACTORS INFLUENCING HYDROTHERMAL ALTERATION

The formation and stability of the hydrothermal minerals is influenced by factors that include (1) temperature, (2) permeability and porosity, (3) rock type, (4) fluid composition, (5) total pressure, and (6) water flow and time for reaction.

Temperature, rock composition, and permeability are probably the most important factors in static systems. It is apparent from table 3 that the temperature at which a mineral first forms varies from drillhole to drillhole, due to other influences. In most cases, however, there is a temperature range for the Ohaki-Broadlands system outside which a mineral will not form or persist under the natural hydrothermal conditions, and table 3 indicates this range. For example, it is apparent that calcite and pyrite are less sensitive to temperature than are zeolites, clays, siderite, cristobalite, and albite.

Below 4000 ft (1219 m) depth, temperatures may reach 292°, but over most of the active part of the field, including production zones, temperatures vary between 220° and 270°. The phase diagrams (figs. 7-12) discussed below, referring to a temperature of 260°, are applicable to the most common measured subsurface conditions. Temperature generally increases with depth, but several inversions occur, notably in Br-6 where at a depth of 200 ft (61 m) the temperature is 160°, but at 2200 ft (670 m) it is only 49°.

Over the depths drilled the moderate pressures of up to about 200 atm in excess of water vapor pressures are unlikely to have a major effect on formation of mineral assemblages. However, White and Sigvaldason (1963) suggested epidote formation may be a function of depth. Indirectly, total pressure is a very important variable as it determines the depth and temperature of boiling, a process that changes fluid composition and in turn affects mineral stabilities.

Permeability has an important control on the formation of hydrothermal minerals, since mineralogical changes are for the most part not isochemical, and although some water is available in pore spaces, the rocks must be open for the addition and removal of constituents. It is apparent that in places the more dense, impermeable rocks, such as rhyolite and ignimbrite are little altered, even at high temperatures. For example, in some places there is incomplete alteration of andesine to calcite, clay, quartz, or albite, whereas in cores from more porous, permeable zones, reaction is complete. In some fissure zones, for example, Br-7 at about 2758 ft (840 m) and Br-2 at 1660 to 2080 (506-634 m), where there is good permeability and a continuous flow of fluid, quartz, calcite, and adularia are abundant. These are zones of boiling, and as discussed below these minerals precipitate through the water trying to adjust its composition toward that for an equilibrium assemblage stable at the higher pH and a lower temperature.

At Ohaki-Broadlands the influence of rock type on hydrothermal alteration is mainly through texture and porosity variations affecting permeability. Most of the rocks are chemically and mineralogically similar, containing primary quartz and andesine but not K-feldspar, and thus variation in the original rock chemistry is not especially significant during hydrothermal alteration. However, the maximum quantity of

albite, which may form during alteration, is controlled by the amount of primary plagioclase originally present in the rock.

CORRELATION OF MINERALOGY AND WATER CHEMISTRY

Temperature estimation.—Mahon (1966) and Fournier and Rowe (1966) showed that the deep hot waters in geothermal areas contain silica concentrations at a level for equilibrium with quartz, and this fact may be used to estimate underground temperatures from silica analyses on waters discharged from drillholes. In a hydrothermal system containing sodium and potassium feldspars in the mineral alteration assemblage, there is an inverse relationship between temperature and Na/K ratio in the waters (Ellis, 1969, and discussion below). In table 4, temperatures estimated from the silica and the Na/K methods are compared with the maximum temperatures measured in individual drillholes by the New Zealand Ministry of Works.

TABLE 4

Hole no.	Max temp measured	T_{SiO_2}	$T_{Na/K}$
1	278	225-235	200-210
2	276	260	280-290
3	281	256	275-290
4	265	266	270-280
5	244	—	195
6	170	—	190
7	279	—	250-260
8	268	260	300
9	290	260	290
10	270	244	245
11	271	260	290
13	258	255	280

It has been observed in geothermal systems that the solution/quartz equilibrium adjusts more rapidly with changing temperatures than does the solution Na/K mineral equilibrium. Ohaki-Broadlands temperatures by the Na/K method are often higher than those obtained by the silica method, particularly in the more permeable zones. Maximum measured temperatures before production are closest to the Na/K temperatures, but the silica temperatures are more in line with measurements at the production levels. The higher Na/K temperatures may be a memory effect reflecting characteristics acquired by the waters at deep levels in the field.

Mineral equilibria.—The usefulness of these two simple mineral-water equilibrium considerations encouraged a more detailed examination of the relationship between water chemistry and hydrothermal alteration minerals. In this respect the work of Hemley and Jones (1964) on the solution ratios of m_{Na^+}/m_{H^+} and m_{K^+}/m_{H^+} for equilibrium with sodium potassium feldspars, micas, and clays is of particular significance. Helgeson (1967) showed how this experimental information, together

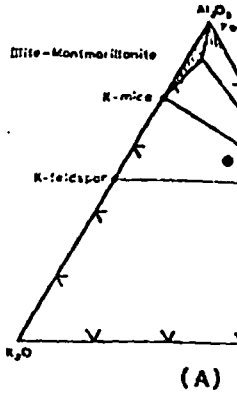

(A)

Fig. 7. Compositic
join coexisting miner
region.

with the composi
aquifers in whicl
used to construct
tions in the water
not directly appli
use of the same
area have been de

Figures 7A, E
in hydrothermal
Wairakei hydrotl
average rhyolite
given as a solid p
freely in a hydrot
tion of the rock.
plicity, interlayer
discrete phases—i

Figure 8A is
alteration, constr

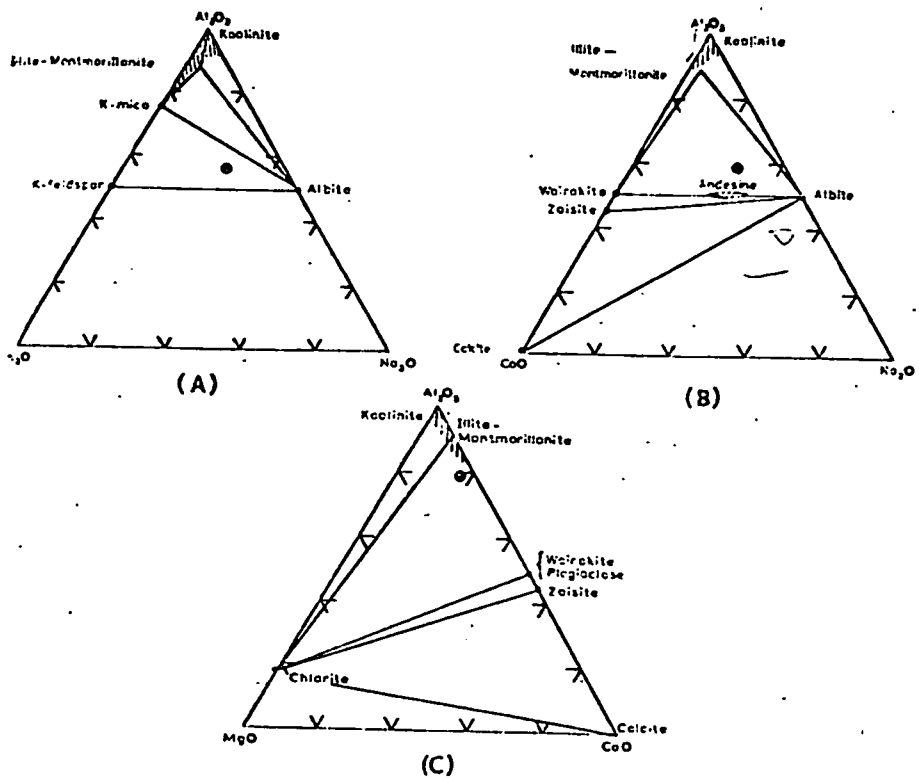

Fig. 7. Compositions of minerals occurring in the Ohaki-Broadlands field. Tie-lines join coexisting minerals. A solid point gives the average rhyolite composition in the region.

with the composition of waters taken at measured temperatures from aquifers in which equilibrium mineral assemblages existed, could be used to construct mineral stability diagrams in terms of ionic concentrations in the water. His diagrams for the Salton Sea geothermal area are not directly applicable to New Zealand geothermal areas, but through use of the same principles, mineral phase diagrams for the Broadlands area have been developed.

Figures 7A, B, C give the composition of the various minerals found in hydrothermally altered zones in the Ohaki-Broadlands and the Wairakei hydrothermal areas, and tie lines show their associations. An average rhyolite composition for the Wairakei-Broadlands district is given as a solid point, but element transport, which in some cases occurs freely in a hydrothermal area, may markedly change the overall composition of the rock. Here and in most later diagrams, for the sake of simplicity, interlayered illite-montmorillonite is considered to consist of two discrete phases—illite and montmorillonite.

Figure 8A is a Hemley–Helgeson K–Ca–H diagram for Broadlands alteration, constructed from published experimental information on the

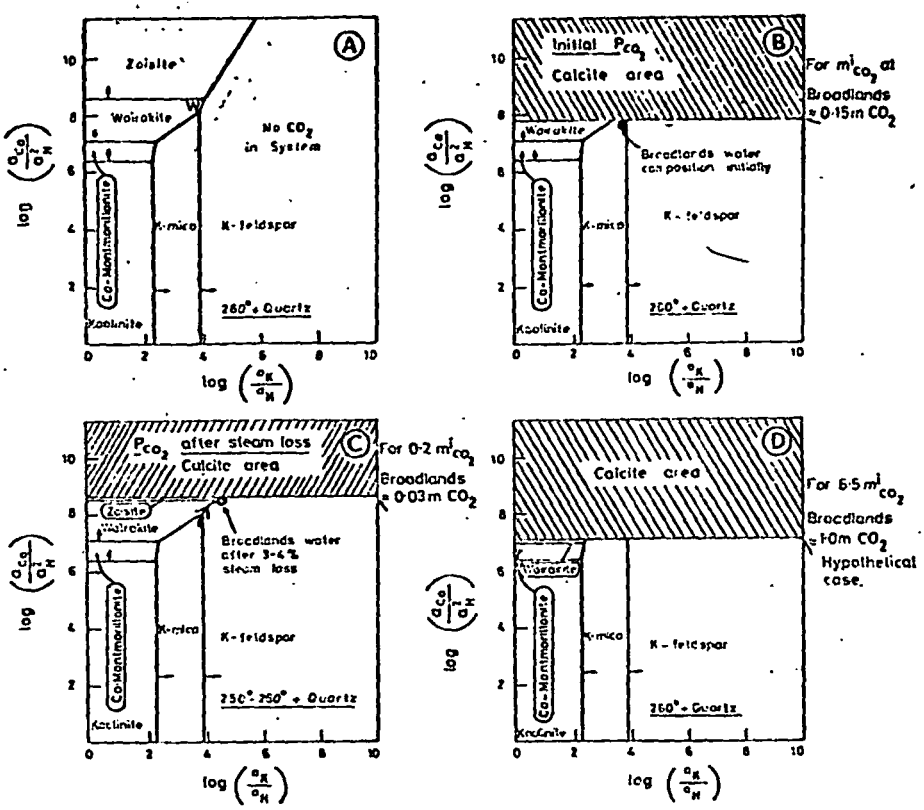

Fig. 8. Mineral stability diagrams for calcium and potassium minerals at 260°, in terms of solution ion ratios and various m_{CO_2} values.

potassium mineral system (Hemley and Jones, 1964), from drill-core mineralogy, and from analytical data for calcium, potassium, and hydrogen ion concentrations in the waters. The figure is drawn for 260°, for although higher temperatures have been measured in the area, this is the average temperature in the most productive zones (see table 4). The main calcium and potassium minerals occurring in the Broadlands system are calcite, epidote (zoisite), wairakite, calcium montmorillonite, K-mica, and K-feldspar. In the discussion that follows quartz is assumed always to be present.

Hemley and Jones' mineral equilibrium boundaries in terms of ratios of concentrations of univalent ions (m_{K^+}/m_{H^+}, m_{Na}/m_{H^+}) were equated to ion activity ratios. Boundaries were adjusted for the lower pressure conditions of the Broadlands system, for example, the value of log (a_{K^+}/a_{H^+}) for the K-mica, K-feldspar equilibrium increases by 0.15 per 1000 bars pressure rise.

To obtain values of the solution ratios a_{Na^+}/a_{H^+}, $a_{Ca^{++}}/a_{H^+}{}^2$, et cetera, values of a_{H^+} were calculated from water analyses and acid-base equilibria (Ellis, 1967). The activity coefficient of univalent ions was taken to be

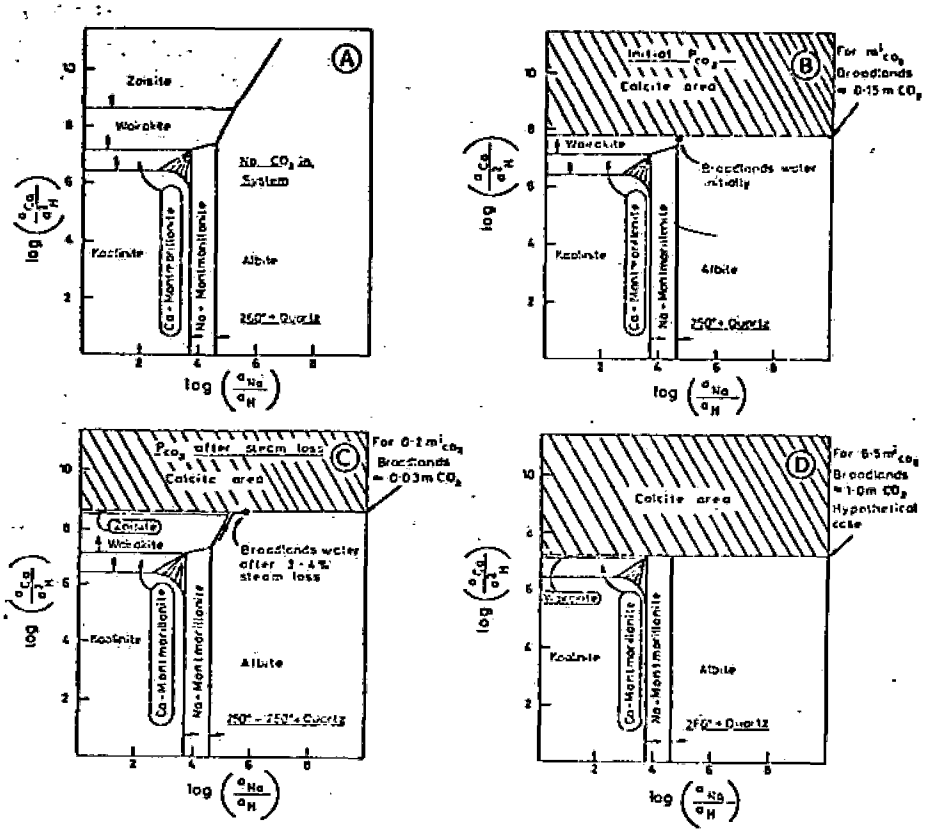

Fig. 9. Mineral stability diagrams for calcium and sodium minerals at 260°, in terms of solution ion ratios and various m_{CO_2} values.

0.70, and for calcium and magnesium ions, 0.25 (the solution ionic strength is about 0.04 m).

Figures 9A, 10A, and 11 are diagrams for the Na–Ca–H, the Ca–Mg–H, and Na–K–H systems respectively, relevant to the Broadlands mineralogy and water chemistry. The effect of intersubstitution of ions has been neglected (straight line phase boundaries) except for the Na–Ca montmorillonites. (The Ohaki-Broadlands and Wairakei montmorillonites are as the calcium form.)

Each of the diagrams represents a particular element combination plane in a more complex phase diagram. The stability conditions in figure 8A for example, are those in the presence of particular solution concentrations of other elements such as sodium, magnesium, and iron. Except for calcite the phase boundaries for the calcium and magnesium minerals are only approximate but are chosen to give the best fit with the observed chemistry and mineralogy. The diagrams themselves give no new information but provide a convenient means of following the reasons for differing mineralogy at various levels and positions in the field.

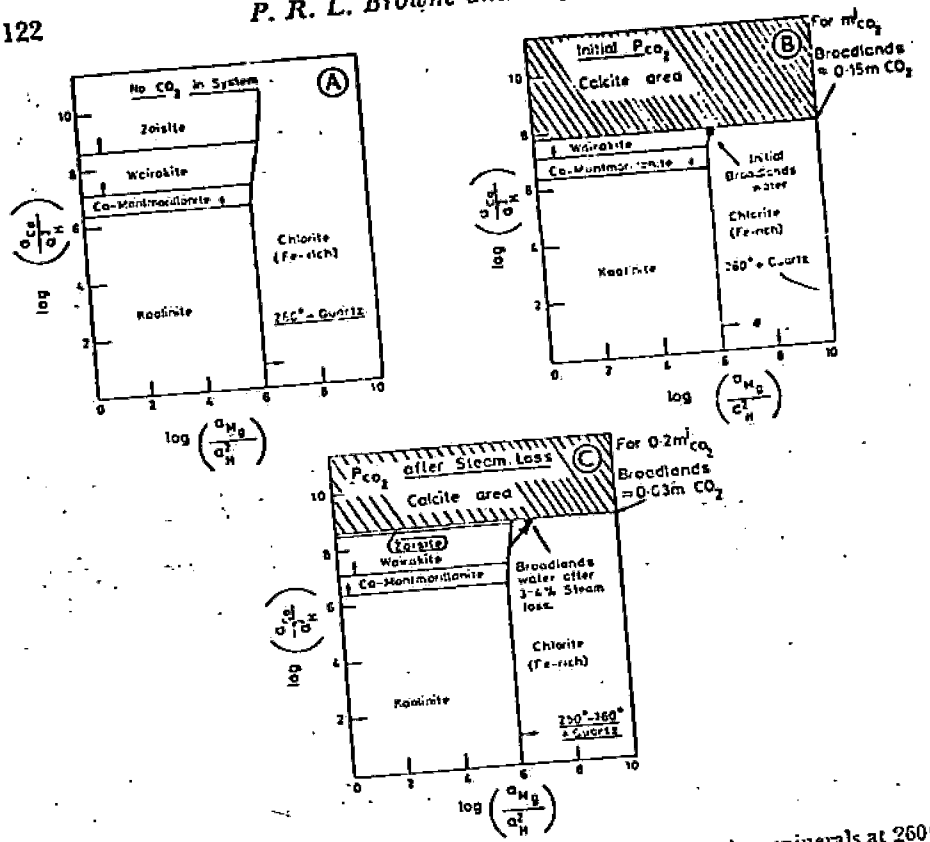

Fig. 10. Mineral stability diagrams for calcium and magnesium minerals at 260° in terms of solution ion ratios and various m_{CO_2} values.

The reason for the rarity of epidote and wairakite in the Ohaki-Broadlands hydrothermal alteration compared with Wairakei alteration may be sought in terms of variations in carbon dioxide concentration.

With the addition of carbon dioxide to a rock-water system, bicarbonate and carbonate ions are formed, and at a particular carbon dioxide concentration on the diagrams with log (a_{Ca}/a_H^2) as their ordinate a horizontal line can be drawn representing the value at which calcite precipitates (experimental solubility data of Ellis, 1963). For example figure 8B shows the calcite line for the original Broadlands m_{CO_2} value of 0.15. In the upper area of these diagrams lie values of log (a_{Ca}/a_H^2) which are prohibited by calcite precipitation. This calcite "blind" is lowered down the range of (a_{Ca}/a_H^2) values as the concentration of carbon dioxide in the system is increased. As can be seen in figure 8C, at $m_{CO_2} = 0.03$, zoisite (epidote) still appears as a stable mineral under certain solution conditions, but it does not appear at 0.15 m CO_2 (fig. 8B). At higher m_{CO_2} values (fig. 8D; m = 1.0) the wairakite field would

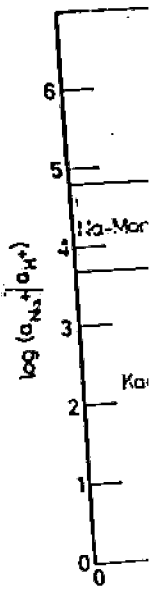

Fig. 11. Mineral sta
terms of solution ion co

also disappear. The
in other geological
can also be interpre
trations (Zen, 1961).
Although chlo
magnesium ion con
as an iron-rich vari
also contains appr
lonite-illites has be

Figures 8B, 9
the deep Broadla
diagrams (solid pc
chlorite, wairakit
of the original w
with calcite may
The fact tha
mineral gives no
in addition to t
nucleate as a ne
the mineral alte
diagrams provid
in mineral assem

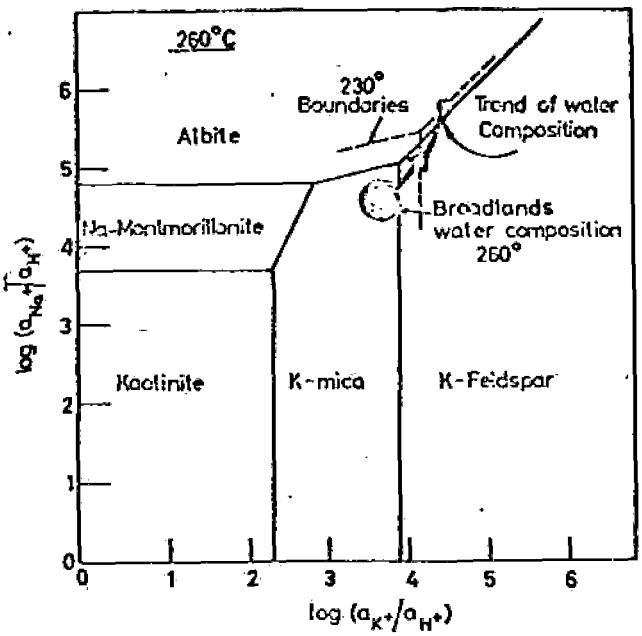

Fig. 11. Mineral stability diagram for sodium and potassium minerals at 260° in terms of solution ion concentration ratios (broken lines show 230° boundaries).

also disappear. The presence or absence of calcium epidote or wairakite in other geological settings such as in low grade regional metamorphism can also be interpreted in terms of the associated carbon dioxide concentrations (Zen, 1961).

Although chlorite is interpreted in the phase diagrams with the magnesium ion concentration as a major control on its stability, it occurs as an iron-rich variety both at Broadlands and Wairakei, and the epidote also contains appreciable iron. The composition range of montmorillonite-illites has been hatched in on figures 7A, B, C.

HYDROTHERMAL ALTERATION SEQUENCES

Figures 8B, 9B, 10B, and 11 show that the average composition of the deep Broadlands water falls in a position on the mineral stability diagrams (solid point) close to equilibrium for K-mica, K-feldspar, albite, chlorite, wairakite, calcite, and quartz. Compositions and temperatures of the original waters will vary slightly from place to place. Saturation with calcite may not always be achieved.

The fact that the water composition falls in the stability field of a mineral gives no indication of the quantity of the mineral present, since in addition to the factors already discussed, the ability of a phase to nucleate as a new mineral and the rate of crystal growth also influence the mineral alteration assemblage. Nevertheless, the mineral equilibrium diagrams provide a convenient base on which to examine the variations in mineral assemblages with depth and water conditions.

Changes in water temperature cause changes in the positions of phase boundary lines, so that a mineral assemblage stable at a given water composition and temperature may be unstable at a higher or lower temperature. Trends in water pH which accompany the loss of steam and carbon dioxide caused through boiling of the deep water also give rise to consequent changes in the mineralogy. Other changes, such as those due to condensation of CO_2-rich steam into a water phase or to dilution, can also be interpreted on the diagrams.

With the exception of the potassium/sodium system there is no quantitative information on the movement of phase boundaries with temperature. On figure 11, the phase boundaries for 230° are given as a dashed line for comparison with the 260° potassium/sodium mineral boundaries, but boundaries on other diagrams have a short arrow which suggests their direction of movement with decreasing temperatures.

The effect of steam boiling off from the deep 260° water phase is first considered. On figures 8 to 11 a short heavy line with an arrowhead gives the general trend in water composition with steam loss. For a few percent steam loss, concentration of the ions by evaporation can be neglected, and the important effects are a rise in water pH and a slight cooling of the water.

With increasing steam loss from the deep 260° water (and with rising pH) the diagrams suggest that the water rising through the field would tend to impose the following sequence of hydrothermal alteration minerals into the rocks, and the sequence would usually be one of diminishing depth. All assemblages include quartz.

1. Water at 260° in equilibrium with albite, K-mica, K-feldspar, calcite, wairakite, and chlorite.
2. With slight steam loss and pH rise the water composition point would move in the direction shown by the arrow line. On figure 8C, K-feldspar and wairakite would be stable minerals, on figure 9C the water composition would lie along the albite-wairakite boundary, while figure 10C shows that chlorite would remain stable. Calcite would be precipitated, as the calcite "blind" rises proportionally to pH change, but the water composition point rises proportionally to twice the pH change. Due to the shift of phase boundaries with temperature, growth of K-feldspar is necessary to remove potassium ions in excess of those for equilibrium two-feldspar conditions (fig. 11). Depending on the direction of movement with temperature of the wairakite-K-feldspar and the wairakite-albite boundaries, the slight cooling with continuing steam loss would cause growth of one or other of each mineral pair so as to maintain the water composition at equilibrium Ca/K or Ca/Na ratios, respectively, for the two-phase boundary conditions. Growth of chlorite would occur.
3. With a few percent steam loss the same trends would follow, except that epidote (zoisite) growth would be initiated (figs. 8C

and 9C). Calcite and K-feldspar would continue to be formed, and the mineral assemblage would at this stage trend toward K-feldspar, albite, calcite, epidote, and chlorite.

After about 3 to 4 percent steam loss by boiling, the carbon dioxide concentration in solution would be then about 0.2 of the original or about 0.03 m. The water composition would trend toward a point for equilibrium with calcite and K-feldspar (fig 8C), albite and calcite (fig. 9C), and chlorite and calcite (fig. 10C). However, the rock-mineral system has a buffering action toward the changes which the rising water pH tries to bring about. The trends in mineralogy are certain, but the extent to which changes are brought about in a homogeneous rock at a particular level depends on the volume of water of the particular composition that passes through the rock, the rock porosity and permeability, and the reactivity of various minerals.

The preceding discussion considered steam boiling from a homogeneous aquifer of slowly rising hot water. In contrast, a flow of water rising in a fissure and rapidly boiling off steam would produce secondary mineralogy about the fissure dominated by the first minerals formed through the water trying to adjust its composition toward that for an equilibrium mineral assemblage at the higher pH and lower temperature. Buffering effects from the rock would be minimal, and the main minerals formed about the fissure would be K-feldspar, calcite, and quartz through a continuous supply of elements from the water flow. This relationship between alteration and permeability has been used as an aid to estimate steam and water production of individual drillholes (Browne, in preparation). Meyer and Hemley (1967) also discuss this type of mechanism. Formation of wairakite (or chlorite) in fissures at the level of first boiling, followed by epidote (or chlorite) at a higher level would also be consistent with the phase diagrams.

The case of water heated by the condensation into it of steam rich in carbon dioxide may be considered. The phase diagrams show that the lower pH conditions would cause a trend toward mineral assemblages such as albite, K-mica, wairakite, or montmorillonite, K-mica, wairakite.

The diagrams show kaolinite to be stable at temperatures of the order of 260°, only under low pH conditions. Clays of this type are often found near surface levels where acid conditions occur through hydrogen sulphide oxidation, although the diagrams of Hemley and Jones (1964) show that at lower temperatures very acid conditions are not necessary for their formation.

The diagrams also suggest that certain mineral associations are not possible if chemical equilibrium is attained. Ca-montmorillonite + K-feldspar, epidote + Ca-montmorillonite, epidote + K-mica, and calcite + Ca montmorillonite should be incompatible pairs at equilibrium. Of these, the first two have not been observed. Small amounts of calcite occasionally coexist with Ca-montmorillonite but at comparatively low

temperatures. In a few rocks, epidote and K-mica coexist, suggesting that at these places the minerals have not attained equilibrium.

Broadlands hydrothermal alteration.—Further brief comments on rock alteration at various depths at Ohaki-Broadlands can be made with reference to the stability diagrams and, where appropriate, figures 3 to 6. These comments are intended to show how observed hydrothermal mineral assemblages in individual holes may be related to subsurface fluid behavior, for although the stability diagrams are drawn for average 260° conditions, their general form will apply over a range of temperatures.

Hole Br-1. Alteration is slight at higher levels although temperatures in some places are in excess of 200°, but below about 2800 ft (853 m), albite and K-mica occur. This alteration corresponds to water compositions likely in impermeable rocks under static aquifer conditions, and this conclusion is supported by the fact that the hole does not produce.

Hole Br-2. Below a depth of 2300 ft (701 m), albite, adularia, chlorite, calcite, and very minor epidote coexist (fig. 3), and this assemblage could be formed by water rising to these levels and boiling off a few percent steam (and CO_2). Between 1650 ft (502 m) and 2000 ft (609 m) the rocks are highly silicified and in addition to abundant hydrothermal quartz contain adularia and calcite but not albite. This suggests that this is a zone of vigorous boiling, with rapidly rising pH and cooling of the water flow. A similar but smaller zone of this kind also occurs between 750 and 1000 ft (229-305 m), but the remainder of the alteration above 1600 ft (488 m), characterized by illite, could be attributed to the cooler conditions at higher levels, caused by considerable steam loss, and possibly also to some conduction and convection. In this situation, as the pH rise of the water is limited to the effect caused by the loss of most of the CO_2 from solution, the effect of cooling in moving the K-mica, K-feldspar boundary to higher a_{K^+}/a_{H^+} values could cause K-mica to become stable, overriding the opposing effect of pH-rise. Under cooler near-surface conditions, the rates of mineral growth may be more important than trends toward an equilibrium mineral assemblage.

Hole Br-4. Figure 4 shows that at about 3300 ft (1006 m) minor adularia occurs with illite and chlorite, indicating a cooling zone, but the absence of calcite or epidote suggests that this cooling is by convection or conduction rather than by boiling.

From 2300 to 3300 ft (701-1006 m) the hydrothermal minerals are dominantly albite, illite, chlorite, and calcite. This and the absence of adularia except for traces in the upper level of this section may indicate levels where water rises in temperature by conduction.

From about 1500 to 2300 ft (457-701 m) there is a broad zone of albite, adularia, calcite, chlorite, and illite which suggests this is an aquifer of water containing appreciable carbon dioxide. The disappearance of albite at the top of these levels may be caused by boiling, but the persistence of illite suggests that sufficient contact of water with rock surfaces was retained to hold the system on the K-mica, K-feldspar

boundary line; that is, the conditions are those of a porous aquifer rather than a fissure flow. A narrow zone of adularia at a depth of about 1100 ft (335 m), but without calcite, epidote, or albite and containing illite, suggests that this is a zone of cooling, but not one of major fissure flow of boiling water.

Hole Br-6. The distribution of minerals in this hole and the measured downhole temperature are shown in figure 5. The persistence of primary minerals below 2400 ft (730 m) and absence of adularia suggest that impermeable conditions occur over most of the hole, but the small amount of albite in some cores below 3000 ft (914 m) may indicate that there is minor conductive heating. In the shallower levels of the hole, the irregular distribution of some hydrothermal minerals allied with temperature reversals implies that there is cooling water circulating laterally between rhyolite flows.

Hole Br-7. Mesozoic graywacke and argillite basement rocks from below 3100 ft (945 m) contain albite, illite, chlorite, and calcite (Browne, 1969), but some of these minerals may have formed by burial metamorphism preceding geothermal activity. However, a temperature increase below 3100 ft (945 m) points to conductive heating. From 2300 to 3000 ft (701-914 m), abundant adularia, quartz, and minor calcite with little albite and illite (sericite) reveals this to be a zone with a flow of boiling water. The persistence of minor illite (sericite) suggests that the flow, however, is not sufficiently great in comparison with the surface area of exposed rock to raise the water pH above the illite-K-feldspar phase boundary. Between about 900 and 1700 ft (274 and 518 m), unaltered plagioclase shows that there has been little access of water to allow reaction with the mainly impermeable Broadlands dacite, but above a depth of 900 ft (274 m) there is abundant montmorillonite which may have formed by reaction between rocks and circulating river water.

Hole Br-9. At the deepest levels the hydrothermal minerals present in dense ignimbrite are quartz, calcite, chlorite, illite, and albite (fig. 6), an assemblage that suggests reaction under rather impermeable conditions of rising water temperatures.

From 2500 to 3200 ft (762-976 m), albite, adularia, calcite, and quartz with an absence of illite, reveal a lower aquifer in which a few percent of steam boils from water as it moves through the zone.

The appearance of illite and wairakite and the disappearance of calcite and feldspars at about 2100 ft (640 m), just above the Broadlands rhyolite, suggest a water of lower pH, possibly due to steam (+ CO_2) condensing into it.

DIFFERENCES BETWEEN ROCK ALTERATION AT WAIRAKEI AND AT BROADLANDS

As shown by Steiner (1953 and 1968) the most common hydrothermal alteration minerals at highest temperatures and deep levels in the Western Wairakei field are albite, K-feldspar, K-mica, epidote, quartz, and wairakite.

A major difference between Wairakei and Broadlands high temperature alteration is that calcite is common at Broadlands and much less common at Wairakei, while the opposite situation applies for wairakite and epidote. The reason for this can be interpreted by means of the phase equilibrium diagrams (figs. 8-11) and lies in the position of the deep water composition point with respect to the epidote, wairakite, K-mica, and calcite stability fields, at the particular carbon dioxide concentration.

As shown by Ellis (1969) the Wairakei water composition with $m_{CO_2} = 0.01$ is near the wairakite, epidote, K-feldspar coexistence point[2]. The composition is shown as W on figure 8A, and it is appreciably below the calcite solubility line that occurs at $\log (a_{Ca}/a_H^2) = 9.1$ for 0.01 m CO_2 concentration. Slight separation of steam and pH rise would bring the water on to the epidote (zoisite), K-feldspar stability line, and an appreciable steam separation would be required before the composition point reached the calcite line.

Broadlands, however, has a deep water composition point close to the K-mica, K-feldspar, and wairakite coexistence point and to the calcite line. With steam separation, calcite would be precipitated, and although the composition point would subsequently follow along the wairakite, K-feldspar boundary, it is unlikely wairakite would nucleate and grow with any efficiency while calcite was forming.

For a given temperature there is a particular concentration of carbon dioxide in the underground water above which calcite will precipitate as the calcium mineral phase with first steam separation, and below which a calcium silicate phase forms or remains stable with steam separation. At 260° this carbon dioxide concentration is about the Broadlands value (0.1 m). Calcium silicate phases are unlikely to nucleate in drill-pipes, whereas calcite can do so. Slight calciting of drillholes occurs at Broadlands but not at Wairakei. Reasoning along these lines may make it possible to distinguish at an early stage of development the geothermal fields which could give trouble with calcite precipitation caused by first flashing of steam from hot water. The CO_2 concentration of the deep water is a key factor.

Iron sulphide phases.—The equation relating the relative stabilities of pyrrhotite and pyrite to measurable parameters, P_{H_2S} (partial pressure of H_2S) and P_{H_2} (partial pressure of hydrogen) is as follows:

$$FeS_2 + H_2 = FeS + H_2S$$

In figure 12, $\log (P_{H_2S}/P_{H_2})$ for coexistence of the minerals is drawn versus temperature, showing the pyrite field at high H_2S/H_2 ratios and the pyrrhotite field at low ratios.

The concentration ratio H_2S/H_2 in the steam phase of a drillhole discharge is obtained from gas analyses. The solubility of hydrogen sulphide is ten times that of hydrogen at 260° (Ellis, 1967) so that if it is

[2] Unfortunately, in Ellis (1969) values of m_{Ca} were used in error for a_{Ca} values, so that the vertical scale on the diagram differs from the present diagrams by 0.6.

log (P_{H_2S}/P_{H_2}) boundary line

Fig. 12. The bou
drogen and hydrogen
are given for five drill
in terms of H_2S and
thermodynamic data.

certain that the dr
phase at depth, th
liquid can be cal
draw on a two-pha
enthalpy discharge
run, had enthalpi
inflow, but before
the enthalpy had
sulphide is much n
steam boiled from

Taking the H
points are marked
(S_1/S_2) for drillhol
and Br-9 will not
water but should
original P_{H_2S}/P_{H_2}
field.

Country rock
instead of pyrite b
residual water aft
favors pyrite. Whe
material may caus
into the pyrrhotit
Br-4 from 2200 to

We thank N.
Wainwright of N

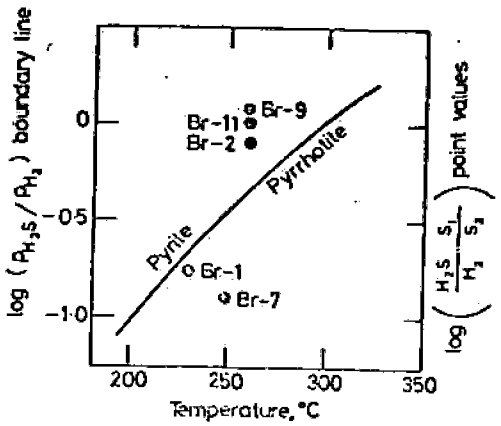

Fig. 12. The boundary between pyrite and pyrrhotite stabilities in terms of hydrogen and hydrogen sulphide partial pressures. Point values of log ($H_2S/H_2 \cdot S_1/S_2$) are given for five drillholes (see text). The pyrite/pyrrhotite boundary is recalculated in terms of H_2S and H_2 pressures, from Toulmin and Barton (1964), using standard thermodynamic data.

certain that the drillhole discharge is derived from a single 260° liquid phase at depth, the partial pressure ratio of the gases in the original liquid can be calculated. Unfortunately, most Broadlands drillholes draw on a two-phase steam-liquid mixture at depth, with consequent high enthalpy discharges. Some drillholes such as 2 and 9 and 11, when first run, had enthalpies that could be reconciled with a simple hot water inflow, but before analyses for hydrogen were done for Br-2 and Br-9, the enthalpy had risen to a two-phase inflow condition. As hydrogen sulphide is much more soluble than hydrogen, drillholes that draw excess steam boiled from water in the country have a low H_2S/H_2 ratio.

Taking the Henry's Law solubilities of H_2S and H_2 to be S_1 and S_2, points are marked on figure 12 for the logarithm of the product (H_2S/H_2). (S_1/S_2) for drillholes 1, 2, 7, 9, and 11. The values for Br-1, Br-2, Br-7, and Br-9 will not correspond to log (P_{H_2S}/P_{H_2}) values for unboiled deep water but should do so for hole 11. Below holes 1, 2, 9, and 11, the original P_{H_2S}/P_{H_2} ratios for unboiled waters would be within the pyrite field.

Country rock exposed to separated steam may produce pyrrhotite instead of pyrite because of the low P_{H_2S}/P_{H_2} ratios in the steam, whereas residual water after steam separation has a high P_{H_2S}/P_{H_2} ratio and so favors pyrite. Where organic-rich sediments occur, breakdown of organic material may cause a local, low P_{H_2S}/P_{H_2} pressure and bring the system into the pyrrhotite field. This process may operate for example in hole Br-4 from 2200 to 2600 ft (670-793 m) and in Br-13 at 1601 ft (488 m).

ACKNOWLEDGMENTS

We thank N. D. Dench, A. C. L. Fooks, W. B. Stillwell, and D. K. Wainwright of New Zealand Ministry of Works for making drillhole

information available; also W. A. J. Mahon and J. B. Finlayson, Chemistry Division, for providing chemical data. G. A. Challis, G. W. Grindley, and A. Wodzicki, New Zealand Geological Survey, and W. A. J. Mahon gave helpful comments on the manuscript, while technical assistance was provided by D. Clyma, C. P. Collard, M. W. Gardner, J. L. Hunt, L. E. Klyen, N. Orr, H. R. Pringle, A. G. Rhode, J. B. Ross, and R. Soong.

References

Browne, P. R. L., 1969, Sulphide mineralization in a Broadlands geothermal drillhole, Taupo Volcanic Zone, New Zealand: Econ. Geology, v. 64, p. 156-159.

Coombs, D. S., Ellis, A. J., Fyfe, W. S., and Taylor, A. M., 1959, The zeolite facies with comments on hydrothermal synthesis: Geochim. et Cosmochim. Acta, v. 17, p. 53-107.

Ellis, A. J., 1960, Mordenite synthesis in a natural hydrothermal solution: Geochim. et Cosmochim. Acta, v. 19, p. 145-146.

———— 1963, The solubility of calcite in sodium chloride solutions at high temperature: Am. Jour. Sci., v. 261, p. 259-267.

———— 1967, The chemistry of some explored hydrothermal systems, *in* Barnes, H. L., ed., Geochemistry of Hydrothermal Ore Deposits: New York, Holt, Rinehart & Winston, p. 465-514.

———— 1969, Present-day hydrothermal systems and mineral deposition: Commonwealth Mining and Metallurgy Conf., 9th, London 1969, Mining and Petroleum Geology Sec., Paper 7, p. 1-30.

Ewart, A., 1966, Review of mineralogy and chemistry of the acidic volcanic rocks of Taupo Volcanic Zone, New Zealand: Bull. volcanolog., v. 29, p. 147-172.

Fournier, R. O., and Rowe, J. J., 1966, Estimation of underground temperatures from silica content of water from hot springs and wet-steam wells: Am. Jour. Sci., v. 264, p. 685-697.

Garrels, R. M., and Christ, C. L., 1965, Solutions, Minerals and Equilibria: New York, Harper and Row, 450 p.

Grindley, G. W., 1960, Taupo geological map of New Zealand, 1: 250,000, 1st ed.: Wellington, New Zealand Dept. Sci. Indus. Research, sheet 8.

———— 1961, Taupo geological map of New Zealand 1:63, 360, 1st ed.: Wellington, New Zealand Dept. Sci. Indus. Research, sheet N94.

———— 1965, The Geology, Structure, and Exploitation of the Wairakei Geothermal Field, Taupo, New Zealand: New Zealand Geol. Survey Bull., new ser., v. 75, 131 p.

Grindley, G. W., and Browne, P. R. L., ms, 1968, The sub-surface geology of the Broadlands geothermal field: New Zealand Geol. Survey Rept. 34 (unpub. open file rept.).

Healy, J., ms, 1968a, Geological Report on Broadlands geothermal field: New Zealand Geol. Survey Rept. 34 (unpub. open file rept.).

———— ms, 1968b, Broadlands geothermal investigations for period June to October, 1968: New Zealand Geol. Survey Rept. (unpub. open file rept.).

Helgeson, H. C. 1967, Solution chemistry and metamorphism, *in* Abelson, P. H., ed., Researches in Geochemistry, v. 2: New York, John Wiley & Sons, p. 362-404.

Hemley, J. J., and Jones, W. R., 1964, Aspects of the chemistry of hydrothermal alteration with emphasis on hydrogen metasomatism: Econ. Geology, v. 59, p. 538-569.

Honda, S., and Muffler, L. J. P., in press, Hydrothermal alteration in core from research drillhole Y-1, Upper Geyser Basin, Yellowstone National Park.

Mahon, W. A. J., 1966, Silica in hot water discharged from drillholes at Wairakei, New Zealand: New Zealand Jour. Sci., v. 9, p. 135-144.

Meyer, Charles, and Hemley, J. J., 1967, Wall rock alteration, *in* Barnes, H. L., ed., Geochemistry of Hydrothermal Ore Deposits: New York, Holt, Rinehart & Winston, p. 167-235.

Muffler, L. J. P., and White, D. E., 1969, Active metamorphism of Upper Cenozoic sediments in the Salton Sea geothermal field and the Salton Trough, Southeastern California: Geol. Soc. America Bull., v. 80, p. 157-182.

Ribbe, P. H., and Smith, J. V., 1966, X-ray emission microanalysis of rock-forming minerals IV. Plagioclase feldspars: Jour. Geology, v. 74, p. 217-233.

Schoen, Robert, and White, D. E., 1965, Hydrothermal alteration in GS-3 and GS-4 drillholes, Main Terrace, Steamboat Springs, Nevada: Econ. Geology, v. 60, p. 1411-1421.

Shaw, H. R., and Meyer, Charles, 1959, Phase studies in the Fe-rich carbonates of the Bunker Hill mine, Idaho [abs.]: Geol. Soc. America Bull., v. 70, p. 1674-1675.

Sigvaldason, G. E., 1963, Epidote and related minerals in two deep geothermal drillholes, Reykajavik and Hveragerdi, Iceland: U.S. Geol. Survey Prof. Paper 450-E, p. 77-79.

Sigvaldason, G. E., and White, D. E., 1962, Hydrothermal alteration in drillholes GS-5 and GS-7 Steamboat Springs, Nevada: U.S. Geol. Survey Prof. Paper 450-D, p. 113-117.

Steiner, A., 1953, Hydrothermal rock alteration at Wairakei, New Zealand: Econ. Geology, v. 48, p. 1-13.

———— 1963, The rocks penetrated by drillholes in the Waiotapu Thermal Area, and their hydrothermal alteration: New Zealand Dept. Sci. Ind. Research Bull. 155, p. 26-34.

———— 1968, Clay minerals in hydrothermally altered rocks at Wairakei, New Zealand: Clays and Clay Minerals, v. 16, p. 193-213.

Taboadela, M. M., and Ferrandis, V. A., 1957, The mica Minerals *in* Mackenzie, R. C., ed., The Differential Thermal Investigation of Clays: London, Mineralog. Soc. p. 165-190.

Tatlock, D. B., 1966, Rapid modal analysis of some felsic rocks from calibrated X-ray diffraction patterns: U.S. Geol. Survey Bull., v. 1209, 10 p.

Toulmin, Priestly, 3d., and Barton, P. B., Jr., 1964, A thermodynamic study of pyrite and pyrrhotite: Geochim. et Cosmochim. Acta, v. 28, p. 641-671.

White, D. E., and Sigvaldason, G. E., 1963, Epidote in hot-spring systems, and depth of formation of propylitic epidote in epithermal ore deposits: U.S. Geol. Survey Prof. Paper 450-E, p. E80-E84.

Weissberg, B. G., 1969, Gold-silver ore-grade precipitates from New Zealand thermal waters: Econ. Geology, v. 64, p. 95-108.

Zen, E-an, 1961, The zeolite facies: an interpretation: Am. Jour. Sci., v. 259, p. 401-409.